UILU-ENG-96-2011

CIVIL ENGINEERING STUDIES

STRUCTURAL ENGINEERING SERIES NO. 613

CONNECTIONS TO CONCRETE-FILLED STEEL TUBES

By

YOUSEF MOHAMMED ALOSTAZ

and

STEPHEN PATRICK SCHNEIDER

A Report on Research Sponsored by the

NATIONAL SCIENCE FOUNDATION

NSF CMS 93-00682

DEPARTMENT OF CIVIL ENGINEERING

UNIVERSITY OF ILLINOIS AT URBANA-CHAMPAIGN

OCTOBER 1996

CONNECTIONS TO
CONCRETE-FILLED STEEL TUBES

By

YOUSEF MOHAMMED ALOSTAZ

and

STEPHEN PATRICK SCHNEIDER

A Report on Research Sponsored by the

NATIONAL SCIENCE FOUNDATION

NSF CMS 93–00682

DEPARTMENT OF CIVIL ENGINEERING

UNIVERSITY OF ILLINOIS AT URBANA-CHAMPAIGN

OCTOBER 1996

ABSTRACT

CONNECTIONS TO CONCRETE–FILLED STEEL TUBES

The objective of this research program was to study connections to concrete–filled steel tubes. This research focused on the connection to circular steel tubes, because this shape presents more detailing difficulties compared to the square counterpart. To accomplish the goals of this study, the research was divided into three phases: prototype frame design and analysis, a finite element analysis of several connections, and an experimental study on six large–scale connection specimens. In the first phase, two prototype moment–resisting steel frames were designed to satisfy the *1991 NEHRP Provisions*. The inelastic performance of these frames was studied, and the connections with the highest ductility demand were isolated. The second phase of the research was devoted to the inelastic finite element analysis of several connection details. A 3–D finite element model was developed for each connection detail. The parameters used in the analytical study included: the diameter–to–tube wall thickness ratio, the applied axial load on the column, the moment–to–shear ratio of the girder, and the yield strength of the steel tube. In the third phase of the research, six $^{2}/_{3}$rd–scale specimens were fabricated and tested with the quasi–static method. The flexural strength of the connection was the primary concern in this study. The analytical models and each experimental specimen were a T–shape configuration. A monotonic load was applied to the analytical finite element models. For the test specimens, a predetermined cyclic displacement was imposed at the girder tip, and the specimens were tested to destruction.

Analytical and experimental results suggest that connections which attach exclusively to the tube wall exhibit large distortion of the tube wall in the connection vicinity, thus preventing the development of the girder flexural strength. Using external diaphragms improved the simple connection behavior, however, the performance was susceptible to the geometry of the diaphragm. The behavior was significantly improved when part of the girder forces was transferred to the concrete core. However, the improvement in behavior depended on the connection detail. Continuing the girder through the concrete–filled steel tube was the most effective method to develop the full plastic hinge in the connected girder.

ACKNOWLEDGMENT

This research was funded by the National Science Foundation under Grant No. **NSF CMS 93 – 00682** with Dr. S.C. Liu as the program director. This support is gratefully acknowledged. Opinions stated in this report are those of the author and do not necessarily reflect the opinions of the NSF.

TABLE OF CONTENTS

LIST OF FIGURES

LIST OF TABLES

LIST OF SYMBOLS

The following symbols were used in this report:

A_b = cross section area of an individual bar (in^2),

A_c = cross section area of the concrete core,

A_s = cross section area of the pipe,

A_{so} = shank area of the stud (in^2),

b_f = girder flange width,

C = connection stiffness,

D = outer diameter of the steel tube,

d = girder depth,

d_h = head diameter of the stud (in),

E = modulus of elasticity of the girder,

f'_c = uniaxial compressive strength of the concrete,

F_y = yield strength of the steel tube,

F_{yb} = reinforcement yield strength (psi),

F_{yf} = yield strength of the girder flange,

f'_s = ultimate tensile strength of the stud (psi),

I = moment of inertia of the girder cross–section,

k = effective length factor,

l = girder length measured to the CFT center–line,

l_{db} = bar embedded length (in),

l_e = embedment length of the stud (in),

M = moment on the girder,

M_p = plastic bending strength of the girder,

M/V = moment–to–shear ratio for the girder load,

P = column compressive load,

P_y = squash load of the concrete–filled steel tube column,

P'_U = pull–out capacity of the stud (lb),

R = steel tube radius,

t = steel tube wall thickness,

t_f = girder flange thickness,

V = shear force on the girder,

V_p = shear force needed at the cantilever tip to form a plastic hinge at column face,

V'_U = ultimate shear strength of connection *Type IV*,

V_y = shear strength of the of the connection,

δ = deflection at the tip of the cantilever girder,

θ = angle over which the girder forces are distributed in the simple connection,

τ_{up} = shear strength of the pipe wall.

CHAPTER 1

INTRODUCTION

1.1 STEEL–CONCRETE COMPOSITE CONSTRUCTION

Composite steel–concrete structures are used in civil engineering projects worldwide. Applications include buildings, bridges, foundations, and special structures (Bridge *et. al.* 1992; Faschan 1992; Griffis *et. al.* 1992; Viest 1992). Steel–concrete composite systems combine the advantages of a ductile steel frame with the stiffness of concrete components to control drift. Figure 1.1 shows a possible composite construction sequence, in which the erection of the steel frame precedes placement of the concrete. Provided the steel frame can support construction loads, composite construction can reduce the time of construction.

Steel–concrete composite columns are among the most common type of composite structural system. There are two types of composite columns: concrete encased structural steel columns and concrete–filled tubes (CFTs). Concrete–filled steel tubes have many advantages over other types of columns, including: *1)* the tube eliminates the column formwork during construction, *2)* the tube provides longitudinal and confining reinforcement, so that usual reinforcement for concrete columns is often not used, *3)* the steel pipe prevents spalling of the concrete, and *4)* the concrete prolongs the local buckling of pipe wall. Also, CFTs possess more strength, lateral stiffness, and ductility relative to reinforced concrete columns of similar size.

Although the CFT can be an economical form of composite construction, their use has been limited due to the complexity of the beam–to–column connections and the limited construction experience. Extensive experimental and analytical work has been done to study the behavior of CFTs under different loading conditions, however, research on connections to tubular columns is limited. Therefore, a better understanding of the inelastic behavior of connections is needed to make concrete–filled tube columns a viable alternative in composite construction.

1.2 RESEARCH OBJECTIVE

The object of this research was to investigate the behavior of connections to concrete–filled tube columns experimentally and analytically, with special focus on connections that develop the flexural strength of the connected girder. Although, specimens were tested under slow cyclic displacement, the elastic connection behavior results will benefit the design of frames controlled by wind forces. Only connections to circular steel tubes were considered since these connections present several detailing difficulties not generally associated with the square tube counterpart.

To study the inelastic behavior of connections, this research was divided into three phases:

1) Design and evaluate the seismic behavior of prototype frames using CFTs in the lateral–load resisting system.
2) Develop several connection alternatives and study factors that may influence connection performance using 3–D nonlinear finite element models.
3) Test several large–scale connection specimens identified in phases 1 and 2.

1.3 PREVIOUS RELATED WORK AND LITERATURE REVIEW

CFTs are usually designed for composite behavior (*US–JAPAN planning groups* 1992), which requires shear transfer between the steel tube and the concrete core. Therefore, welding of the girder directly to the tube wall is possible. On the other hand, bond stresses are not generally developed in CFTs in which the steel tube is designed for confinement only. Therefore, part of the girder force should be transferred to the concrete core using shear connectors. Generally, composite action can be achieved with stocky CFTs with diameter–to–thickness (D/t) ratio less than 60, while confinement is realized in slender tubes with $D/t > 100$ or 150. Therefore, connection performance depends significantly on the behavior of the CFT column. Consequently, it is necessary to discuss the most important features in the behavior of concrete–filled steel tubes.

1.3.1 Composite Columns

The current specifications for the analysis and design of composite columns are based on a 1979 Structural and Stability Research Council (*SSRC*) report (*SSRC* 1979). In this report, composite columns were defined as elements with rolled or built up structural steel shapes, or tubing and concrete acting together to resist compression or compression plus bending. To qualify as a composite column, the area of the steel cross section must be at least 4% of the total cross section area of the column, otherwise, the column must be treated as a reinforced concrete column. Further, the D/t ratio of a concrete–filled circular tube must be limited to :

$$D/t = \sqrt{\frac{8E}{F_y}} \tag{1.1}$$

where D is the outer diameter of the pipe, t is the pipe wall thickness, E is the modulus of elasticity of the steel pipe, and F_y is the yield strength of the steel pipe. These composite column provisions apply to steel cross sections with yield strength less than 379 MPa (55 ksi). The purpose of limiting the yield strength of structural steel in composite columns to 379 MPa (55 ksi) is to ensure strain compatibility between concrete and steel.

In response to their experimental work, Kenny *et. al.* (1994) suggested that the yield strength limit could be increased to 552 MPa (80 ksi). In their research, six concrete–filled circular tubes with yield stress in excess of 552 MPa (80 ksi) were tested. The specimens were categorized into two groups: the first group had a D/t ratio of 13.9 with length–to–diameter (L/D) ratios of 5.1 and 17.4, and the second group had a D/t ratio of 15.2 with L/D ratios of 6.5 and 21.8. Five of the six columns tested sustained ultimate loads in excess of the predicted nominal strength. At ultimate load, the steel tubes maintained their cross sectional shape, and no distress of the concrete was observed. Therefore, the recommendation from this research was to increase the yield strength from 379 MPa (55 ksi) to 552 MPa (80 ksi) for CFT columns. However, the limitation on the yield strength is valid for concrete encased steel columns.

Experimental research by Boyd *et. al.* (1995) suggested that the limit on the D/t ratio given by Eq. 1.1 is not justified. Five concrete–filled circular steel tubes were loaded axially, and cyclic lateral deformations were applied at one end. The results illustrated that a pipe with higher D/t ratios had lower ultimate strength and dissipated less energy than did a column with lower D/t ratio, however, the tube with higher D/t ratio had greater ductility. High–strength concrete in the column core resulted in higher ultimate load than columns with normal strength concrete, however, the high–strength concrete core produced greater strength degradation and lower energy dissipation. Tubes with headed studs, welded to the interior side of the tube wall, had higher ultimate strength, less degradation in strength, and a higher dissipation of energy than tubes without studs. Further, the column ductility was slightly increased due to the presence of the studs. However, fracture of the tube wall occurred earlier in tubes with studs, which was attributed to the welding process.

Tomii *et. al.* (1988) suggested that the post–yield behavior for vertical load may be characterized as either: *1)* strain–hardening, *2)* perfectly–plastic, or *3)* degrading stiffness type.

Circular and some octagonal shapes were classified as either type *1* or *2*, while some of the octagonal and all of the square cross sections were classified as type *3*. At high axial loads, circular and many octagonal cross sections confined the concrete core, this resulted in the strain–hardening characteristics for these specimens. Square tubes offered little confinement of the concrete core because the wall of the square tube must resist the concrete pressure by plate bending, instead of hoop stresses, hence there was no axial load increase due to triaxial effects.

Concrete–filled tubes have shown favorable seismic behavior, and they may significantly reduce the construction time. However, a primary obstacle to the use of such columns is the complexity of connections between columns and girders. The following section discusses research work on composite connections.

1.3.2 Related Connections for Composite Construction

The most common type of connections for composite construction consists of a steel girder attached to a structural steel column using web and seat angles. Composite behavior is due to the concrete deck. This kind of composite connections has been the subject of many previous studies (Daniels *et. al.* 1970; Lindsy *et. al.* 1985; Plumier *et. al.* 1993; Anderson *et. al.* 1994; Xiao *et. al.* 1994; and Leon 1994). Other composite connections may consist of steel girders attached to reinforced concrete columns or to structural steel sections encased in reinforced concrete columns. Several studies have been completed on this connection type by Ansourian *et. al.* (1976), Sheikh *et. al.* (1989), Deirlein *et. al.* (1989), and Tschemmernegg *et. al.* (1992). Guidelines for the design of composite joints were published by the ASCE Task Committee on Design Criteria for Composite Structures in Steel and Concrete (1994). However, these guidelines do not cover connections to concrete–filled steel tubes.

Steel elements embedded in a reinforced concrete column were used to connect precast concrete members, such as columns and beams. The *PCI design handbook (1971)* published several provisions for the design and detailing of such connections. There are some detailing similarities between precast connections and connections to tubes, therefore, it is advantageous to review some of the research work available for this connection type.

A typical precast connection is shown in Figure 1.2. For the connection to function properly, the concrete around the embedded steel elements should be consolidated and well confined. Raths

(1974) discussed the importance of holes in the web of the embedded structural section and headed stud anchors attached to the web. Holes in the web, larger than 25.4 mm (1.0″) in diameter, guarantee good concrete consolidation between the flanges of the embedded steel section, and enhance the composite action. Headed studs welded to the web of the embedded member ensure bearing confinement of the concrete between the flanges as well as distribution of bearing stresses.

Marcakis and Mitchell (1980) tested a total of twenty five precast connections incorporating embedded steel members. The parameters for this study included, the column axial load, the effective width of the connection, the amount of reinforcement welded to the connection, the shape of the embedded element, and the eccentricity of loading. The results of the study showed that wide–flange sections embedded in the column were stiffer, and had an 11.0% larger shear strength than embedded hollow structural steel shapes. Further, high axial load in the column reduced the ductility of the connection compared to low axial load. Finally, the results showed that welding reinforcing bars to the embedded structural steel sections significantly increased the capacity and the stiffness of the connection.

Hawkins *et. al.* (1980) connected steel beams to reinforced concrete columns using end–plates and headed studs embedded in the concrete column. Twenty two specimens were tested, and all of them represented an interior joint with a girder on each side of the column. Typical specimens are shown in Figure 1.3. The primary test parameters included the embedded length of the headed studs (101.6 and 152.4 mm), the layout pattern for the studs, and the moment–to–shear ratio (M/V) of the applied load. The results showed that the flexural strength of the connection was severely limited by the tensile strength of the studs and their vertical spacing. Large moments caused relatively brittle failure if the tension studs were not deeply embedded. The connection was ductile when the shear force was high and the moment was low. Severe cyclic loading reduced the ultimate strength of the connection and produced a deteriorating stiffness.

Connections between I–beams and concrete–filled circular tubes were tested by Valbert (1968). These connections were fabricated by welding the girder directly to the tube. During the test, an axial load was applied to the column, and the beam was loaded to failure in monotonic shear. The supports became unstable during testing, and therefore only qualitative results were reported. It was observed that the presence of the concrete core postponed local buckling in the steel pipes. Eventually, the specimens failed by tube wall tearing in the vicinity of the tension flange.

Ansourian (1976) tested connections between wide–flange beams and concrete–filled rectangular tube columns. A total of nine specimens were tested, and all specimens represented exterior joints with the girder on one side of the column only. Some of the connections are shown in Figure 1.4. Eight CFT specimens were tested with an axial–to–squash load ratio between 0.15 to 0.75. A ninth connection specimen was tested as an empty tube, and the load ratio was 0.53. Two specimens were fabricated with welded and plated joints similar to those used in connections to wide–flange columns. These specimens failed by fracture of the V–butt weld connecting the tension flange plate to the tube. Another two specimens had welded connection, but the tension flange force was applied as a compression force to the back side of the tube. The remaining specimens contained shop welded elements, but the connections were assembled using high strength friction bolts. Most of these specimens failed by panel zone collapse after extensive yielding of the tube and varying damage to the connection. However, these details did not account for load reversal, nor did they account for additional elements framing into the joint.

Connections between I–beams and concrete–filled steel tubes were studied by Kanatani *et. al.* (1987). As shown in detail by Figure 1.5, these connections were fabricated by welding end–plates to the girder, and attaching these end–plates to the tube using high strength bolts. A variation of this detail used structural WT–section in place of the end–plates. The girder flanges were bolted to the WT–stem, and the WT–flanges were attached to the column using continuous bolts. For comparison, two other details were fabricated with through and exterior diaphragms as shown in Figure 1.5. Two groups of specimens were tested, one group was subjected to monotonic loading and the other group was subjected to cyclic loads. The results of the test suggest that all connections were able to develop the plastic moment of the connected girder. Most specimens failed by local buckling of the tube wall, and all specimens showed similar behavior regardless of the concrete strength.

Tests on full–scale connections between wide–flange beams and rectangular hollow sections were performed by Dawe *et. al.* (1990). Figure 1.6 illustrates the two connection groups studied. The first connections group was fabricated using tension and compression plates with web clip angles. The second connections group was fabricated using tension plates and seat angles. In both groups, doubler plates were used to stiffen the walls of the hollow section. The experimental program consisted of ten specimens, and all specimens were subjected to monotonic loading only. Note that the tubes were not filled with concrete. Semi–empirical equations were developed to predict the strength of each connection. The results of the study showed that the walls of a hollow section can be reinforced with doubler plates so that full beam capacity can be obtained. Compression flange plates on beams should be avoided or checked against sudden failure by compression buckling. The tube wall thickness must be adequate to withstand the shear developed at the doubler plate periphery.

Connections to hollow steel tubes were also investigated by Shanmugam (1994). Several details were investigated using finite element models, and some connections were tested experimentally. As shown in Figure 1.7, flat plates, angles, or WT–sections were used to stiffen the connection. Flat plates and angles produced high stress concentration in the tube wall, however, connections stiffened with WT–sections showed higher rigidity and ultimate capacity. The best behavior was obtained when the girder flange forces were transferred to the web of the box column.

Azizinamini *et. al.* (1992) tested a connection in which the beam was passed through the CFT column. This required that an I–shaped slot to be cut in the tube wall. After passing the beam through the column, the slot was welded to the beam. Figure 1.8 shows the specimen and the test set–up. To reduce concrete and steel pipe stresses, deformed steel bars were welded to the beam flanges within the column. One cruciform specimen was tested, which was subjected to monotonic loading only. Results suggested that the beam web within the joint experienced a shear type deformation, thereby activating a concrete compressive strut. This strut acted as a diagonal stiffener to assist the beam web in resisting joint shear. A finite element analysis was performed to analyze the proposed detail, and tentative guidelines for the design of such joints were proposed.

Kato *et. al.* (1992) investigated a simple steel beam–to–column moment connection, as shown in Figure 1.9. The connection consisted of external stiffening rings fillet welded to the tube wall to which the beam flanges were welded. A design formula for this connection was proposed, and the validity of this formula was confirmed by a tested connection subassembly. The specimen was designed such that yielding of the beam occurred before yield in the beam–to–column connection. It was shown that properly designed connections can develop the flexural strength of the connected girder. The connection exhibited stable cyclic behavior and excellent energy dissipation capacity.

Morino *et. al.* (1992) tested planar and three dimensional specimens that consisted of wide–flange beams connected to concrete–filled steel tubes. Diaphragm plates, with thickness matching the beam flange, passed through the column and had openings for proper concrete placement. Beam flanges were welded to those diaphragms. Figure 1.10 shows the test set–up and the details of these connections. The specimens were designed for two types of failure modes: shear failure of the panel zone, and flexural failure of the composite column. The study showed that the panel–failing specimens were more stable and exhibited more energy dissipation capacity compared to the column failing specimens. The strength of the three–dimensional panel failing specimens increased after the panel yielded, and the plastic hinge formed in the column. This increase was not observed in the planer specimens, and it was attributed to the confinement of the concrete and strain–hardening of the steel tube. Although some of these connections performed favorably under laboratory conditions, connections similar to this, but without the concrete core, were damaged by the *1995 Hyogoken–Nambu* earthquake near Kobe, Japan (Toyoda 1995). The weld attaching the steel tube to the diaphragm plates fractured, which minimized the lateral–load resisting capacity of the column.

Prion and McLellan (1992) proposed a connection which consisted of end–plates attached to the end of the beam, and each end–plate was attached to the column using through–depth bolts. Results suggested that good shear capacity was obtained from the through–depth bolts. However, it was noted that the bolts were subjected to shear and bending stress due to large eccentricities.

Shakir (1992) tested eight full–scale composite connections. In these connections, shear tabs were used to attach the steel beams to the columns. The shear tabs were fillet welded to the tube skin, and were bolted to the girder web. Cruciform specimens were subjected to a symmetric pattern of loads, which were applied to each beam end and to the CFT simultaneously. Loads were increased proportionally until failure occurred. A typical specimen is shown in Figure 1.11. The use of shear connectors in some specimens increased the failure load by about 7%. No concrete crushing was observed, and the only damage in the connection was the bearing failure of the bolt holes.

It is more convenient to connect the girder directly to the steel tube without using any embedded members. However, this detail produces high local stresses in the steel pipe which may irreparably damage the skin of the steel tube. Connections that utilize embedded components may distribute the girder loads to the concrete core, and consequently may improve behavior compared to connections welded to the tube skin exclusively.

Behavior of connections in previous research suggests that some connections to CFT columns may be considered semi–rigid. This connection restraint has great influence on the behavior of steel frames. Therefore, the following section reviews some main features in the behavior of steel frames with semi–rigid connections.

1.3.3 Steel Frames with Semi–Rigid Connections

Semi–rigid connections were identified in the steel specifications in the *U.S.* since 1946 as *Type III* construction (Lorenz 1985), and were identified as *Type II* in the current *AISC/LRFD* specifications. Beam–to–column connections are classified in *EUROCODE IV* (Johnson 1994) by rotational stiffness needed for elastic analysis, and by the bending capacity which is relevant to the strength of the frame at ultimate load. For stiffness, there are three classes according to the *EUROCODE*: *1)* rigid connections, *2)* semi–rigid connections, and *3)* nominally pinned connections. The nominally pinned connection is designed not to develop a significant moment. The elastic stiffness of the connection is limited by the following equation:

$$C \leq 0.5\left(\frac{E\,I}{L}\right)_b \tag{1.2}$$

where C is the stiffness of the connection, E is the modulus of elasticity of the beam, I is the moment of inertia of the beam, and L is the beam span.

For flexural strength there are three connection type categories: *1)* a full–strength connection should be able to develop a sufficient rotation capacity (*this condition is waived if the strength of the connection is 20% higher than the plastic strength of the beam*), *2)* partial strength connections, and *3)* nominally pinned connections which can not develop more than 25% of the plastic strength of the beam.

Structural engineers are reluctant to design frames with semi–rigid connections (Lorenz 1985). One reason is that the current engineering curricula does not include any topics related to the design of semi–rigid connections. Hence, engineers are trained to design either a simple, pinned–connection or a fully rigid connection. Another deterrent to the use of semi–rigid connection is that the connection must be shown capable of providing the predicted end restraint. So without evidence of this semi–rigid capability, the semi–rigid connections can not be used in a steel frame. Another concern for semi–rigid connections is the need to design stable frames within specified drift limits. In fact, the effect of semi–rigid connections on the stability and drifts of steel frames is not yet fully realized. The need for reliable moment–rotation models for the semi–rigid connections is another obstacle that hinder engineers when designing semi–rigid connections in moment–resisting frames.

Several investigators have recognized the need to understand the behavior of semi–rigid connections (Lindsy *et. al.* 1985; Popov 1985; Kishi *et. al.* 1990; King *et. al.* 1993; Kishi 1993; Wexlar 1993; King *et. al.* 1994; Mander 1994; Sherbourn 1994; Stefano 1994). Most of the work done on semi–rigid connections have focused on steel beams connected to structural steel columns. The design of frames with semi–rigid connections requires special considerations not generally needed for frames with rigid joints.

To design columns in frames, an appropriate value of the effective length factor “K” must be selected. This value is based upon the degree of restraint provided by the joints at both ends of the column. The current steel design specifications use the G–factor method, which is the ratio of the flexural stiffness of the columns to that of the beams at a joint. The values of the G–factor at the upper and lower joints of the column are used to find the appropriate value of “K”. However, this value of “K” is valid only for rigid frames and it does not apply for frames with semi–rigid connections. In order to select a correct value of “K” for columns with semi–rigid connections, it is necessary to know the stiffness of the connections and their influence on the strength of the columns.

Lindsey *et. al.* (1985) suggested some guidelines for the design of steel frames with semi–rigid connections. Lateral drift can be a major problem even in low–rise buildings (2 story) with semi–rigid connections. Frames with semi–rigid connections are vulnerable to stability problems, so it is recommended that columns with fixed bases should be used. The critical issue in the design of any frame with semi–rigid connections is the moment–rotation ($M–\theta$) relationship of the connection. If the $M–\theta$ is not representative of true connection behavior, then the analytical results may be not conservative. The shape of the $M–\theta$ curve has great impact on the overall performance of the frame, $M–\theta$ curves with perfectly plastic behavior may cause serious drift and stability problems.

Leon (1985) performed a test on a full–scale floor subassemblage. The specimen consisted of a two–bay frame with W14×120 columns and W14×38 beams. A 76 mm (3″) light weight concrete composite slab on 50 mm (2″) formed metal deck was used. The connection consisted of a seat–angle and double web angles. The results suggested that the connections had rigidities similar to rigid frames. More over, these connections provided excellent ductility and energy dissipation. The presence of the reinforced composite slab limited the story drift and increased the ultimate strength of the frame.

Some of the factors that may affect the behavior of steel frames with semi–rigid connections were studied analytically by Poggi *et. al.* (1985). This study investigated only one story, one bay steel frames. The results showed that a trilinear representation of the $M–\theta$ relationship of the semi–rigid connection was sufficiently accurate. A bilinear model of the $M–\theta$ relationship was more convenient, but it overestimated the frame strength by about 1.5–6.8%, and underestimated the displacements by more than 30%.

Basu *et. al.* (1989) studied the effects of semi–rigid connections and loading arrangements on frame stability. For these frames the effective length factor for columns in a portal frame were evaluated for different kinds of connections. To study this, a computer program was developed for the large–displacement elastic–plastic stability analysis of plane frames with flexible beam–to–column connections. The results of the analysis showed that flexible connections increased the effective length factor. Moreover, with the same connection flexibility, this increase was more severe in the case of unbraced frames than braced frames. For frames with rigid connections, "K" values obtained with joint loading differ significantly from those obtained for member loading. Effective length factors for semi–rigid connected frames were less affected by applied loads.

Yau *et. al.* (1994) developed a computer program for the nonlinear analysis of steel frames with semi–rigid connections. Two springs connected in series were used to model the semi–rigid connection. One of the springs represented the effect of girder yielding, and the other spring was used to account for the connection flexibility. The computer program was used to investigate the response of one, two, and six–story unbraced frames. It was found that the nonlinear effect for joint stiffness was more profound in frames with loads along beam spans. This was attributed to the induced large rotation at the beam–to–column connection.

From this research, it is clear that moment–resisting steel frames with semi–rigid connections are susceptible to stability problems, and the overall performance of the frame is greatly influenced by the connection behavior. However, in the current engineering practice, the connection is often disregarded until all members in the frame have been sized. Even once the connection is designed, it is cost prohibitive, and often quite difficult, to re–analyze the frame to investigate the consequences of connection behavior on overall building performance.

1.4 REPORT OVERVIEW

Chapter 2 describes the design of two prototype frames to satisfy the *1991 NEHRP* requirements. The inelastic program DRAIN–2DX was used to investigate the seismic behavior each frame to a variety of seismic events. The results from this analysis were essential to isolate the most critical connections in each frame, and identify values for various parameters needed for testing. Different connection details were developed, and a detailed 3–D nonlinear finite element model was created for each detail. A parametric study was performed to investigate the factors that influence the performance of each detail. This finite element analysis is presented in *Chapter 3*. Based on the analytical results, six connection details were selected for experimental testing. The fabrication of the specimens, and the test procedure are presented in *Chapter 4*. A discussion of the test results from the six specimens is given in *Chapter 5*. Practical implications of the results of this research program are presented in *Chapter 6*. Finally, conclusions and recommendations from this research are presented in *Chapter 7*.

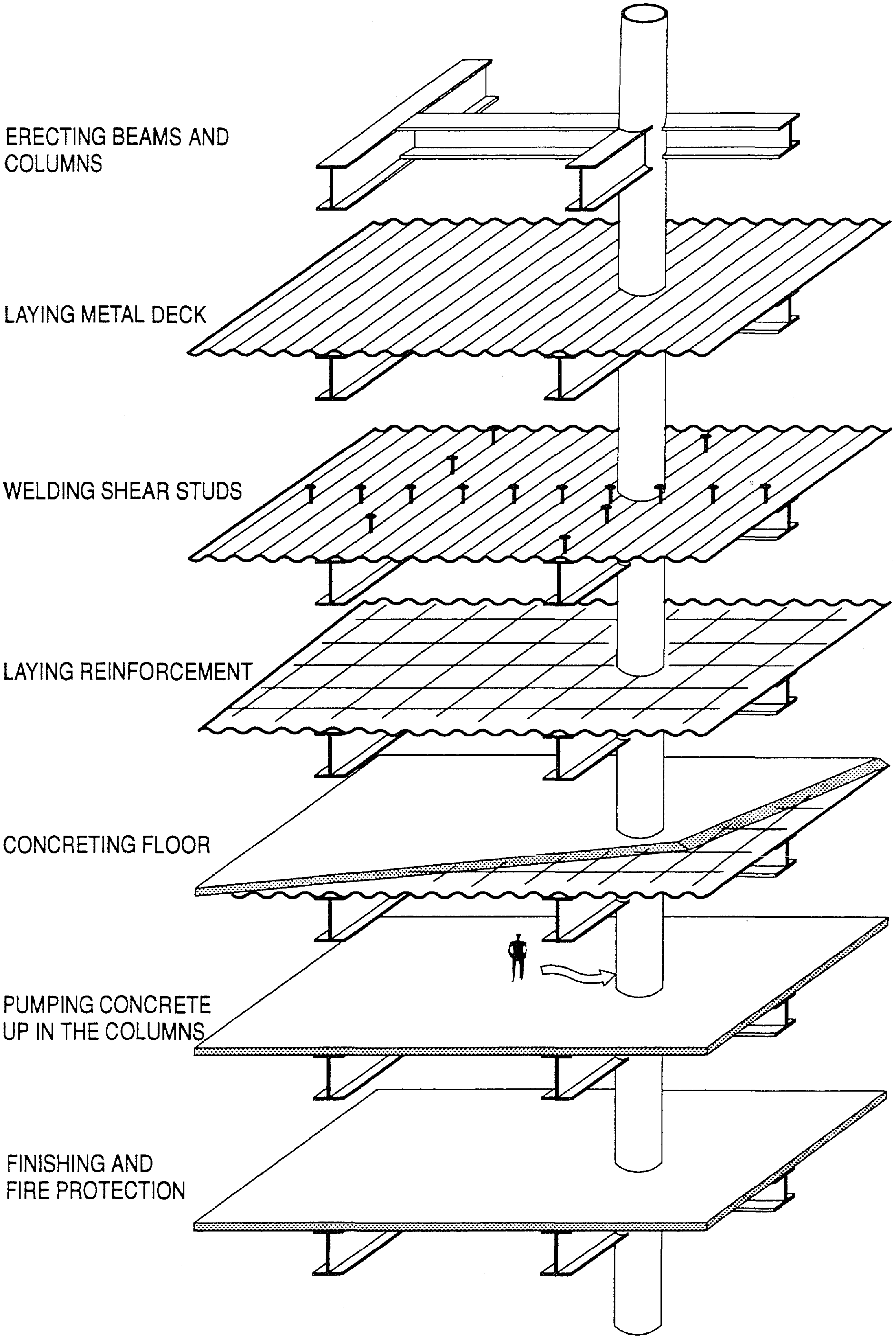

Figure 1.1. Construction Method, Bridge *et. al.* (1992)

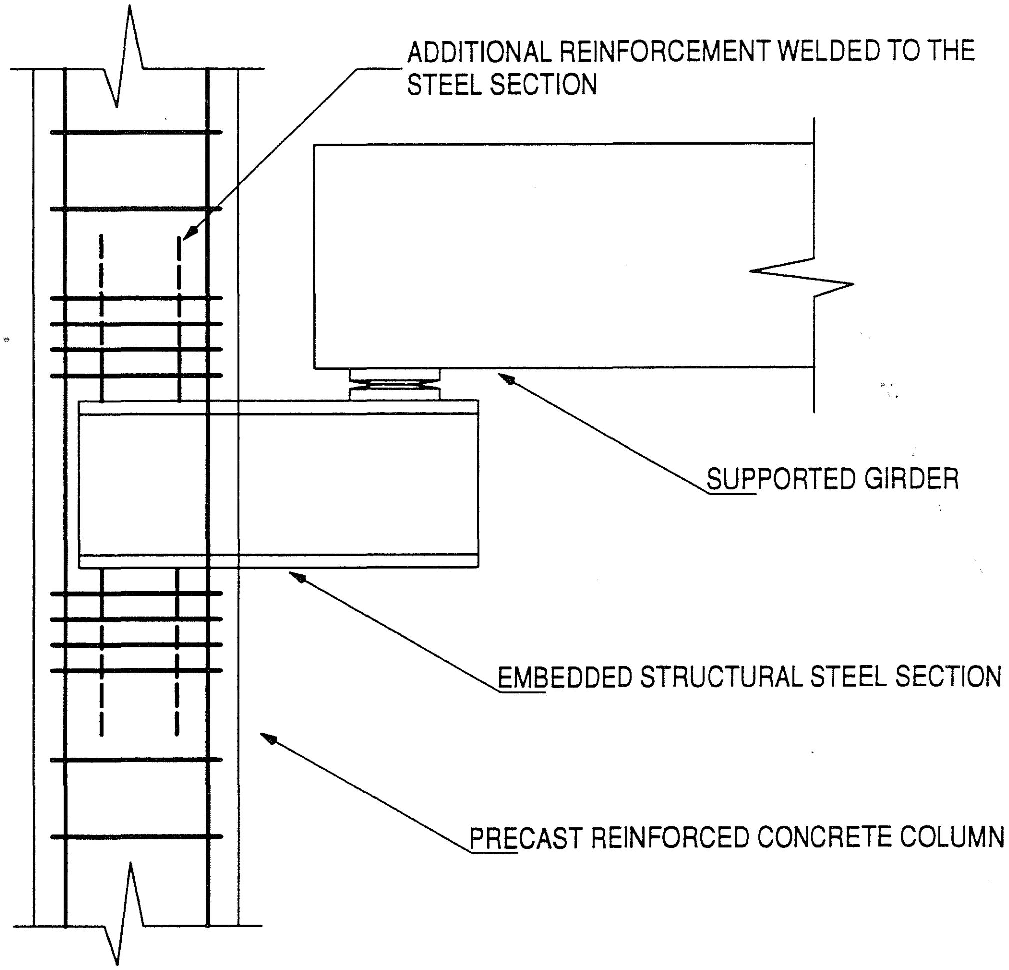

Figure 1.2. A Typical Precast Connection

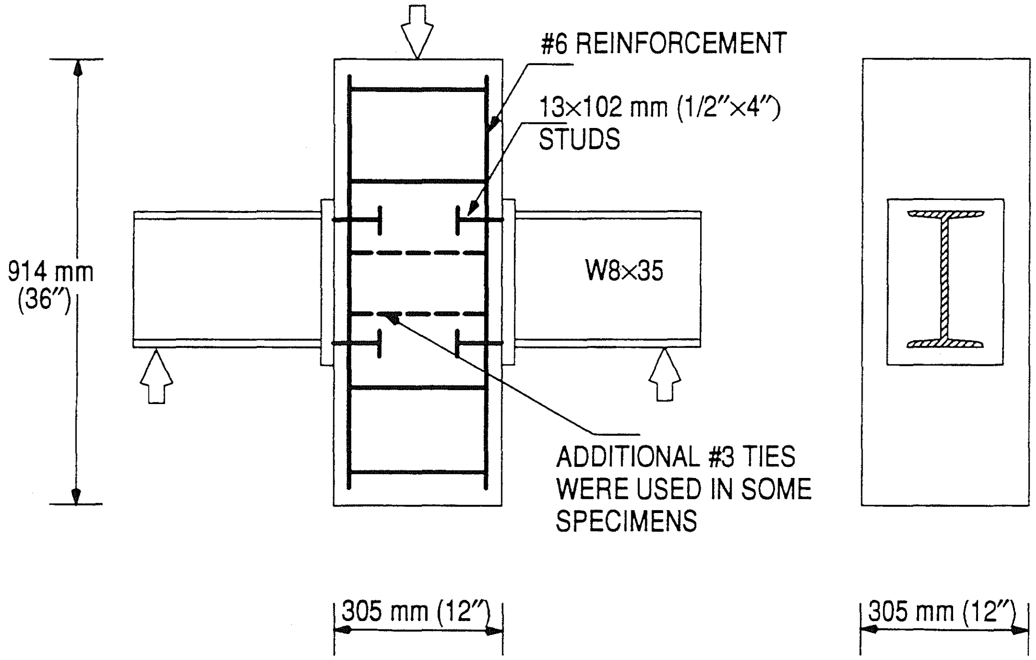

a.) Details of Typical Group I Specimen.

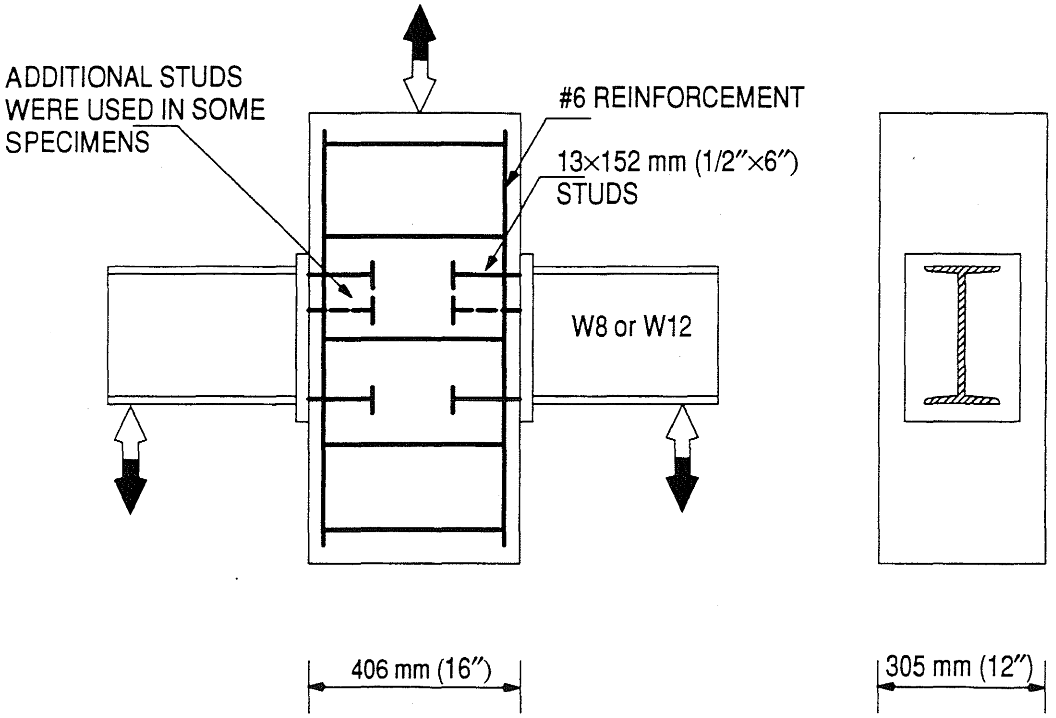

b.) Details of Typical Group II Specimen.

Figure 1.3. Connections to Reinforced Concrete Columns, Hawkins *et. al.* (1980)

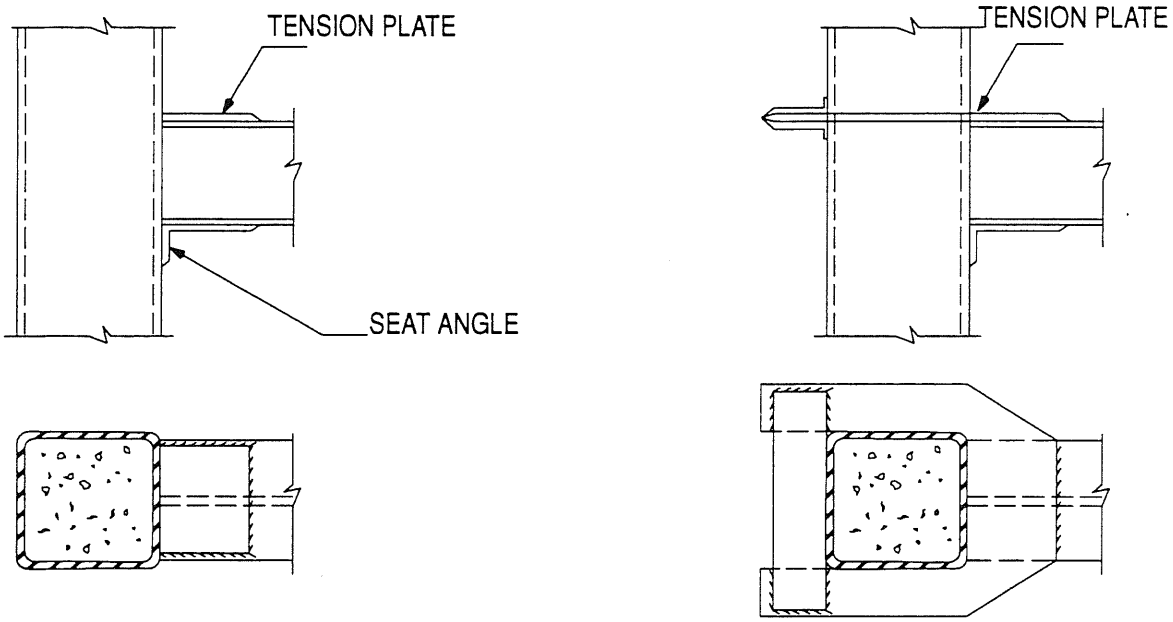

a.) Specimen 1.

b.) Specimen 3.

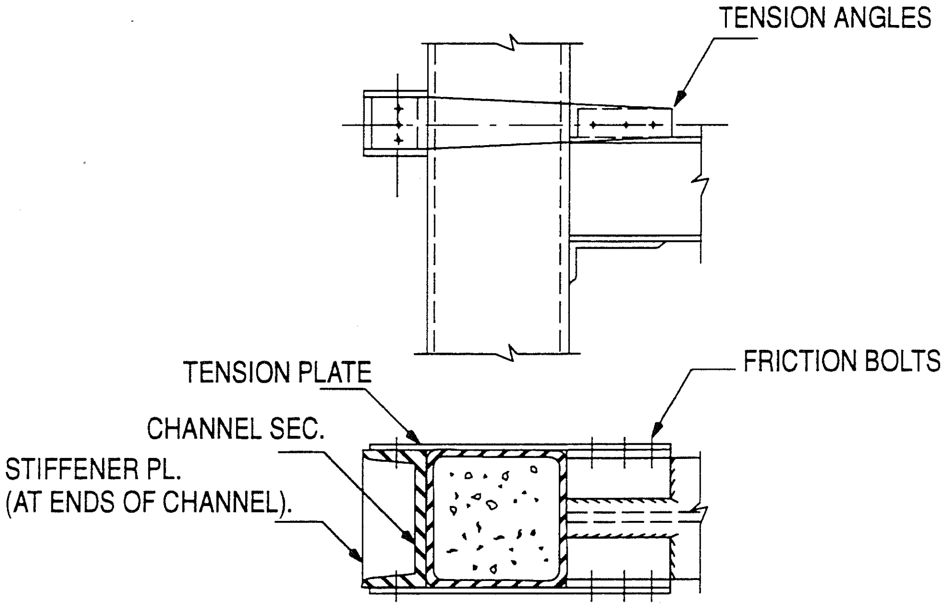

c.) Specimen 7.

Figure 1.4. Some Connection Details Tested by Ansourian (1976)

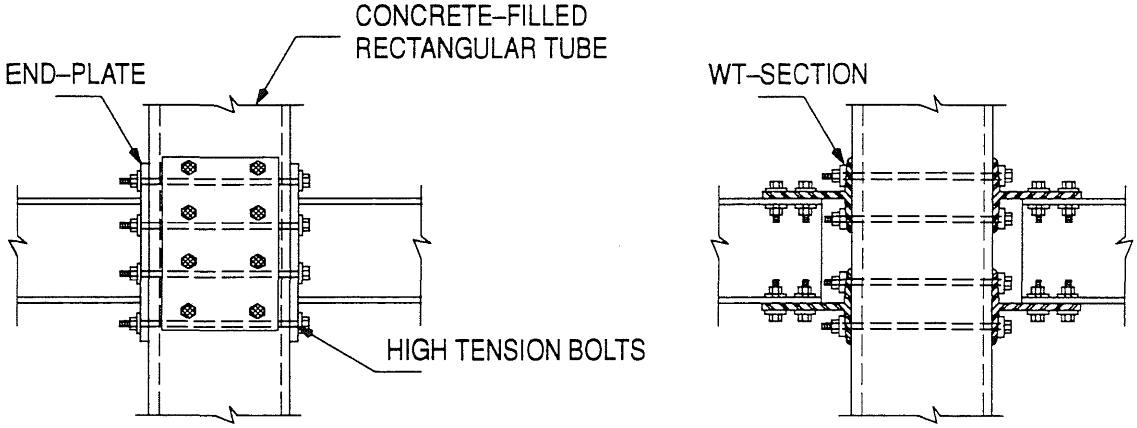

a.) Connection w/ End–Plates.

b.) Connection w/ WT–Sections.

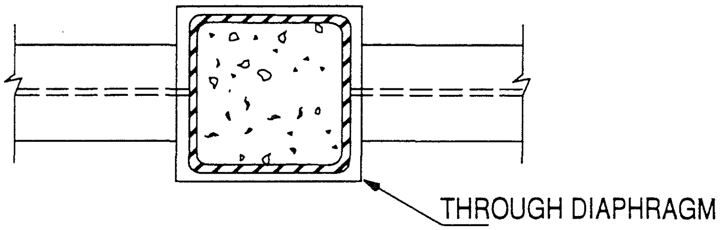

c.) Connection w/ Through Diaphragm.

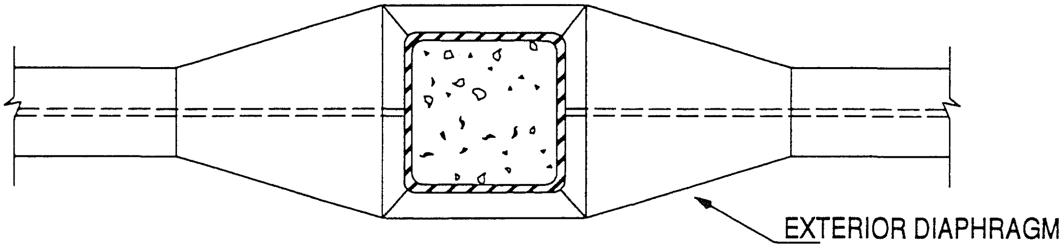

d.) Connection w/ Exterior Diaphragm.

Figure 1.5. Connection Details Studied by Kanatani *et. al.* (1987)

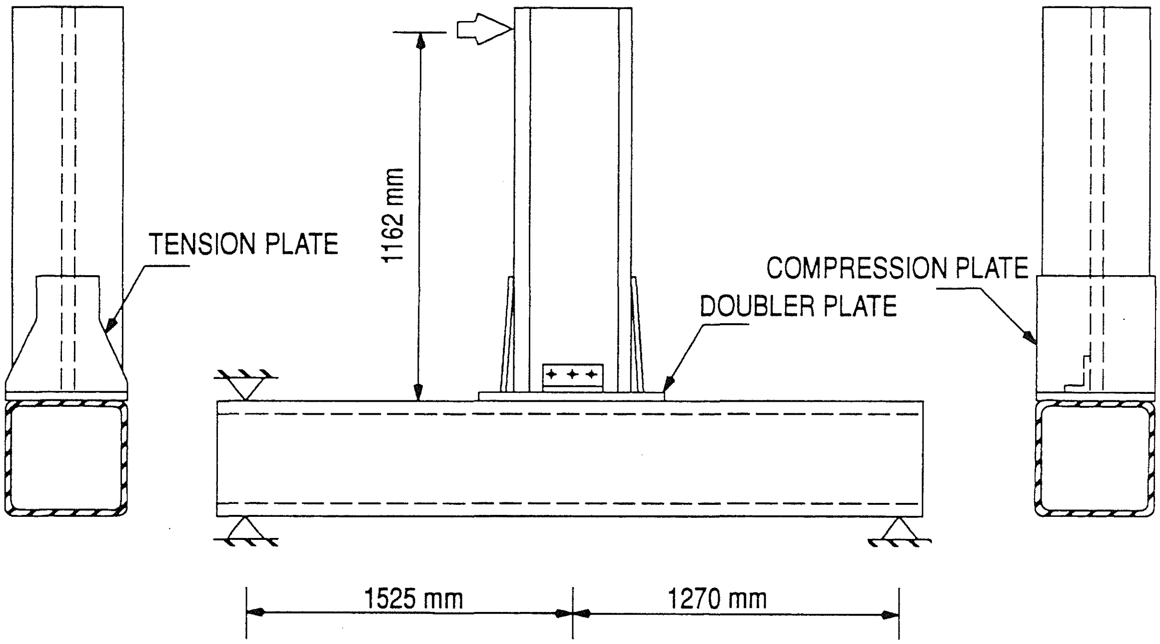

a.) Connection with Tension Plate.

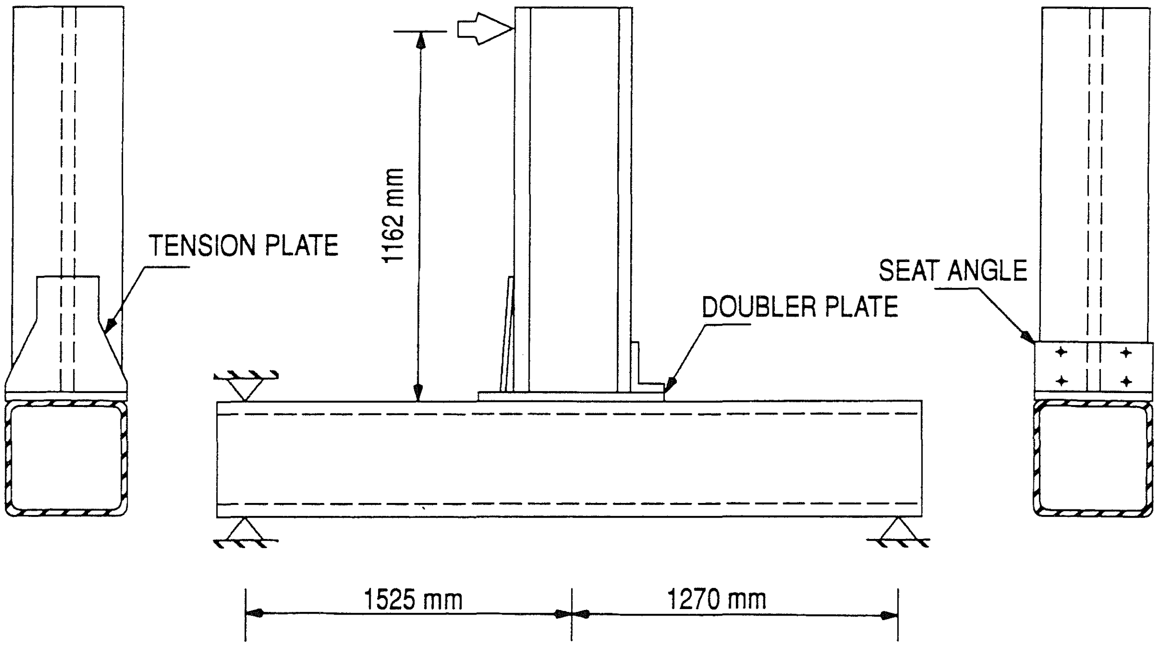

b.) Connection with Tension Plate and Seat Angle.

Figure 1.6. Connections to Rectangular Tubes. (from Dawe *et. al.* 1990)

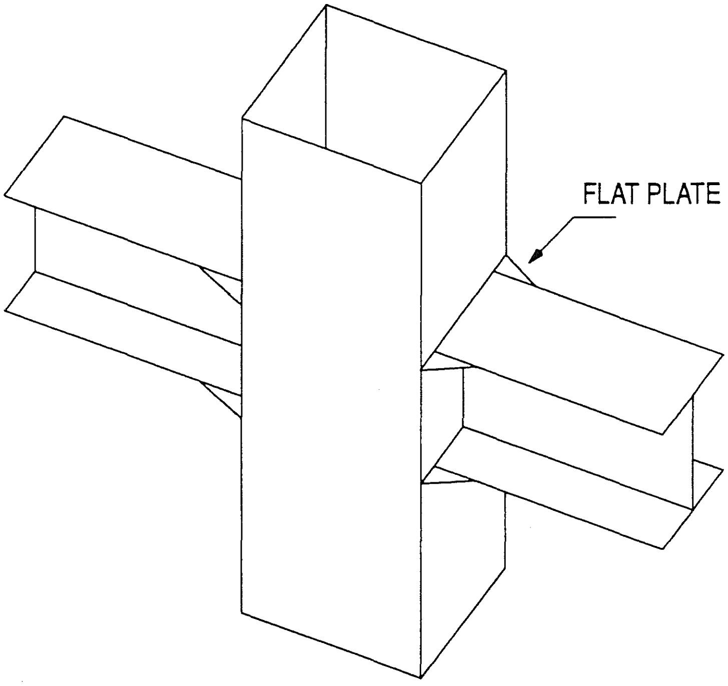

a.) Connection Stiffened with Flat Plates.

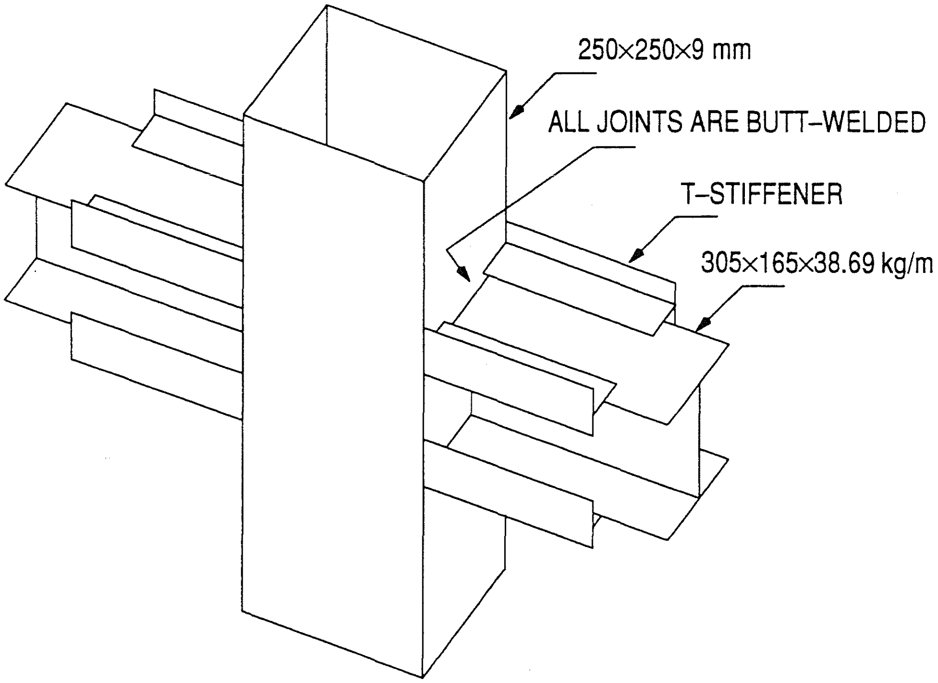

b.) A Typical Specimen with T–Stiffeners.

Figure 1.7. Connections to Tubular Columns, Shanmugam (1994)

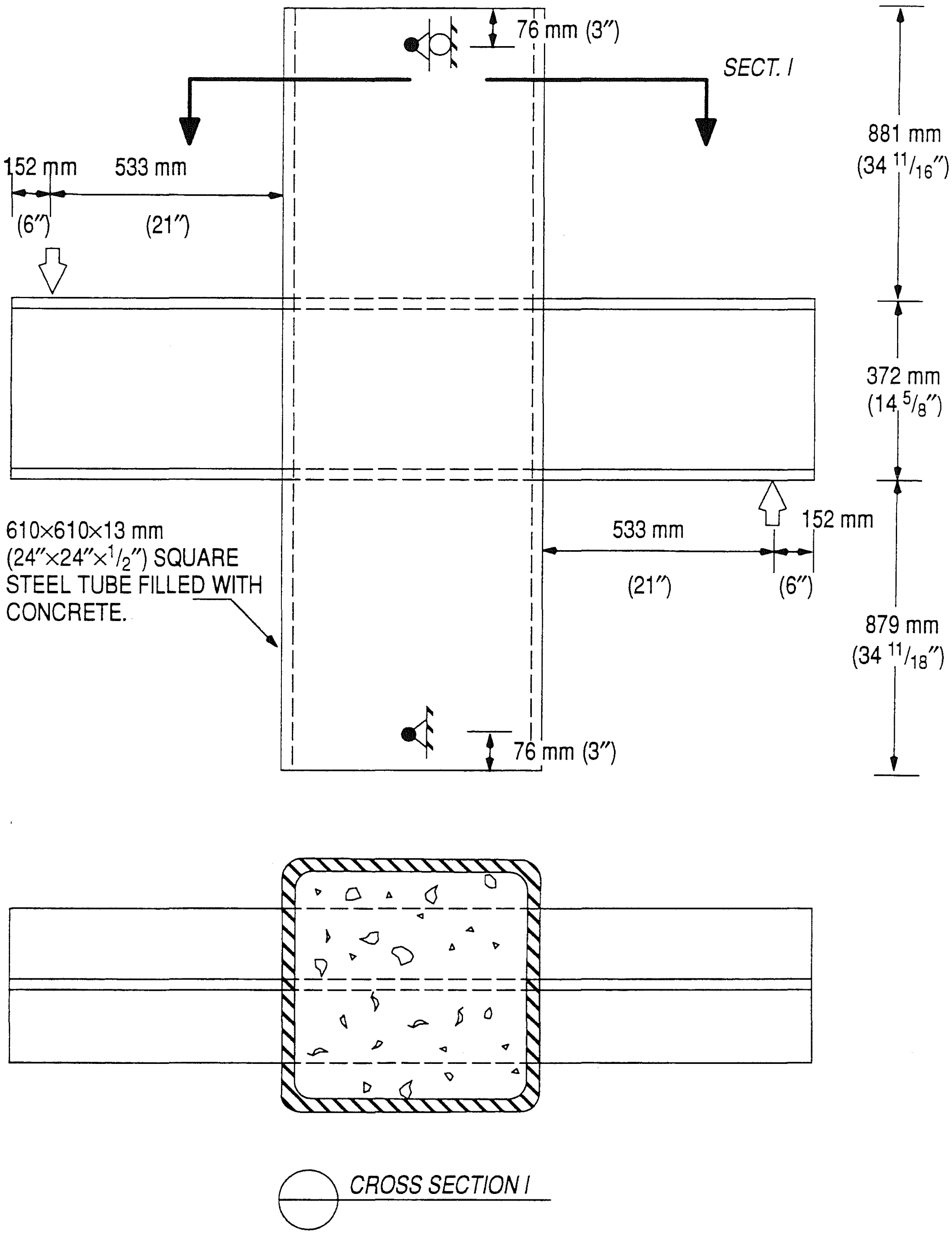

Figure 1.8. Test Specimen used by Azizinamini *et. al.* (1992)

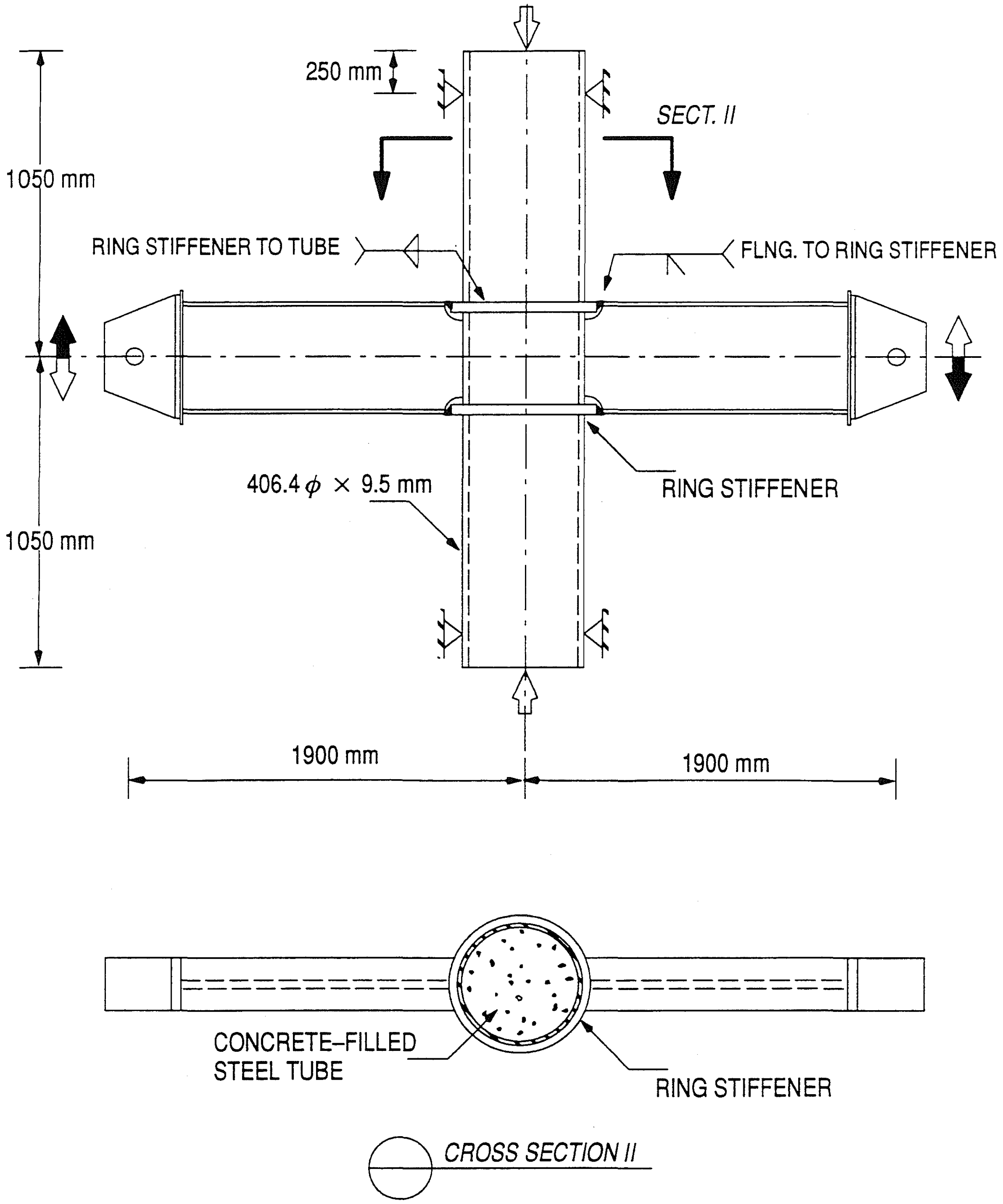

Figure 1.9. Connection to Tubular Column using Ring Stiffener, Kato *et. al.* (1992)

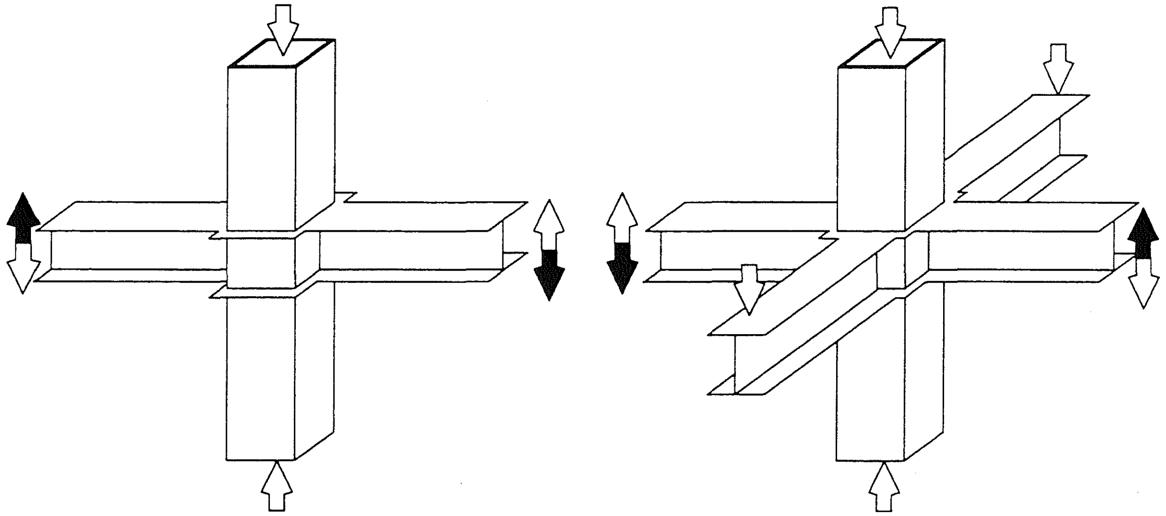

a.) Planer Specimen.

b.) 3–D Subassemblage.

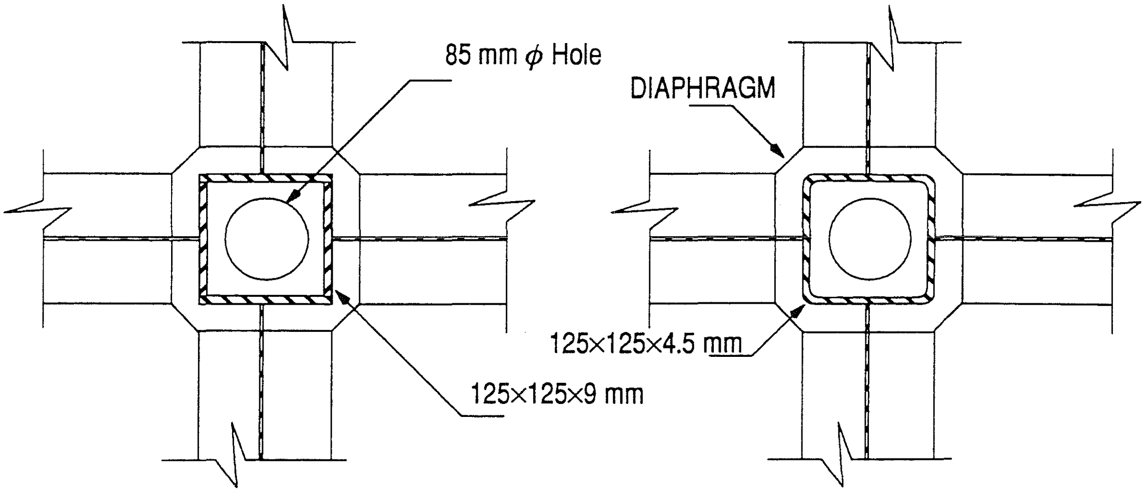

c.) Column Failing Specimens.

d.) Panel Zone Failing Specimens.

Figure 1.10. Connections to Concrete–Filled Rectangular Tubes, Morino *et. al.* (1992)

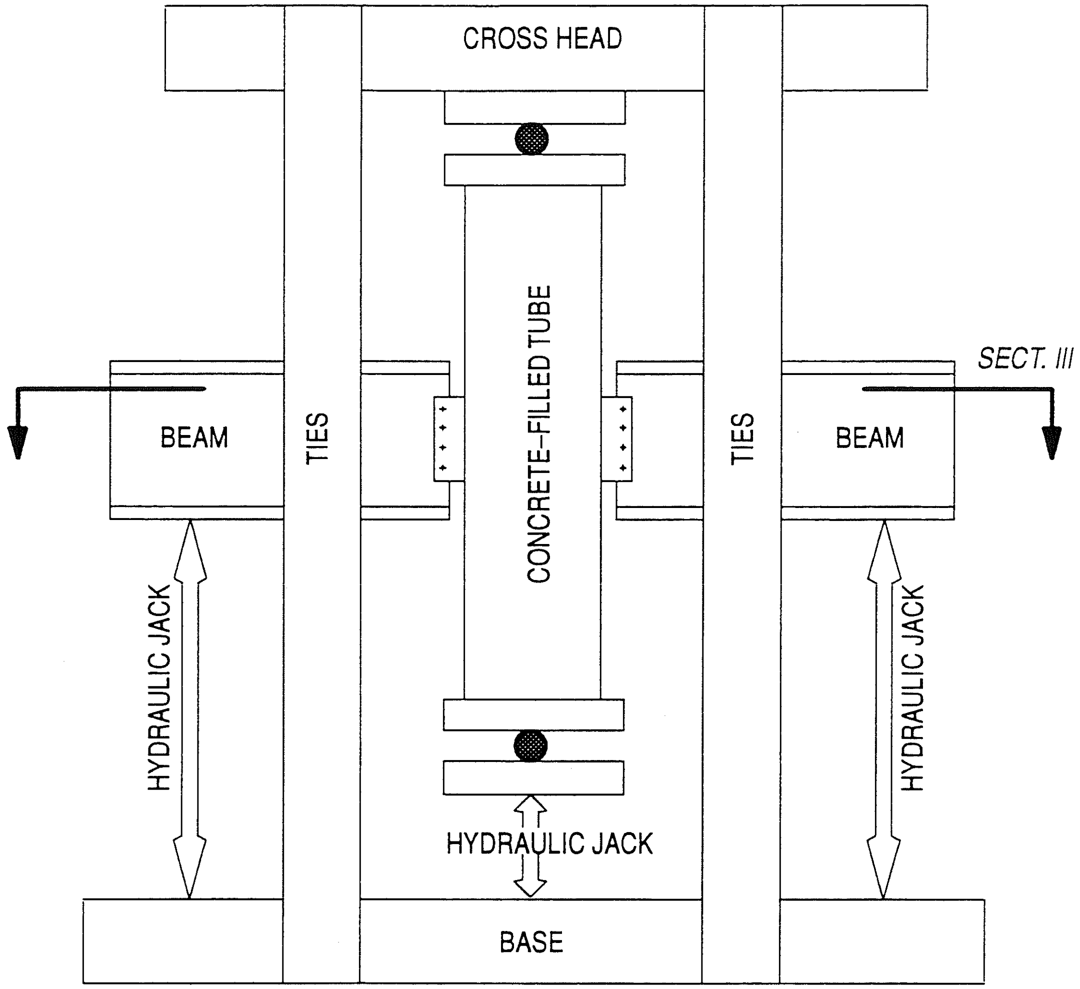

a.) Test Set–Up, Elevation View.

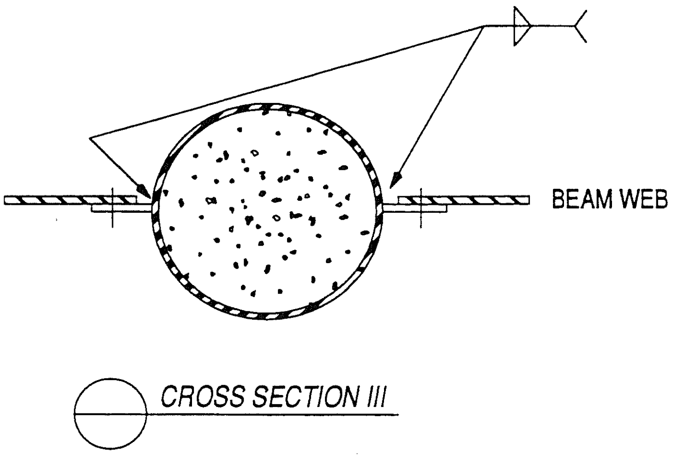

Figure 1.11. Beam–to–Column Connection Using Finplates, Shakir (1992)

CHAPTER 2

PROTOTYPE STEEL FRAMES

2.1 *INTRODUCTION*

Prototype frames were needed to study the essential characteristics of moment–resisting composite frame behavior with concrete–filled steel tubes. These frames were used for the inelastic seismic analysis, and determined approximate sizes and parameters needed for the experimental work. This chapter presents the design parameters and the original inelastic seismic performance of these frames.

2.2 *DESIGN OF THE PROTOTYPE FRAMES*

Prototype frames were selected to be regular and symmetric to avoid any complications that may arise from torsional deformations or from plan and vertical building irregularities. Two moment–resisting steel frames were considered for this project. In order to investigate the influence of the height–to–width ratio of the frame on the structural performance, an 8 story, 5 bay frame, and a 14 story, 3 bay frame were designed. Each structure made use of the perimeter frame concept, in which only the columns around the perimeter participate in lateral load resistance. Figure 2.1 shows the plan view of each frame, and Figure 2.2 depicts the elevations of each frame. Each building was square in plan with a 7.3 m (24′) bay width. The first story was 4.6 m (15′) high, and the subsequent stories were 3.7 m (12′) high. CFT column splices were placed at 1.5 m (5′) above each floor level for convenience during construction. The only CFT elements in the frames were the columns along the perimeter. All other columns were designed as wide–flange sections, and they were not intended to participate in resisting lateral loads. The diameter of the concrete–filled pipes remained constant for all columns along the same column–line. This was done for convenience of column splicing. Column bases were assumed to be fixed. Wide–flange shapes were used for all girders in the prototype buildings.

Each frame was designed assuming a typical office building occupancy. Self weight of the structure consisted of a composite floor with 63.5 mm ($2^{1}/_{2}''$) normal weight concrete on a 50.8 mm (2″) formed steel deck (2.16 kPa, 45 psf), an average of 0.48 kPa (10 psf) for the concrete fill, and

0.72 kPa (15 psf) for the steel framing. Floor sustained dead loads consisted of 0.96 kPa (20 psf) for partitions, and 0.48 kPa (10 psf) for mechanical, electrical and architectural ceiling and floor coverings. Floor live load was 2.39 kPa (50 psf) and these loads were reduced as applicable according to the *UBC* code. Roof dead load was 3.83 kPa (80 psf) and the roof live load was 1.20 kPa (25 psf). The cladding load was 0.96 kPa (20 psf) and it was assumed that the cladding was supported at each floor level. Mechanical, elevator, and other heavy equipment were not considered in the design. The design loads were consistent with loads used in many frame studies as found in the literature.

The building site was selected to be on the fringe of a suburb (*Wind Exposure Group B)* and located in seismic zone *4*. Wind pressures were determined by the *ASCE 7–93 Minimum Design Loads for Buildings and Other Structures*. The following parameters were used to calculate the wind loads:

- Importance factor: I= 1.0
- Wind Speed: v= 128 km/hr (80 mph).

The seismic loads were calculated according to the *1991 NEHRP Recommendation for Seismic Provisions*. The following parameters were used in the calculations of the seismic base shear:

- Effective peak velocity–related acceleration: A_v= 0.4.
- Soil condition Factor: S= 1.4 (between S_2, and S_3 soils).
- Response modification factor: R= 8.

For design purposes, the perimeter frame was separated into four independent plane frames. However, the seismic forces were increased by about 30% to account for the orthogonal effects. It was assumed that each two opposite frames participated in resisting the lateral loads which were in the plane of these frames. Because of symmetry, only one frame needed to be designed. The loads that contributed to the seismic mass were 100% of the floor and roof dead loads from half the total floor plan area, and the cladding weight of half the building perimeter. The mass and stiffness centers of each building coincided with each other. However, the code requires that a minimum accidental eccentricity of 5% of the building dimension must be considered in the frame design. This was done by increasing the seismic mass distributed to the frame by 10%. The portion of the seismic mass due to the cladding weight was not increased. Design story shears for wind and seismic forces are shown in Figure 2.3. Clearly, the seismic forces controlled the design of both frames. The final design of the structural elements was done according to *the 1994 AISC/LRFD* specifications. The element sizes for each frame are shown in Figure 2.2.

An average strength concrete of f_c'= 34.5 MPa (5.0 ksi) was used for the CFTs. The steel pipes were designed for a yield strength of F_y= 317 MPa (46 ksi), and for preliminary design, the design charts provided by the *American Institute for Hollow Steel Sections* were used. Since steel pipe yield strength ranges between 248 and 317 MPa (36 – 46 ksi), the yield strength of the tube was among the parameters studied using finite element models. While F_y= 317 MPa (46 ksi) was used for the tubes, A36 steel (F_y= 248 MPa) was used for all other structural elements. The stiffness of each concrete–filled steel tube was calculated according to the *1994 AISC/LRFD* specifications. The story drift was limited to the 1.5% of the story height as required by the *1991 NEHRP Provisions*. Serviceability controlled the design of some structural elements.

2.3 INELASTIC SEISMIC ANALYSIS OF THE PROTOTYPE FRAMES

DRAIN–2DX (Kanaan and Powel 1973) was used to investigate the inelastic seismic performance of the the prototype frames, and a modal analysis was done to calculate the natural periods of these structures. The mode shapes for the first three modes of vibration for each frame are shown in Figure 2.4. The modal analysis showed that the fundamental periods of vibration were T_{MA}= 1.65 and 2.61 seconds for the 8 and 14 story frames, respectively, while the approximated *NEHRP* periods of vibration were T_{NEHRP}= 1.10 and 1.66 seconds. So the fundamental natural periods of vibration calculated using the modal analysis were approximately 50–57% higher than the approximate values.

The beam–column element (*element type 2*) of DRAIN–2DX was used to model the moment frame members. This element does not account for stiffness deterioration or for plastic shortening due axial loads. Plastic behavior occurs only at the nodes which are located at the element ends. Bilinear load–deformation relations were used for each element, and 2% strain–hardening was assumed. Viscous damping for each frame was assumed to be 2% of critical damping.

The axial load–moment (*P–M*) interaction curve requires the specification of both negative and positive yield moments as well as ultimate axial loads in tension and compression. For girders, the plastic bending capacity (M_p) was calculated as the yield stress (F_y) times the plastic section modulus (Z_x), *i.e.* $M_p = F_y Z_x$. Negligible axial forces were assumed in the girders, hence, the beam yield surfaces were used for these elements. The behavior was quite different for columns which were made of steel pipes filled with concrete. Figure 2.5a shows a typical axial load–moment interaction curve used for concrete–filled steel tube. Many relationships to model the axial load–moment interaction curves for concrete–filled steel tubes have been proposed by different researchers. However, these models are not widely used. Therefore, the axial load–moment interaction relation was determined using the *1994 AISC/LRFD Specifications*. Although this interaction relationship is conservative, and it might produce early yielding in the CFT column, this relation is sufficient for the present research.

The ultimate axial load for a composite column in tension (P_{yt}) was calculated based on the steel area (A_s), while the contribution of the concrete was ignored, *i.e.* $P_{yt} = A_s F_y$. The ultimate axial load in compression was calculated according to *Section H* of the *1994 AISC/LRFD specifications*. At ultimate moment, it was assumed that the pipe yielded and the concrete on the compression side had crushed. The concrete stresses were approximated using the *ACI* stress block, and an iterative procedure was used to solve for the plastic bending capacity. The contribution of the concrete on the tension side was ignored.

Due to symmetry, only one side of the total perimeter frame system was analyzed. Horizontal and vertical eccentricities were assumed at each beam–to–column connection, see Figure 2.6.

Since each prototype frame was designed for a region of high seismicity, the inelastic dynamic behavior of each frame was evaluated using various ground motion records that occurred in a seismic zone *4* region. Each frame was subjected to the following unmodified acceleration records:

- 1940 El Centro (5/18/1940) : Imperial Valley Irrigation District, S 00°E,
- 1952 Taft (7/21/1952) : Lincoln School Tunnel, N 21°E,
- 1971 Pacoima Dam (2/9/1971) : San Fernando Earthquake,

- 1979 Imperial Valley (10/15/1979) : Imperial Valley College, Array 7, N 230°E,
- 1989 Loma Prieta (10/17/1989), and
- 1994 Northridge (1/17/1994) : Santa Monica–City Hall, Channel 1: 90 DEG.

These earthquake records are shown in Figure 2.7. It is believed that seismic events with large velocity pulses may produce a large ductility demand on moment–resisting steel frames (Schneider *et. al.* 1992). Therefore, the ground velocities, obtained by integrating the acceleration records, for each earthquake record are shown in Figure 2.8.

2.4 RESULTS OF THE INELASTIC SEISMIC ANALYSIS

The inelastic seismic behavior of each prototype frame was investigated using each ground motion record. Some of these records produced similar results. In general, the 1952 Taft had very low peak acceleration, and hence resulted in negligible inelastic deformations. On the other hand, the 1979 Imperial Valley record produced the largest inelastic deformations. This is consistent with previous research in which the seismic behavior was found to be significantly dependent on the ground acceleration record used in the study (Schneider *et. al.* 1992). One seismic event may cause an almost even distribution of the dissipated energy in the frame elements. However, the same frame may exhibit a concentration of damage in only few floors when subjected to a different seismic event.

Moment–resisting frames are usually designed for the hinging girder conditions in which the plastic deformations are concentrated in the connections and the connected girders. Therefore, the focus of this research is on the connection performance, not the joint behavior. For the current study, the response of connections to exterior columns is sufficient.

2.4.1 Drift and Ductility

The story drift envelopes for each frame are depicted in Figure 2.9. In both frames, the 1940 El Centro and the 1994 Northridge earthquakes caused an almost uniform drifts in all floor levels, and these drifts were less than the 1.5% limit specified by the *1991 NEHRP Provisions*. A strong seismic event like the 1979 Imperial Valley caused larger story drifts of up to 6% in a low–rise frame. However, taller frames were less susceptible to larger drifts. It appeared that the *1991 NEHRP Provisions* were not sufficient to control the drift of moment–resisting steel frames when subjected to strong ground motion records.

Comparison of the drifts between the two frames showed that the short frame had a significant change in drift distribution along the frame height. The first floor in the 8 story frame was subjected to the largest drift. Drift response of the two stories with the highest drift in each frame are shown in Figures 2.10 through 2.13 for various ground motion records. It is clear that some permanent inelastic deformation may occur under strong earthquakes. The tall frame showed story drifts which were closer to the 1.5% drift limit compared to the short frame. Generally, the story drift controlled the design of the tall frame more than the short frame. This is among the reasons that make short structures susceptible to large story drifts.

The story drift is an indication of the ductility demand at that story. The ductility demand, or the ratio of the maximum inelastic to initial yield rotation, for joints at the exterior column in each frame is depicted in Figure 2.14. This figure illustrates that the 1971 Pacoima Dam and the 1979 Imperial Valley earthquakes produced the highest ductility demand in both frames. However, the frames had different response to these two seismic events. For the tall frame, the 1979 Imperial Valley earthquake produced an almost uniform ductility demand of 4 times the yield displacement up to the 7th floor. Above the 7th floor, the ductility demand decreased almost linearly with increased height in the frame. The Pacoima Dam earthquake imposed a maximum ductility demand of about 3 on the tall frame. For the short frame, the ductility demand decreased almost linearly from a maximum value of about 7 at the first floor to almost zero at the roof level.

For the 8 story frame, the ductility demand decreased gradually from a maximum value at the first floor. The 1979 Imperial Valley earthquake produced a ductility demand of approximately 7 times the yield displacement, while the 1971 Pacoima Dam record yielded a value of about 4. From the results shown in Figure 2.14, it was observed that almost all seismic events, considered in this research, imposed higher inelastic deformations on the short frame than the tall frame.

The deformed shape of both prototype frames during the 1979 Imperial Valley earthquake is shown in Figures 2.15 and 2.16. Both frames experienced large displacements during the second largest pulse of the ground velocity, which occurred between 11.4 and 12.0 seconds. During this interval, about 86% and 89% of the plastic hinges were formed in the tall and the short frame, respectively. Therefore, both frames sustained considerable damage during the first moments of this earthquake. Such damage and extreme story drift could seriously reduce the lateral resistance of these frames, hence, make them susceptible to total collapse before the end the earthquake or during after shocks.

2.4.2 Hysteretic Energy Dissipation

Comparison of Figures 2.17 through 2.21 clearly illustrates the dependency of the seismic response of a structural frame on the ground motion record. These figures show the percentage of the total energy dissipated by the frame at each floor.

For the the 14 story frame, the largest energy demand resulted from the 1979 Imperial Valley earthquake, and 78.0% of this energy was almost evenly distributed to floors 1 through 7. The same frame dissipated almost one–third of this energy for the 1971 Pacoima Dam earthquake, and some concentrated damage was observed in the first two floors. On the other hand, the 1940 El Centro earthquake resulted in larger damage to the beams between the 7th and the 10th floors which dissipated about 44% of the energy. For this frame, it was clear that it had the largest inelastic energy demand during the 1979 Imperial Valley earthquake.

Figures 2.17 through 2.20 illustrate the symmetry of the energy distribution along each column line, and they show that the majority of the plastic hinges were developed in the girders. For the 14 story frame, story drift and ductility demand from the 1971 Pacoima Dam earthquake were higher than those from the 1989 Loma Prieta earthquake. However, the reverse was true for the total dissipated energy. This was primarily due to the fact that the 1971 Pacoima Dam earthquake produced a single large cycle of inelastic deformations followed by smaller cycles. On the other hand, the 1989 Loma Prieta earthquake imposed many cycles of inelastic deformations, but with smaller amplitude.

The short frame showed a concentrated damage to the first floor during the 1979 Imperial Valley and the 1940 El Centro earthquakes. However, during other seismic events, the first three floors dissipated the majority of the inelastic energy, and the energy distribution to these floors was almost uniform. Again, this illustrates the dependency of the frame behavior on the seismic event. At least 14% of the total energy was dissipated by the plastic hinges at the bottom end of the first floor columns. In general, the short frame dissipated significantly more energy than the tall frame. Most of this energy was dissipated by members in the lower floors of the 8 story frame. This behavior was due to the fact that these floors experienced large story drifts.

2.4.3 Base Shear Demand

The base shear demand from various seismic events is shown in Figure 2.22 for both prototype frames. This shear represents the maximum shear calculated in the first floor columns at any time step during the seismic response. The ultimate shear capacity of each frame is also shown in the same figure. Figure 2.23 shows a push–over analysis of both frames. For this analysis, a static lateral load consistent with *1991 NEHRP Provisions* was applied to each frame.

The ultimate shear capacity was calculated using the Upper Bound Limit Theorem. This theorem requires an assumption of a kinematically admissible dynamic mechanism. The prototype frames can be characterized as strong column–weak beam frames, hence, the plastic hinges were likely to develop in the girders. Further, the DRAIN–2DX analysis clearly showed that most of the plastic hinges were developed in the girders, refer to Figures 2.17 through 2.20. Plastic hinges should develop at the bottom of the first floor columns, this is necessary to have a complete admissible failure mechanism. Therefore, a sway "panel" mechanism was assumed for both frames. Distribution of seismic forces is related to the mass and the linear acceleration of each floor. The linear acceleration at each story is proportional to the angular acceleration (*the second derivative of the frame rotation with respect to time*). But since each floor has the same mass, then the distribution of seismic forces should be linear.

The ultimate shear capacity of the 8 story frame was 3,738 kN (840 kips), and it was 1,753 kN (394 kips) for the 14 story frame. These frames were designed for base shear of 1,446 and 654 kN (325 and 147 kips), respectively. This shows that there is a considerable amount of reserve shear strength in both frames with a safety factor of 2.6 for the 8 story frame and 2.7 for the 14 story frame. Results shown in Figure 2.22, suggest that both frames have developed a full plastic mechanism.

2.4.4 Moment–Rotation Relationships for Frame Elements

The moment–rotation diagrams for girder ends connected to the exterior columns are shown in Figures 2.24 through 2.26. These girder ends were selected because they exhibited highest ductility demands under most of the ground motion records used in this study. The 1979 Imperial Valley earthquake produced the largest inelastic rotations at the beam ends in both frames. For the 14 story frame, the 1979 Imperial Valley earthquake produced a maximum inelastic rotation of about 0.040 radians, while the 1971 Pacoima Dam and the 1989 Loma Prieta earthquakes resulted in about

0.026 and 0.020 radians, respectively. The 1971 Pacoima Dam acceleration record imposed a single large cycle of inelastic rotation followed by several small cycles, and no reversal of deformations were observed. The other two earthquakes imposed several cycles of inelastic deformations. Evidence from previous research (Schneider *et. al.* 1992) indicates that the demand due to some earthquakes like the 1971 Pacoima Dam earthquake, may produce local instability (*such as local buckling in the flanges*) in the wide–flange girder. Consequently, rapid deterioration in the flexural strength of an actual wide–flange beam may occur.

For the 8 story frame, the 1979 Imperial Valley record produced a single large cycle of plastic rotations and several other cycles of considerable magnitude. No deformation reversals were noted. The maximum inelastic rotation for this earthquake was about 0.060–0.070 radians. The 1971 Pacoima Dam and the 1989 Loma Prieta earthquakes resulted in a maximum inelastic rotation of 0.032 and 0.027 radians, respectively.

In general, strong seismic events, such as the 1979 Imperial Valley and the 1971 Pacoima Dam earthquakes, tend to impose a few large cycles of plastic deformations with very little reverse deformations. Previous research (Schneider *et. al.* 1992) raised some doubts on the ability of actual wide–flange beams and connections to provide large rotation capacities. Therefore, only experimental study can fairly address these issues.

2.5 SUMMARY OF INELASTIC DYNAMIC RESULTS

This analysis assumed frames with rigid connections. Connection rigidity is highly susceptible to the connection detail and is often not considered in the design process. The results of this inelastic study showed that story drift can be much greater than the current *NEHRP Provision* limit of 1.5%. This was most noticeable in the short frame. It was expected that this problem will be more serious if actual connections exhibit semi–rigid moment–rotation behavior.

Clearly, for these frames, strong earthquakes will impose high ductility demands on the connections. This may lead to significant damage to the connections and to the frame. Therefore, the focus of this research concentrates on the design and detailing of these connections.

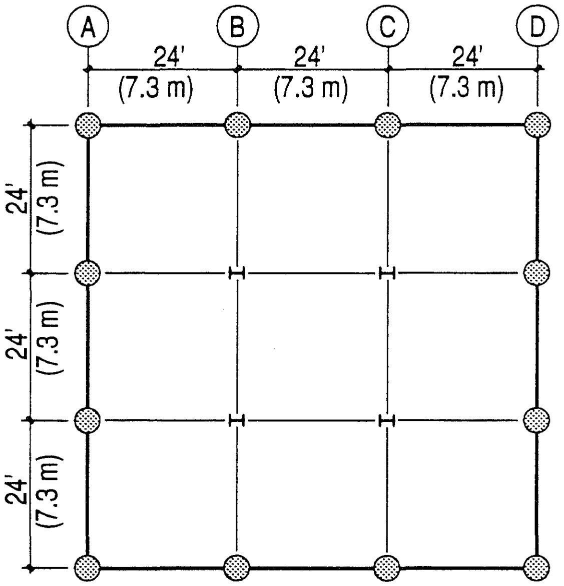

a.) 14 Story Frame, Plan View.

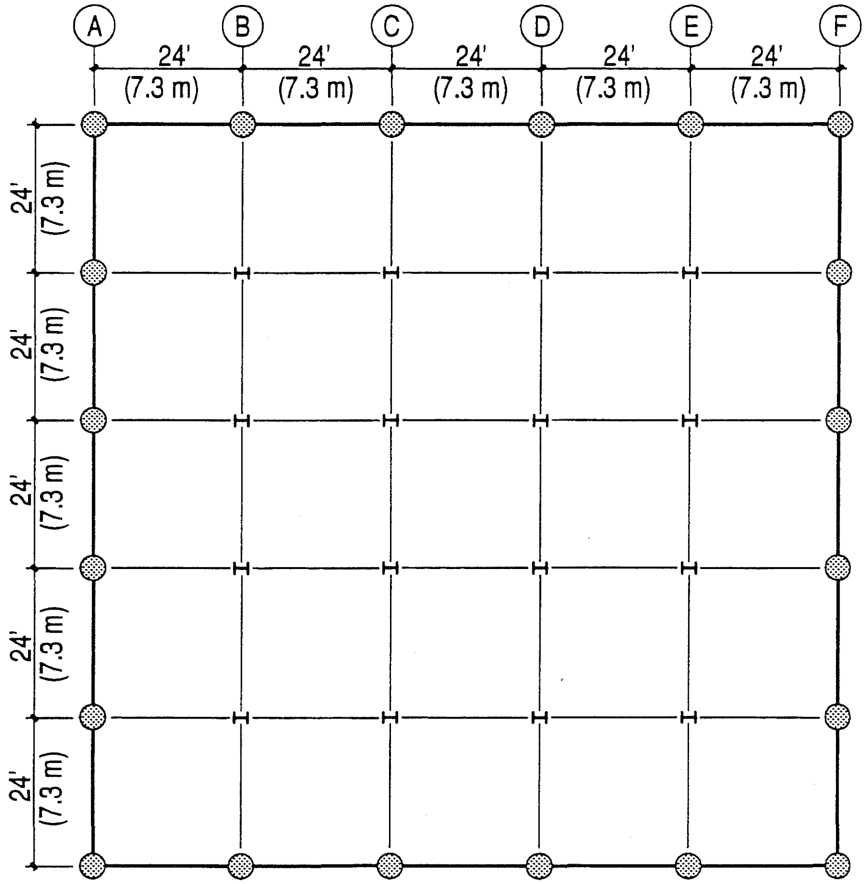

b.) 8 Story Frame, Plan View.

Figure 2.1. Plan View of the Prototype Buildings

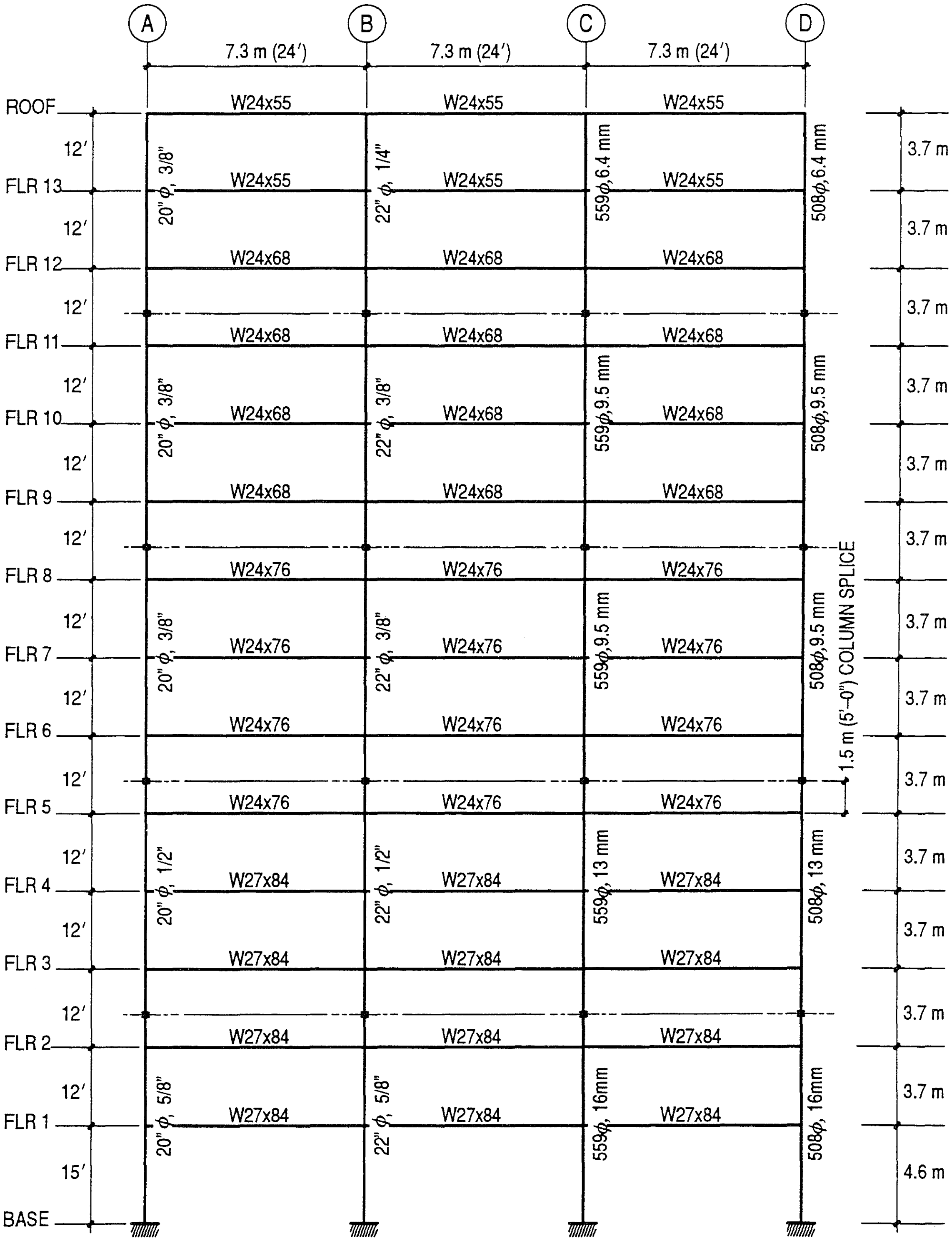

Figure 2.2a. 14 Story Perimeter Frame, Elevation

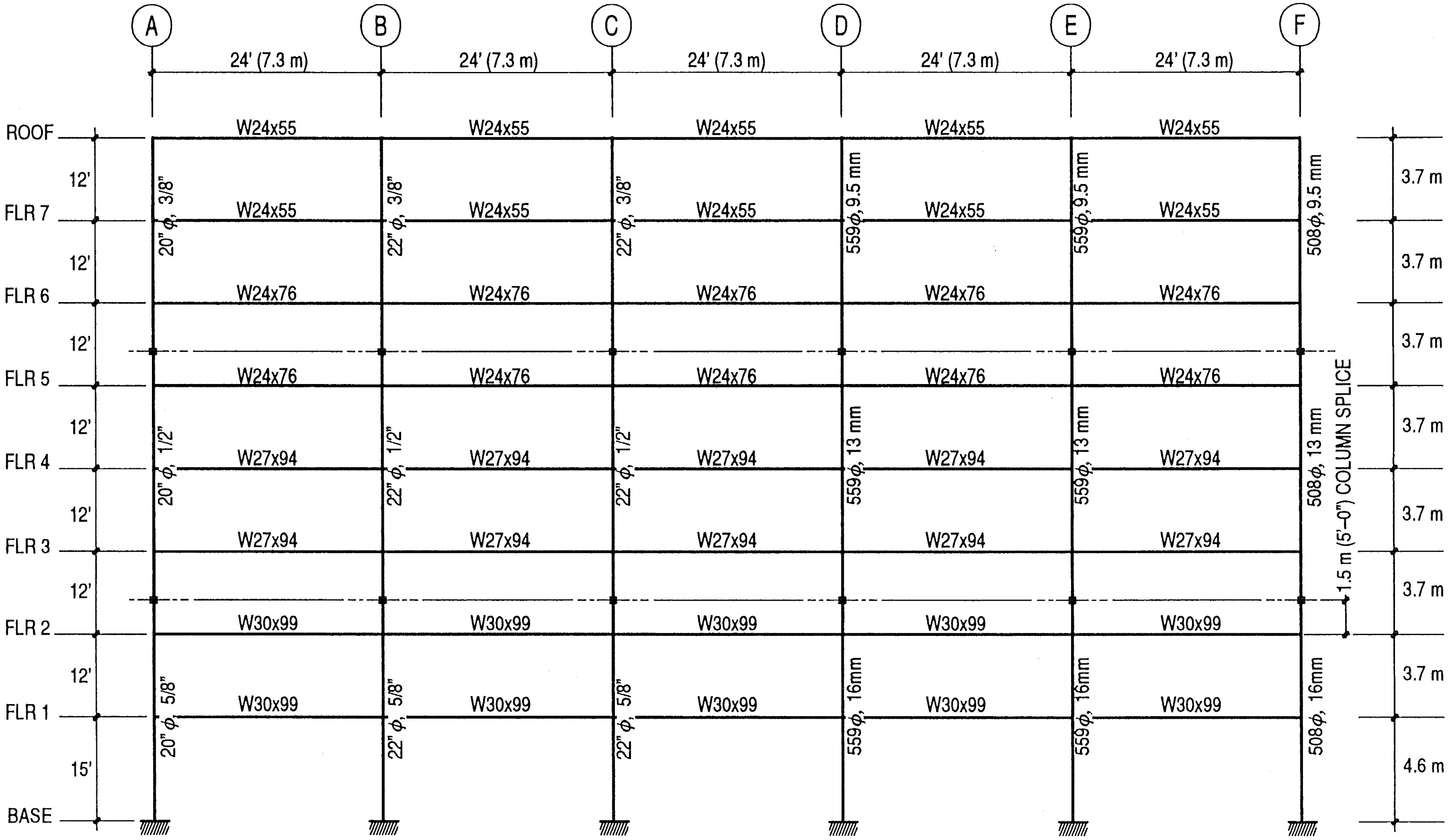

Figure 2.2 b. 8 Story Perimeter Frame, Elevation

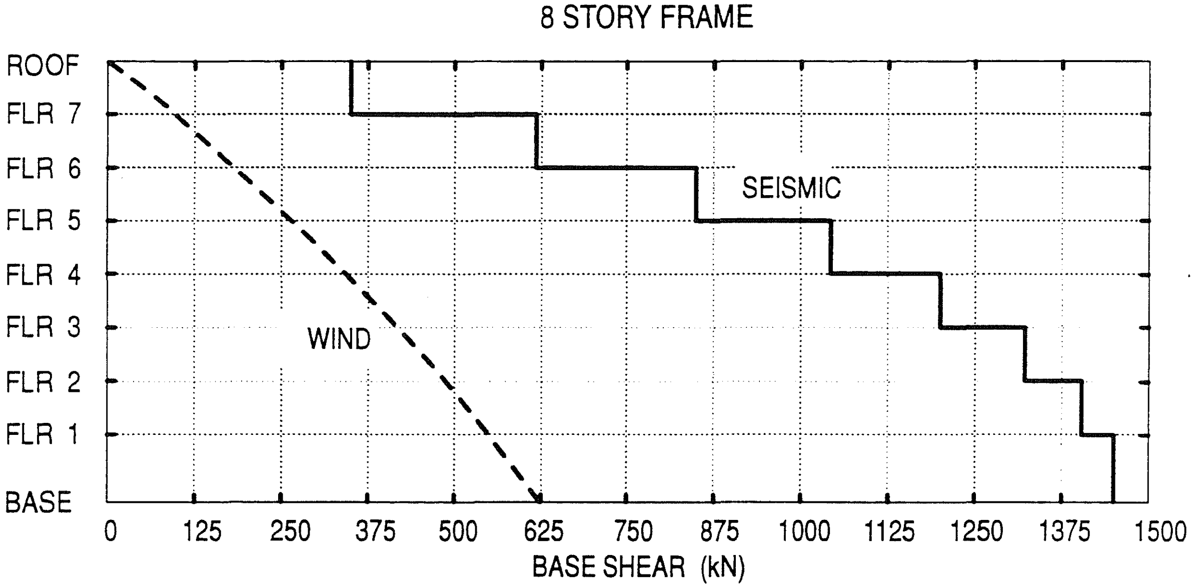

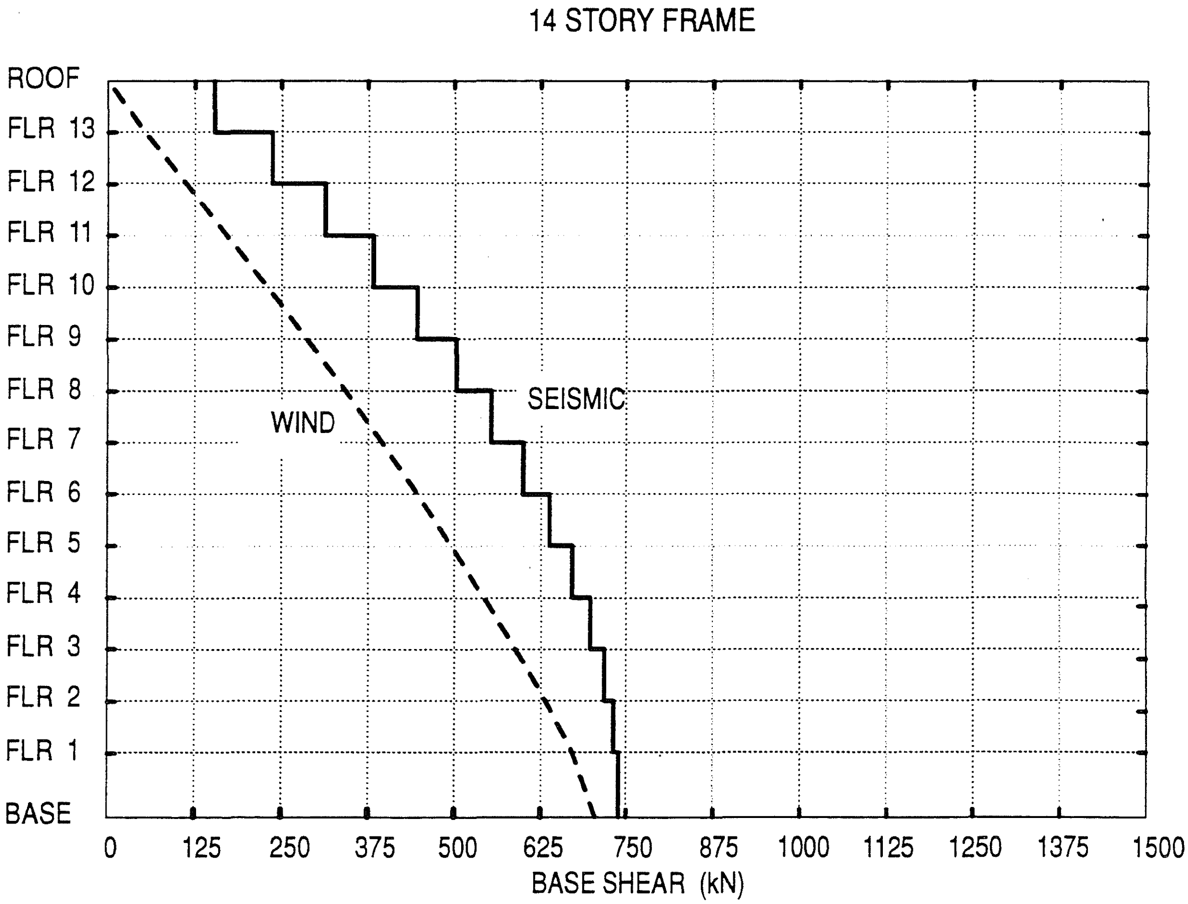

Figure 2.3. Design Story Shears for Seismic and Wind Loads

8 STORY FRAME

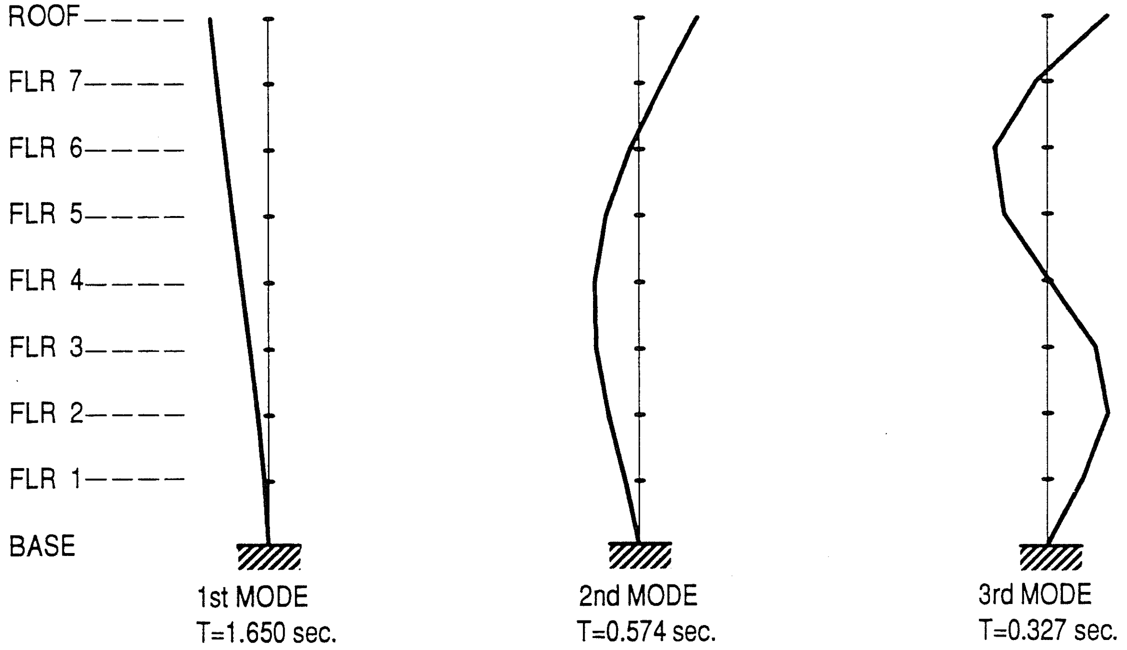

14 STORY FRAME

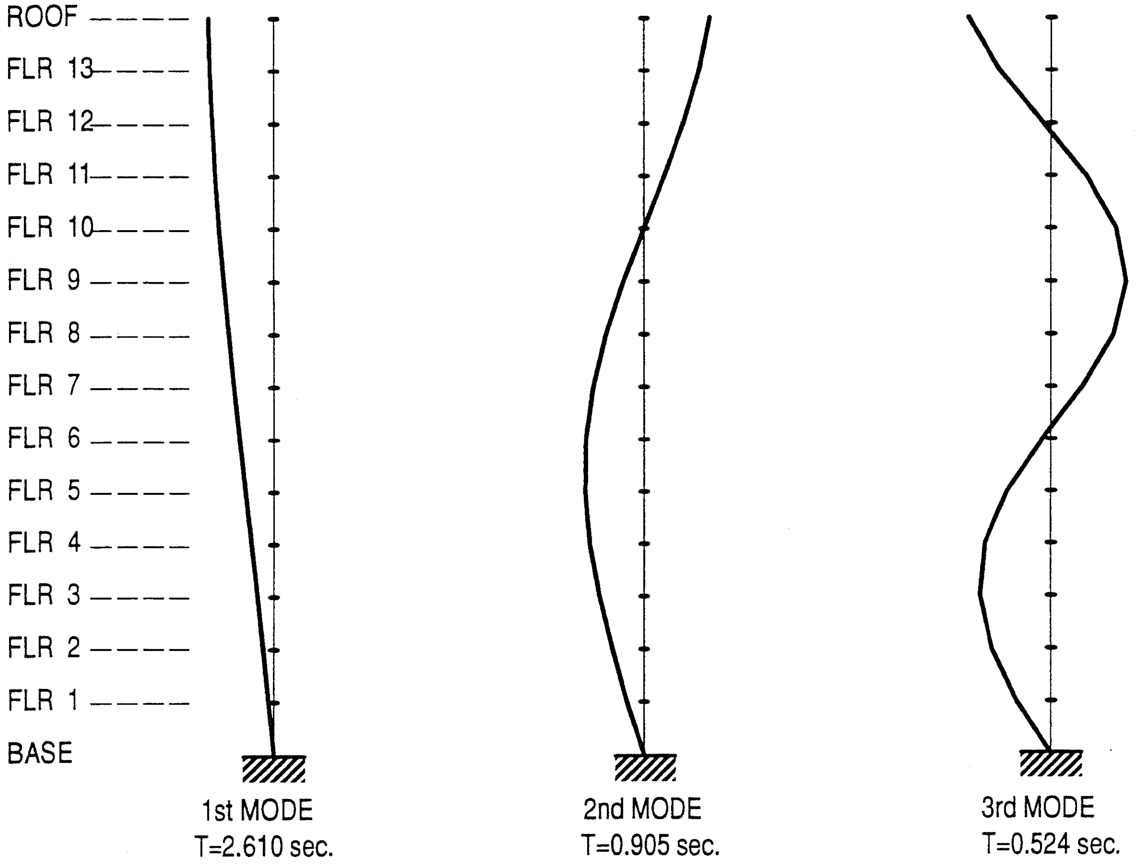

Figure 2.4. Periods and Mode Shapes

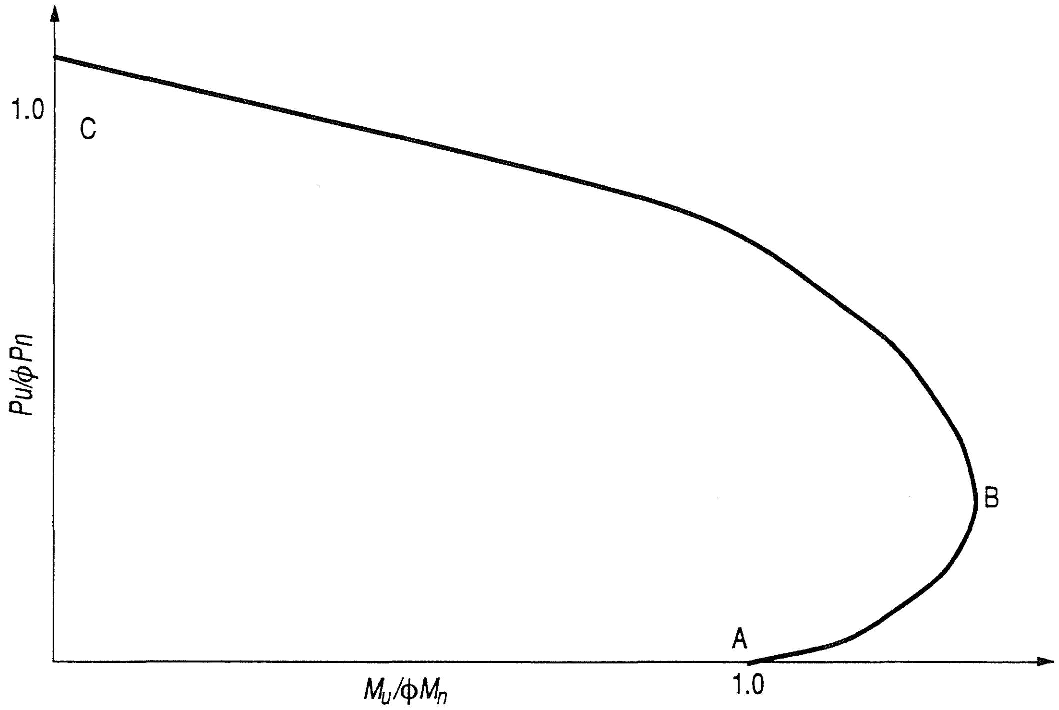

a.) Typical Interaction Curve for Composite Columns, (Narayanan 1988).

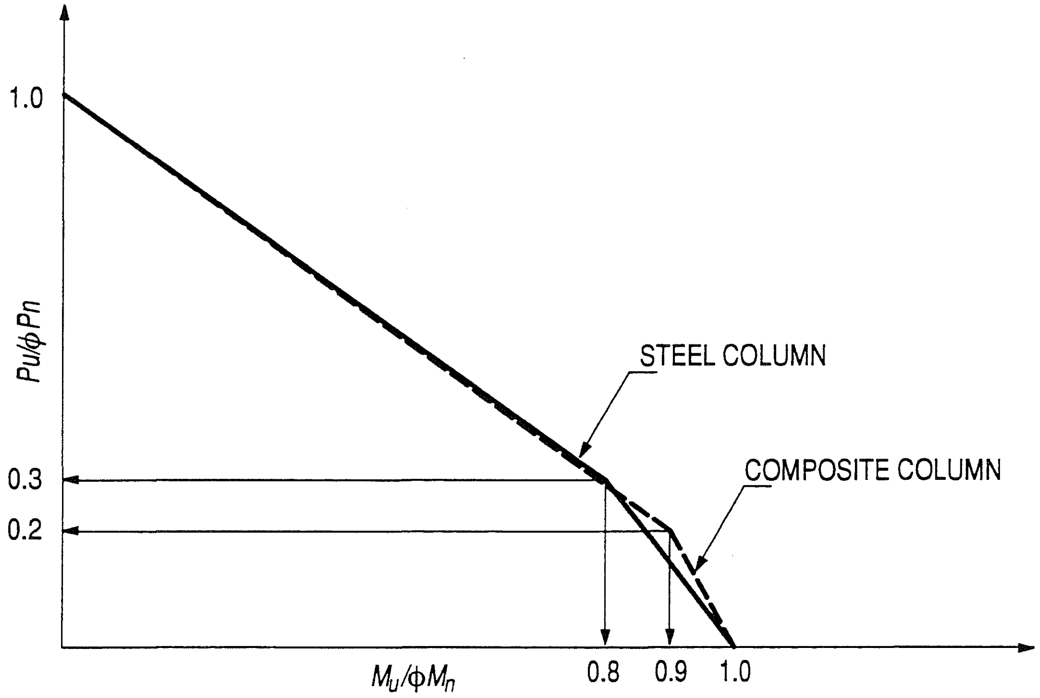

b.) The *1986 AISC/LRFD* Interaction Curves for Composite and Steel Columns.

Figure 2.5. Axial Load–Moment Interaction Relations for Steel and Composite Columns

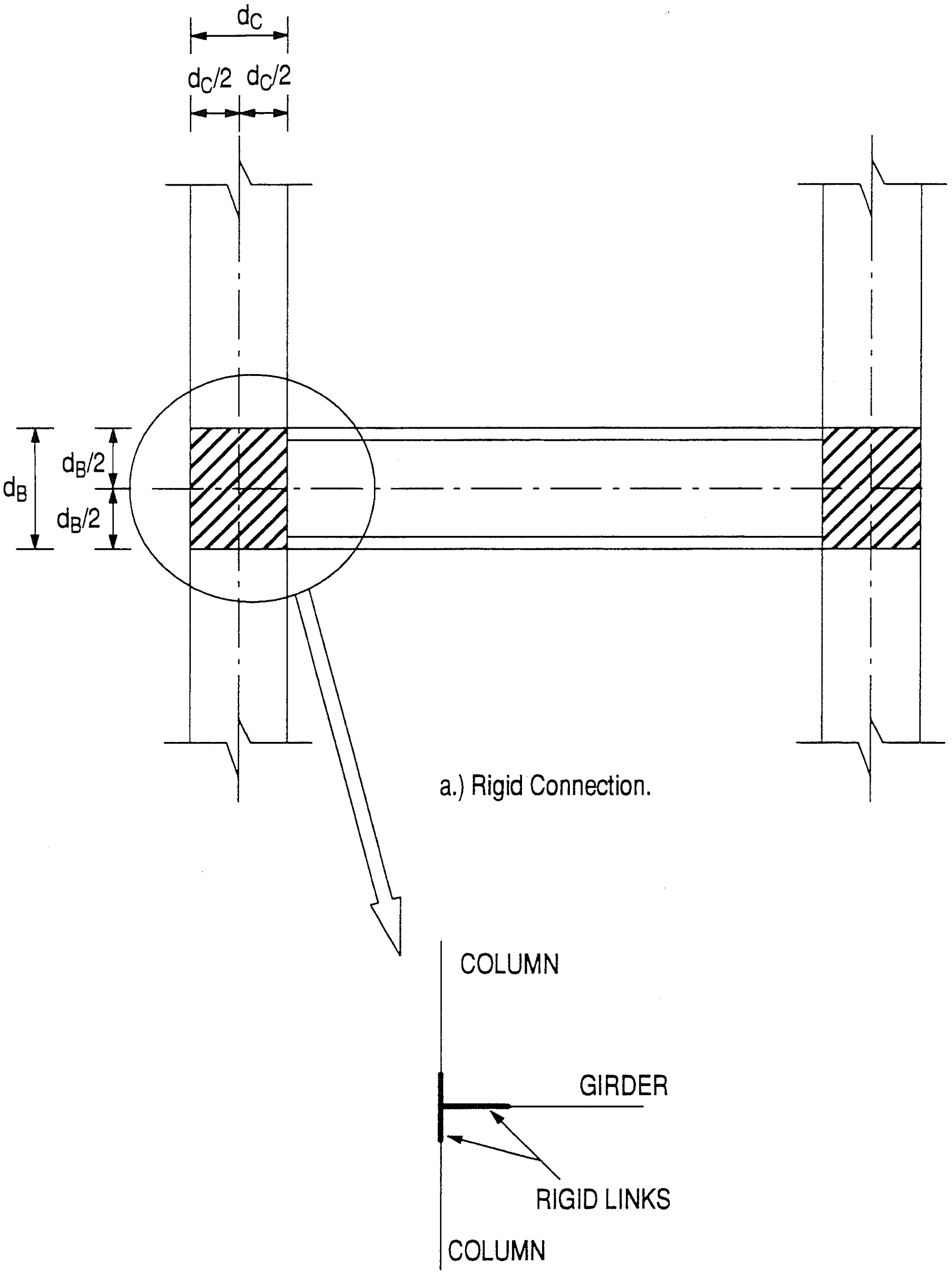

a.) Rigid Connection.

b.) Analytical Model.

Figure 2.6. Joints with Finite Size

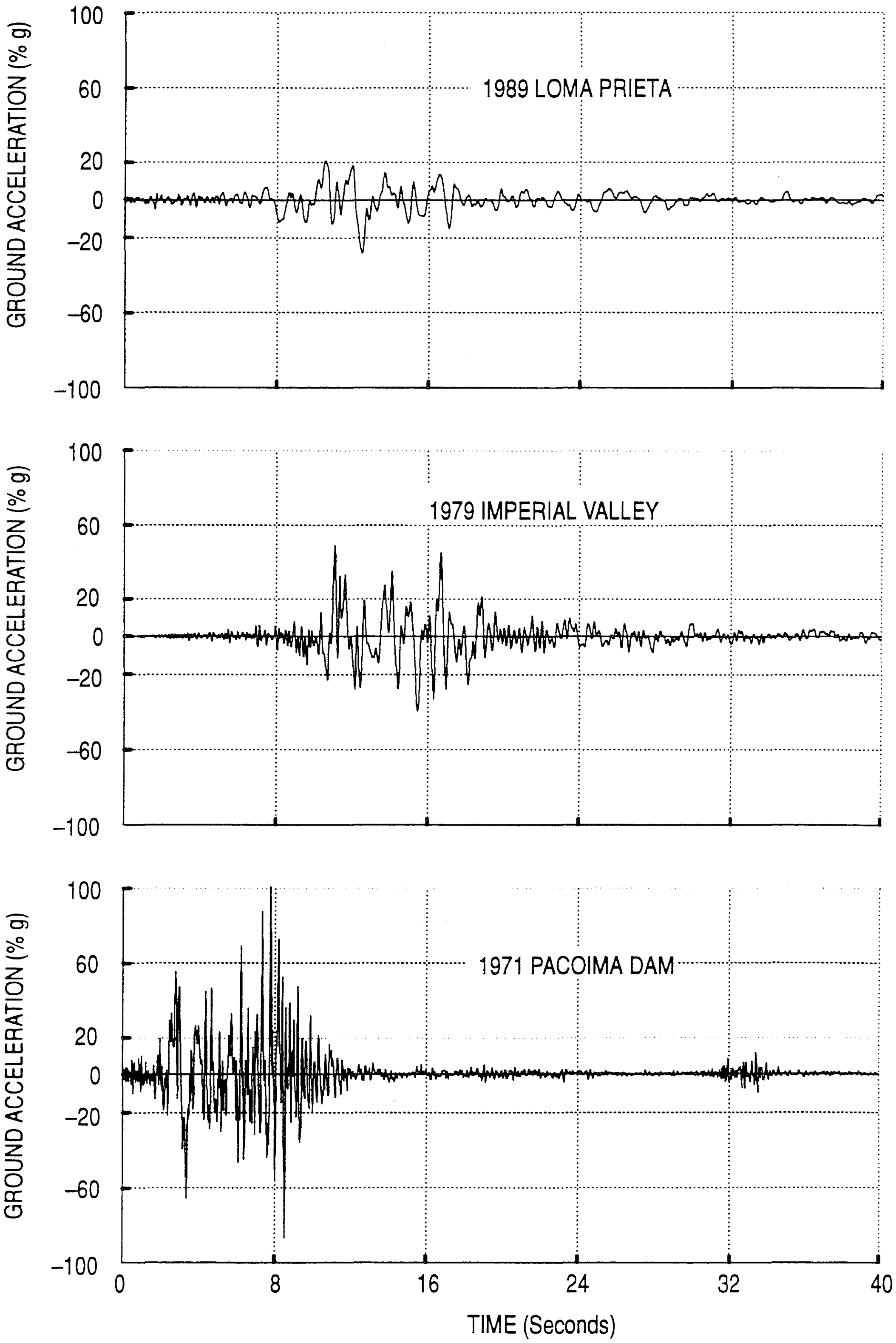

Figure 2.7 a. Earthquake Records used in the Current Study

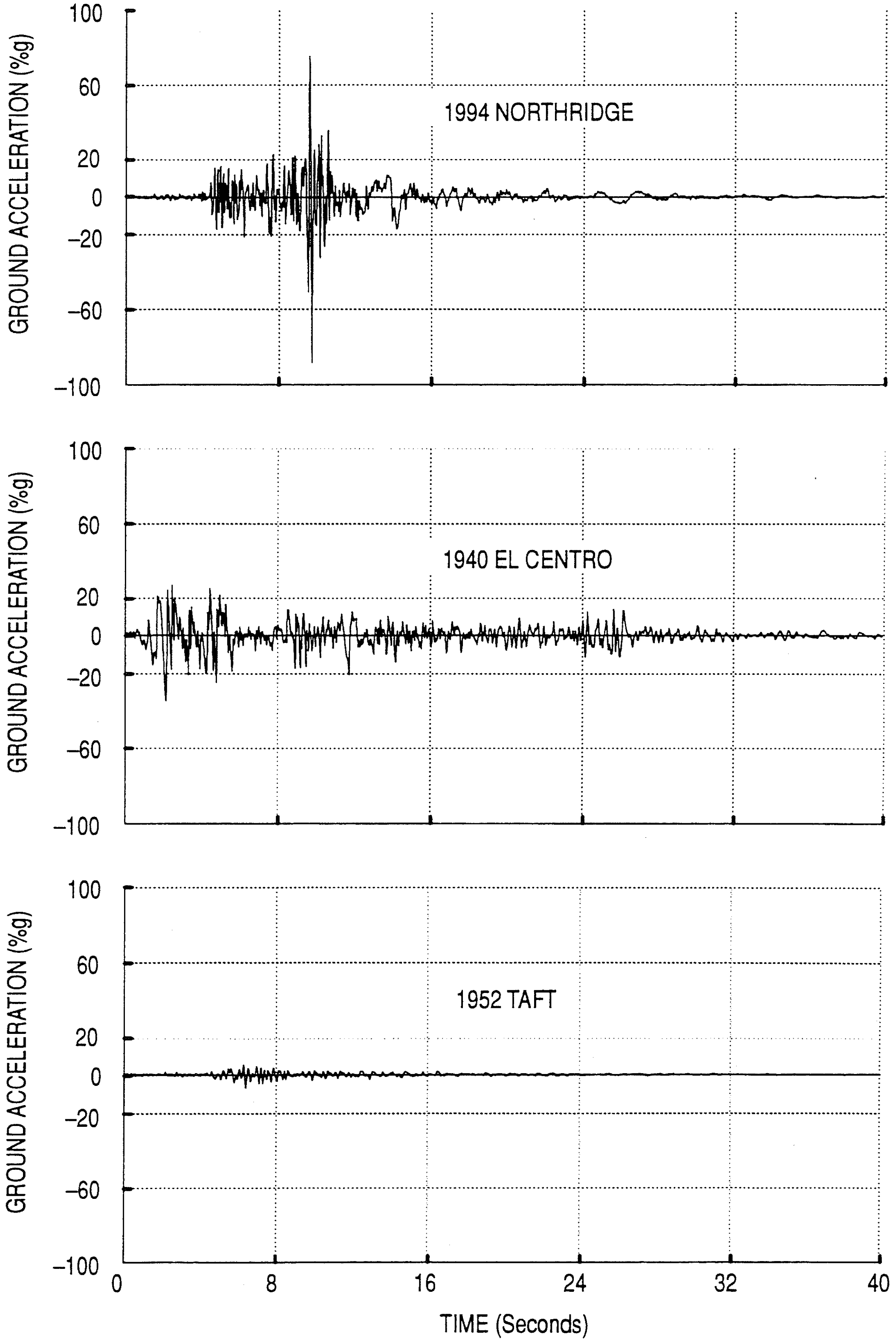

Figure 2.7 b. Earthquake Records used in the Current Study

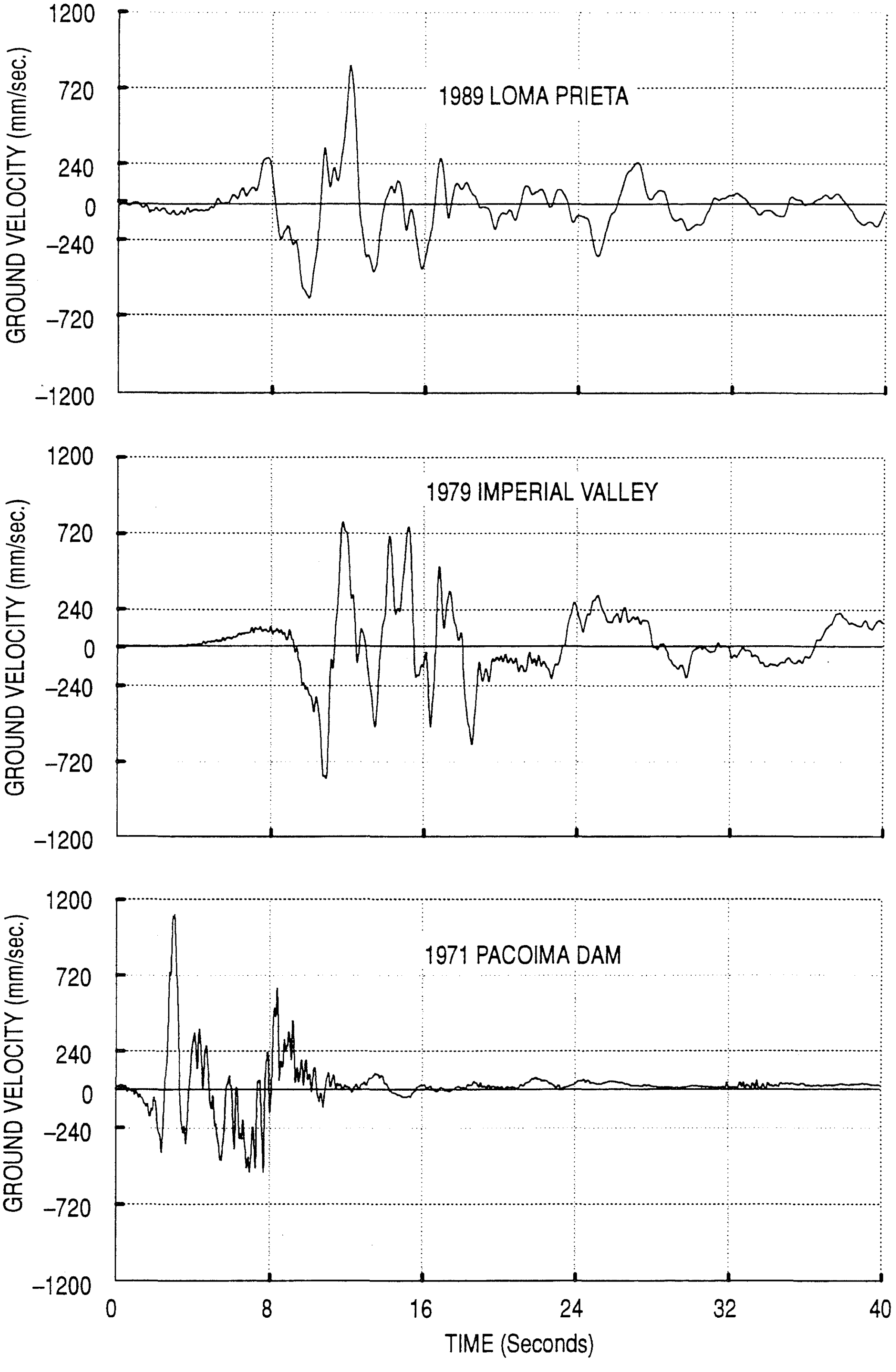

Figure 2.8 a. Ground Velocities

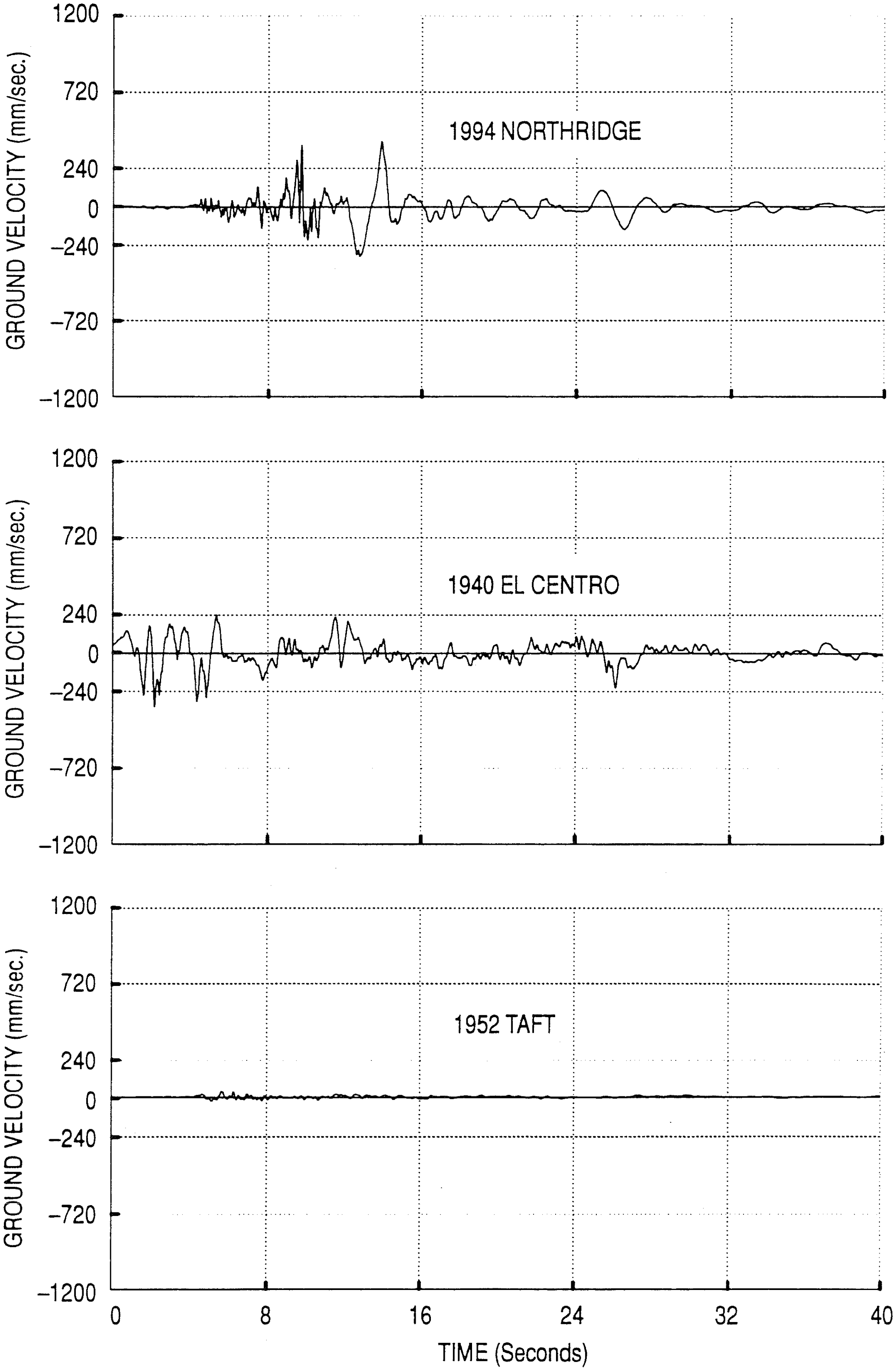

Figure 2.8 b. Ground Velocities

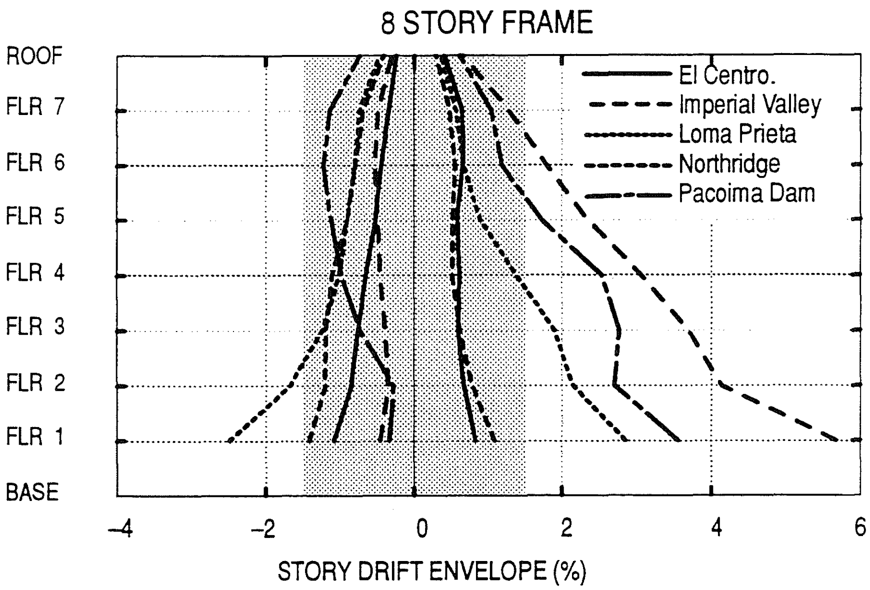

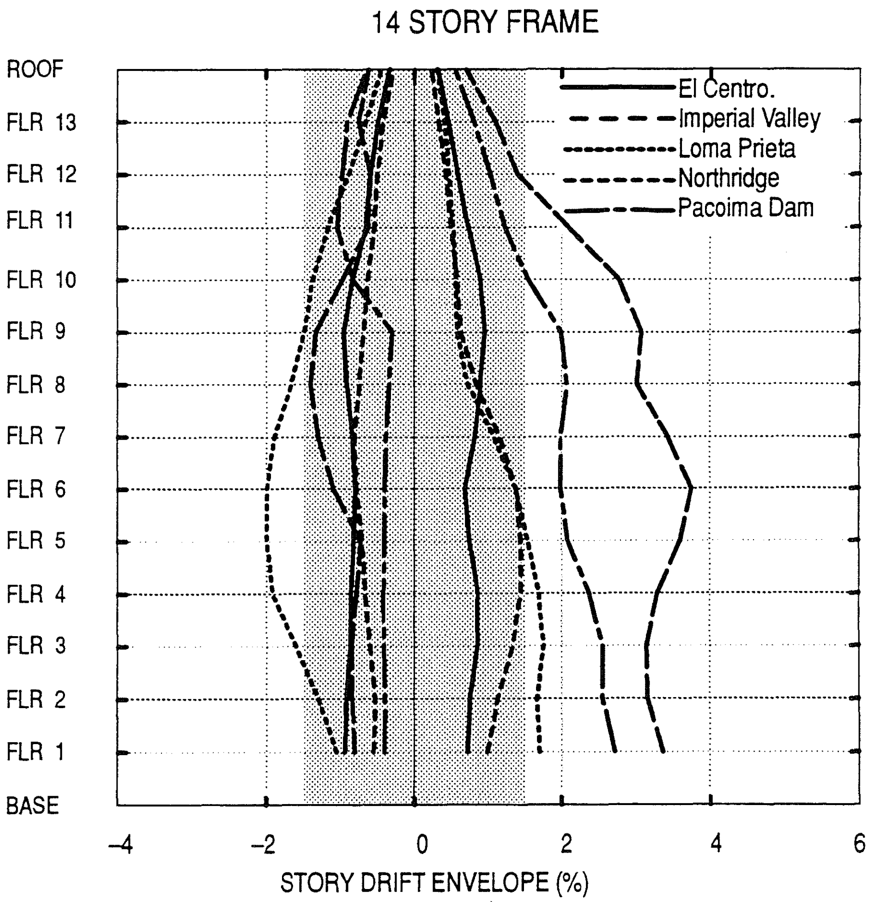

Figure 2.9. Story Drift Envelopes

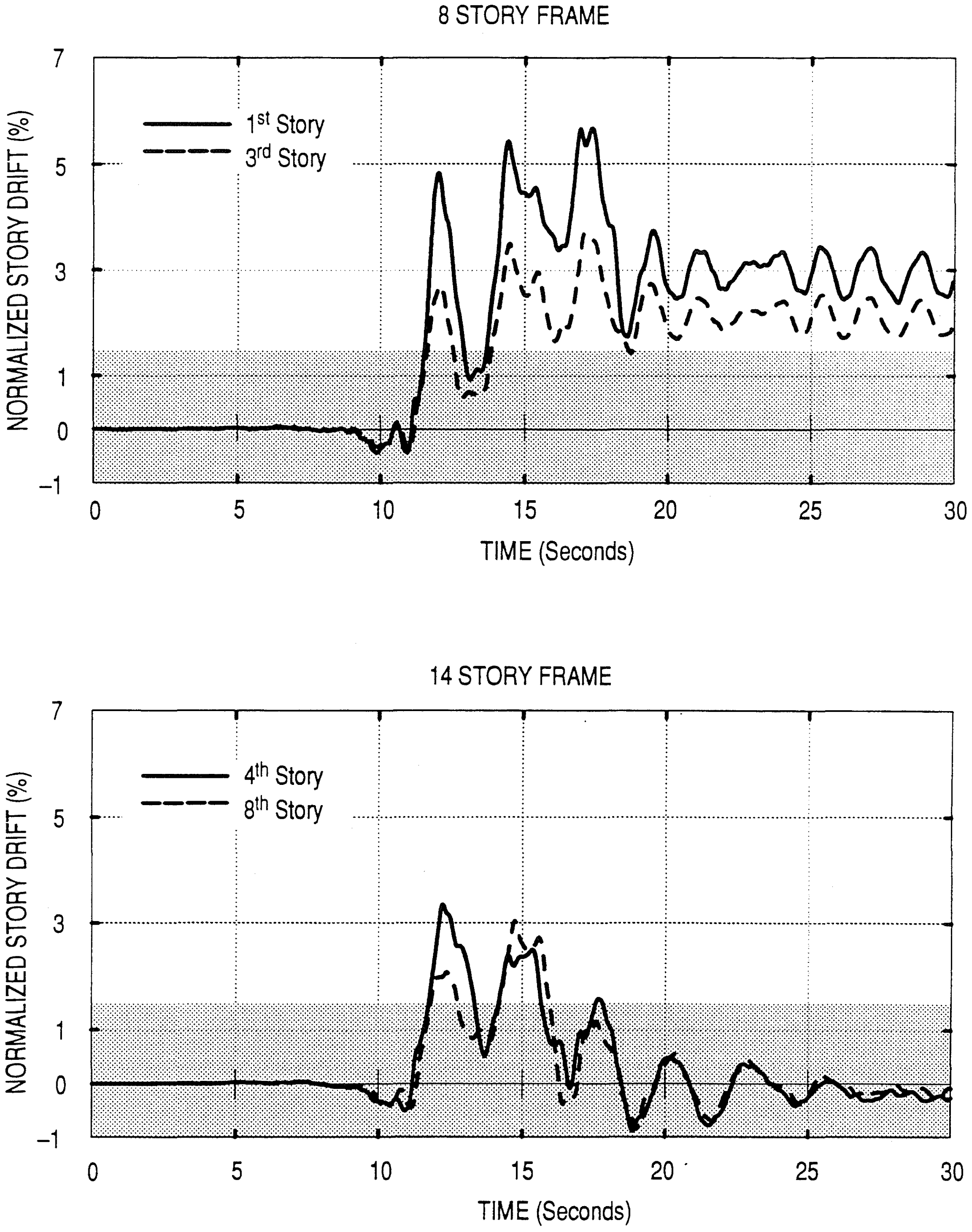

Figure 2.10. Story Drift for the Prototype Frames with the 1979 Imperial Valley Record

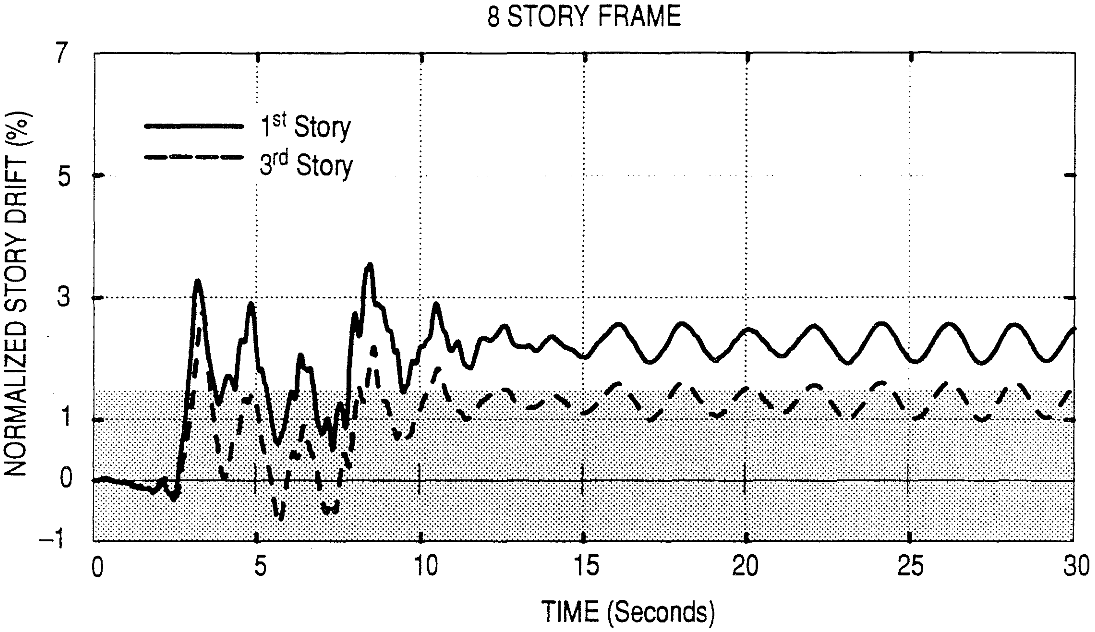

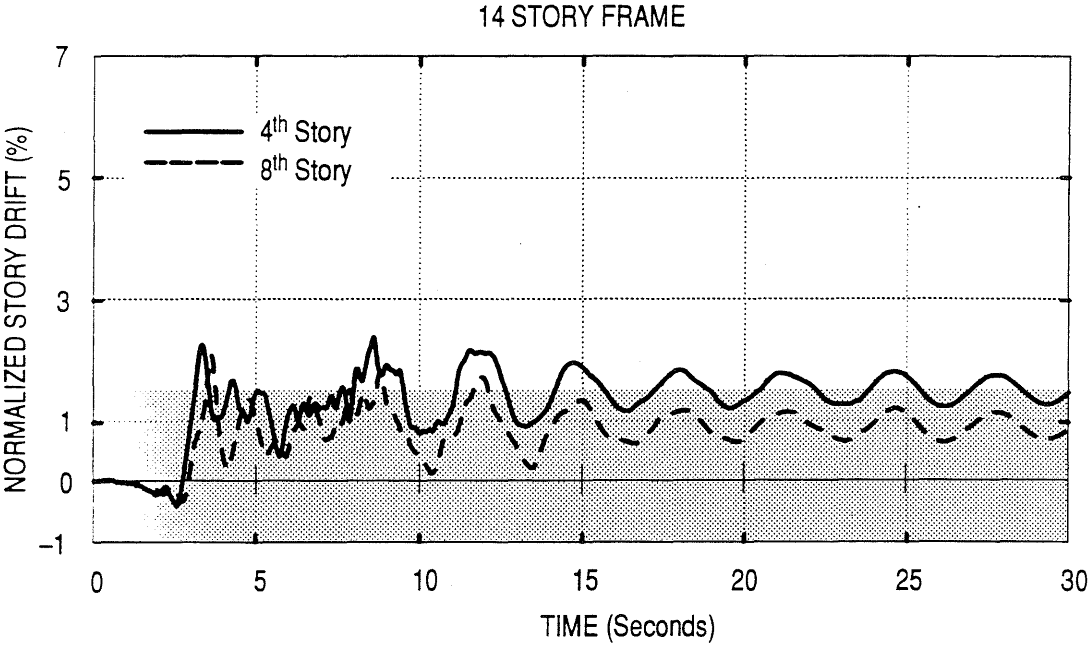

Figure 2.11. Story Drift for the Prototype Frames with the 1971 Pacoima Dam Record

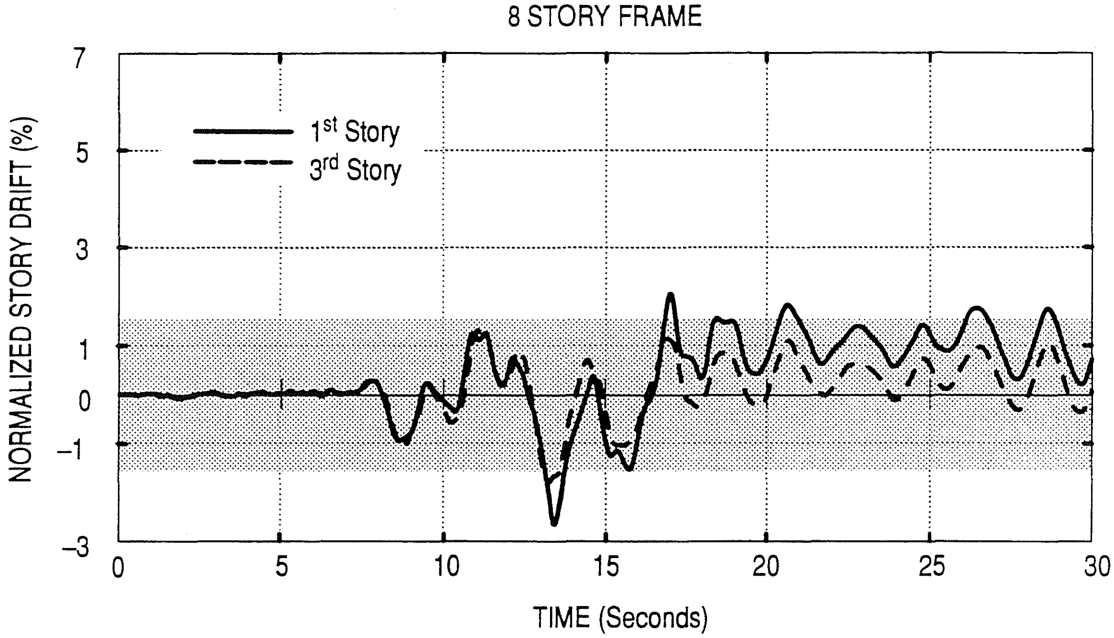

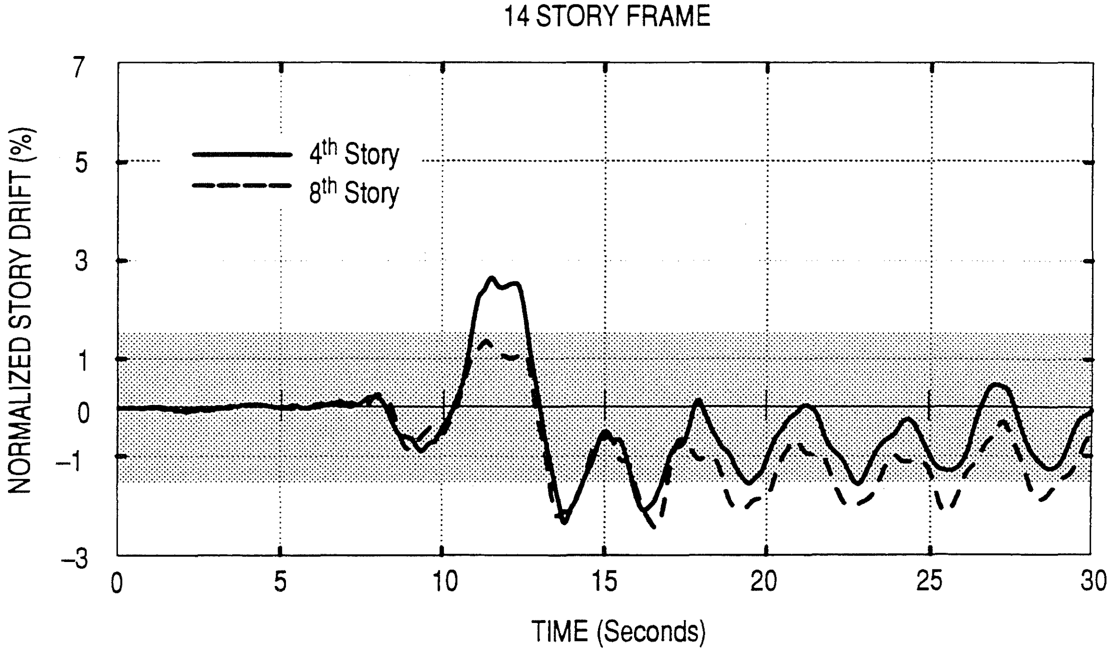

Figure 2.12. Story Drift for the Prototype Frames with the 1989 Loma Prieta Record

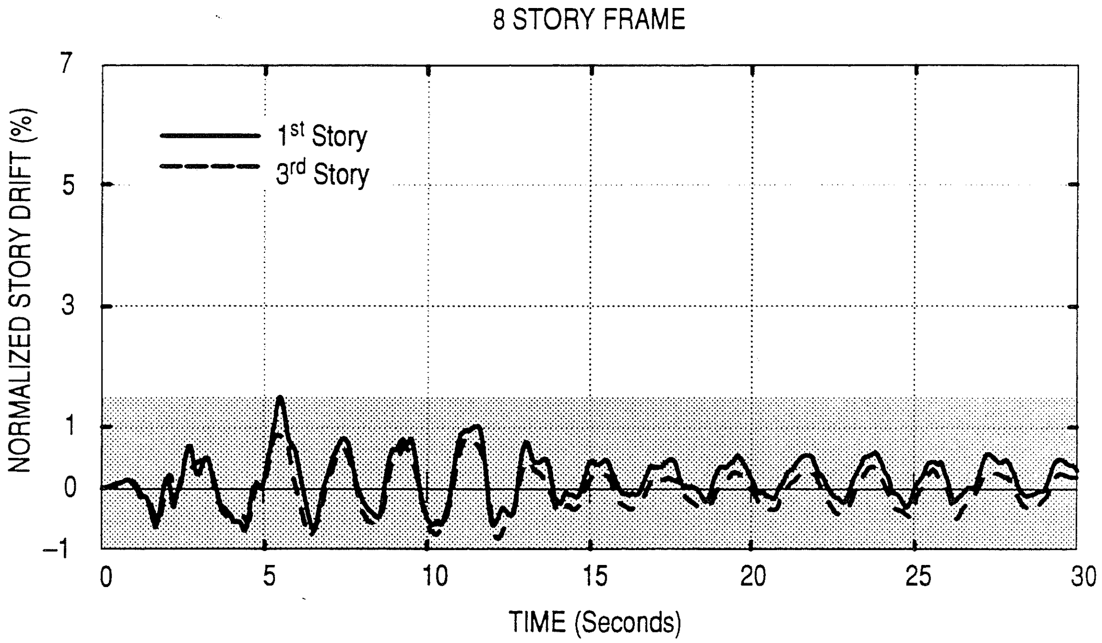

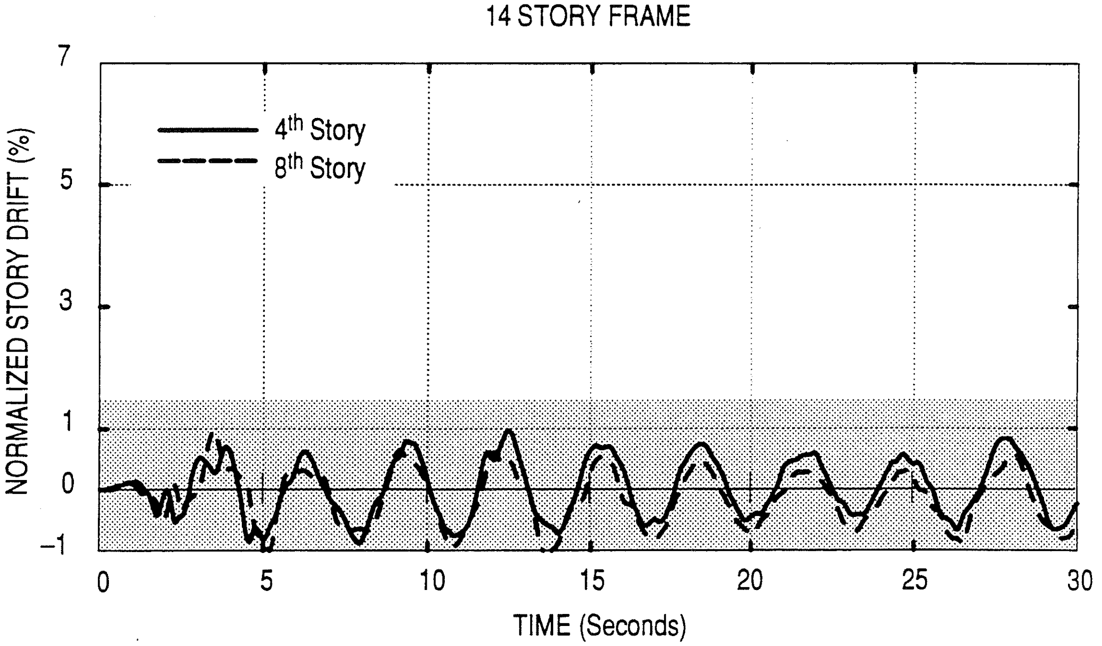

Figure 2.13. Story Drift for the Prototype Frames with the 1941 El Centro Record

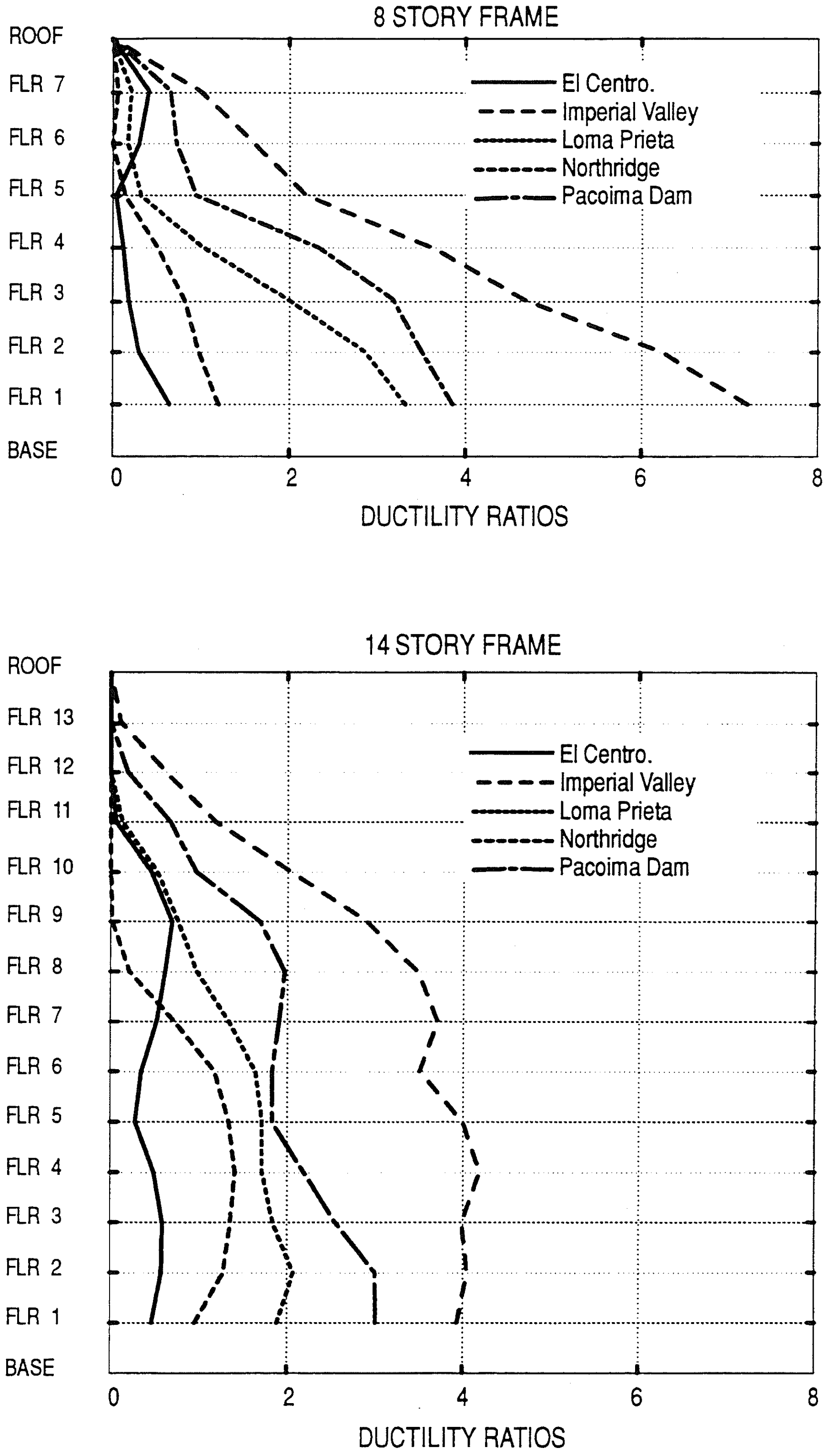

Figure 2.14. Ductility Ratios of Beam Ends Connected to an Exterior Column

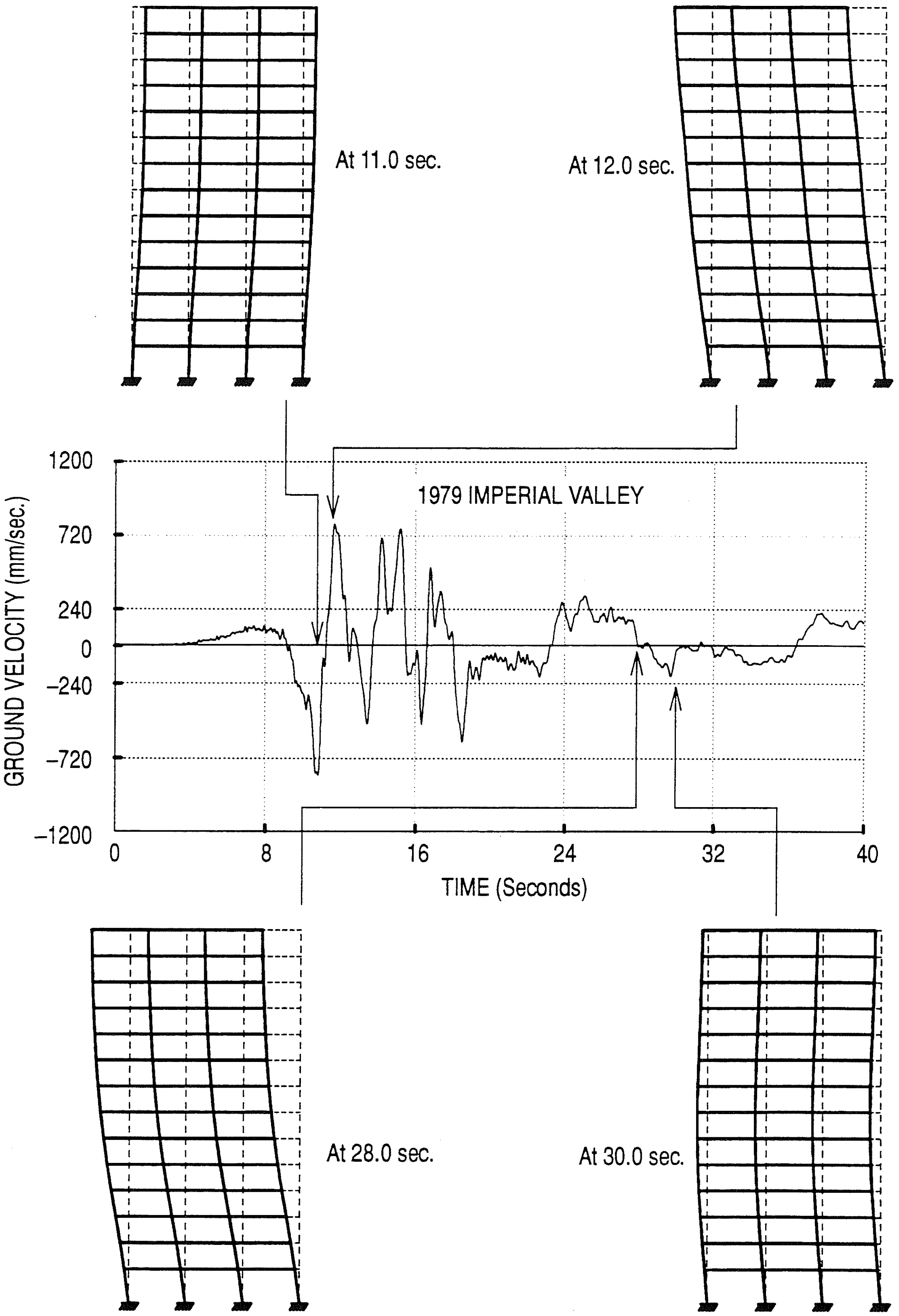

Figure 2.15. The Deformed Shape of the 14 Story Frame During the 1979 Imperial Valley Earthquake

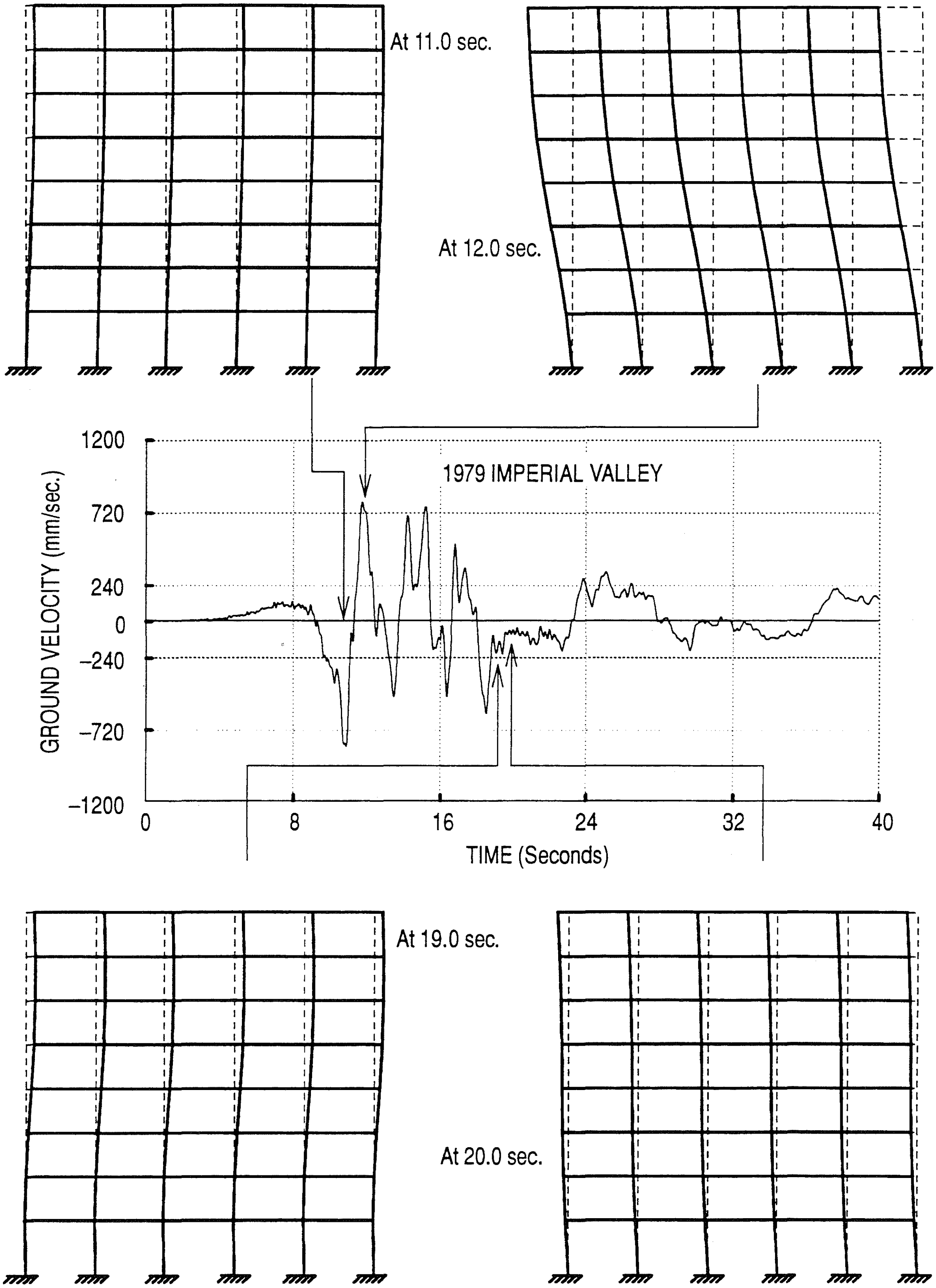

Figure 2.16. The Deformed Shape of the 8 Story Frame During the 1979 Imperial Valley Earthquake

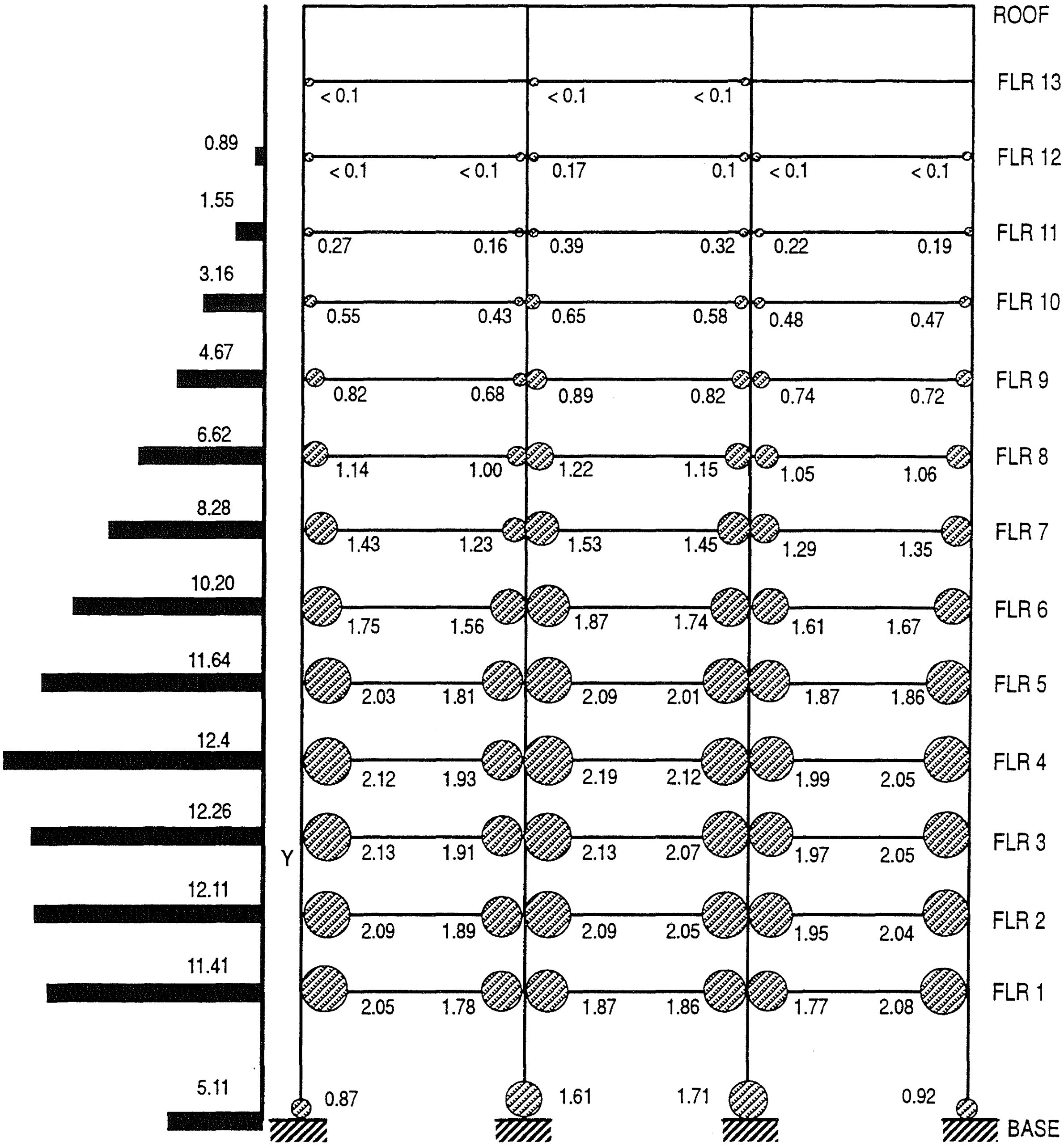

NOTE: 1)–Numbers represent % of total dissipated energy.
2)–'Y' Indicates that the column has just yielded at this location.
3)–Total dissipated energy is 3785 m–kN (33500. inch–kip).
4)–8% of the plastic hinges formed at 10.8 seconds,
31% of the plastic hinges formed at 11.4 seconds, and
61% of the plastic hinges formed after 11.7 seconds.

Figure 2.17. Distribution of Energy Dissipation for the 14 Story Frame with the 1979 Imperial Valley Earthquake

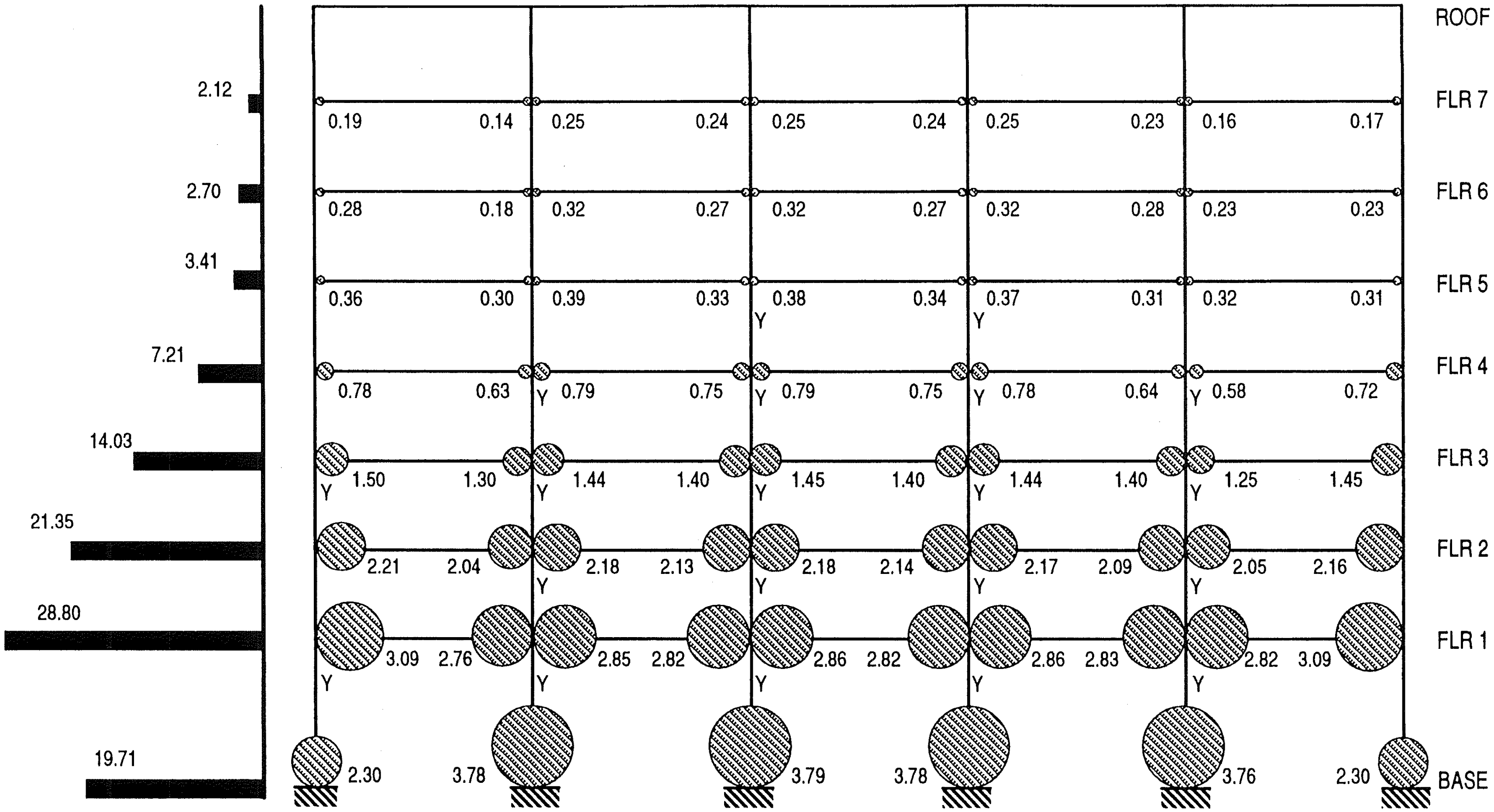

NOTE: 1)–Numbers represent % of total dissipated energy.
2)–'Y' Indicates that the column has just yielded at this location.
3)–Total dissipated energy is 5694 m–kN (50400 inch–kip).
4)–79 % of the plastic hinges formed at 11.4 seconds,
9% of the plastic hinges formed at 11.8 seconds, and
12% of the plastic hinges formed after 14 seconds.

Figure 2.18. Distribution of Energy Dissipation for the 8 Story Frame with the 1979 Imperial ValleyEarthquake

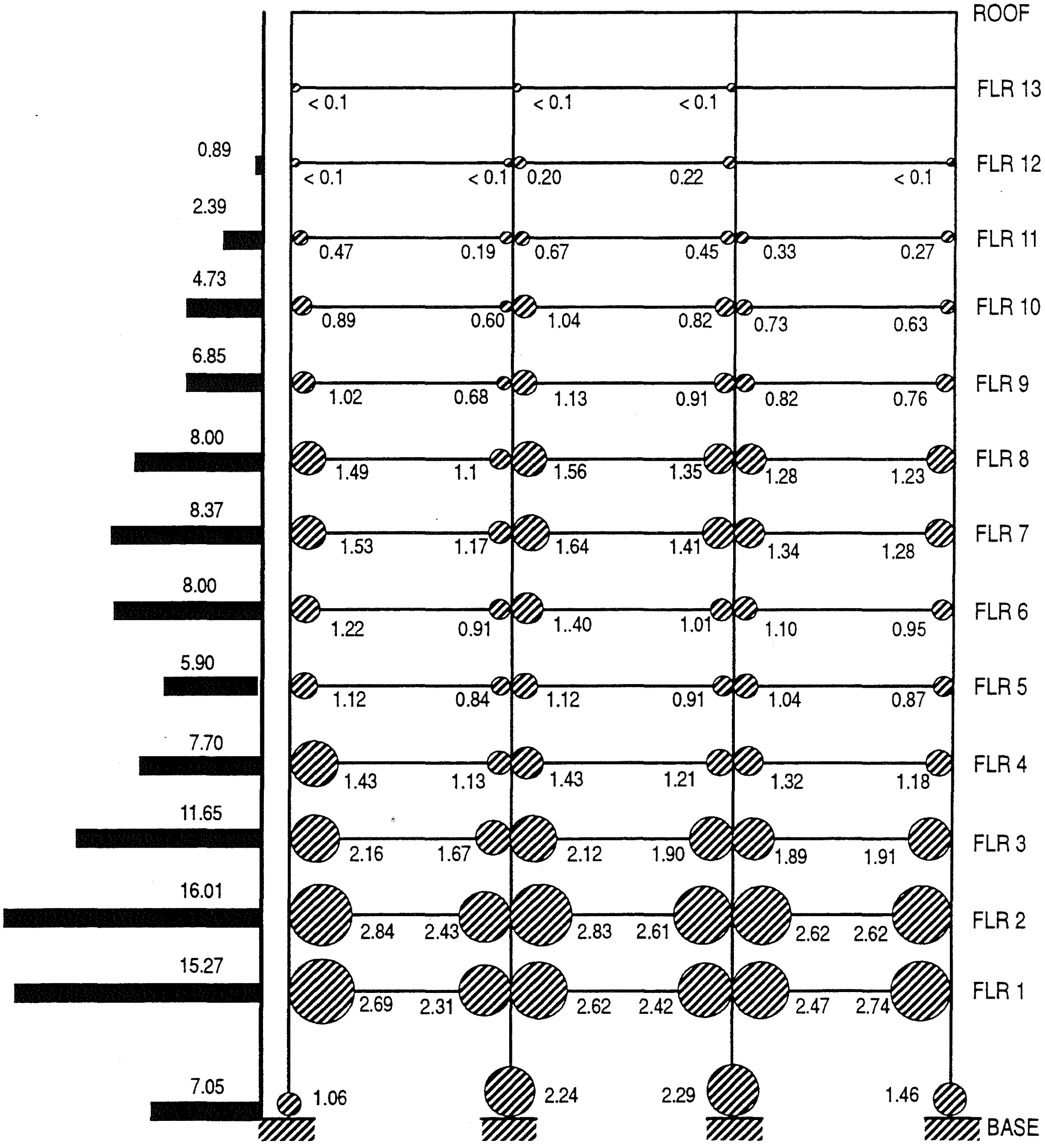

NOTE: 1)–Numbers represent % of total dissipated energy.
2)–Total dissipated energy is 1186 m–kN (10500 inch–kip).
3)–16% of the plastic hinges formed at 2.8 seconds,
32% of the plastic hinges formed at 3.0 seconds,
23% of the plastic hinges formed at 3.2 seconds, and
29% of the plastic hinges formed after 3.3 seconds.

Figure 2.19. Distribution of Energy Dissipation for the 14 Story Frame with the 1971 Pacoima Dam Earthquake

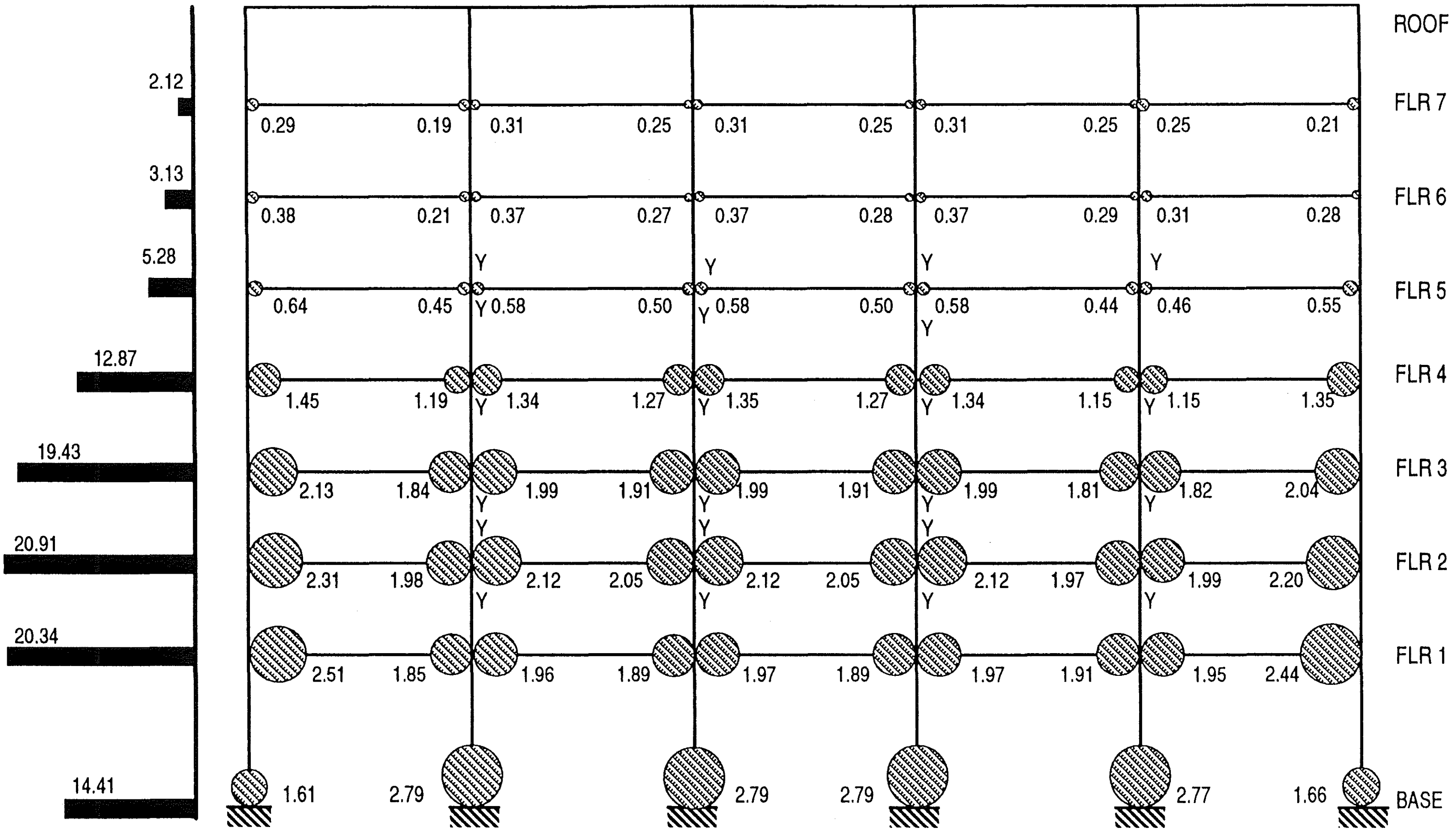

NOTE: 1)–Numbers represent % of total dissipated energy.
2)–'Y' Indicates that the column has just yielded at this location.
3)–Total dissipated energy is 2994 m–kN (26500 inch–kip).
4)–27% of the plastic hinges formed at 2.8 seconds,
49% of the plastic hinges formed at 3.0 seconds, and
24% of the plastic hinges formed after 3.2 seconds.

Figure 2.20. Distribution of Energy Dissipation for the 8 Story Frame with the 1971 Pacoima Dam Earthquake

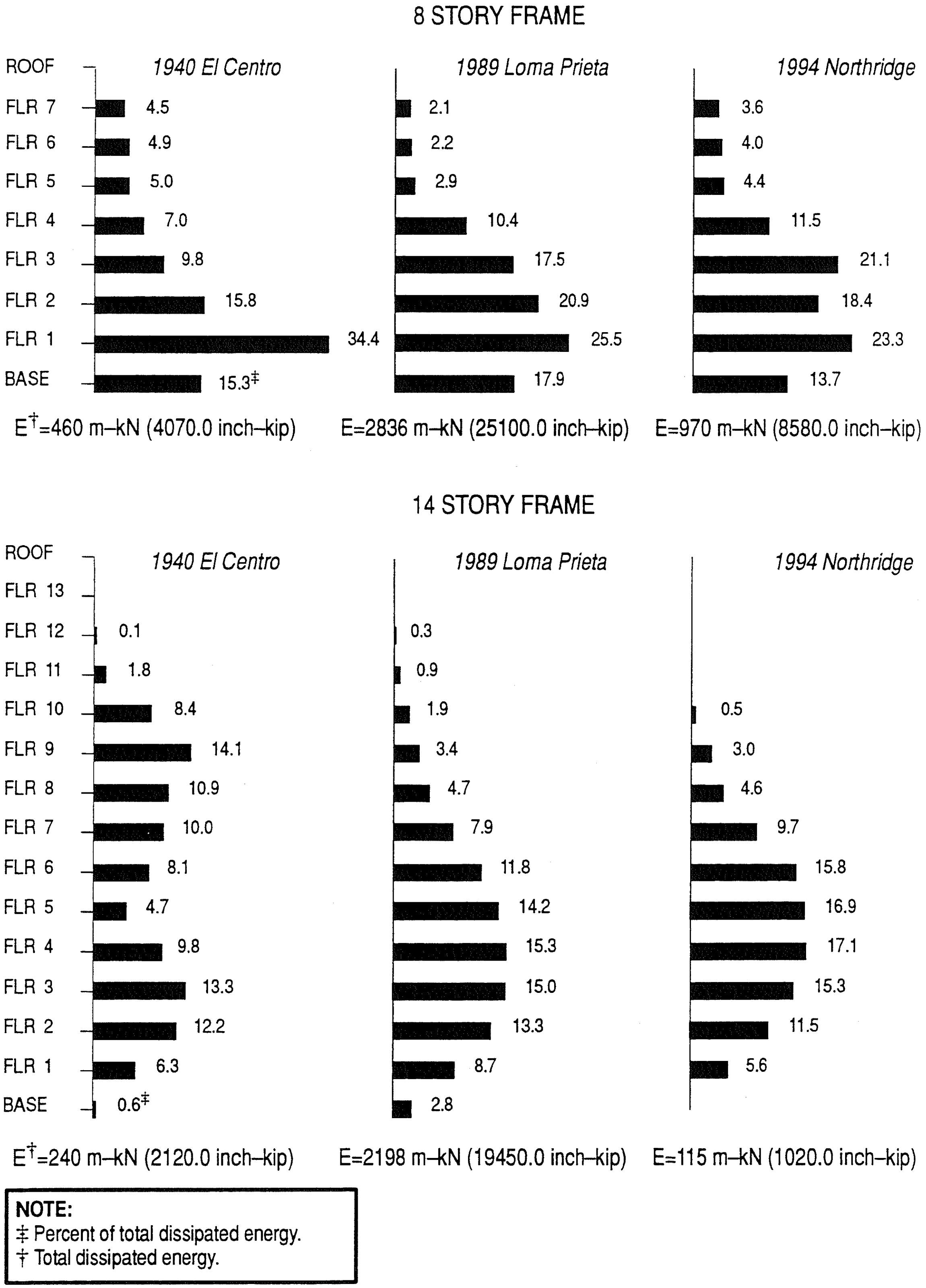

Figure 2.21. Distribution of Total Dissipated Energy with Different Seismic Events

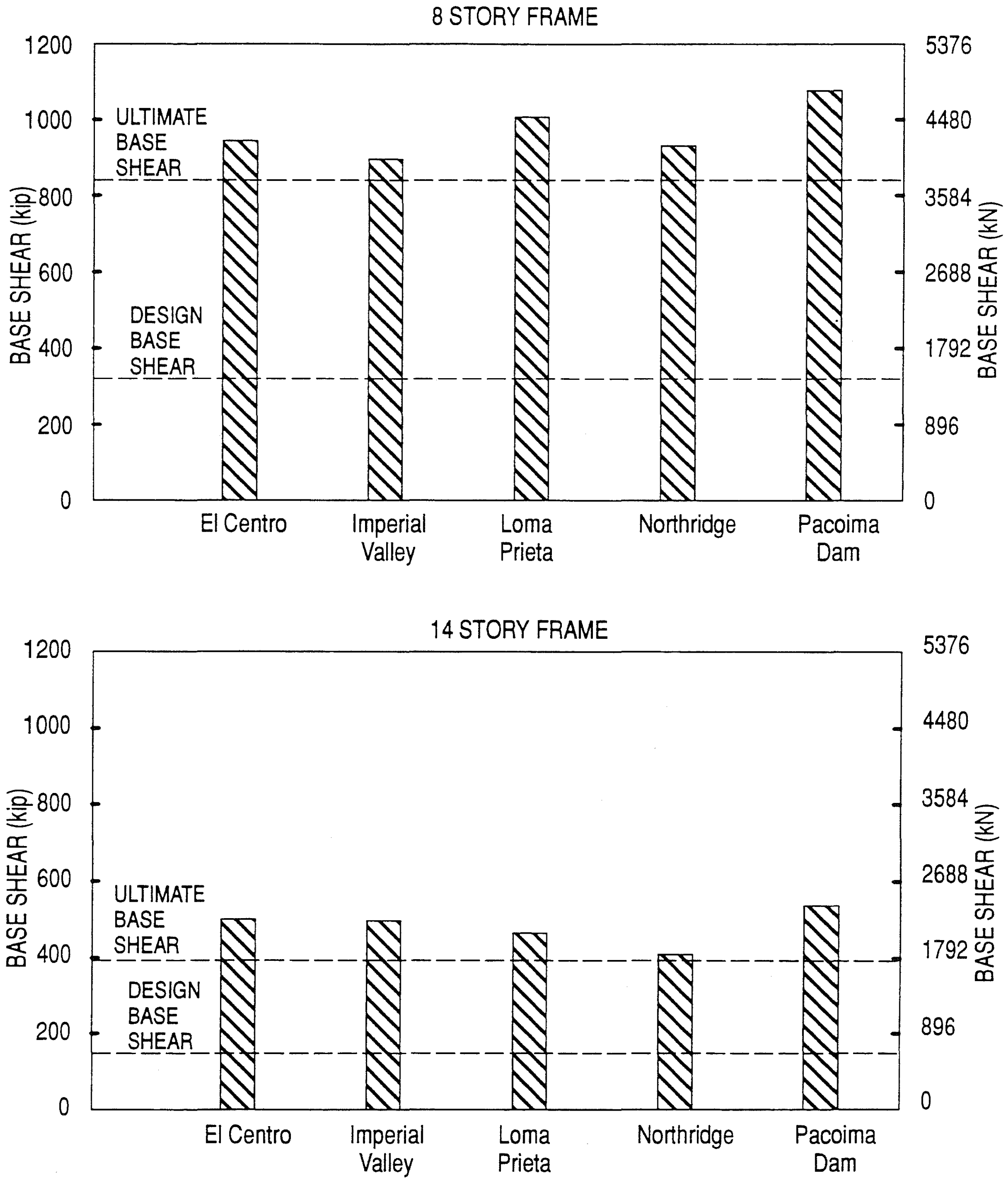

Figure 2.22. Base Shear Demand for Different Seismic Events

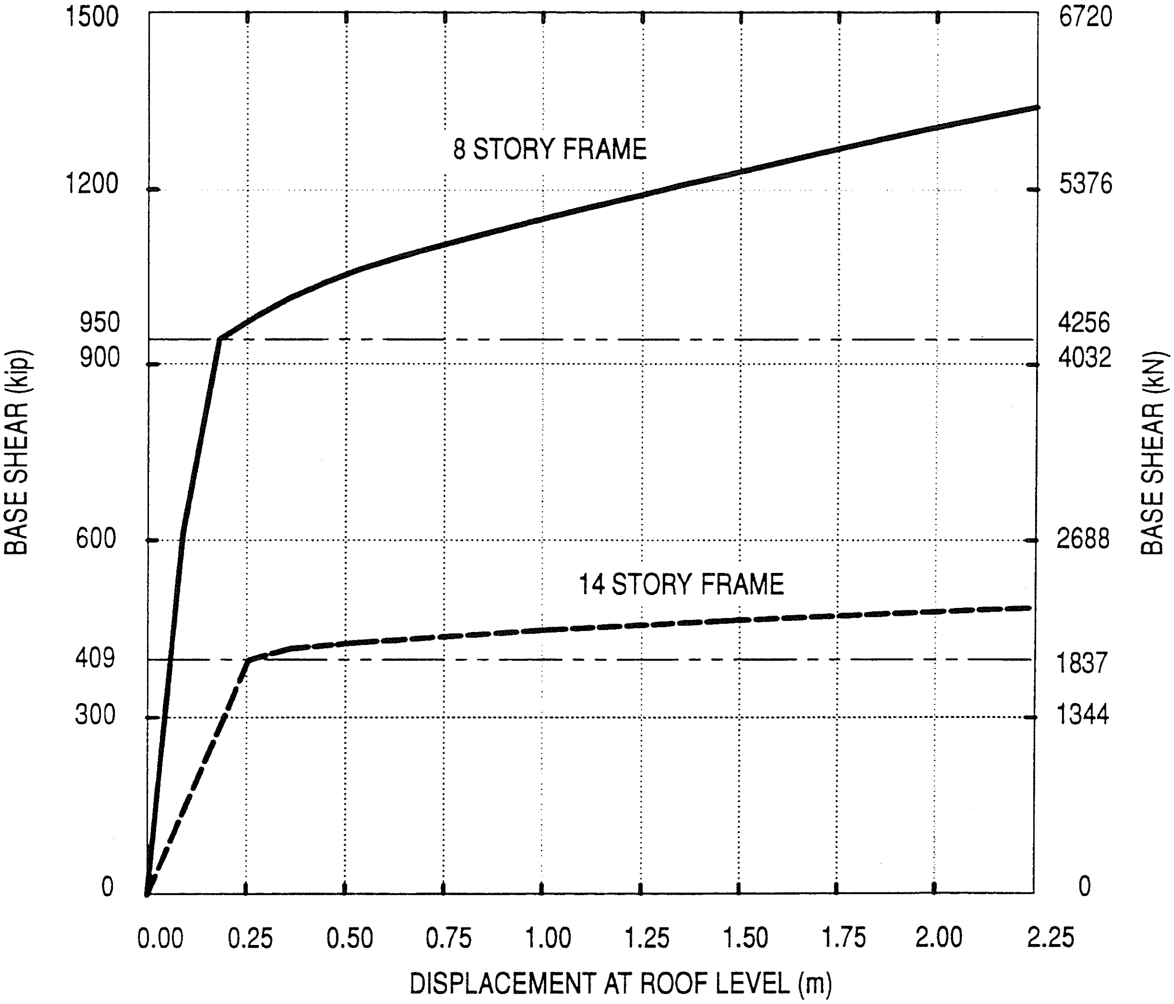

Figure 2.23. Push–Over Analysis of the Prototype Frames

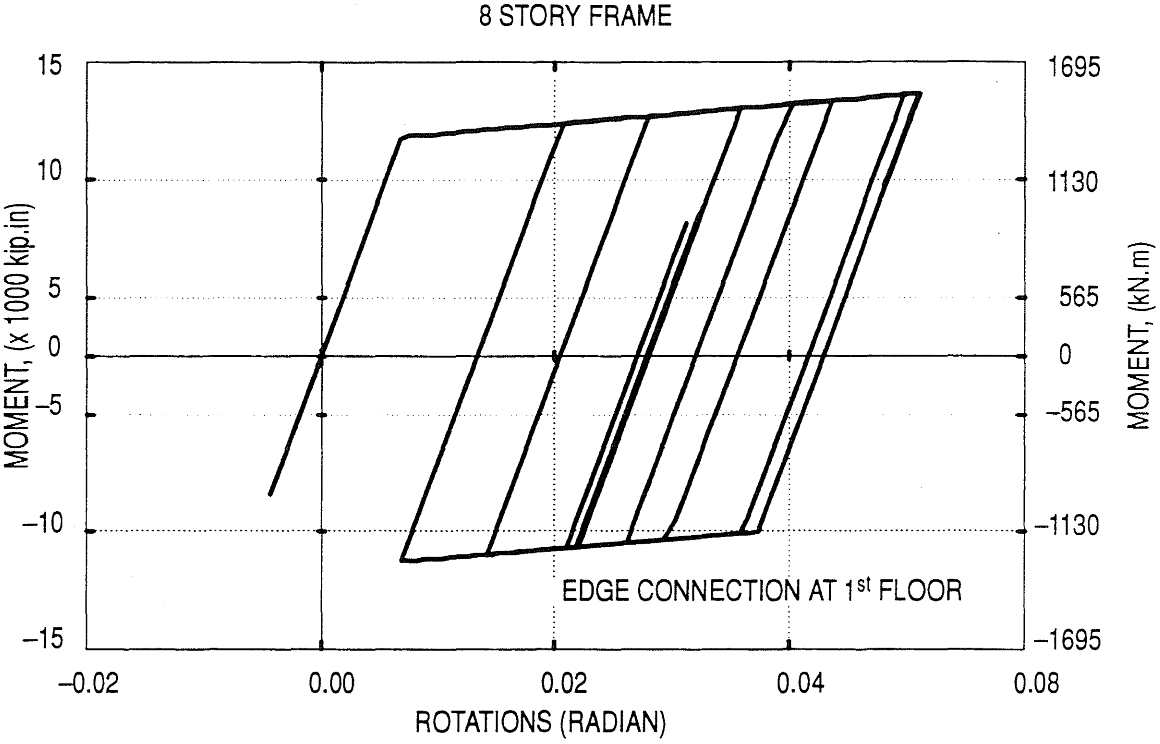

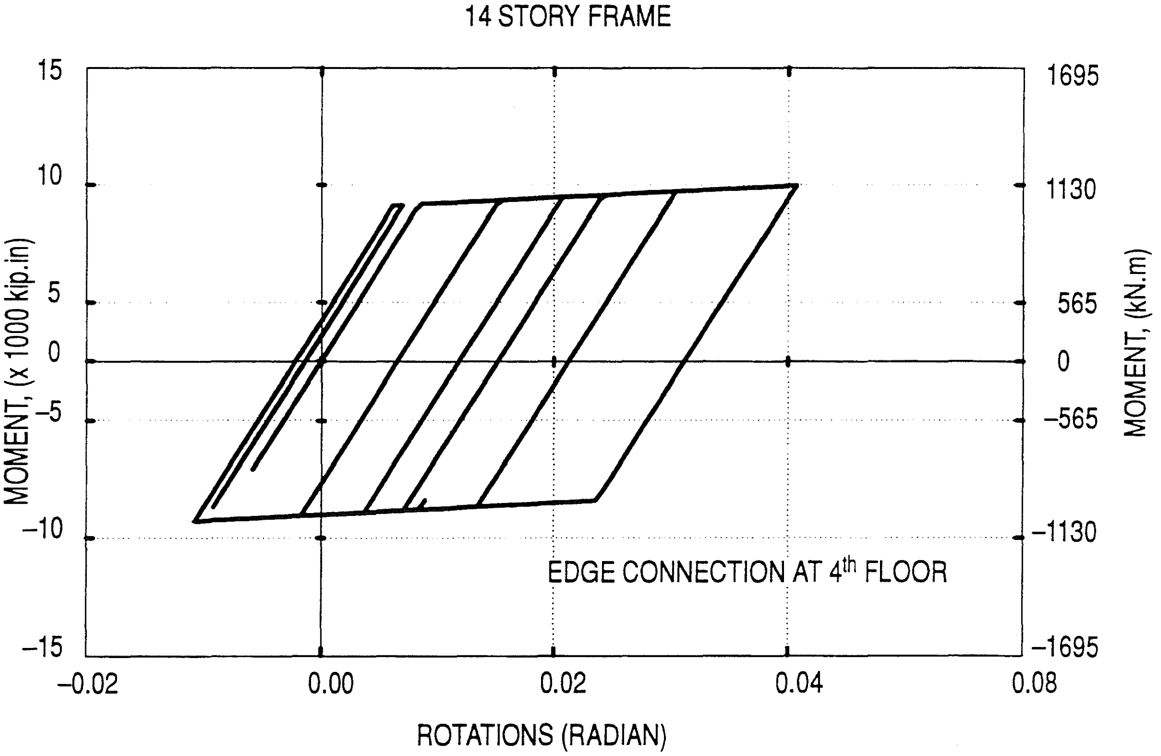

Figure 2.24. Girder Moment–Rotation Relations for the 1979 Imperial Valley Earthquake

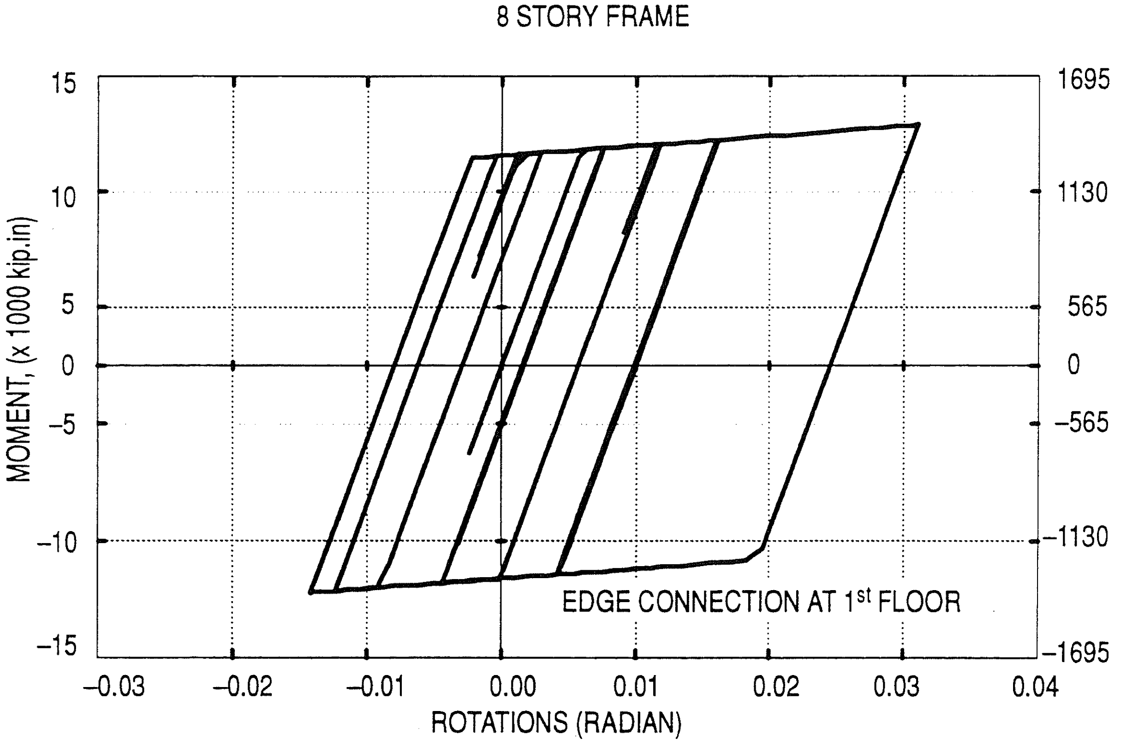
8 STORY FRAME

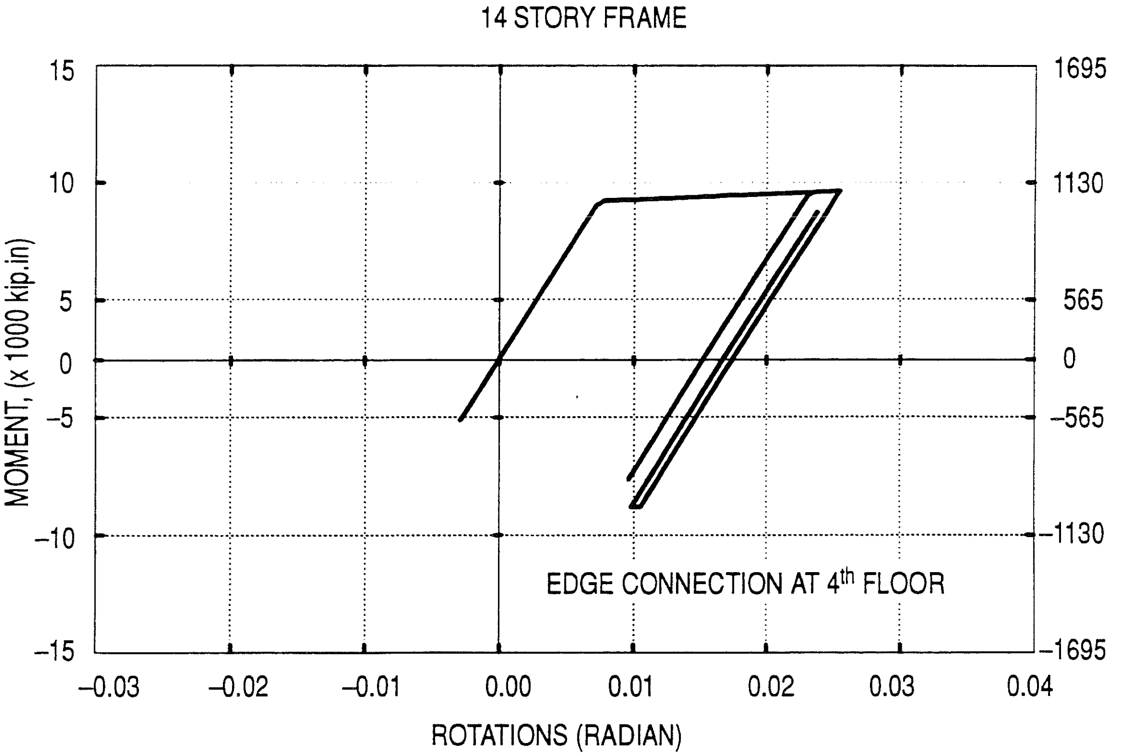
14 STORY FRAME

Figure 2.25. Girder Moment–Rotation Relations for the 1971 Pacoima Dam Earthquake

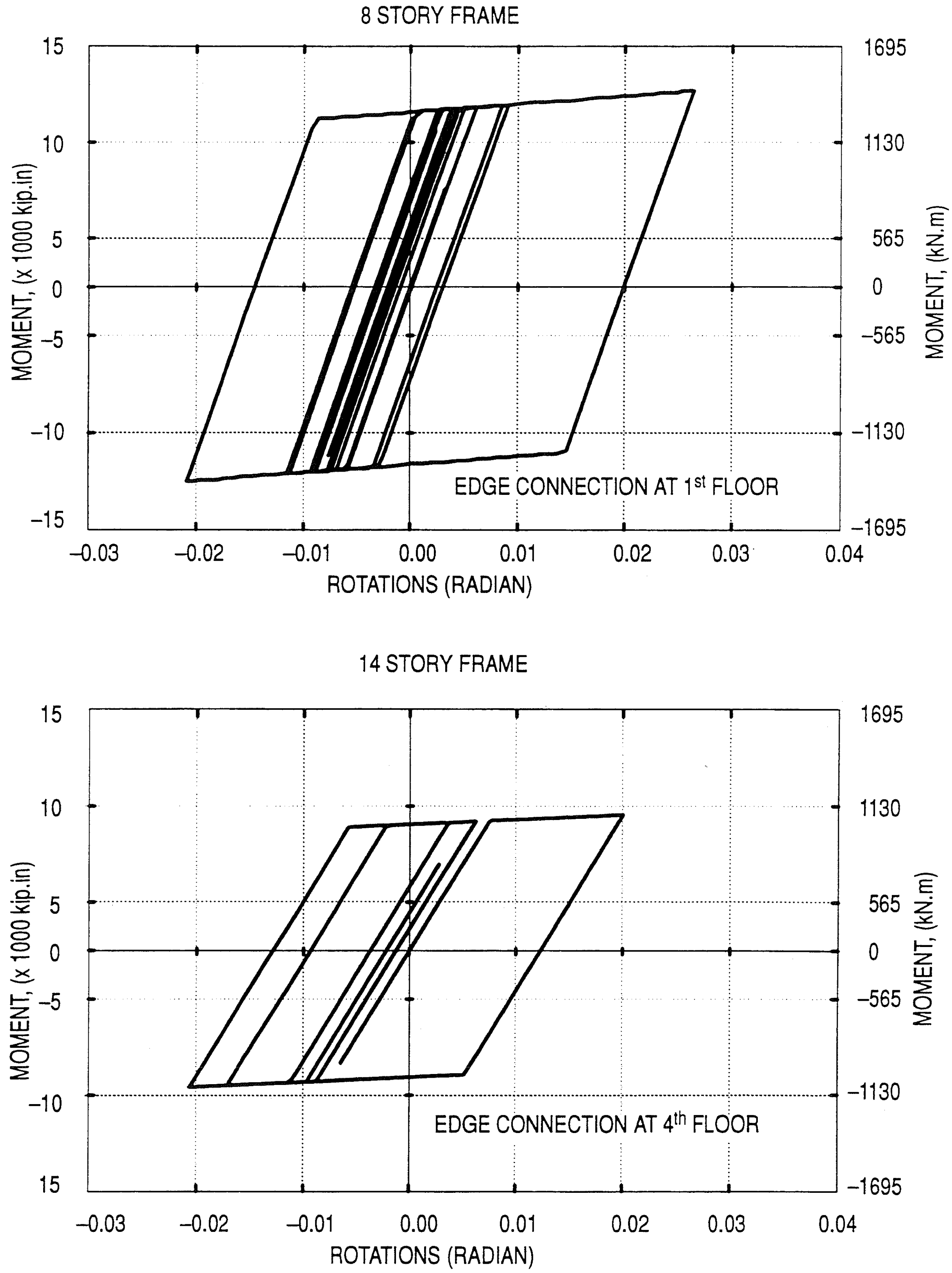

Figure 2.26. Girder Moment–Rotation Relations for the 1989 Loma Prieta Earthquake

CHAPTER 3

ANALYTICAL INVESTIGATION

3.1 INTRODUCTION

Several connection details were designed to offer a wide range of rigidities for flexural behavior. A comprehensive finite element model was generated for each of these connection details. These finite element models were used to investigate the contribution of the various detail components to enhance the flexural resistance of each connection. Eventually, these models will be compared to results obtained from the testing of several large–scale connections. Connection details that exhibited favorable analytical performance were selected as experimental specimens.

3.2 CONNECTION DETAILS

A variety of details have been used in previous construction projects to connect steel girders to tubular columns. Connection details range from a very simple connection, like that shown in Figure 3.1, to complex details, like those shown in Figure 3.2. Connections to concrete–filled steel tubes can be categorized into two basic groups: *1*) connections that load the steel tube wall only, and *2*) connections that penetrate the steel skin and have embedded connectors into the concrete core. Both connection groups were represented by the details investigated in this research program. Seven potential connection details were selected for analytical investigation. These details, *Type I* through *VII*, are shown in Figures 3.3 through 3.9. The connections were arranged roughly in the order of increased fabrication difficulty and increased disruption of the steel tube core. It was also expected that this coincided with the order of increased flexural strength. Because of the welded connection failures noted after the *1994 Northridge* earthquake in California, and the *1995 Hyogoken–Nambu* earthquake near Kobe, Japan, each connection was designed using a beam connection stub. This connection stub was intended to be fabricated in the shop in which higher quality control existed compared to field construction. In the field, steel girders were expected to be bolted and/or welded to these beam stubs.

3.2.1 Simple Connection, Type I

For this connection, the beam stub was welded to the skin of the tube, thus transferring girder forces directly to the steel tube. Some forces, however, were transferred to the concrete core through the bond between the tube wall and the concrete. For a smooth tube, the bond was developed due to friction and chemical adhesion between the two materials. However, this bond was very small, and it will likely vanish when the tube wall separates from the concrete core. Because of this lack of stress transfer from the tube to the concrete core, this connection may impose high strength demand of the tube wall. To better distribute these local stresses, the flanges of the connection stub were flared. The assumed mode of failure was considered to be shear yield through the thickness of the steel tube wall. Therefore, the angle over which the flange stresses were distributed, as shown in Figure 3.3, was given by the following equation:

$$\theta = \frac{F_{yf}\, t_f\, b_f}{R\, t\, \tau_{up}} \tag{3.1}$$

where θ in radians, F_{yf} is the yield strength of the girder flange, t_f and b_f are the thickness and width of the girder flange, respectively. R is the average radius, t is the thickness, and τ_{up} is the shear strength of the steel tube wall.

It was expected that this detail would impose high ductility demand on the tube wall at the girder tension flange elevation, which might cause severe damage to the steel tube or connection. To alleviate this high stress concentration on the tube wall, the connection stub was expanded to an external diaphragm.

3.2.2 Connection with External Diaphragms, Type II

Connections with external and internal diaphragms have been used in east Asian countries in moment–resisting steel frames. The fabrication of a connection with internal diaphragms is labor intensive. Moreover, the *1995 Hyogoken–Nambu* earthquake exposed many flaws in the design, detailing, and construction of such connections for hollow steel tube columns. For convenience of fabrication, a connection using external diaphragms, as depicted in Figure 3.4, was investigated. The intent of the diaphragm was to distribute the girder forces around the circumference of the pipe, thus alleviating the stress concentration on the steel tube skin. This external diaphragm was detailed using a square plate. The corners of the plate were cut to match the girder flange width. The diaphragm was selected such that its width was equal to the outer diameter of the pipe plus the girder flange width. This was considered to be the absolute minimum diaphragm size.

Because the performance of the external diaphragm may depend on its ability to allow the girder flange forces to flow around the steel tube, an alternative diaphragm was detailed. A modification to the minimum external diaphragm was investigated by shifting the girder farther from the column face. This modified connection was denoted as connection *Type IIA*.

Connection *Types I* and *II* distribute the girder forces to the skin of the steel pipe. This might raise several concerns including: transferring the girder tensile forces to the tube wall may separate the tube from the concrete core, and welding steel elements to the relatively thin tube wall may result in high residual stresses. Therefore, details that transfer load to both the steel tube and the concrete core were proposed.

3.2.3 Connection with Deformed Bars, Type III

This detail represented very little disruption of the steel tube. Holes were drilled in the tube wall, and weldable deformed bars were inserted into the concrete core and welded to the top and bottom flanges. No connection was provided between the tube wall and the weldable deformed bars. The needed embedded length was calculated according to the following equation (*ACI 318–89*):

$$l_{db} = \frac{0.04\ A_b\ F_{yb}}{\sqrt{f'_c}} \tag{3.2}$$

where l_{db} is the bar embedded length (in), A_b is the cross section area of an individual bar (in^2), F_{yb} is the deformed bar yield strength (psi), and f'_c is the uniaxial compressive strength of concrete (psi). The presence of the axial compressive load in the column and the confinement provided by the steel tube might reduce the required embedded length. However, the embedded length calculated from Eq. (3.2) was not reduced, or modified.

3.2.4 Connection with Headed Studs, Type IV

This connection was similar to connection *Type I*, however, headed studs were attached inside the tube wall to distribute flange forces to the concrete core. Fabrication of this connection was more labor intensive than the simple *Type I* connection. A section of the tube was cut in order to weld the headed studs to the inside of the tube wall. The removed portion of the steel tube was replaced and attached to the column using full penetration weld. This detail improved the composite behavior between the steel tube and the concrete core compared to the simple connection. Several rows of headed studs might be needed to develop the required axial and shear forces of the girder.

Due to the lack of provisions that govern the design of studs embedded in concrete–filled steel tubes, the *PCI Design Handbook 1971* provisions were used to perform an approximate design of connection *Type IV.* The pull–out strength of a headed stud cast into concrete was assumed to be governed by the shear cone or by the tensile strength of the stud. The *PCI Design Handbook 1971* gives the following equations to calculate the axial capacity of a stud embedded in concrete:

$$P'_U = \phi 16(l_e + d_h)\sqrt{f'_c}\ l_e$$

or (3.3)

$$P'_U = 0.9A_{so}\, f'_s$$

where P'_U is the pull–out capacity of the stud (lb), $\phi = 0.85$, l_e is the embedment length of the stud (in), d_h is the head diameter of the stud (in), A_{so} is the shank area of the stud (in^2), and f'_s is the ultimate tensile strength of the stud (psi).

Although used primarily for tension, it was possible for the stud to experience shear. Therefore, the axial load–shear interaction became relevant. For combined tension and shear on headed studs, the ultimate capacity was determined by the following equations (*PCI 1971*):

Concrete capacity:

$$\left(\frac{P_U}{P'_U}\right)^{4/3} + \left(\frac{V_U}{V'_U}\right)^{4/3} \leq 1.0 \qquad (3.4)$$

Stud capacity:

$$\left(\frac{P_U}{P'_U}\right)^{2} + \left(\frac{V_U}{V'_U}\right)^{2} \leq 1.0 \qquad (3.5)$$

Headed studs 19 mm ϕ, 89 mm long ($^3/_4'' \phi \times 3.5''$), with 414 MPa (60 ksi) yield strength, were used. The concrete strength was 34.5 MPa (5 ksi), and the moment–to–shear (*M/V*) ratio was 7,620 mm (300″). Therefore, according to the above equations, at least three rows, with 5 studs/row, were needed for each flange of the W24×76 girder used in this analytical study. The failure of the connection was controlled by the shear failure of the concrete around the studs. When shear forces dominated the design of this connection, it was found that only five studs arranged in one row at the level of each flange were enough to develop the shear strength of the girder. This was the basic design for the connection with headed studs. Other alternatives were also considered.

3.2.5 Connection with Web Plate and Headed Studs, Type V

The fabrication of this connection required cutting away a portion of the steel tube. This cutting required a significant degree of precision, since this provided alignment of the beam and column center–lines. The girder moment was to be resisted by the forces developed by shear in the headed studs times the distance between them. For this to occur, the web plate must be stiff and strong enough to transfer the girder forces to the concrete core.

3.2.6 Continuous Flanges, Type VI

The weldability of the deformed bars, and the clearance between them were among the critical issues in connection *Type III*. To resolve some of these problems, connection *Type VI* was developed. Slots were cut in the tube wall, and flange plates were continued through the concrete–filled tube. The flange plates and the shear tab were fillet welded to the steel tube.

3.2.7 Continuation of the Girder through the Column, Type VII

In this detail, an I–shaped slot was cut in the tube wall, a beam stub was passed through this slot, and it was fillet welded to the steel tube. The girder and column center–lines were in alignment. For simplicity, no additional detailing was introduced to enhance additional composite behavior. This was considered to be the minimum effort for the continuous connection.

3.3 FINITE ELEMENT ANALYSIS

A comprehensive finite element model was generated for each connection type. These analytical models were generated to investigate the influence of various detail components on the connection flexural behavior. *PATRAN 2.5* (PDA Eng. 1990) was used to create the finite element models, and *ABAQUS v5.4* (HKS 1994) was used to analyze the 3–D nonlinear finite element models of the proposed details. All numerical calculations were performed on the HP720 machines in the Department of Civil Engineering at the University of Illinois at Urbana–Champaign.

3.3.1 Material Models

The reliability of these finite element analyses depended, among other factors, on how accurately the material properties were mathematically modeled. Each analytical model had three basic types of elements: concrete, steel, and the interface between the steel and the concrete.

For a concrete–filled steel tube, confinement of the concrete core was not fully understood. At low to moderate axial loads, the steel tube might offer little confinement. However, near ultimate load of the concrete–filled steel tube, the concrete might be well confined, and hence under a triaxial state of stress. Many numerical models have been developed to describe the stress–strain relationship of concrete under various loading conditions (Bangash 1989). Further many failure criteria for concrete elements have been suggested. A good concrete model should account for the cohesive strength of the cement paste and the frictional adhesion of the aggregate.

ABAQUS was selected for all finite element computations, because of its available 3–D inelastic concrete material model. This model was designed for cases when the concrete was subjected to monotonic strain with relatively low confinement. When the principal stresses were predominantly compressive, the concrete was modeled by an elastic–plastic theory using a simplified yield surface.

Cracking was assumed to be the most important aspect of the material behavior, therefore, adjusting strength and stiffness when cracks occur was critical. Cracking was assumed to occur when the stresses reached the failure surface, which was taken to be a simple Coulomb line. ABAQUS used a smeared crack model, which did not track individual macro–cracks, but adjusted the strength and stiffness at each integration point within the finite element model. Smeared crack models might introduce a mesh sensitivity in the results, in the sense that the finite element solution does not converge to a unique value as the mesh is refined. For this case, the utilization of the fracture energy concept eliminated most of the mesh sensitivity effects. The fracture energy concept was concerned only with the energy required to open a unit area of crack, and neglected the elastic deformation of the material. Neglecting the elastic deformations was justified because the deformations of a concrete specimen under tension were mainly due to crack opening, and the elastic deformations were small. The post–cracking behavior was controlled by tension stiffening, which determined how much tensile stresses can transfer across a given crack. In order to minimize the mesh sensitivity effect, the tension stiffening behavior was defined by utilizing a fracture energy criterion, in which the stress–displacement response of the concrete was used.

The concrete stress–strain model shown in Figure 3.10 was used to describe the uniaxial behavior of concrete. This model had a linear elastic part with the same stiffness in compression and tension. Crushing was assumed to occur at point C, after which, the behavior of concrete depended on the confining pressure. Because confinement of the concrete core was not well understood, particularly in the connection vicinity, it was assumed that there would be some strength deterioration of the concrete under large compressive strains. For tension in the concrete material, the behavior was linear up to its tensile strength. This tensile strength was assumed to be 10% of the uniaxial compressive strength. Since cracks in plain concrete can not transfer tensile stresses, the post tensile strength stiffness, line FG in Figure 3.10, was quite steep. Sudden failure in the material model, however, caused numerical problems during the finite element analysis, so it was assumed that only cracks wider than 2.54 mm (0.1″) were not capable of transferring tensile stresses.

Shear retention was used to describe the reduction in the shear modulus associated with the concrete cracking. It was assumed that the shear response was not affected by cracking. This assumption was reasonable, and in many cases, the overall response was not strongly dependent on the amount of shear retention.

For the analytical study, the concrete strength was 34.5 MPa (5 ksi), which produced an elastic modulus of 27,790 MPa (4,030 ksi). The ratio of the ultimate biaxial compressive stress to the ultimate uniaxial compressive stress was specified as 1.2.

An isotropic elasto–plasticity model was used to simulate the elastic and inelastic behavior of all steel components. Von Mises' yield criteria defined the material yield surface, and Prandtl–Reuss flow rule was used to determine the plastic deformation. Figure 3.10 shows the uniaxial constitutive relationship used to model the steel material. It was assumed that the steel behavior under tension was identical to that under compression. The Young's modulus of steel was assumed to be 200 GPa (29,000 ksi). The yield strength of the deformed bars and the headed studs was 414 MPa (60 ksi), and the girder yield stress was 248 MPa (36 ksi).

The bond between the smooth pipe and the concrete core was due to chemical adhesion and friction between the two materials. It was assumed that this bond had no tensile capacity allowing the two materials to separate without significant resisting forces. Two finite element models were considered for the interface material between the steel and concrete: the first model used the gap element in ABAQUS, and the second model used a soft material placed between the concrete core and the steel pipe. The gap element can transfer compressive and frictional forces only. However, due to the nonlinearity of the gap element compounded with the nonlinearity associated with the concrete cracking, it was difficult for the solution to converge. To extend the analysis further into the inelastic region, the second model was considered. This included a thin layer of 20–node brick element, which was given a very low stiffness and tensile strength.

The second interface model resulted in aspect ratios as high as 1:50 for the solid interface elements. To investigate the effect of this high aspect ratio on the finite element results, another model was created with a 1:6.5 aspect ratio. A comparison between different models of the interface layer is shown in Figure 3.11. The soft layer interface model exhibited solution convergence at much larger deformations compared to the gap element model. Further, a comparison over the range of deformation prior to the instability of the gap element solution showed that there were no significant differences between the connection behavior observed for the two interface models. The stress gradients across the width of the interface elements were small. Moreover, these elements were subjected to simple loading that did not include significant bending or torsion. Therefore, the interface element aspect ratio did not have significant effect on the analytical results. Using a small aspect ratio for the interface layer resulted in extremely large analytical model which required extensive computational effort. Consequently, the aspect ratio of the interface elements was allowed to reach a maximum value of 1:50. The strength and stiffness of the interface layer were assumed to be 27.6 MPa (4 ksi) and 172 MPa (25 ksi), respectively. These numbers were based on a previous study on the bond–slip behavior in reinforced concrete girders (Alostaz 1992), and they were on the conservative side.

3.3.2 Finite Elements

Twenty–node brick elements (*C3D20 of ABAQUS*) with three translational degrees of freedom at each node were used to model the concrete core, the deformed bars, and the headed studs. Also the interface between the concrete core and the steel pipe was modeled using the 20–node brick elements, however, reduced integration procedure was used for these elements. Eight–node shell elements (*S8R5 of ABAQUS*) with five degrees of freedom at each node were used to model the steel tube and the girder. Both elements incorporated material and geometric nonlinearities in their formulation. Nodal displacement compatibility was enforced between the solid and shell elements. However, no rotation compatibility was enforced between the two element types.

Convergence of the numerical solution was checked by varying the number of elements and nodes in each model. Based on these convergence studies, the type of finite elements and the size of the finite element mesh were selected.

Since little research has been done on connections to concrete–filled steel tubes, it was not possible to calibrate the finite element models against experimental results. However, the suggested finite elements and material models were used to analyze several concrete–filled steel tubes which were tested experimentally by other researchers (Kenny *et. al.* 1994). A sample comparison is shown in Figure 3.12. This figure illustrates that the finite element models, as proposed in the present research, were capable of predicting the elastic and inelastic behavior of concrete–filled steel tubes reasonably well under axial compression. The finite element models will be verified using the experimental results of this research project.

3.3.3 Three–Dimensional Finite Element Models

While some connections were conducive to large dimensional CFTs, other connections were more suitable for small diameter pipes. For example, the simple connections might be more appropriate for a large diameter CFT, while the diaphragm plates were perhaps more suitable for small diameter pipes. Although the type of connection may depend on the pipe diameter, this research attempted to investigate the behavior of a broad range of details on moderate size CFTs. Therefore, the pipe diameter remained constant in this study such that a comparison could be made between the behavior of various connection details. The sizes of the column and girder were selected such that they represent average member sizes used in the prototype frames designed in Chapter 2. Hence, the column was selected to be a 510 mm $\phi \times 9.5$ mm ($20'' \phi \times {}^{3}/_{8}''$) concrete–filled steel tube, and the beam was a W24×76 girder.

For convenience, the X–axis aligned with the longitudinal axis of the girder, the Z–axis aligned with the longitudinal axis of the column, and the Y–axis was perpendicular to both longitudinal axes of the column and girder. Due to symmetry in the X–Z plane, one half of the connection was modeled. Nodes at the column top were restrained from translation in the X and Y directions, and the displacement along the Z–direction was not restrained to allow for the application of the column axial forces. Nodes at the other end of the column were restrained from translation in the X, Y, and Z directions. To eliminate boundary influence, the length of the girder was selected to be about 2.5 times its depth. To achieve the proper M/V ratio, shear was applied to the girder web, and longitudinal stresses were imposed on the girder flanges to simulate the bending moment needed at that location. Figures 3.13 through 3.18 show the connection details and the finite element model of each detail.

The applied load did not stress the column beyond the elastic range, therefore, the full magnitude of the axial force was applied in one increment to the top of the column. Then, the girder was loaded incrementally to failure. The Newton–Raphson procedure was used during the elastic behavior, and the Riks procedure was used for the inelastic analysis. The Riks procedure allowed for a unique solution of the equilibrium equations even when the model exhibited strength deterioration. The finite element models were loaded monotonically to a point where solution convergence was not possible.

3.4 FINITE ELEMENT RESULTS

The behavior of a concrete–filled steel tube may be affected by many factors, including: shape of the tube cross section, the length–to–depth ratio (L/D) of the column, the axial–to–yield load ratio (P/P_y), the yield strength of the tube, and the D/t ratio. Furthermore, the performance of connections to tubular columns may be influenced by the moment–to–shear ratio (M/V).

A parametric investigation was performed to expose the most critical elements in the design and detailing of connections to concrete–filled steel tubes. For each connection detail, the following parameters were studied:

1) D/t ratios of 40.0, 53.3, and 80.0. These ratios were in the range where column behavior might exhibit the greatest benefit from composite action, and were in the practical range for moderate–height structural systems. Limitations on D/t were suggested by some model codes to prevent buckling of the tube wall. For instance, *EUROCODE 4* (Johnson 1994) limited $D/t \leq 66.0$ for a steel pipe with $F_y = 317$ MPa (46 ksi), and the equivalent limitation in *AISC/LRFD 1986* was $D/t \leq 71.0$. However, D/t ratios as large as 200 were successfully used in actual building structures (Boyd *et. al.* 1995, Bridge *et. al.* 1992).

2) Axial load ratios of P/P_y = 0.0%, 6.0%, 36.0% were investigated. These values were consistent with P/P_y ratios used in previous experimental work found in the literature, and were also within the practical limits as determined by prototype frame design. The squash load, P_y, was calculated as follows:

$$P_y = A_s\, F_y + A_c\, f'_c \qquad (3.6)$$

where A_s is the cross section area of the steel pipe, F_y is the yield strength of the pipe, and A_c is the cross section area of the concrete core.

3) Yield stress limits of F_y = 248, and 317 MPa (36 & 46 ksi) were considered to account for the available steel pipes.

4) Moment–to–shear ratios of M/V = 0.50, 1.27, and 7.62 m (20″, 50″, and 300″). For some connections, a ratio of M/V= 0.66 m (26″) was investigated. Concrete–filled tubes may desirable in eccentrically braced frames, therefore, the M/V ratio of the connection becomes critical. The length of a link in an eccentrically braced frame was calculated per the *1991 NEHRP Provisions.* For a W24×76 structural steel section, this length is about 0.95 m (38″). So M/V ratios of 0.5 and 0.66 m (20″ & 26″) are for connections with shear as the dominant force, while M/V values of 1.27 and 7.62 m (50″ & 300″) are for connection dominated by flexure. While flexural connections were the primary interest of this research, it was also desirable to investigate the performance of each connection in shear.

5) This research focused on connections to exterior columns, however, some details were studied in an interior joint configuration with a girder connected to each side of the column along a single plane.

The need for the analytical modeling was to expose the advantages and disadvantages of the individual connection types. In response to the performance obtained from these analytical studies, certain connections were analyzed with various changes. Some of these changes included adding or eliminating headed studs inside the tube wall, strengthening and stiffening the tube wall with a sleeve, and altering the embedment of some connection components. Some of these modifications resulted in a hybrid of two or more of the basic connection types.

Only parameters that showed significant influence on connection performance will be emphasized by this report. The standard reference connection had the following parameters: D/t=

53.3, P/P_y= 6%, M/V= 7,620 mm (300″), and F_y= 317 MPa (46 ksi). Unless otherwise noted, the discussion in this chapter will focus on the standard parameters for each connections. More complete results from the finite element analyses are shown in *Appendix A*.

The analytical moment–rotation behavior for some of the basic connection types is shown in Figure 3.19. The rotation shown in this figure was the total rotation of the joint. The rotation of the column center–line accounted for approximately 10 – 15% of the total joint rotation. Connection *Type VII* developed the highest flexural strength, while the lowest strength was developed by connection *Type V*. It is worth mentioning that the nonlinear behavior observed from the numerical analysis did not necessarily indicate connection ductility. A detailed discussion of each connection type follows.

3.4.1 Simple Connection, Type I

As shown in Figure 3.20, flexure on the girder creates high local stresses on the tube wall in the vicinity of the tension flange. The severe distortion of the tube wall shown in Figure 3.21, suggests that the tube wall may be highly susceptible to fracture. The tube wall distortions and high stresses account for the flexibility of the connection and for the fact that it could only develop 92% of the girder flexural strength. This flexible connection has significant consequences on frame performance, since it might lead to large drifts in moment–resisting frames. At ultimate strength, a plastic hinge is expected to occur. However, from these analytical results it is clear that the connection strength might be limited by the through–thickness shear strength of the tube wall.

Because of the significant tube wall distortion, the shear stresses in the tube wall are expected to increase towards the tips of the girder flange. This was confirmed by the the finite element analysis as shown in Figure 3.22. This figure shows that the shear stress through the pipe wall thickness at the flange tip is more than twice its value near the girder web. The high stress concentration at the flange tip makes the pipe wall and the flange tip susceptible to fracture.

Figure 3.23 illustrates that the connection performance was influenced by the tube wall thickness. Increasing the D/t ratio from 40 to 80 reduced the M–θ initial stiffness by 30%, and only 5% drop in the strength was observed. Hoop stresses as high as 345 MPa (50 ksi) were observed adjacent to the tension flange for a pipe with D/t= 80. These high stresses increased the demand on the tube wall significantly. Because of the high local distortions and stress concentrations, the joint was reinforced with a sleeve resulting in a D/t= 22.8 compared to D/t= 53.5 used for the original detail. The reinforcing sleeve increased the elastic stiffness by about 86% compared to the basic simple connection. However, the strength increase was only about 7%. Figure 3.23 illustrates that maintaining the same D/t ratio in the connection vicinity while varying the wall pipe thickness away from the connection region did not significantly affect the connection performance.

The yield strength of the pipe had no significant effect on the elastic behavior of this connection. Connections with lower pipe yield strength, yielded earlier and showed less strain hardening behavior.

The M–θ behavior was not significantly affected by the different axial load ratios. However, high axial loads created significant axial shortening of the column which may be exacerbated under cyclic loading. The elastic axial shortening of a tubular column subjected to 6% of the squash load was about 0.31 mm (0.012″). The finite element analysis gave a 50% higher axial deformation under the same axial load, refer to Figure A.3. This difference was due to the fact that both materials were highly stressed in the connection vicinity. As a consequence, the axial stiffness of the column was reduced.

Figure 3.24 shows the analytical behavior of a simple connection with different moment–to–shear ratios. The flexural strength and the shear strength for a W24×76 cantilever can be approximately developed if M/V= 0.79 m (31″). The analytical results showed that the connection was able to develop approximately 50% of the girder shear strength for M/V= 1.27 m (50″), and only 41% of the girder bending strength was developed. For M/V= 0.5 m (20″), the connection might exhibit a rapid strength deterioration after reaching its maximum flexural capacity. Numerical results suggest that simple connections with long shear spans might exhibit more flexible behavior compared to those with shorter shear span. This behavior was attributed to the flexibility resulting from excessive distortion of the tube wall.

The ultimate flexural strength of an exterior joint was about 7% higher than that of an interior joint with moment reversal across the column. The reduction in the strength of the interior joint was due to the high diagonal tensile stresses, which were approximately 65% – 78% of the tube yield strength, that developed in the steel pipe. These tensile stresses flow between the tension flanges on either side of the pipe. Stresses in this range can seriously reduce the pipe strength. Both exterior and interior joints have almost the same elastic behavior. Although interior joints have almost twice the shear force there was no concrete crushing apparent in the panel zone region.

3.4.2 Connection with External Diaphragms, Type II

External, through and internal diaphragms are sometimes used to stiffen the tube walls in the connection region. Through and internal diaphragms require extensive welding and disruption to the steel tube. Furthermore, strong seismic events exposed potential problems in connections with through or internal diaphragms for hollow steel tube columns (Toyoda 1995). External diaphragms may be more practical, therefore, they were studied in this analytical research. Two diaphragm configurations were considered as shown in Figure 3.25. Dimensions were selected such that the minimum distance between the pipe wall and the plate edge was at least equal to half the girder flange width. The diaphragm plates had the same thickness as the girder flange.

Figure 3.25 shows the analytical moment–rotation behavior of this connection, and the Von mises' stresses are shown in Figure 3.26. Connection *Type II* was not able to develop the plastic strength of the girder. Further, the initial elastic stiffness was approximately the same as for the simple connection *Type I*. Shifting the girder farther from the face of the CFT, however, improved connection performance significantly. In this study, shifting the girder was accomplished by changing the angle of the diaphragm plate about the top edge. This resulted in a more direct path in which the girder flange stresses could flow around the CFT. In this example, the girder for *Type II* was at a distance of *1.45R* from the center of the column, where *R* was the steel tube radius. For connection *Type IIA* the girder was *2.18R* from the column center. The detail with *Diaphragm Type IIA* exhibited much more stiffness and strength than for the minimum size diaphragm plate detail. Also, shifting the girder farther from the CFT face resulted in development of almost the full plastic bending strength of the girder.

The stresses and deformations for both types of the diaphragm plates, are shown in Figures 3.27 and 3.28. These figures illustrate the differences observed in the diaphragm connection behavior. For the minimum size diaphragm, the tube wall distortion prevented the gradual flow of girder flange stresses into the diaphragm plate. Stresses exceeding the material yield strength remain localized in the diaphragm plate adjacent to the girder flange. Further, the strains, shown in Figure 3.28b, are highly localized in the diaphragm plate due primarily to the distortion of the steel tube. Since the overall behavior was similar to the simple connection *Type I*, this connection performance was also sensitive to the tube wall thickness. Therefore, this type of connection was susceptible to the same type of failure that was exhibited by connection *Type I*. On the other hand, shifting the girder farther from the face of the CFT improved the elastic and inelastic behavior significantly. *Diaphragm Type IIA* resulted in much less distortion of the plate around the CFT compared to the basic *Type II* connection. As shown in Figure 3.27, stresses in the extended diaphragm plate were better distributed than for the minimum diaphragm plate size, while the very large strains predominantly remained within the girder flange. Consequently, *Diaphragm Type IIA* exhibited a stress and strain behavior necessary for a plastic hinge to form in the girder.

The strain contours illustrate that the diaphragm was susceptible to a fracture, which was likely to initiate at point A. For diaphragm *Type IIA*, the fracture might propagate through the weld between the diaphragm and the girder. On the other hand, for connections with diaphragm *Type II*, the fracture was likely to propagate through the diaphragm itself until it reached the tube wall.

High compressive stresses were observed along the outer edge of the minimum size diaphragm. Such stresses could initiate local plate instability, which would increase the demand on the tube wall. These stresses were not observed in diaphragm *Type IIA*.

3.4.3 Connection with Deformed Bars, Type III

This connection detail was identical to connection *Type I*, except holes were drilled in the steel pipe above and below the beam flanges. Weldable deformed bars were inserted into the openings and welded to the girder flanges. Figure 3.29 illustrates the Mises' stresses in the pipe and the girder of connection *Type III*. Results suggest that the girder flanges began to yield around the deformed bar region, indicating that the girder was beginning to develop the plastic bending capacity. Figure 3.19 shows that the connection might have a reasonable post–yield behavior. This detail became nonlinear at about 78% of the girder flexural strength, and it was able to develop almost 90% of the plastic bending strength of the connected girder. The initial elastic stiffness, however, was still only 57% of the ideal rigid connection condition.

The embedded deformed bars relieved the high stress concentration from the tube wall compared to the simple connection *Type I*. This suggests that part of the girder flange forces were transferred to the concrete core using the embedded deformed bars. The finite element analysis indicated that the amount of axial forces transferred to the deformed bars was independent of the thickness of the pipe wall as illustrated in Figure 3.30. It was estimated that 71% of the flange tensile forces were transferred to the tension deformed bars, and 65% of the flange compressive forces was resisted by the compression bars. As shown in Figure 3.31, the 3–D finite element model of this connection clearly indicated that the deformed bars were subjected to local bending which forced the extreme fibers on one side of the bar to yield.

Since the pipe stresses remained mostly in the elastic range, the behavior of the connection was not affected by the yield strength of the tube. The elastic slope of the M–θ curve was almost the same for connections with different axial loads. However, connections with higher axial load ratios showed lower ductilities.

Figure 3.32 shows that the connection was susceptible to the M/V ratio. For a shear span of 1.27 m (50″) the connection was able to develop about 55% and 35% of the flexural and shear strength of the girder, respectively. The behavior was linear up to about 20% of the bending strength of the girder, and strength deterioration occurred after the maximum strength was reached. For $M/V=$ 0.50 m (20″), the connection developed 80% of the girder shear strength, the behavior was linear up to about $0.25M_p$, and no strength deterioration was observed. When compared to the simple connection *Type I*, it was clear that the deformed bars improved the connection performance even in cases where shear was the dominant force.

Details for interior joints were also examined. The deformed bars were extended continuously through the pipe, and the behavior was studied under anti–symmetric loading. The bars in this arrangement reduced the embedded length, hence, they were susceptible to bond failure. In such cases, independent weldable deformed bars on each girder, with standard hooks could be used to anchor the bars in the concrete core. This configuration was selected because it represented the most critical case for this detail. Figure 3.33 illustrates the moment–rotation behavior of this detail. The connection yielded at 50% of the plastic strength of the girder compared to 88% for an exterior joint. Exterior joints exhibited stiffer elastic behavior, however, both connections had almost the same flexural strength.

An alternative to this connection was investigated in which the girder flanges were not welded to the tube wall. This allowed the girder to be connected with a simple connection and deformed bars to resist flange forces. Analytical results suggest that bar buckling will occur between the end of the flange and the tube wall, as shown in Figures A.17 and A.18. Moreover, since the deformed bars were designed to develop the full flange strength, this detail might result in too much congestion violating the minimum clearance requirements specified by *ACI 318–89* code. These specifications require that the minimum clearance between reinforcing bars shall be equal to one bar diameter, but not less than 25.4 mm (1.0″).

For the current study, the ratio between the bar axial capacity and the flange axial capacity (F_b/F_f) was about 87%. Analytical results suggest that this strength ratio was enough to develop more than 90% of the flexural strength of the girder.

3.4.4 Connection with Headed Studs, Type IV

This connection was intended to improve compatibility of the tube and the concrete core, and to reduce local distortions of the tube wall compared to the simple connection. Figure 3.19 illustrates that linear moment–rotation behavior was exhibited until the strength reached the girder yield moment. The elastic stiffness of connection *Type IV* was almost twice that of connection *Type I*, yet it was still 48% of the assumed ideal rigid connection condition. Further, this connection was linear up to about 93% of the ultimate bending strength of the girder.

There were two possible failure modes considered for the headed stud subjected to tensile forces: tensile failure of the stud shank, or concrete cone shear failure if the stud had insufficient embedment or clearance between other studs. Stresses along the longitudinal axis of the headed studs are shown in Figure 3.34. It is clear that the axial stress in the studs at the tension flange exceeded the yield stress considerably, indicating development of the full tensile strength of the stud. In these analytical studies, it was assumed that the ultimate tensile strength of the stud is 50% larger than its yield strength. Due to the high local stresses in the concrete surrounding the studs, convergence problems were encountered, and it was not possible to capture the full inelastic behavior of this connection.

As depicted by Figure 3.35, local bending stresses exist in the studs, this introduced additional stresses that were not accounted for in the design of the connection. About 4% of the girder shear was resisted by the tension studs, and about 39% was resisted by the compression studs. Due to the curvature of the tube wall, the studs farther away from the web of the girder were at an increasingly skewed angle. The larger the skew for the stud, the less the participation of the stud in resisting the girder flange forces. To study this influence, the studs on the outside edge of the girder flange were eliminated, resulting in three studs at each girder flange. The analytical behavior of the modified detail was almost identical, exhibiting only about 3% drop in its flexural strength compared to the original detail. Therefore, adding studs above and below the girder flanges might provide better resistance to flexural behavior than adding studs on the extreme flange edges.

The connection exhibited some sensitivity to the tube wall thickness. For $D/t= 40$ the connection was able to develop more than 90% of the girder flexural strength, however, for $D/t= 80$ the strength was only about 80% of M_p. Therefore, doubling the thickness of the pipe resulted in about 13% increase in the connection strength. Consequently, the strength of this connection was limited primarily by the strength of individual studs. The elastic stiffness of the $M–\theta$ curves was slightly decreased as the load ratio was increased from 0 to 36%, and more inelastic behavior was exhibited at higher axial load ratios.

The behavior of this connection was significantly affected by the moment–to–shear ratio as shown in Figure 3.36. Connection with small moment–to–shear ratios became inelastic at a much smaller moment, and exhibited a lower elastic stiffness. After reaching the maximum capacity, connections with low M/V ratios experienced a slight decrease in flexural strength. Research on end–plate connections of steel girders to reinforced concrete columns (Hawkins *et. al.* 1980) exhibited behavior similar to this connection type. For connections with high M/V ratios, a pull–out failure mode occurred, in most cases, with small stud embedment lengths. This explained the brittle failure mode observed in connections with large M/V ratio. On the other hand, connections with low M/V ratios exhibited a ductile shear failure of the studs. Under cyclic loading, the connection showed rapid strength deterioration. The presence of the tube in connection *Type IV* provided additional redundancy that did not exist in the end–plate connections. However, the finite element analysis suggests that the studs were significantly overstressed. If the studs fail, high forces will be transferred suddenly to the tube wall. If the studs fracture from the inside, this will reduce to behavior similar to that of the simple *Type I* connection.

3.4.5 Connection with Web Plate and Headed Studs, Type V

The moment–rotation behavior for connection *Type V*, shown in Figure 3.19, exhibited an initial elastic stiffness of about 28% of the ideal rigid connection. This connection developed the least bending strength of any of the connections investigated, at only 72% of the plastic bending strength of the girder.

Results of this basic connection type suggested that there was little participation of the headed studs in resisting the girder moments. Therefore, a variation of this connection was investigated, in which the web was continued through the steel tube and no headed studs were attached to the embedded plate. Eliminating the headed studs might significantly reduce fabrication costs associated with this connection. Comparison of the M–θ behavior between these connection types is shown in Figure 3.37. The simple connection *Type I* was similar to the variation on connection *Type V* since the primary change was extending the web plate through the steel tube. Thus, the simple connection *Type I* was shown in Figure 3.37 for comparison. The high flexibility of this connection was due to the flexibility of the web plate. The flange plates of connection *Type VA* were continued to the pipe, but in the original detail, they were discontinued at 38 mm (1.5″) from the pipe wall. Connection *Type VA* produced high stress concentrations at the location of the flange plate–tube wall intersection, which resulted in large local deformations. As shown in Figure 3.38, transferring the girder moment to the web plate produced high flexural stresses in this plate, this might make the connection susceptible to local instabilities. Clearly, it was advantageous to continue the flanges to the steel tube wall, reducing the potential for instability in this part of the connection. However, local instabilities were not observed in the analytical models because the web plate was in the plane of symmetry of the connection.

The behavior of this connection was dominated by that of the web plate. Therefore, the D/t ratio, the yield strength of the tube, and the axial load ratio had little effect on the connection behavior.

3.4.6 Continuous Flanges, Type VI

This detail was proposed in order to overcome some of the problems associated with connection *Type III*. However, the force transfer mechanism between the steel and the concrete core was the major issue in this new detail. This became more critical in the case of interior joints subjected to cyclic loading.

As shown in Figure 3.39, connection *Type VI* had distinct trilinear behavior. The first portion of the trilinear response, represented the elastic behavior of this connection. At approximately 55% of the flexural strength of the girder, slip occurred between the embedded flanges and the concrete core. This slip represented the second stage of the analytical behavior. Due to this slip, most of the girder flange forces were transferred to the tube wall. The third portion of behavior was initiated by yielding of the connected girder. Bond failure prevented the analytical model from exhibiting a significant strain hardening behavior, hence, the maximum strength developed by this connection was approximately $1.0M_p$.

The variation of the girder flange forces along the axis of the girder is shown in Figure 3.40. The flange stresses decreased significantly as it entered the tube, suggesting that the majority of these stresses were transferred to the tube wall. The behavior of this connection was influenced by the interaction between the embedded flanges and the concrete core. Therefore, the pipe yield strength, the axial load ratio, and the pipe wall thickness had little effect on the connection performance.

3.4.7 Continuation of the Girder through the Column, Type VII

Figure 3.19 indicates that this connection best represented ideal conditions, *i.e.* full connection restraint. The elastic stiffness was within 96% of the rigid connection, and it produced the plastic bending strength of the steel girder. The finite element results clearly indicated that the strength of this connection was limited by the capacity of the steel girder and not the region interior to the CFT.

Due to the rotation of the girder, the steel pipe may be overstressed and the concrete in direct contact with the flanges may crush. A solution to this problem was to weld deformed bars to the beam flanges within the tube (Azizinamini *et. al.* 1993). However, this required an access opening to be cut in the steel pipe. In the present research no reinforcing bars were used, because high stresses were not observed in the steel pipe. Shear stresses as high as 0.70 MPa (0.10 ksi) were observed at the interface between the tension flange and the surrounding concrete. Previous research (Roeder 1984, Wium *et. al.* 1994) indicated that the bond stress between a structural steel section and encasing concrete may range from 0.22 to 3.80 MPa (0.03 & 0.55 ksi). This suggests that bond failure and slip are not likely to occur for the girder in an exterior joint configuration.

Connections with higher axial loads showed stiffer elastic behavior in the moment–rotation relationships. The distribution of the contact stresses between the embedded flanges and the surrounding concrete is shown in Figure 3.41. Axial load ratio of 36% resulted in no tension stresses for the compression flange, with a 50% increase in the concrete stresses, hence the maximum concrete compressive stress was approximately $0.7f'_c$. A thicker tube wall stiffened the elastic response of the connection, however, no increase in the bending capacity was observed. This emphasized that the connection strength was related primarily to the girder strength. The thickness of the tube had no significant influence on the longitudinal flange stresses. However, these stresses decreased to approximately 30% of their original value as the girder entered the tube. A considerable amount of flange forces was transferred directly to the steel tube wall, however, Figure 3.42 shows no signs of overstressing in the steel tube wall.

Since this connection may be very sensitive to a girder on the opposite side, an interior joint was investigated. Exterior joints were 12% stronger and 60% stiffer than interior joints. The needed bond stresses between the flange and concrete nearly doubled for interior joints. Although this is close to the minimum slip stress observed in previous studies, it still does not appear to be overly critical.

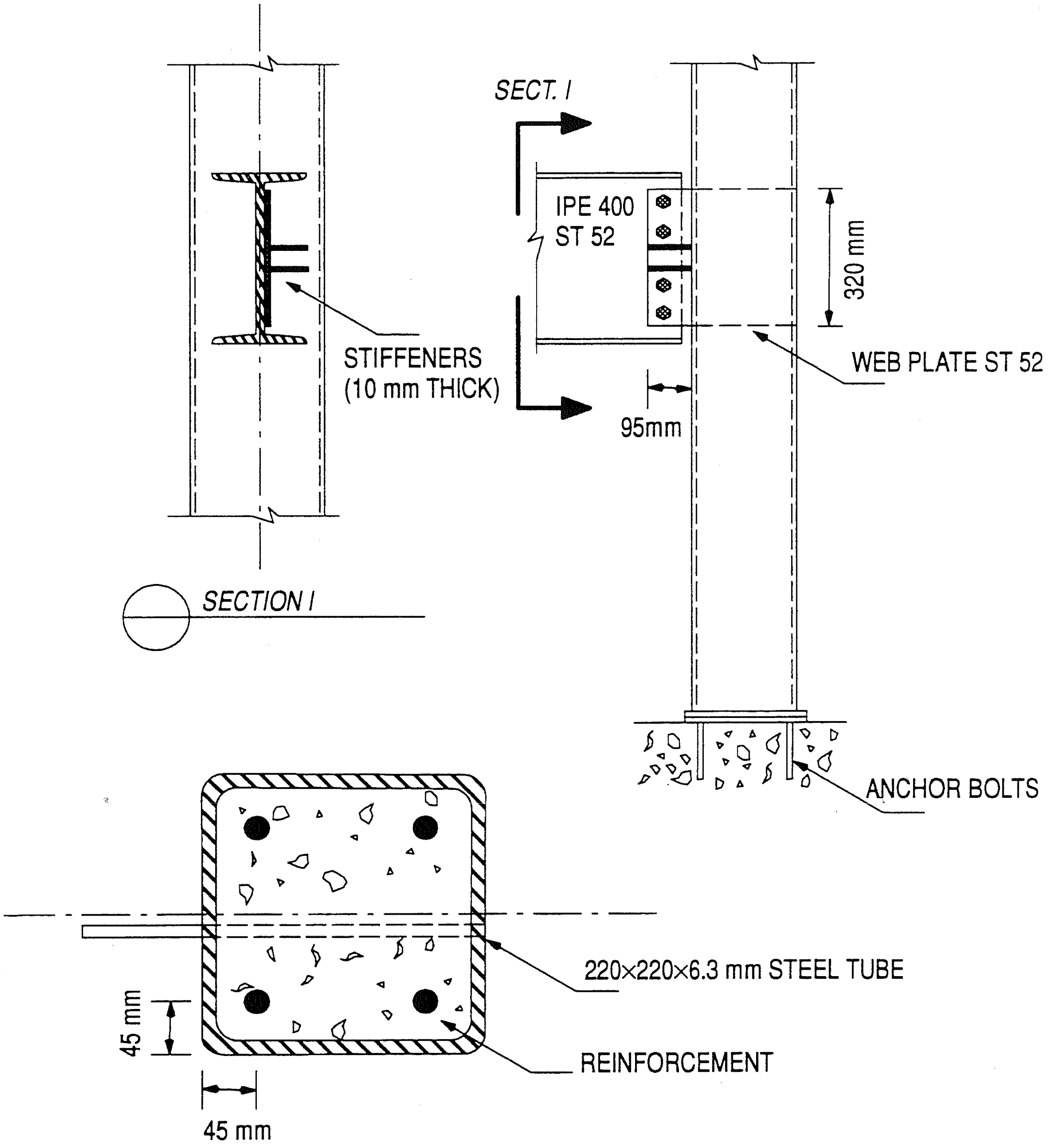

Figure 3.1. Simple Connection used in the Industrial Bureau Building in Bielefeld, Germany, Roik *et. al.* (1985)

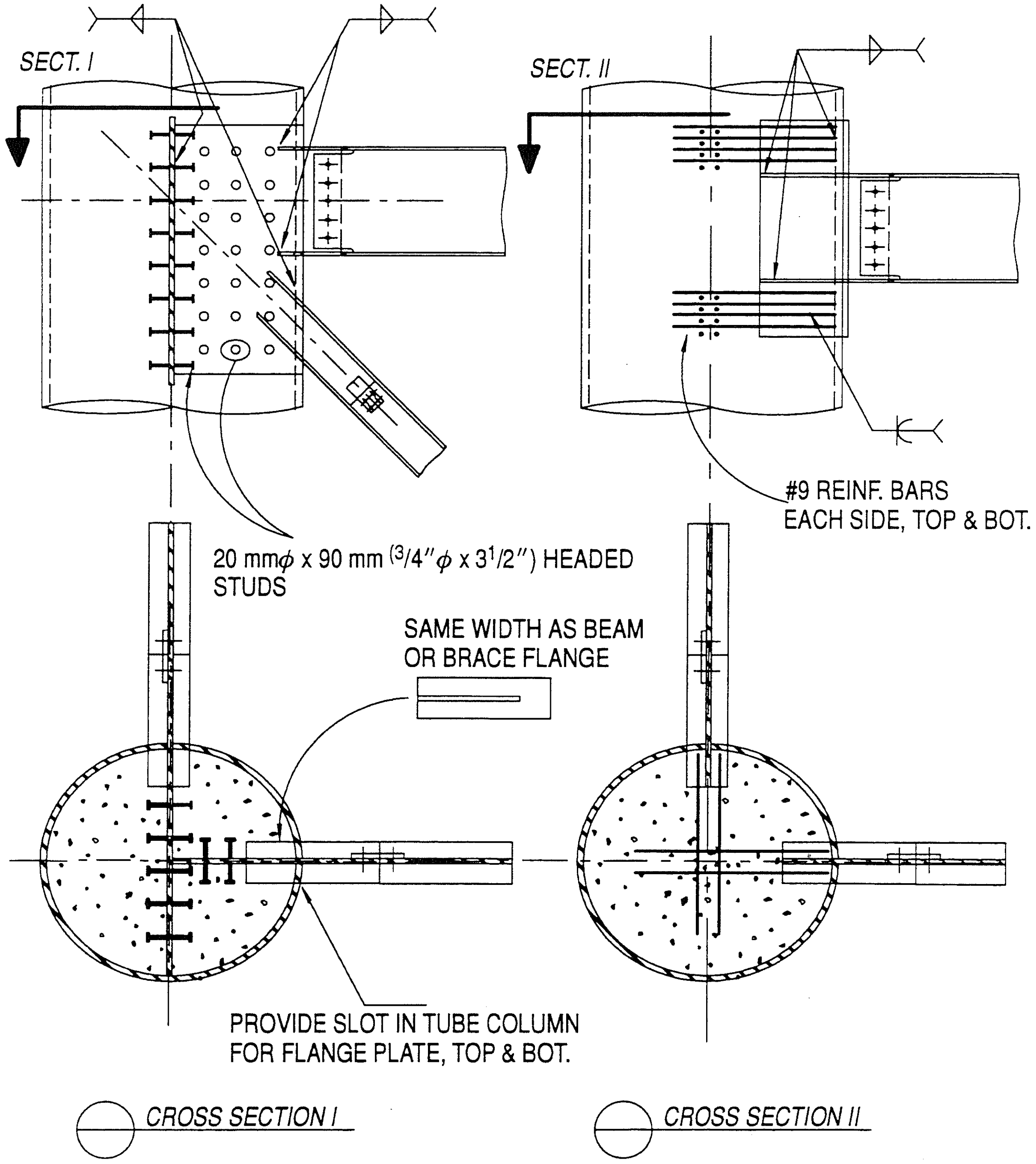

a.) Connection with Headed Studs.

b.) Connection with Reinforcing Bars.

Figure 3.2. Typical Connection Details for Large Diameter Steel Tubes

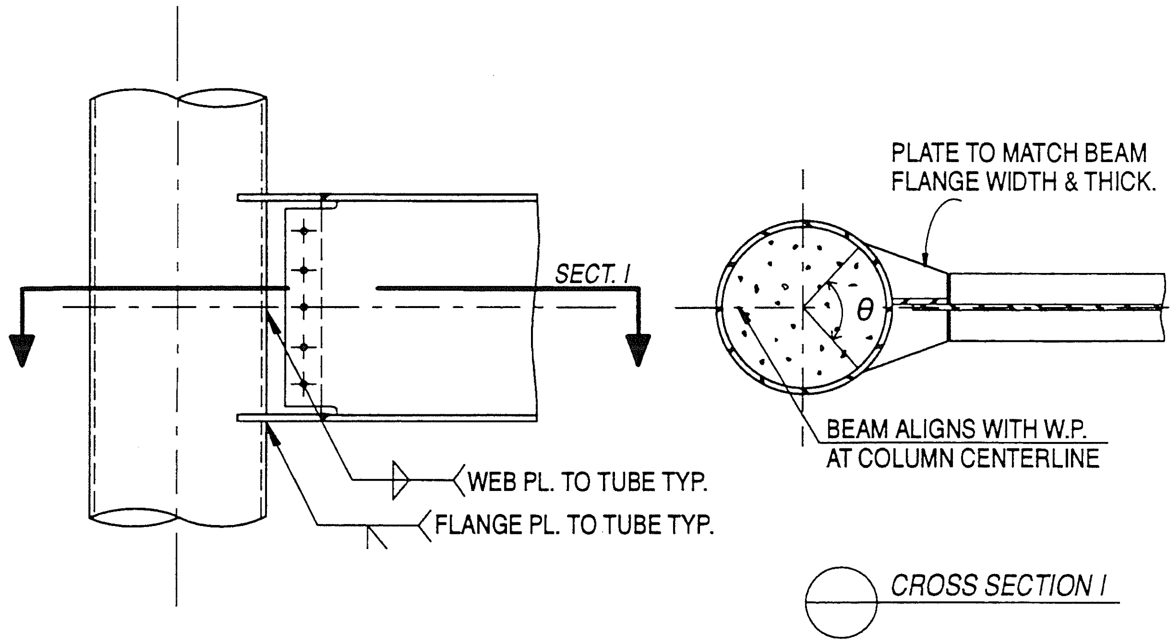

Figure 3.3. Simple Connection, *Type I*

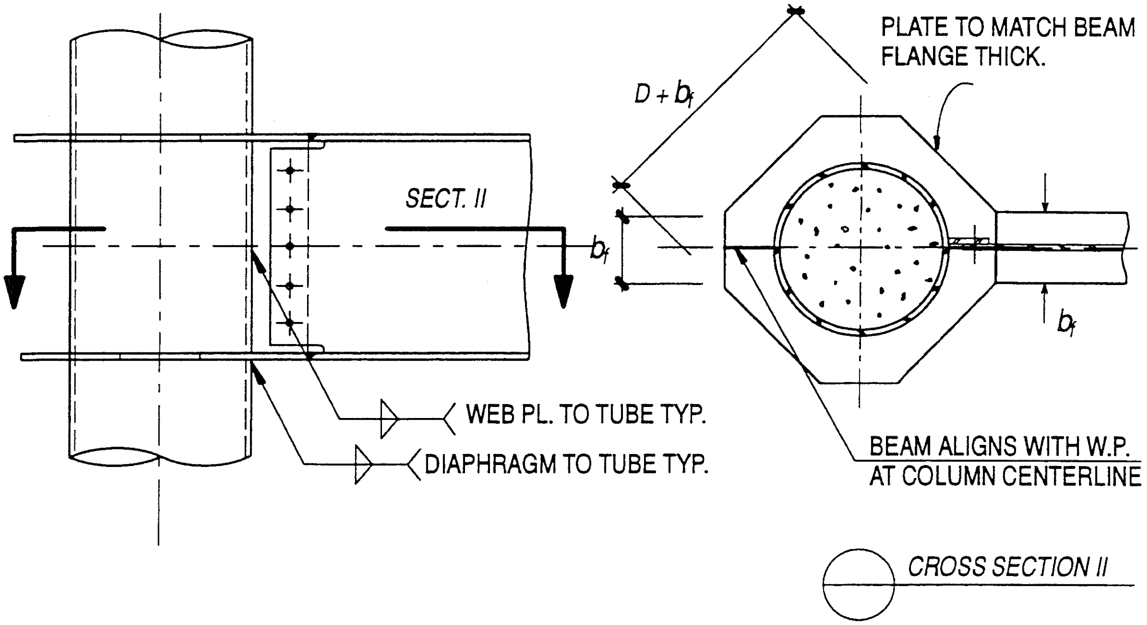

Figure 3.4. Diaphragm Plates, *Type II*

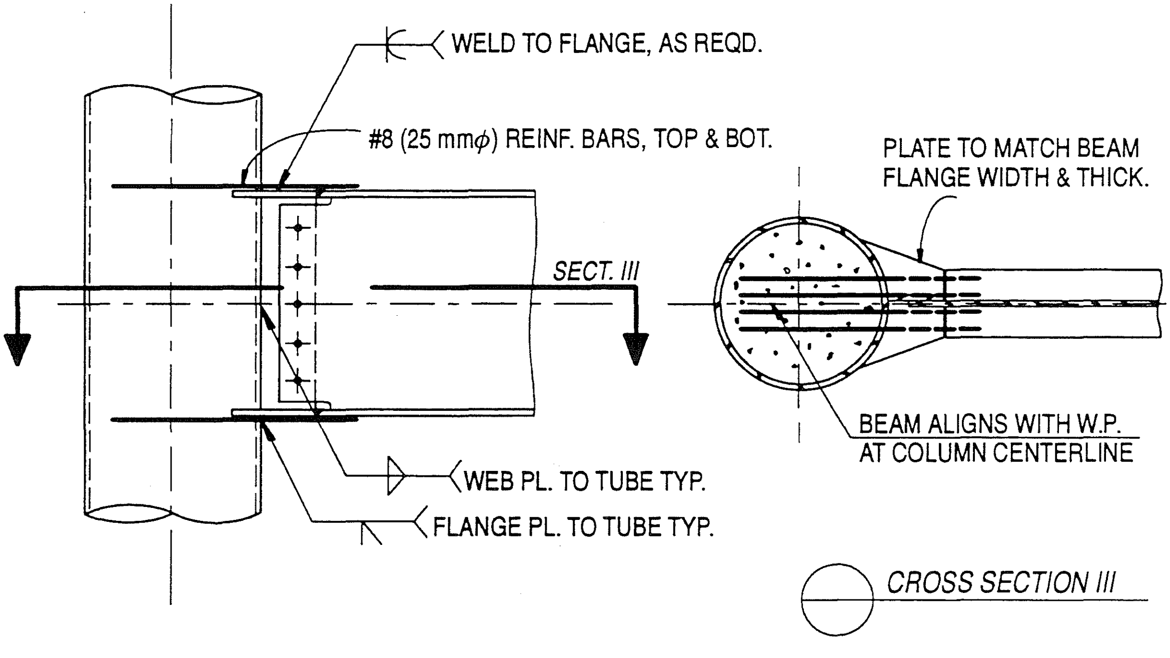

Figure 3.5. Joint with Deformed Bars Embedded in Concrete Core, *Type III*

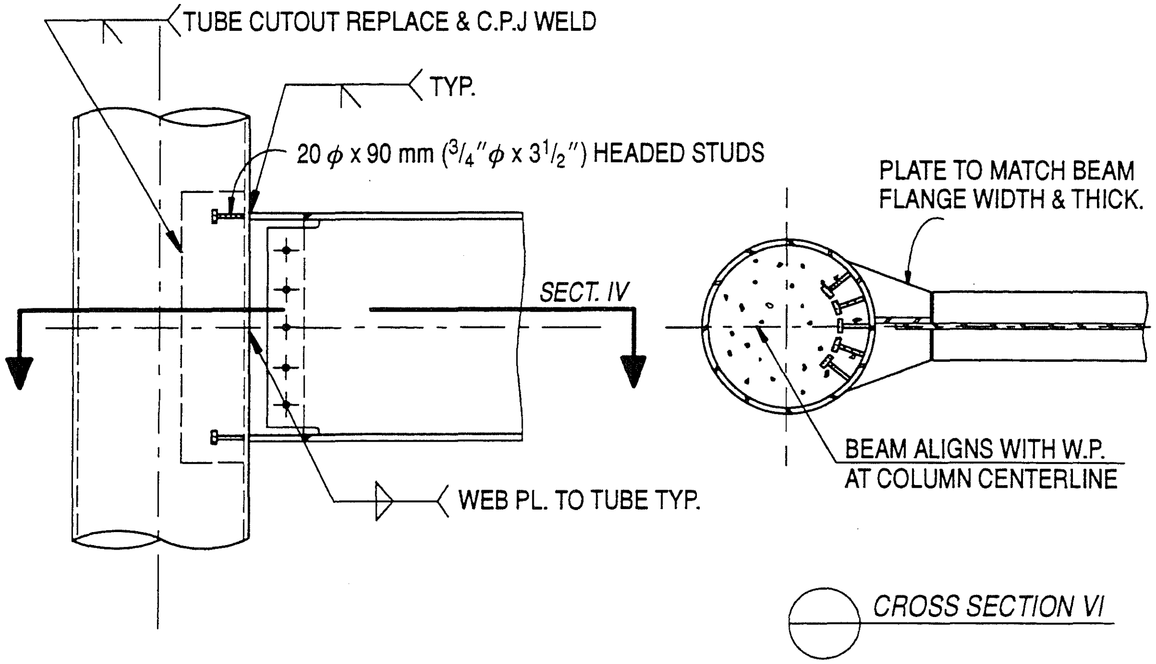

Figure 3.6. Joint with Headed Studs, *Type IV*

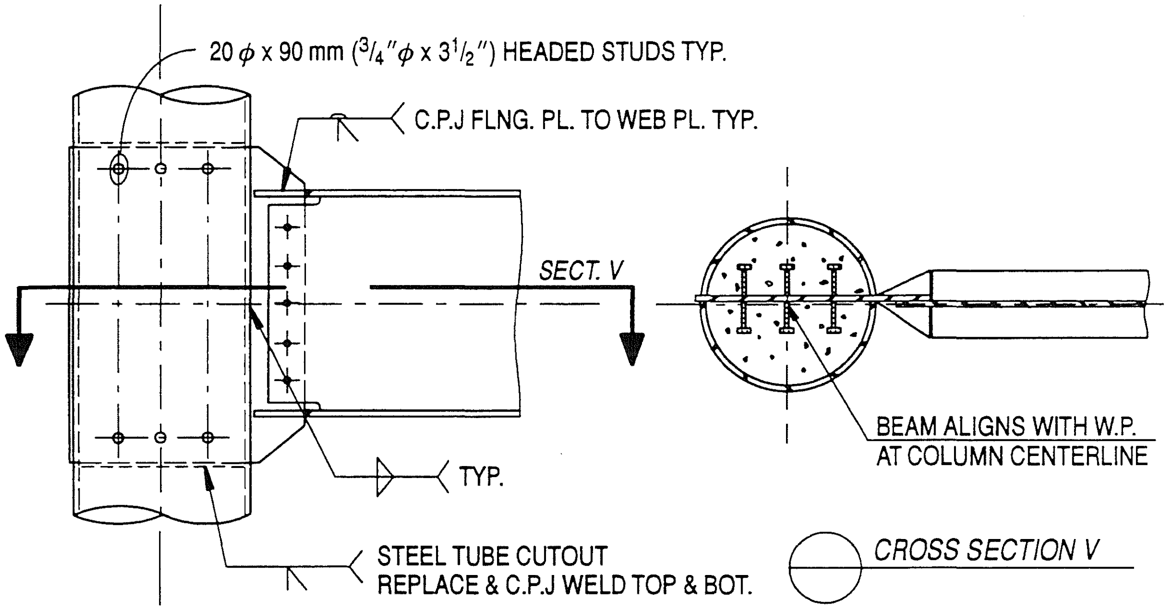

Figure 3.7. Joint with Plate and Shear Studs, *Type V*

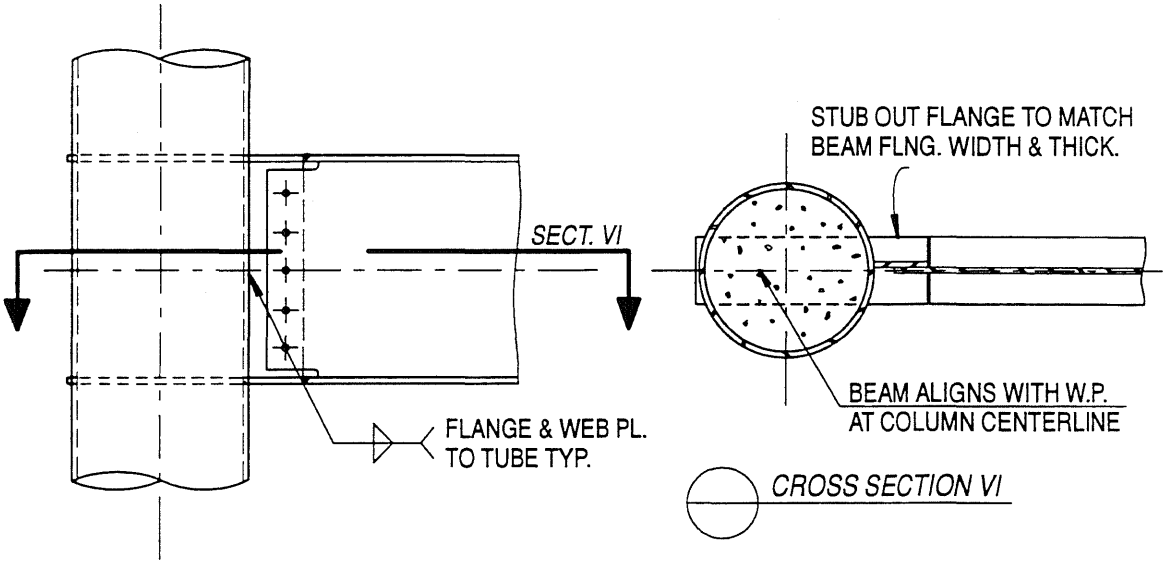

Figure 3.8. Connection with Continuity Plates, *Type VI*

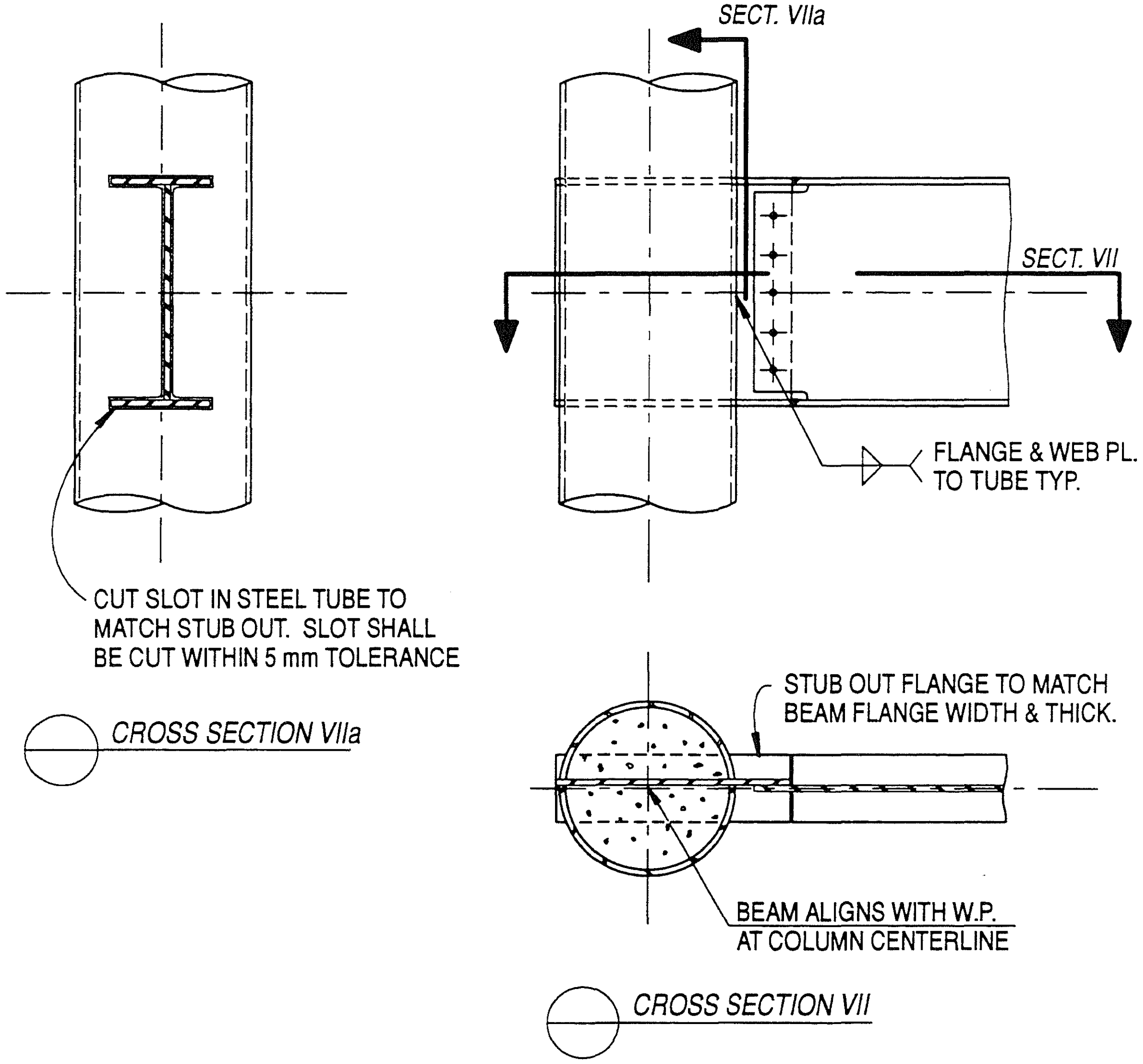

Figure 3.9. Continuation of Cross Section through Tube Column, *Type VII*

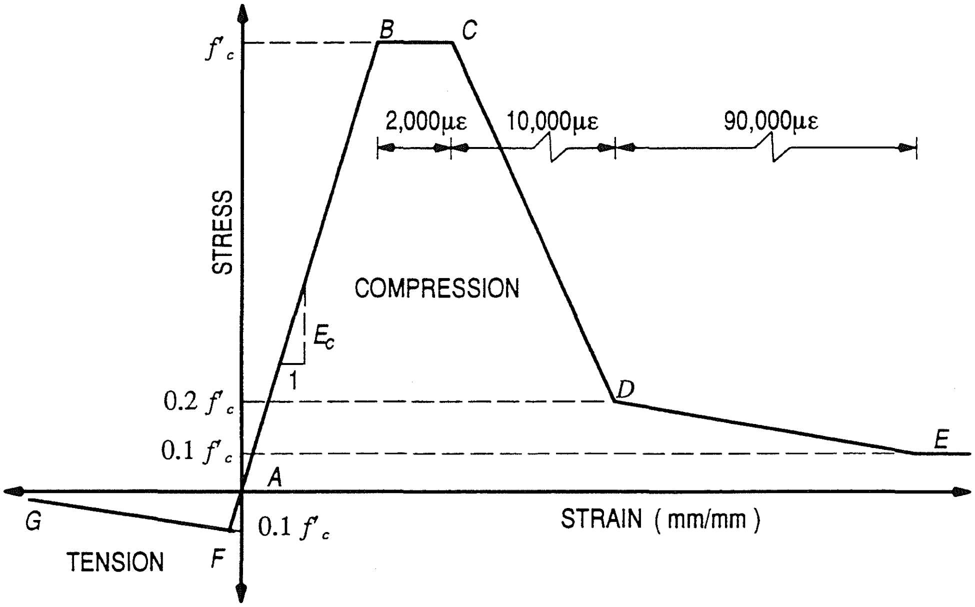

a.) The Stress–Strain Relationship for Concrete.

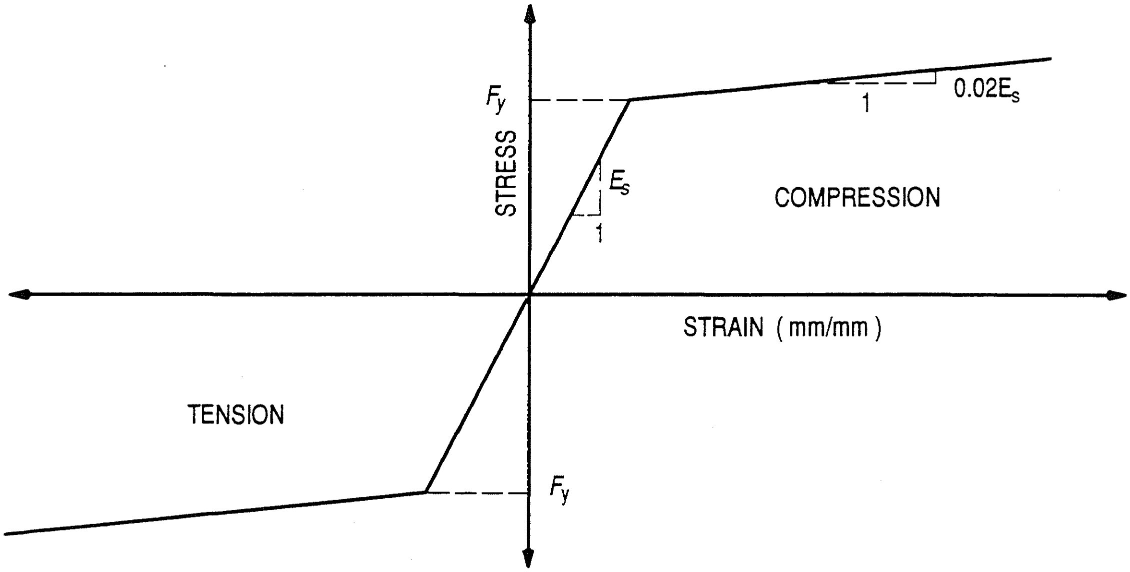

b.) The Stress–Strain Relationship for Steel.

Figure 3.10. The Material Constitutive Relations used in the Present Research

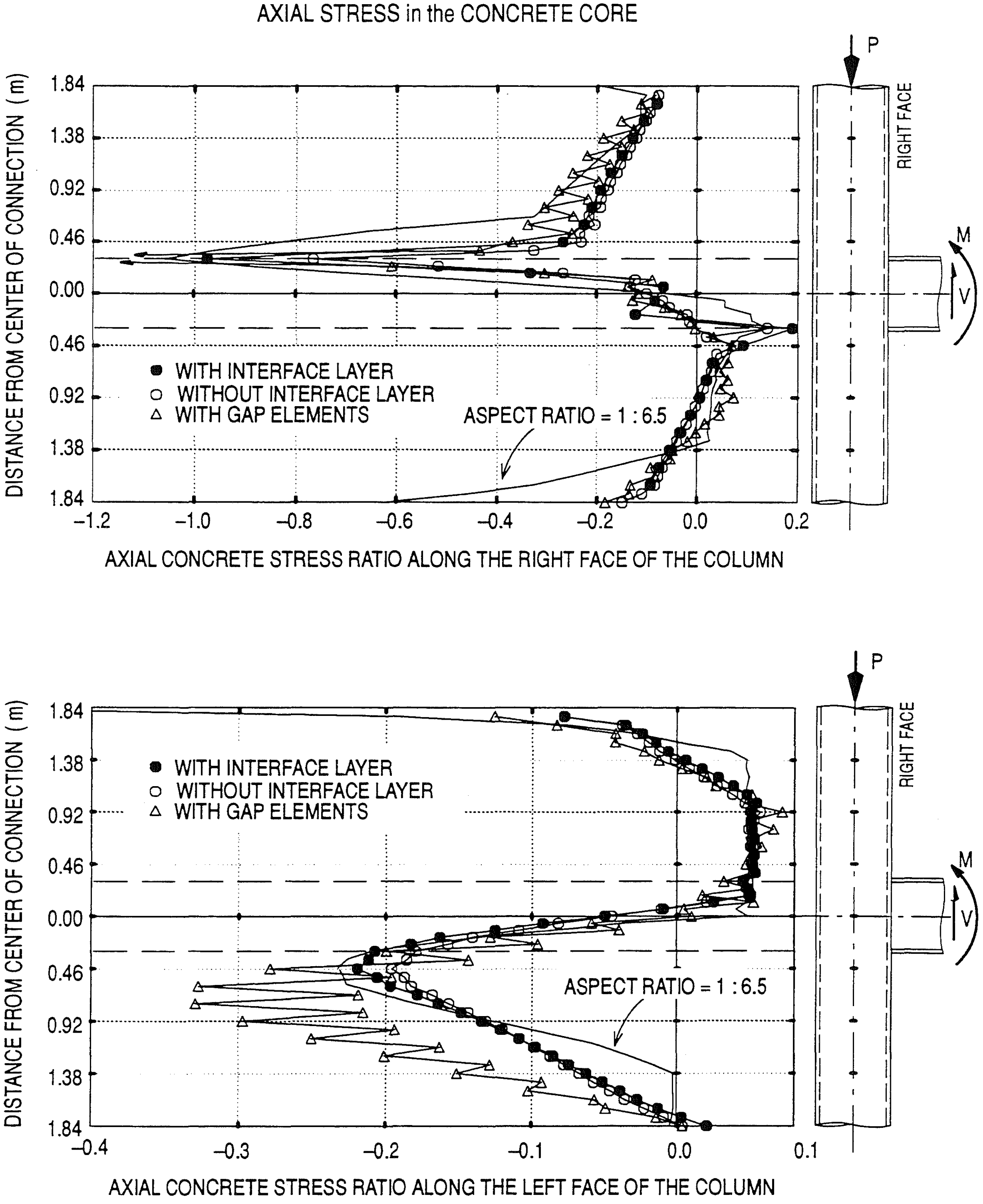

Figure 3.11 a. Numerical Results for Different Interface Models: Concrete Stresses

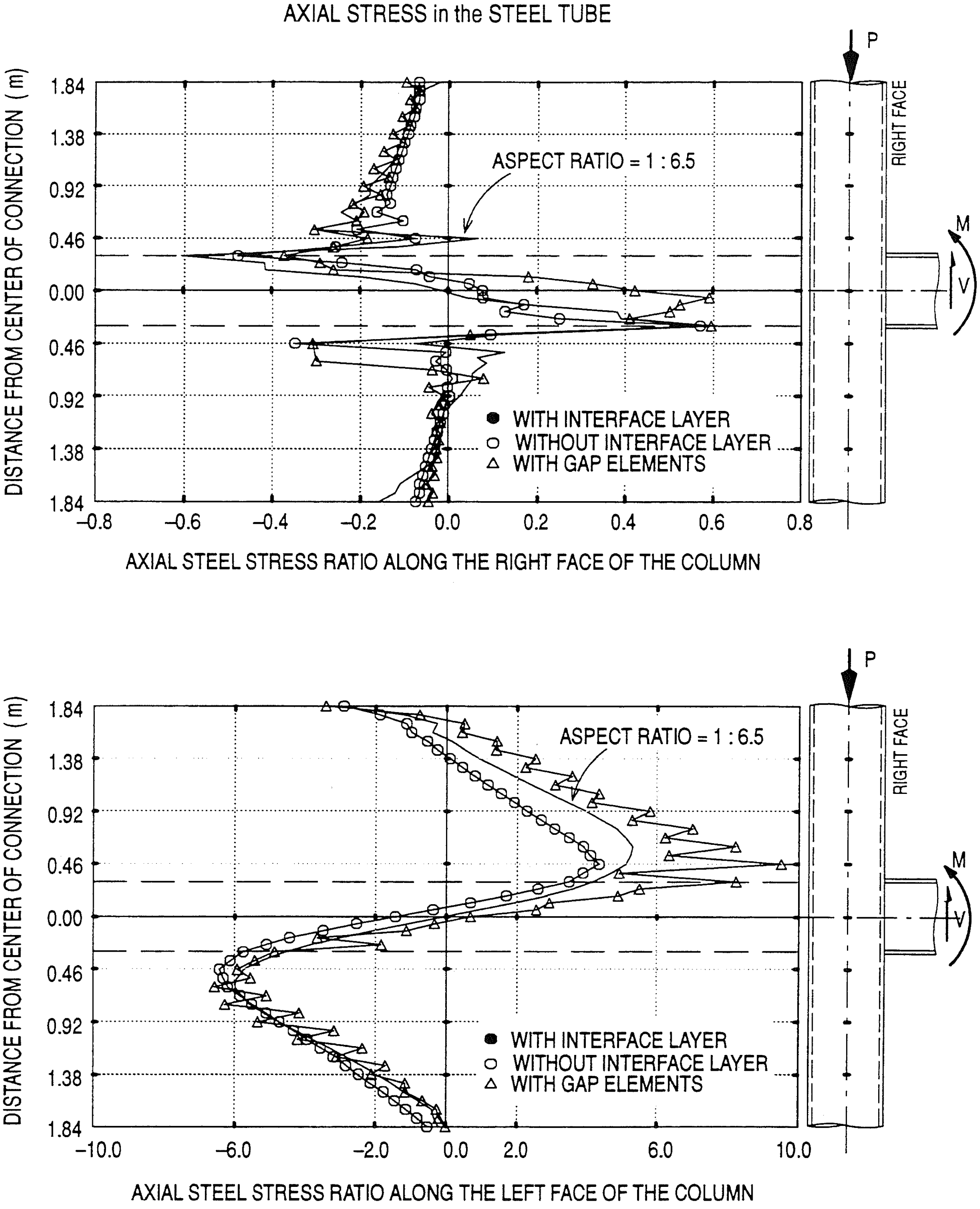

Figure 3.11 b. Numerical Results for Different Interface Models: Steel Stresses

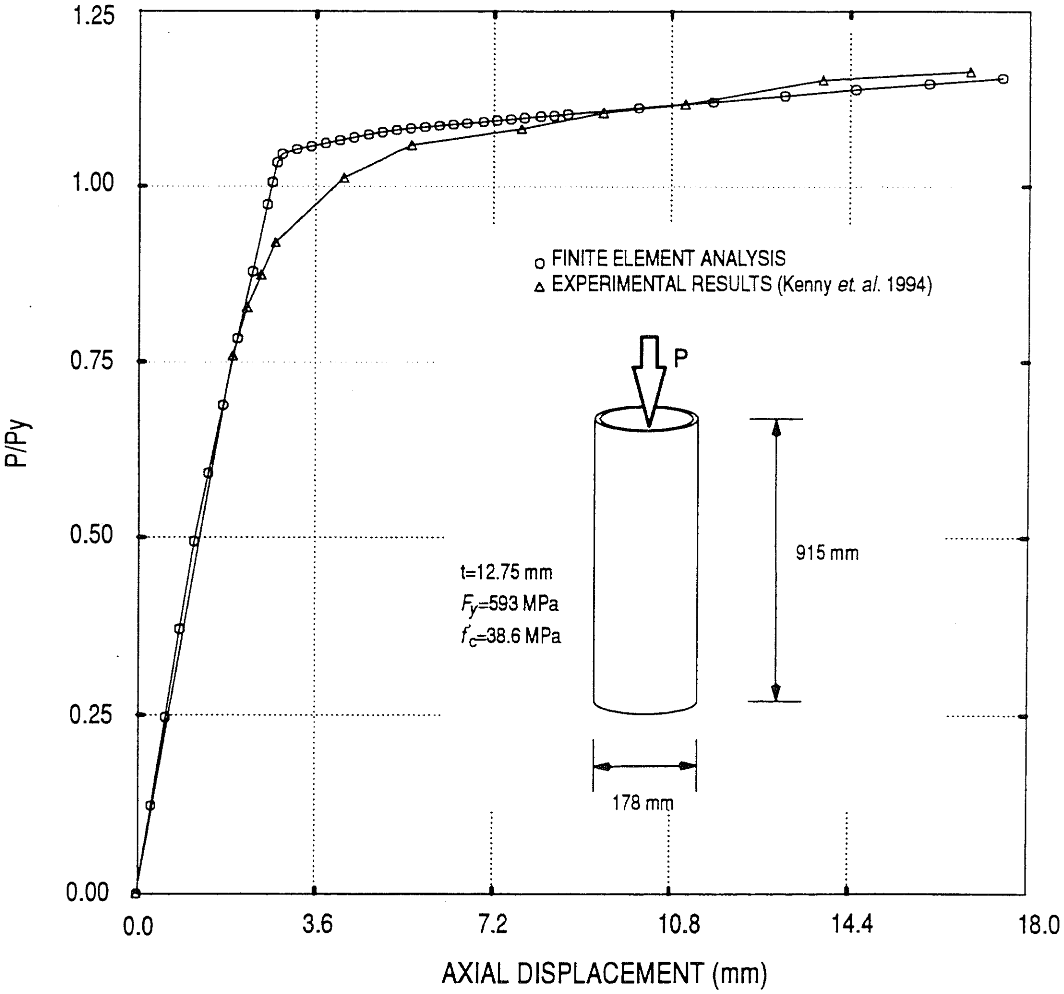

Figure 3.12. Analytical and Experimental Response of a Concrete–Filled Steel Tube

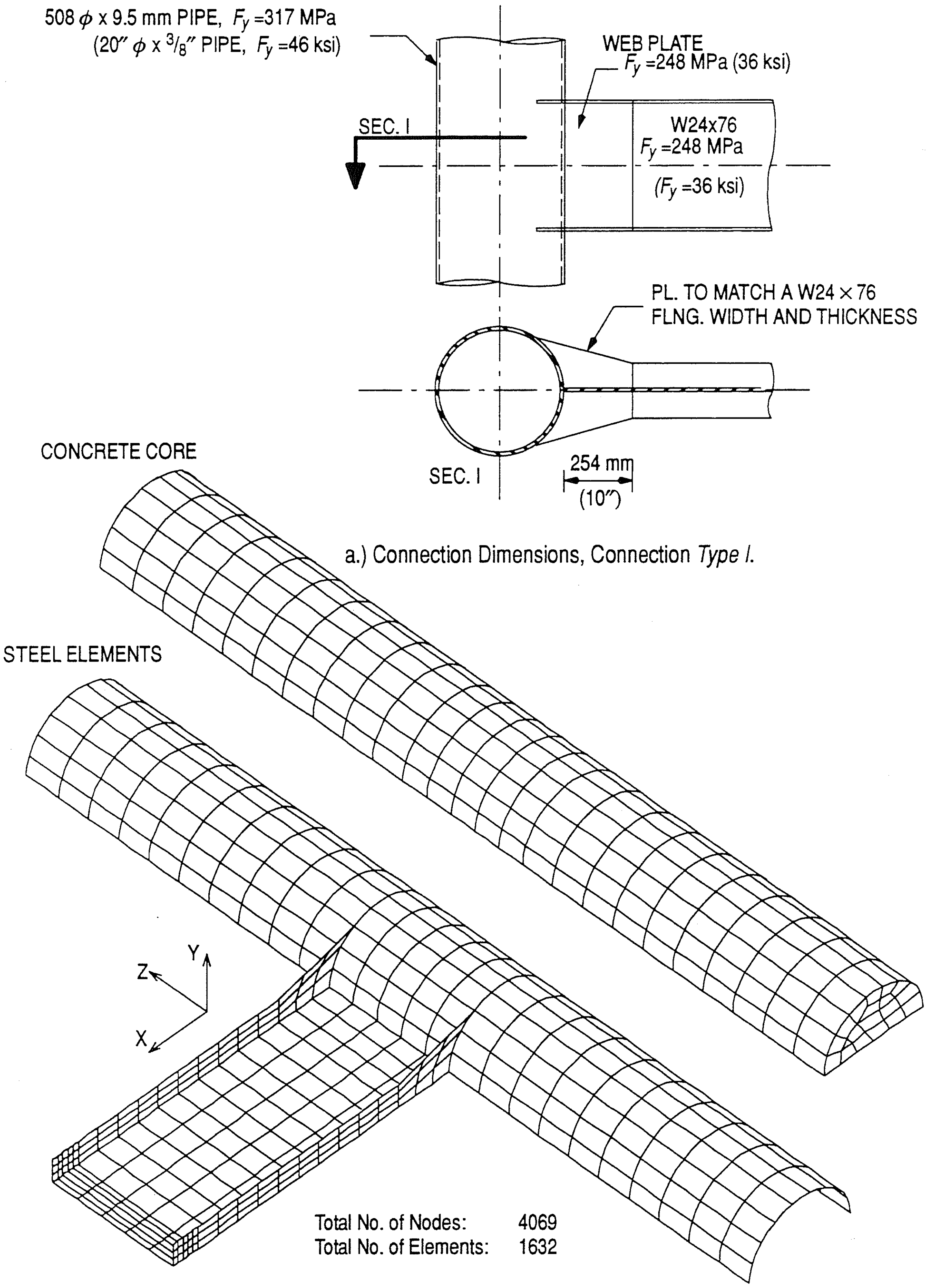

a.) Connection Dimensions, Connection *Type I*.

Figure 3.13. 3–D Finite Element Model for Connection *Type I*

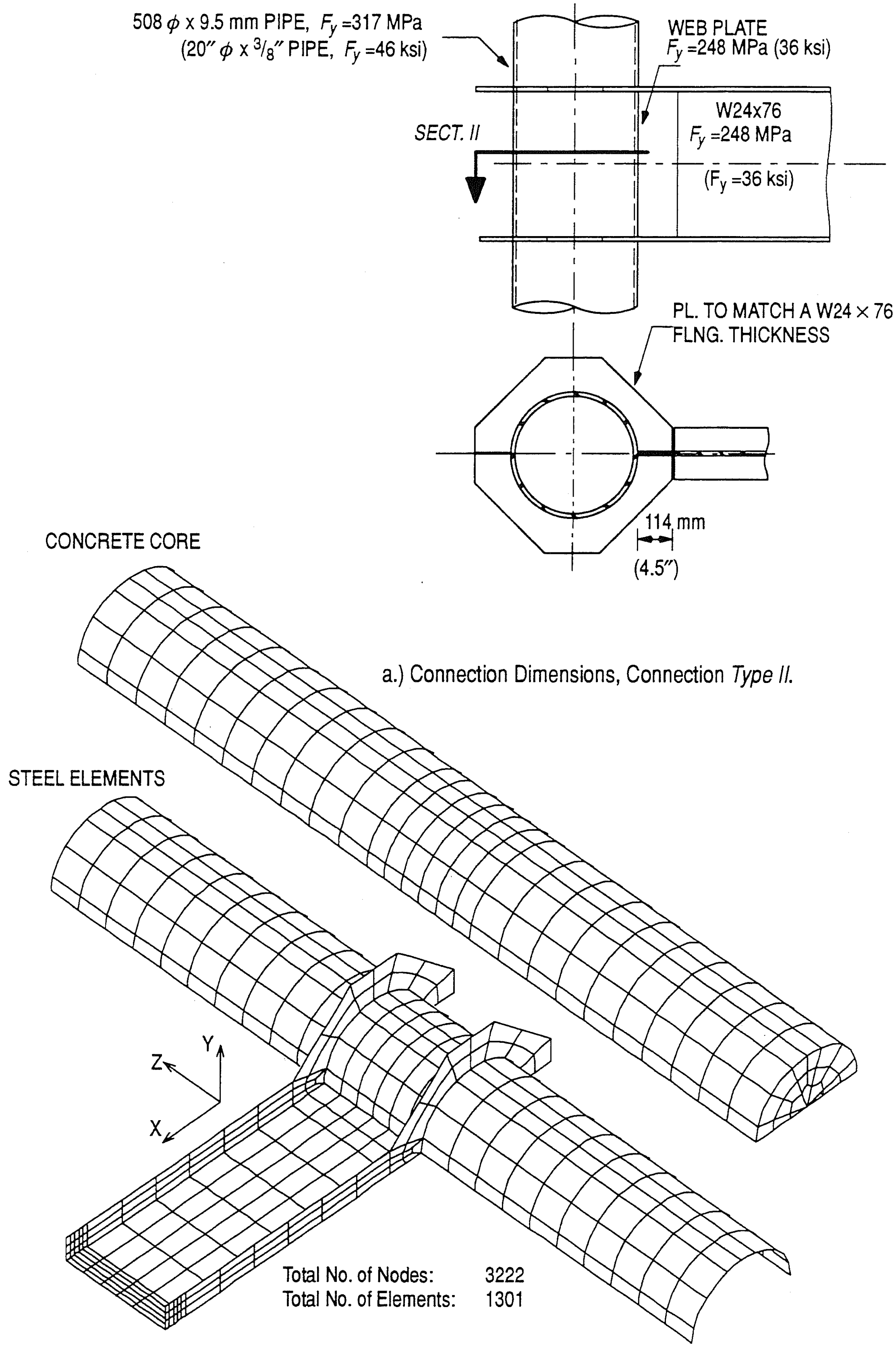

a.) Connection Dimensions, Connection *Type II.*

Figure 3.14. 3–D Finite Element Model for Connection *Type II*

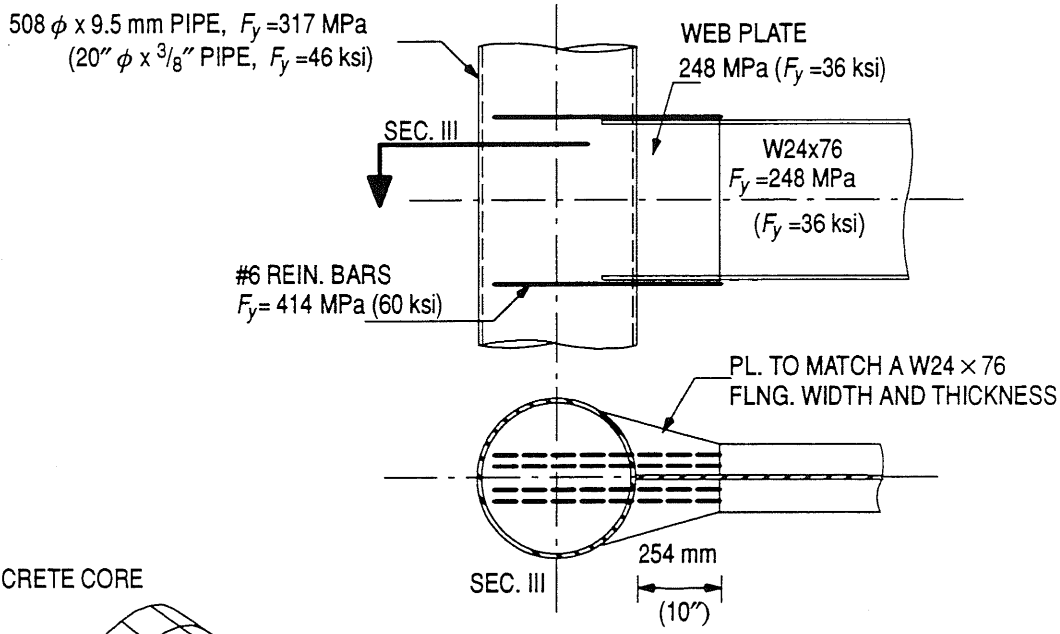

a.) Connection Dimensions, Connection *Type III.*

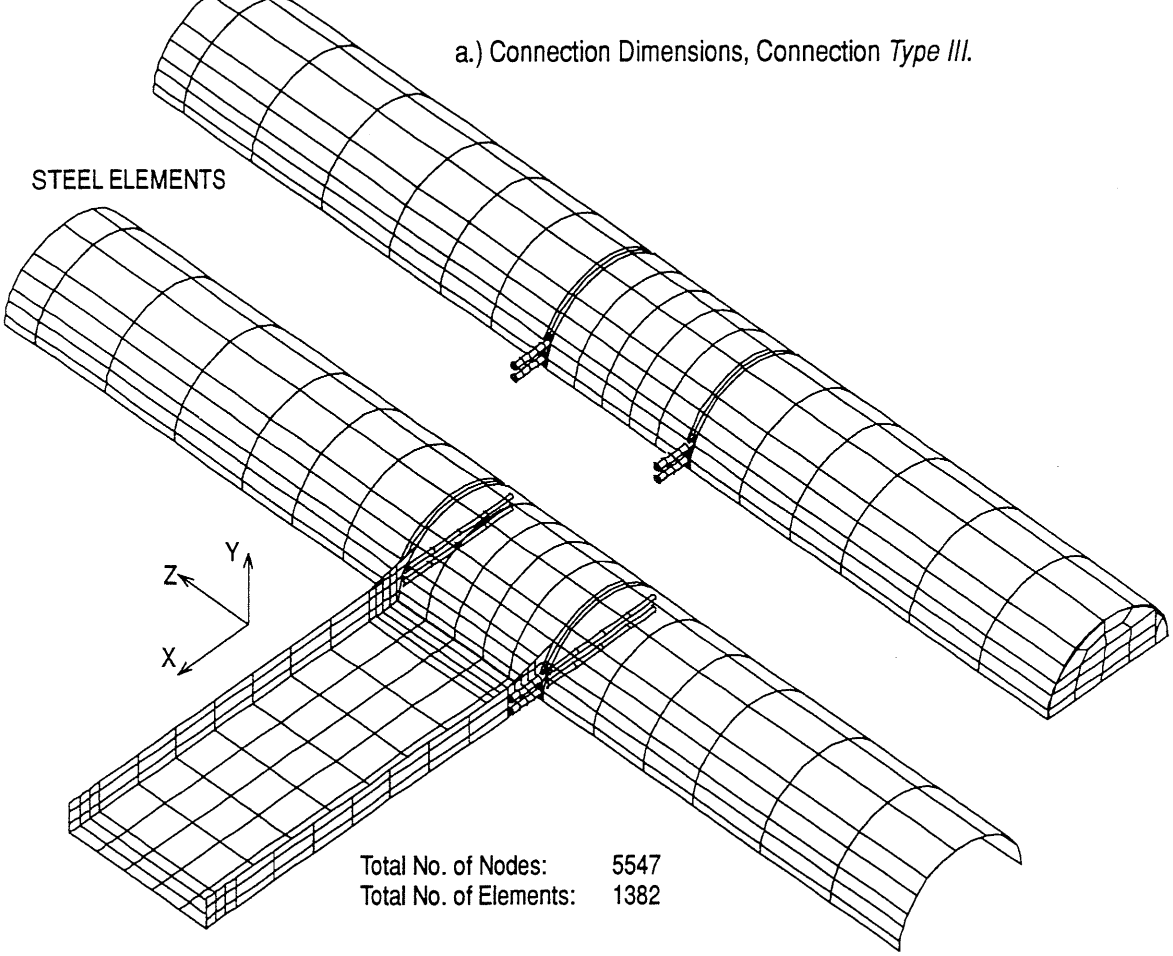

Figure 3.15. 3–D Finite Element Model for Connection *Type III*

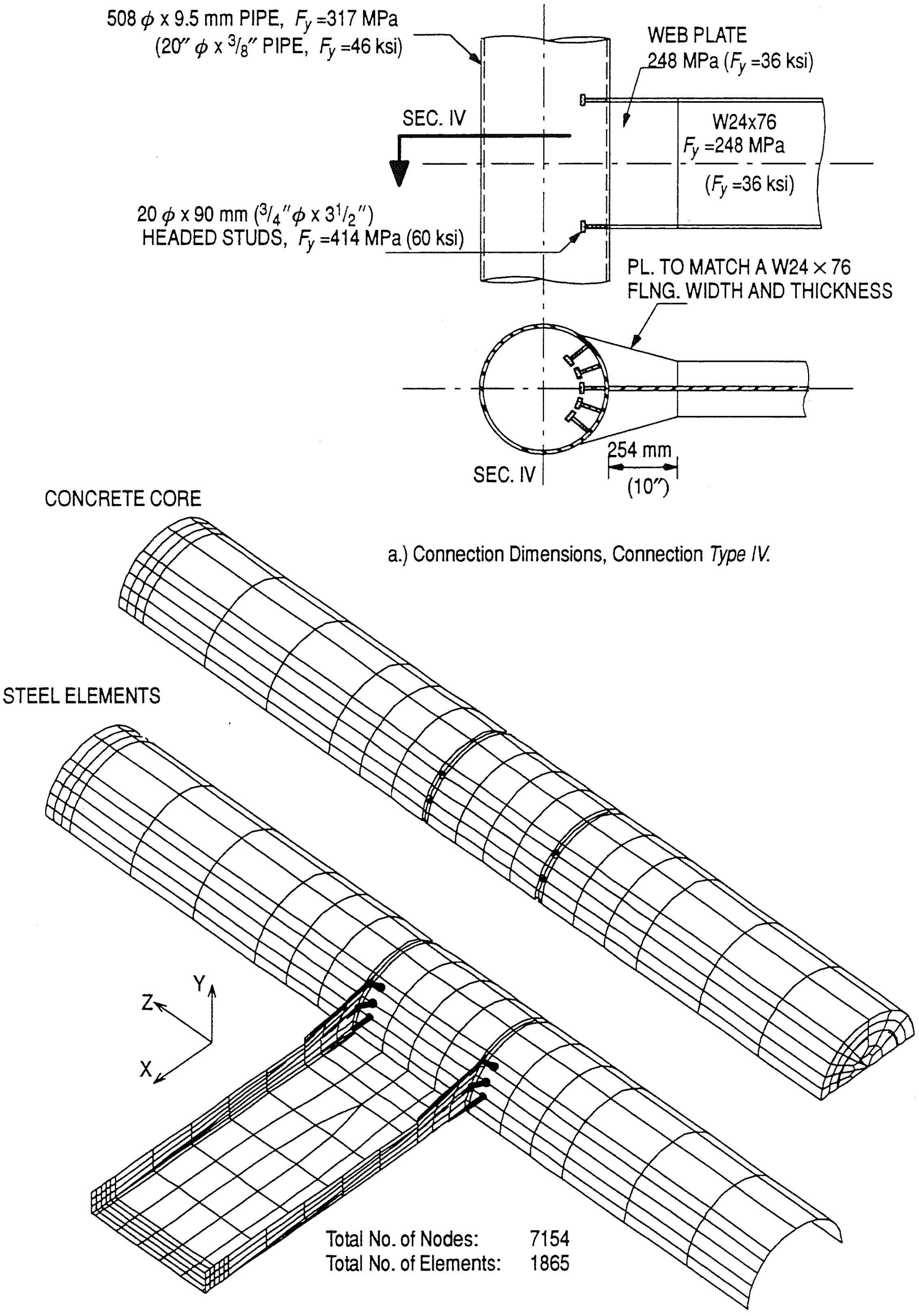

a.) Connection Dimensions, Connection *Type IV.*

Figure 3.16. 3–D Finite Element Model for Connection *Type IV*

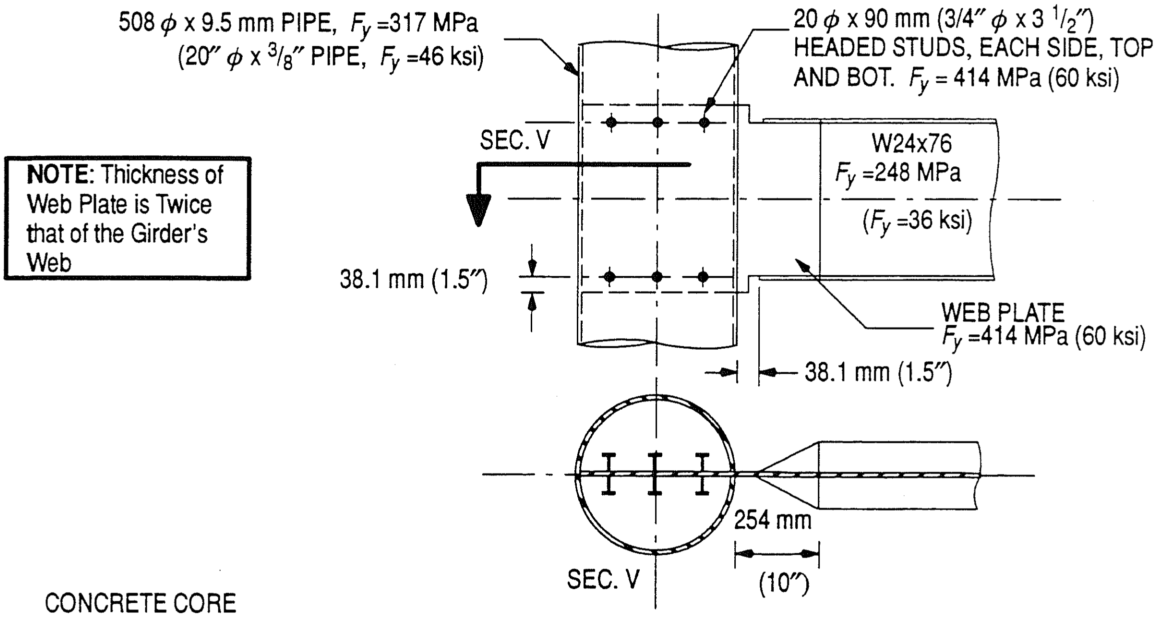

a) Connection Dimensions, Connection *Type V.*

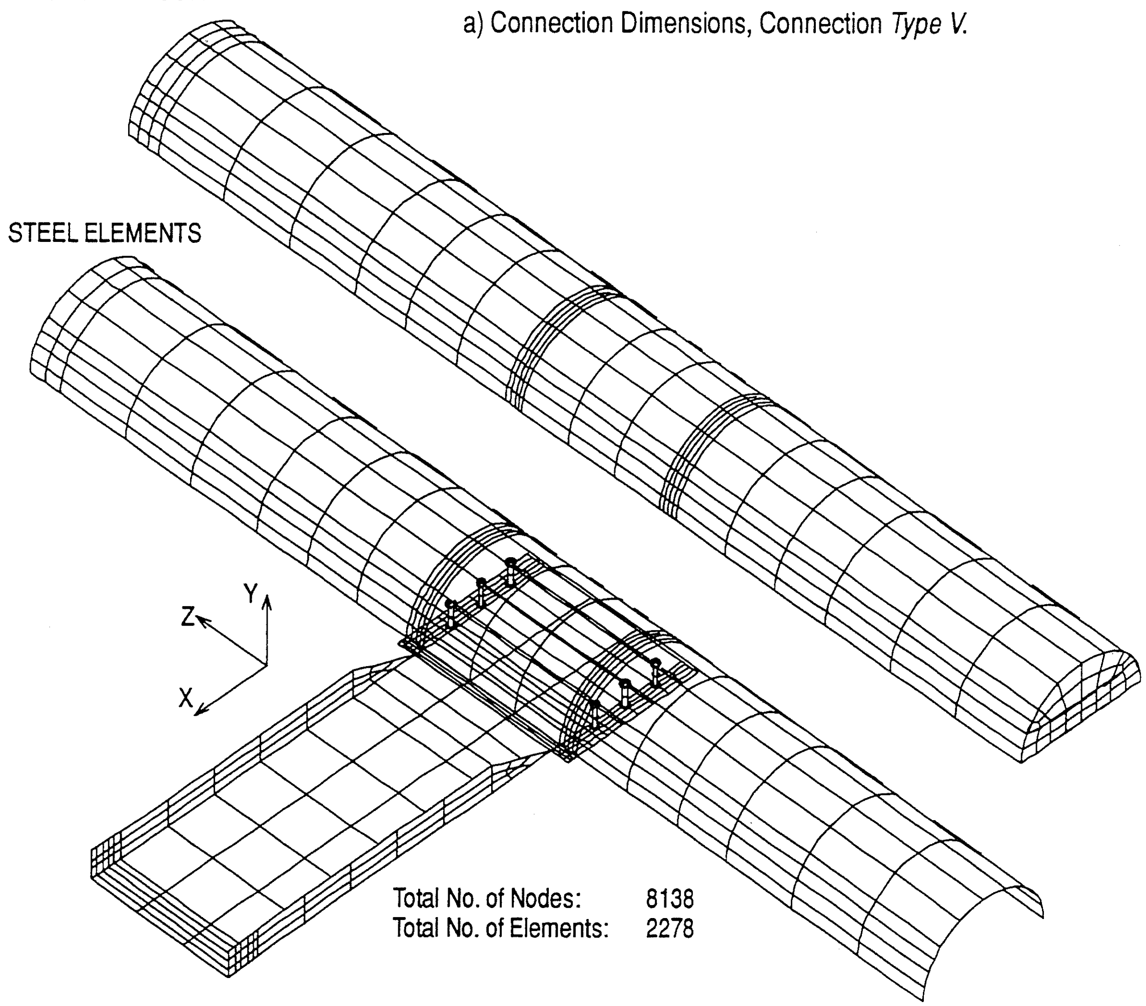

Figure 3.17. 3–D Finite Element Model for Connection *Type V*

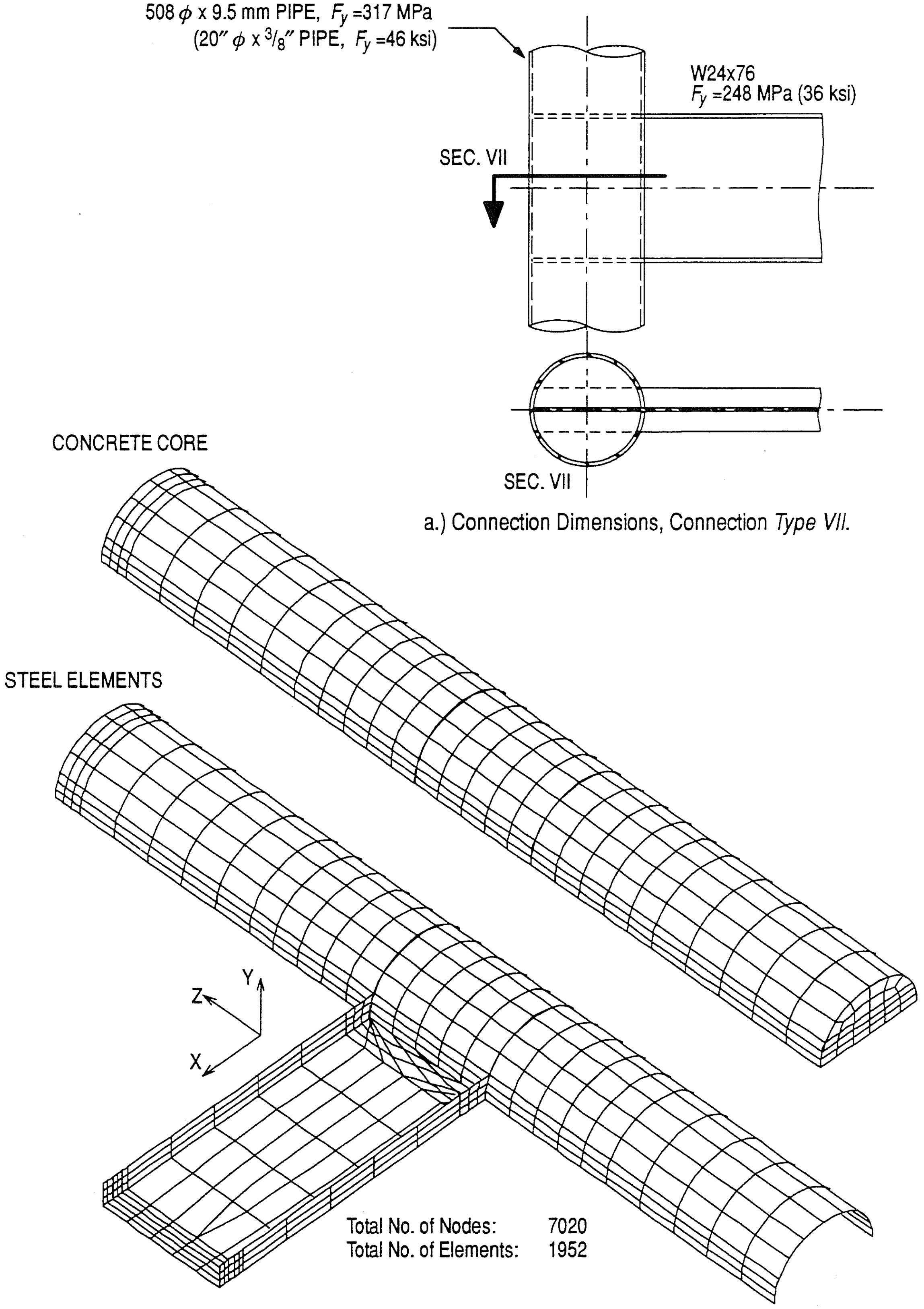

a.) Connection Dimensions, Connection *Type VII.*

Figure 3.18. 3–D Finite Element Model for Connection *Type VII*

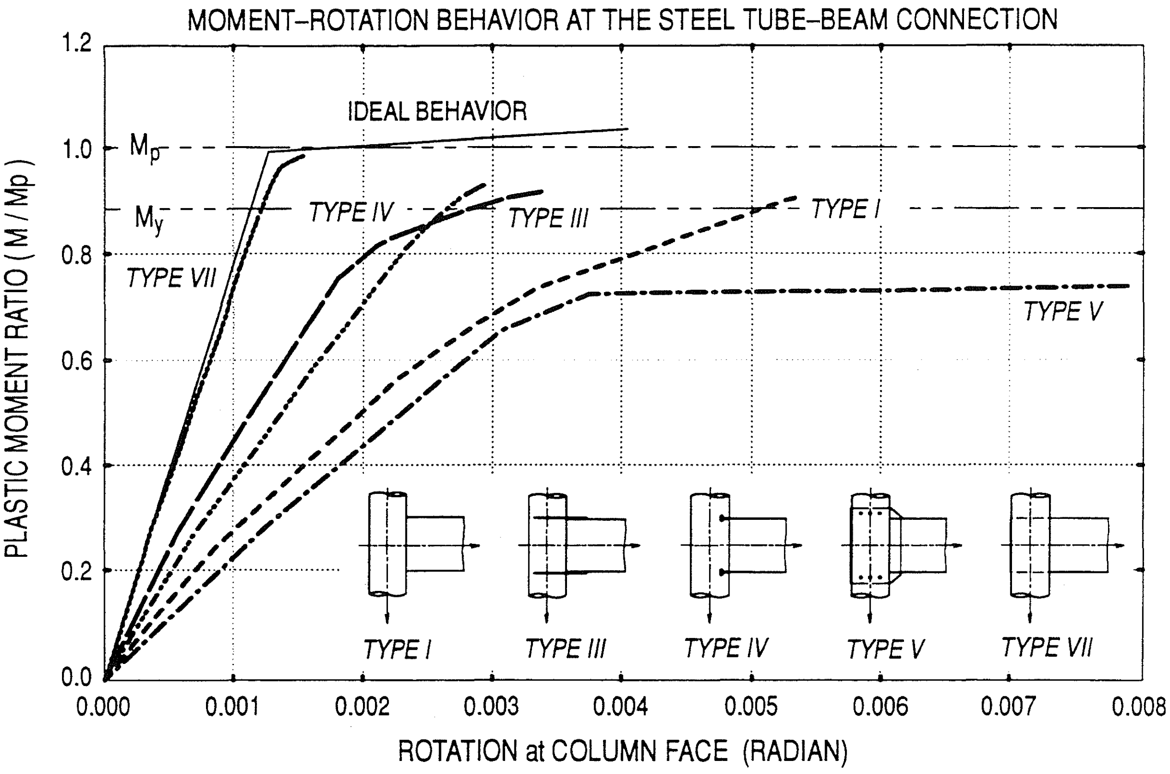

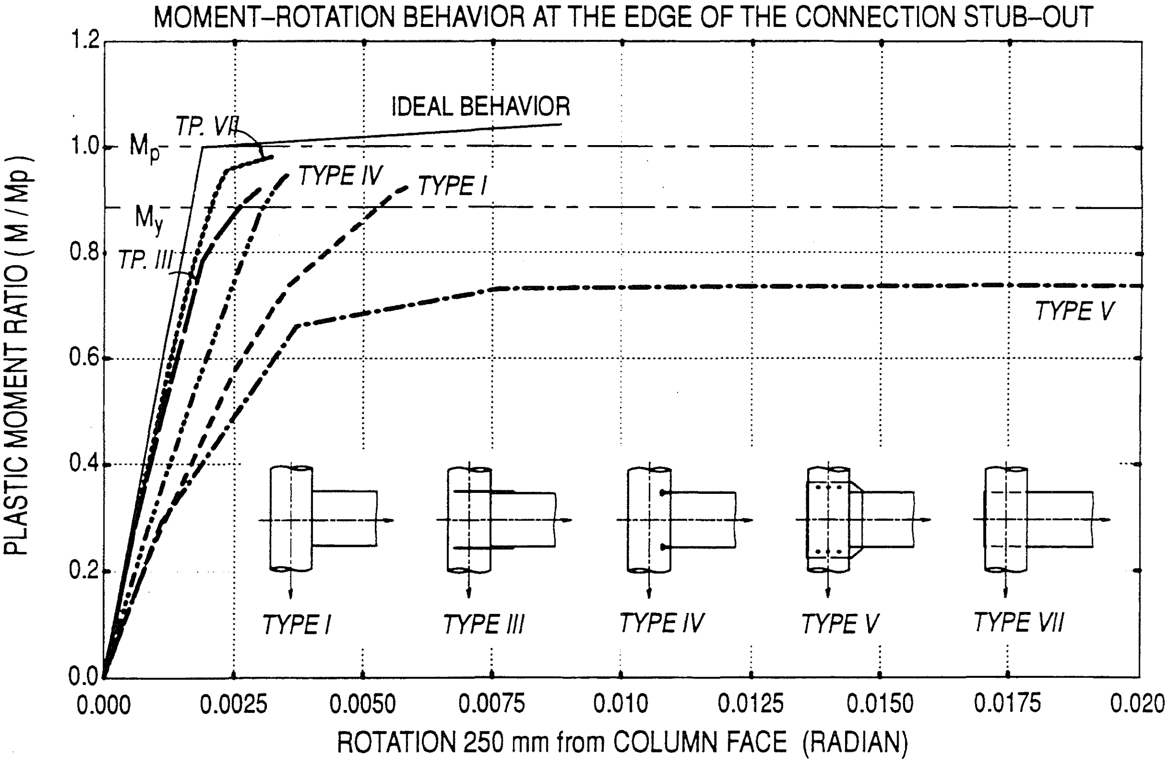

Figure 3.19. Analytical Moment–Rotation Behavior for some of the Basic Connections

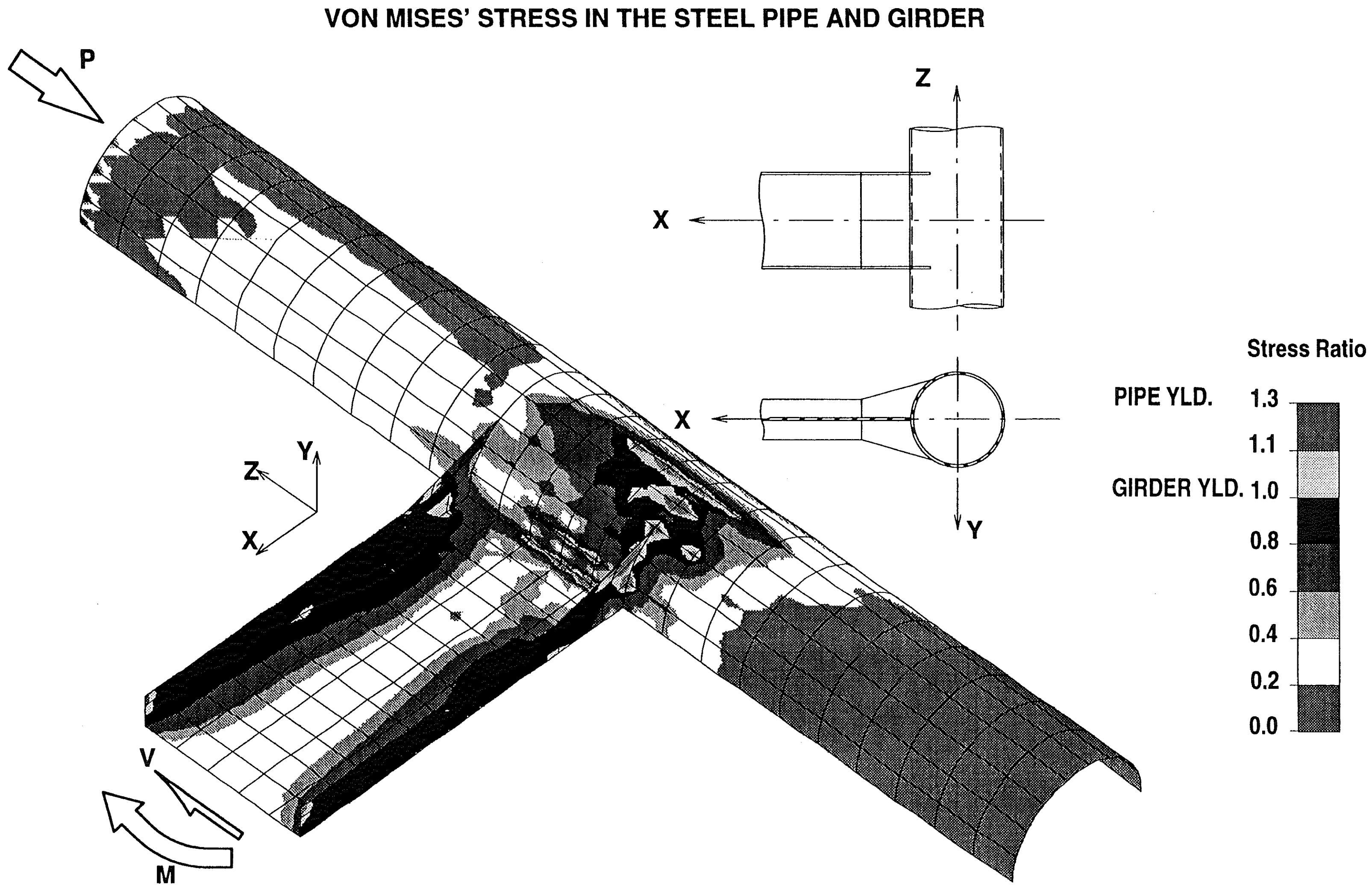

Figure 3.20. Von Mises' Stresses in the Pipe and the Girder, Connection *Type I*

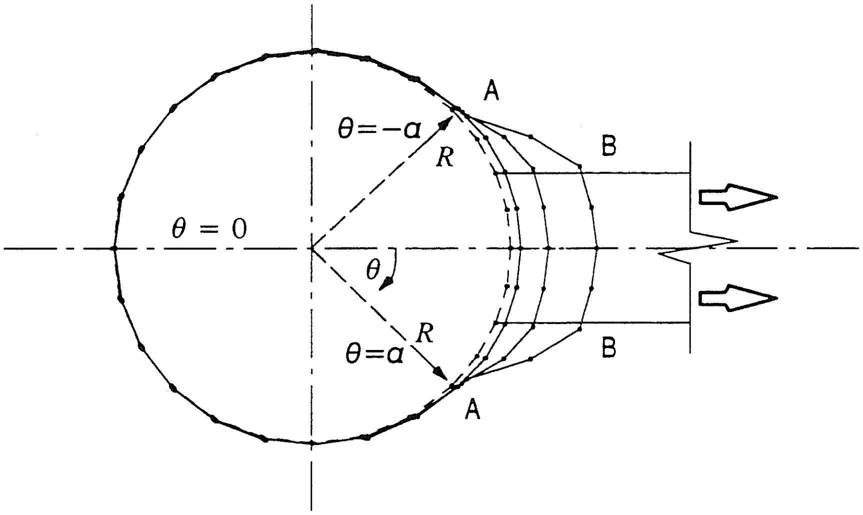

a.) Deformed Shape of the Pipe Cross Section at Level of Tension Flange.

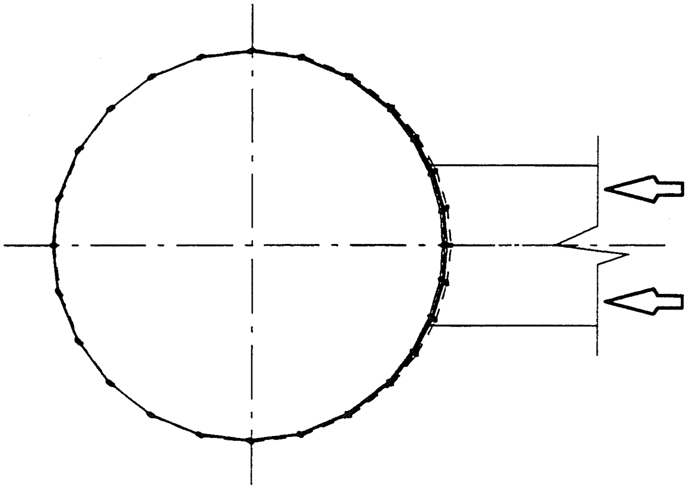

b.) Deformed Shape of the Pipe Cross Section at Level of Compression Flange.

Figure 3.21. Deflected Shape of a Column Section at Level of Girder Flange

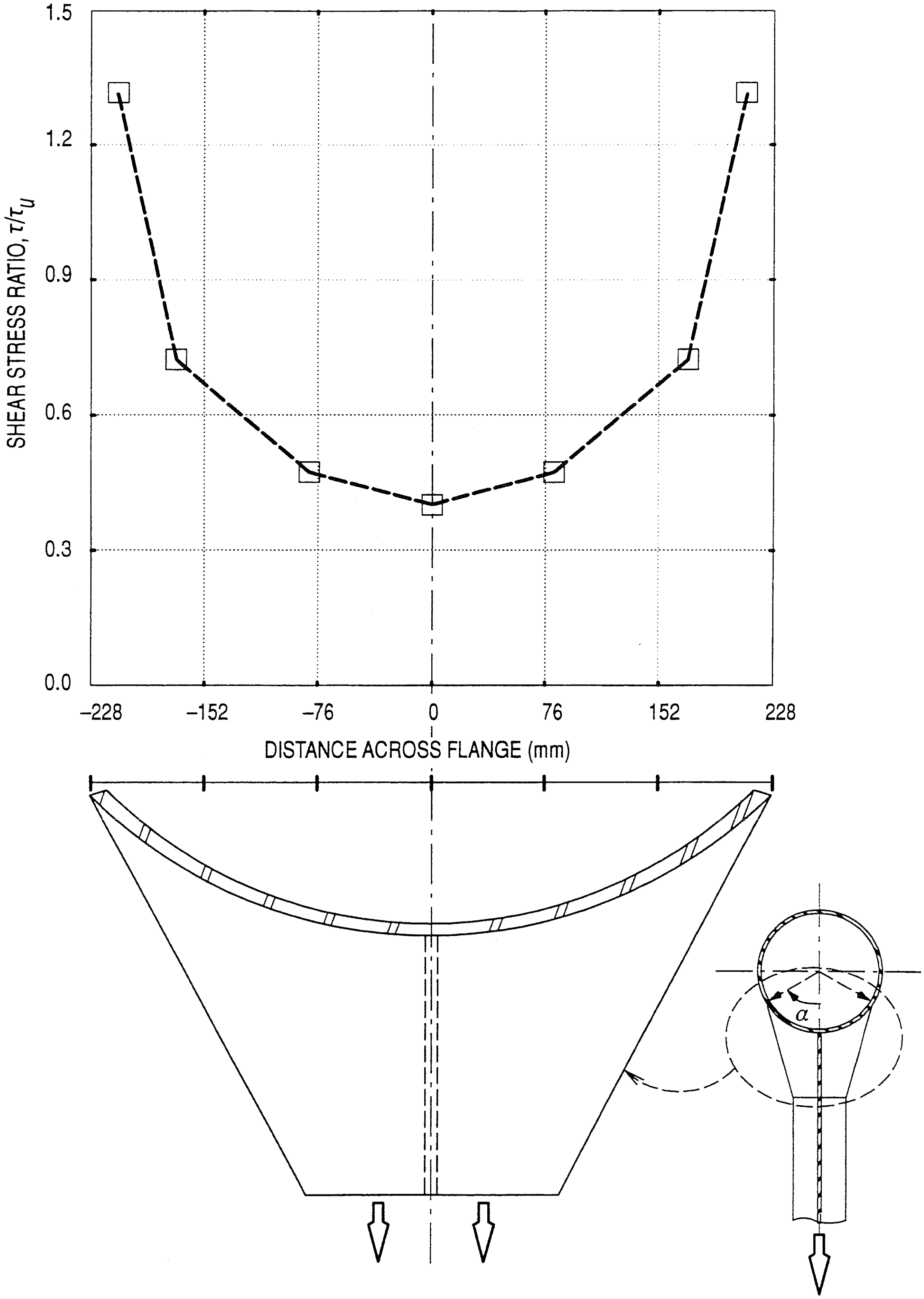

Figure 3.22. Pipe Shear Stress Distribution at the Tension Flange Level

MOMENT–ROTATION BEHAVIOR AT THE STEEL TUBE–BEAM CONNECTION

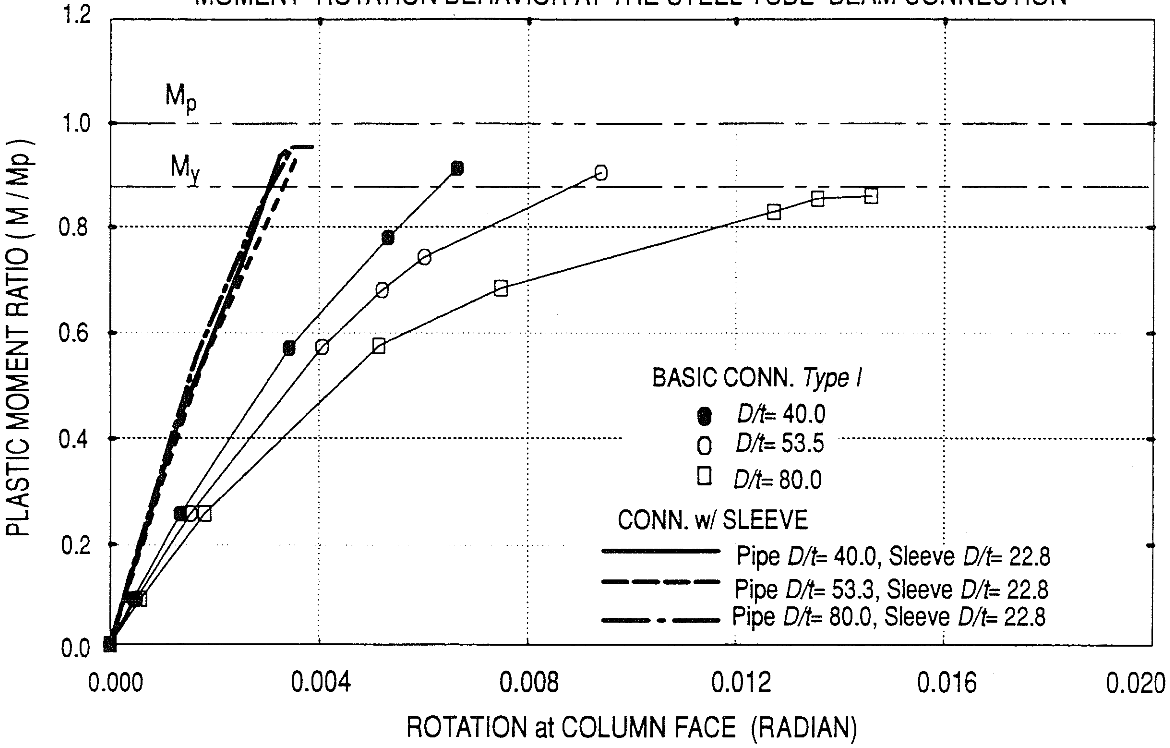

MOMENT–ROTATION BEHAVIOR AT THE EDGE OF THE CONNECTION STUB

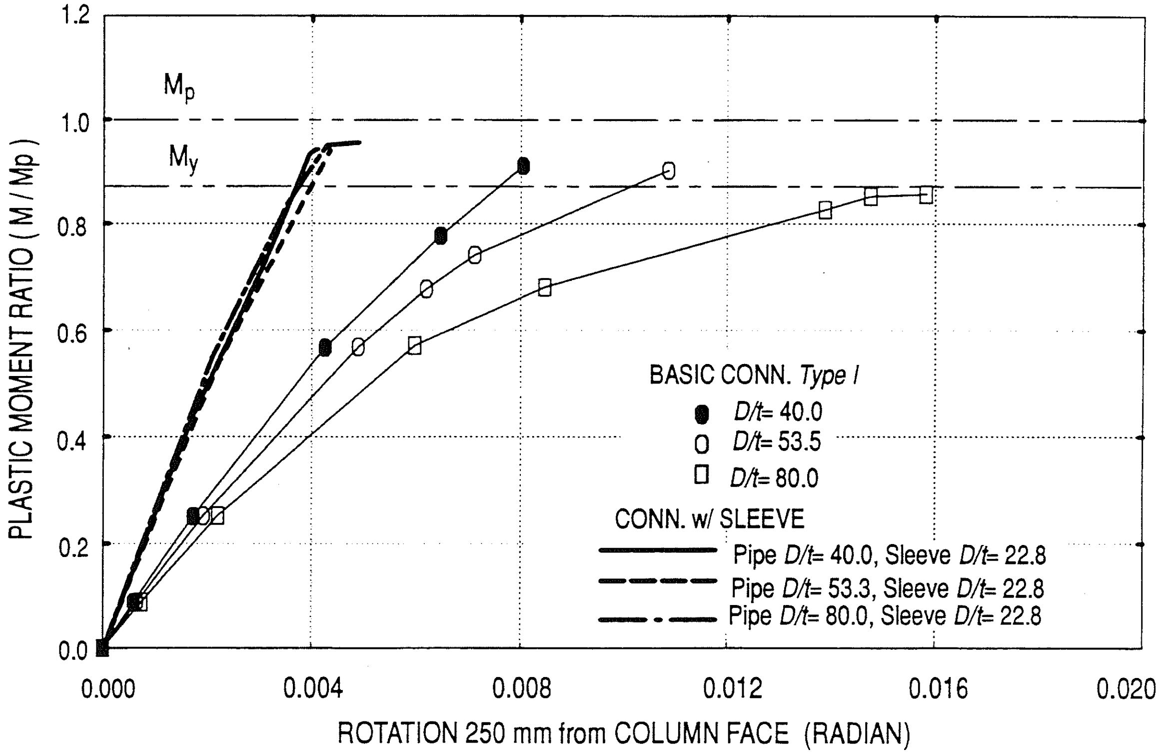

Figure 3.23. Analytical Moment–Rotation Behavior for a Simple Connection, *Type I*

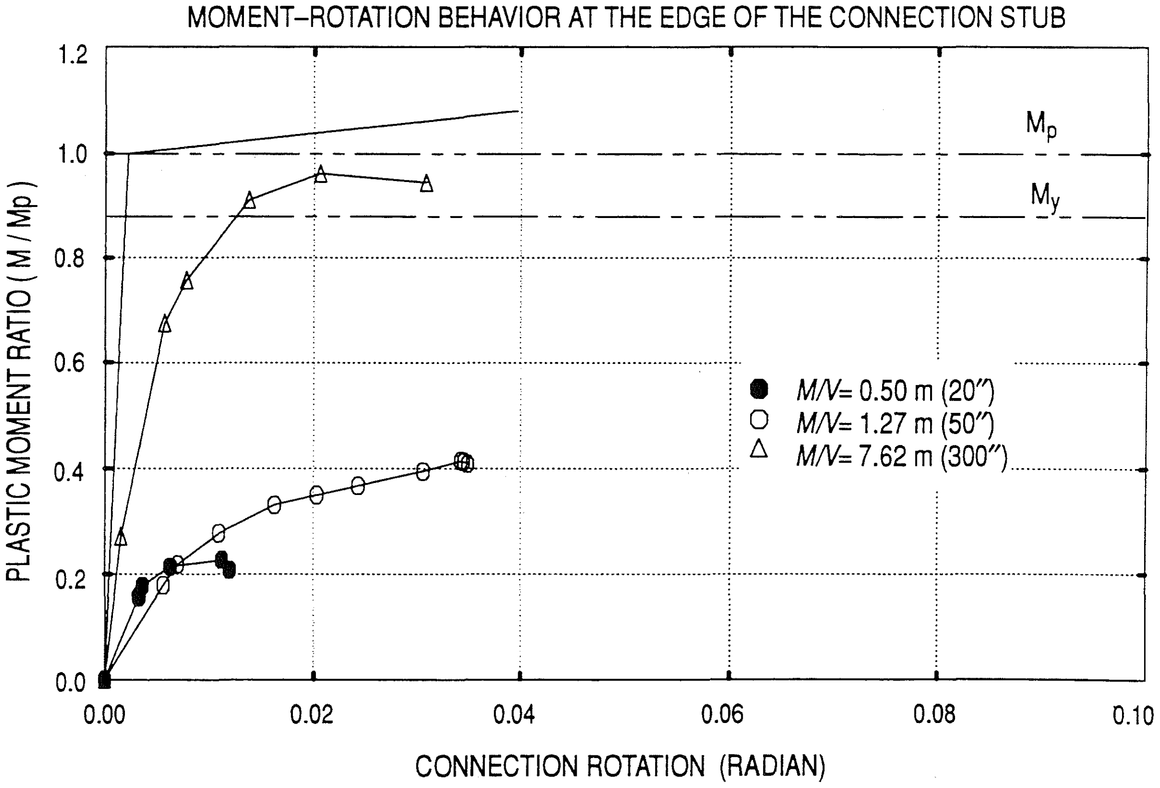

Figure 3.24. Analytical Moment–Rotation Behavior for a Simple Connection w/ Various *M/V* Ratios

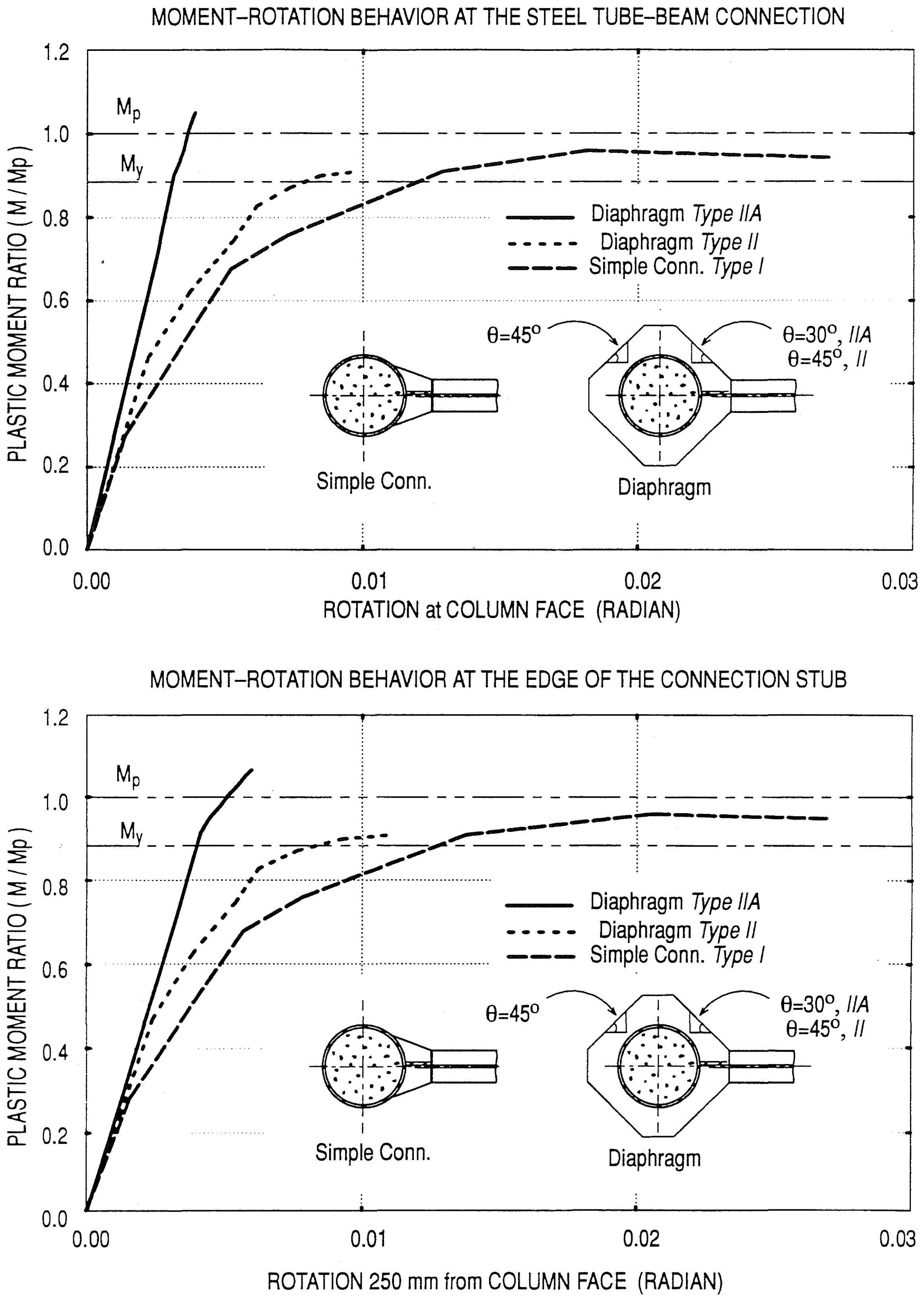

Figure 3.25. Analytical Moment–Rotation Behavior for Connections that Load the Tube Alone

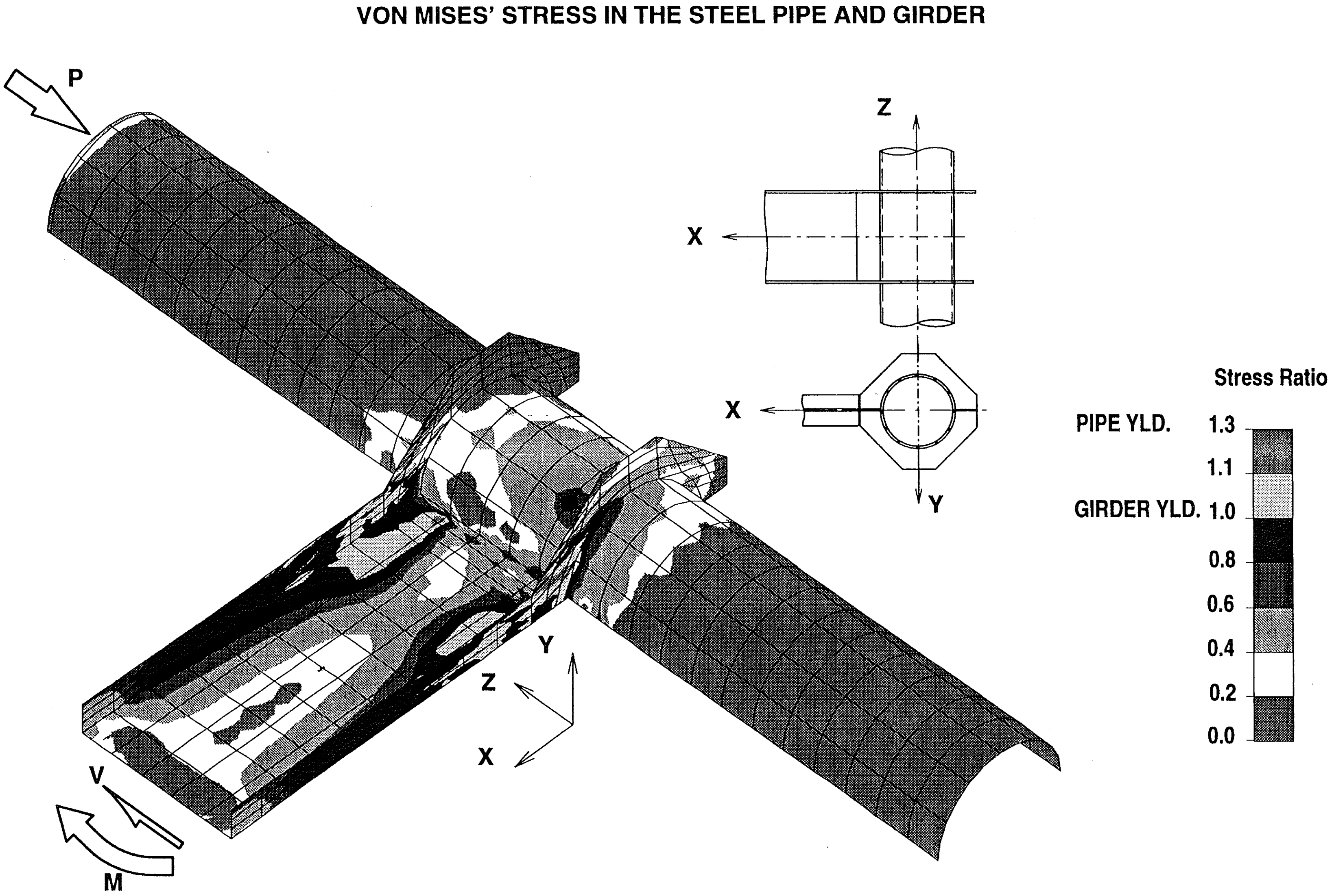

Figure 3.26. Von Mises' Stresses in the Pipe and the Girder, Connection *Type II*

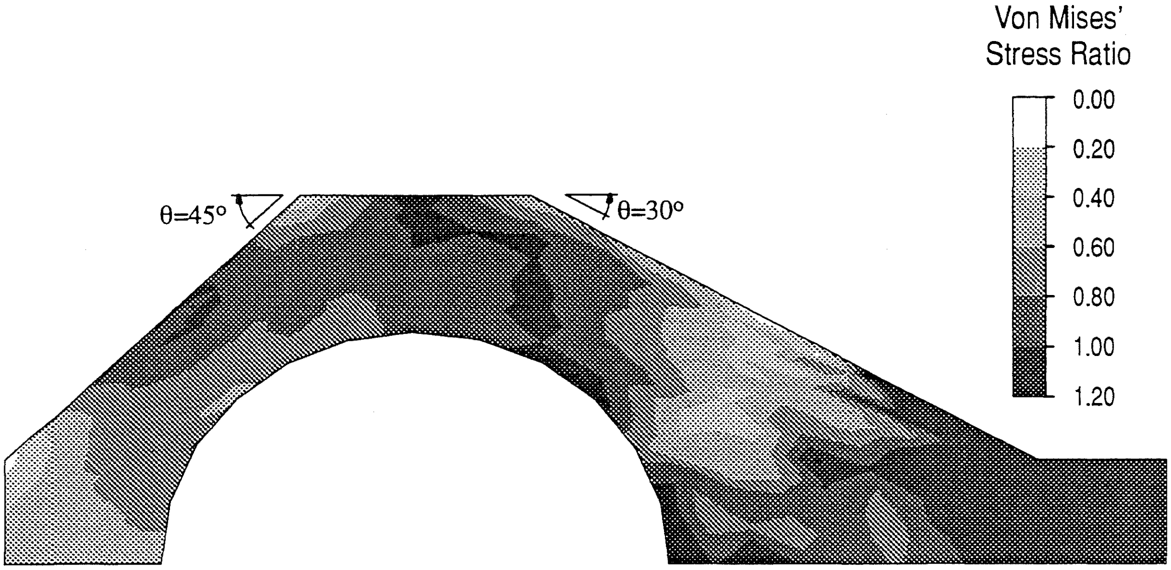

a) Von Mises' Stress Ratio.

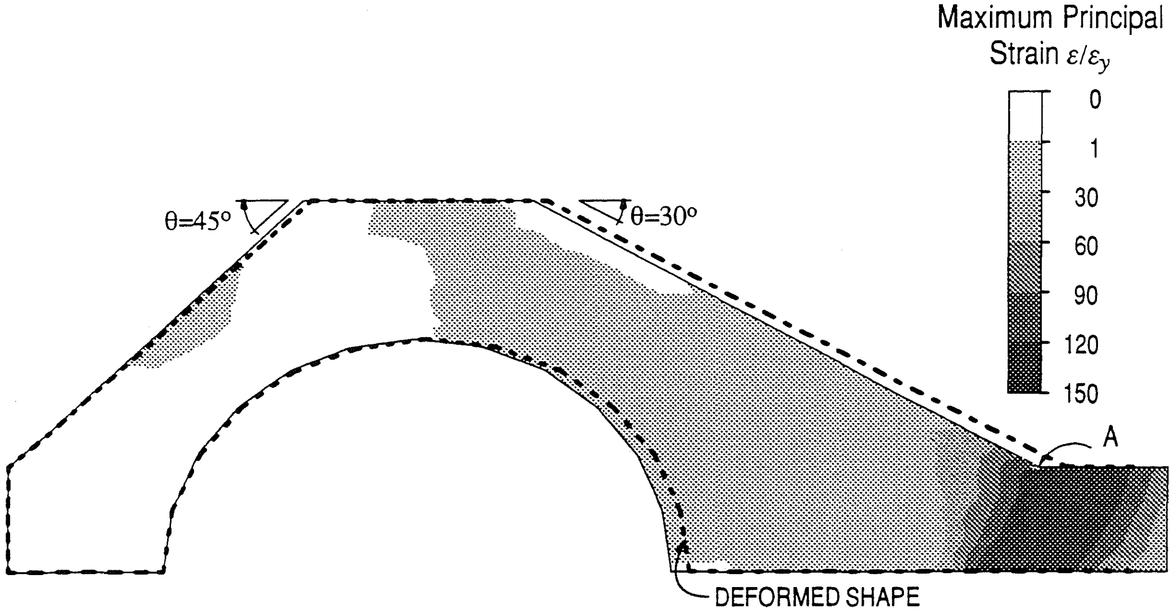

b) Maximum Principal Strain Value ($\varepsilon/\varepsilon_y$).

Figure 3.27. Stress and Strain Behavior of Tension Diaphragm Plate; Connection *Type IIA*

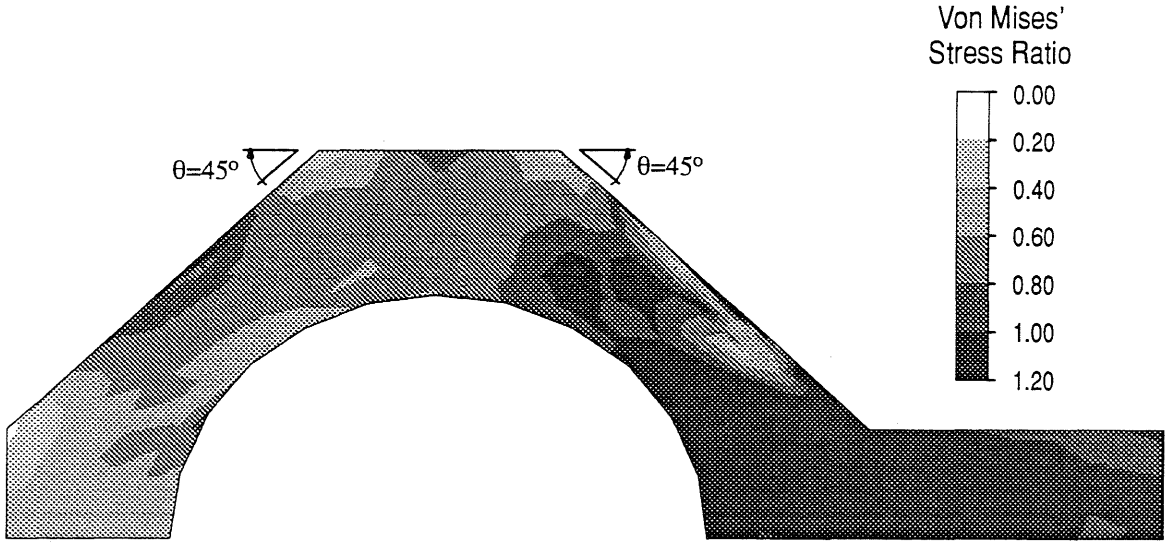

a) Von Mises' Stress Ratio.

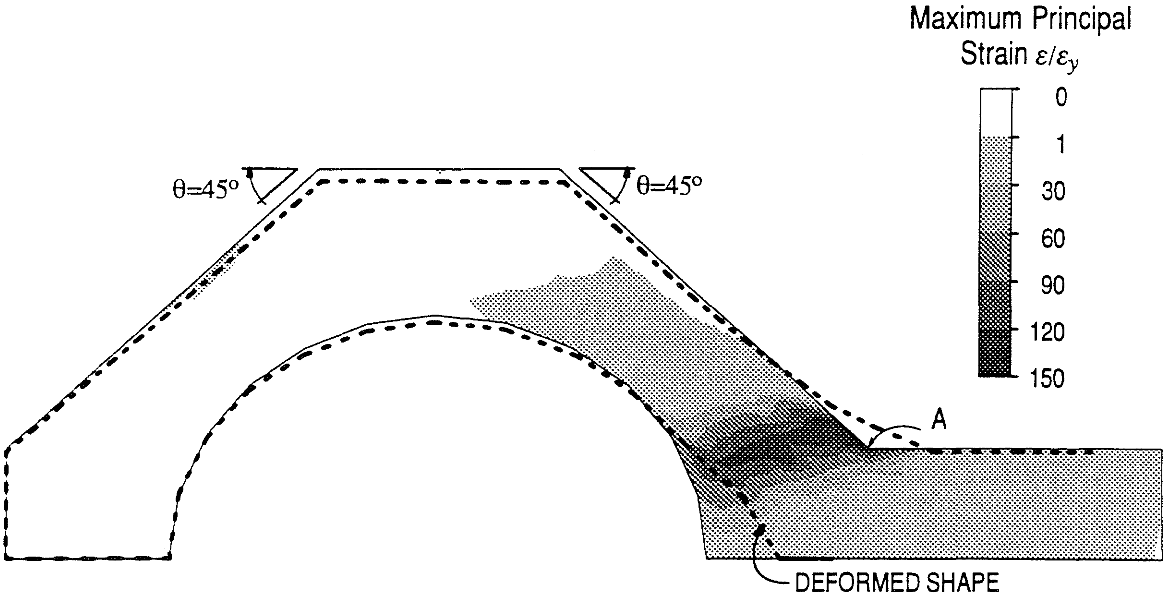

b) Maximum Principal Strain Value ($\varepsilon/\varepsilon_y$).

Figure 3.28. Stress and Strain Behavior of Tension Diaphragm Plate; Connection *Type IIB*

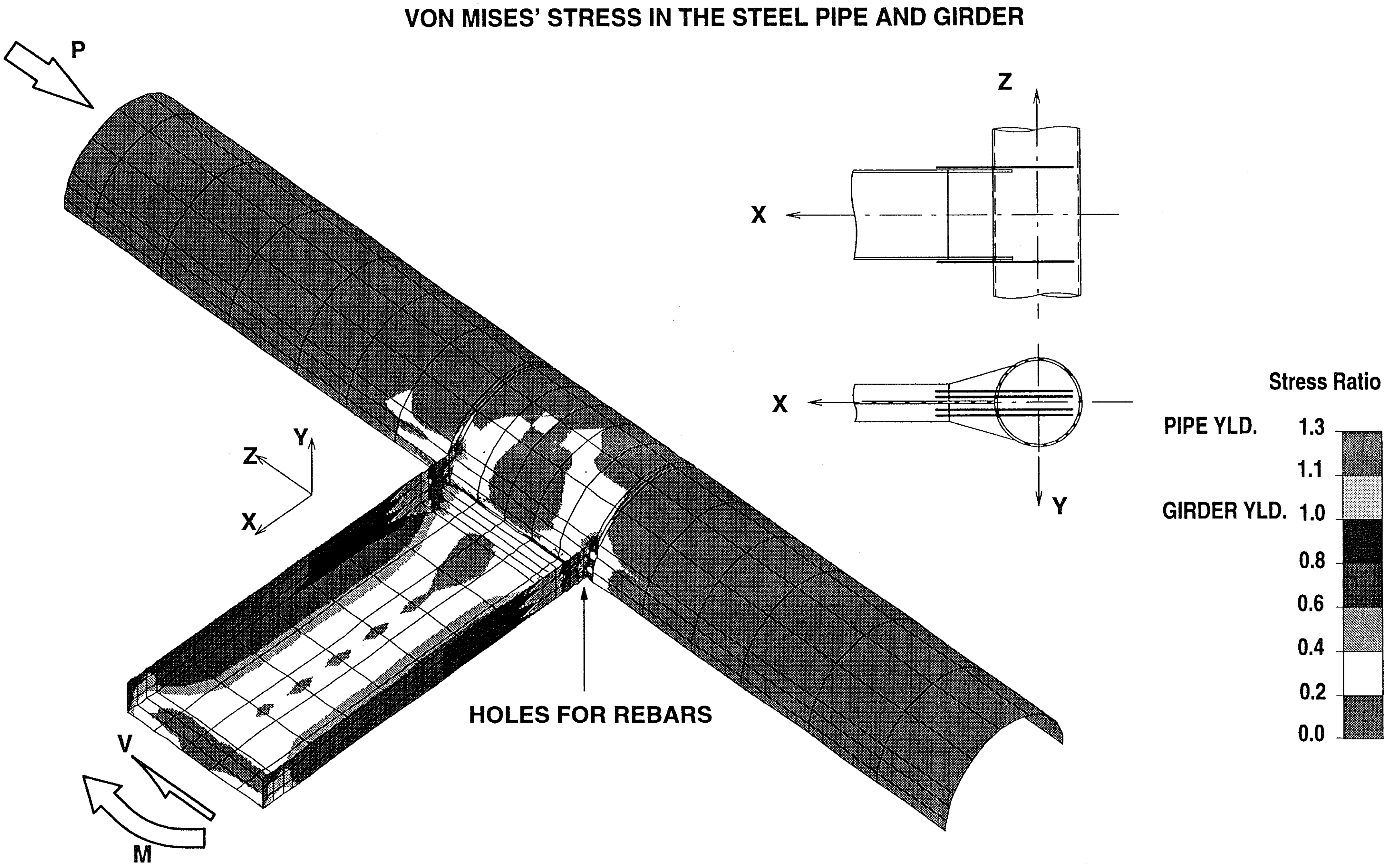

Figure 3.29. Von Mises' Stresses in the Pipe and the Girder, Connection *Type III*

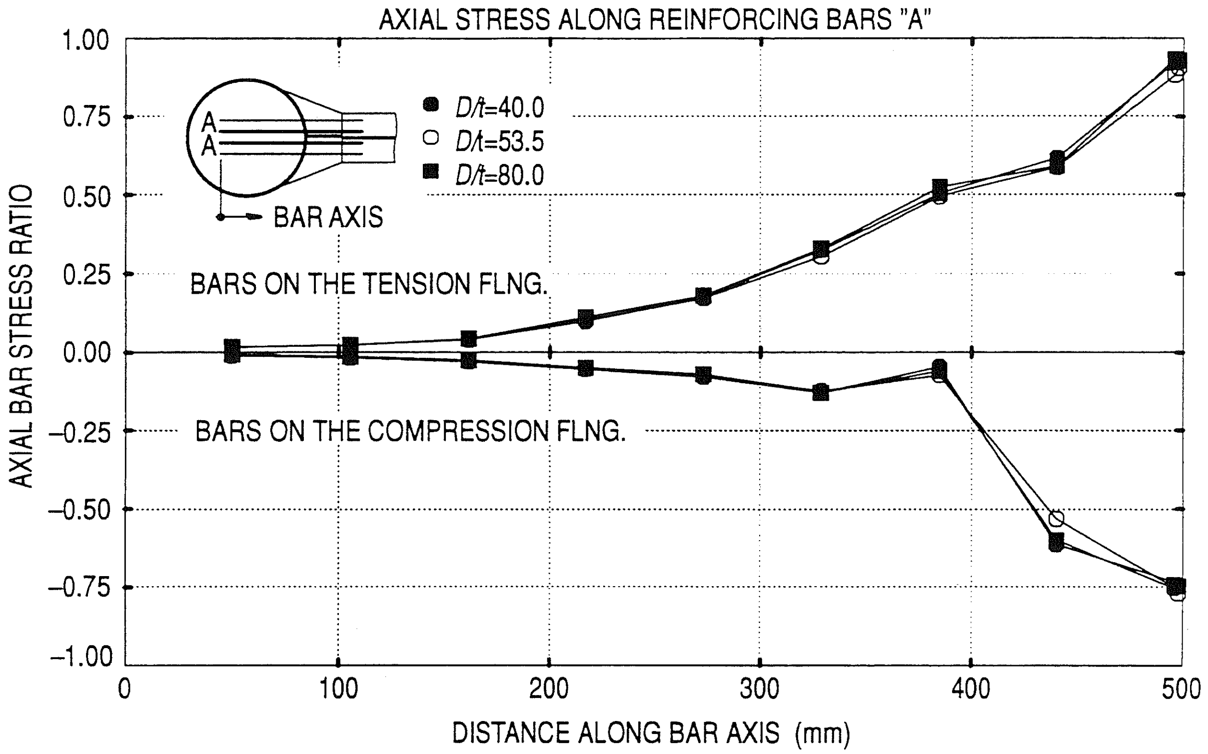

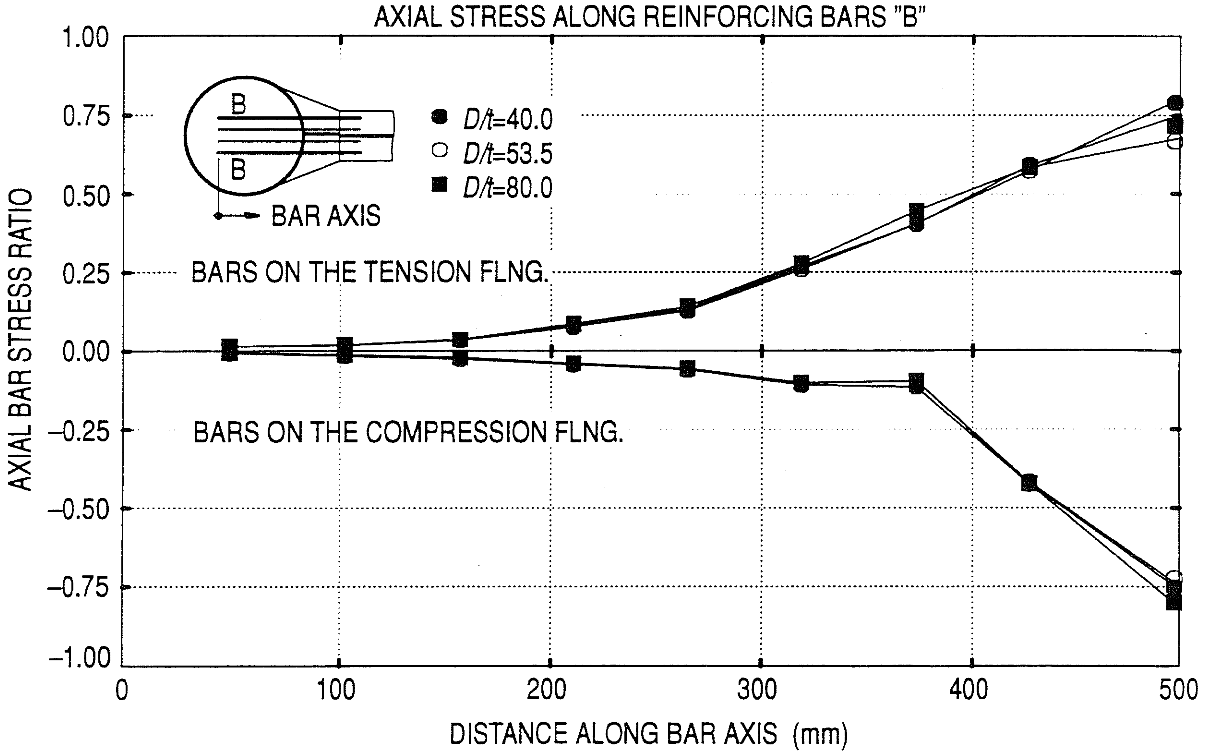

Figure 3.30. Variation of Axial Stress in the Deformed Bars

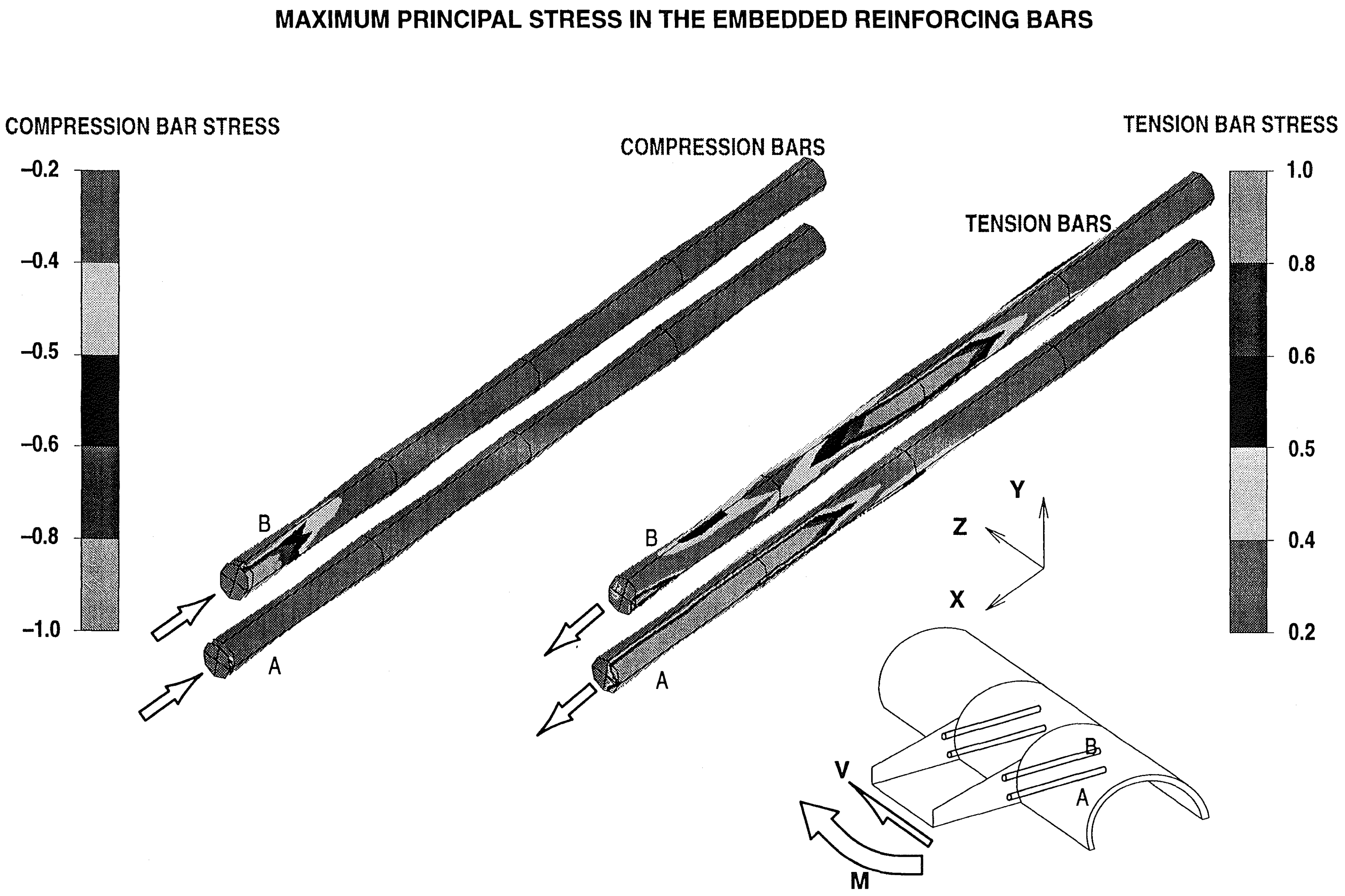

Figure 3.31. Axial Bar Stress, Connection *Type III*

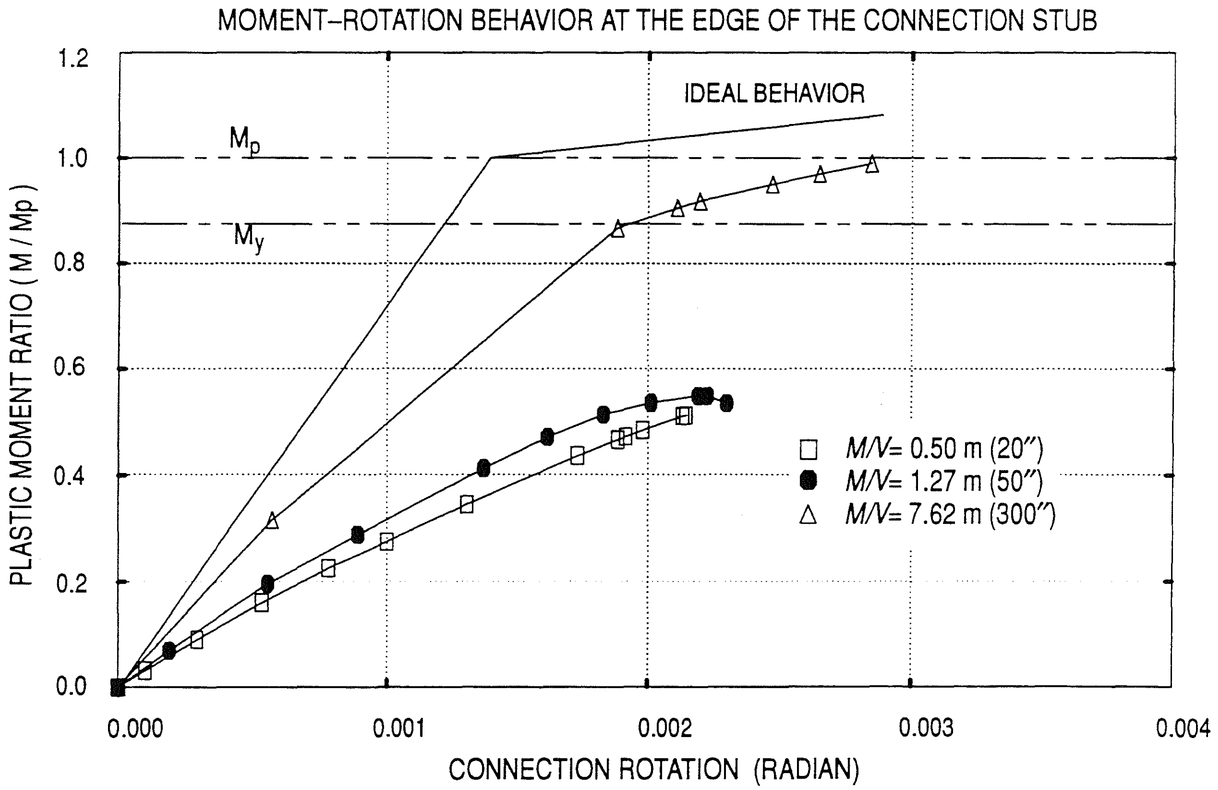

Figure 3.32. Analytical Moment–Rotation Behavior for Connection *Type III* w/ Different *M*/*V* Ratios

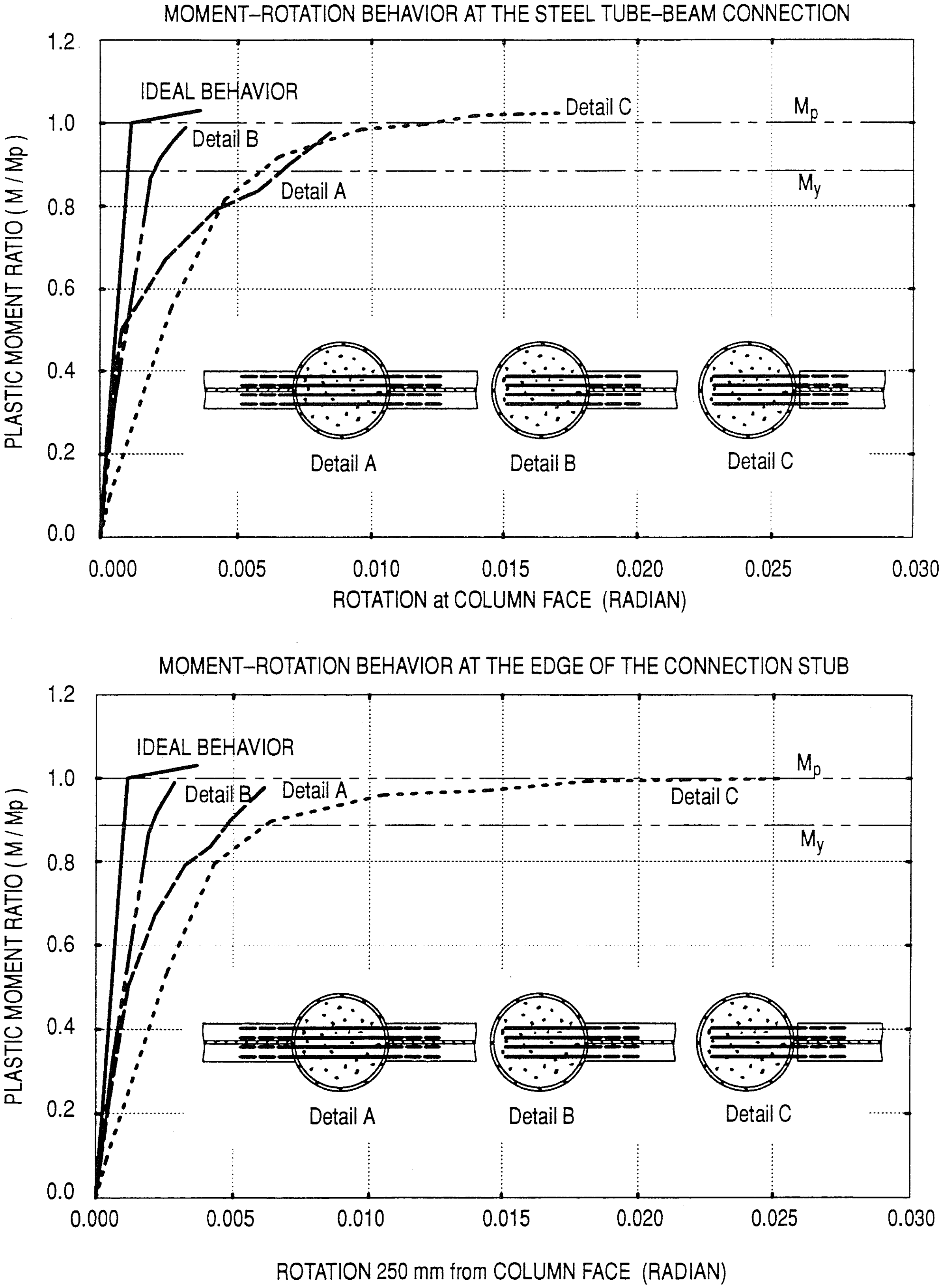

Figure 3.33. Analytical Moment–Rotation Behavior for Different Configurations of Connection *Type III*

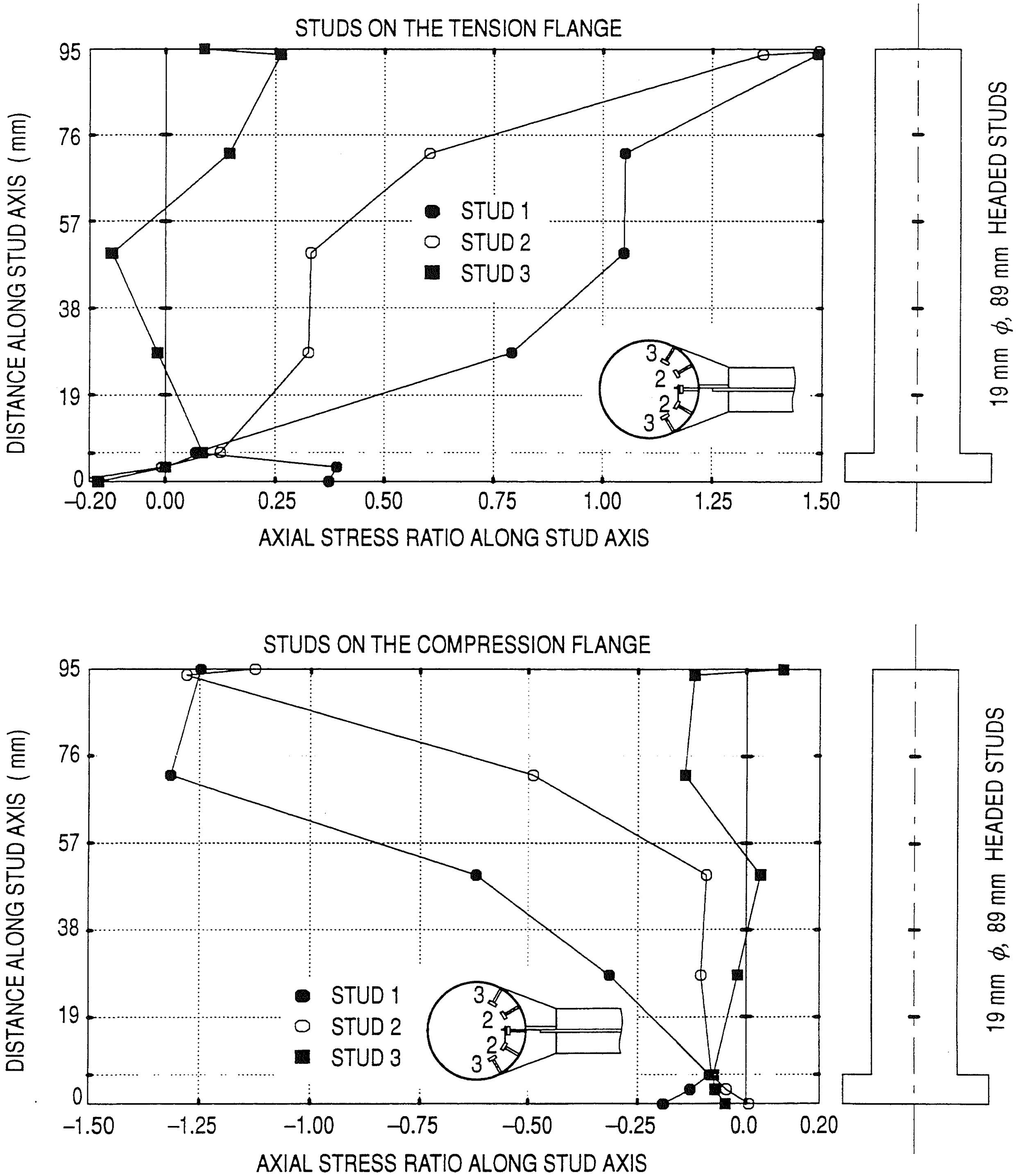

Figure 3.34. Axial Stresses in the Studs, Connection *Type IV*

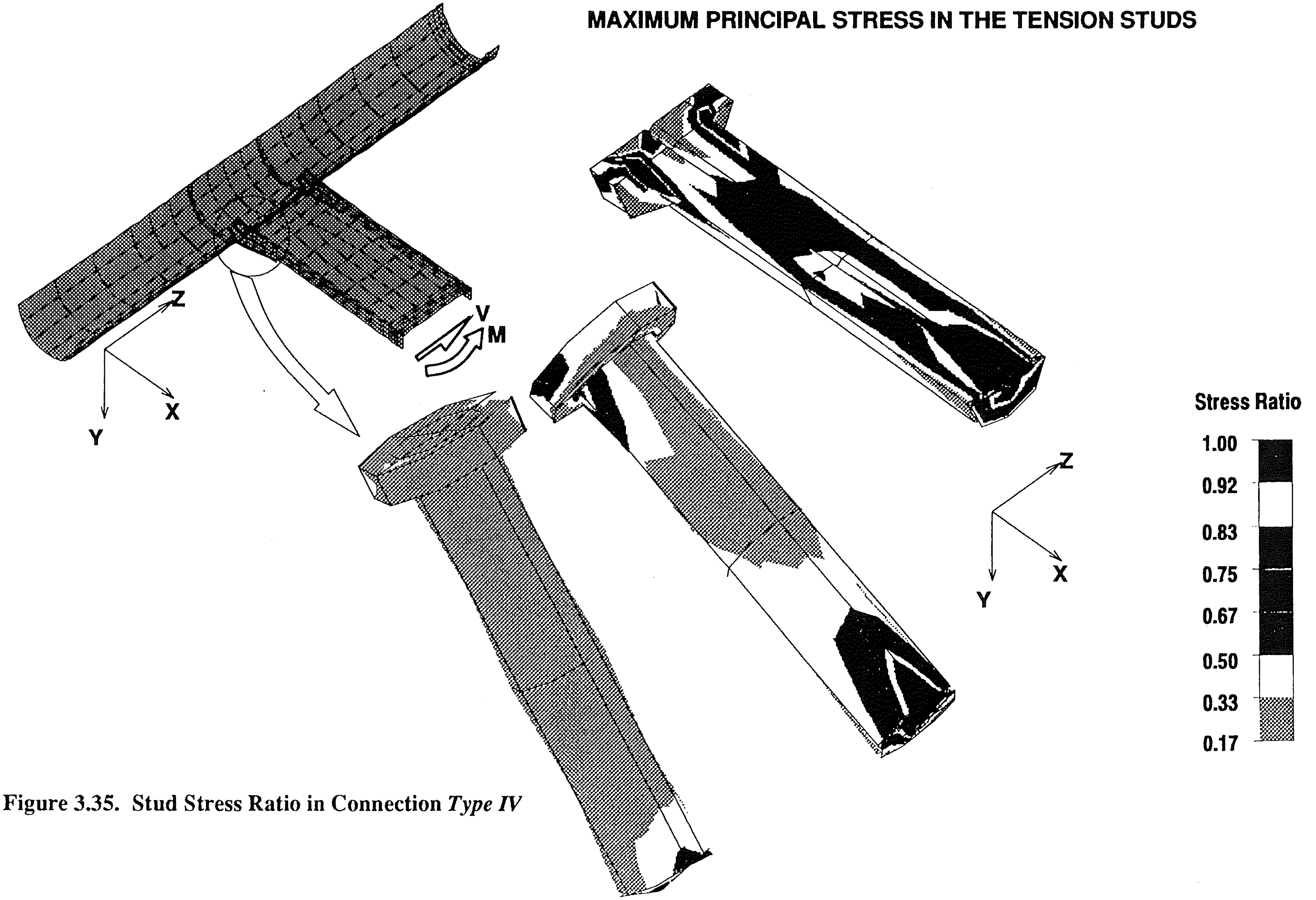

Figure 3.35. Stud Stress Ratio in Connection *Type IV*

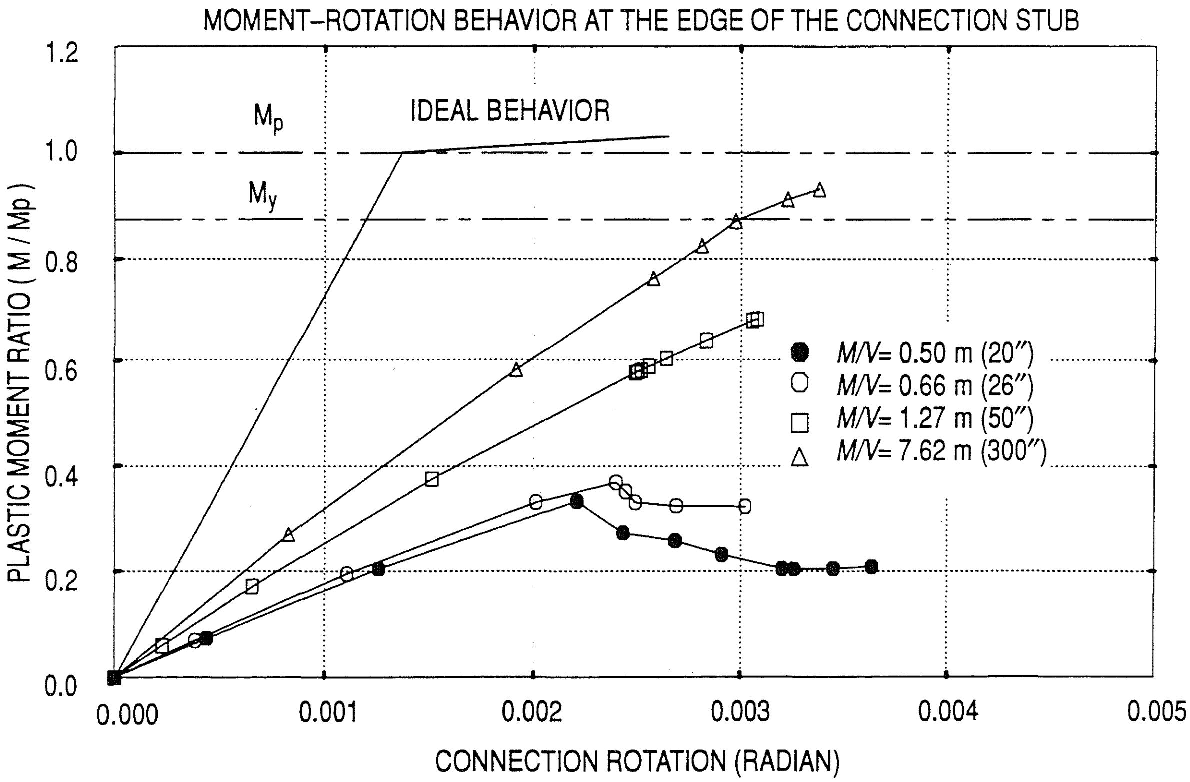

Figure 3.36. Analytical Moment–Rotation Behavior for Connections w/ Headed Studs, *Type IV*

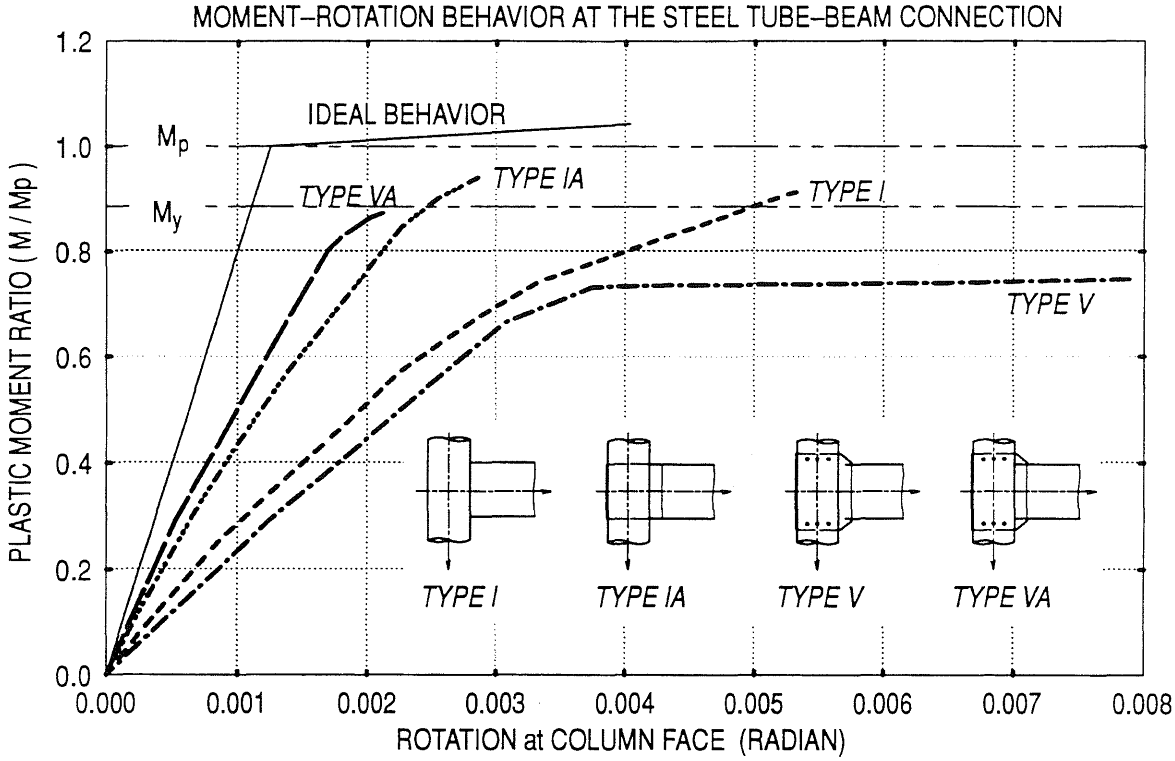

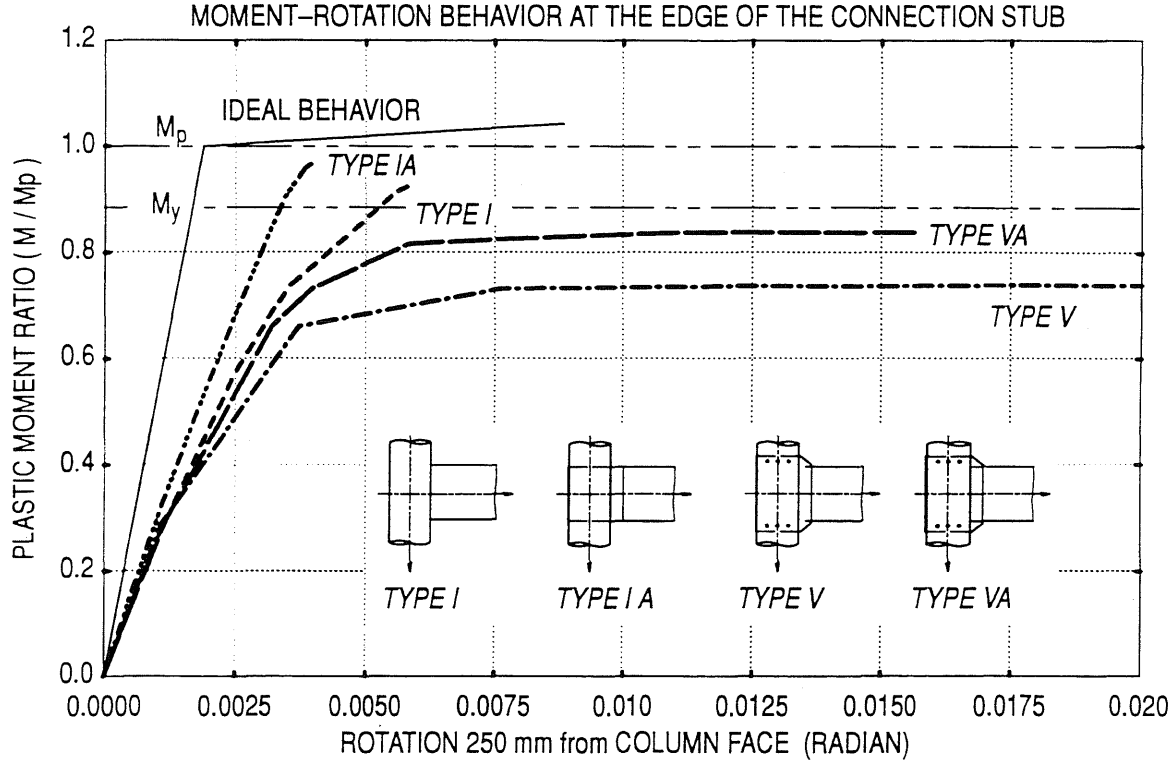

Figure 3.37. Analytical Moment–Rotation Behavior for Connection *Type V*

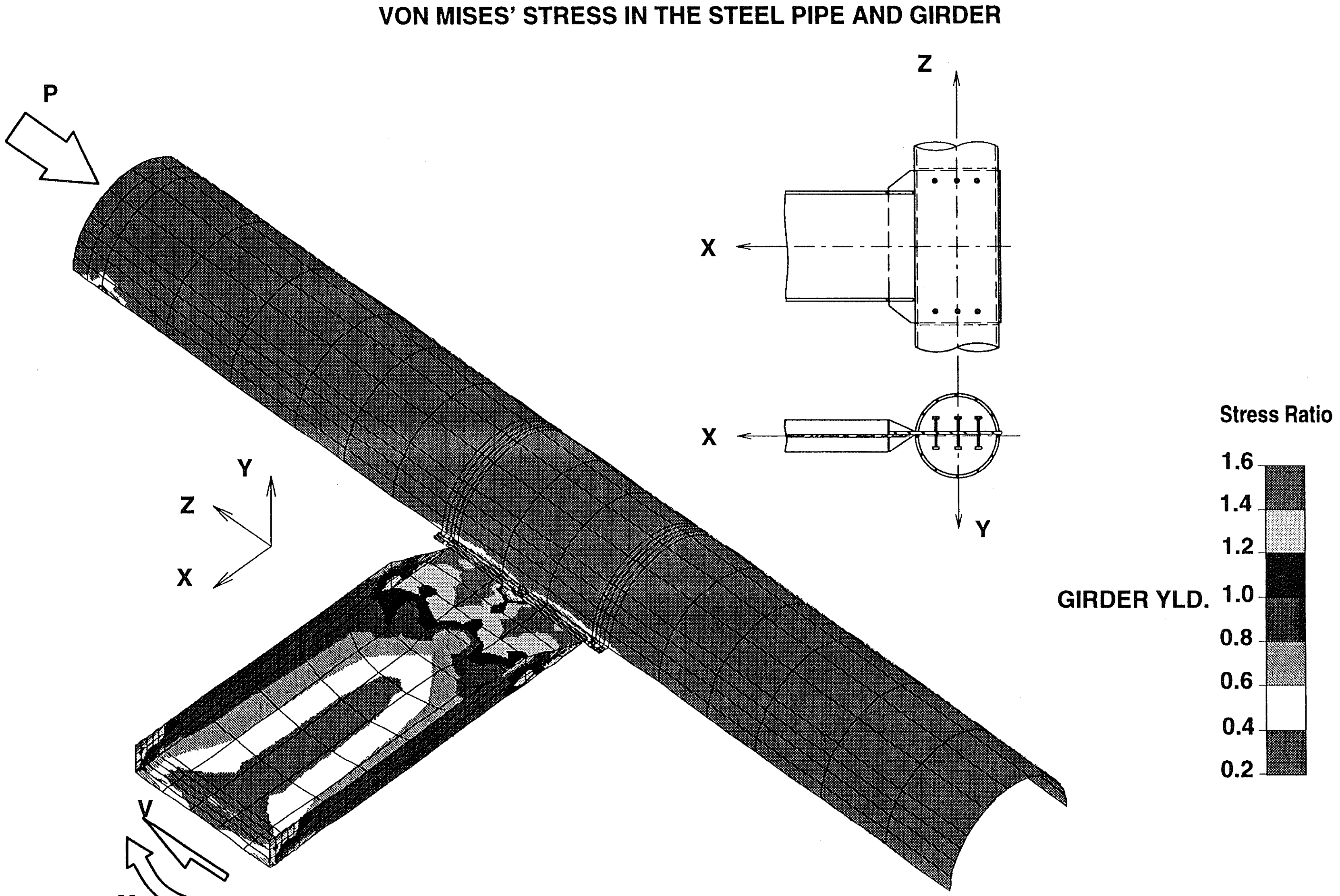

Figure 3.38. Von Mises' Stresses in the Pipe and the Girder, Connection *Type V*

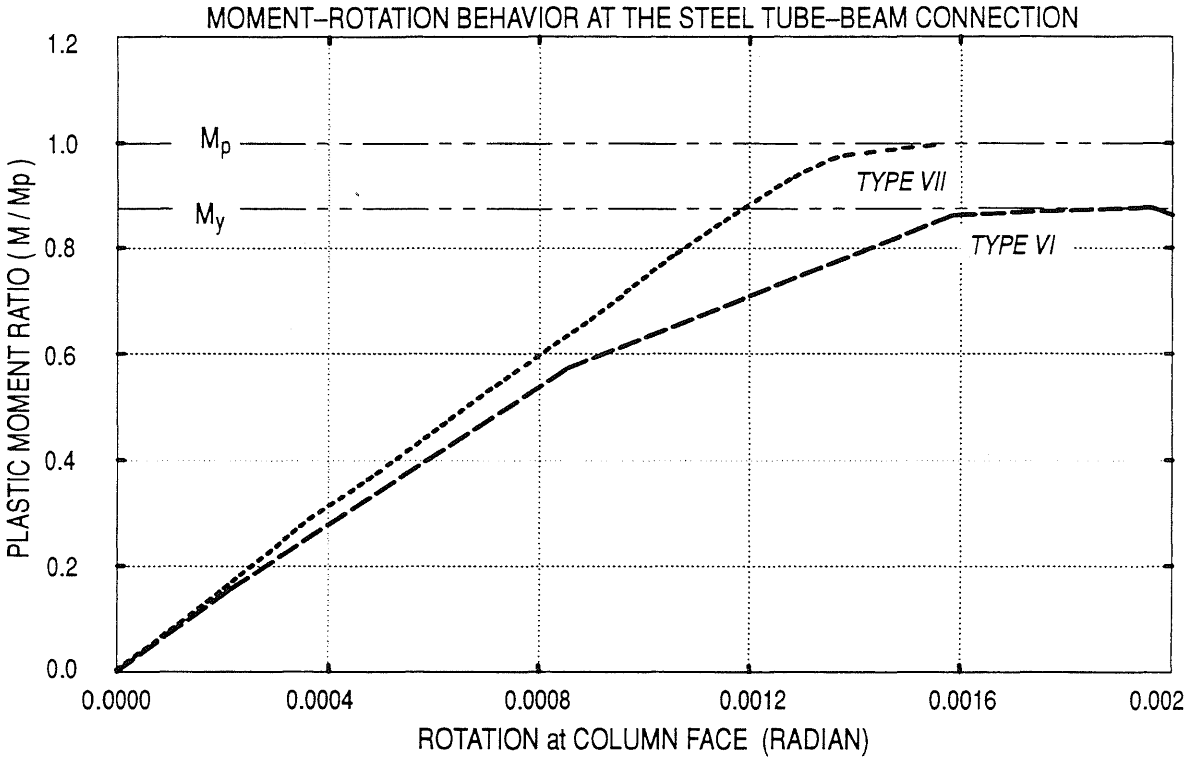

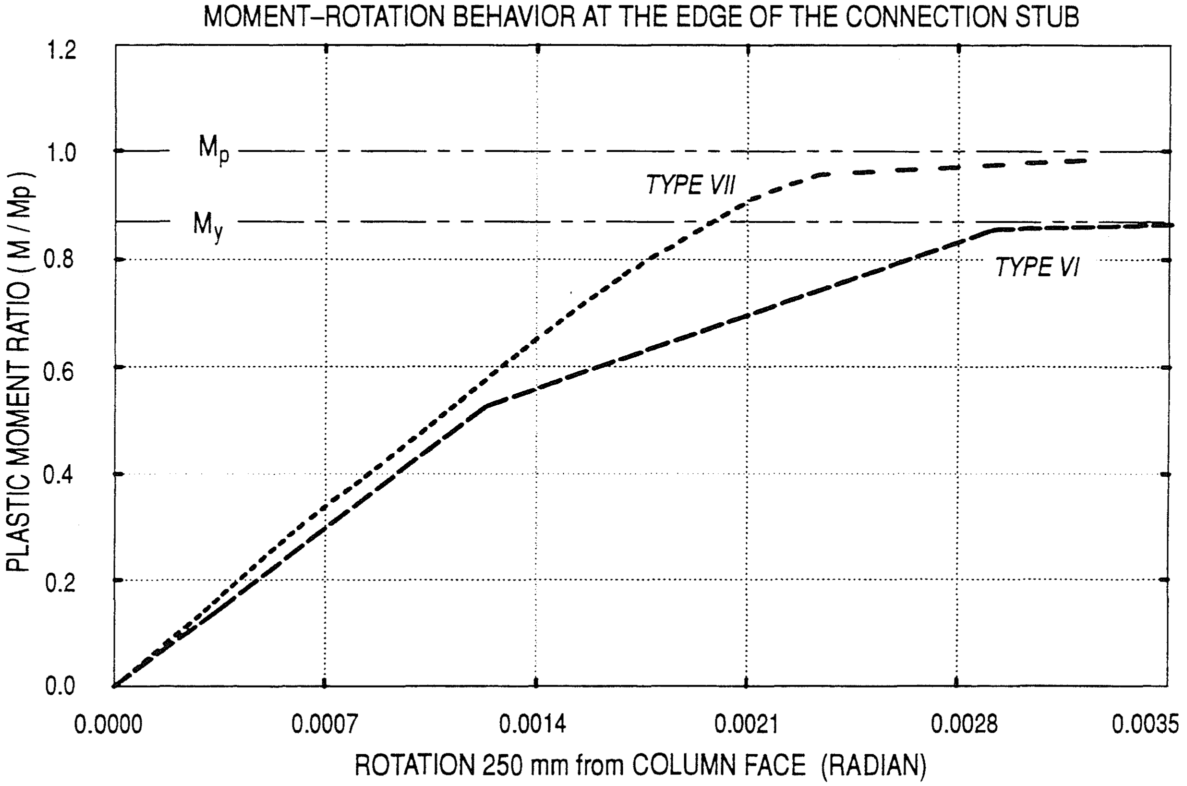

Figure 3.39. Analytical Moment–Rotation Behavior for Connection *Type VI*

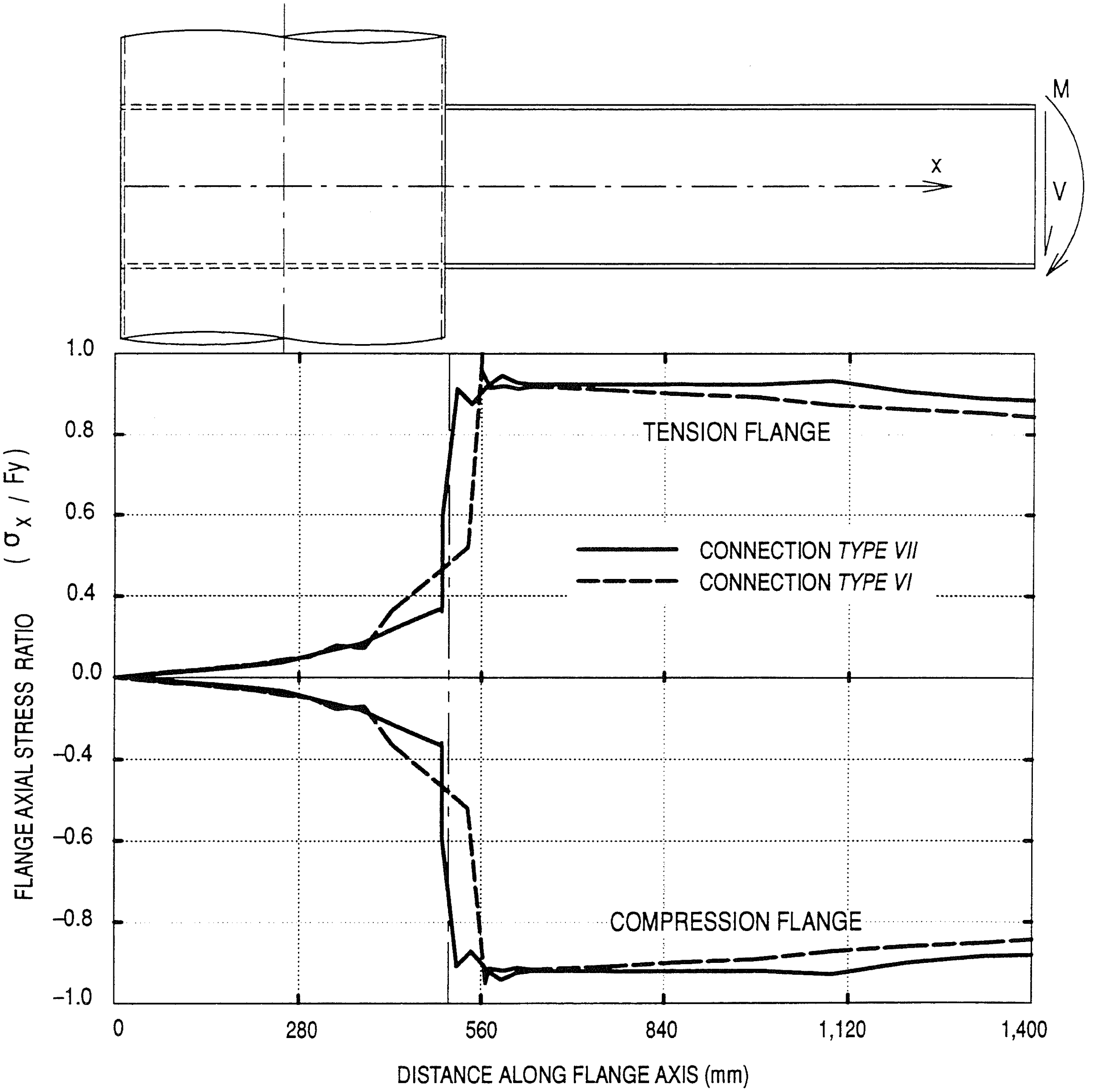

Figure 3.40. Variation of Flange Forces Along the Girder Axis

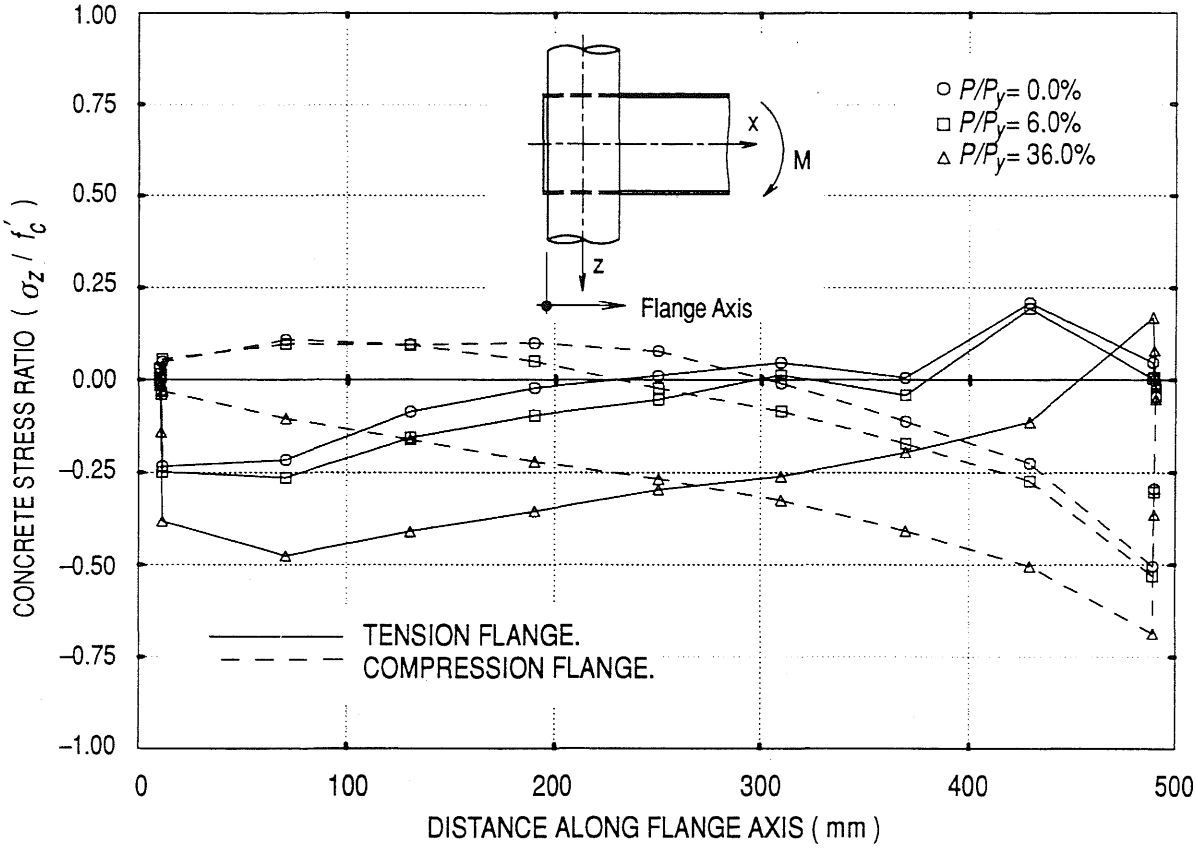

Figure 3.41. Bearing Stresses between the Flanges and the Concrete Core, Connection *Type VII*

VON MISES' STRESS IN THE STEEL PIPE AND GIRDER

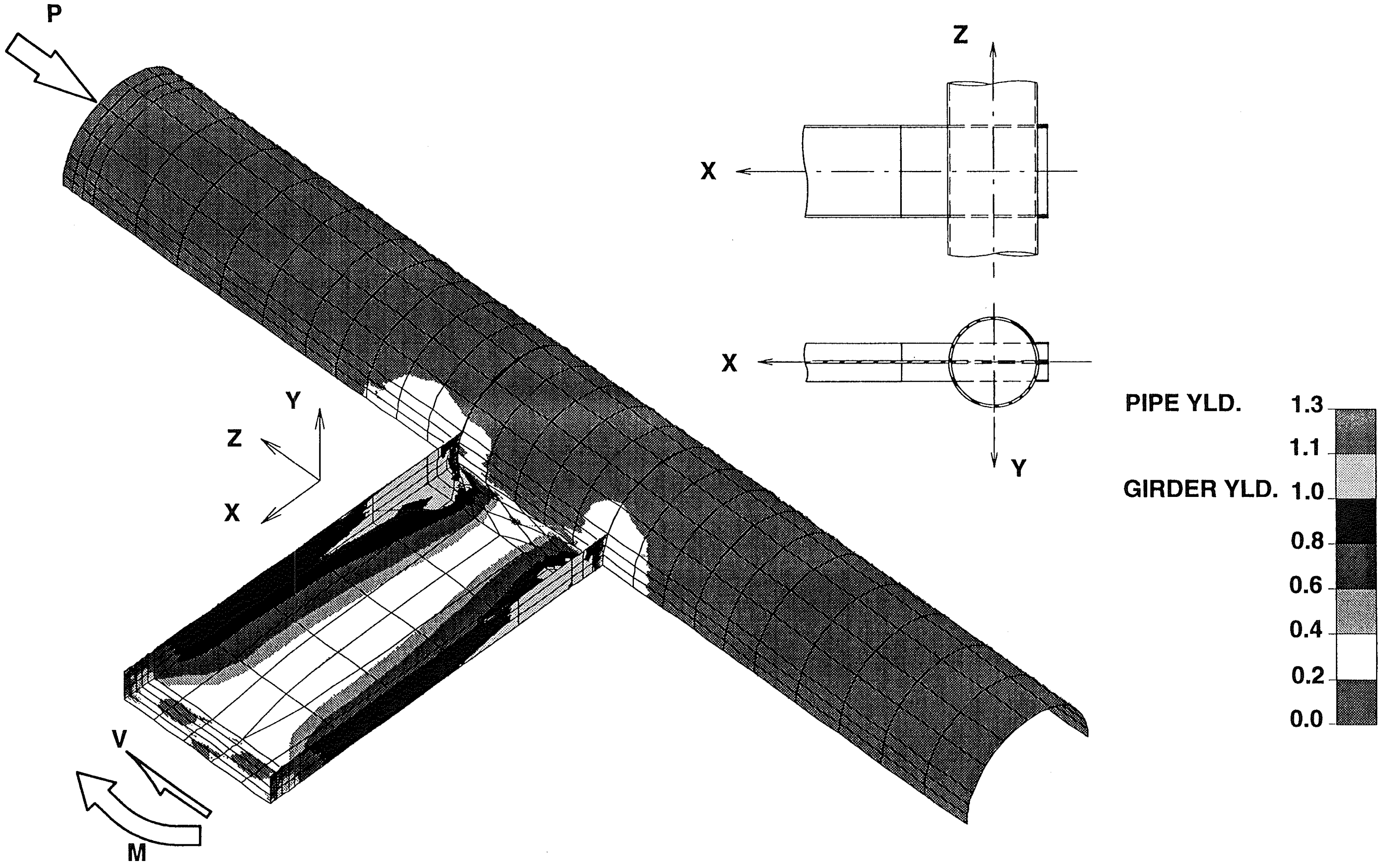

Figure 3.42. Von Mises' Stresses in the Pipe and the Girder, Connection *Type VII*

CHAPTER 4

TEST SPECIMENS AND TEST SET–UP

4.1 INTRODUCTION

The primary objective of this study was to investigate the flexural behavior of various connections to concrete–filled tubes. Since connections were the primary concern, and not joint or panel zone behavior, all specimens represented an exterior joint, in which a single girder was attached to one side of the CFT. A total of six large–scale specimens were tested in this research program. The fabrication and the testing of all specimens were performed in the Newmark Laboratory at the University of Illinois at Urbana–Champaign.

Connections using 510 mm $\phi \times 9.5$ mm thick ($20'' \phi \times {}^{3}/{}_{8}''$) pipes and W24×76 girders were analyzed, however, testing connections of this size was not economically feasible. Therefore, connections between 356 mm $\phi \times 6.4$ mm thick ($14'' \phi \times {}^{1}/{}_{4}''$) pipes and W14×38 girders were tested. These sizes represented approximately ${}^{2}/{}_{3}$–scale compared to the element sizes needed for the prototype perimeter frames. All structural steel sections were obtained by a local steel supplier.

4.2 FABRICATION OF SPECIMENS

All connections were designed with beam stubs which were considered to be shop fabricated. The girders were bolted and/or welded to these stubs in the field. Connection *Types I*, *II*, *III*, and *VII* exhibited the broadest range of moment–resisting behavior, hence, these connections were tested. The connections with continuous web and continuous flanges, *Types IA* and *VI*, respectively, were tested to investigate the influence of the web and the flanges of connection Type *VII*. ER70S–3 electrode was used for all welding, and all elements were preheated before the welding process.

For each specimen a 510×510×13 mm ($20'' \times 20'' \times {}^{1}/{}_{2}''$) plate was welded to one end of the pipe. This plate was necessary for concrete placement, and was used to attach the composite column to the test apparatus.

4.2.1 Simple Connection, Type I

This specimen, shown in Figure 4.1, consisted of a 2,108 mm (6′–11″) long, 356 mm $\phi \times$ 6.4 mm (14″ $\phi \times {}^1/_4$″) pipe and a beam stub welded to the pipe. The flange and web plates of the connection stub were attached to each other using a continuous 6.4 mm (${}^1/_4$″) fillet weld on both sides of the web plate. At the tube face, the flange plates were flared to form a central angle of 120°, and the width of the plates was decreased gradually over a 254 mm (10″) distance to match that of the girder flanges.

The beam stub was connected to the girder using a full penetration weld. While it was anticipated that field connection might be bolted, the object of this research was to study the connection to CFT columns and not the connection between beam stubs and girders. Therefore, a fully welded girder to stub connection was used.

4.2.2 Continuous Web Plate Connection, Type IA

To continue the web through the tube, a vertical slot on opposite sides was cut in the tube wall. The web plate was fillet welded to the tube, and it was bolted and welded to the girder web. A calibrated wrench was used to tighten the bolts to about 70% of their axial strength. This specimen is depicted in Figure 4.2. This detail may be considered as a hybrid between the simple connection *Type I* and the through connection *Type VII*.

4.2.3 Connection with External Diaphragms, Type II

In the analytical study, two types of diaphragms were investigated. For the purpose of this research program, the absolute minimum external diaphragm connection was investigated. The behavior of these connections will indicate the validity of diaphragm connections for further investigation.

A square plate, with a thickness equal to that of the girder flange, was used as a diaphragm in this detail. The dimensions of the plate were selected such that the width was equal to the diameter of the pipe plus the width of the girder flange. For convenience during fabrication, the diaphragm was cut into two halves which were groove welded together during the connection assembly. The diaphragm was fillet welded to the pipe wall on both sides of the plate. The web plate was connected to the girder web in the same manner as in connection *Type IA*. Figure 4.3 illustrates the details of this specimen.

4.2.4 Connection with Deformed Bars, Type III

The specimen shown in Figure 4.4 is identical to connection *Type I*, except that holes were drilled in the pipe to insert weldable deformed bars into the core of the tube. Four 19 mm ϕ (#6), deformed bars were welded to each flange. The attachment of each bar was approximately 50% more weld than needed to develop the bar strength in tension. Each bar extended 300–330 mm (12″–13″) in the concrete core, or approximately 10% longer than that required by the *ACI 318–89 code*.

To monitor the bar forces, some deformed bars were instrumented with strain gages. The location of these gages is shown in Figure 4.5.

4.2.5 Continuous Flanges, Type VI

For this connection type, embedded elements were used in an attempt to transfer part of the beam forces away from the tube wall and into the concrete core. As shown in Figure 4.6, plates that matched the width and thickness of the girder flange were continued through the pipe, and they were fillet welded to the pipe wall. A shear tab was fillet welded to the tube skin, and it was bolted and welded to the girder web. No effort was made to enhance the bond between the embedded flanges and the concrete core.

4.2.6 Continuation of the Girder through the Column, Type VII

To fabricate this connection, an I–shaped slot was cut in the tube wall, as shown in Figure 4.7. The beam stub was fillet welded to the pipe on both sides of the flanges. However, only one side of the web was fillet welded to the tube, and a full penetration groove weld was used to attach the girder to the beam stub. Strain gages were applied on the connection stub within the pipe. The location of these strain gages is shown in Figure 4.8. Again, no effort was made to improve the bond between the embedded connection stub and the concrete core.

4.3 MATERIALS

4.3.1 Concrete

Concrete mixing was done using a 0.56 m^3 ($^3/_4$ yd^3) horizontal pan concrete mixer. The mix was designed according to the *ACI* absolute volume method, and the 28 day target design strength was 34.5 MPa (5.0 ksi). The mix proportioning is shown in Table 4.1. All specimens were cast in the vertical position, and a high frequency, internal rod vibrator was used to consolidate the concrete. Although, one batch could provide concrete for three specimens. There was concern that the weight of the mix was larger than the mixer capacity. Therefore, a separate concrete batch was prepared for each specimen. The same mix proportioning was used for each specimen. Four 150 mm $\phi \times 300$ mm long ($6'' \phi \times 12''$) cylinders were sampled from each batch. These cylinders were used to evaluate the uniaxial compressive strength of the concrete core at the day of testing. The concrete strength test was done according to *ASTM C469–87*, and the results are shown in Table 4.2. To prevent loss of water, the open ends of the pipes and cylinders were covered with plastic sheets. The specimens and the compression cylinders were left to cure in the ambient temperature and humidity of the structures laboratory.

Sand and crushed lime stone were selected as fine and coarse aggregates, respectively. The aggregate physical properties are shown in Table 4.3. Unit weight, specific gravity, and gradation of the aggregates were obtained according to *ASTM C29*, *C127*, and *C136*, respectively. The maximum aggregate size was 19 mm ($^3/_4''$), this size satisfied *ACI 318–89* section 3.3.2. The fine aggregate's absorption was found according to *ASTM C128*. The gradation of both aggregates is shown in Figure 4.9. Ordinary, type I, portland cement, was used in all specimens, and no chemical admixtures were used.

4.3.2 Steel

Three samples from each steel element were tested in tension according to *ASTM A370*. The coupons were sampled near the ends of the pipe and the tip of the cantilever. Although tensile coupons were cut from the test specimens after testing, the coupon location experienced minimum strain demand, confirmed by the strain gages applied at these regions. The gage length of each coupon was 203 mm (8″) long by 38 mm (1.5″) wide. The stress–strain relationship for each steel component is shown in Figure 4.10, and the mechanical properties are summarized in Table 4.4.

4.4 TEST SET–UP AND PROCEDURE

To study the potential seismic performance of different connection types, each specimen was tested using the quasi–static test method. The quasi–static test method imposed a predetermined cyclic deformation history on the test specimen. These cyclic deformations were well into the inelastic range of behavior for each specimen. Potential seismic performance was inferred from the inelastic cyclic response of each specimen.

4.4.1 Test Apparatus

A plan view of the test set–up is shown in Figure 4.11. A set of rollers were used to guide the girder between the MC beams in the horizontal plane. This bracing system, shown in Figure 4.12, was designed to prevent out–of–plane and lateral–torsional deformations of the girder end.

Another lateral bracing system was provided at the axial actuators position. This was to provide the pinned–end inflection point needed at the column top. This system consisted of a pair of MC 9×25.4 beams, and a concrete reaction block. Slots parallel to the longitudinal axis of the column were provided in each channel section to allow the axial deformation of the column. The 76.5 mm ϕ (3″ ϕ) pin was guided by these slots, and the shear force was transferred through direct bearing of this pin on the channel sections. The region of the channel section which contained the slots was reinforced with a 12.7 mm (0.5″) thick, A441 plate. An end–plate was welded to each channel, and was bolted to the concrete reaction block. A schematic of this bracing system is shown in Figure 4.13.

Hinges were assumed at the column ends to represent inflection points at mid–column length in the prototype frame. As shown in Figures 4.14 and 4.15, each hinge consisted of two 76.5 mm (3″) thick plates with a 76.5 mm (3″) diameter pin between them. To reduce the bearing stresses between the pin and the plate, and to provide a convenient way to align the pin, two semi–circular grooves were milled in each plate. In order to transfer shear forces, the pin was bolted to one plate and inserted through two circular holes made in two 13 mm (0.5″) thick plates. These plates were bolted to the top and bottom of the 76 mm (3″) plate. Plastic pads were used to reduce friction developed during the rotation of the pin assembly. Aluminum shims were used to compensate for the additional thickness from the plastic pads.

All reaction blocks were anchored to the strong floor using high strength rods. Each rod was pretensioned to 445 kN (100 kips). One of the column ends was secured between two 76.5 mm (3″) thick semi–circular plates, shown in Figure 4.14. This arrangement was detailed for convenience during installation and removal of the test specimens. A 12.7 mm (0.5″) thick plate was welded to the other end of the column before the casting of concrete, this plate was bolted to the pin assembly as shown in Figure 4.15.

4.4.2 Instrumentation

Electrical resistance, foil type strain gages were applied to the tested specimens, and their properties are shown in Table 4.5. Each strain gage was wired to a Wheatstone quarter–bridge configuration. Linear variable displacement transducers (*LVDTs*), with direct current excitation, were used to monitor the deformations of the specimen and the test apparatus. Calibrated load cells were used to monitor the loads applied by the different actuators used in the test.

A constant 445 kN (100 kips) axial load was applied to the steel tube and the concrete core of each specimen simultaneously. Two manually operated hydraulic jacks, with a total capacity of 890 kN (200 kips) and a maximum stroke of 25.4 mm (10″), were used to apply the axial load to the composite column. The hydraulic jacks were aligned with the longitudinal axis of the pin. This arrangement was needed to eliminate any differences in the actuator forces due to the rotation of the end plate.

A 445 kN (100 kip) *MTS*, uniaxial, servo–controlled hydraulic actuator was used to apply predetermined cyclic displacement at the tip of the cantilevered girder. Cyclic deformations were controlled using an *8500 plus Instron* controller. The displacement control during the test utilized an external ± 127 mm (± 5″) *LVDT* attached to the hydraulic actuator as shown in Figure 4.16. To eliminate the influence of the flexibility of the piston assembly and the deformation of the test apparatus, the external *LVDT* was used to control the imposed displacement at the girder tip. The external *LVDT* was placed in one of the two positions shown in Figure 4.16. However, there was no significant difference between the readings from the internal *LVDT* on the hydraulic actuator and the external *LVDT*.

Electrical resistance strain gages were applied along the longitudinal axis of the column to study the distribution of axial stresses along the pipe. Also, a set of strain gages were applied in the panel zone area to study the state of stresses in this region. Very small hoop strains were observed in the test of the simple connection, *Type I*. Hence, no circumferential strain gages were applied to the remaining specimens.

Column deformations were measured using a set of *LVDTs* distributed along its length. Four *LVDTs* were used to calculate the connection rotation relative to the column center line, and their results were used to develop the moment–rotation hysteresis of the connection. Figure 4.17 shows the locations of the strain gages and *LVDTs*.

The displacements of the reaction blocks and the lateral bracing system were monitored using *LVDTs* and dial gages. These deformations were measured relative to the strong floor. The column was assumed to be rigidly connected to the end plate which was bolted to the pin assembly. Therefore, any rotations of the column about its longitudinal axis can be calculated from two *LVDTs* attached to the end plate.

Voltage outputs from the strain gages were collected using *Strain Gage Conditioner and Amplifier (2100 System).* All data from the measurement sensors were recorded electronically by *LABVIEW* software mounted on a Quadra 650 *Apple Macintosh* computer. A 16 bit analog–to–digital converter board was used to transfer the data from the measurement sensors to the *LABVIEW* software.

4.4.3 Test Parameters

Prototype frame design and the inelastic dynamic analysis provided values needed for the test parameters. Because of the perimeter frame concept, the composite column axial load was relatively small. Therefore, axial force for each test specimen column was 10% of the squash load.

Cyclic deformations were imposed according to *ATC–24 : Guidelines for the Seismic Cyclic Testing of Components of Steel.* The amplitude of the yield displacement was needed for the imposed cyclic deformation, which was determined for each specimen from the finite element analysis. The analytical load–deflection curves for four of the six connection details are shown in Figure 4.18. The behavior shown is for actual dimensions and material properties of the specimens. A typical set of imposed cyclic displacements is shown in Figure 4.19. Each set of inelastic cycles was followed by two elastic cycles of amplitude $0.5\delta_y$. These small–amplitude cycles were used to investigate the deterioration of the elastic stiffness of the connection. The specimens were loaded until clear failure of the connection was apparent. The cycles were imposed at the frequencies shown in Figure 4.19, and the data from the strain gages, *LVDTs*, and load cells were recorded every 0.5–1.0 second.

Table 4.1. Concrete Ingredients

	Cement kg/m^3 (lb/yd^3)	Water kg/m^3 (lb/yd^3)	Sand kg/m^3 (lb/yd^3)	Gravel kg/m^3 (lb/yd^3)	Slump mm (in)
Weight	436 (659)	209 (316)	452 (683)	1176 (1777)	114 (4.5″)

Table 4.2. Concrete Core Compressive Strength

	Specimen					
	I	*IA*	*II*	*III*	*VI*	*VII*
Cast Date	04/06/1995	04/01/1996	12/22/1995	04/06/1995	12/22/1995	04/06/1995
Test Date	08/15/1995	05/01/1996	03/20/1996	08/22/1995	03/27/1996	09/05/1995
f'_c, MPa (ksi)	56.5 (8.2)	53.8 (7.8)	57.2 (8.3)	55.9 (8.1)	54.5 (7.9)	56.5 (8.2)

Table 4.3. Aggregate Properties

Property	Coarse Aggregate	Fine Aggregate
Maximum Aggregate Size, mm (in)	19.00 ($^3/_4$″)	——
Fineness Modulus	7.97	2.82
Bulk Specific Gravity, SSD†	2.65	2.29
Absorption Capacity, (%)	1.80	2.23
Moisture Content, (%)	0.08	0.13
Unit Weight, kg/m^3 (lb/yd^3) ‡	1663 (2513)	1621 (2449)

†SSD: Saturated Surface Dry.

‡This is the stock unit weight.

Table 4.4. Mechanical Properties of the Steel Elements

		Yield Strength MPa (ksi)	Modulus of Elasticity GPa (ksi)	Ultimate Strength MPa (ksi)	Thickness mm (in)
Steel Pipe		396.5 (57.5)	222 (32289)	540 (77)	6.850 (0.269)
Girder	Flange	305.5 (44.3)	207 (29993)	455 (66)	13.437 (0.529)
	Web	358.5 (52.0)	221 (32073)	490 (71)	7.950 (0.313)
Stub Beam	Flange	332.3 (48.2)	220 (31945)	490 (71)	12.395 (0.488)
	Web	271.7 (39.4)	217 (31500)	415 (59)	8.128 (0.320)
Deformed Bars, #6		379.3 (55.0)	171 (24809)	605 (86)	....

Table 4.5. Strain Gage Properties

Supplier	Measurements Group, INC. NC, USA
Designation	EA–06–250BG–120
Gage Length	6.35 mm
Gage Factor	2.075 ± 0.5%
Resistance	120.0 ± 0.15%
Temperature Range	–75° to 175° C
Strain Limit	5%

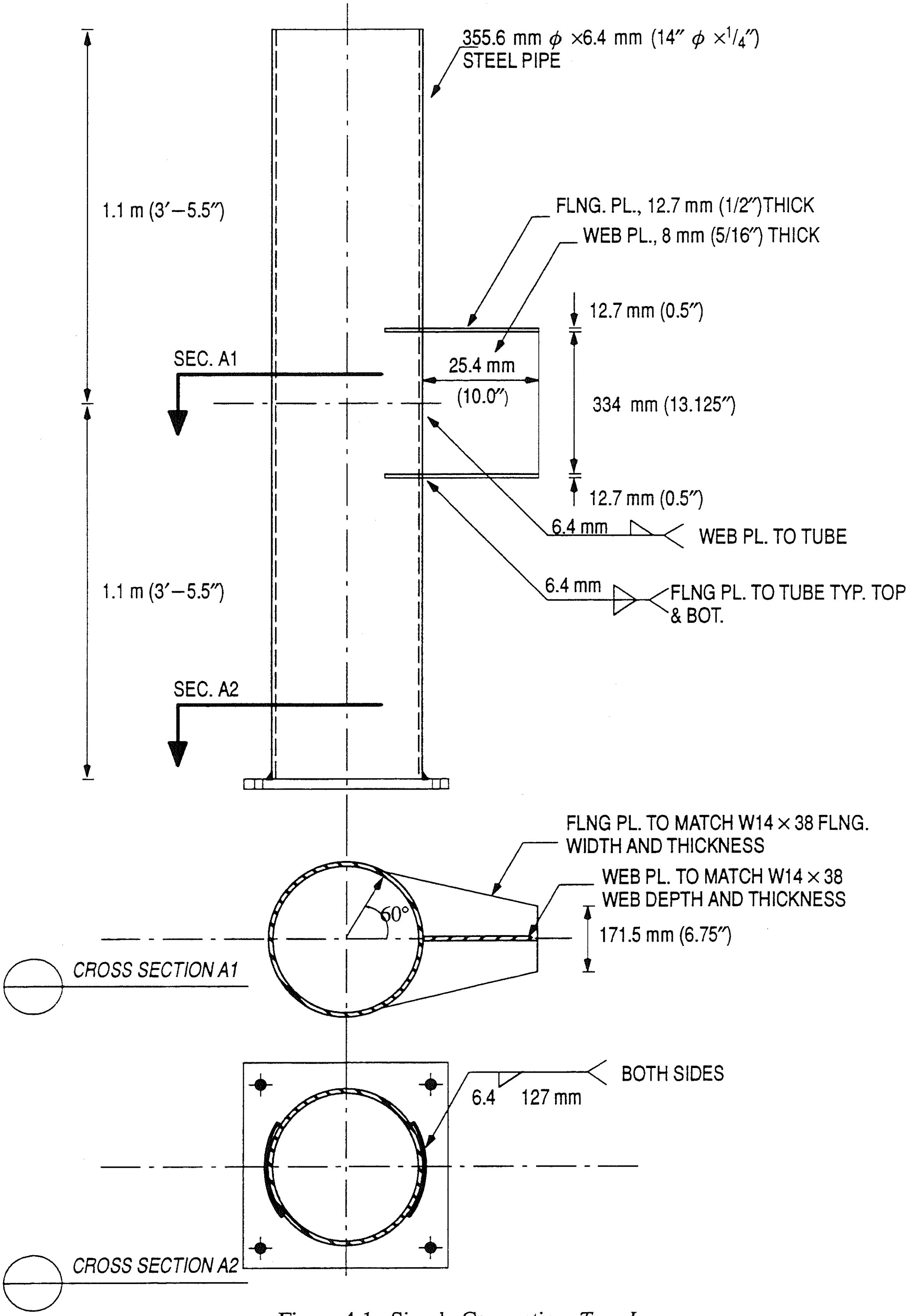

Figure 4.1. Simple Connection, *Type I*

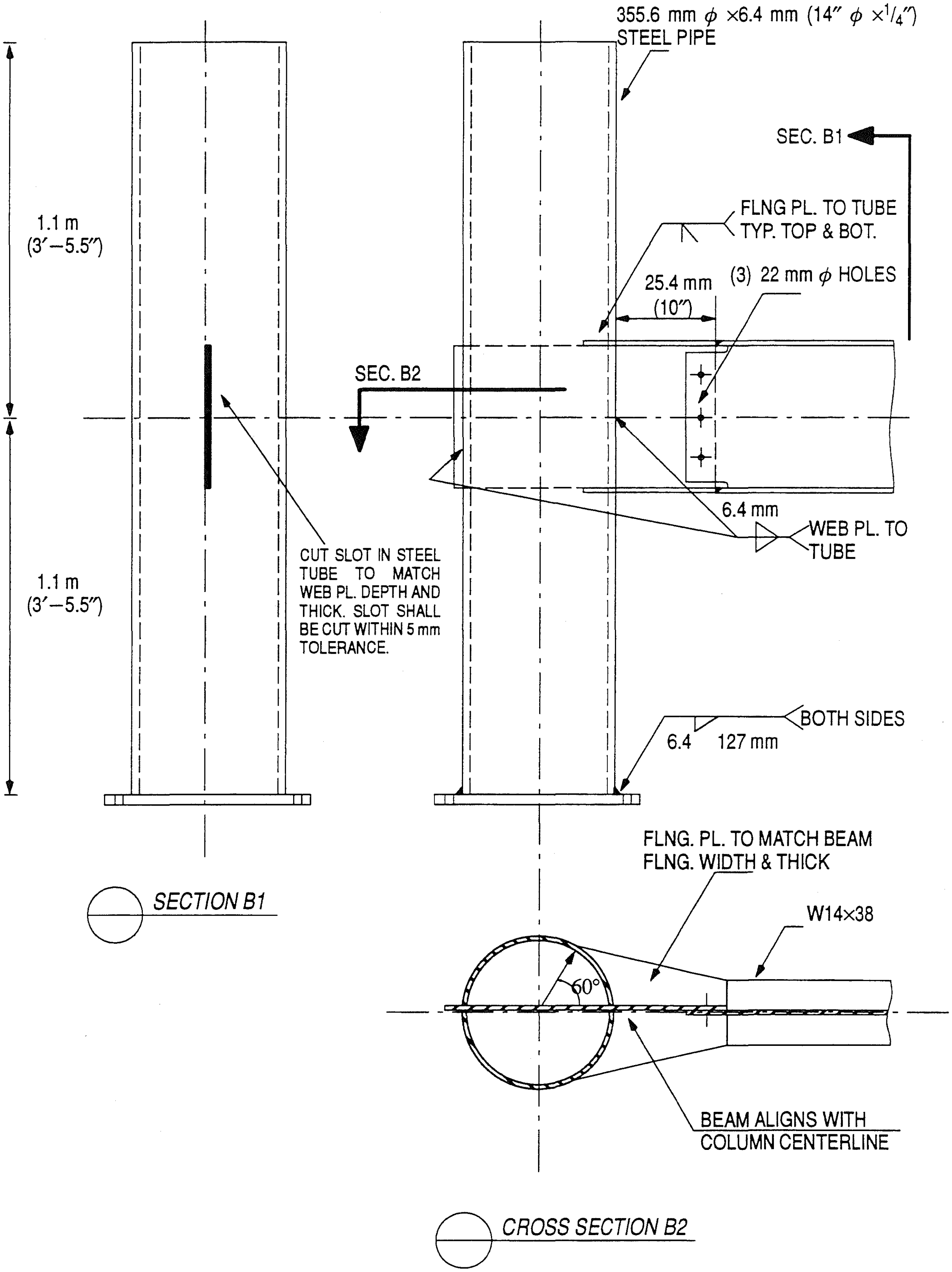

Figure 4.2. Simple Connection with Continuous Web Plate, *Type IA*

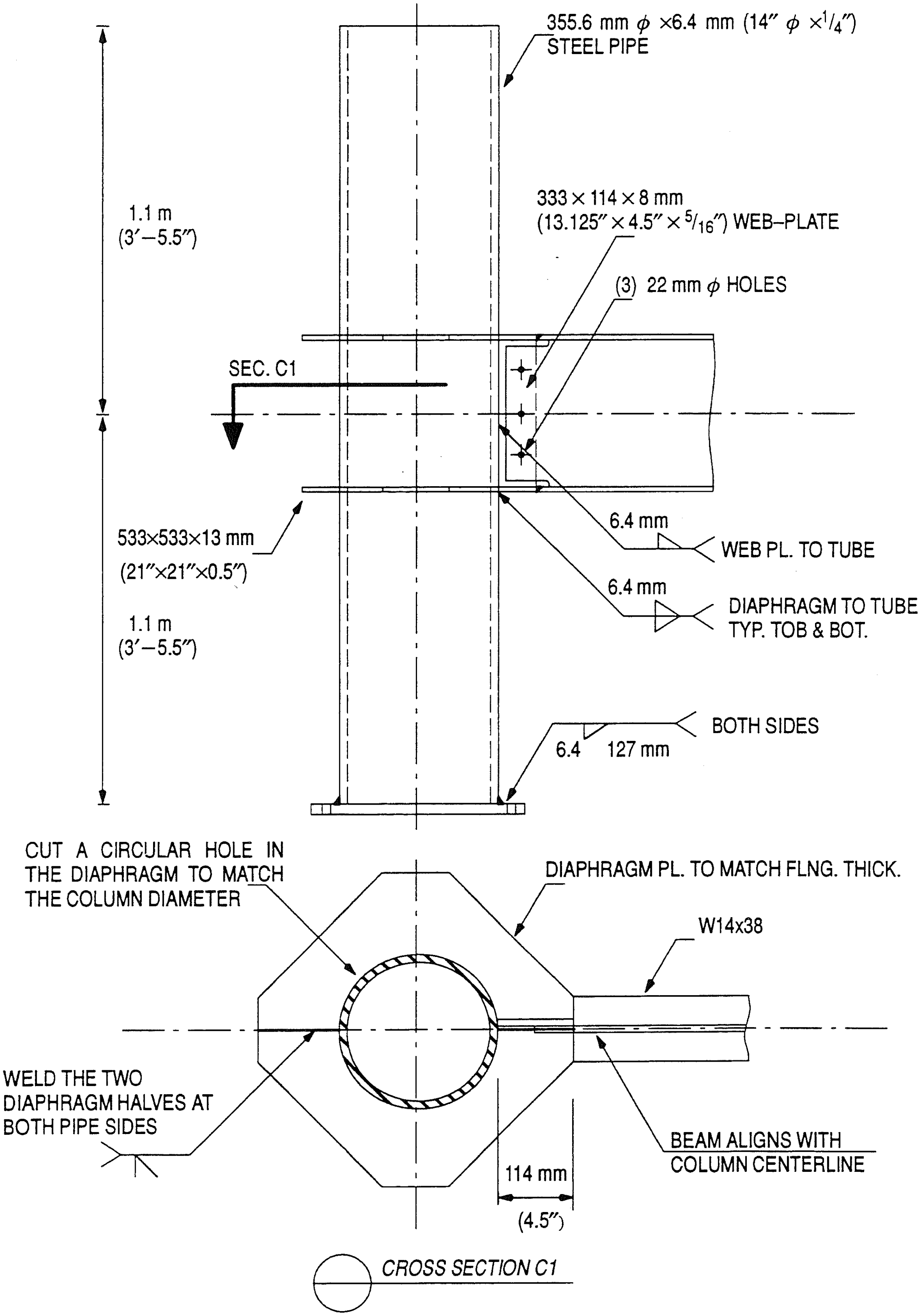

Figure 4.3. Connection w/ External Diaphragms, *Type II*

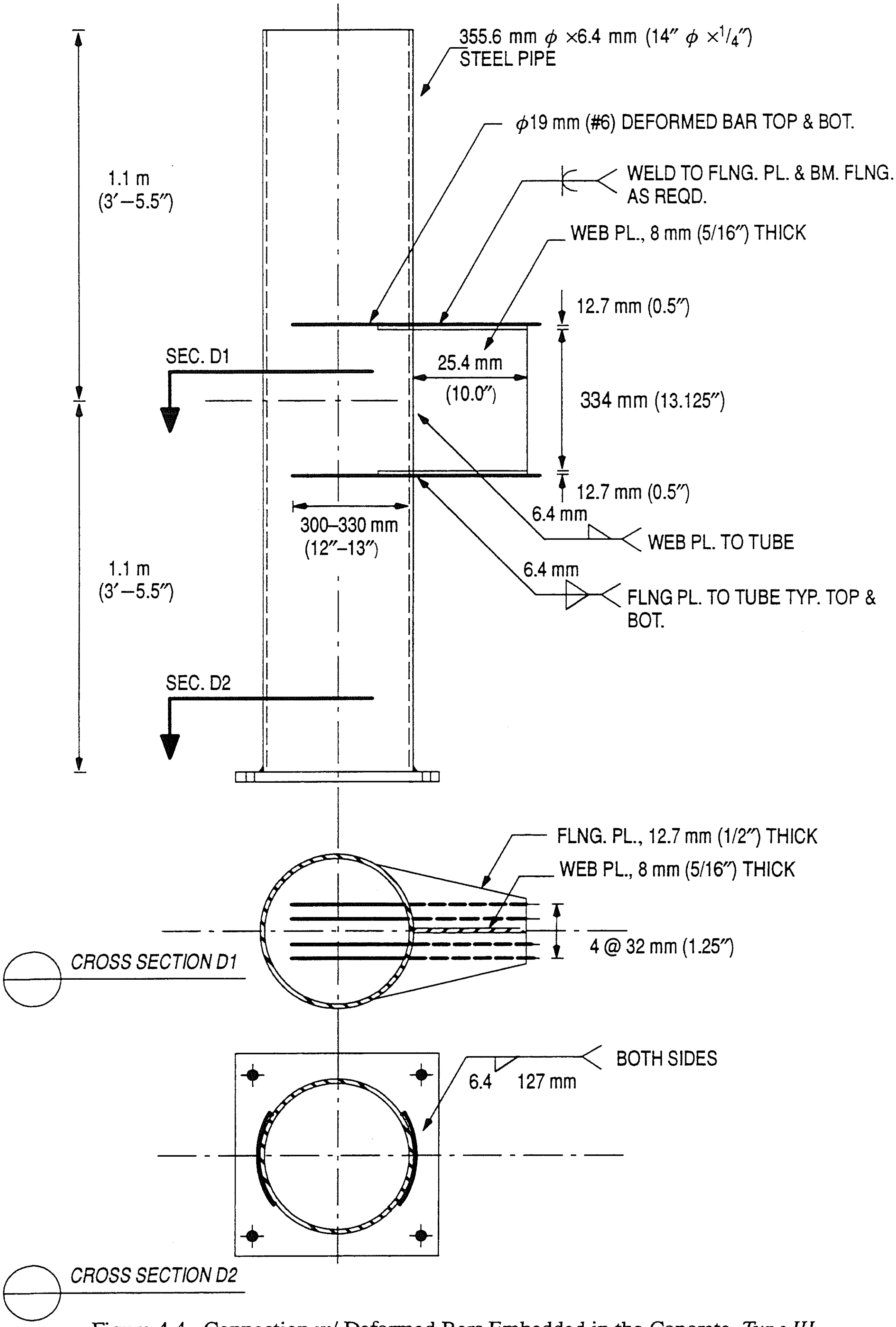

Figure 4.4. Connection w/ Deformed Bars Embedded in the Concrete, *Type III*

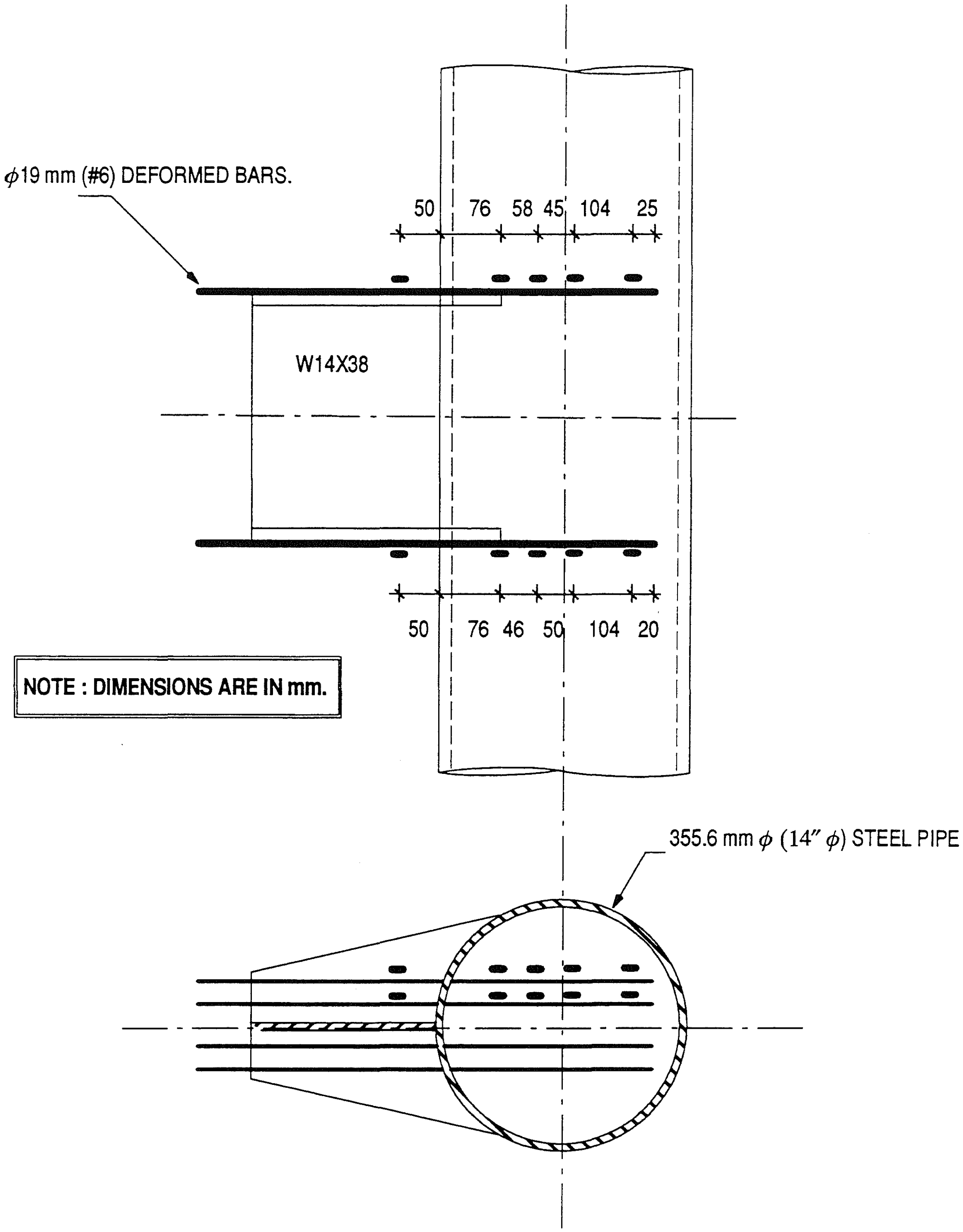

Figure 4.5. Deformed Bar Instrumentation, Connection *Type III*

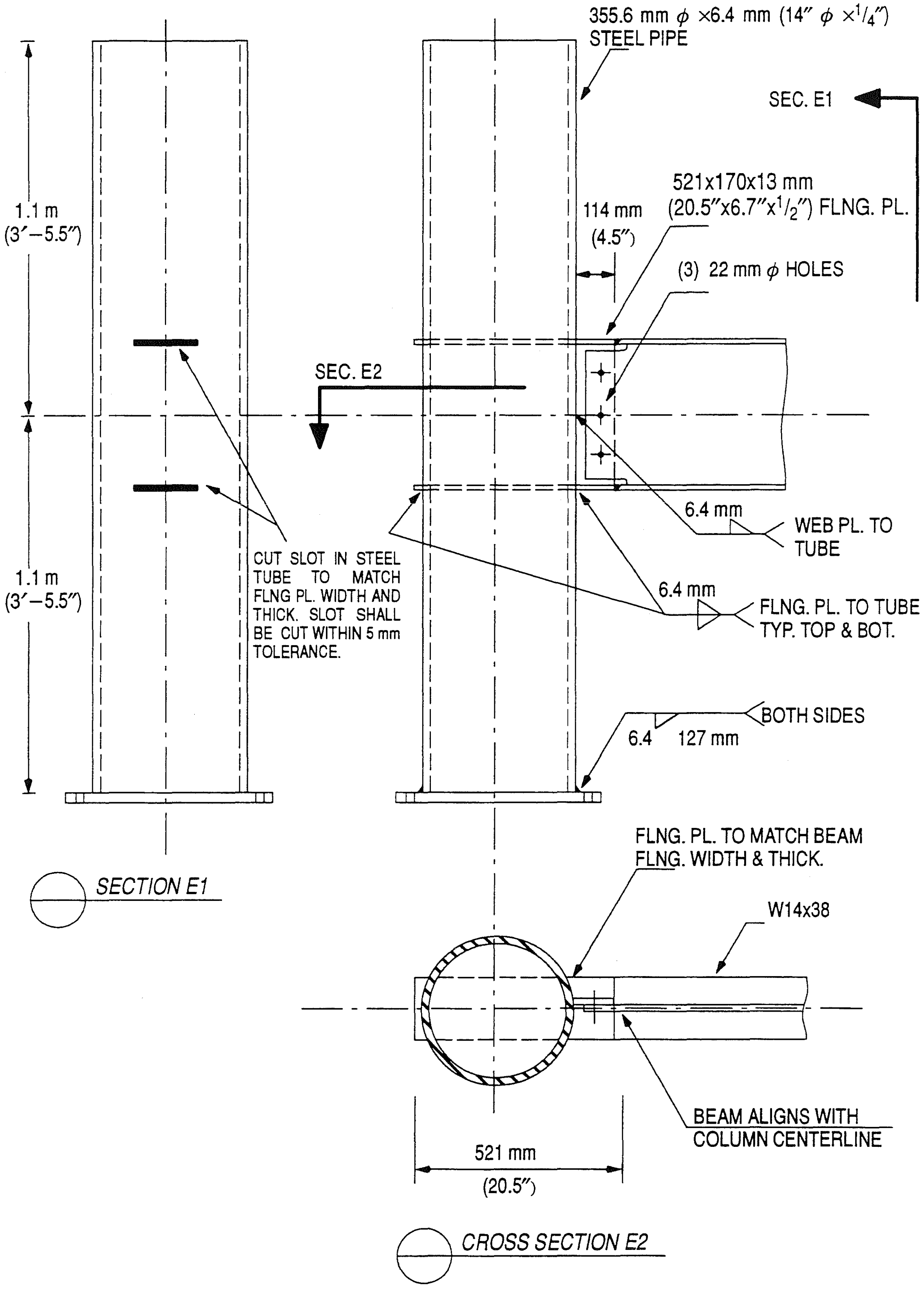

Figure 4.6. Continuous Flanges, *Type VI*

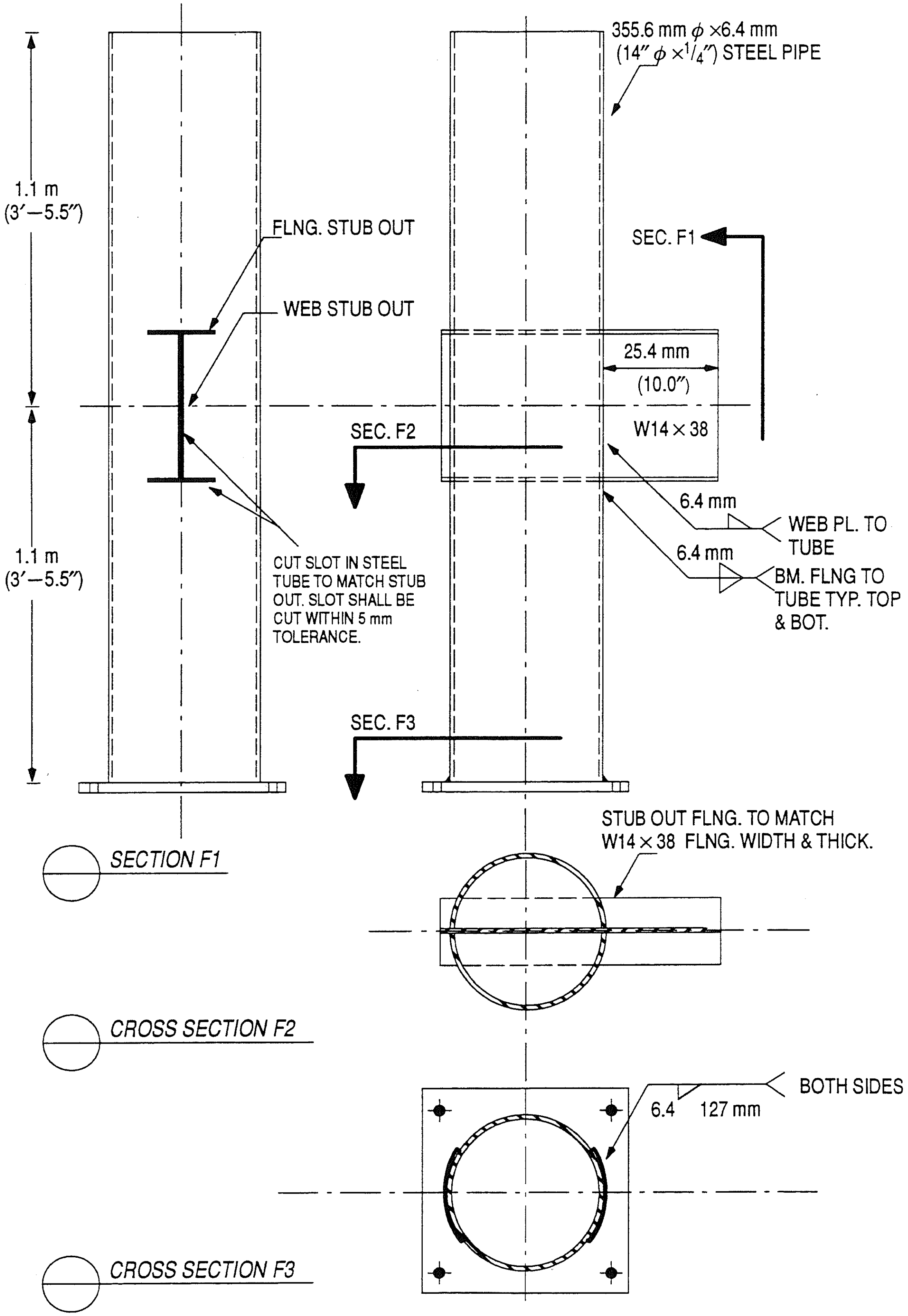

Figure 4.7. Continuation of Cross Section through Tube Column, *Type VII*

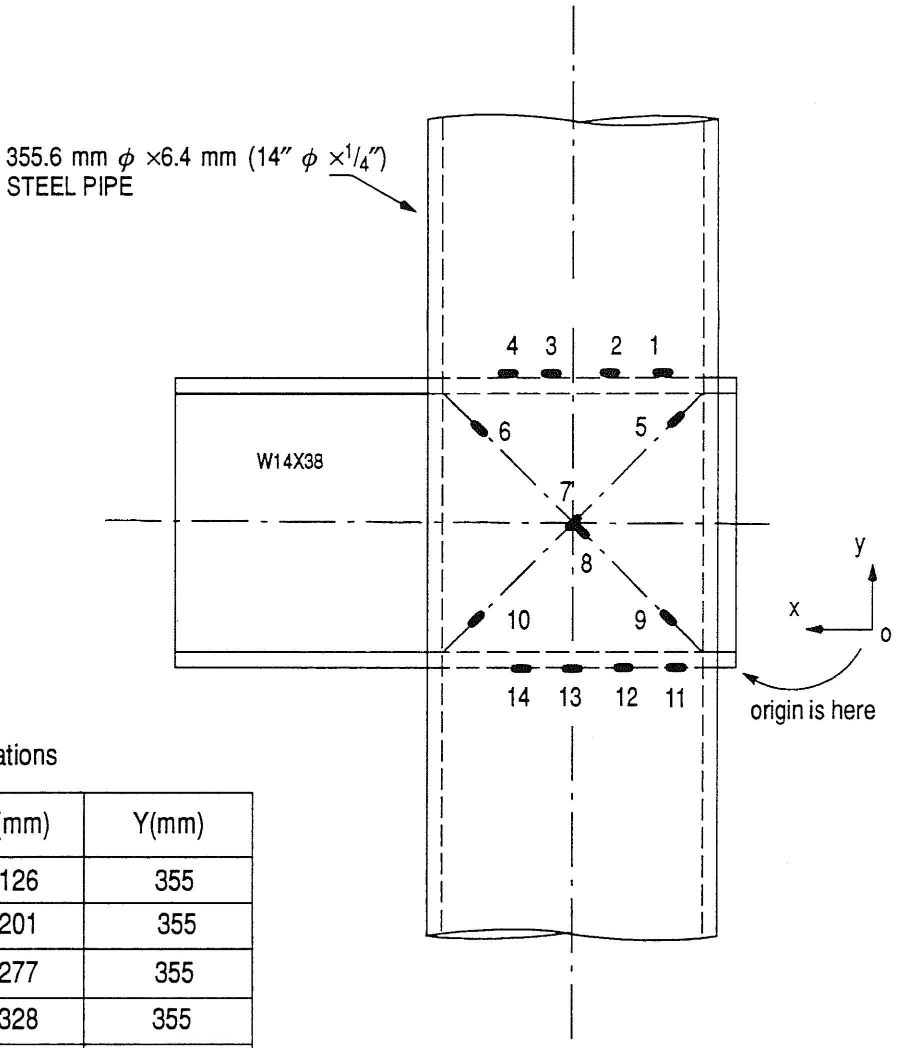

Strain Gauge Locations

Strain Gage	X (mm)	Y(mm)
1	126	355
2	201	355
3	277	355
4	328	355
5	85	307
6	382	318
7	220	187
8	210	167
9	75	48
10	375	51
11	124	0
12	200	0
13	270	0
14	328	0

Figure 4.8. Instrumentation of the Beam Stub within the Column, Connection *Type VII*

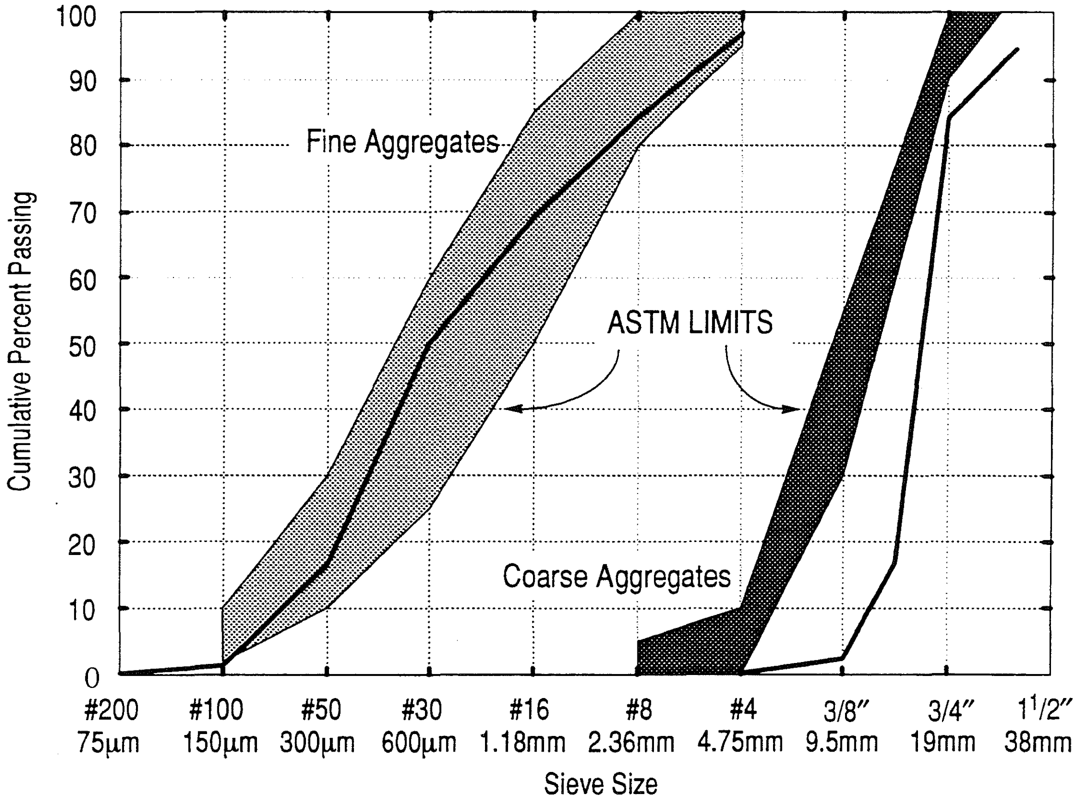

Figure 4.9. Gradation of the Aggregate

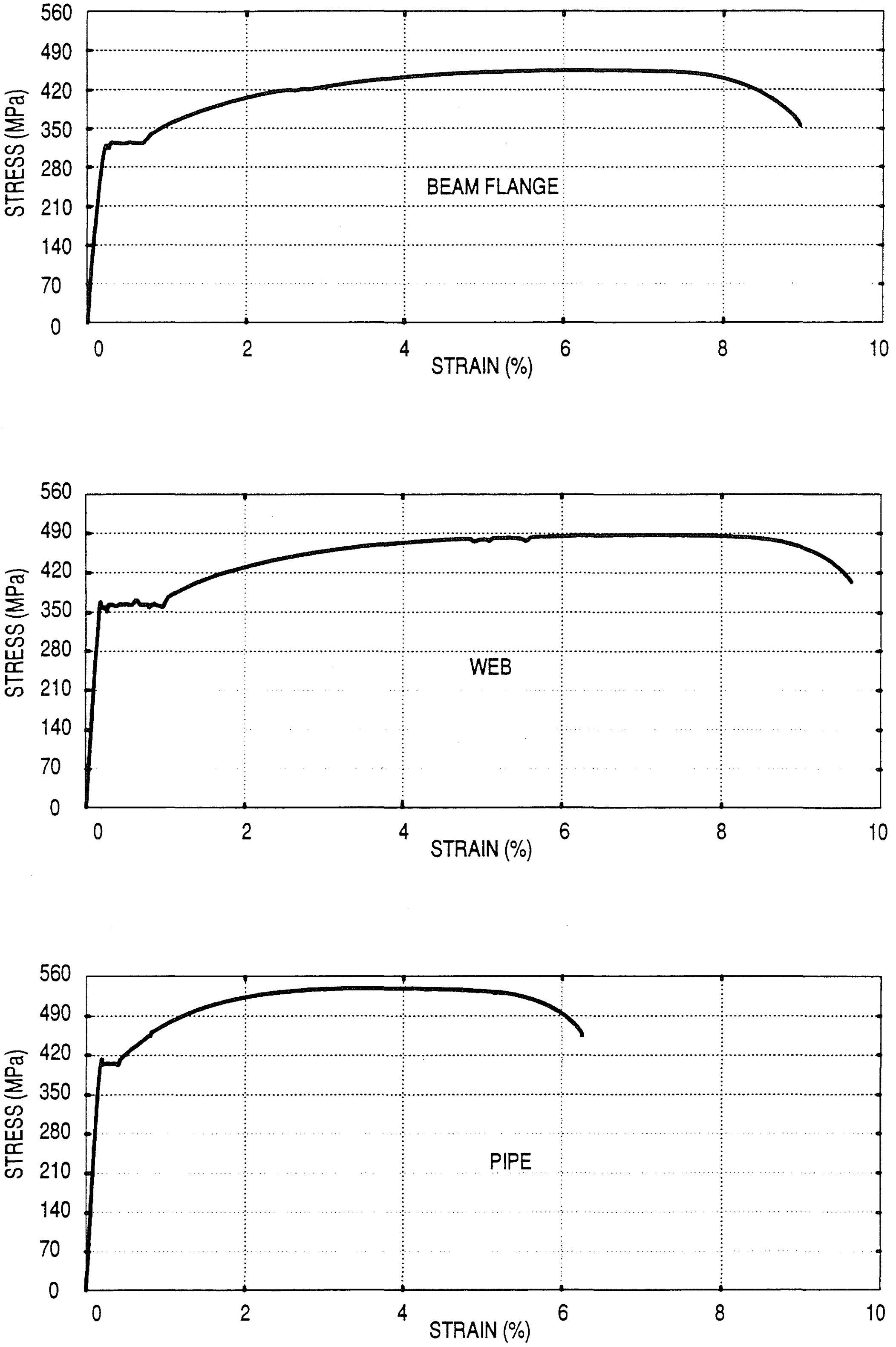

Figure 4.10. Stress–Strain Relationships for the Steel Elements

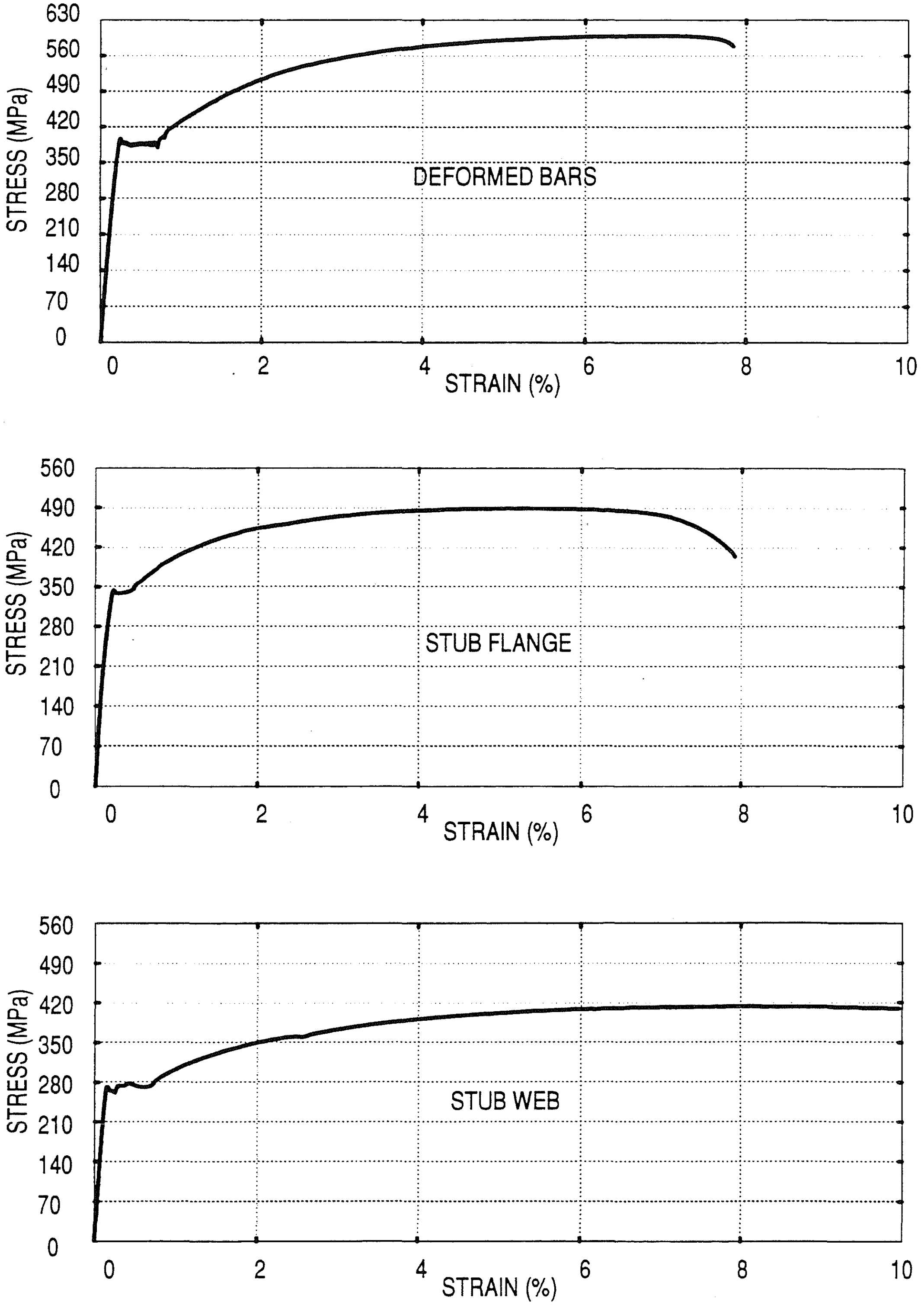

Figure 4.10. Stress–Strain Relationships for the Steel Elements, *Continued*

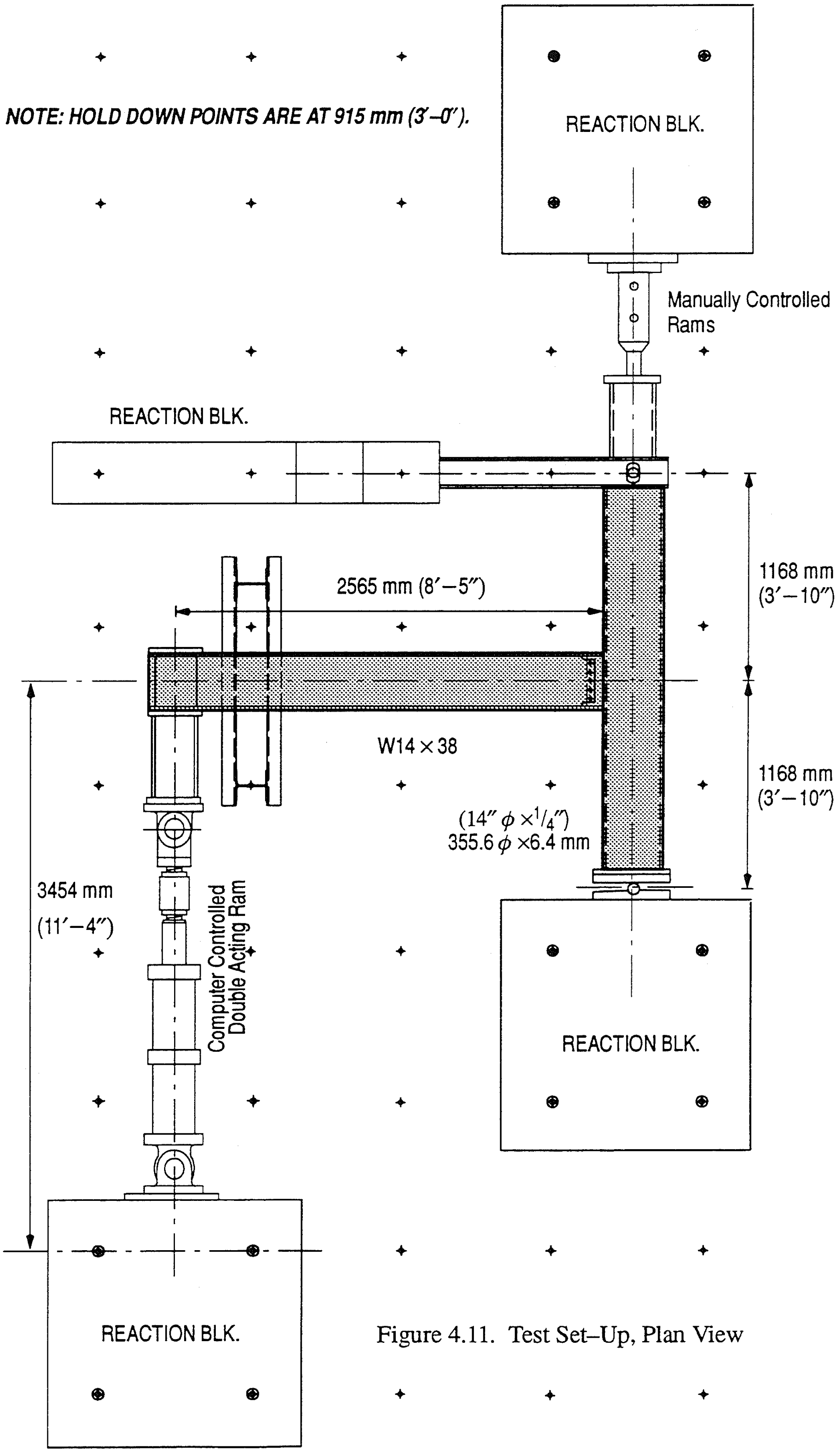

Figure 4.11. Test Set–Up, Plan View

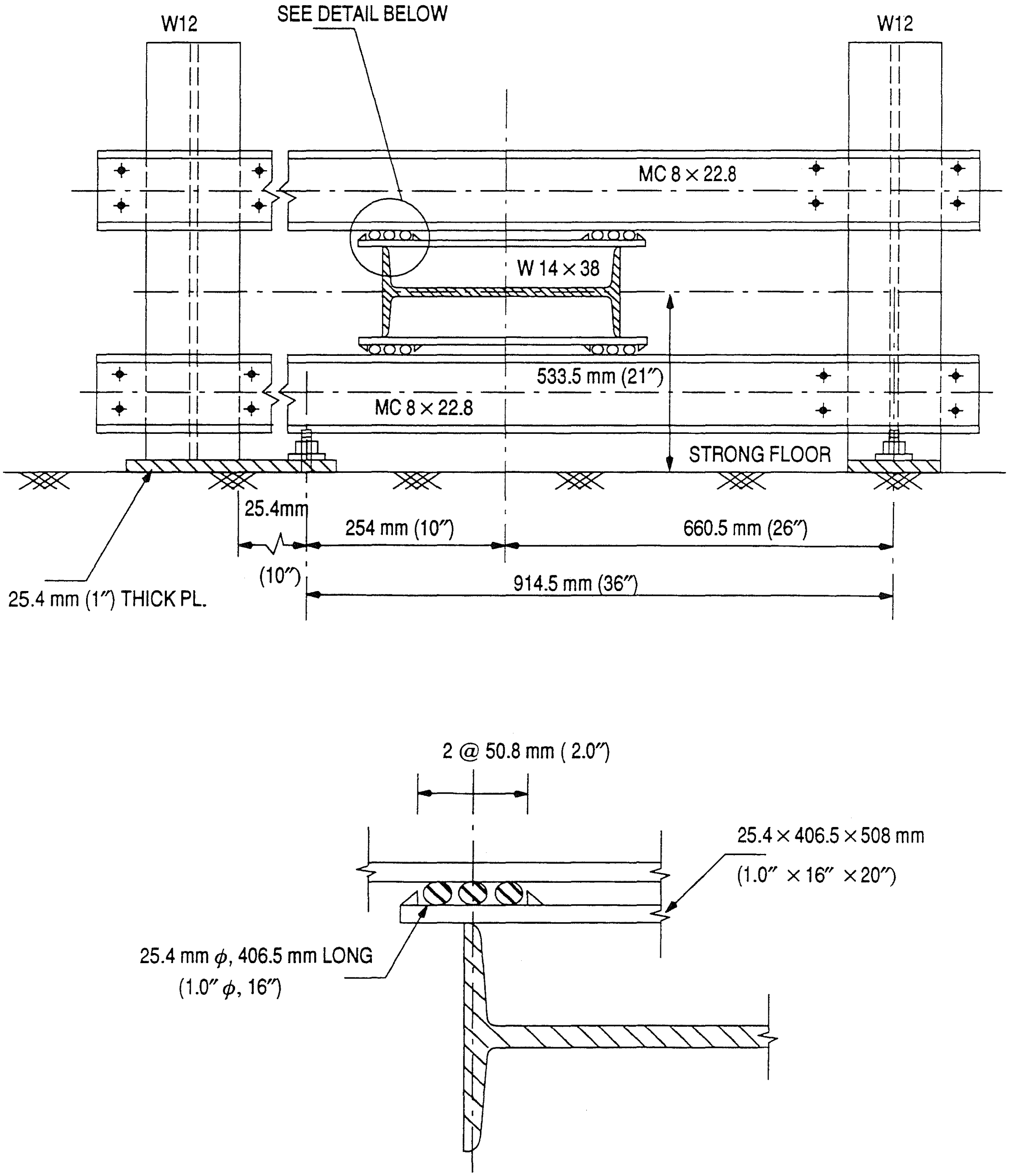

Figure 4.12. Lateral Support for the Girder

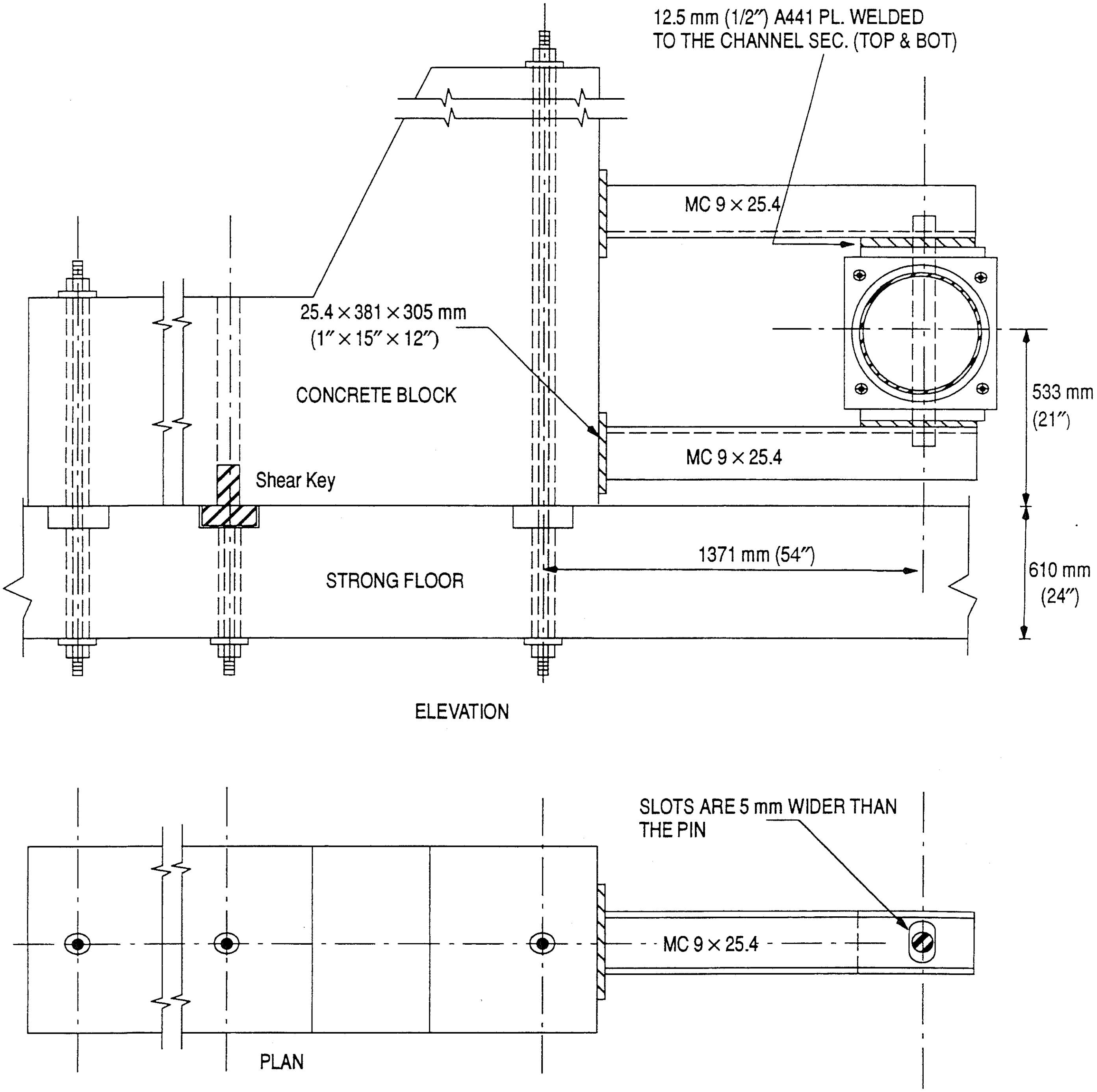

Figure 4.13. Lateral Support at Axial Actuator

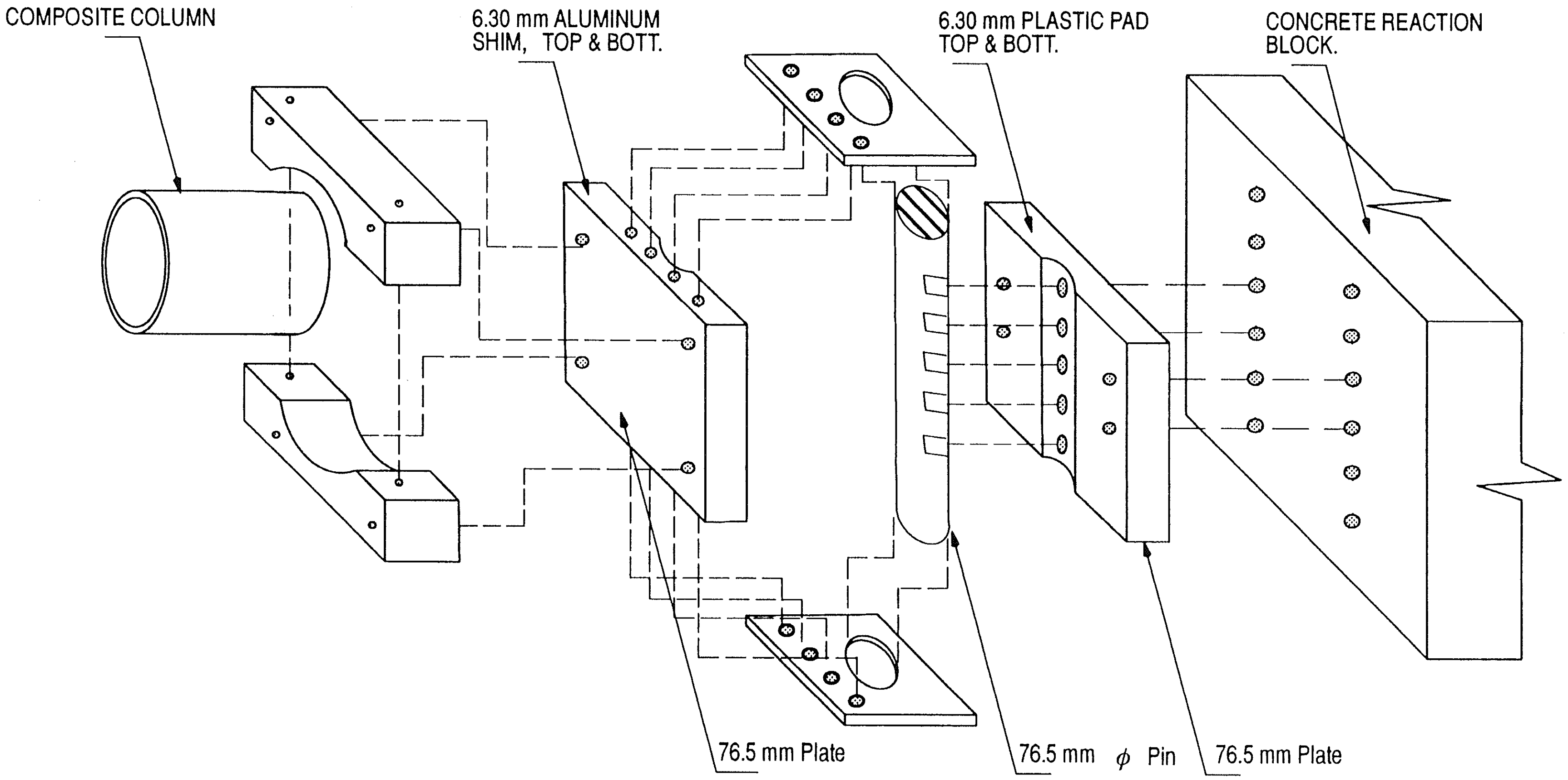

Figure 4.14 Pin Support at One End of the Column

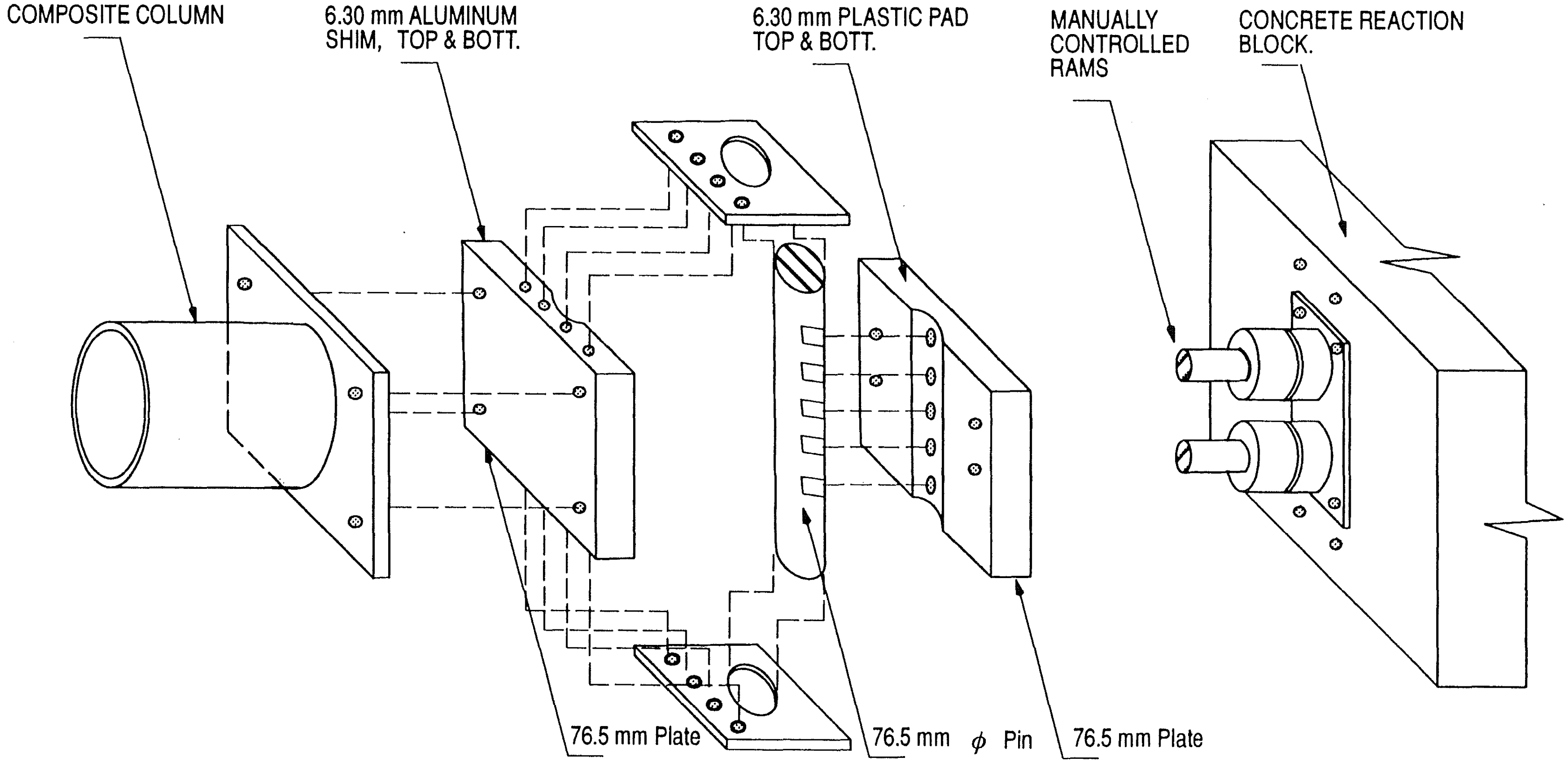

Figure 4.15. Pin Support at the Other End of the Column

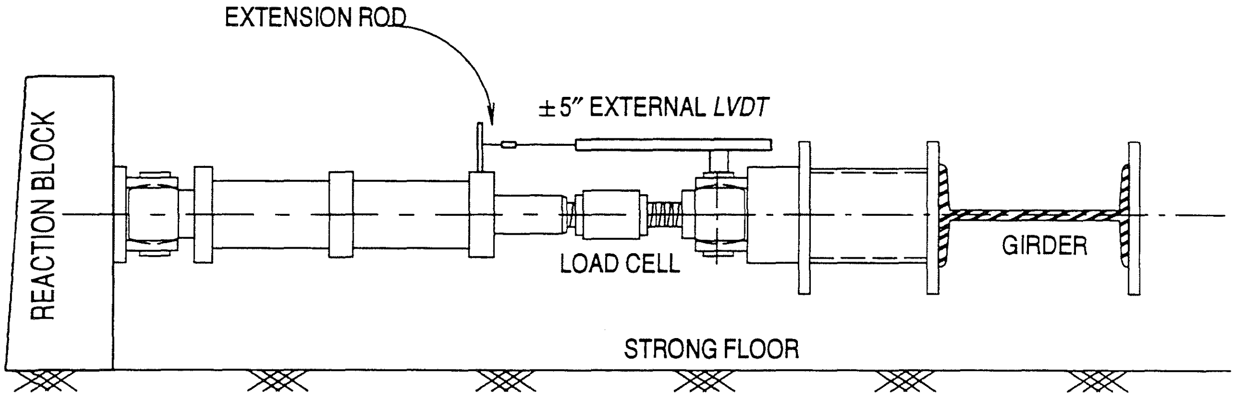

a.) External *LVDT* on Top of the Actautor.

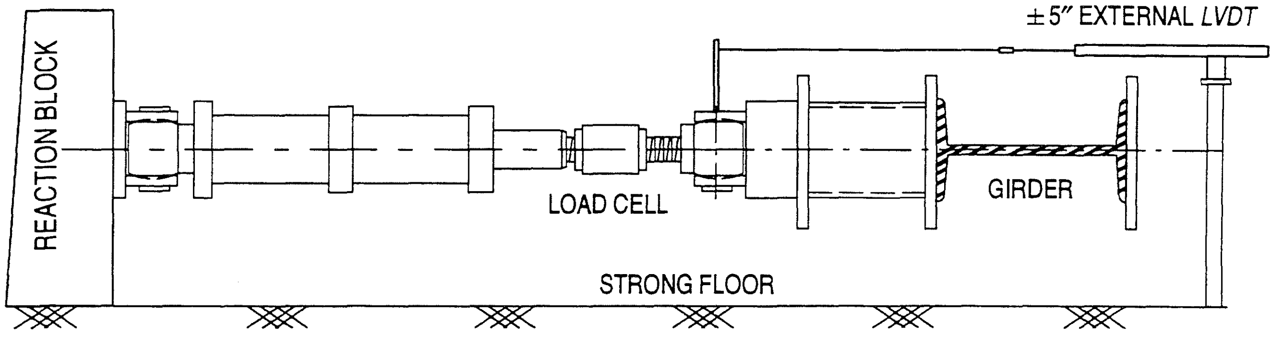

b.) External *LVDT* fixed to the Strong Floor.

Figure 4.16. External *LVDT* Positions

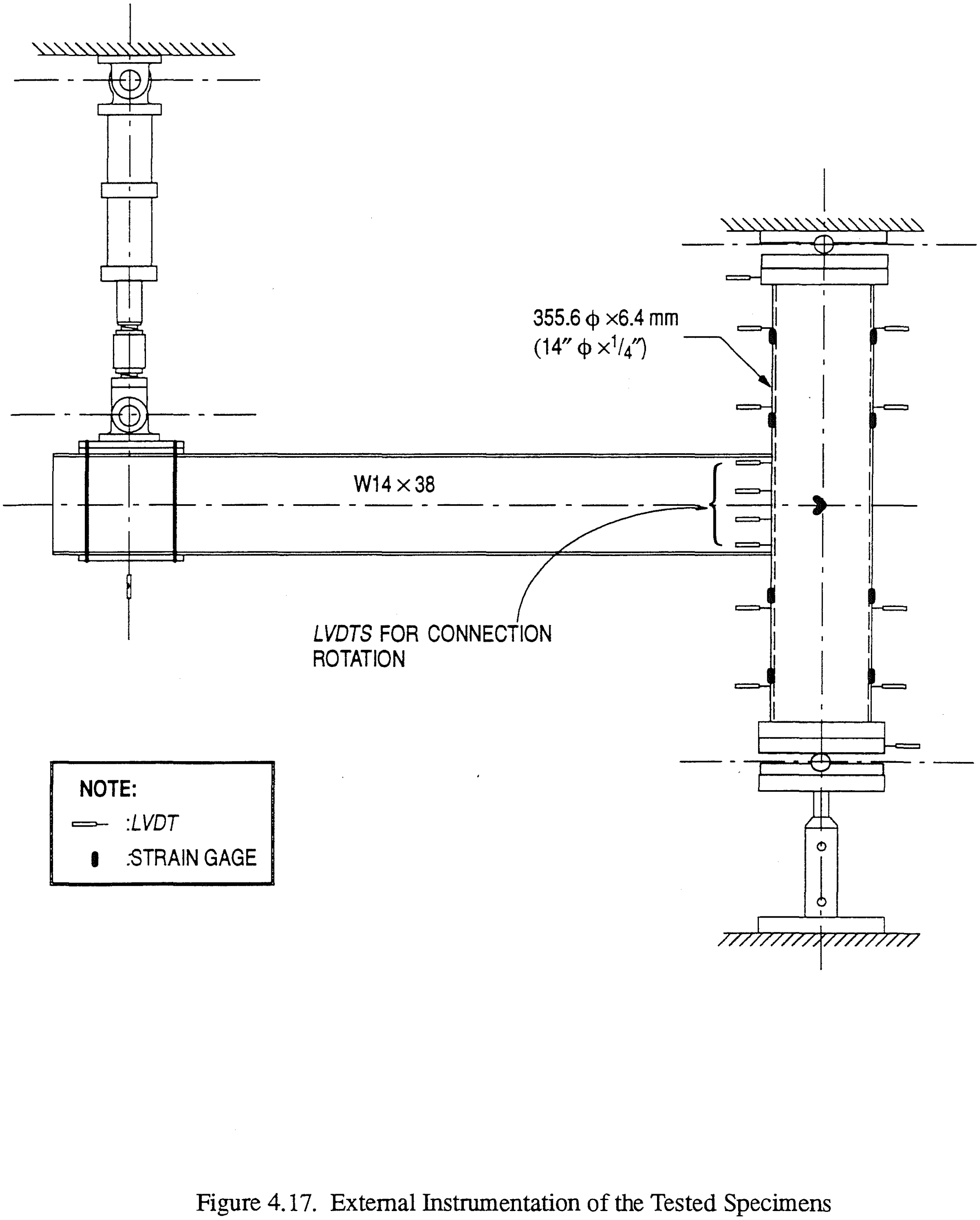

Figure 4.17. External Instrumentation of the Tested Specimens

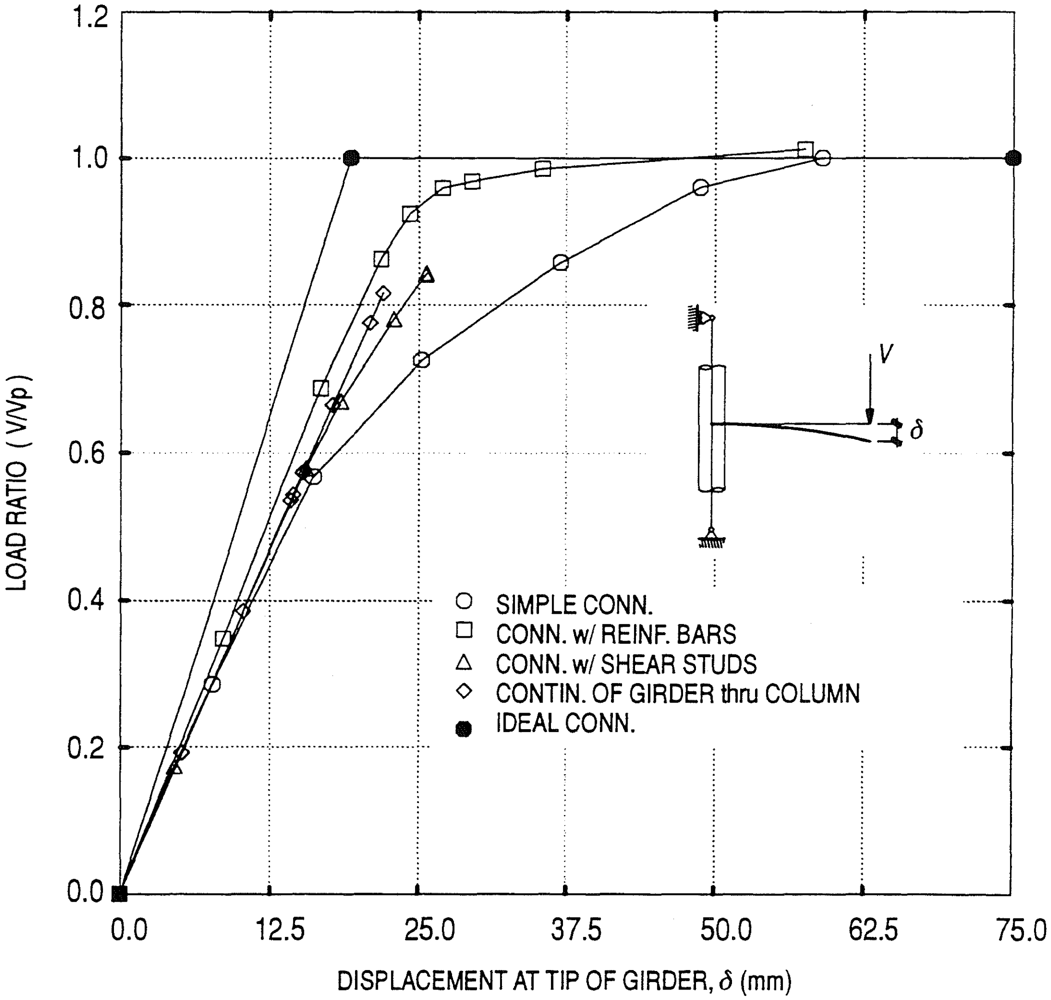

Figure 4.18. Analytical Load–Deflection Curves for some of the Tested Connections

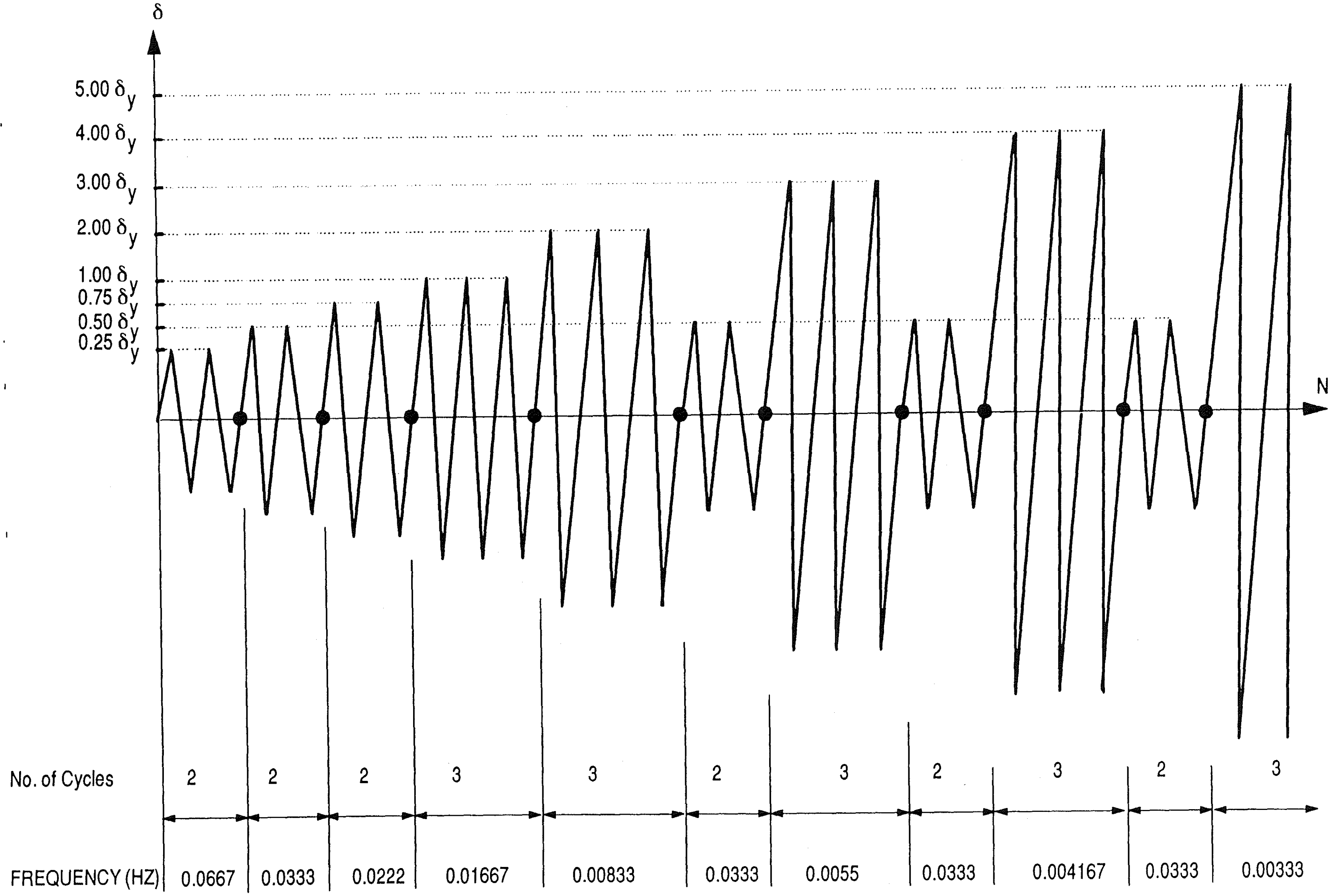

Figure 4.19. Load History Imposed on the Test Specimens

CHAPTER 5

ANALYSIS OF THE EXPERIMENTAL RESULTS

5.1 INTRODUCTION

While the analytical study can identify the potential efficiency of various details to resist bending, an experimental program was needed to determine the inelastic, cyclic behavior of the more promising connection details. Therefore, six large–scale specimens were tested in this research program. These specimens represented connection *Types I, IA, II, III, VI*, and *VII* shown previously. This chapter presents the measured cyclic response of each specimen. In many cases, when possible, analytical results will be shown for comparison.

5.2 SIMPLE CONNECTION, TYPE I

Figure 5.1 shows the hysteretic force–displacement behavior of the simple connection, *Type I*. The imposed displacement at the girder tip was normalized by the cantilever length measured to the center–line of the CFT column. The girder load was normalized by the shear force, V_p, needed to develop the plastic moment, M_p, in the girder at the face of the CFT column.

The elastic response of this connection stiffened slightly compared to the initial conditions. Several causes might have participated in this behavior: it might have been caused by shrinkage of concrete from the pipe wall, a weak layer of concrete in direct contact with the tube wall, or tolerance of the connections in the test set–up. However, the variation of the stiffness was not significant.

This detail barely developed the girder yield strength in only one direction of the cyclic load. During the second cycle of 1.50% displacement of the girder tip, the flange tip on the connection stub fractured in the heat affected zone. By the end of the third cycle at this deformation level, the connection strength decreased by about 20%. Failure of this connection occurred due to this crack, initiated at the flange tip, eventually propagating into the tube wall. Only one flange fractured, while the weld and the tube wall at the other flange remained primarily intact. This resulted in lop–sided cyclic behavior, and the connection exhibited clear unsymmetric behavior. The fracture in this flange continued to propagate each time it was subjected to tension during the cyclic deformation. Strength and stiffness continued to deteriorate with further crack propagation. The other flange, however, did not fracture. Therefore, the force–displacement behavior was reasonably stable when this flange was stressed in tension. In this direction, the connection shear strength increased 10% as the cantilever tip displacement increased from 1.50% to 2.75%.

During the second cycle of 2.25% normalized displacement, initial signs of pipe fracture and weld fracture between the pipe and the flange were observed. This flange failure is shown in Figure 5.2. As a result of this flange fracture, the shear strength of the connection decreased to about 60% of the girder shear strength. Upon subsequent deformation cycles at 2.75%, significant deformation demand was imposed on the web plate as the fracture propagated in the connection flange. This caused the fillet weld between the web plate and the pipe to fracture, as shown in Figure 5.2b. Consequently, the connection lost most of its shear capacity during the second cycle, and it was clearly evident that the connection had no more shear strength during the third cycle of 2.75% tip deformation. This represented clear failure of the specimen, and hence, the test was stopped. The other flange showed no visible signs of fracture, and the shear strength did not deteriorate when this flange was loaded in tension. However, tube wall distortion was evident locally, and the mill scale flaking was apparent around the tube and stub flange surfaces.

The concrete core in the connection region, was examined through the tearing in the pipe wall, and by removing part of the tube skin in the connection vicinity after the test was completed. The concrete exhibited no signs of distress or crushing.

The moment–rotation relationship for this connections is shown in Figure 5.3 and the analytical behavior of the connection is also shown for comparison. Computed connection rotation was calculated relative to the composite column center–line. Four *LVDTs* were mounted across the depth of the girder at the beam stub edge, and were used to calculate the connection rotation. The moment–rotation relationship provides a good indication of the connection behavior, since it provides better information on localized behavior of the connection stub.

In general, the moment–rotation relationship reflected the force–displacement relationship. One notable difference, however, between the shear force–deformation and the moment–rotation behavior was the unsymmetric behavior of the rotation amplitudes. Displacements were imposed at the cantilever tip, and therefore cyclic deformations were symmetric. However, cyclic rotations were not symmetric because of the unsymmetric fracture of the connection. Due to the modest local buckling of the pipe wall around the girder flanges, and to the fracture of some of the jointed elements in the simple connection, rotations as large as 0.038 radian were obtained. However, the maximum rotation was 0.022 radian when the load reversed. Finally it should be noted that the connection developed 87% of the plastic flexural strength of the girder when the fractured flange was in tension, but produced almost the full strength when the load reversed.

5.3 CONTINUOUS WEB PLATE CONNECTION, TYPE IA

Behavior of the previous simple connection, *Type I*, illustrated that once the flange fractured, the shear capacity deteriorated rapidly. Therefore, for the simple welded detail the loss of shear strength quickly followed the loss of the flexural capacity. In an effort to mitigate this shear capacity loss, the web plate was continued through the pipe in connection *Type IA*.

The nonlinear force–displacement behavior of this connection is shown in Figure 5.4. This figure illustrates that the continuous web detail exhibited significant improvement in behavior compared to the simple detail, *Type I*. For this connection, mill scale flaking on the girder flanges was observed at 0.75% cantilever tip displacement. Mill scale flaking on the steel tube, above and below the girder flanges, occurred at 1.5% cantilever tip displacement. However, the force–displacement behavior indicated that the connection continued to strain–harden up to the first cycle of 3.0% girder tip deformation. Prior to this displacement amplitude, hysteresis behavior for each cycle with same deformation amplitude was almost identical.

At approximately 3.0% tip deformation, the force–displacement behavior began to deteriorate. This deterioration coincided with tube wall tearing and weld fracture. During the first half of the second imposed 3.0% deformation cycle, the pipe fractured at the tip of the tension flange. As this second cycle of 3.0% deformation reversed, another fracture occurred in the pipe, as well as the groove weld between the tension flange and the tube wall. Each fracture was less than 25 mm (1″) in length, and this tube wall fracture resulted in about an 8% decrease in the connection shear strength. Each tube wall fracture flared out from the connection stub flange tip, above and below the flange. By the end of the third cycle at this 3.0% deformation amplitude, a 20% decrease in the shear strength of the connection was observed. In addition to the pipe wall fracture at the flange tips, the pipe wall fractured near the center of the connection. This fracture occurred directly above each flange. Tearing propagated exclusively in the tube wall as shown in Figure 5.5.

Local flange buckling was observed during the first cycle of 3.25% girder tip displacement. These local buckles were small, and the flange buckling generally recovered upon load reversal. A 38 mm (1.5″) fracture in the web plate was observed during the second cycle of 3.25% tip deformation. This fracture initiated at the flange–web intersection on the tension side of the connection, and propagated toward the connection center. This web fracture caused a 16% decrease in the shear strength compared to the first cycle of 3.25% tip displacement. At this deformation level, the pipe wall tearing was sufficiently wide enough to expose the web plate inside the steel pipe. It was clear that web tearing adjacent to the opposite flange, just inside the tube wall, initiated in previous deformation cycles. This web fracture also propagated toward the connection center, yet it remained inside the tube wall. Both web plate fractures, the one outside the steel tube and the one inside, propagated until they approached the girder center. The only visible damage to the pipe occurred adjacent to the connection. No damage was observed at the side of the pipe opposite to the connection.

The moment–rotation hysteresis of this connection, shown in Figure 5.6, closely resembled its force–displacement behavior. This connection detail was able to sustain rotations of less than 0.014 radian before the flexural strength deteriorated rapidly. The flexural strength of the connection was approximately 25–30% higher than the plastic bending strength of the girder. The maximum rotation was approximately 0.045 radian, however, only 35% of the plastic bending strength of the girder remained. Behavior was not symmetric, upon load reversal, the maximum rotation was about 0.039 radian, and only 25% of the plastic bending strength remaining.

5.4 CONNECTION WITH EXTERNAL DIAPHRAGMS, TYPE II

Applying the girder tensile forces directly to the face of the pipe had detrimental effects on the simple connection performance. External diaphragm plates were used in this connection in an effort to distribute the girder flange tensile forces to the back side of the pipe. As shown in Figure 5.7, this connection continued to strain–harden up to about 2.75% cantilever tip displacement. The connection shear strength was approximately 22% higher than the girder shear strength. However, the connection behavior was not quite symmetric, and the maximum shear strength for load reversal was about $1.13V_p$.

At 2.75% cantilever tip displacement, mill scale flaking was clearly evident on the diaphragm and the girder. The presence of the re–entrant corner between the diaphragm and the girder created high local stresses. These were most likely compounded by large residual stresses due to the full penetration groove weld at that location. These stress concentrations led to a 38 mm (1.5″) long fracture in the tension diaphragm during the first half of the second cycle of 2.75% deformation. Upon load reversal, a similar fracture was observed in the same location on the opposite diaphragm plate. These fractures propagated, to about 50–64 mm (2–2.5″) in length, by the end of the third cycle of 2.75% tip displacement. By the end of these imposed cycles, the remaining shear strength of the connection was approximately 80% of the shear strength of the girder.

As the deformation amplitude increased to 3.25%, the original fractures that were in the flange propagated to the pipe wall. A second fracture occurred in the pipe wall, initiated directly above the diaphragm plate. Figure 5.8 shows the fracture in the diaphragm for this specimen. The tearing in the pipe wall caused an additional 30% decrease in the shear strength. Increasing the displacement amplitude to 3.75% initiated a third fracture in the pipe wall, eventually joining the existing fracture in the diaphragm plate. At the end of the three cycles of imposed 3.75% deformation, the connection had lost about 50% of the girder shear strength. The opening and closing of these cracks, upon subsequent deformation cycles, explains the pinching of the hysteresis loops.

At large–amplitude displacements, the full joint penetration groove weld, between the connection stub and the girder flange, fractured. This fracture propagated across half the flange width. Further, the pipe wall fractured along the full depth of the beam web at these high deformation levels. This pipe fracture occurred in the heat affected zone adjacent to the fillet weld that attached the web plate to the pipe. At approximately 4.0% tip displacement, local buckling was observed in one of the diaphragms when it was subjected to tension. This happened because the diaphragm was subjected to high shear distortions resulting from the various fractures that occurred in the connection region. However, the connection did not exhibit significant strength deterioration between 4.5% and 5.5% girder tip displacement. The concrete core was observed through the pipe fractures, and there were no apparent signs of crushing of the concrete core behind the web or the diaphragm plates. Due to the extensive damage to the connection, the test was stopped at about 5.5% normalized girder tip displacement.

Figure 5.9 illustrates the *M–θ* behavior of this connection. Because of the unsymmetric failure of the connection, the shape of the hysteretic curves were quite different than the force–displacement behavior. The connection was able to sustain only rotations less than 0.01 radian before it lost more than one–third of its flexural strength. This sharp decrease in the flexural strength occurred at the onset of the diaphragm fracture. The strength continued to deteriorate gradually as fractures propagated in the diaphragm and the pipe wall. At high deformation cycles, the connection behavior stabilized, and very small strength deterioration was observed. The maximum rotation was approximately 0.038 radian at $0.50M_p$. Upon load reversal, the connection sustained a maximum rotation of approximately 0.048 radian at $0.25M_p$.

To investigate the force transfer mechanism in the diaphragm plates, strain gages were applied to one diaphragm plate. Strain gage locations are shown in Figure 5.10. Strain gages at locations *2* and *3* indicated that the portion of the diaphragm, reasonably far away from the girder flange, did not experience significant compressive strains. Even the strain gage at location *1* experienced very small compressive strains. Therefore, most of the girder flange compressive forces were distributed directly to the concrete core in bearing. However, due to the flexibility of the tube wall, the girder tensile stresses were transferred to the diaphragm plates. The gage at location *1* recorded a maximum tensile strain of about 80% of the yield strain, while only one–fifth this value was recorded at strain gage locations *2* and *3*. This illustrated the need to increase the length of the diaphragm by shifting the girder farther from the CFT column. Analytical results indicate that creating a more direct path for tensile stresses produced a better distribution of the girder flange forces to the diaphragm.

5.5 CONNECTION WITH DEFORMED BARS, TYPE III

Cantilever tip deformation relative to the shear force for this connection is shown in Figure 5.11. As indicated by this figure, adding deformed bars improved the behavior of the simple *Type I* connection significantly, while the increase in the fabrication cost was approximately 25%. This connection exhibited stable strain–hardening behavior. Further, little stiffness deterioration was observed up to failure of the deformed bar. At 3.0% tip displacement, mill scale flaking was observed on the surface of the girder flanges. Initial wall tearing occurred at a tip displacement of approximately 3.75%, however, this tearing was located only in the tube wall between the openings for the deformed bars. This minor wall tearing did not affect the inelastic performance of this connection. Local flange buckling was also observed at a deformation level of approximately 3.75%. This buckling occurred outside the region of the deformed bars. This suggests that the connection was strong enough to initiate significant strains in the girder beyond the connection stub.

Upon subsequent cycles, the connection stub integrity began to deteriorate. One deformed bar buckled between the tube wall and the second weld that attached the bar to the flange. Failure of this connection was due to fracture of the deformed bars. Three of the four bars failed by tension rupture, while one bar pulled out of the concrete core. Each deformed bar that failed in tension ruptured between the tube wall and the first weld location that attached the bar to the girder flange. The bar pull–out was accompanied with bar buckling as the load reversed. The bar buckling did not have significant effect on the connection strength or stiffness. This indicates that once buckling occurred, the connection relied on direct bearing to distribute the flange compressive forces to the concrete core.

Failure of the deformed bars placed high flexural demand on the web plate, which led to the fracture of the fillet weld between the pipe wall and the web plate. The failure of this connection is shown in Figure 5.12. This connection exhibited stable behavior up to a cantilever tip displacement of approximately 4.0%. No significant stiffness or strength deterioration was observed prior to the fracture of the deformed bars.

The moment–rotation behavior, shown in Figure 5.13, illustrates the benefits of using deformed bars to transfer some of the girder flange forces to the concrete core. Compared to the simple connection behavior shown in Figure 5.3, connection *Type III* exhibited stable, strain hardening behavior, with full hysteresis curves. The strength of the connection developed well in excess of the girder strength, reaching a maximum value of $1.70M_p$ at 3.75% rotation. Further, the connection sustained approximately 5% rotation without showing significant strength or stiffness deterioration, and the connection strength just before failure was approximately 50% higher than the bending strength of the girder.

Figure 5.14 illustrates strains measured at selected locations along the weldable deformed bars. Clearly, these measured strains indicate that the deformed bars developed significant tension and compression. The maximum recorded tensile strain was approximately 30% higher than the bar yield strain, while the maximum compressive strain was about $0.75\varepsilon_y$ at gage location *1*. These strains suggest that over 67% of the flange tensile force was resisted by the weldable deformed bars, and about 50% of the flange compressive force was transferred by the bars. Very little difference was noted between strain gage measurements at locations *1* and *2*. Since the deformed bars developed strains beyond yield, this suggests that the bars were fully developed. Even at gage location *3* tensile strains as high as $1.30\varepsilon_y$ were recorded. This explains the pull–out which characterized the failure mode of this specimen. It is interesting to note that the same bar on the other flange had a maximum tensile strain of about $0.75\varepsilon_y$ at gage location *6*. This indicates that while the first bar experienced slip, the second bar was still anchored in the concrete core.

5.6 CONTINUOUS FLANGES, TYPE VI

One draw back to connection *Type III* might be the use of weldable deformed bars to transfer the girder flange forces. Therefore, a fifth test specimen was fabricated with embedded plates that matched the width and thickness of the girder flanges. No attempt was made to enhance the bond between the embedded plates and the concrete. This lack of bond impacted the hysteretic performance of this connection, as shown in Figure 5.15, compared to other connection types. Due to the significant flange forces, the fillet weld that attached the flanges to the pipe wall fractured at low amplitude cyclic deformations. As the embedded plate was subjected to tension, it slipped through the concrete core without a significant resistance. However, as the fillet weld fragments and the pipe wall interlocked upon load reversal, the strength increased to almost $1.2V_p$.

Mill scale flaking on the girder surface was observed at approximately 1.75% girder tip displacement. Fracture of the weld between the embedded flanges and the pipe also occurred at this displacement amplitude. The fillet weld on the outside of each flange fractured, however, the weld on the opposite side of the flange remained primarily intact. Since the inside weld maintained its integrity, the tube wall fractured upon subsequent load reversals. The pipe wall fracture initiated at both flange tips, and propagated towards the inside of the connection as shown in Figure 5.16. The tube fracture did not cause significant strength decrease, however, the stiffness deterioration was rapid. This resulted in significant pinching of the hysteretic behavior, since the flange plate resisted force only when it stopped sliding. For example, at large displacements, the resisting shear force of the connection averaged about 20% of V_p. However, once the flange engaged at the new displacement amplitude, the shear strength jumped to approximately $0.85V_p$.

The moment–rotation behavior of this connection is shown in Figure 5.17. The maximum connection rotation was between 0.03 to 0.04 radians. Again, although the connection developed about 1.2 times the plastic bending strength of the girder, the hysteretic loops were very pinched. The envelope of the moment–rotation curves of all cycles appears sufficient. However, the pinched hysteretic curves may prevent the satisfactory performance during a seismic event. Due to the slippage of the embedded flanges, no significant strain hardening was observed.

5.7 CONTINUATION OF THE GIRDER THROUGH THE COLUMN, TYPE VII

In the previous specimen, only the flanges were continuous through the concrete core, and serious bond problems were encountered. In this specimen, the entire girder cross section was continued through the pipe. The force–displacement behavior of this connection, as shown in Figure 5.18, exhibited stable strain hardening up to about 4.0% girder tip displacement.

Mill scale flaking appeared on the connection stub flange surface at a deformation amplitude of 1.5%. Upon subsequent load reversals mill scale flaking migrated towards the girder. Local flange buckling in the connection stub occurred at approximately 3.75% normalized cantilever tip displacement, and mill scale flaking was observed at 510 mm (20″) from the steel tube face. The flange buckles straightened when the flange was subjected to tension, but returned upon load reversal.

The fillet weld that attached the beam stub to the pipe fractured during this 3.75% deformation amplitude. This weld fracture initiated at the middle of the stub flange and propagated towards the flange tips. Consequently, larger flange forces were transferred to the back side of the CFT column. This led to the fracture of the fillet weld at the tube back side at 4.0% tip deformation. Web buckling was also observed at 4.0% displacement amplitude.

Deterioration of the inelastic characteristics were observed after the onset of the web buckling. Continued cyclic loading led to tearing in the beam stub flange at 5.5% normalized girder deformation. During the first cycle of 6.0% displacement amplitude, a distinct fracture in the stub flange was apparent. This tearing eventually propagated through the full flange width, and continued into the web during the second cycle of this deformation amplitude. The fracture of the beam stub is illustrated in Figure 5.19.

This connection sustained several cycles of deformation at large displacements, and was able to develop the plastic bending strength of the girder. No significant post–yield stiffness deterioration was noted prior to the buckling of the connection stub web at extreme cyclic deformations. However, once flange buckling occurred, the shear strength of the connection deteriorated by about 30% of the maximum strength. After the test, the steel skin was removed from the concrete core in the region around the connection. No crushing of the concrete core was apparent, and the tube wall did not display signs of mill scale flaking or local buckling.

Figure 5.20 shows that this connection developed 1.25 times the plastic flexural strength of the girder, and had stable inelastic rotations over 0.12 radians. This connection detail sustained rotations up to 0.04 radian before strength deterioration was apparent. Although strength deterioration was apparent, the flexural strength was still equivalent to the plastic bending strength of the girder through almost all of the cyclic deformation history. Further, the hysteretic loops were full and stable even at large rotations.

Measured strains of the embedded flange are depicted in Figure 5.21. Strain measurements at gage location *2*, 136 mm (5.4″) from the tube face, indicated that the girder flange at that location just reached yield. However, this strain was about 45% lower than the axial flange strain just outside the tube wall. This suggested that part of the flange stresses were transferred to the concrete core and the steel pipe. Note that the tensile and compressive strains were on the same order of magnitude, which indicated less participation of the concrete core in resisting the embedded flange forces. At gage location *3*, 206 mm (8.1″) from the pipe face, the tensile strain in the embedded flange decreased by about 20%, and an additional 10% decrease was observed at gage location *4*, 282 mm (11.1″) from the steel pipe face. At gage location *4*, the maximum tensile strain in the flange was almost $0.70\varepsilon_y$, while the compressive strain was approximately $0.30\varepsilon_y$. Relative to the flange tensile strains, the flange compressive strains decreased faster when moving farther away from the steel tube face.

It is interesting to note that the flange tensile strains were nearly linearly related to the girder shear. On the other hand, the flange compressive strains tended to stabilize or decrease with an increase in the girder shear. This might be explained by the force transfer mechanism shown in Figure 5.22. The applied girder shear created compressive stresses in the concrete core near the end of the embedded section. Since the concrete was still in its elastic range, these compressive stresses increased as the girder shear increased. These compressive stresses enhanced the bond due to friction between the concrete core and the embedded flanges. Therefore, more flange stresses could transfer to the concrete core. Further, the interlock between the fillet weld fragments and the tube slots provided a support for the girder flange, thus minimizing the amount of compressive forces transferred to the embedded flanges.

The embedded web strain gage locations and measurements are shown in Figure 5.23. These strain gages were aligned with the diagonal of the connection stub web to monitor potential strut forces that might have developed in the steel section. At gage location *5*, the maximum measured tensile and compressive strains were about $1.0\varepsilon_y$ and $0.8\varepsilon_y$, respectively. At the approximate web center (*gage location 7*), the maximum tensile strain was almost twice as large as the compressive strain. This might be a result of a redistribution of strain in the steel to the concrete by friction or bond, or it could be due to a wider distribution of the strut force at the web center. Clearly, this strut helped the beam web in resisting some of the diagonal compressive forces.

5.8 CONCRETE–FILLED STEEL TUBE RESPONSE

5.8.1 Simple Connection, Type I

During each test, the lateral deformations of the concrete–filled steel tube were measured by *LVDTs* attached along the column center–line. These *LVDTs* were located on each side of the column in the plane of deformations. Strains were used to determine local behavior at different locations along the axis of the column. For convenience, the measured pipe strains were normalized by the pipe yield strain, and they were plotted against the normalized shear in the girder. All strain curves intersected the load axis at a value that corresponds to the initial constant strain resulting from the axial load applied to the composite column prior to the cantilever tip deformations. For all specimens, this constant axial strain was approximately $95\mu\varepsilon$ or $0.05\varepsilon_y$. All strain and deformation curves for each CFT column are shown in *Appendix B*.

Since the girder was welded directly to the steel tube skin in the *Type I* detail, this connection damaged the pipe significantly compared to other specimens. However, the axial strains on the pipe outside the connection region were well below the yield strain. Figure B.1 illustrates that while the steel tube strains approached yield, all strain ratios ($\varepsilon/\varepsilon_y$) remained less than 1.0. Therefore, the severe distortion and damage of the tube wall was localized around the connection region. The maximum measured axial strain in the pipe, far away from the connection region, was approximately

40% of the yield strain. However, axial strains as high as $0.70\varepsilon_y$ were recorded at 126 mm (5″) above the connection stub flange. Strain gages located along the neutral axis of the column away from the connection region, showed that behavior of the steel pipe was primarily axial, with little flexural behavior of the CFT column. These gages measured a maximum axial strain of about $0.10\varepsilon_y$ suggesting the axial load did not change significantly during load reversals. Subtracting the strain due to the applied axial load on the CFT, and assuming a uniform distribution of the axial strain in the CFT, this represented approximately 93% of the maximum applied girder shear. This suggested that only 7% of the girder shear was transferred to the concrete core through bond stresses. It is of interest to note that the steel pipe axial stresses due to the girder shear were at most 5% of the yield stress of the steel pipe.

Small values of the hoop strains were recorded in the vicinity of the connection. These hoop strains appear to be due mostly to Poisson's ratio. This is best illustrated by comparing strain readings at gage locations *3* & *7*, and *12* & *13* in Figure B.1. From these strain measurements, the axial–to–hoop strain ratio was approximately 0.3. Therefore, flexure on the CFT column did not develop significant hoop stresses in the pipe.

Gages at locations *8* through *11* in Figure B.1, demonstrated that part of the flange tensile forces might be resisted by diagonal stresses in the steel pipe. Therefore, maximum tensile strains recorded at these locations were up to $0.70\varepsilon_y$. Comparison of gage locations *8* through *11* suggest that the compression strains are more likely to be distributed to the CFT above and below the connection than it is to be distributed between the connection flanges in the steel tube. Due to the connection failure, smaller diagonal tensile strains were recorded at gage location *11* compared to gage location *8*.

Due to the high stiffness of the composite column, measured deformations of the CFT resulting from flexure were very small. Lateral deformations were equivalent on each side of the connection, and were approximately 2 mm (0.08″). It should be noted that the lateral bracing at the manual hydraulic jacks for the axial load was stiffer when subjected to compression than to tension. This explains some of the non–symmetrical nature of the measured lateral deformations of the pipe. The small hysteresis shown in Figure B.2 is due to the tolerance of the slotted pin connection at the axial load location. This influenced *LVDTs* closer to the column top than the bottom. The effect of these deformations was eliminated from the test data.

5.8.2 Continuous Web Plate Connection, Type IA

Transferring the girder shear to the concrete core using the continuous web plate, as done in connection *Type IA*, did not significantly affect the axial strains as shown in Figure B.3. Gages located along the column axis suggested linear behavior of the CFT, only gages located near the connection exhibited some localized effect from the girder shear transfer to the steel tube. Locally, it appeared that most of the girder shear load transferred to the column through the steel tube. The maximum diagonal strain measured on the steel tube in the panel zone region was approximately $0.40\varepsilon_y$. This value was comparable with those measured in other specimens at this location.

For this specimen, the maximum lateral deformation for the column was less than 1.5 mm (0.06″). While significant damage was noted in the connection region at high imposed displacements, the lateral deformations of the pipe did not increase significantly during large–amplitude displacements. As in all connection tests, behavior of the CFT column was linear.

5.8.3 Connection with External Diaphragms, Type II

Because of suspected bolt slip, the testing of connection *Type II* was stopped prematurely while the specimen was in the elastic range. While handling the specimen, some strain gages were damaged which precluded useful results when the test resumed. However, strains for this specimen, shown in Figure B.5, were recorded up to about 75% of the girder flexural strength. Once again, higher axial strains were recorded in the vicinity of the connection. However, different strain values were obtained at the front and back sides of the pipe. Axial strains at the connection side were almost twice those at the opposite side of the column, and were on the order of $0.25\varepsilon_y$. Measured strains decreased to almost half these value at 600 mm (23.5″) away from the connection. The maximum diagonal strain of the steel tube in the panel zone region was approximately $0.25\varepsilon_y$. All strain curves were stable, and no translation of the hysteresis loops was observed.

5.8.4 Connection with Deformed Bars, Type III

The axial strains in the steel pipe of this connection, as shown by Figure B.7, were comparable with those observed in the previous specimens. The maximum measured values were less than $0.30\varepsilon_y$ at 635 mm (25″) from the connection center–line. Axial strains were on the same order of magnitude on each side of the pipe. These strains suggest that early bond failure in some of the deformed bars on the girder flange resulted in more flange forces transferred to the pipe. This produced high diagonal tensile and compressive strains on the pipe in the panel zone region, and the maximum strain value was about $0.40\varepsilon_y$.

5.8.5 Continuous Flanges, Type VI

Longitudinal column strains measured in the connection region, shown in Figure B.9, for connection *Type IV* were 25% higher than strains measured away from the connection. In this connection, the girder shear was transferred exclusively to the steel pipe, yet the maximum axial strain recorded in the connection vicinity was approximately $0.30\varepsilon_y$. The maximum diagonal strain on the pipe measured in the panel zone region was about $0.30\varepsilon_y$, and the panel zone strains seemed to stabilize as the girder shear increased. Note that the damage in this connection was almost symmetric, therefore, panel zone tensile and compressive strains were on the same order of magnitude.

5.8.6 Continuation of the Girder through the Column, Type VII

The rotation of the continuous connection stub detail, *Type VII,* induced axial strains as high as $0.70\varepsilon_y$ in the steel tube 305 mm (12″) away from the connection center–line. However, the axial strains of the steel tube decreased to approximately $0.3\varepsilon_y$ at 661 mm (26″). These axial strains were comparable with those recorded for other specimens. In the vicinity of the connection, the hysteretic curves progressively shifted in the negative strain direction. This might suggest the presence of some residual compressive strains in the pipe wall. Diagonal strains measured on the steel tube in the panel zone region were about $0.40\varepsilon_y$, and were higher in tension than in compression.

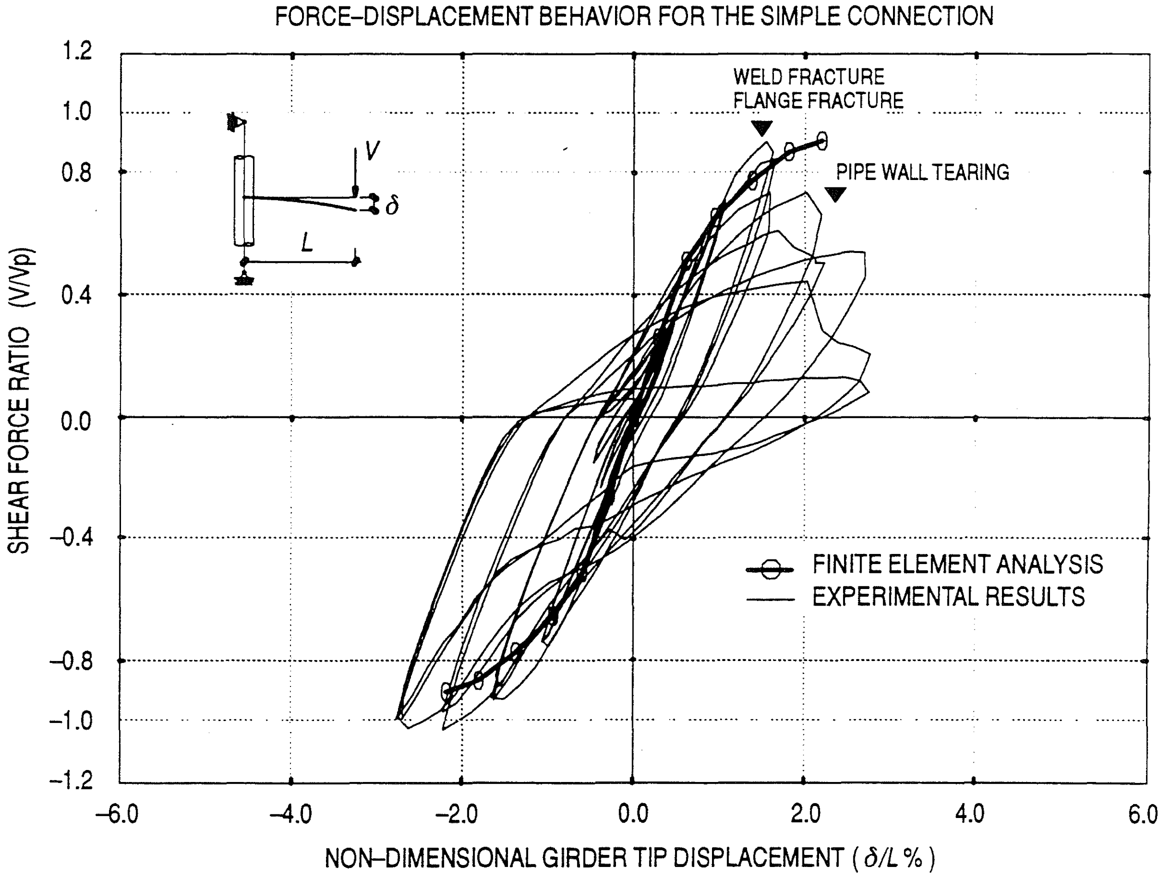

Figure 5.1. Experimental and Analytical Force–Displacement Behavior of Connection *Type I*

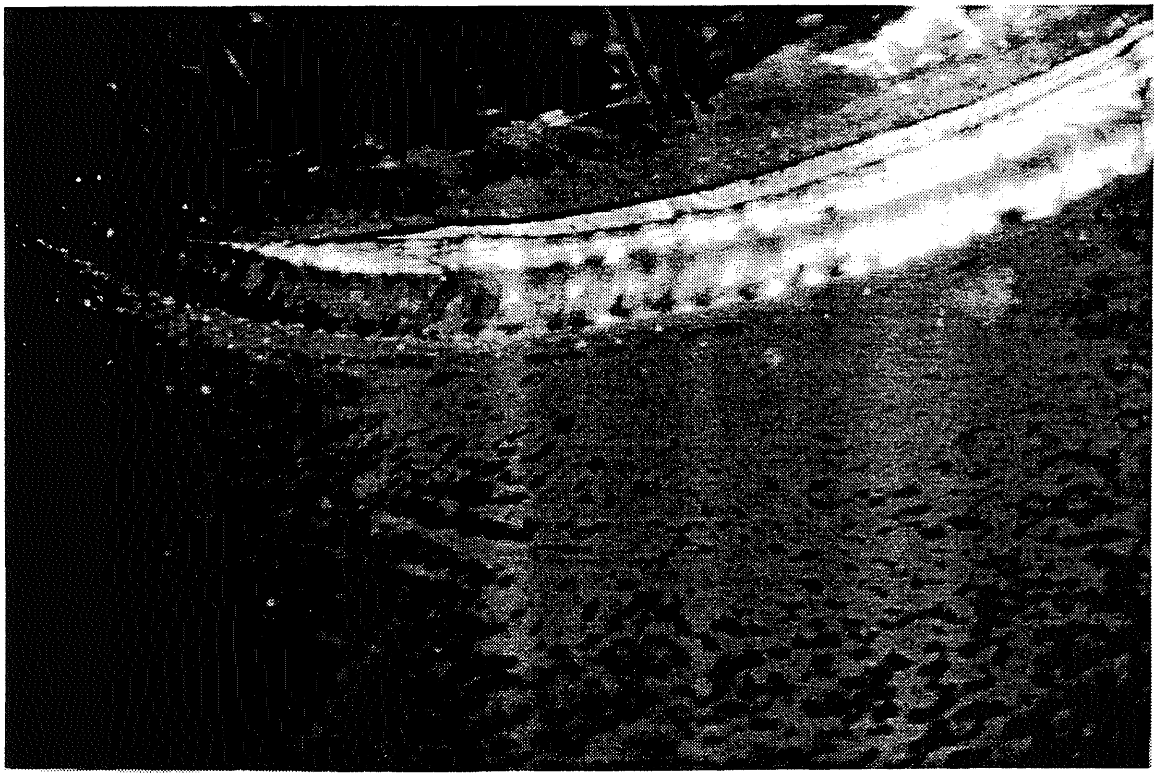

Figure 5.2 a. Failure of Connection *Type I:* Pipe Tearing

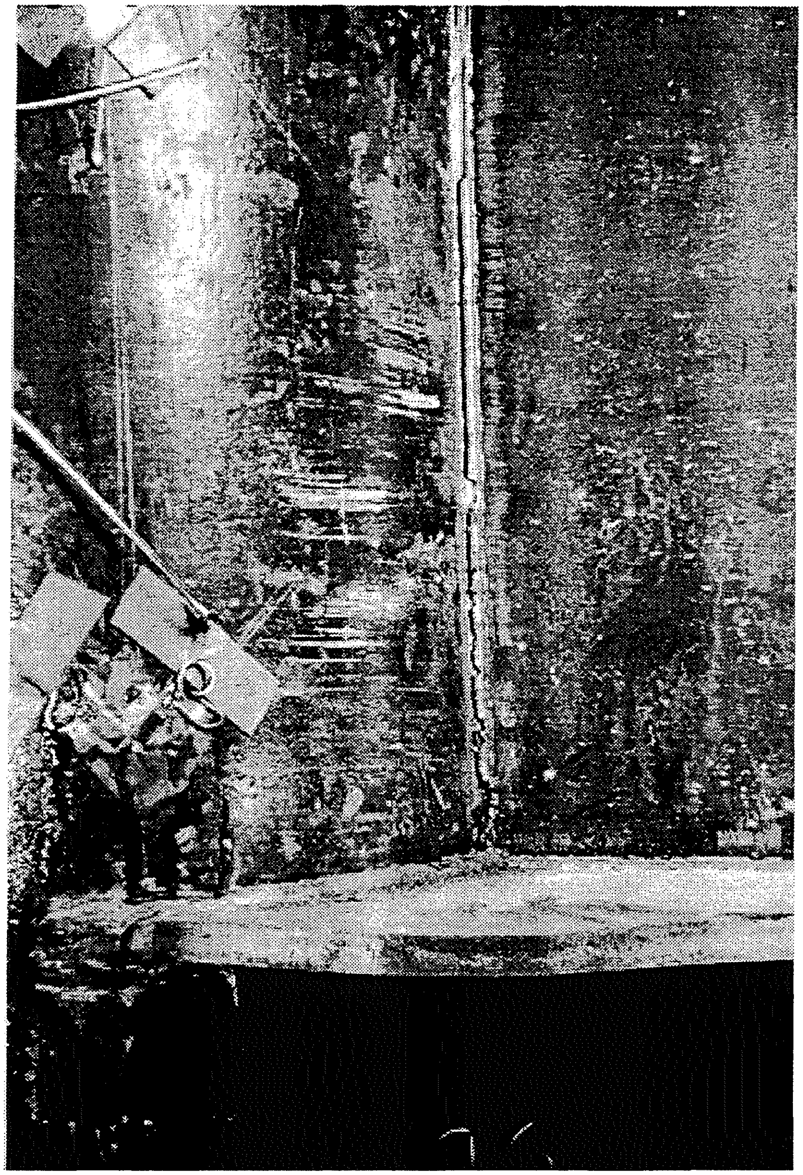

Figure 5.2 b. Failure of Connection *Type I:* Weld and Flange Fracture

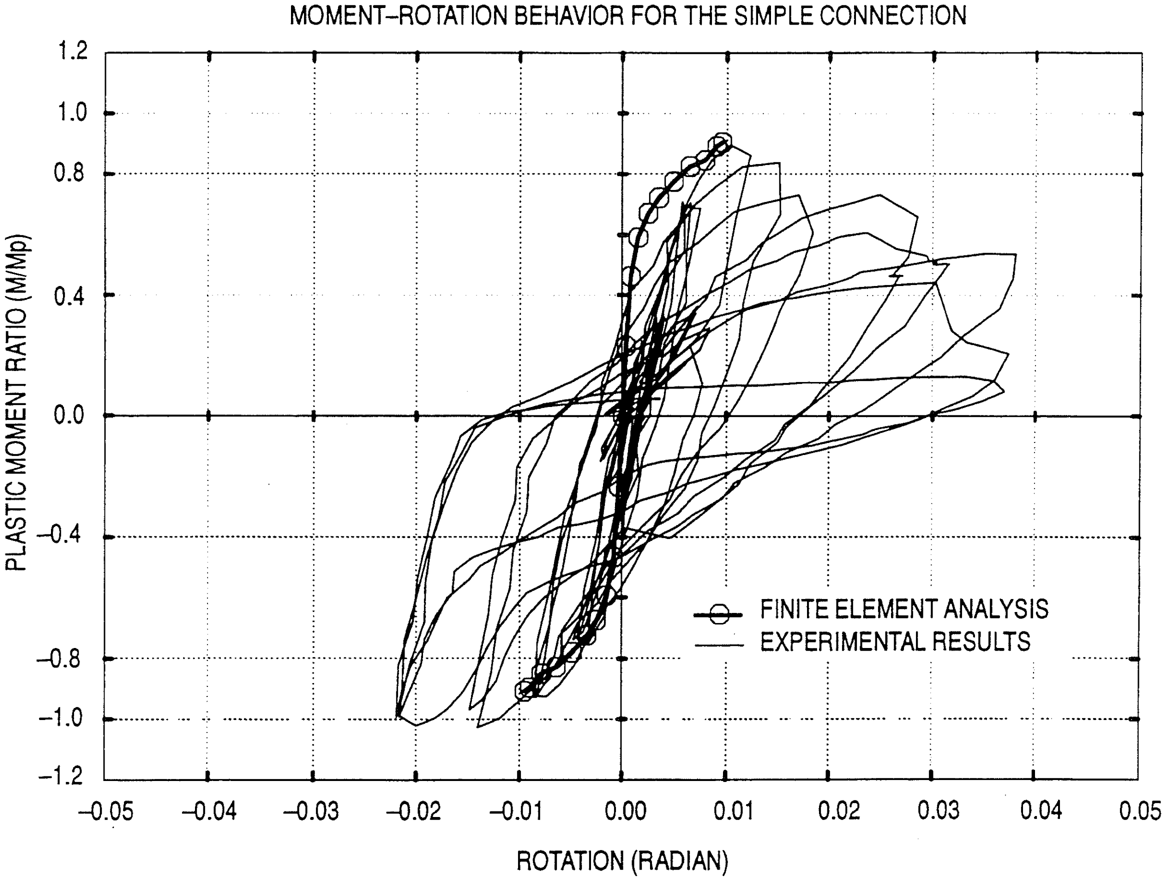

Figure 5.3. Experimental and Analytical Moment–Rotation Behavior of Connection *Type I*

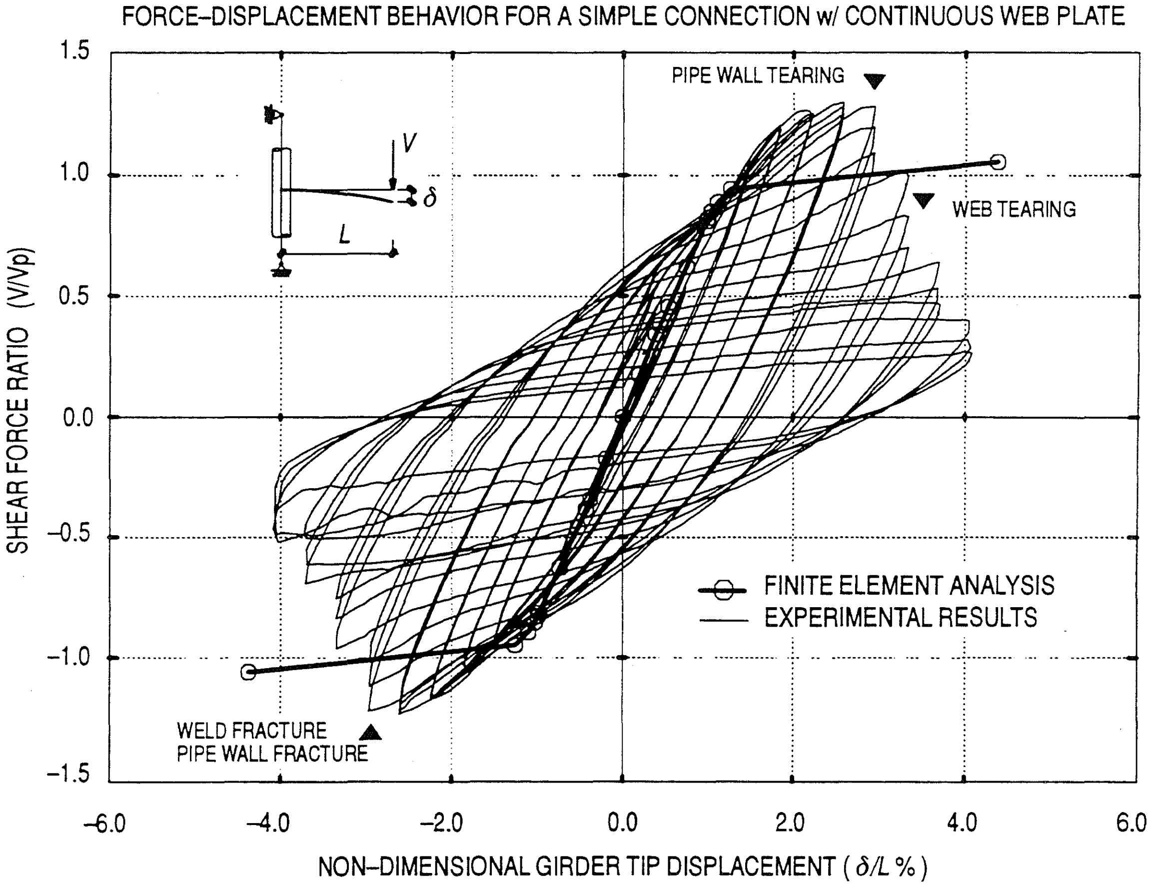

Figure 5.4. Experimental and Analytical Force–Displacement Behavior of Connection *Type IA*

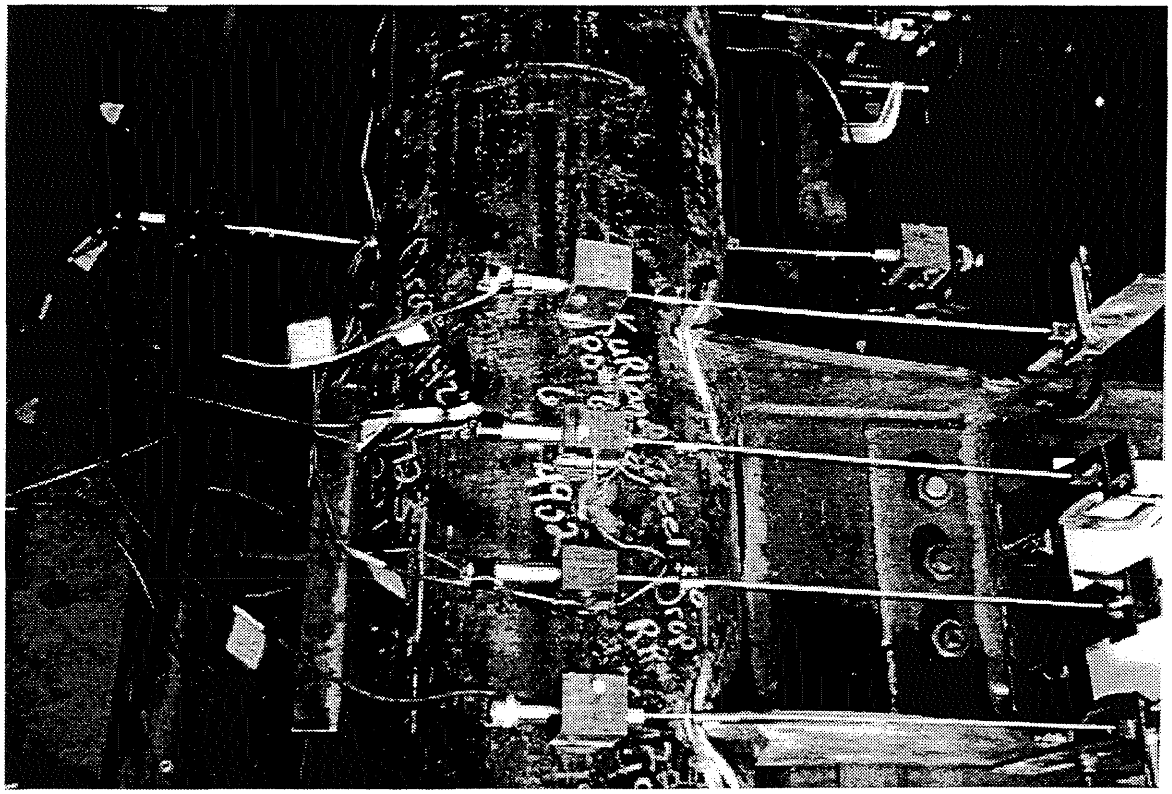

Figure 5.5 a. Failure of Connection *Type IA: General View*

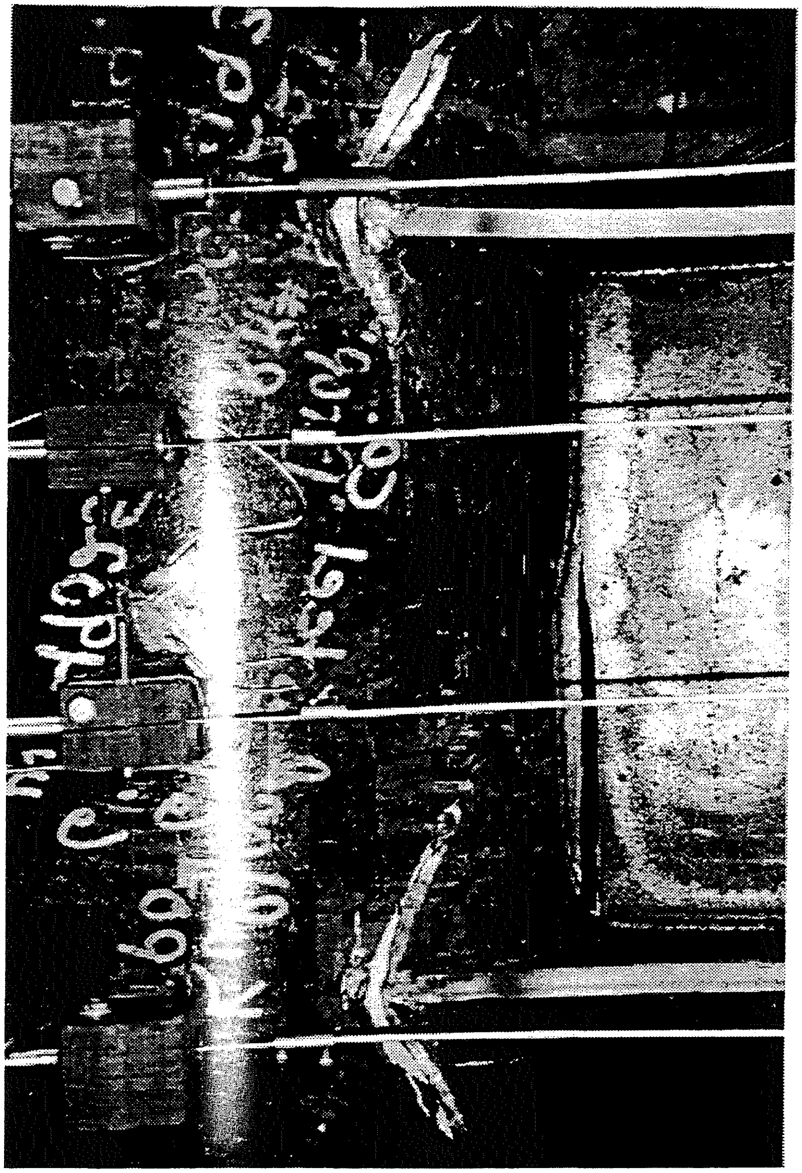

Figure 5.5 b. Failure of Connection *Type IA: Closer View*

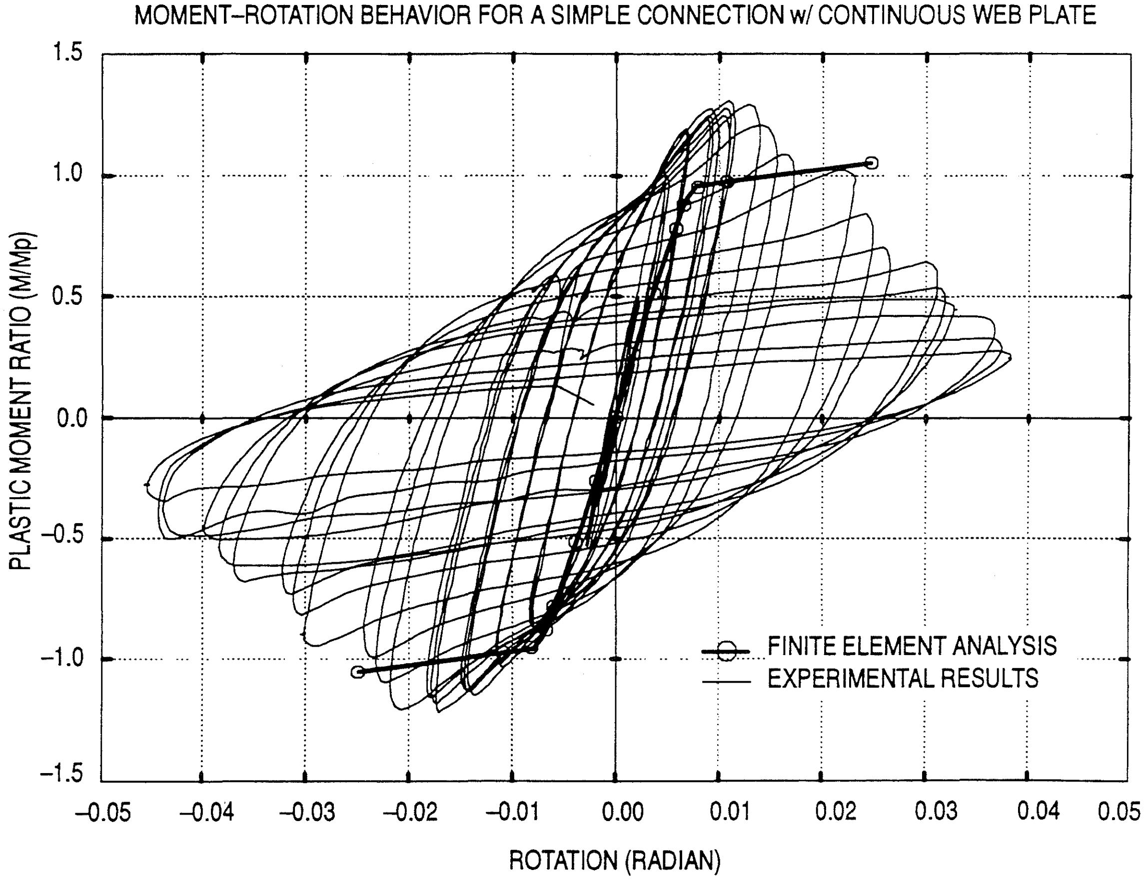

Figure 5.6. Experimental and Analytical Moment–Rotation Behavior of Connection *Type IA*

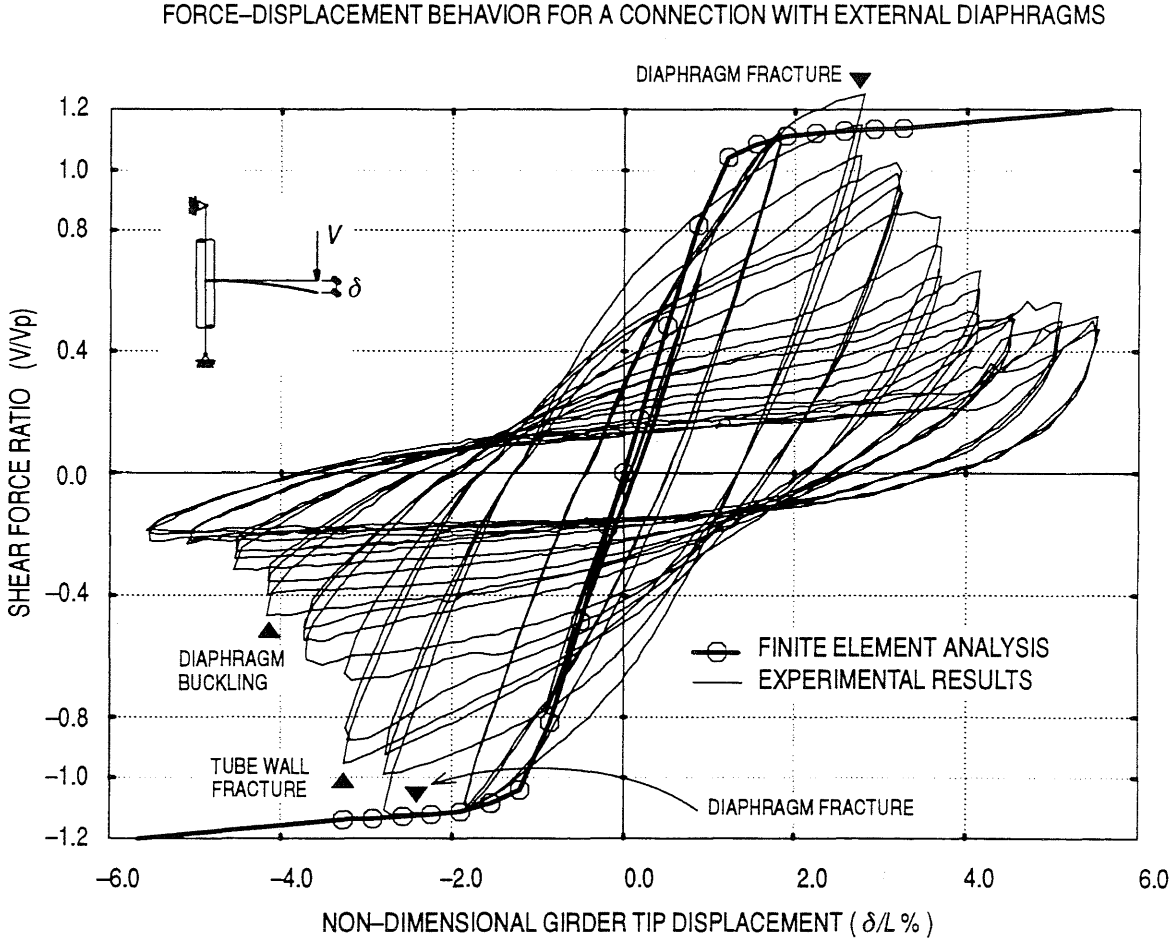

Figure 5.7. Experimental and Analytical Force–Displacement Behavior of Connection *Type II*

Figure 5.8 a. Failure of Connection *Type II:* Diaphragm and Pipe Fracture

Figure 5.8 b. Failure of Connection *Type II:* Diaphragm Buckling

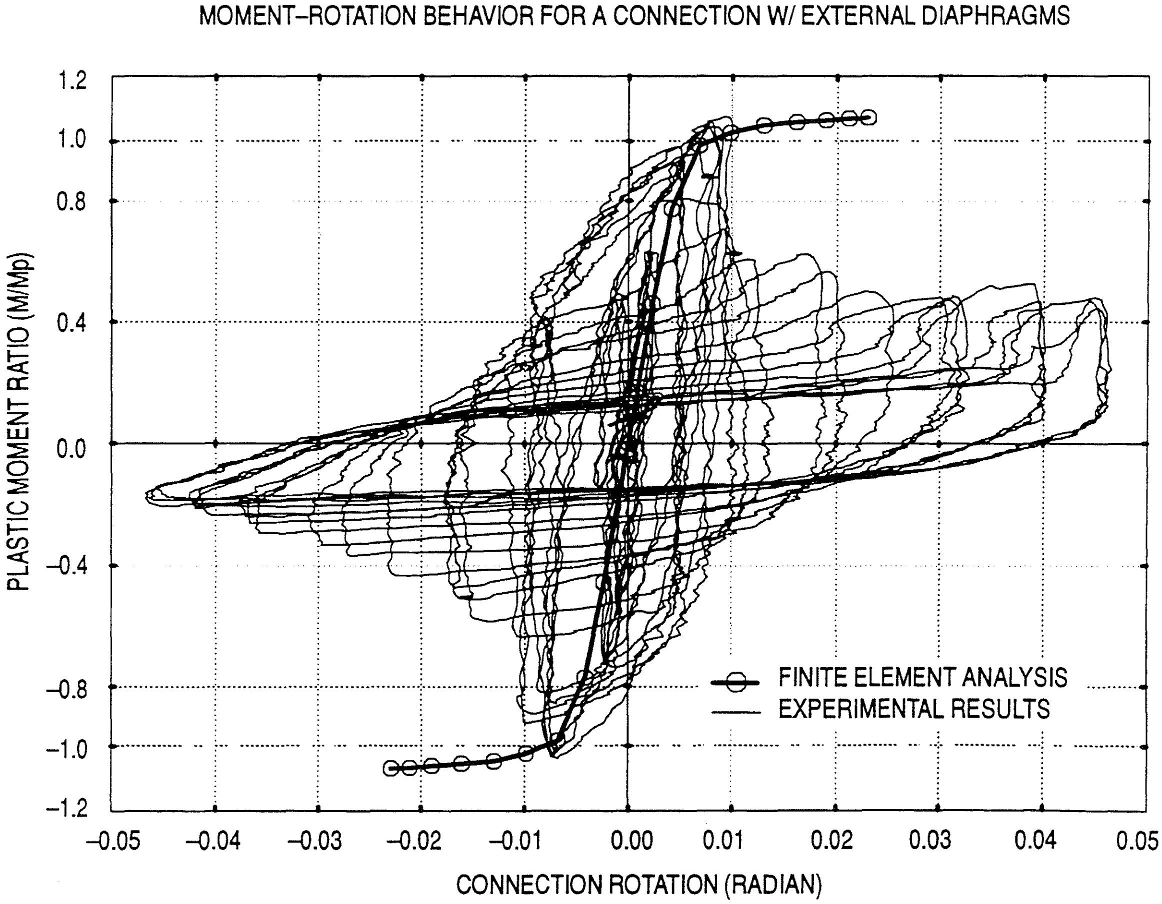

Figure 5.9. Experimental and Analytical Moment–Rotation Behavior of Connection *Type II*

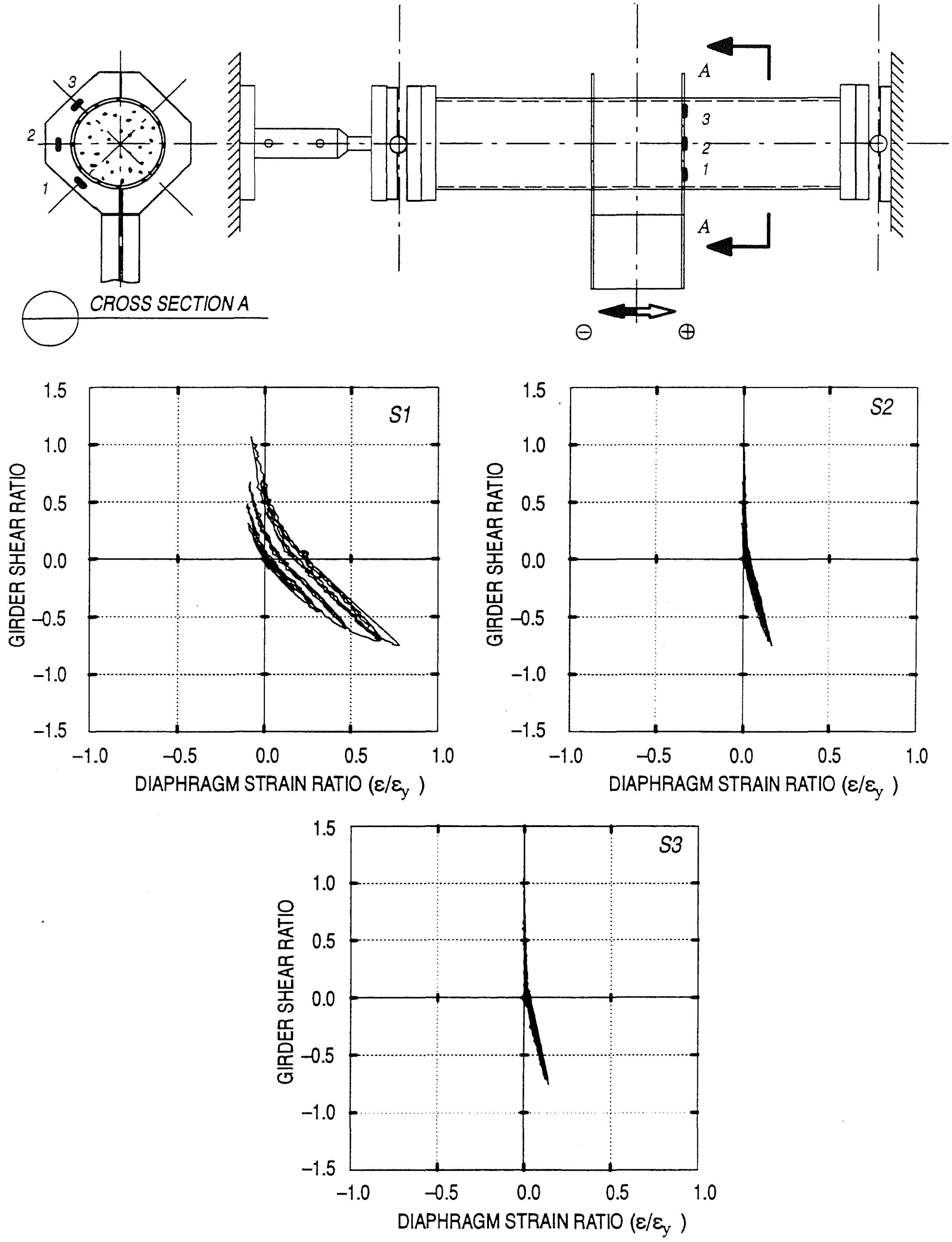

Figure 5.10. Measured Diaphragm Strains, Connection *Type II*

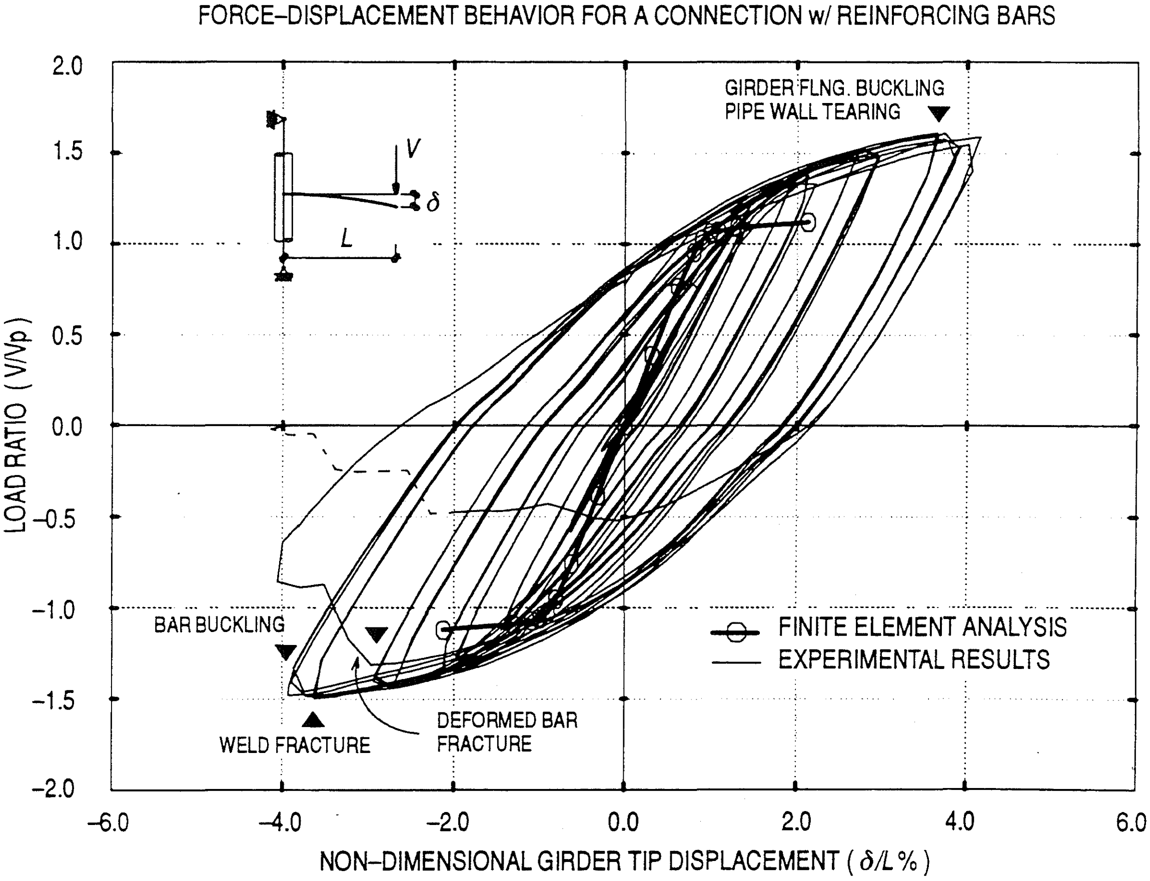

Figure 5.11. Experimental and Analytical Load–Displacement Behavior of Connection *Type III*

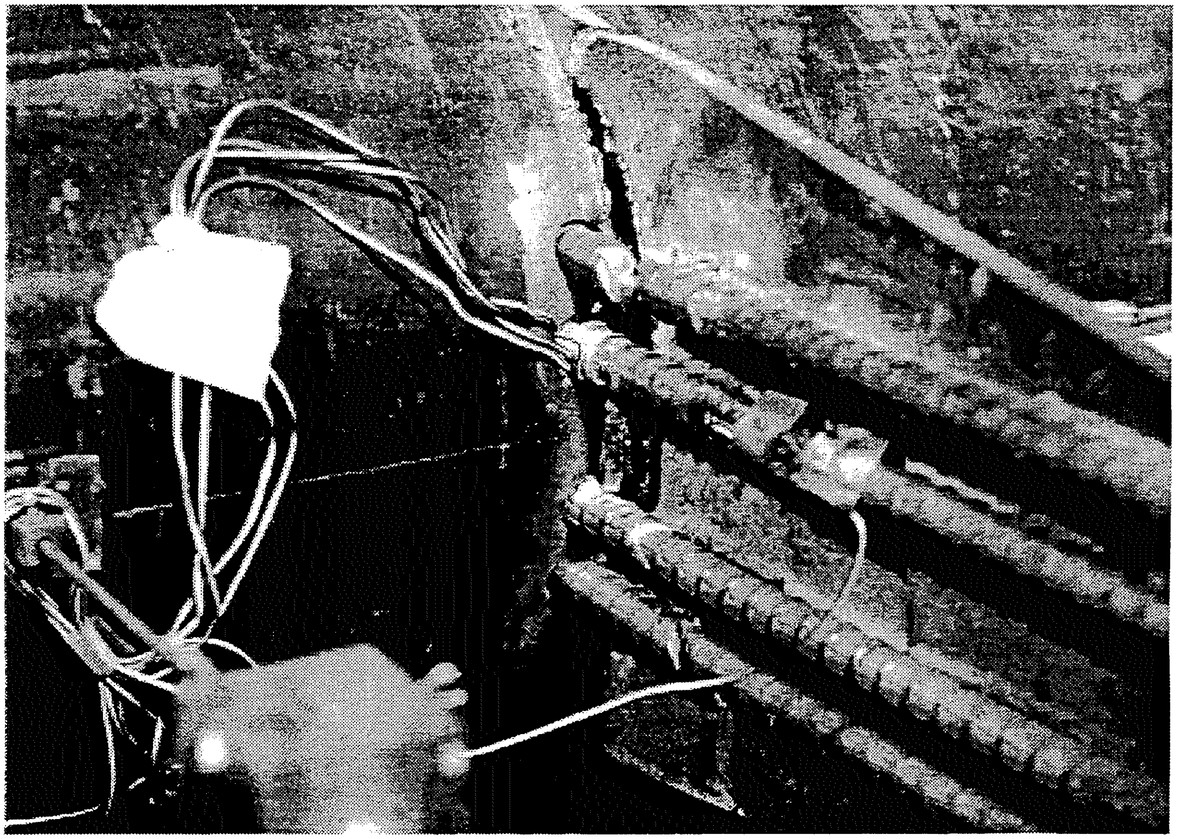

Figure 5.12 a. Failure of Connection *Type III:* Deformed Bar Failure

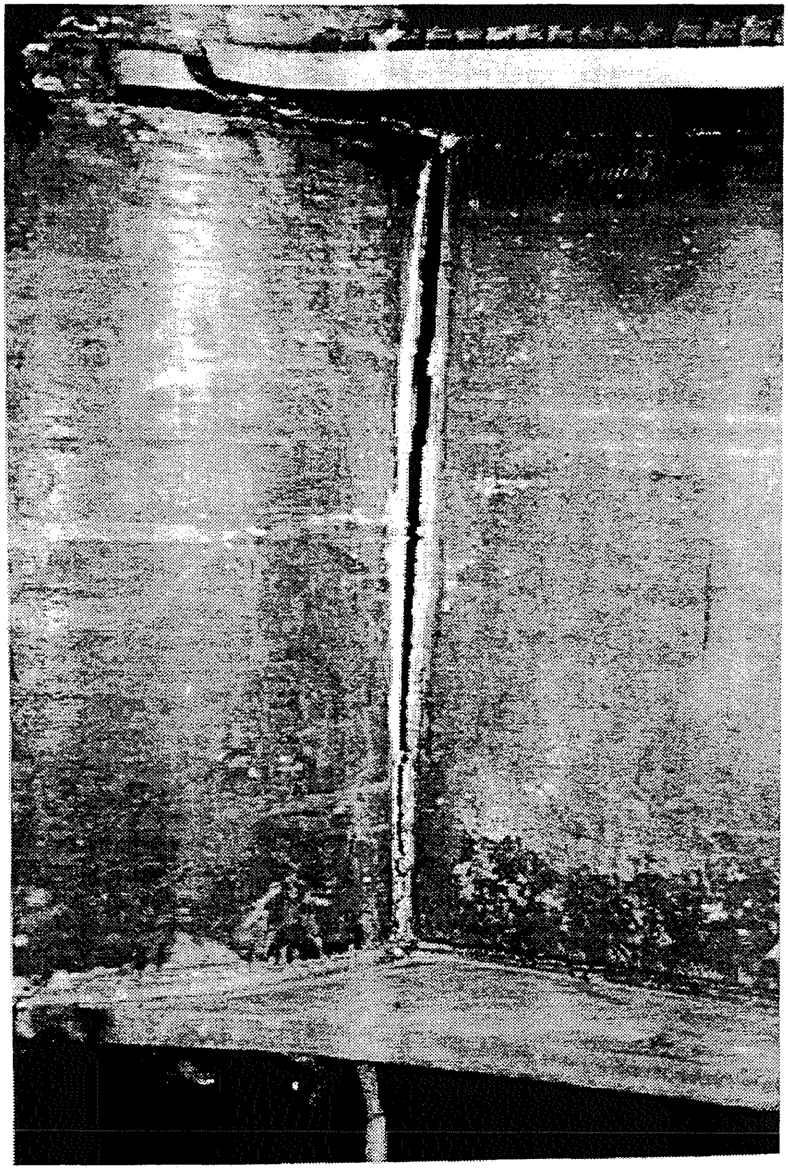

Figure 5.12 b. Failure of Connection *Type III:* Weld and Flange Fracture

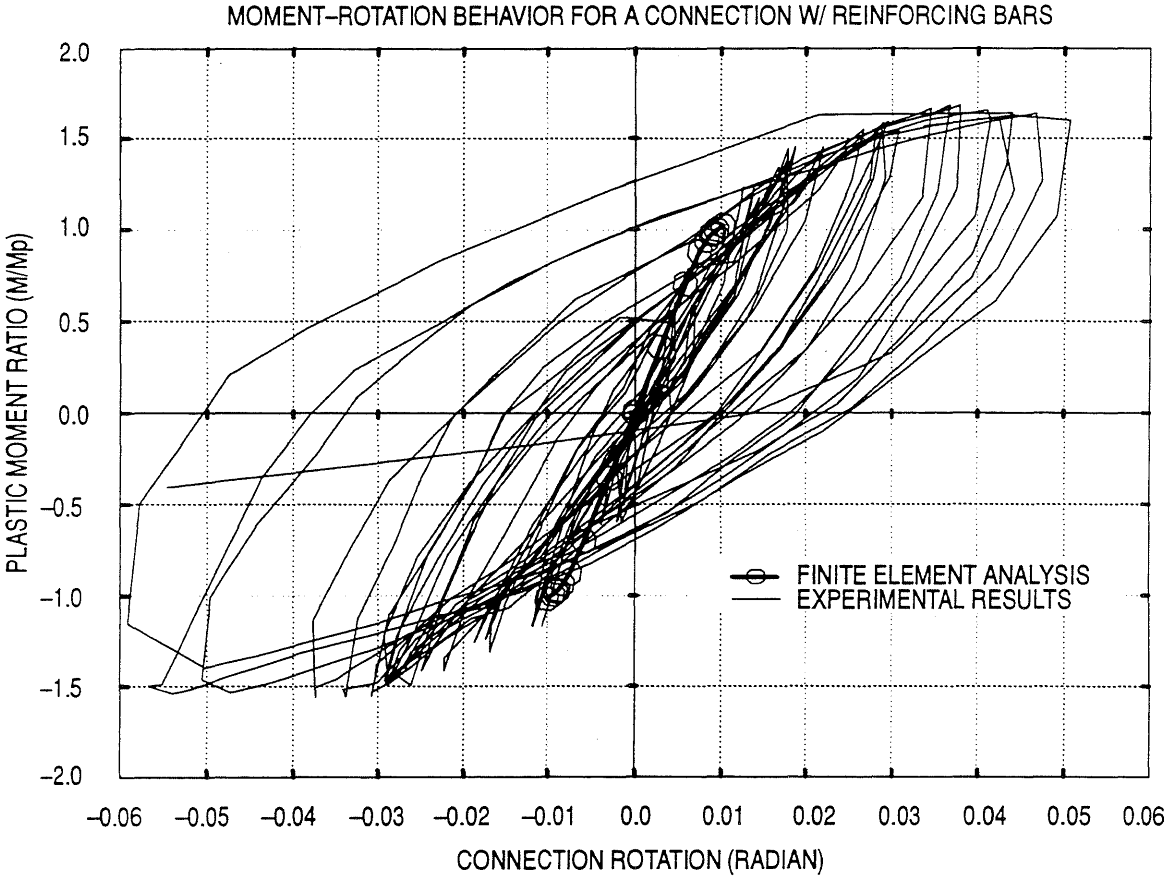

Figure 5.13. Experimental and Analytical Moment–Rotation Behavior for Connection *Type III*

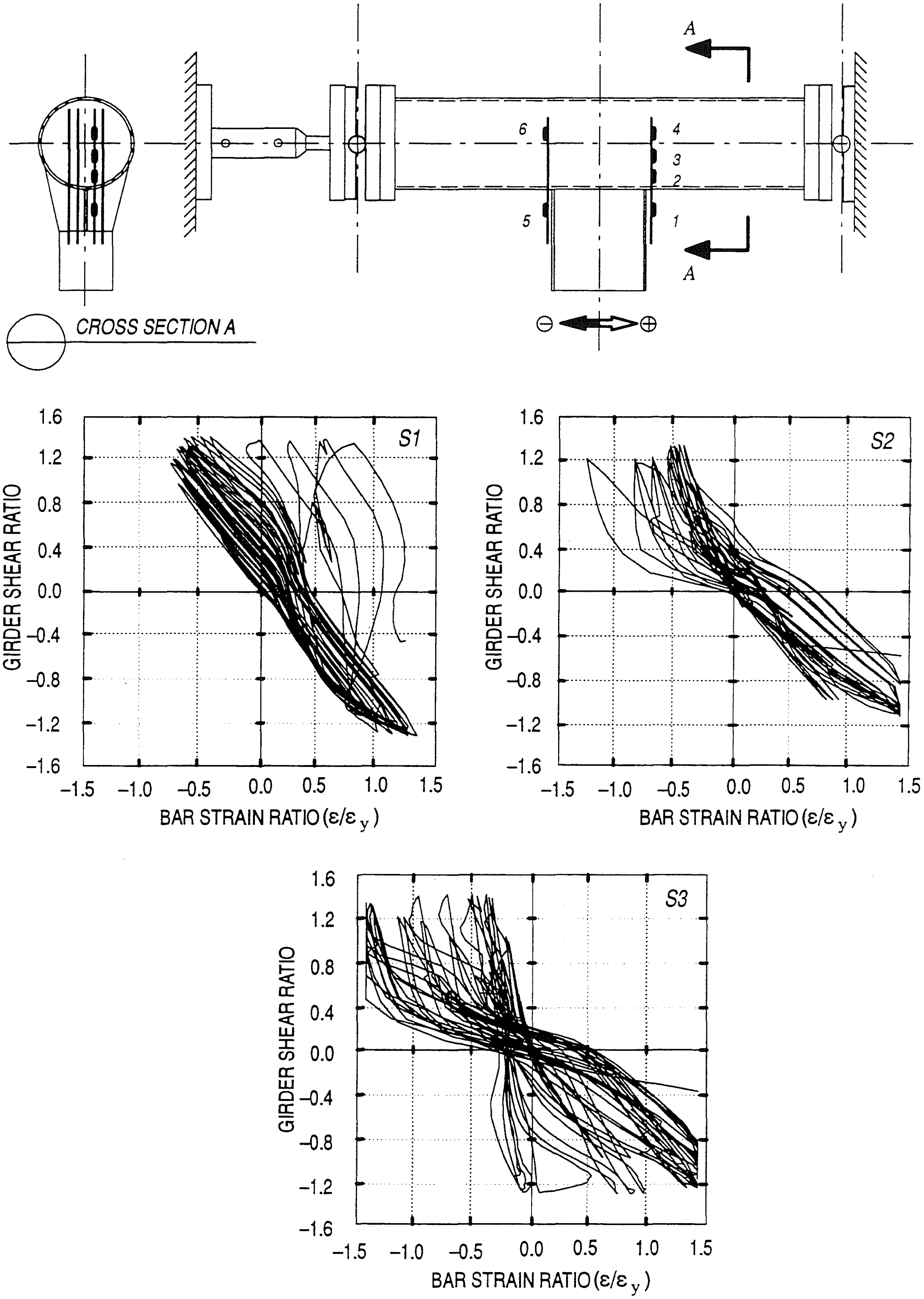

Figure 5.14 a. Measured Axial Strains in the Embedded Bars of Connection *Type III*

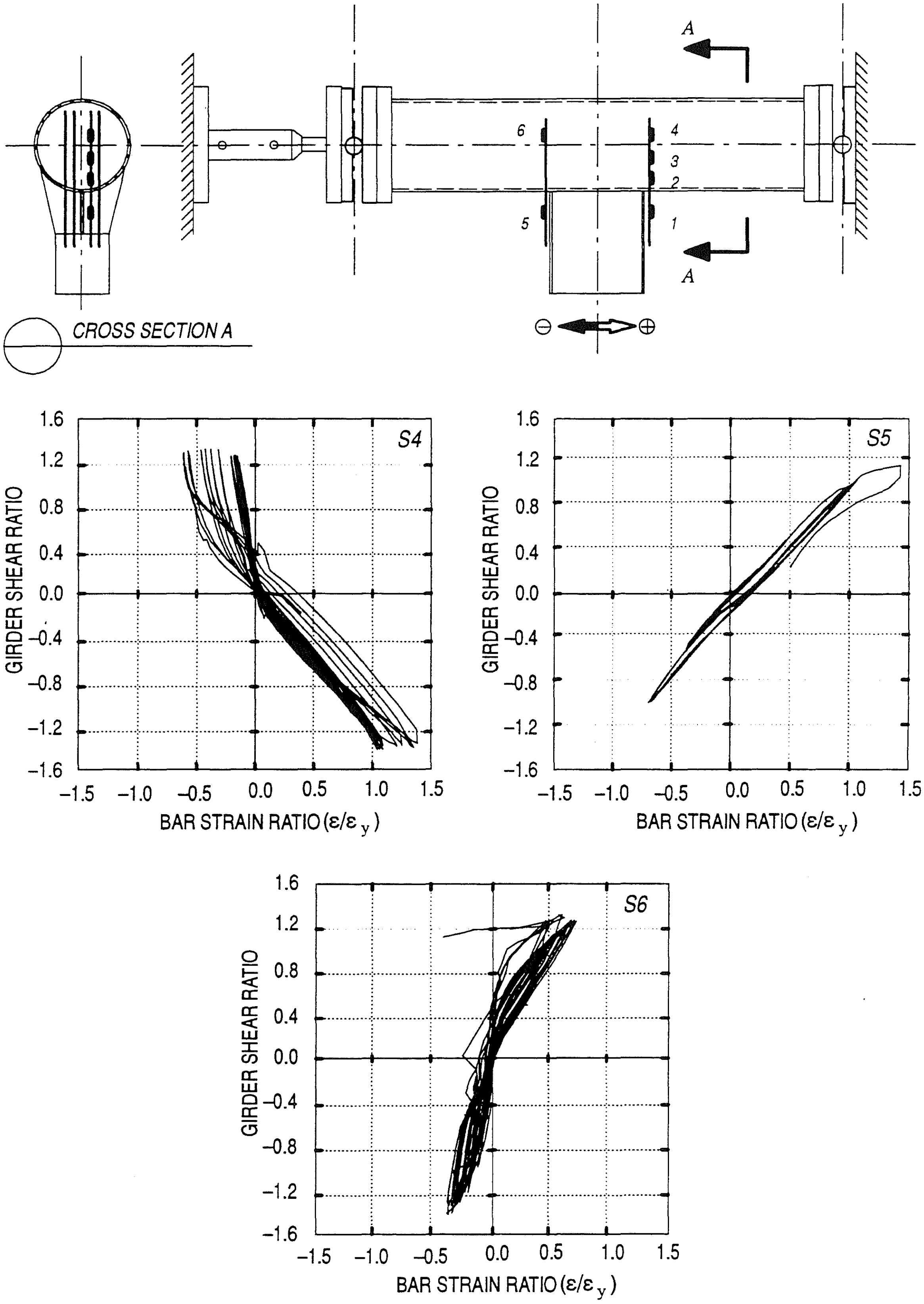

Figure 5.14 b. Measured Axial Strains in the Embedded Bars of Connection *Type III*

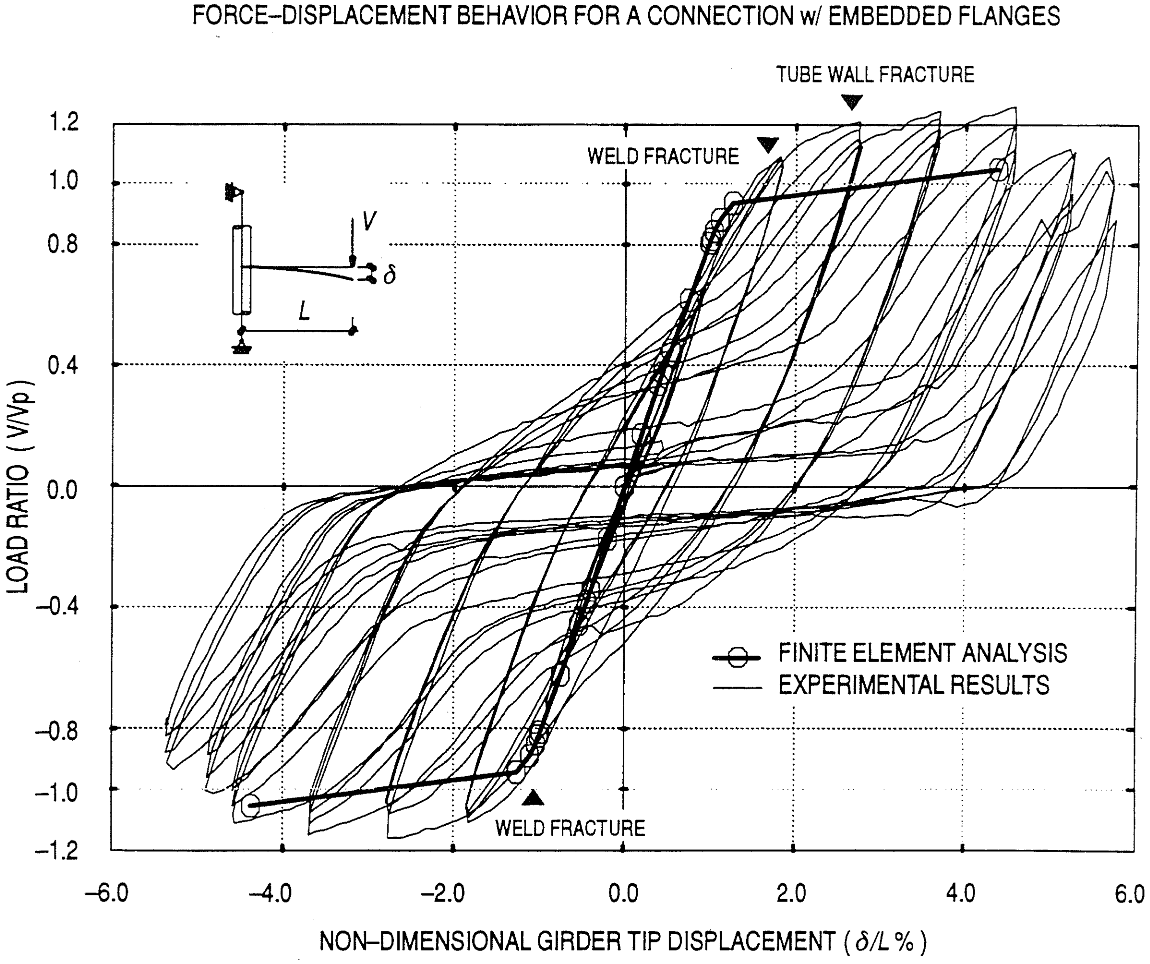

Figure 5.15. Experimental and Analytical Load–Displacement Behavior of Connection *Type VI*

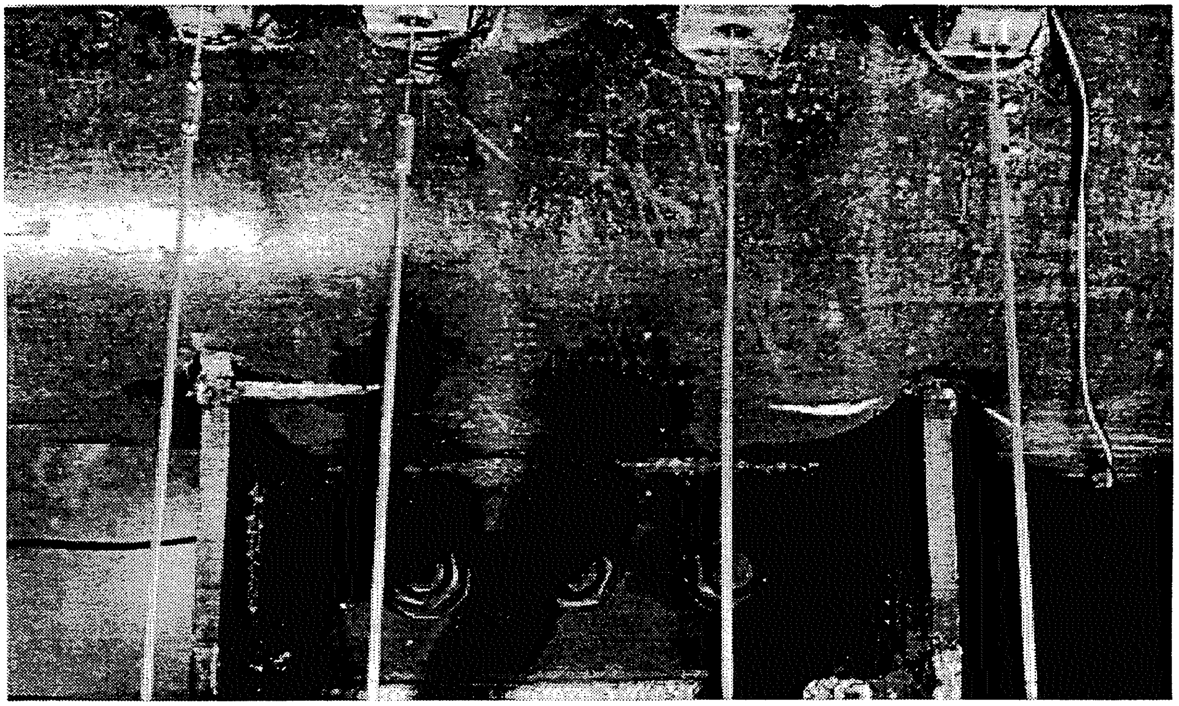

Figure 5.16. Failure of Connection *Type VI*

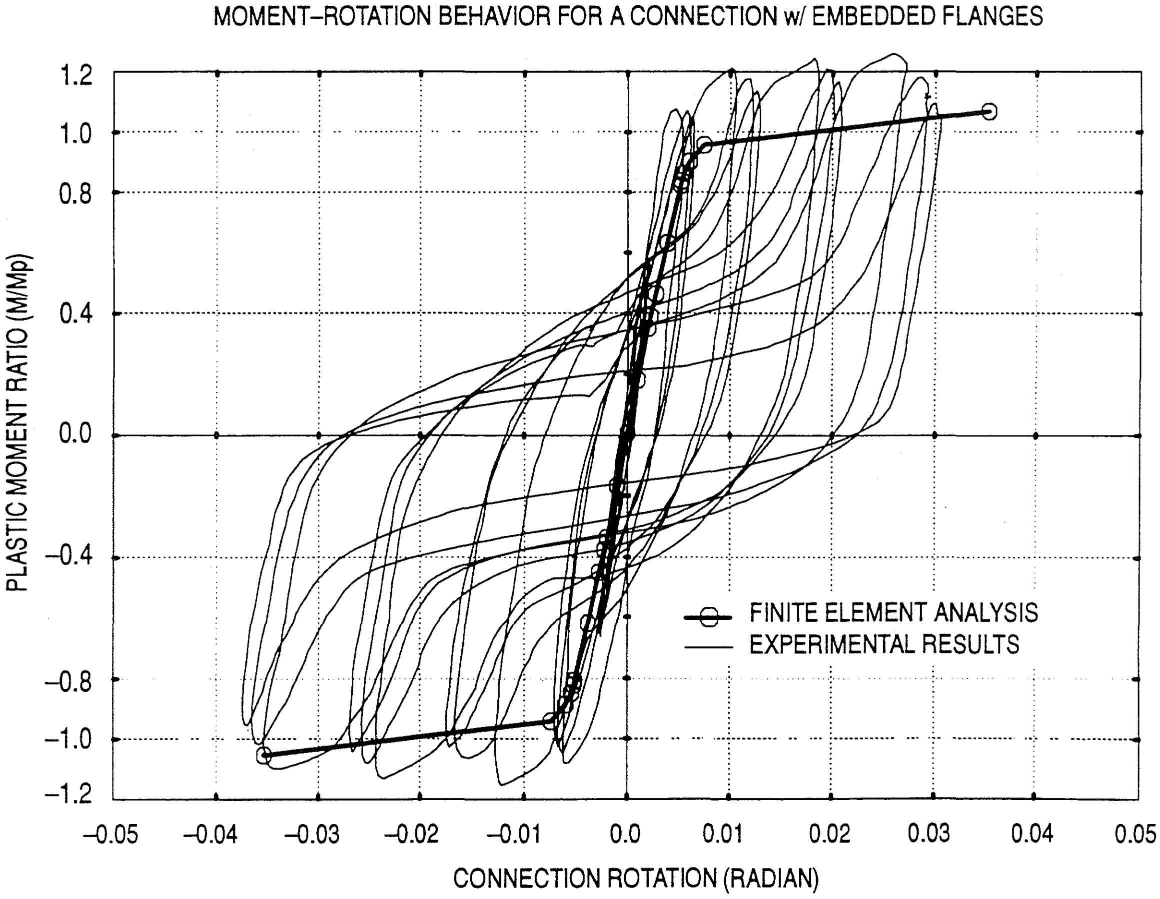

Figure 5.17. Experimental and Analytical Moment–Rotation Behavior of Connection *Type VI*

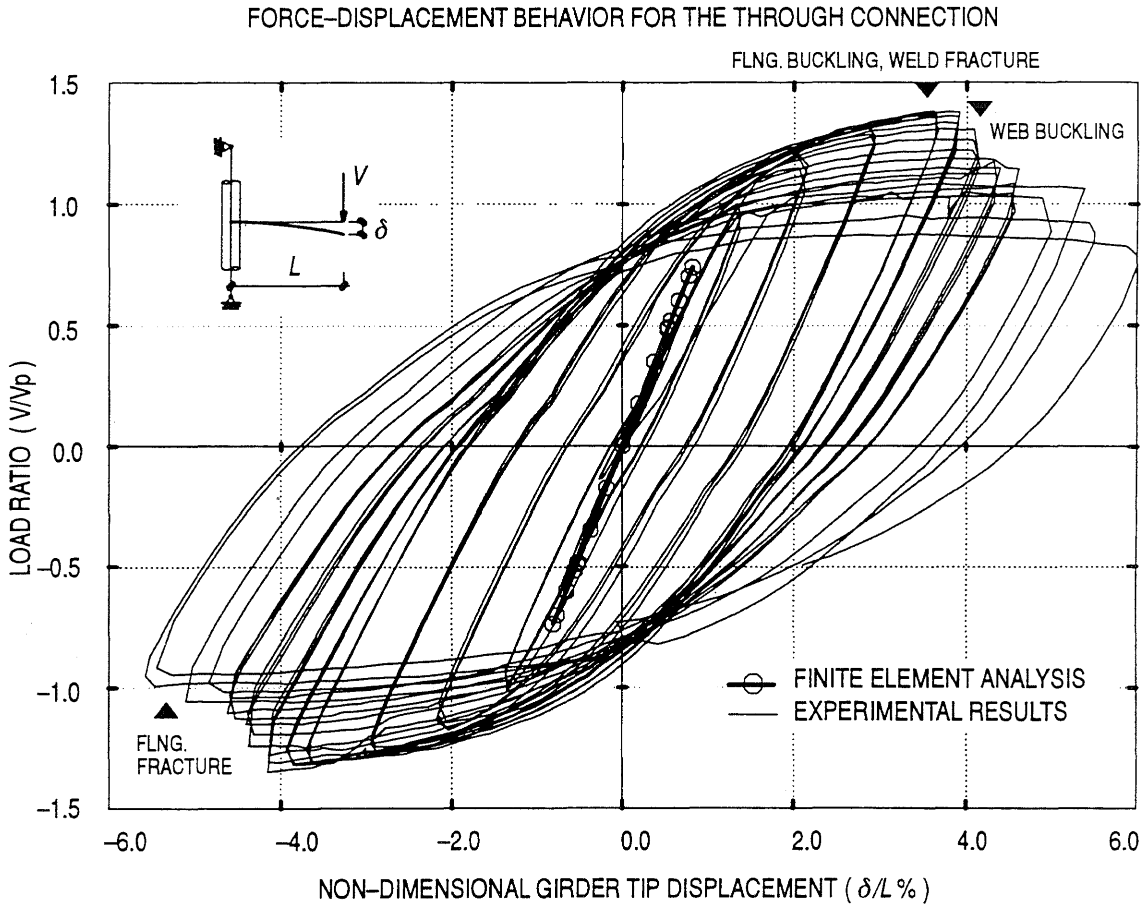

Figure 5.18. Experimental and Analytical Load–Displacement Behavior of Connection *Type VII*

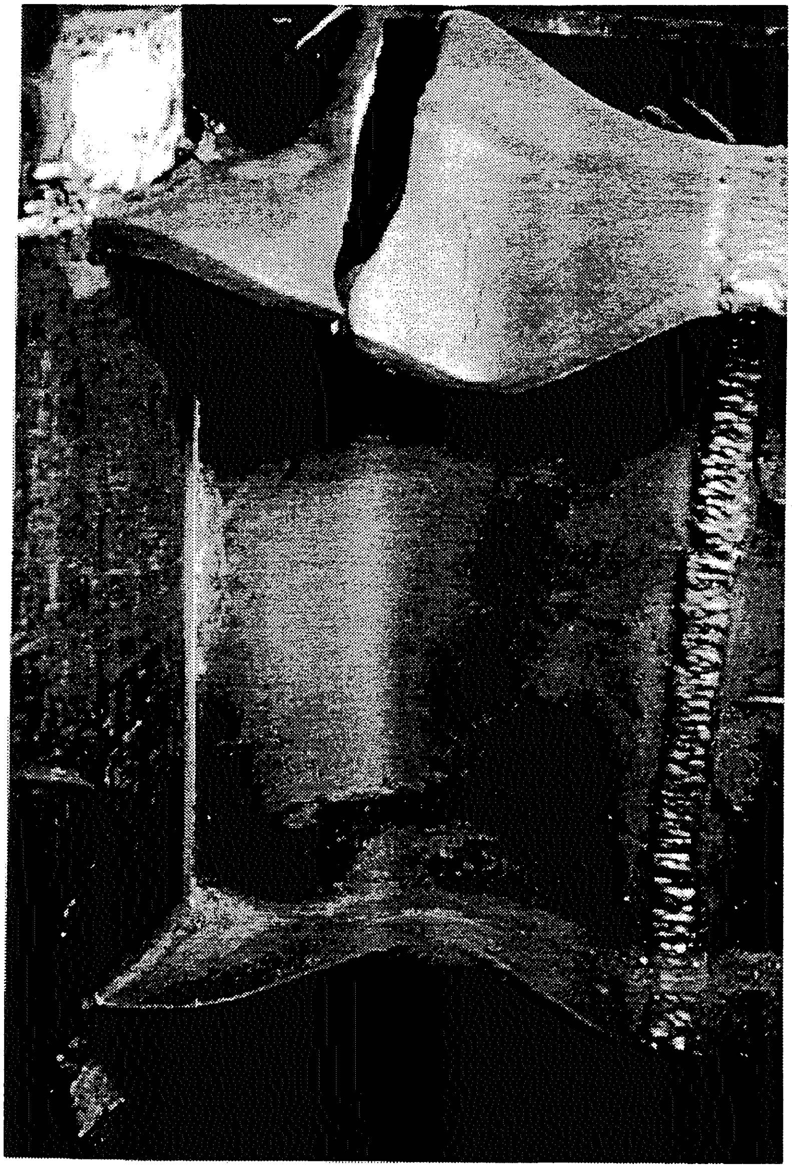

Figure 5.19 a. Failure of Connection *Type VII*

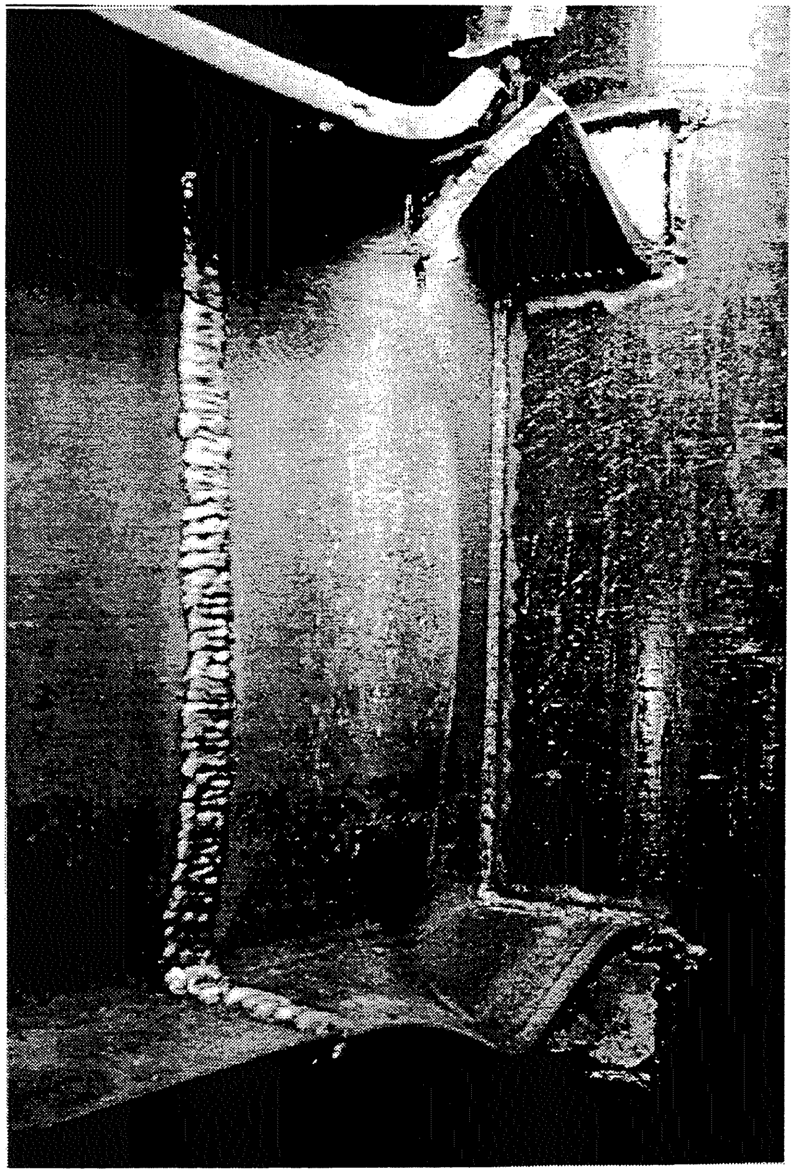

Figure 5.19 b. Failure of Connection *Type VII*

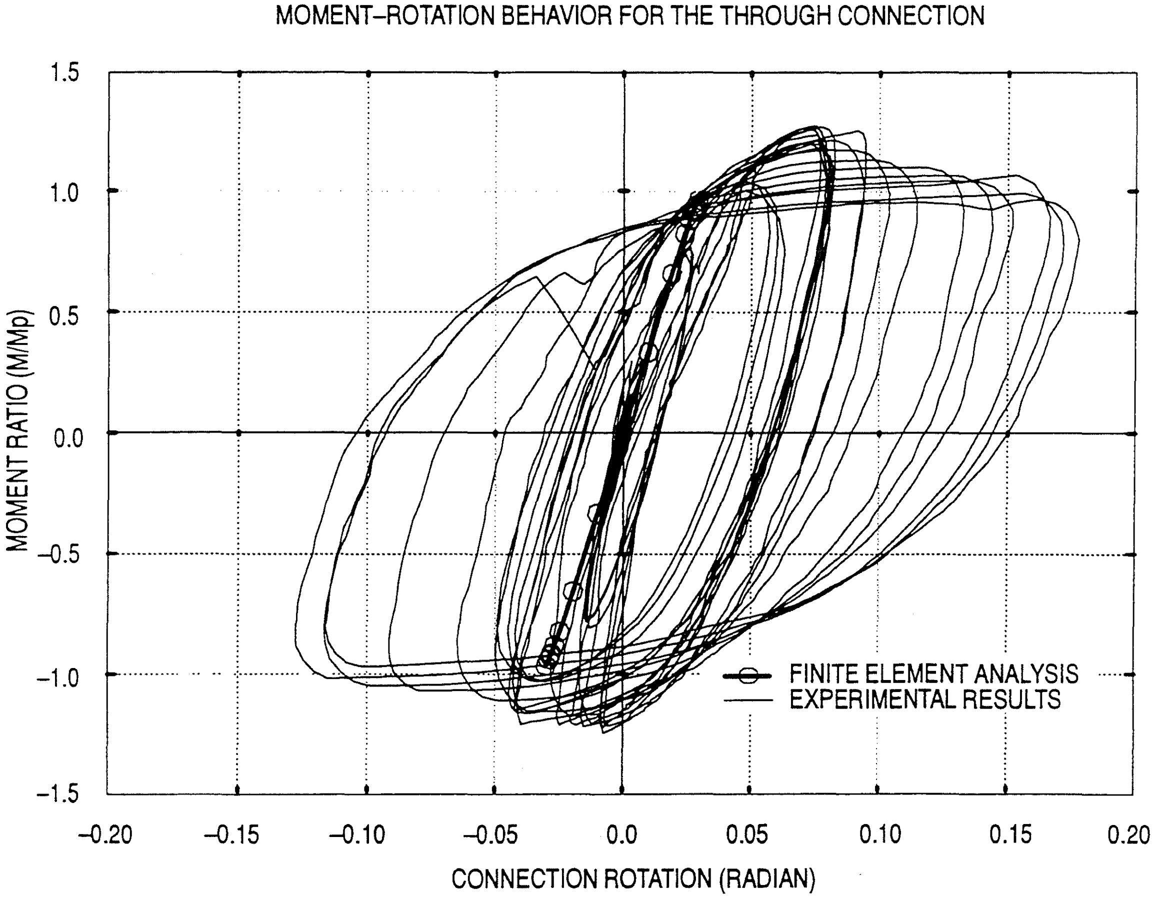

Figure 5.20. Experimental and Analytical Moment–Rotation Behavior of Connection *Type VII*

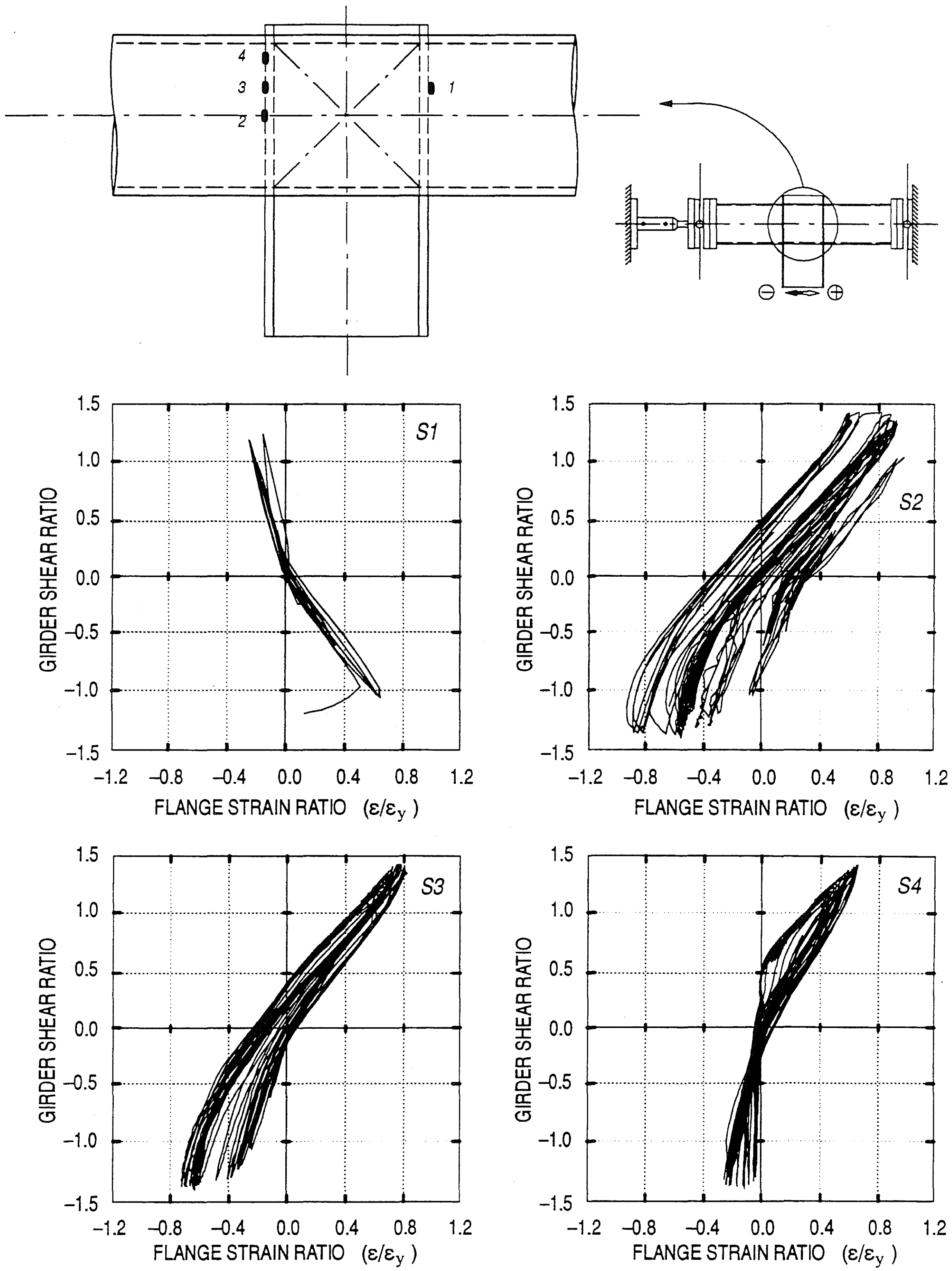

Figure 5.21. Measured Strains in the Embedded Flanges, Connection *Type VII*

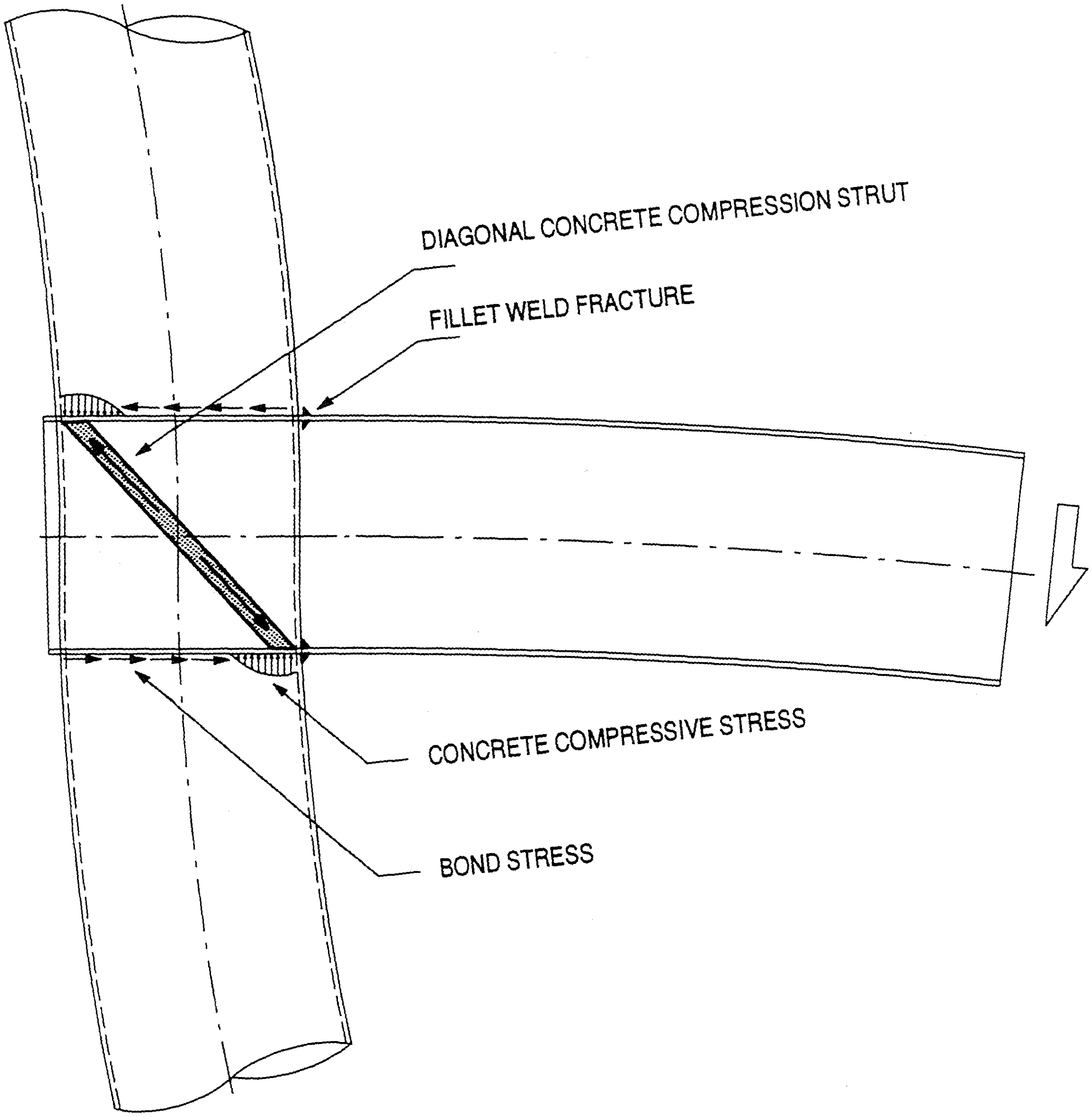

Figure 5.22. A Possible Force Transfer Mechanism in Connection *Type VII*

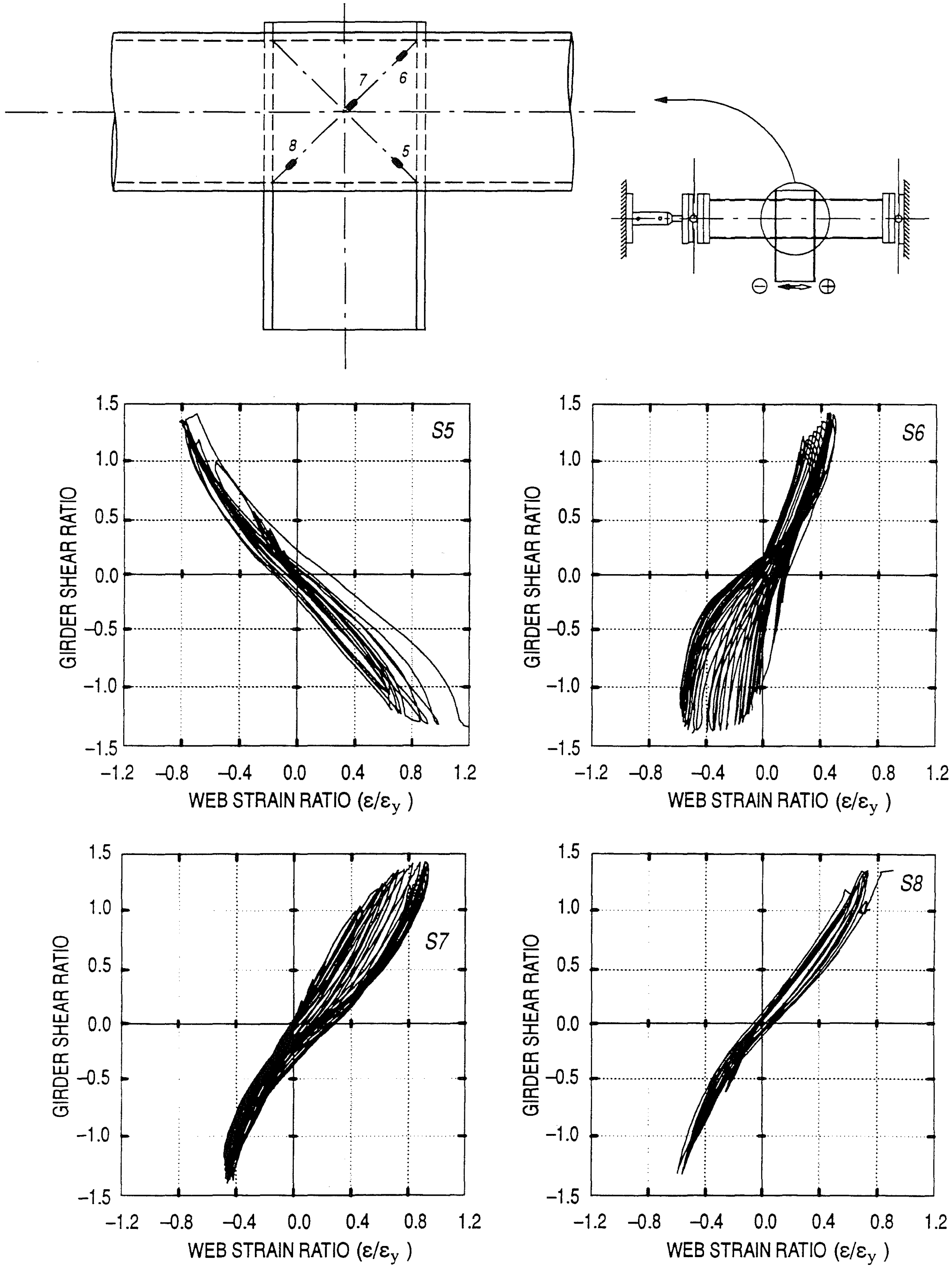

Figure 5.23. Measured Strains in the Embedded Web, Connection *Type VII*

CHAPTER 6

PERFORMANCE OF CONNECTIONS TO CONCRETE–FILLED STEEL TUBES

6.1 SUMMARY OF THE TEST RESULTS

A summary of the force–displacement and moment–rotation tests results are shown in Figures 6.1 and 6.2, respectively. These envelope curves suggest the relative inelastic performance of each connection with respect to the other details tested. The 3% rotation magnitude of the moment–rotation behavior, as indicated in Figure 6.2, has particular significant to the study of the inelastic performance of connections. Because of the problems noted with connection fracture in steel frames after the 1994 Northridge earthquake (SAC 1995), a value of 3% rotation has become the standard of minimum ductility for construction in a region at high seismic risk. This includes a minimum plastic rotational capacity of 2% rotation, with an approximate 0.67% elastic behavior. While some of these connections appeared to satisfy this minimum requirement, others did not. The following is a more complete summary of the inelastic behavior of each connection relative to strength, stiffness, and ductility.

A summary of the tangent stiffness for each connection type is shown in Figure 6.3. The tangent stiffness was determined by the elastic cycles imposed between each set of three large–amplitude inelastic cycles. This tangent stiffness was checked against the unloading stiffness of the large–amplitude deformations imposed prior to the elastic–level displacements. Results between the two methods appeared to be in close agreement.

In general all connections, except connection *Type I*, exhibited an initial elastic tangent stiffness comparable to that of a rigid connection. The ideal rigid connection condition is assumed by most practitioners in the design process. These results suggests that initial conditions of frame performance may have rigid connection behavior for all tested details except the simple connection. However, for several connection details tested, this stiffness deteriorated rapidly. Therefore, it cannot be assumed that the connection has the stiffness of the ideal rigid connection through even moderate drift levels. The tangent stiffness curves indicate the elastic performance that can be expected from each connection type after a specified level of displacement has been imposed. This is particularly important for a post–earthquake evaluation of the structural integrity of frames using these types of connections.

Due to the inelastic behavior implied by seismic provisions for model building codes, the ability of a connection to maintain its structural integrity during an earthquake depends significantly on its ductility. Therefore, a Flexural Ductility Ratio (FDR) was defined as follows:

$$FDR = \frac{\delta_{max}}{\delta_{yield}} \tag{6.1}$$

where δ_{max} is the maximum displacement at the girder tip prior to failure, and δ_{yield} is the yield displacement obtained experimentally. The maximum displacement, δ_{max}, was considered to be the deformation at which the shear strength of the connection was 80% of the peak strength obtained during the test, or 80% of the girder strength, whichever was lower. If the connection failed prior to sufficient decrease in strength, the maximum imposed displacement was δ_{max}. The yield displacement, δ_{yield}, was determined by the force–displacement behavior of the connection. The value of the displacement at the intersection of the initial tangent stiffness of the force–displacement behavior and the plastic flexural strength of the girder defined the yield displacement. This definition of the ductility ratio is consistent with that introduced by Roeder *et. al.* (1996).

Flexural Ductility Ratios for the connections tested in this research program are given in Table 6.1. As a comparison, moment–resisting steel frame designed per the *Uniform Building Code* (1988) with an R_w value of 12.0, or $R = 8$ according to the *NEHRP Recommendations for Seismic Design*, will have an effective ductility demand of about 4.0–6.0 (Roeder *et. al.* 1996). Therefore, the FDR is an indicator of what can be expected from a connection during an extreme seismic event. However, this value clearly cannot be the only measure. For instance, the continuous flange connection, *Type VI*, had the second largest FDR value, at 3.76, of any of the connections tested. However, the hysteretic curves were quite pinched and it is likely this connection may not perform well during a severe seismic event.

Six different connection details were tested in the experimental phase of this research program. These connections ranged from a very simple detail that attached the girder to the tube skin as in connection *Type I*, to a more complicated detail in which the girder was passed through the tube core as represented by connection *Type VII*. Due to the premature failure of the pipe wall and the connection stub flange, the simple connection survived a limited number of inelastic cycles and it could not develop the plastic flexural strength of the girder. Moreover, once the connection failed in flexure, its total collapse was inevitable. Most seismic design philosophies do not attempt to prevent minor structural damage. However, serious damage that leads to the collapse of the structure must be prevented. In an attempt to prevent the total collapse of the simple connection, the web plate was extended through the concrete core in connection *Type IA*. The hysteretic behavior of this modified connection exhibited significant improvement compared to the original simple connection. *Type IA* connection was able to develop approximately 1.26 times the flexural plastic strength of the girder, and the initial elastic stiffness was comparable to the ideal rigid connection. Once the connection flanges were not able to develop significant tensile forces, the connection behavior deteriorated rapidly. The flange failure imposed high demand on the connection stub web, leading to the fracture of the web. Another way to improve the simple connection behavior was accomplished by expanding the connection stub flanges to form external diaphragms, as illustrated by connection *Type II*. The hysteretic performance of the connection with external diaphragms improved relative to the simple connection *Type I*. This resulted in a connection strength of approximately 17% higher than the girder bending strength. It seemed that the geometry of the diaphragm was a critical issue in the behavior of this detail, for example, the sharp re–entrant corner between the diaphragm and the girder created large stress concentration which initiated a fracture in the diaphragm. This fracture, which occurred at approximately 1% rotation, interrupted the flow of forces from the girder flanges to the diaphragms, and caused rapid deterioration in the connection performance. Although connection *Type IA* had higher strength, its strength deteriorated at faster rate compared to the connection with external diaphragms. This explains the higher ductility associated with connection *Type II* compared to *Type IA*.

Transferring the flange forces to the steel tube, as in connection *Types I*, *IA*, and *II*, led to unfavorable connection performance. Therefore, the remaining three specimens utilized embedded elements that distributed part of the girder flange forces to the concrete core. Transferring 80–85% of the girder flange force to the concrete core via deformed bars, improved the hysteretic performance of the simple connection. Connection *Type III* exhibited stable strain–hardening behavior up to failure, and it developed approximately 1.5 times the girder bending strength. The connection ductility was approximately 3.5 compared to only 1.9 for an identical connection but without the deformed bars. The clearance, the weldability of the deformed bars, and the configuration of the weld on the bars are among the critical issues in this detail. In an attempt to resolve some of these problems, the stub connection flanges were continued through the concrete core in connection *Type VI*. The hysteretic curves were very pinched due to the lack of bond between the embedded flanges and the concrete core. On the other hand, the envelope curve of this connection seemed to be satisfactory. One way to improve this connection performance was achieved through continuing the full cross section of the girder through the tube core. The new connection, *Type VII*, developed a full plastic hinge in the girder, and it had satisfactory hysteretic performance. The following paragraphs emphasis the impact of the design assumptions for each connection detail on the connection performance.

6.1.1 Simple Connection, Type I

The simple connection *Type I* had the lowest flexural strength among all of the connections tested. This connection barely developed the plastic bending strength in one direction of loading, and produced less than 87% of the flexural strength when loaded in the opposite direction. The strength of this connection was primarily limited to the through thickness shear strength of the tube wall. Deterioration in the strength of this connection initiated at approximately 1.0% rotation. Further, the flexural strength deteriorated to 80% of its original peak strength by 1.5% rotation. This was well under the minimum performance threshold developed as a result of the connection problems noted after the Northridge earthquake.

For this connection, the shear capacity was lost shortly after the failure of the flanges in flexure. Once the flanges fractured, the rotational demand was placed on the web of the connection stub. Without rotational restraint, this connection became an effective pinned end, much like girders connected to CFTs that are not intended to be moment–resisting. The test demonstrated that under imposed cyclic deformations, the connection web failed by tearing away from the steel tube wall. Therefore, if the shear tab is simply welded to the skin of the tube, which might be the case in a simple connection type, the connection will unlikely sustain large deformations experienced by the frame during seismic excitations. This indicates a potential problem with this type of moment–resisting connection, as well as a simple pinned–end connection with a shear tab welded to the face of the tube wall.

Connection *Type I* was the most flexible of all the connection details, starting at an initial value of 85% of the ideal rigid connection condition. Further, this connection exhibited the earliest decay in tangent stiffness, starting at about 0.60% normalized cantilever tip displacement. It decayed to less than 50% of the rigid connection stiffness within approximately 2% girder tip deformation. This flexibility was clearly due to the excessive deformation of the tube wall.

This connection type had the lowest FDR of any of the connections tested by this study. A value of FDR = 1.88 is well below the threshold value of 4.00 expected for a frame designed in a region at high seismic risk. Therefore, this connection could not be expected to provide the sufficient ductility compared to the demands of a major seismic event.

The design of this connection was based on the assumption that the girder flange forces must be distributed such that the through–thickness shear strength of the tube wall was not exceeded. However, only 87% of the flexural strength was obtained in one load direction, therefore it is possible that this design assumption was not conservative enough. The failure mode of this connection detail was by tearing of the connection stub flange, the weld, and the tube wall. Because of the high strains noted in the analysis, and the experimental work, the tips of the flanges fractured first. The tearing eventually propagated into the tube wall. Because of strain compatibility of the girder near the web flange intersection, it is likely that the tube wall would have to be thickened significantly. However, the analytical parameter study showed that a thicker tube wall increased stiffness of the connection, but not necessarily the flexural strength. Further, a thicker tube wall, either locally around the connection, or continuous along the column height, will be costly for little improvement in connection performance.

Clearly, the use of connection *Type I* in a frame with CFT columns will produce substantially more drift than predicted by a simple frame model assuming rigid behavior at each girder–to– column connection. Further, the lateral strength of the frame may be over–estimated if these connections were used in the frame. Therefore, the simple connection should not be used in moment–resisting frames with CFT columns in regions of moderate or high seismic risk.

It is possible that the inelastic behavior of this connection type can be improved. For large diameter pipes, where the pipe interior can be accessed by a welder, headed studs may be attached to the inside of the tube wall. This connection type was investigated analytically, connection *Type IV*, but was not considered further because of the diameter of pipe used in the experimental study.

For the small diameter pipes the tube must be cut to gain access to the tube interior to attach the studs behind the girder flanges. The cut tube section must then be replaced by partial– or full–joint penetration groove welds. Further, the skewed angle of the headed studs closer to the flange tip in small diameter pipes were not effective in resisting the forces generated by the flanges along the longitudinal axis of the girder. Both of these concerns diminish for large diameter pipes. Headed studs might be attached without disrupting the tube wall, and because of less curvature in the pipe each stud will be more effective. The analytical study suggested that the performance of this simple connection improved significantly when headed studs were attached to the inside of the tube wall. The stiffness increased by approximately 65% and the strength appears to approach the full plastic bending strength of the girder. If one row of headed studs is insufficient, it might be possible to use two rows of studs to improve performance. This may require thicker tube walls.

This connection type was similar to connections of girders that have headed studs welded to end–plates which are embedded into concrete walls or columns. End–plate connections had favorable ductile failure when the moment–to–shear ratio was small, and they exhibited rapid strength deterioration when subjected to cyclic loading. It is presumed that CFT connections with headed studs attached inside the tube wall has more redundancy than embedded end plate details.

Another method to improve behavior of the simple connection is to add vertical fin plates, connected to both the connection stub flanges and the tube wall. This connection type was not addressed by this analytical study, but has been tested through the SAC program to improve pre–Northridge type welded connections. This connection type has shown to alleviate some of the high stress concentrations on the column.

6.1.2 Continuous Web Plate Connection, Type IA

The high flexural demand imposed on the connection stub web in the simple *Type I* detail, once the flanges and tube wall fractured, precipitated tearing of the shear tab from the column face. To mitigate this kind of failure, the web was extended through the concrete core for connection *Type IA*. The steel tube was slotted to allow the web to pass through the column, and a 6 mm ($^1/_4$″) fillet weld on each side of the web attached the web to the steel tube. Otherwise, this detail was identical to the simple *Type I* connection.

Extending the web plate inside the concrete core, increased the flexural strength of the simple connection to approximately 1.2 times the plastic hinge strength of the girder. However, this strength was only maintained to an approximate rotation of 1.4%. The strength began to rapidly deteriorate at 1.3% rotation, and reached 80% of the peak flexural strength at 2.5% rotation. When the test concluded at the final imposed rotations of 4.5%, this connection only had 50% of the girder bending strength remaining.

This continuous web connection detail, *Type IA*, also improved the stiffness of the simple connection detail. The initial tangent stiffness for connection *Type IA* averaged between 94% to 98% of the ideal rigid connection conditions. This tangent stiffness was sustained up to approximately 2.7% rotation, which was almost 4.5 times the deformation before the deterioration of the simple *Type I* connection.

An FDR value of 2.55 was a significant improvement over the simple connection *Type I* detail, however, it was still below the minimum ductile behavior expected from a moment–resisting frame.

Although the continuous web detail was an attempt to improve the potential shear behavior of connection *Type I* once the flanges failed, significant web tearing was still noted. Once the flanges of this connection failed, this exacerbated the high strain demands on the extreme web fibers. Due to the embrittlement of the web in the heat affected zone, tearing initiated close to the fillet weld that attached the web to the pipe wall. Therefore, continuing the web still imposed extremely high ductility demand on the web for flexure. Variations of an embedded web plate must be studied to obtain an appropriate condition to sustain shear behavior of the connection after significant flexural damage has occurred. It should be mentioned that for the W14 × 38 section used as the girder in these tests, 76% of the plastic bending strength was associated with the flanges. Therefore, the web contributed 24% of the bending strength. Careful consideration must be given to cross sections in which the web contributes more to the plastic strength of the girder, since the web is subjected to significant deformation demands once the flexural capacity diminishes.

Adding headed studs to the continuous web plate in an attempt to develop the flexural capacity of the girder does not improve performance. This was investigated by connection *Type V* in which the web with attached shear studs was to develop the flexural capacity. The finite element analysis suggested that the headed studs contributed very little to the flexural capacity of the W14 cross section. Therefore, although there might be a significant cost increase to detail the connection with studs on the interior of the concrete–filled tube, the improvement in the inelastic performance is minimal.

6.1.3 Connection with External Diaphragms, Type II

External diaphragm plates, if properly designed, can improve the inelastic performance of the simple *Type I* connection. Therefore, external diaphragms should be used in lieu of the *Type I* detail. Diaphragm plates are much more practical for small diameter CFTs, and can be used to attach other girders at the joint.

The external diaphragm connection, *Type II,* produced 10%–15% more strength than the shear capacity of the girder, and the strength deterioration rate was lower compared to connection *Types I* and *IA*. However, deterioration in the flexural strength initiated at 1.0% rotation. At a rotation of 1.0% this connection had 80% of its peak flexural strength, and at the completion of the test, at approximately 4.6% rotation, the connection provided only 20% of the flexural capacity of the W14 girder.

External diaphragms also exhibited reasonably stiff tangent behavior at low displacement amplitudes. Initially, the tangent stiffness was almost 100% of the ideal rigid conditions, however, deterioration of this stiffness was noted almost immediately. At approximately 3.0% rotation, the tangent stiffness was almost 70% of the ideal rigid behavior, and rapidly decreased to slightly less than 20% by the end of the test.

This diaphragm plate detail showed very little improvement in the FDR value, of 2.88, compared to continuous web detail. Therefore, it is probable that this connection also lacks the ductility capacity to sustain the inelastic demand of a large seismic event.

For the minimum size diaphragm that was tested, the re–entrant corner between the diaphragm and the girder flange created a region of high local stresses and strains. This high deformation demand led to the initial fracture of the diaphragm, eventually propagating into the steel tube wall. Significant tearing was noted throught the welded region of the diaphragm plates. Because of the extensive tearing, the minimum size diaphragm was not effective in alleviating the severe distortions on the tube wall noted by the simple *Type I* connection.

The minimum size diaphragm was intended to transfer the full tensile force in the flange to the backside of the CFT column. However, extensive tearing of the diaphragm eventually led to high deformation demand on the tube wall, similar to what was observed in the *Type I* connection. Analytically, this behavior exhibited significant improvement when the girder was shifted further away from the CFT column face. This reduced the sharp re–entrant corner between the diaphragm and the girder flange, and provided an improved stress flow path around the CFT column for the girder flange forces. The minimum throat area, or the diaphragm plate area at the location of minimum distance between the CFT face and the plate edge, did not significantly affect the inelastic behavior. In this study, the diaphragm plate with the 30° edge, *Diaphragm IIA*, had a minimum throat area 6% larger than for the 45° plate edge. Therefore, the path of the stress flow appeared to be more critical.

It should be noted, however, while the flow of tensile stresses might improve when the girder is removed farther from the face of the column, the compressive behavior might become an issue. The extended diaphragm resulted in a large width–to–thickness ($b_f/2t_f$) ratio of 21.0 at the pipe face through the largest throat area of the diaphragm. The *1994 AISC/LRFD* requires the width–to–thickness ratio of a compact section to be less than $65/\sqrt{F_y}$, which reduces to $52/\sqrt{F_y}$ for a cross section that might be subjected to significant inelastic deformations. These values correspond to a width–to–thickness ratio for the flanges of 9.5 and 7.6, respectively, for the material strength used in this study. Thus, the value of $b_f/2t_f = 15.5$ for the tested diaphragm connection, and 21.0 for the improved diaphragm exceed this limit by a minimum of 63%. Diaphragms with a larger yield strength will clearly be much more susceptible to the local instability. As a comparison, the width–to–thickness ratio for non–compact sections given as $106/\sqrt{F_{yw}-16.5}$, which ensures the yield strength be obtained in the cross section, was 22.0 for the material strength used in this study. Thus, the extended diaphragm plate just barely satisfied non–compact section requirements. However, the width–to–thickness ratio can be improved using vertical stiffeners.

6.1.4 Connection with Deformed Bars, Type III

Weldable deformed bars embedded into the concrete core, and attached to the girder flange, improved the behavior of connection *Type I* significantly. If the simple *Type I* connection is desired, embedded deformed bars will improve behavior and should be used if construction is in a region of moderate to high seismic risk.

The deformed bar connection *Type III* exhibited the largest strength among all of the tested connections. The ultimate strength was 50% larger than the plastic bending strength of the girder, and approximately 70% larger strength in the opposite load direction. Further, this connection exhibited reasonably stable strain–hardening until failure of the specimen. However, at approximately 5% rotation, this detail experienced sudden failure.

Weldable deformed bars also improved the tangent stiffness of the simple connection significantly. The stiffness of this connection was actually higher than the ideal rigid connection assumption, indicating an increased moment of inertia around the connection due to the weldable deformed bars. The tangent stiffness for this connection ranged between 98% to 106% of the rigid connection, and did not deteriorate over the entire range of imposed girder deformation. For instance, prior to the abrupt rupture at approximately 5.0% rotation, the connection had a sustained tangent stiffness of 103%.

An FDR value of 3.46 makes this connection borderline from an inelastic energy dissipation standpoint. Considering that it did not reach the minimum threshold of ductility expected from elements in a moment–resisting frame, and the failure of the connection was relatively sudden, this connection is difficult to evaluate strictly on this basis.

Failure occurred by the rupture of three of the four deformed bars in the connection detail, and the fourth bar failed by pull out of the concrete core. The detailing for these weldable deformed bars becomes a critical issue. If the first weld attaching the bar to the girder flange is too close to the column face it may be too short to develop sufficient inelastic behavior needed for the connection. On the other hand, if the distance between the first weld and the face of the column is large, the bar may buckle if it experiences large compressive strains. In the test components, the first weld on each bar was placed at 38 mm (1.5″) from the tube face. The length of this weld was about 50 mm (2″). The second weld was placed 127 mm (5″) from the first weld, and its length was also approximately 50 mm (2″). Finally, the remainder of each deformed bar was welded to the girder flange.

During the inelastic cyclic loading, the weld nearest the column face fractured, for all of the bars that failed by tension rupture. This left three out of four bars with a slenderness ratio (l/r) of about 45. This length did not appear to affect the buckling behavior when those bars were subjected to compression. Upon subsequent deformation cycles, however, the second weld of one of these three bars fractured. Due to the larger slenderness of this bar, it buckled when it was subjected to compression. The bar that did not rupture in tension had strain gages applied to it. The protective coating for these gages reduced the ability of the bar to develop its tensile strength, and hence this bar pulled out of the concrete.

The deformed bars for the tested connection were selected to develop approximately 85% of the girder flange force. Providing enough bars to develop the full strength of the girder flange might require larger bars, which may create problems with weld quality, as well as placement and spacing problems of the bars on the girder flange. Also large bars may create large significant eccentricities between the center of the bar and the flange. This may impose additional stresses on the weld that must be considered in the design of this connection type. Bending stresses were observed in the 3–D finite element models of the deformed bars. Therefore, small diameter bars are recommended for this connection. Further, since there was a 50% increase in the flexural strength of this connection, and a 5% increase in the elastic stiffness compared to the ideal rigid connection condition, it appears that not even 85% of the flange force must be developed. In fact, because of its over–strength and stiffness compared to ideal girder behavior, the percentage of the flange strength needed out of the embedded deformed bars could likely decrease.

In some cases, weldable deformed bars may be undesirable. In lieu of the deformed bars, flat bar stock, or plates, with standard hooks could be used to transfer some of the girder forces to the concrete core. These flat bar elements can be welded and/or bolted to girder flanges. If the flat members were designed to develop the full flange force, then there would be no need to flare the stub flanges. However, as indicated by the analytical work, the stub flange should be attached to the pipe wall in order to prevent local instability in the connection stub. This modified connection can be implemented in different sizes of CFT columns, and will not disrupt other girders connected in orthogonal, or skewed, directions.

6.1.5 Continuous Flanges, Type VI

Flange continuity plates were used in the connection *Type VI* detail in an attempt to develop the tensile strength of the girder flanges. However, while the envelope curves of the force–displacement or moment–rotation behavior appears to be improved compared to other connections tested, the hysteretic behavior was quite pinched. This pinching was due to the slip of the flange plates in the concrete core until a new level of deformation was imposed. The strength increased at each new deformation amplitude, producing a stable appearance to the envelope curves, but the strength diminished significantly upon subsequent same–amplitude deformation cycles. For this connection type, the appearance of the force–displacement, or moment–rotation, envelope values is deceptive. The initial tangent stiffness, however, is a reasonably accurate measure of the tangent stiffness at the various deformation levels.

Continuing the flanges of the connection through the CFT core increased the stiffness of the detail compared to the simple connection *Type I*. The tangent stiffness for this *Type VI* connection was almost 100% of the ideal conditions for rotations less than 0.2%, however, the stiffness decayed significantly at 1.0% rotation. The decay initially was slightly more than the diaphragm plate connection, but in the larger deformation amplitudes the tangent stiffness for these two connection types was almost coincidental.

The large slip of the flange plates precipitated a secondary failure mode. Because top and bottom fillet welds attached the continuous flange plate to the tube wall, on each side of the column, the tube wall experienced significant tearing. Therefore, for this connection to be useful in a region of moderate to high seismicity, the slip of the continuous flange plates must be prevented. This slip will clearly be more critical for an interior joint configuration, in which girders frame to each side of the CFT column.

One method to improve the performance of the this connection detail is to add blocks to the continuous flange plate on each side of the CFT column. These blocks would be needed to transfer tension forces in the flange to bearing stresses on the far side of the CFT column.

Another method to prevent slip might be to drill holes in the continuous flange plates, such that the holes are on the interior of the steel tube. Deformed bars may then be inserted through the holes of the top and bottom flange plates. An access hole may be needed to place the deformed bars for small diameter tubes. The number of deformed bars must be sufficient to distribute the flange forces in bearing to the concrete core. However, for the added expense of this type of detail for this connection, the continuous girder , detail *Type VII*, may become more economical.

6.1.6 Continuation of the Girder through the Column, Type VII

Connection *Type VII* best represented the ideal rigid connection condition, and is preferable for seismic regions. The flexural strength of this connection exceeded 1.3 times plastic bending strength of the girder. Although the connection strength started to deteriorate at approximately 4.0% rotation, the connection strength was maintained at $1.0M_p$ up to failure at approximately 12%. The tangent stiffness for the continuous connection stub, *Type VII*, remained reasonably stable throughout the imposed deformation cycles. This tangent stiffness was initially 100% in the small amplitude deformation cycles, while this stiffness deteriorated to about 90% of the ideal rigid connection conditions by the end of the cycle deformation history. This detail was the only tested connection that produced an FDR value larger than the minimum needed value of 4. At the value of FDR = 4.37, this connection clearly produced sufficient ductility capacity.

Analytical and experimental studies indicated that for the element sizes used in the current study, this connection was limited only by the plastic hinge formation in the girder. Further, neither study exhibited signs of distress in the concrete core adjacent to the connection region, nor the steel tube wall. This type of connection may be sufficient for most column dimensions except for small diameter pipes.

The only difference between connection *Types VI* and *VII* was the continuity of the web plate in detail *Type VII*. Connection *Types IA* and *VII* differed by not continuing the flanges in detail *Type IA*. Therefore, details *Type IA* and *VI* can also be viewed as studying the effect of continuing either the flanges or the web in the continuous connection detail. Because of the full continuity in detail *Type VII* this connection was approximately 12% stronger than the connection with the continuous web *Type IA,* and 15% stronger than the connection with continuous flanges *Type VI*. Further, in the case of connection *Type IA*, the strength began to deteriorate rapidly, while in connection *Type VI* the hysteretic behavior became very pinched. Significant damage to the connection stub and tube wall occurred in connection *Types IA* and *VI* that were not illustrated by detail *Type VII*. Therefore, it may be concluded that embedding both the flanges and the web in the concrete core is important in improving the connection behavior. Clearly, the minimal cost increase of continuing the web and the flanges will result in significant improvement in the inelastic connection performance.

Table 6.1. Flexural Characteristics of the Tested Connections

Detail	$\Delta_{elastic}$ (%)	Δ_{max} (%)	*FDR*[†]	Avg. *FDR*	M_{max}/M_p	Avg. M_{max}/M_p	Initial Stiffness Ratio[‡] (%)
Type I	1.50	2.13	1.42	1.88	0.88	0.97	85
	–1.20	–2.80	2.33		1.06		
Type IA	1.33	3.30	2.47	2.55	1.31	1.26	100
	–1.29	–3.38	2.62		1.22		
Type II	1.33	3.74	2.81	2.83	1.22	1.17	100
	–1.20	–3.43	2.85		1.13		
Type III	1.20	4.18	3.48	3.46	1.63	1.56	106
	–1.17	–3.97	3.43		1.50		
Type VI	1.69	5.78	3.42	3.76	1.25	1.23	100
	–1.33	–5.41	4.10		1.16		
Type VII	1.33	5.54	4.20	4.37	1.38	1.37	100
	–1.24	–5.63	4.53		1.36		

[†] Flexural Ductility Ratio calculated from the force–displacement behavior of the connection

[‡] Relative to the ideal connection

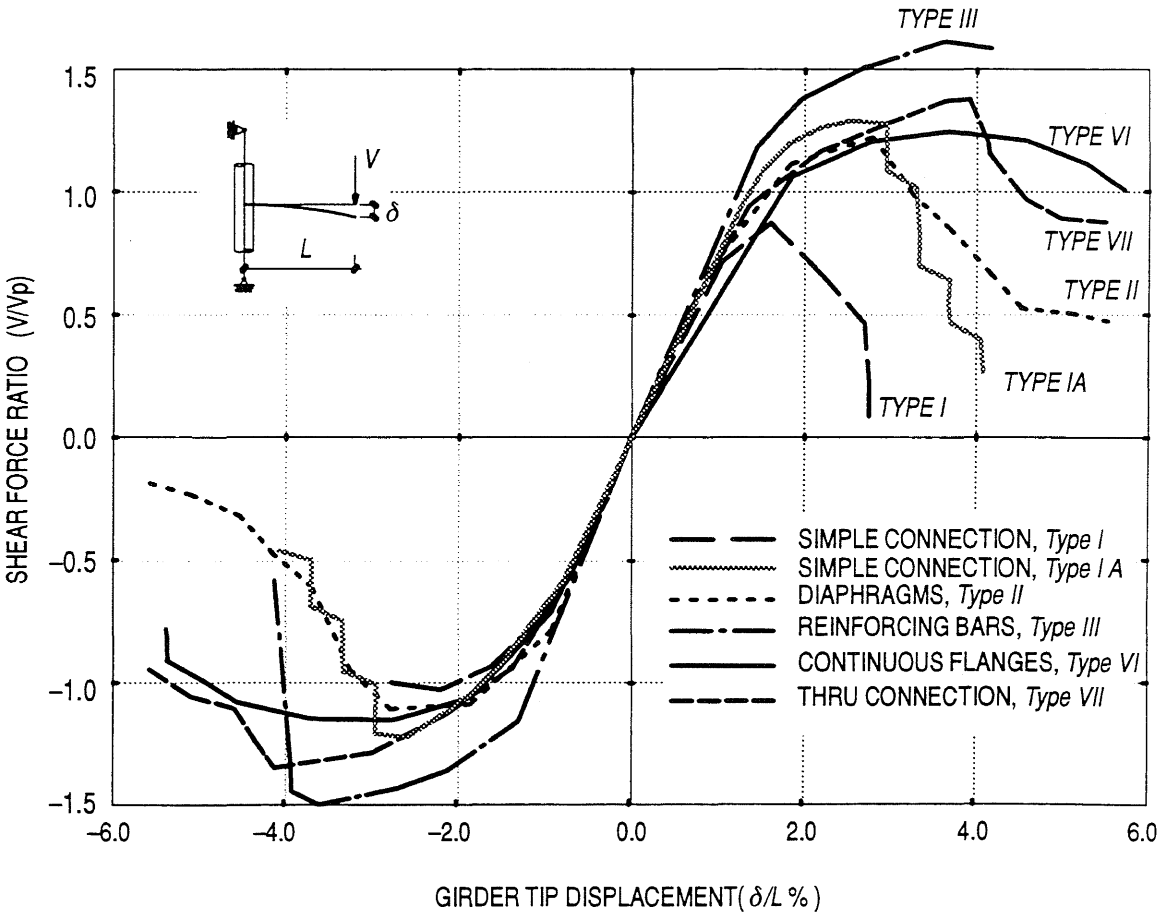

Figure 6.1. Force–Displacement Envelope Curves for the Tested Specimens

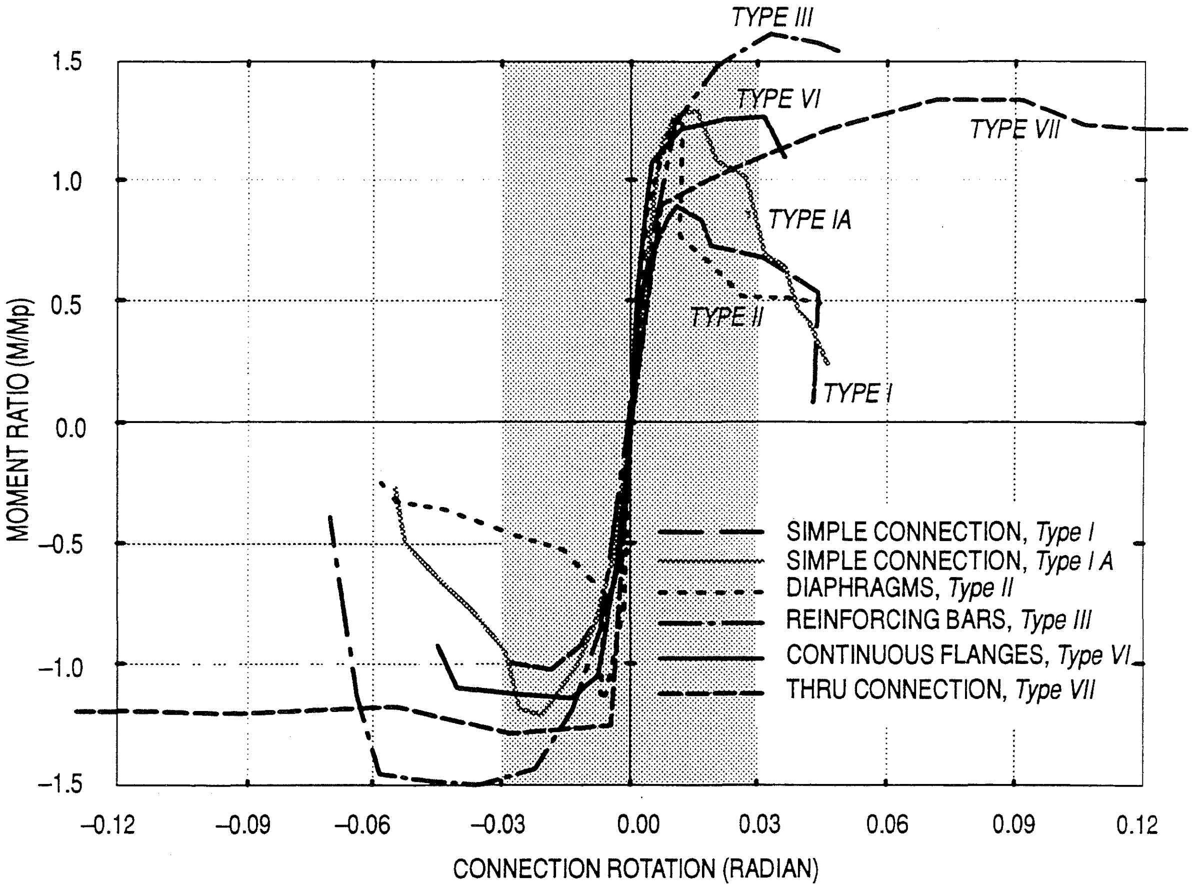

Figure 6.2. Moment–Rotation Envelope Curves for the Tested Specimens

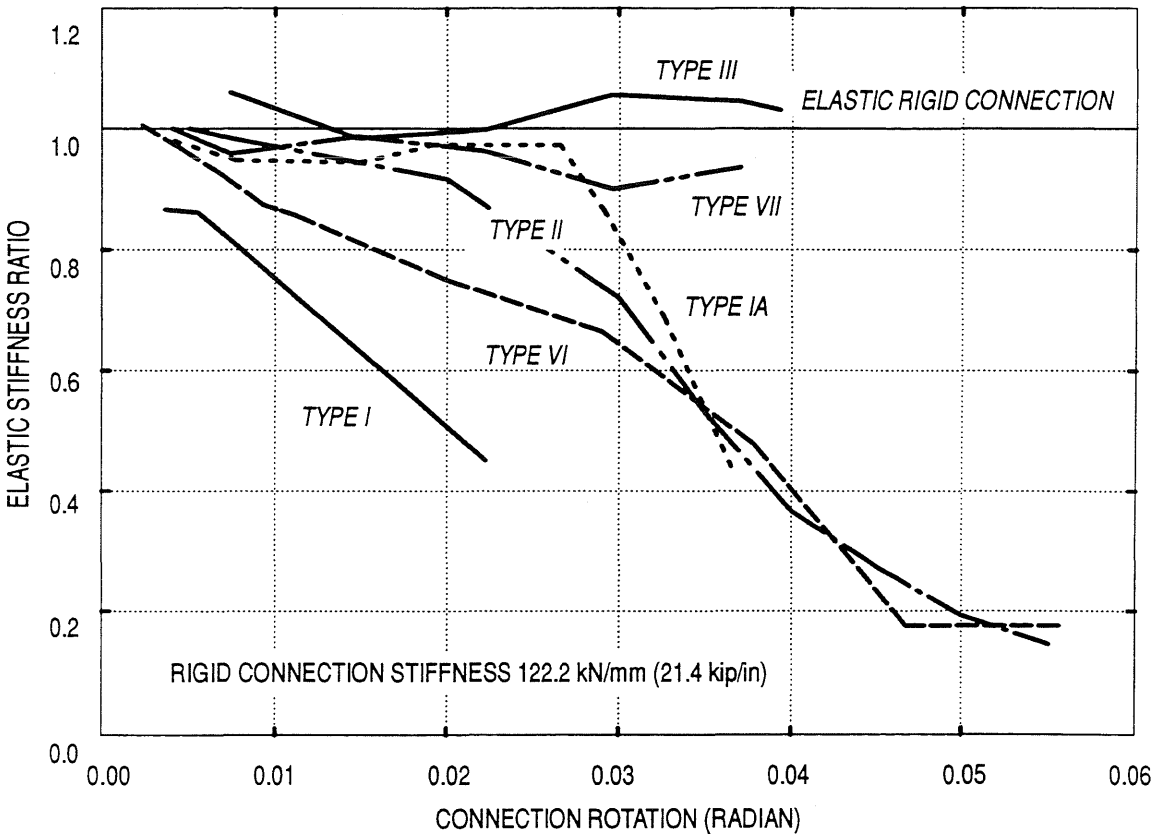

Figure 6.3. Variation of the Elastic Stiffness

CHAPTER 7

CONCLUSIONS AND RECOMMENDATIONS

7.1 SUMMARY

The primary object of this research was to investigate a variety of details that connect steel wide flange sections to circular concrete–filled steel tubes. Because most frames are designed for the hinging girder conditions, the flexural performance of the girder was the critical issue in this study. Since the primary objective of this research program was to investigate the flexural behavior of the connection, and not joint or panel zone behavior, connections to one side of the concrete– filled tube column only were sufficient. Therefore, all joint configurations were considered to be exterior joint configurations. Connection details that covered a broad range of fabrication possibilities were considered. To study these connection details, the seismic demand on moment– resisting frames having concrete–filled tube columns needed to be investigated. Consequently, an 8 story, 5 bay, and a 14 story, 3 bay prototype frames were designed to satisfy the *1991 NEHRP Recommendation for Seismic Provisions*. The inelastic seismic behavior of these frames was investigated using the nonlinear program DRAIN–2DX, and the results of these analyses were used to identify typical section sizes, and loading parameters, for critical joints in each frame. Several connection details were investigated using a 3–D nonlinear finite element model constructed for each connection detail. ABAQUS was used for all finite element modeling. A parametric study was conducted to investigate the factors that affect the performance of each detail. Parameters included: the axial load ratio, the overall depth–to–tube wall thickness, the moment–to–shear ratio, yield strength of the steel tube, and in some cases the effect of the interior joint. Six large–scale specimens were selected and tested using the quasi–static test method. The purpose of the experimental investigation was to further study the inelastic cyclic performance of the more promising connection details identified by the analytical study. Several features from this study are worth noting.

7.2 INELASTIC DYNAMIC ANALYSIS OF THE PROTOTYPE FRAMES

1) The performance of each frame using the steel–concrete composite columns depended significantly on the ground acceleration record used in the study. One seismic event may

cause an even distribution of the dissipated energy in the frame elements. While the same frame may experience a concentration of damage in only few floors when subjected to a different ground motion. This creates great difficulty in determining a critical joint in the frame.

2) Although the frames were designed to satisfy the *1991 NEHRP Provisions*, strong earthquakes caused story drift larger than the 1.5% limit specified by these provisions. The 8 story frame exhibited story drifts as large as 6.0%, while for the 14 story building, the maximum story drift was 3.5%. The short frame also exhibited a greater susceptibility to larger ductility demand than the tall frame.
3) The base shear strength of these frames with composite columns was approximately 2.6 times the base shear strength required by the *1991 NEHRP Provisions*. This excess, or reserve, lateral frame strength beyond minimum required base shear strength was mainly due to the over strength of the girders and composite columns at the base of the structure.
4) In general, the short frame exhibited a concentration of damage to few stories in the structure, while damage was well distributed to many floors in the tall frame.

7.3 CONNECTION DETAIL STUDY

Due to the 1994 Northridge earthquake, and the damage noted in steel frames connections, a minimum standard rotational capacity has evolved through the SAC (1995) program. For moment–resisting steel frames located in large–magnitude, seismic prone regions, the connection is expected to provide at least a minimum plastic rotation of 2.0%. It was also assumed that a minimum elastic rotation was approximately 0.67%. Therefore, the minimum rotational capacity for a severe seismic event should be 3% total without significant deterioration in the structural integrity of the connection. Only connection *Types III*, *VI*, and *VII* had this rotational capacity. Although, the rotation capacity of connection *Type VI* was satisfactory, the cyclic performance was not. The *EUROCODE* (Johnson 1994) requires that the rotation capacity of the connection should be checked. However, this requirement is waived if the connection is 20% stronger than the connected girder.

A second criteria has developed relating the presumed ductility of the system to the implied ductility needed by the *Uniform Building Code* or *NEHRP Provisions*. While this might be an accurate assessment of true behavior, it suggests that the connection must sustain a minimum flexible ductility ratio of 4.0. Based on this criteria, only the continuous connection stub detail, *Type VII*, provided this amount of ductility. Connection *Type III* had significant ductility, yet only produced an FDR = 3.46. However, this connection well exceeded the rotation capacity of 3%.

The following are specific observations of each connection detail.

7.3.1 Simple Connection, Type I

1) Severe tube wall distortions prohibited the development of the full plastic bending capacity of the girder, and fracture of the flange, the weld, and the tube wall was observed in the tested connection. Due to the high stiffness and strength of the CFT column, however, the damage was concentrated locally around the connected region. In fact, damage for all tested specimens was localized around the connected region.
2) The strength of this connection was limited by the through thickness shear strength of the tube wall. The tube wall began to tear as the connection reached its ultimate bending strength equivalent to the plastic hinge strength of the girder.
3) The tested *Type I* detail indicated that only 7% of the girder shear was transferred from the steel tube to the concrete core. Therefore, very little bond strength was available to transfer the girder shear forces to take advantage of the composite behavior.
4) The analytical study showed that the diameter–to–tube wall thickness improved the stiffness of the connection, however, only a marginal increase in flexural strength was observed. Connections with large *M/V* ratio exhibited more flexible behavior compared to connections with smaller *M/V* ratio. High axial loads may cause significant shortening of the CFT column. Finally, the yield strength of the steel tube did not have a significant effect on the connection performance.
5) The flexural strength of the connection exhibited some decrease when the connection was used in an interior joint configuration. This reduction in strength was due to the diagonal stress developing in the steel tube between the tension flanges on the girder on either side of the column. Further, although the shear on the panel zone increased almost 83%, the concrete did not exhibit evidence of excessive stresses or strains. Therefore, for this connection in an interior joint, panel zone behavior did not appear to be significant.

6) Welding the girder directly to the steel tube wall, as in connection *Type I*, should not be used in moment–resisting frames constructed in moderate and high seismic regions.

7.3.2 Continuous Web Plate Connection, Type IA

1) Extending the web plate through the concrete core significantly improved the flexural strength, the stiffness and the ductility compared to the simple connection.
2) High flexural distortion, once the flange fractured, induced high local stresses and strains on the continuous web. A portion of the web fractured outside the tube wall, while the remainder fractured inside the tube wall.
3) While this connection attempted to improve the shear behavior of the simple connection once the flanges fractured, the tearing of the web was prolonged only slightly. These conditions may be exacerbated for cross sections in which the web contributes 25% or more to the fluxural resistance of the girder.
4) While this connection may be used in regions with low frequency, low magnitude seismic activity, this detail may be more suitable for braced frames.

7.3.3 Connection with External Diaphragms, Type II

1) The minimum size diaphragm also improved the inelastic performance of the simple connection *Type I*. The strength, stiffness and ductility were about equivalent to the continuous web detail.
2) Damage to the tested minimum size diaphragm plate connection precipitated at the re–entrant corner between the diaphragm and the girder flange, propagated through the heat affect zone, eventually into the tube wall. Once the fracture initiated, the steel tube wall became subjected to significant deformation demands. Therefore, the diaphragm plate did not necessarily alleviate the severe distortion on the steel tube skin as noted in the simple *Type I* connection.
3) Analytical results suggest that the inelastic performance of the diaphragm plate, connection *Type II*, can be improved when the girder end shifted farther from the face of the concrete–filled tube column. This provided an improved path for the flow of stresses around the concrete–filled steel tube, and resulted in a less sharp re–entrant corner at the flange intersection, compared to the minimum diaphragm plate. Good stress and strain

performance was exhibited for this detail when the girder end was located approximately *2.2* times the pipe radius from the center of the concrete–filled tube column.

4) The analytical performance of this detail was slightly improved as the *D/t* decreased. However, the CFT axial loads and the steel tube yield strength did not have significant effect on the elastic performance of the connection.
5) This connection detail might be useful in low frequency, low magnitude seismic regions.

7.3.4 Connection with Deformed Bars, Type III

1) The inelastic cyclic behavior of the simple *Type I* connection was greatly improved when deformed bars were used to transfer part of the girder force to the concrete core. The flexural strength was more than 50% larger than the plastic bending strength of the girder. Up to failure of the specimen, at approximately 5% rotation, this connection sustained 1.5 times the girder flexural strength.
2) The connection had a stiffness equivalent to, or greater than, that of an ideal rigid connection. This occurred over the entire range of imposed deformations. This was a significant increase compared to the simple *Type I* connection detail.
3) Prior to failure of this specimen, the girder exhibited clear evidence of flange buckling outside the region of the weldable deformed bars. This suggests significant inelastic deformations provided by the connection.
4) Failure of this connection was by tension rupture for three of the four deformed bars on one flange. The fourth bar failed by pull out of the concrete core, in which the pull out failure was attributed to measurement sensors placed on the deformed bar. The tension failure suggests the deformed bars had sufficient development in the concrete core, and the welding to the girder flange was satisfactory.
5) The configuration of the weld and the attachment of the girder flanges to the steel tube are essential to the stability of the connection elements.
6) The amount of flange force transferred to the reinforcing bars was independent of the steel tube thickness. The axial load and the steel pipe yield strength had little effect on the connection performance.
7) This connection could be used in regions at moderate to high seismic risk.

7.3.5 Connection with Headed Studs, *Type IV*

1) Placing headed studs behind each girder flange, as in connection *Type IV*, may also be effective in relieving severe distortions on the steel tube wall of the simple connection *Type I* detail.
2) According to the analytical model, the failure mode of the headed studs is due to tension fracture on the shank of the stud. This was for a stud embedment length of 89 mm (3.5″).
3) Studs further away from the web of the girder are less effective than studs closer to the web in resisting the flange forces. This was due to the high skew angle between the longitudinal axis of the girder, and the axis of the stud. For pipes larger than the 508 mm (20″) diameter pipe used in the analytical study, this problem diminishes.
4) The analytical behavior of this connection showed significant sensitivity to the moment–to–shear ratio on the girder. Connections with small M/V ratio had more ductile behavior compared to those with larger M/V ratios. The strength of the connection was limited by the strength of the studs, so the thickness and yield strength of the pipe did not have significant effect on the connection performance.

7.3.6 Connection with Web Plate and Headed Studs, *Type V*

1) The strength and stiffness of this connection was dominated by the behavior of the web outside the steel tube, which produced the lowest strength and stiffness of any of the connections investigated in this study. The strength of the connection was approximately 72% of the shear strength of the cantilever girder, and the initial tangent stiffness was 28% of the ideal rigid connection conditions.
2) The embedded headed studs did not contribute to the flexural strength of the connection. The analytical models illustrated that the studs experience very little shear resistance at the shank. The flexibility and low strength of the web outside the steel tube prevented the development of large strains on the web inside the concrete core.
3) The connection behavior was controlled by the web plate, therefore, the thickness of the pipe, the M/V ratio, and the yield strength of the steel tube had little effect on the connection performance.

4) This connection type should not be used in regions of high seismic activity. It is possible with detailing modifications, that this connection could be used in braced frame systems.

7.3.7 Continuous Flanges, Type VI

1) The continuous flange plate connection, *Type VI*, exhibited satisfactory ductility, initial tangent stiffness, and strength characteristics. This connection was able to develop approximately 125% of the flexural strength of the girder, and its initial stiffness was equivalent to that of the ideal rigid connection.
2) The failure mode of this connection was by continual slip of the flange plate through the concrete core upon subsequent deformation cycles. Since the continuous flange plates were welded to the steel tube, slipping of the flange plates precipitated significant tube wall tearing.
3) Due to slip of flange plates, the hysteretic behavior became significantly pinched. Therefore, this detail dissipated very little inelastic energy with each cycle of imposed deformation.
4) This detail, as tested, should not be used for a moment–resisting connection in a seismic region, but can be improved with some detailing modifications.

7.3.8 **Continuation of the Girder through the Column, *Type VII***

1) The continuous girder stub produced behavior that best represented ideal connection conditions. The sustained flexural strength was 1.37 times the plastic bending strength of the girder, and the sustained tangent stiffness was between 90% to 100% of the rigid connection condition.
2) The inelastic cyclic behavior of this connection was limited by the connected girder. The steel tube and the concrete core in the connection vicinity did not display obvious signs of distress.
3) Analytical results suggest that larger axial load ratios improve behavior of the connection stub interior to the CFT column. Large axial loads exhibited smaller tension at the interface between the steel section and the concrete core compared to smaller axial loads.
4) Although the interior joint produces almost twice the shear, the concrete core did not appear to be crushing, nor the steel tube near excessive stresses or strains. Further, the panel zone did not appear to be a critical issue for the specimen sizes used in the analytical study.

However, bond stresses appeared to reach the limit of available stress as discussed in the literature.

5) The analytical connection performance was slightly affected by the thickness of the tube and the yield strength of the tube wall.
6) This connection can be used in regions of moderate to high seismic risk.

7.4 RECOMMENDATIONS ON RESEARCH NEEDS

This research program investigated a variety of connection details to develop feasible connections that produce the flexural strength of the girder. Since this study was on a wide range of connection details, many detailing issues for specific connections remain unresolved. Other factors that influence connection behavior include:

- *Interior joints.* The effect of the panel zone behavior may influence performance of the connections because of the added distortions at the connection.
- *Shear strength of the circular concrete–filled tube.* To estimate the panel zone strength, the shear strength of the cross section must be better defined.
- *Bolted connection alternatives.* Steel connections damaged by the 1994 Northridge earthquake demonstrated critical issues concerning the fully welded connection. While the research work on the fractured connection issue will clearly improve the quality of the welding and construction processes, bolted alternative must be considered. Bolted connections to the circular face of the pipe create a significant challenge not associated with the square or rectangular concrete–filled tube counterpart.
- *Braced frame connection details.* Concrete–filled tube columns have significant advantage over conventional steel or concrete column types as members in braced frames. Economical connections are needed to make these composite elements feasible in braced systems. This applies to concentric and eccentric braced frames.
- *Structural system performance.* Significant work must be done to study the effect of these connections on the overall performance of the structure during a seismic event.
- *Concrete slabs.* It is possible that the composite behavior resulting from the floor slab will benefit the performance of details that behave like typical semi–rigid connections. The concrete deck can also become more integral with the CFT column.

- *Analytical finite element models.* This includes more reliable concrete material models, and in particular, interface models to allow larger imposed deformations.
- *Inelastic connection and element modeling.* True seismic performance will be difficult to assess until analytical models of materials and elements incorporate reliable degrading strength, degrading stiffness and failure behavior.

REFERENCES

1). "ABAQUS User's Manual." (1994). Hibbitt, Karlsson, and Sorensen, Inc. Pawtucket, Rhode Island.

2). Adrian, C. A., and Triantafillou, T. C. (1992). "Creep and Shrinkage Analysis of Composite Systems under Axial Load and Biaxial Bending." Materials and Structures, Vol. 25, pp. 543–551.

3). Alostaz, Y. M. (1992). "Bond Slippage in Reinforced Concrete Flexural Members." Master Thesis, Jordan University of Science and Technology, Irbid,The Hashemite Kingdom of Jordan.

4). Anderson, D., and Najafi, A. A. (1994). "Performance of Composite Connections: Major Axis End Plate Joints." Journal of Constructional Steel Research, Vol. 31, No. 1, pp. 31–57.

5). Ansourian, P. (1976). "Connections to Concrete–Filled Tube Columns." International Association of Bridge and Structural Engineers, Vol. 36–I, pp. 1–22.

6). Ansourian, P., and Roderick, J. W. (1976). "Composite Connections to External Columns." Journal of the Structural Division, Proceedings of the ASCE, August, Vol. 102, No. ST8, pp. 1609–1625.

7). ASCE Task Committee on Design Criteria for Composite Structures in Steel and Concrete (1994). "Guidelines for Design of Joints Between Steel Beams and Reinforced Concrete Columns." Journal of Structural Engineering, ASCE, Vol. 118, No. 11, pp. 3036–3054.

8). "ATC–24: Guidelines for Cyclic Seismic Testing of Components of Steel Structures." (1988). Applied Technology Council, Readwood City, California.

9). Azizinamini, A. and Prakash, B. (1993). "A Tentative Design Guidelines for a New Steel Beam Connection Detail to Composite Tube Columns." AISC Engineering Journal, 3rd quarter, pp. 108–115.

10). Bangash, M. Y. H. (1989). "Concrete and Concrete Structures: Numerical Modeling and Applications." Elsevier Applied Science.

11). Basu, P. K., Lee, S. L. (1989). "Steel Structures." ASCE Proceedings of the Session Related to Steel Structures at Structures Congress '89, Ed. Iffland, J. S. B., San Francisco, pp. 185–194.

12). Boyd, P. F., Cofer, W. F. and Mclean, D. I. (1995). "Seismic Performance of Steel–Encased Concrete Columns Under Felxural Loading." ACI Structural Journal, V. 92, No. 3, May–June, pp. 355–364.

13). Bridge, R. and Webb, J. (1992). "Thin Walled Circular Concrete Filled Steel Tubular Columns." Composite Construction of Steel and Concrete II, ASCE, pp. 634–649.

14). Broderick, B. M., Elnashi., A. S. (1994). "Seismic Resistance of Composite Beam–Columns in Multi–Story Structures. Part 2: Analytical Model and Discussion of Results." Journal of Constructional Steel Research, Vol. 30, No. 3, pp. 231–258.

15). "Building Code Requirements for Reinforced Concrete." (1992). ACI 318–89 Revised 1992. American Concrete Institute, Detroit, Michigan.

16). Daniels, J. H., Kroll, G. D., and Fisher J. H. (1970). "Behavior of Composite–Beam to Column Joints." Journal of the Structural Division, Proceedings of the ASCE, March, Vol. 96, No. ST3, pp. 671–685.

17). Dawe, L. J., and Grondin, G. Y. (1990). "W–Shape Beam to RHS Column Connections." Canadian Journal of Civil Engineering, October, Vol. 17, No. 5, pp. 788–797.

18). Elghazouli, A. Y., and Elnashi, A. S. (1993). "Performance of Composite Steel/Concrete Members under Earthquake Loading. Part II: Parametric Studies and Design Considerations." Earthquake Engineering and Structural Dynamics, Vol. 22, pp. 347–368.

19). Elnashi., A. S., and Broderick, B. M. (1994). "Seismic Resistance of Composite Beam–Columns in Multi–Story Structures. Part 1: Experimental Studies." Journal of Constructional Steel Research, Vol. 30, No. 3, pp. 201–229.

20). Faschan, W. (1992). "The Bank of China, Advancing the Art of Composite Construction." Composite Construction of Steel and Concrete II, ASCE, p. 576.

21). Ge, H., and Usami, T. (1992). "Strength of Concrete–Filled Thin–Walled Steel Box Columns: Experiment." Journal of Structural Engineering, ASCE, Vol. 118, No. 11, pp. 3036–3054.

22). Griffis, L. and Maeda, Y. (1992). "Design of a 71–Story Composite Building in Dallas." Composite Construction of Steel and Concrete II, ASCE, pp. 574–575.

23). Hawkins, N., Mitchell, D. and Roeder, C. (1980). "Moment Resisting Connection For Mixed Construction." AISC Engineering Journal, 1st quarter, pp. 1–10.

24). Hunaiti, Y., Wakabayashi, M., and Masuo, K. (1992). "Experimental Evaluation of the Effect of Bond on the Maximum Capacity of Composite Columns." Journal of Constructional Steel Research, Vol. 22, No. 1, pp. 39–55.

25). Johnson, R. P. (1994). "Composite Structures of Steel and Concrete." Vol. I, 2nd edition, Blackwell Scientific Publications.

26). Kanaan, A., and Powell, G. H. (1973). "DRAIN–2D A general Purpose Computer Program for Inelastic Dynamic Response of Plane Structures." Report EERC 73–6, University of California, Berkeley, California.

27). Kanatani, H., Tabuchi, M., Kamba T., Hsiaolien, J., and Ishikawa, M. (1987). "A Study on Concrete Filled RHS Column to H–Beam Connections Fabricated with HT Bolts in Rigid Frames." Composite Construction of Steel and Concrete,ASCE, Edited by Buckner, C. D., and Viest, I. M., Proc. of an Engineering Foundation Conference, New Hampshire.

28). Kato, B., Kimura, M., Ohta, H. and Mizutani, N. (1992). "Connection of Beam Flange to Concrete–Filled Tubular Columns." Composite Construction of Steel and Concrete II, ASCE, pp. 528–538.

29). Kenny, J. R., Bruce, D. A., and Bjorhovde R. (1994). "Removal of Yield Stress Limitation for Composite Tubular Columns." AISC Engineering Journal, Vol. , No. , 1st quarter, pp. 1–11.

30). King, W., and Chen, W. (1993). "LRFD Analysis for Semi–Rigid Frame Design." AISC Engineering Journal, Vol. , No. , 4th quarter, pp. 130–140.

31). King, W., and Chen, W. (1994). "Practical Second–Order Inelastic Analysis of Semirigid Frames." Journal of Structural Engineering, ASCE, Vol. 120, No. 7, pp. 2156–2175.

32). Kishi, N., and Chen W. (1990). "Moment–Rotation Relations of Semirigid Connections with Angles." Journal of Structural Engineering, ASCE, Vol. 116, No. 7, pp. 1813–1834.

33). Kishi, N., Chen, W. F., Goto, Y., and Matsuoka, K. G. (1993). "Design Aid of Semi–Rigid Connections for Frame Analysis." AISC Engineering Journal, Vol. , No. , 3rd quarter, pp. 90–107.

34). Leon, R. T. (1987). "Behavior of Semi–Rigid Composite Frames." Composite Steel Structures; Advances, Design, Construction, ed. R. Narayanan, Elsevier Applied Science, pp. 145–153.

35). Leon, R. T. (1994). "Composite Semi–Rigid Construction." AISC Engineering Journal, Vol. , No. , 2nd quarter, pp. 57–67.

36). Lindsey, S. D. (1985–a). "The Effect of Connection Flexibility on Steel Members and Frame Stability." Connection Flexibility and Steel Frames, ed. Kanamani, ASCE Publications, pp. 6–11.

37). Lindsey, S. D., Ioannides, S. A., and Goverdhan, A. (1985–b). "LRFD Analysis and Design of Beams with Partially Restrained Connections." AISC Engineering Journal, 4th quarter, pp. 157–162.

38). Lorenz, R. F., (1985). "A New Alternative in Steel Construction– Partially Restrained Connections." Connection Flexibility and Steel Frames, ed. Kanamani, ASCE Publications, pp. 1–5.

39). "Load and Resistance Factor Design Specification for Structural Steel Buildings." (1994). American Institute of Steel Construction, Chicago, Illinois.

40). Lui, E. M., and Chen, W. F. (1988). "Behavior of Braced and Unbraced Semi–Rigid Frames." International Journal of Solids Structures, Vol. 24, No. 9, pp. 893–913.

41). Mander, J. B., Chen, S. S., and Pekan, G. (1994). "Low–Cycle Fatigue Behavior of Semi–Rigid Top– and Seat–Angle Connections." AISC Engineering Journal, 3rd quarter, pp. 111–122.

42). Marcakis, K., and Mitchell, D. (1980). " Precast Concrete Connections with Embedded Steel Members." PCI Journal of the Prestressed Concrete Institute, July–August, Vol. 25, No.4, pp. 88–116.

43). Menétrey, Ph., and Willam, K. J. (1995). " Triaxial Failure Criterion for Concrete and its Generalization." ACI Structural Journal, May–June, Vol. 92, No. 3, pp. 311–318.

44). Morino, S., Kawaguchi, J., Yasuzaki, C., and Kanazawa, S. (1992). "Behavior of Concrete Filled Steel Tubular Three Dimensional Subassemblages." Composite Construction of Steel and Concrete II, ASCE, pp. 726–741.

45). Narayanan, R. (1988). "Steel Concrete Composite Structures: Stability and Strength." Elsevier Applied Science.

46). "NEHRP Recommended Provisions for Seismic Regulations for New Buildings." (1991). Seismic Safety Council, Federal Emergency Management Agency (FEMA), Washington, D.C.

47). "PATRAN 2.5." (1990). PDA Engineering, Costa Mesa, California.

48). "PCI Design Handbook, Precast and Prestressed Concrete." (1971). Prestressed Concrete Institute, Chicago, Illinois.

49). Plumier, A., and Schleich, J. B. (1993). "Seismic Resistance of Steel and Composite Frame Structures." Journal of Constructional Steel Research, Vol. 27, No. 1–3, pp. 159–176.

50). Prakash, B. A. (1992). "Development of Connection Detail for Connecting Steel Beams to Composite Columns." Master Thesis, University of Nebraska, Lincoln, Nebraska.

51). Poggi, C., and Zandonini R. (1985). "Behavior and Strength of Steel Frames with Semi–Rigid Connections." Connection Flexibility and Steel Frames, ed. Kanamani, ASCE Publications, pp. 57–76.

52). Popov, E. P. (1985). "Flexibility of Steel Seismic Moment Connections." Connection Flexibility and Steel Frames, ed. Kanamani, ASCE Publications, pp. 101–119.

53). Raths, C. H. (1974). "Embedded Structural Steel Connections." PCI Journal of the Prestressed Concrete Institute, May–June, Vol. 19, No.3, pp. 104–112.

54). Roeder, C. W. (1984) "Bond Stress of Embedded Steel Shapes in Concrete." *ASCE Proceedings of US–Japan Joint Seminar on Composite & Mixed Construction*, Seattle.

55). Roeder, C. W., and Foutch D. (1996). "Experimental Results from Seismic Resistant Steel Moment Frame Connections." Journal of Structural Engineering, ASCE, Vol. 122, No. 6, pp. 581–588.

56). Roeder, C. W., Schneider, S. P., and Carpenter, J. E. (1993). "Seismic Behavior of Moment–Resisting Steel Frames: Analytical Study." Journal of Structural Engineering, ASCE, Vol. 119, No. 6, pp. 1866–1884.

57). Roik, K., and Bergmann, R. (1985). "Composite Columns – Design and Examples for Construction." Composite and Mixed Construction, ed. Roeder, C. W., published by ASCE, pp.267–278.

58). Schneider, S. P., Roeder, C. W., and Carpenter, J. E. (1992) "Seismic Performance of Weak–Column Strong–Beam Steel Moment Resisting Frames." Final Report, University of Washington, Seattle, Washington.

59). Schneider, S. P., Roeder, C. W., and Carpenter, J. E. (1993). "Seismic Behavior of Moment–Resisting Steel Frames: Experimental Study." Journal of Structural Engineering, ASCE, Vol. 119, No. 6, pp. 1885–1902.

60). "Semi–Rigid Connections in Steel Frames." (1993). Council on Tall buildings and Urban Habitat, Committee 43. McGraw Hill, Inc.

61). Shakir–Khalil, H. (1992). "Full Scale Tests on Composite Connection." Composite Construction of Steel and Concrete II, ASCE, pp. 539–554.

62). Shanmugam, N. E. (1994). "Externally Stiffened I–Beam to Box–Column Connections." Structures Congress XII, Vol. 1, Ed. Baker, N. C., and Goodno, B. J., Published by ASCE, pp. 719–724.

63). Steel Moment Frame Connections. Advisory Report No. 3. SAC 95–01. (1995). SAC Joint Venture Partnership, Sacramento, CA.

64). Stefano, M. D., Luca, A. D., and Astaneh–Asl, A. (1994). "Modeling of Cyclic Moment–Rotation Response of Double–Angle Connections." Journal of Structural Engineering, Vol. 120, No.1, pp. 212–229.

65). "Structural Steel Tubing: Composite Load Tables." (19??). American Institute for Hollow Structural Sections, Pittsburgh, PA.

66). Task group 20 Structural Stability Research Council (1979). "A Specification for the Design of Steel–Concrete Composite Columns." AISC Engineering Journal, Vol. 16, No. 4, 4th quarter, pp. 101–115.

67). Tomii, M., Sakino, K. (1988). "Concrete Filled Steel Tubes." Report to the Ministry of Education, Science and Culture, Dept. of Architecture, Kyushu University, Japan, Part I, pp. 1–22.

68). Toyoda, M. (1995). "Failure Experience of Steel Framed Structures Observed from Hanshin Great Earthquake." Department of Welding and Production Engineering, Osaka University, Japan.

69). Tschemmernegg, F. (1992). "The Non–Linear Behavior of Composite Joints." Journal of Constructional Steel Research, Vol. 21, No. 1–3, pp. 59–70.

70). Usami, T., and Ge, H. (1994). "Ductility of Concrete–Filled Steel Box Columns Under Cyclic Loading." Journal of Structural Engineering, Vol. 120, No.7, pp. 2021–2040.

71). Valbert, G. (1968). "Essais d' Assemblages Soudés d'une Solive Sur un Poteau en Tube Rempli de Béton." Construction Métallique, 4 Dec., pp. 27–38. (*in French*).

72). Viest, I., (1992). "Composite Construction Recent Past, Present, and Near Future." Composite Construction of Steel and Concrete II, ASCE, pp. 1–16.

73). Wexler, N. (1993). "Composite Girders with Partial Restraints: A New Approach." AISC Engineering Journal, Vol. , No. , 2nd quarter, pp. 68–75.

74). Wium, J. A., and Lebet, J. P. (1994). "Simplified Calculation Method for Force Transfer in Composite Columns." Journal of Structural Engineering, Vol. 120, No. 3, pp. 728–746.

75). Xiao, Y., Choo, B. S., and Nethercot, D. A. (1994). "Composite Connections in Steel and Concrete. I. Experimental Behavior of Composite Beam–Column Connections." Journal of Constructional Steel Research, Vol. 31, No. 1, pp. 3–30.

76). Yau, C. Y., and Chan, S. L. (1994). "Inelastic and Stability Analysis of Flexibly Connected Steel Frames by Springs–in–Series Model." Journal of Structural Engineering, Vol. 120, No. 10, pp. 2803–2819.

APPENDIX A

ANALYTICAL INVESTIGATION

Chapter 3 presented a comprehensive finite element analysis of selected connections to CFT columns. This appendix contains additional results from this numerical analysis.

The figures presented in this appendix are for the following details:

1. Simple connections, *Type I*,
2. Connections with external diaphragms, *Type II*,
3. Connections with reinforcing bars, *Type III*,
4. Connections with headed studs, *Type IV*,
5. Connections with continuous web plate and shear studs, *Type V*, and
6. Through connection, *Type VII*.

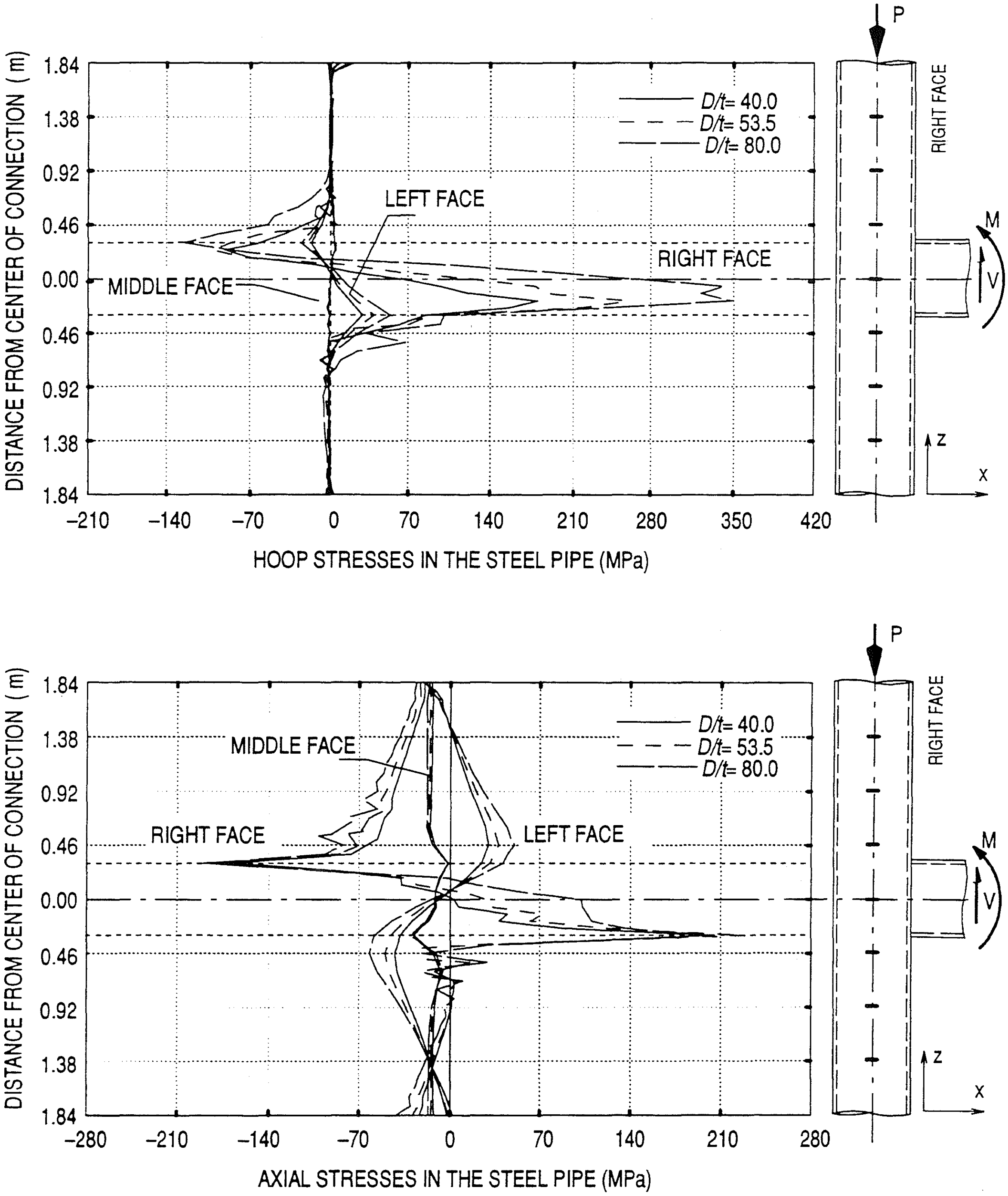

Figure A.1. Steel Pipe Stresses, Connection *Type I: D/t* Effect

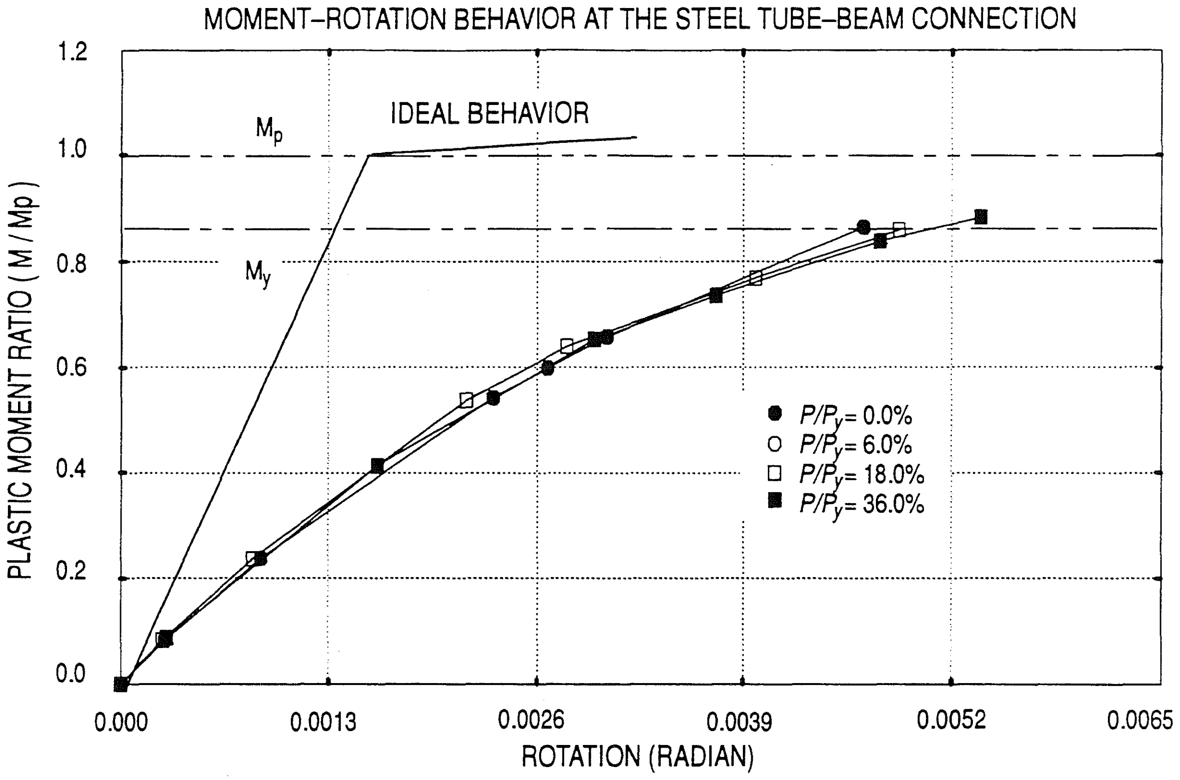
MOMENT–ROTATION BEHAVIOR AT THE STEEL TUBE–BEAM CONNECTION

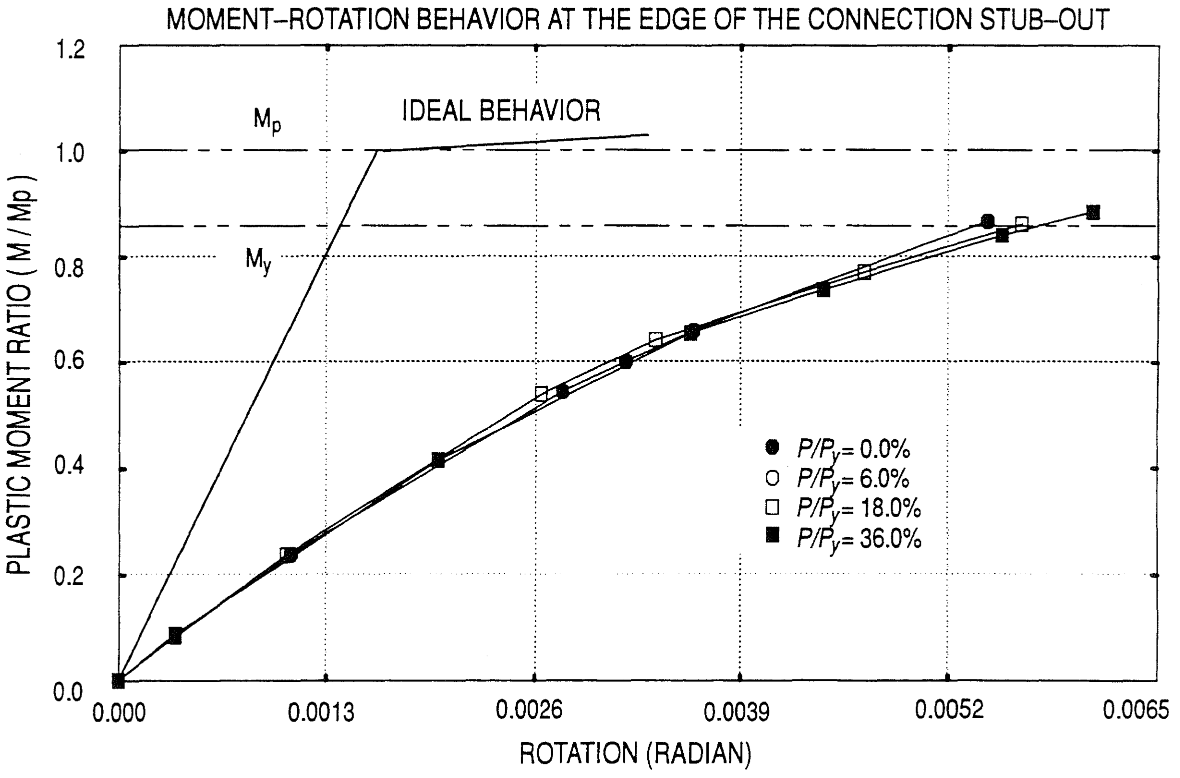
MOMENT–ROTATION BEHAVIOR AT THE EDGE OF THE CONNECTION STUB–OUT

Figure A.2. Analytical Moment–Rotation Behavior for Connection *Type I:* Load Ratio Effect

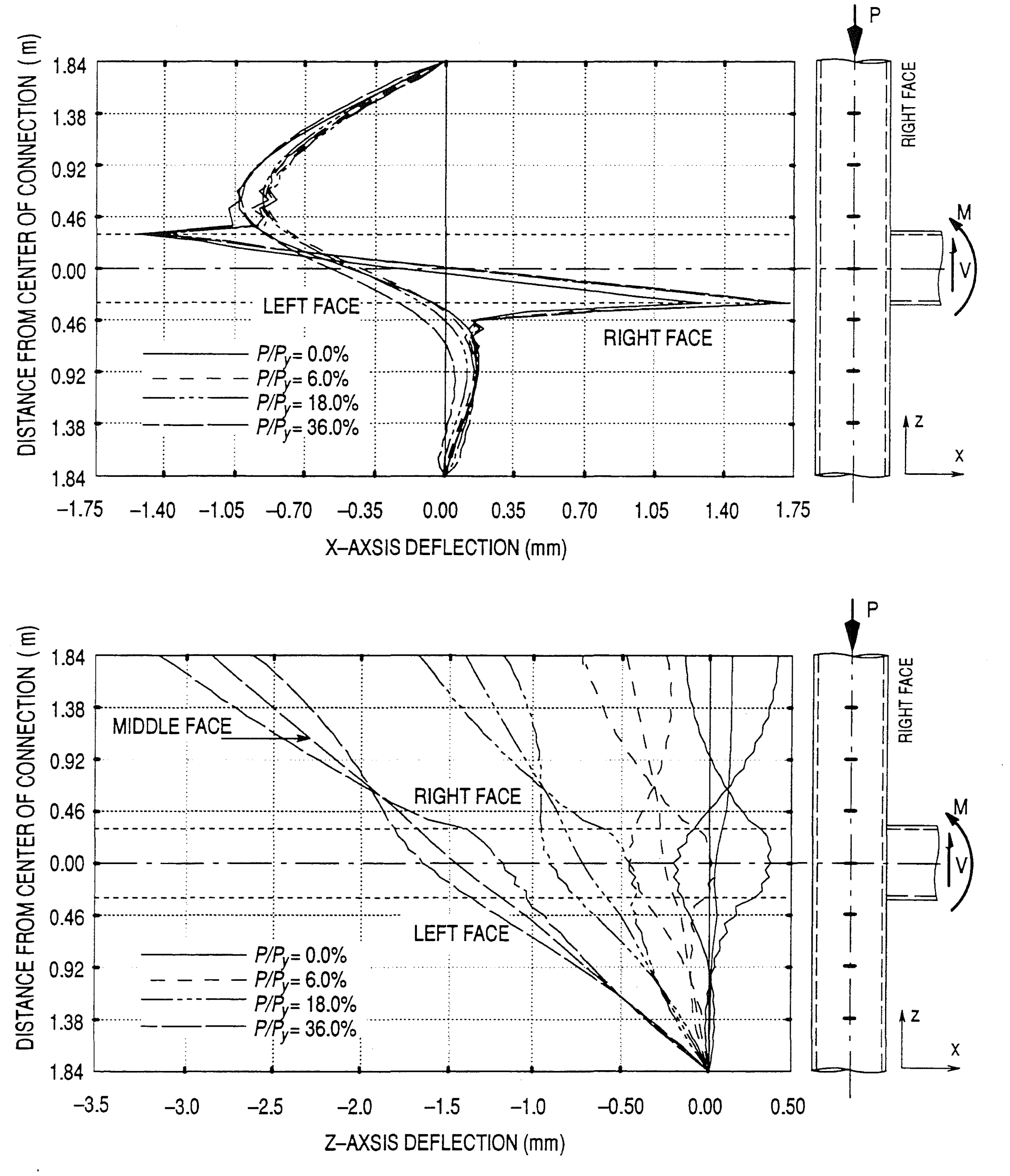

Figure A.3. Displacement of the Steel Pipe, Connection *Type I:* Load Ratio Effect

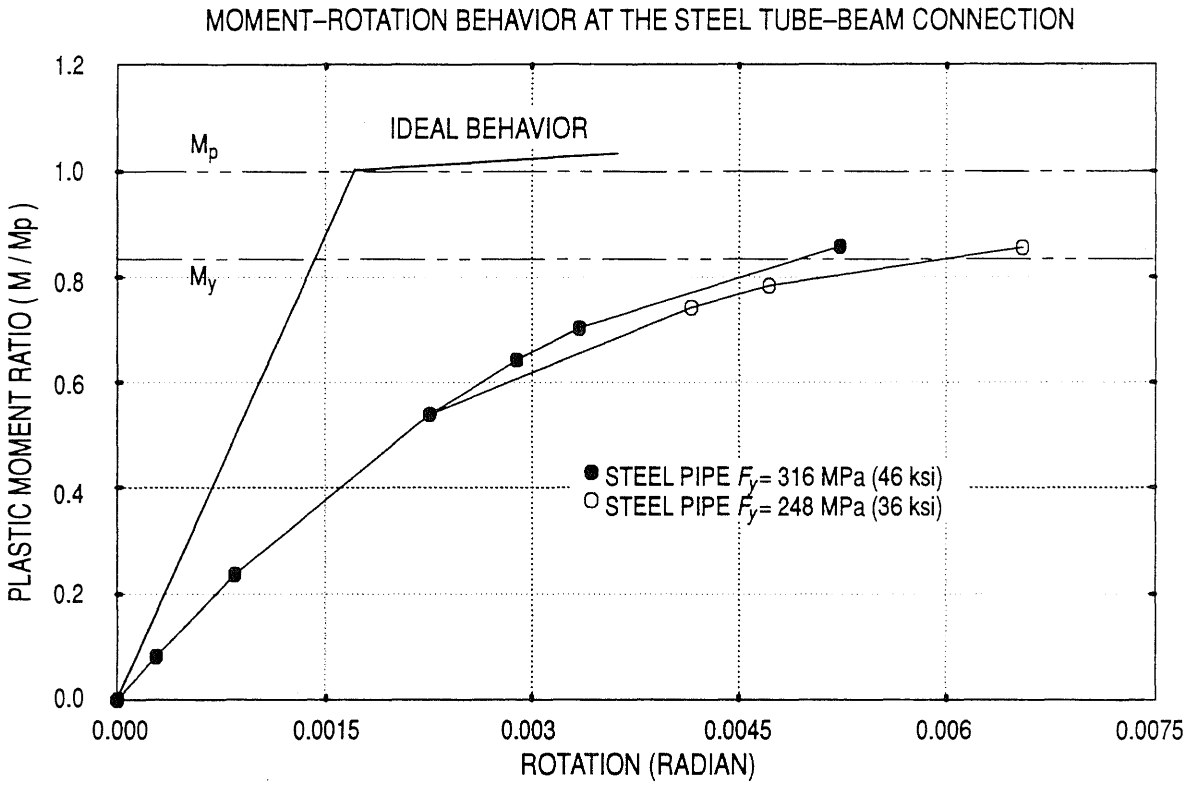

MOMENT–ROTATION BEHAVIOR AT THE STEEL TUBE–BEAM CONNECTION

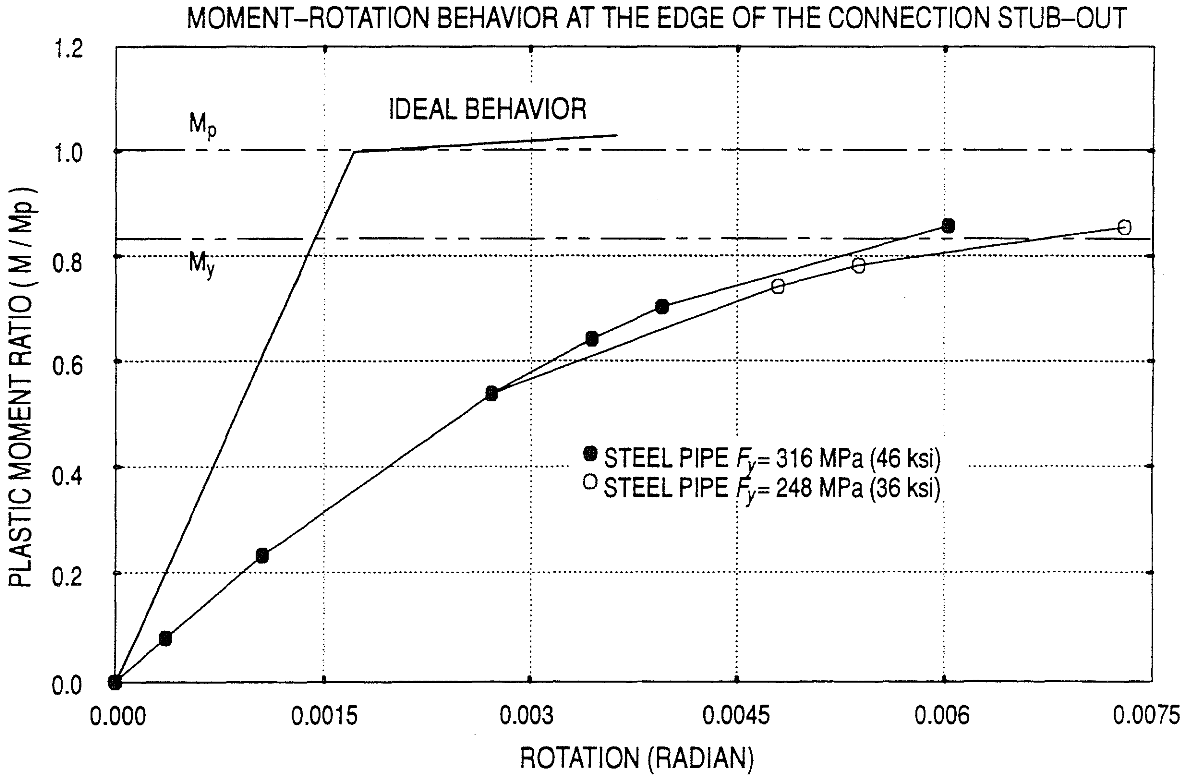

MOMENT–ROTATION BEHAVIOR AT THE EDGE OF THE CONNECTION STUB–OUT

Figure A.4. Analytical Moment–Rotation Behavior for Connection *Type I:* Steel Grade Effect

TOTAL DISPLACEMENT OF THE PIPE AND THE GIRDER

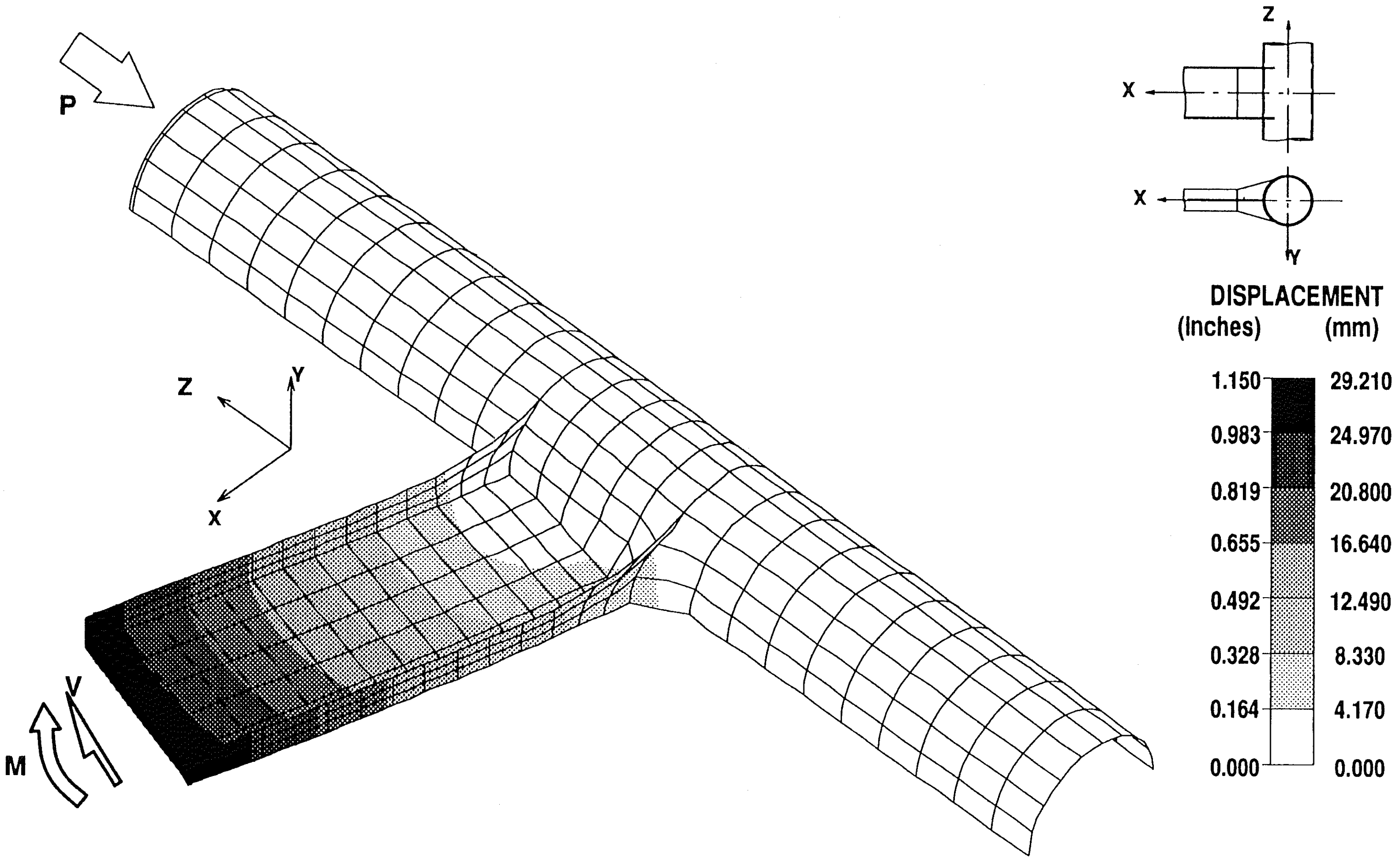

Figure A.5. Total Displacement and Deformed Shape of the Tube and the Girder, Connection *Type I*

CONCRETE CORE MINIMUM PRINCIPAL STRESS

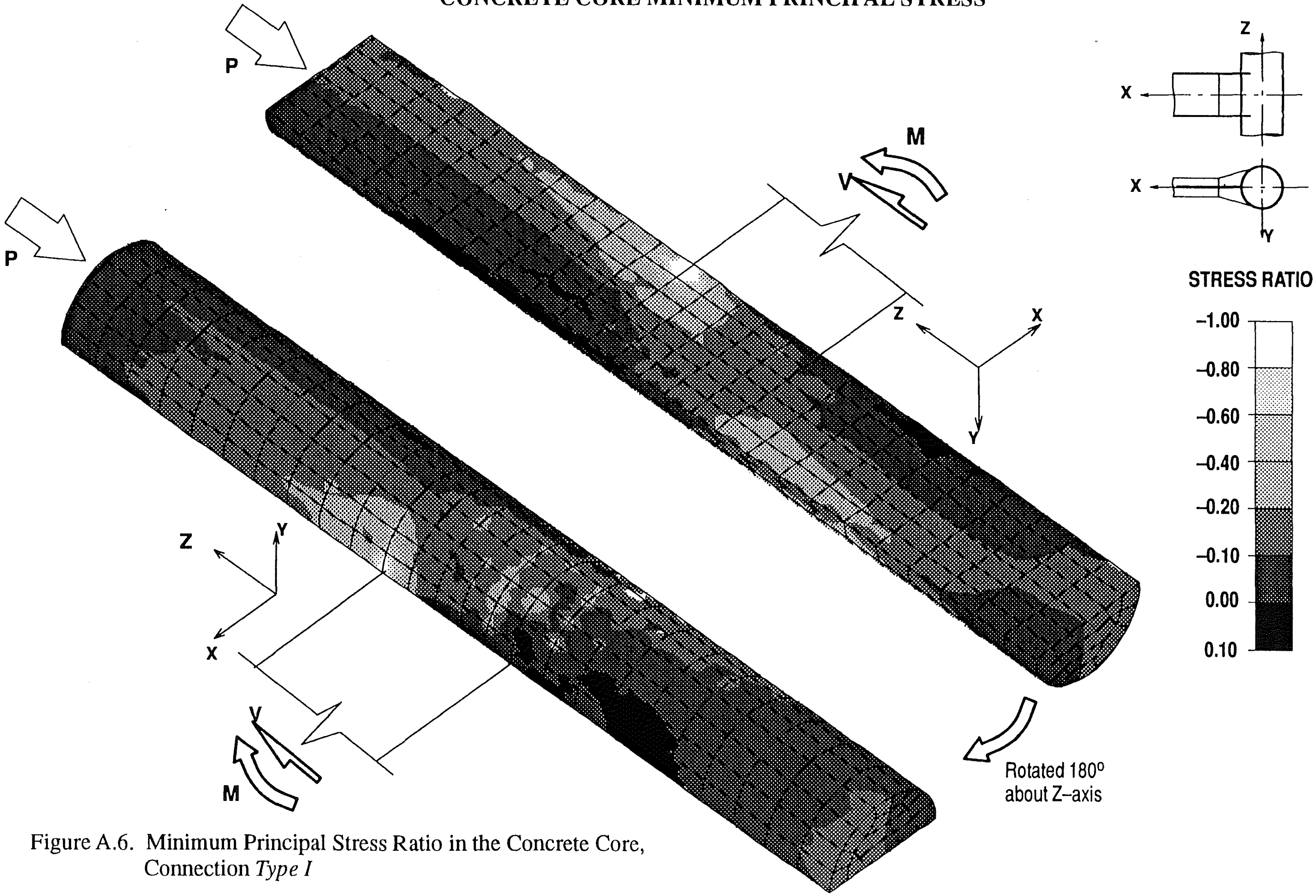

Figure A.6. Minimum Principal Stress Ratio in the Concrete Core, Connection *Type I*

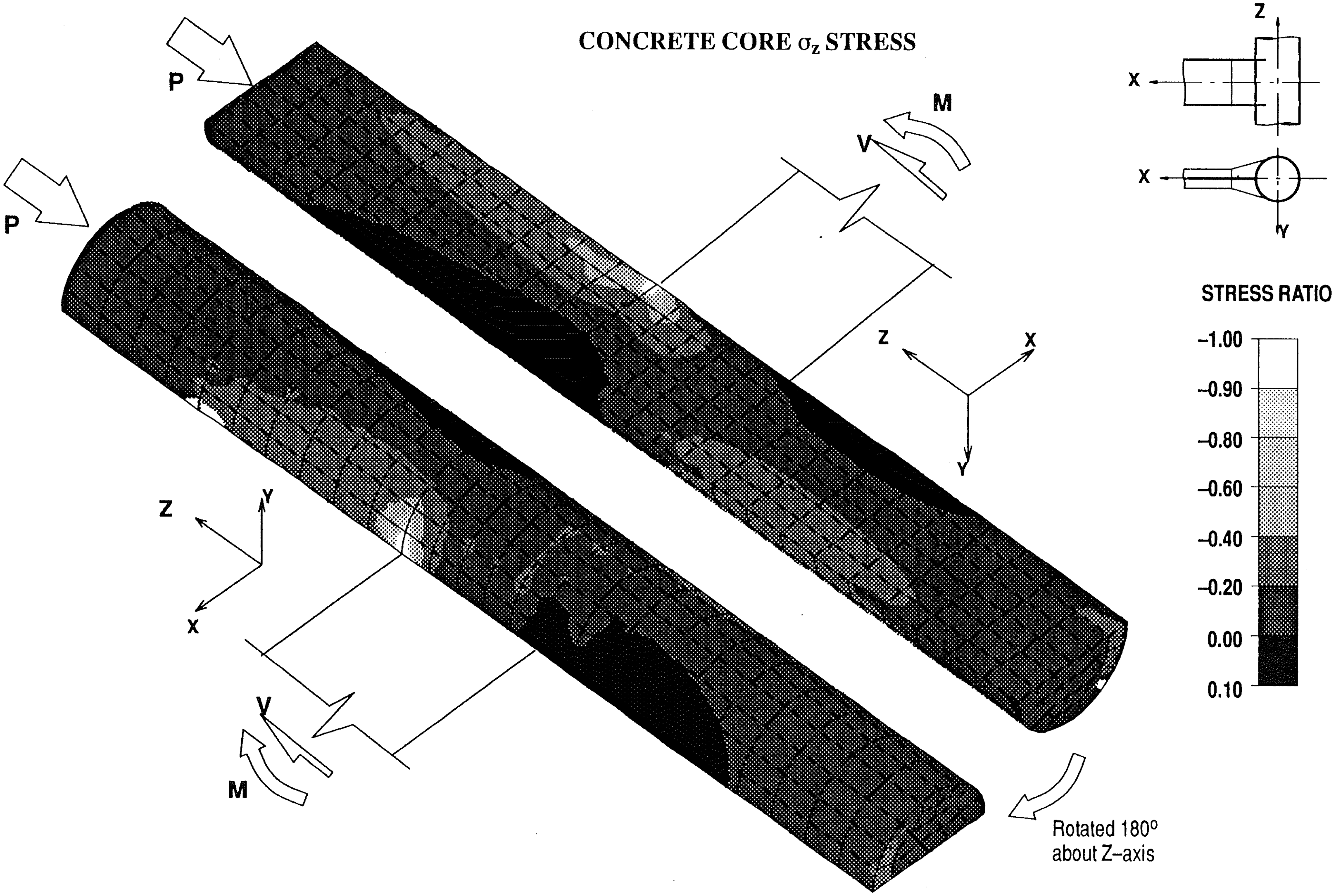

Figure A.7. Longitudinal Stress Ratio in the Concrete Core, Connection *Type I*

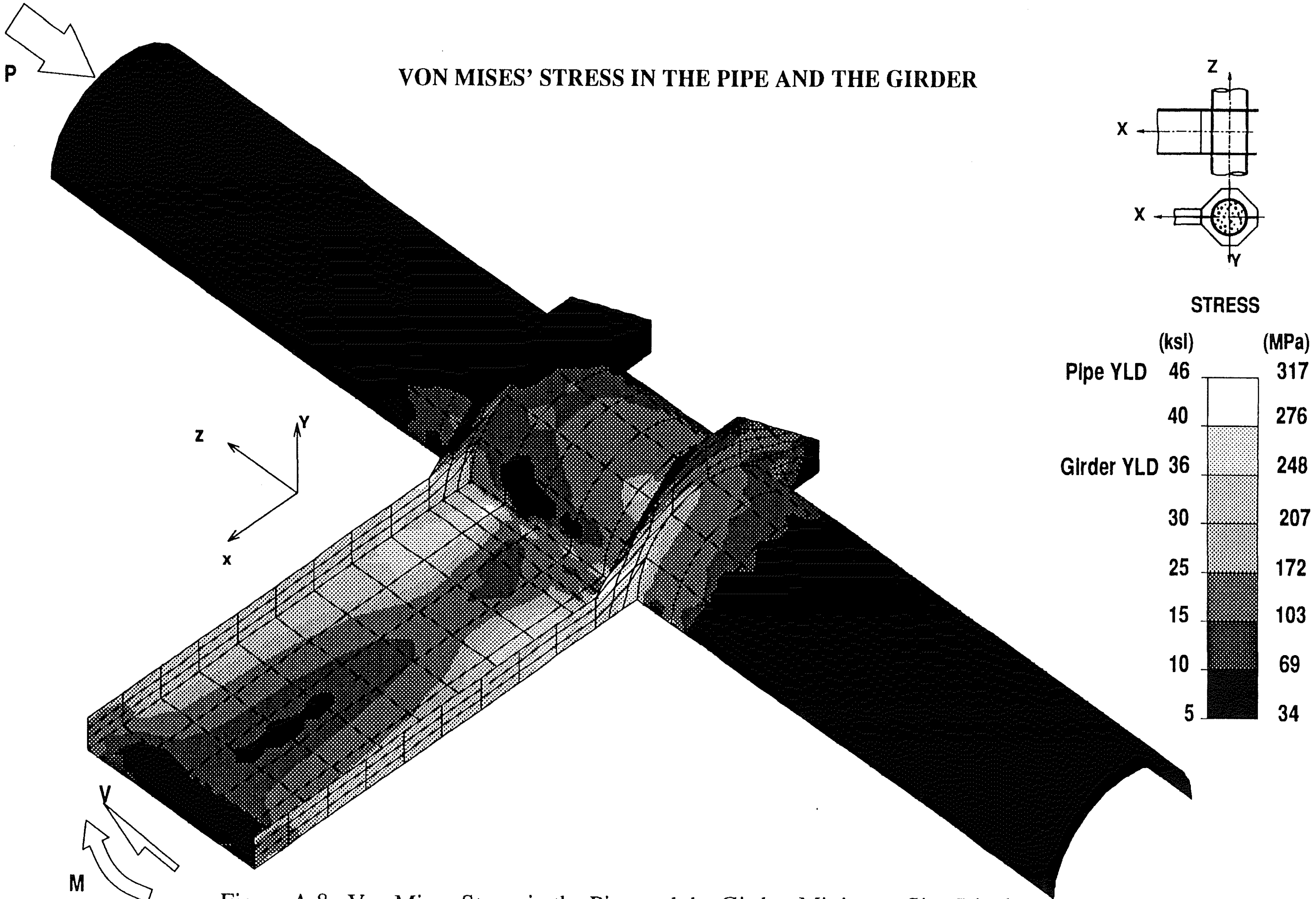

Figure A.8. Von Mises Stress in the Pipe and the Girder, Minimum Size Diaphragm

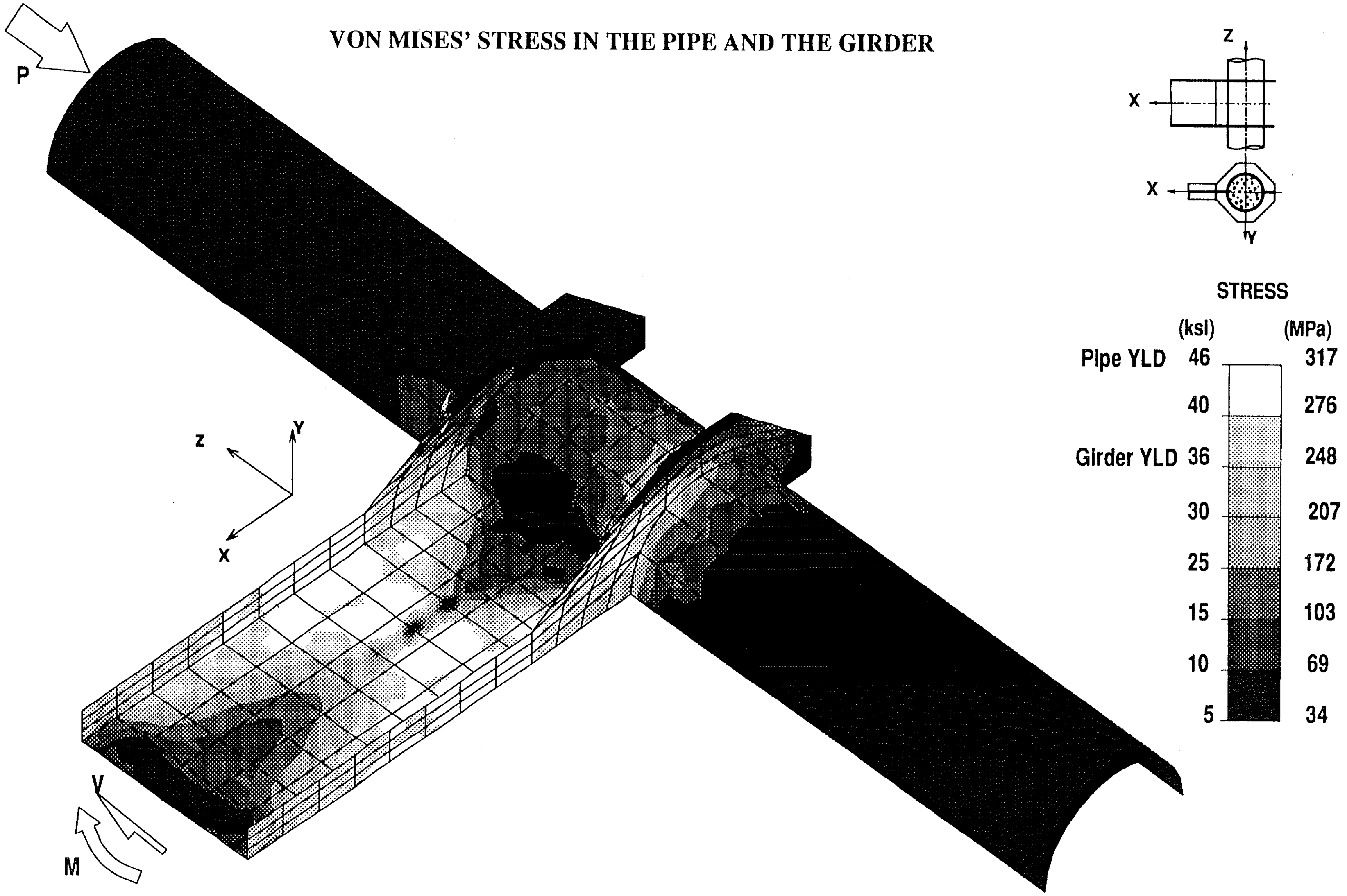

Figure A.9. Von Mises Stress in the Pipe and the Girder, Connection *Type IIA*

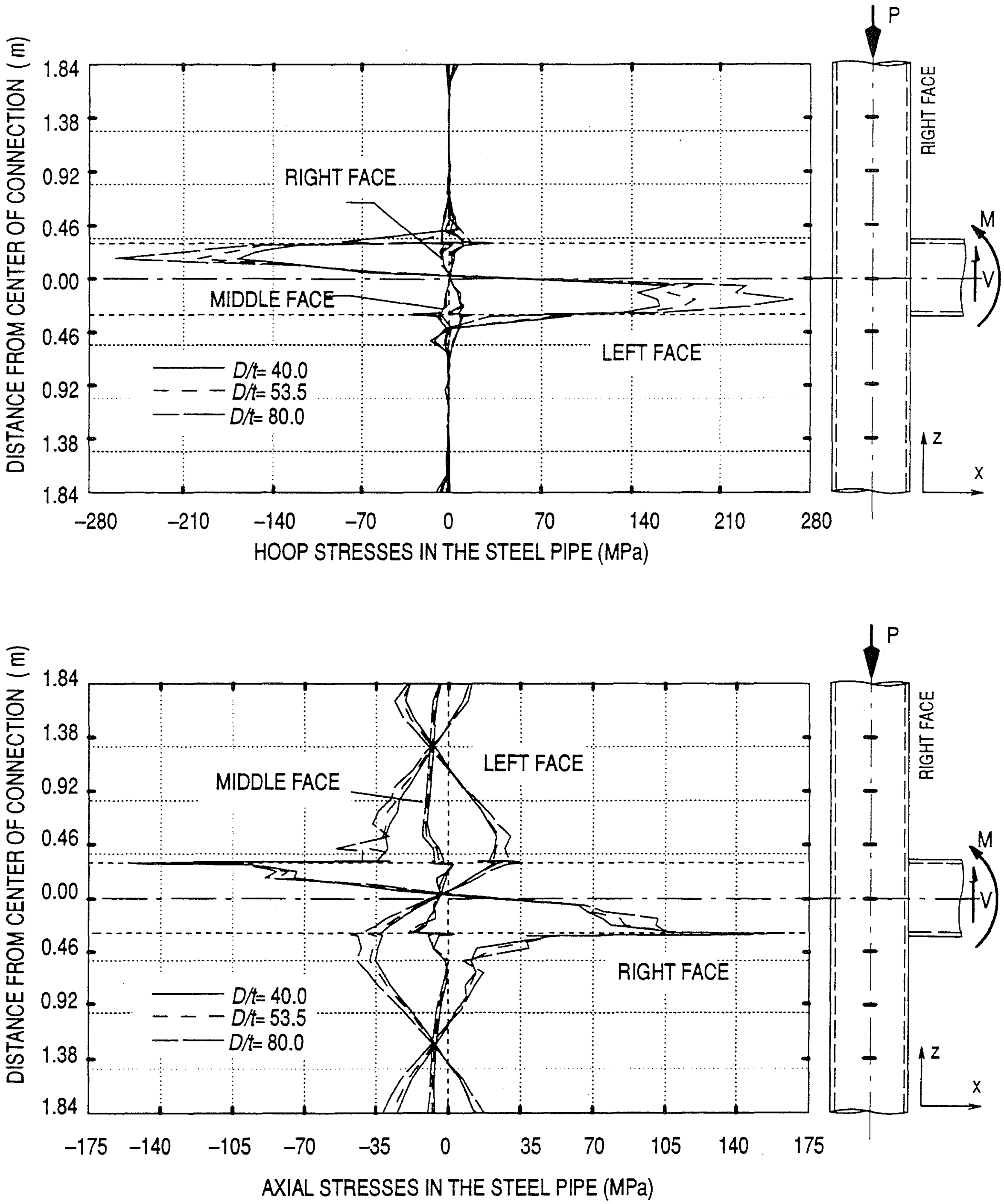

Figure A.10. Steel Pipe Stresses, Connection *Type III: D/t* Effect

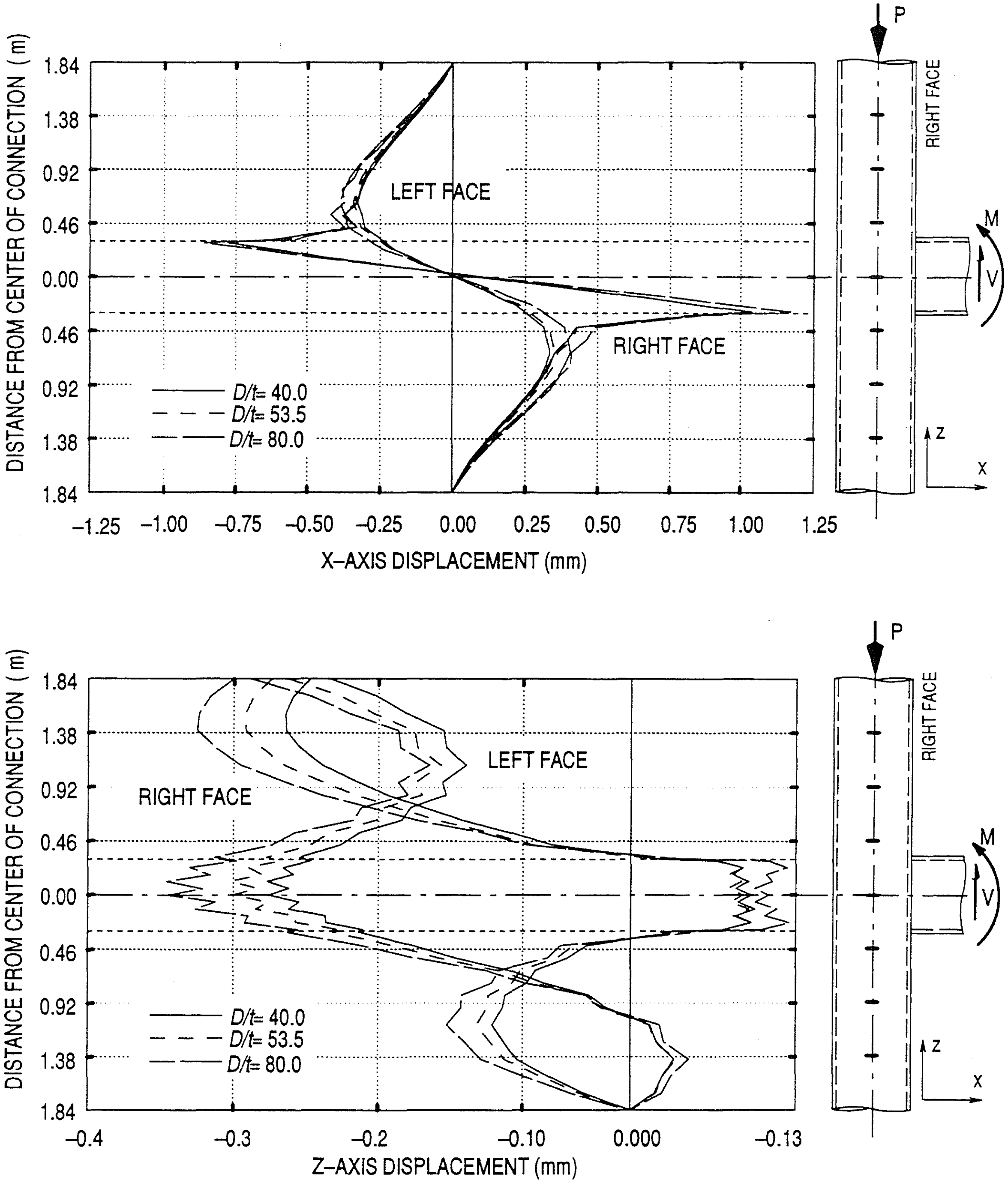

Figure A.11. Steel Pipe Displacements, Connection *Type III: D/t* Effect

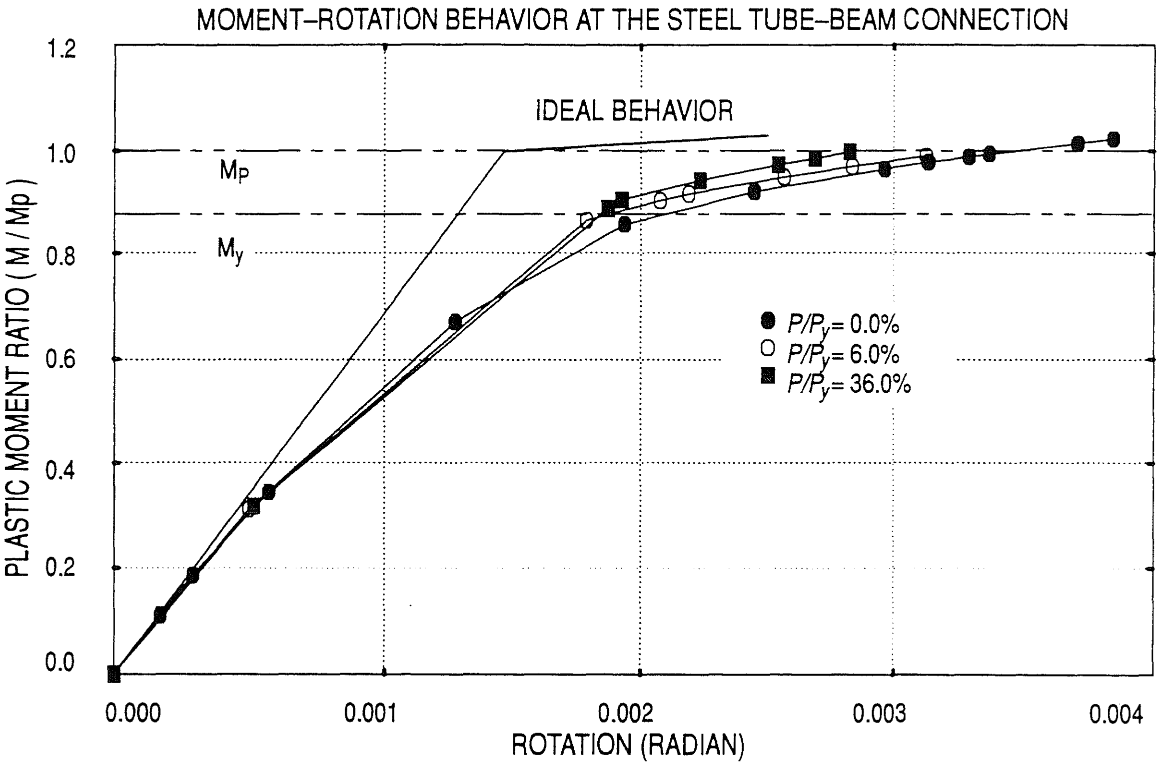

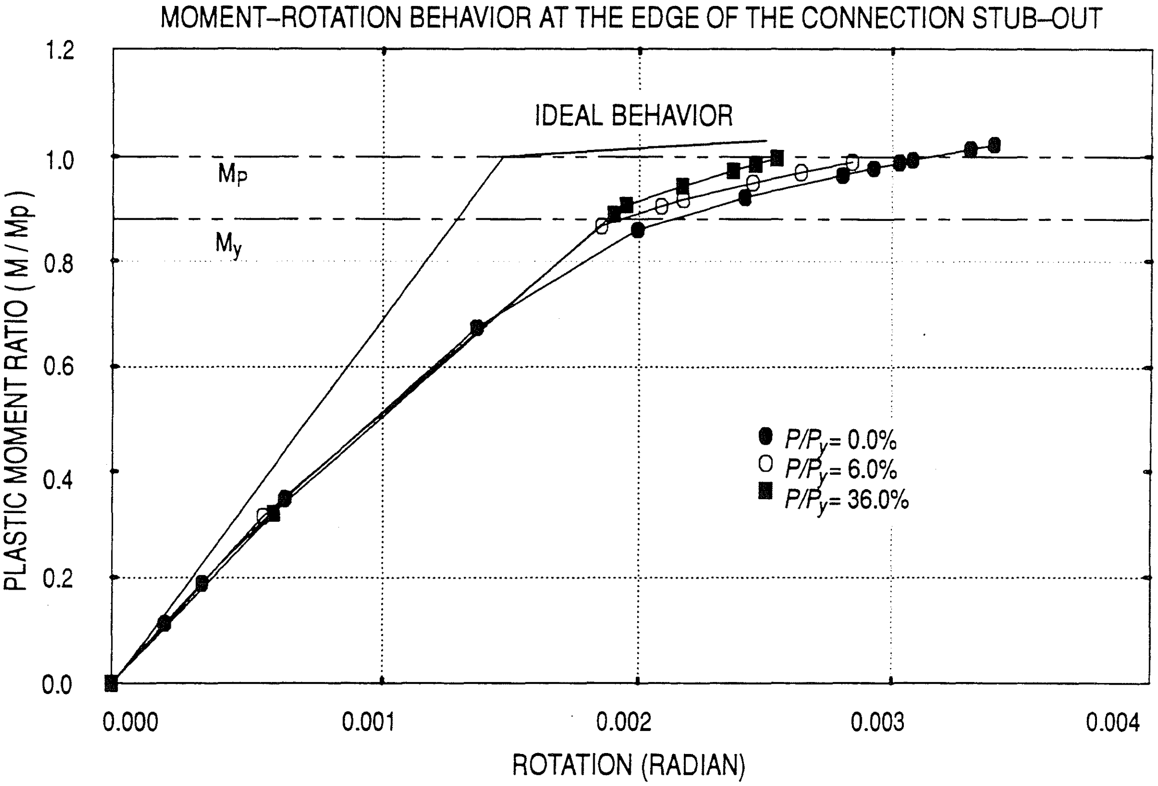

Figure A.12. Analytical Moment Rotation Diagram, Connection *Type III*: Load Ratio Effect

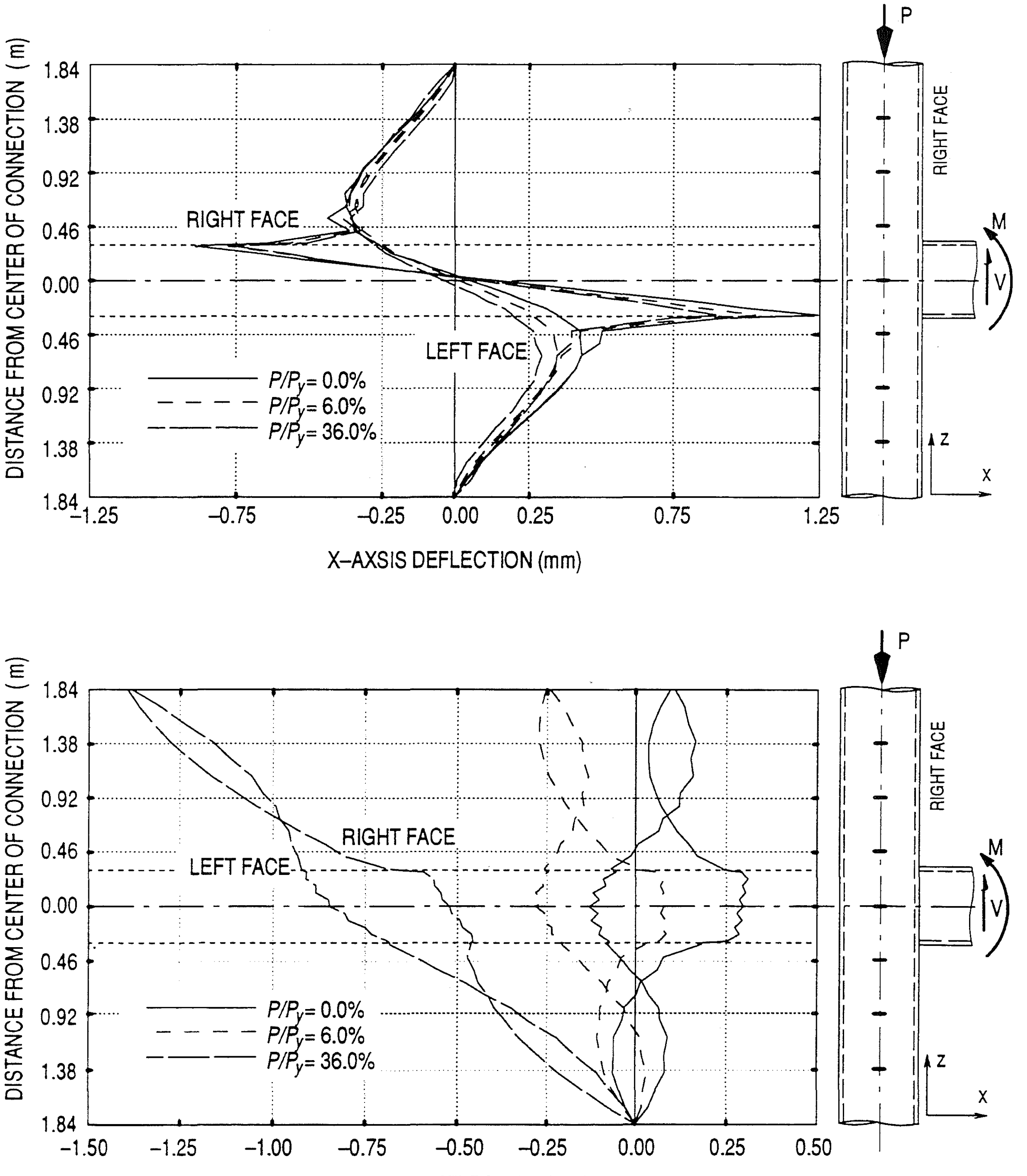

Figure A.13. Displacement of the Steel Pipe, Connection *Type III:* Load Ratio Effect

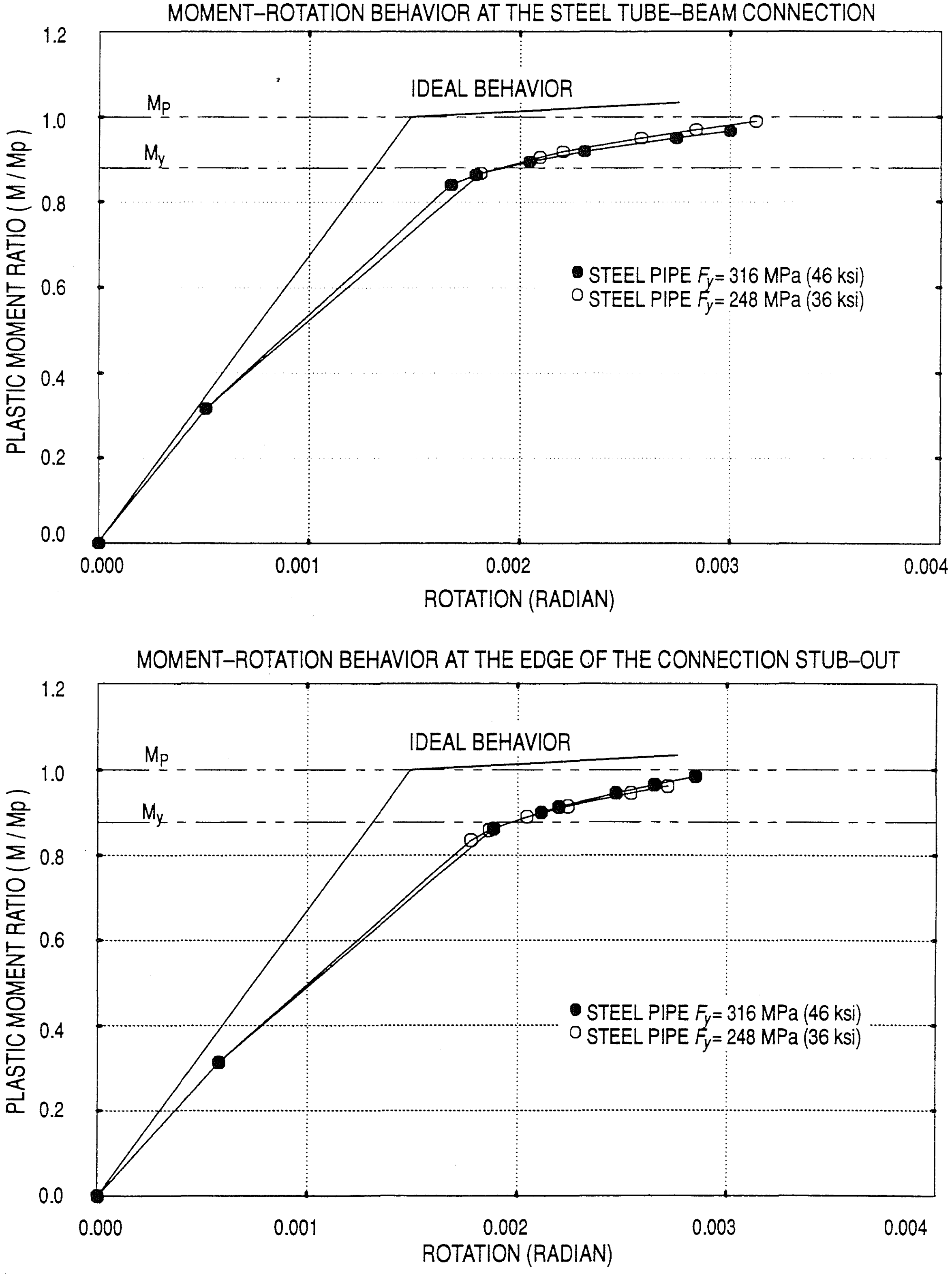

Figure A.14. Analytical Moment–Rotation Behavior, Connection *Type III:* Steel Grade Effect

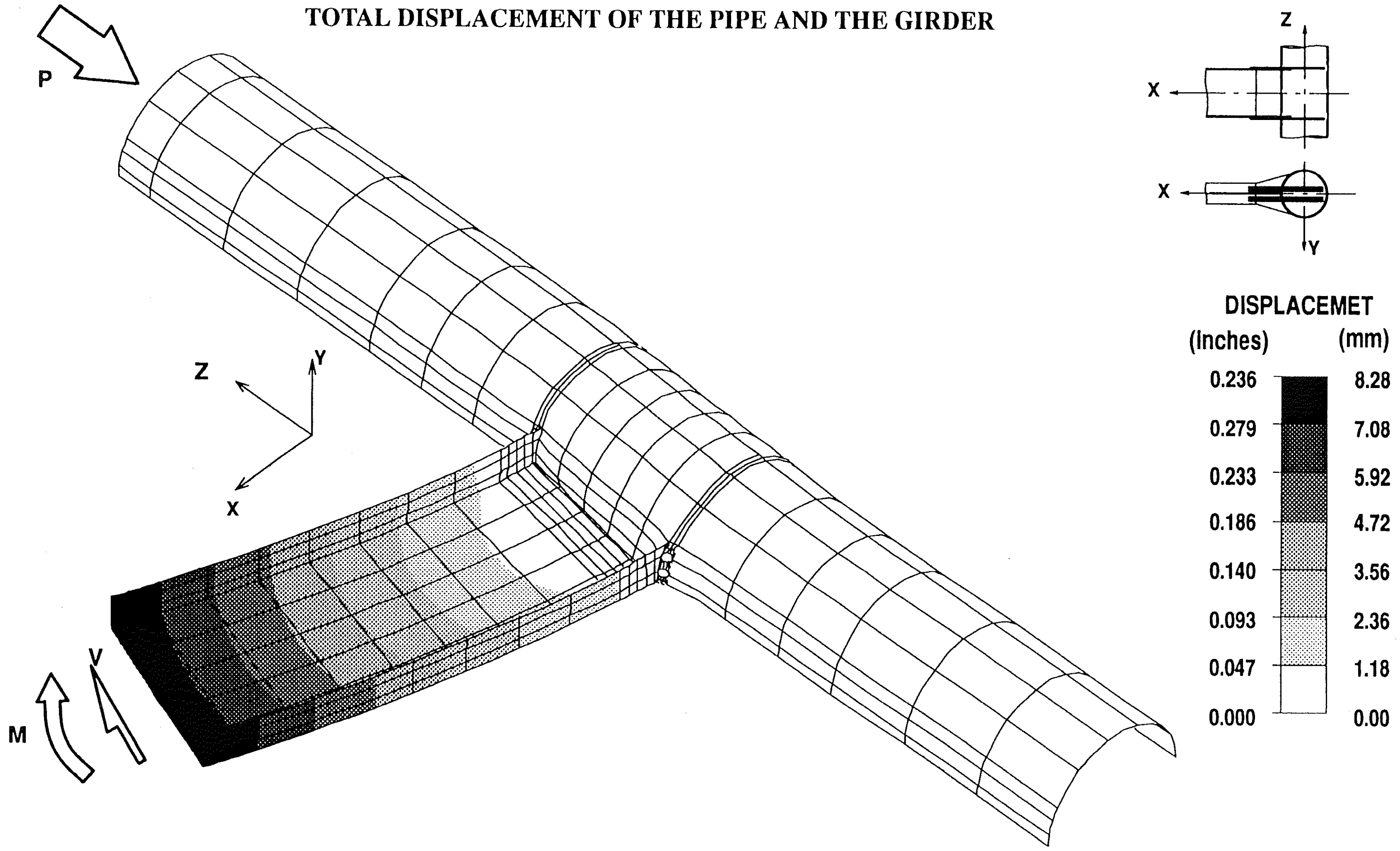

Figure A.15. Total Displacement and the Deflected Shape of the Tube and the Girder, Connection *Type III*

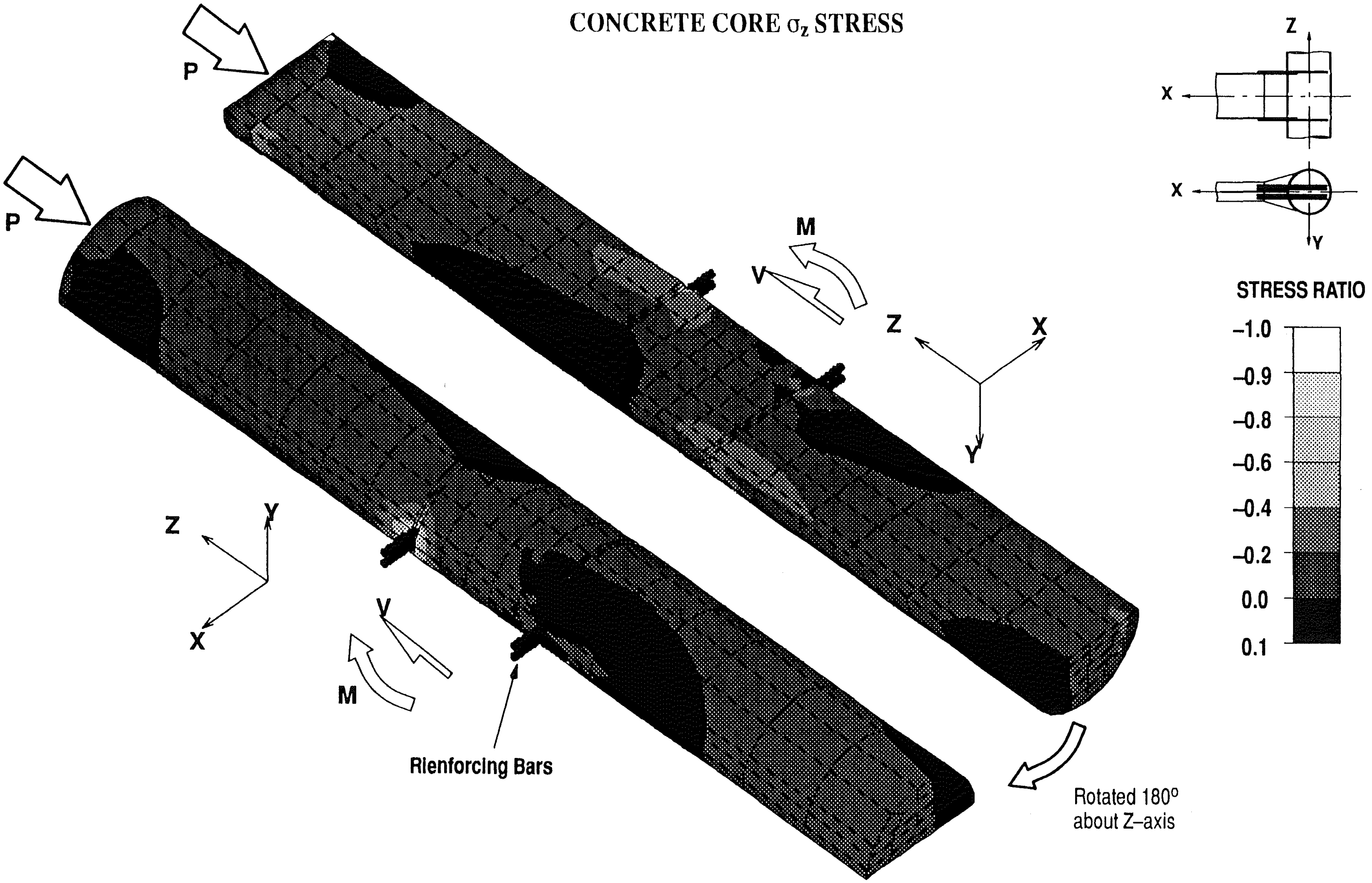

Figure A.16. Longitudinal Stress Ratio in the Concrete Core, Connection *Type III*

LOCAL BAR BUCKLING IN A CONNECTION W/ REINFORCING BARS

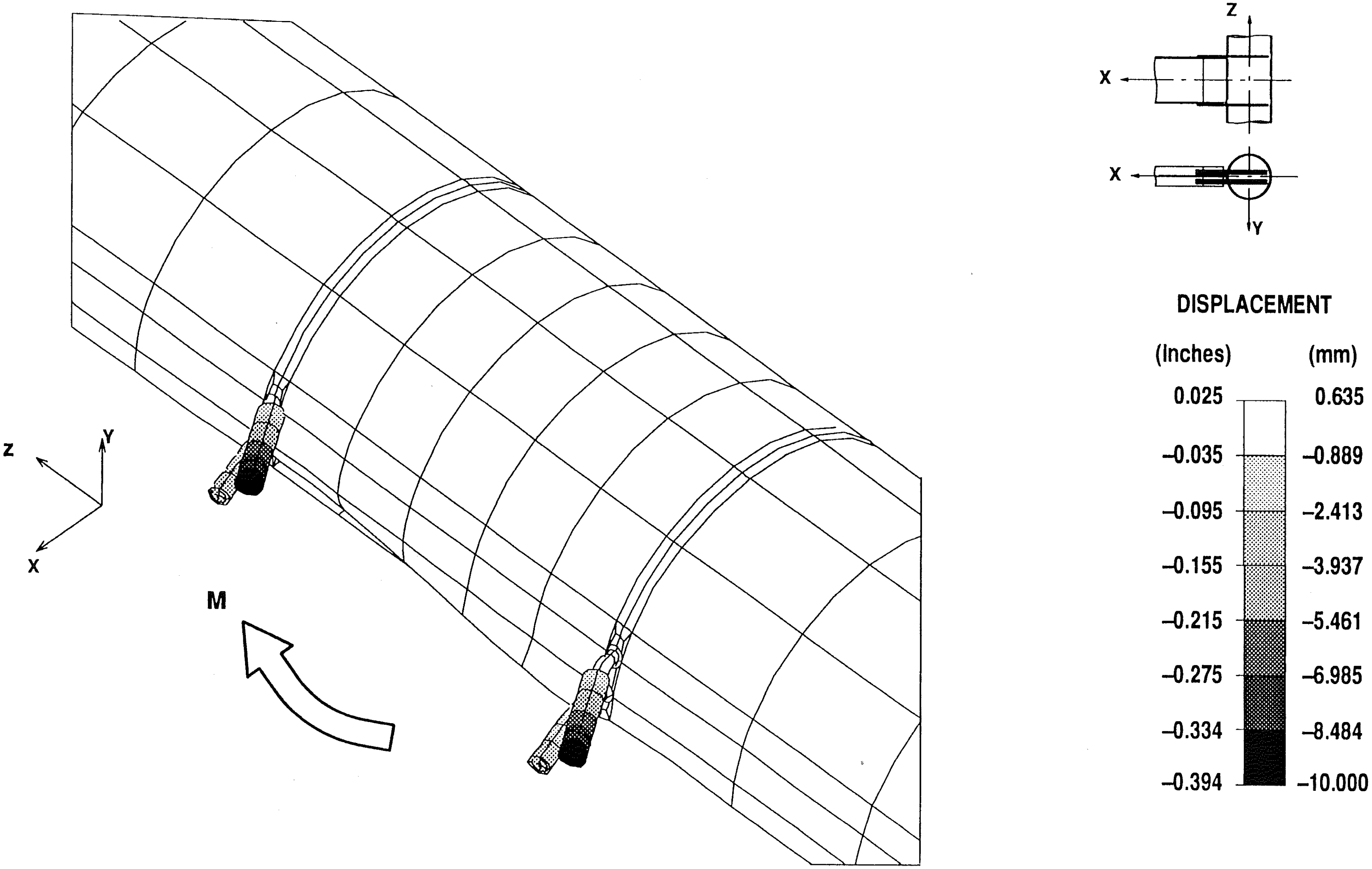

Figure A.17. Z–Direction Displacement and the Deflected Shape of the Bars and the Concrete Core

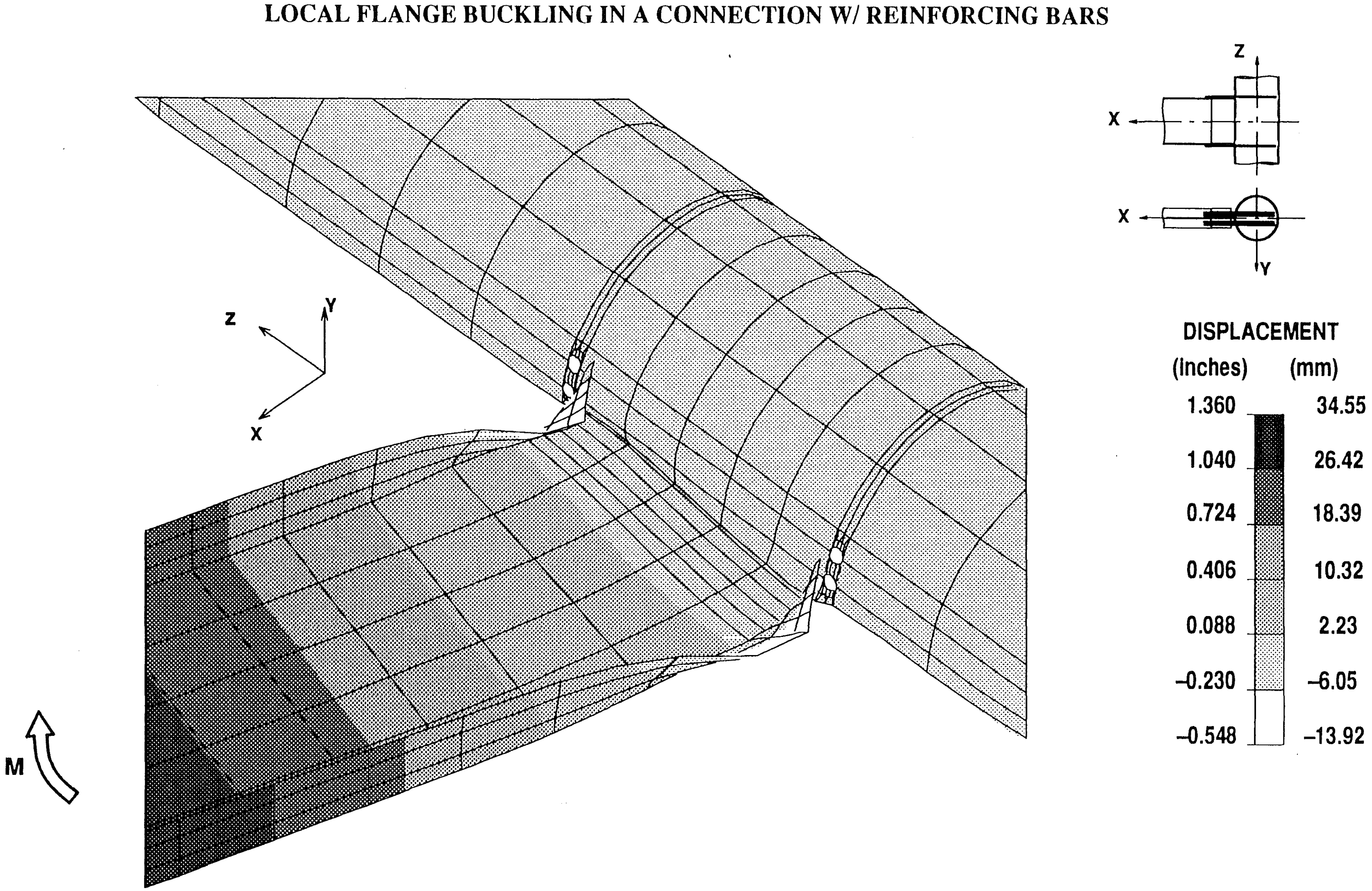

Figure A.18. Z–Direction Displacement and the Deformed Shape of the Girder, Connection w/ Deformed Bars

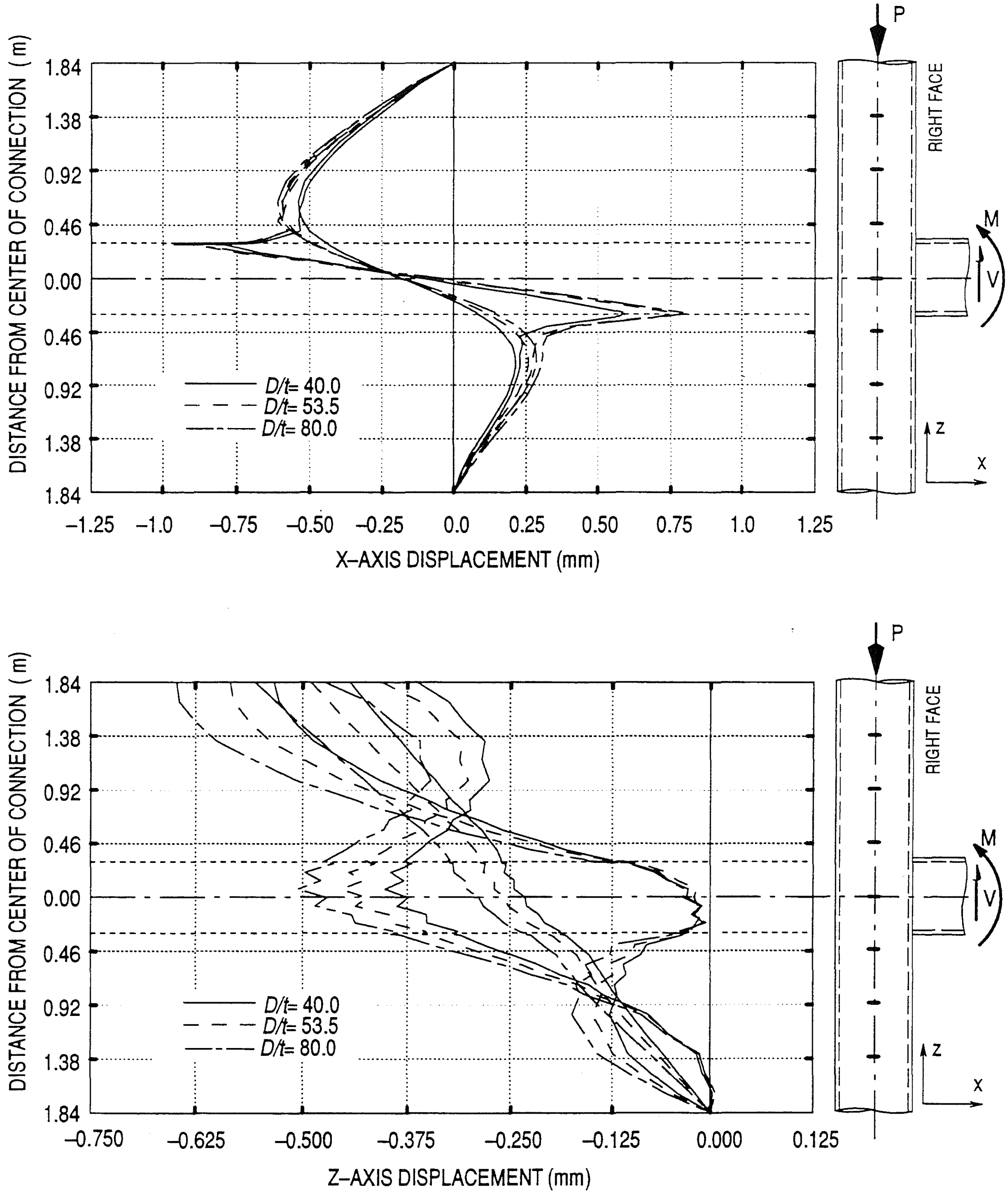

Figure A.19. Displacement of The Steel Pipe, Connection *Type IV: D/t* Effect

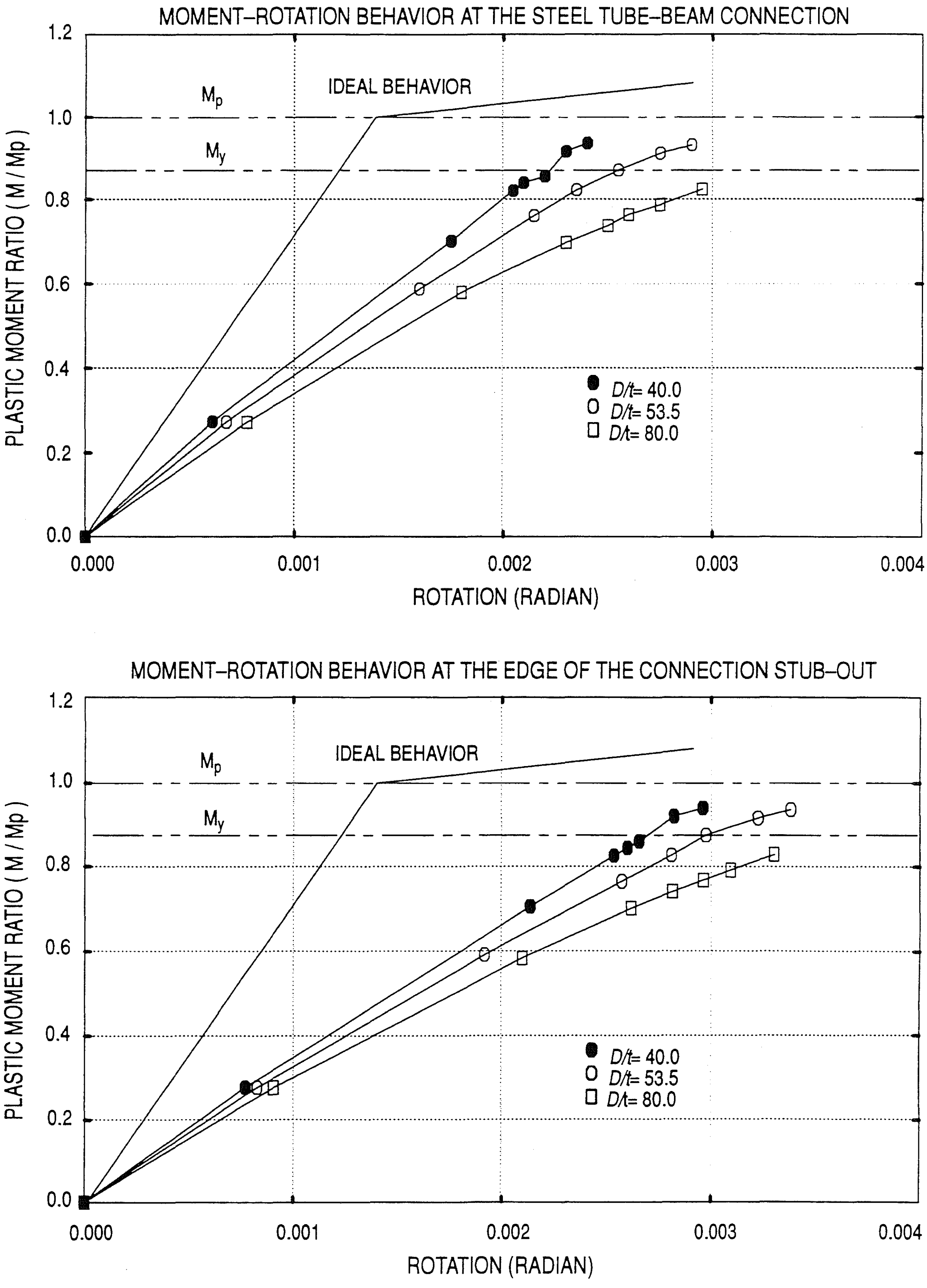

Figure A.20. Analytical Moment–Rotation Behavior, Connection *Type IV: D/t* Effect

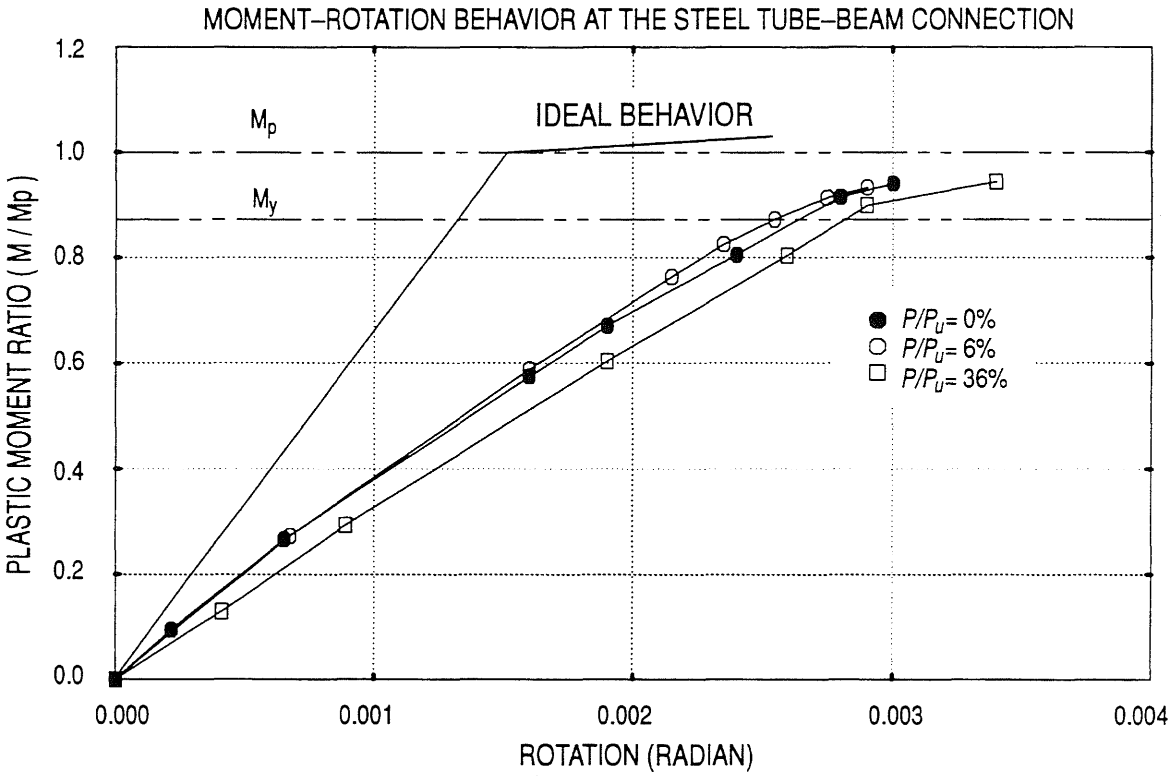

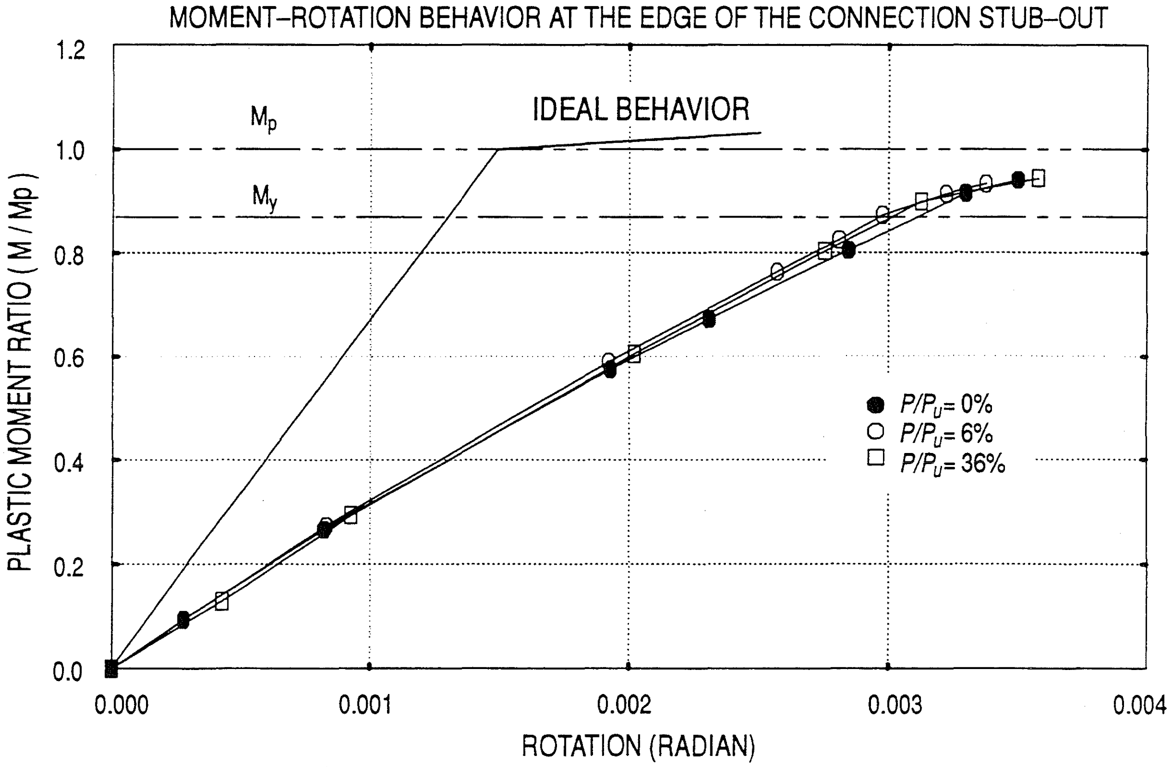

Figure A.21. Analytical Moment Rotation Behavior, Connection *Type IV:* Load Ratio Effect

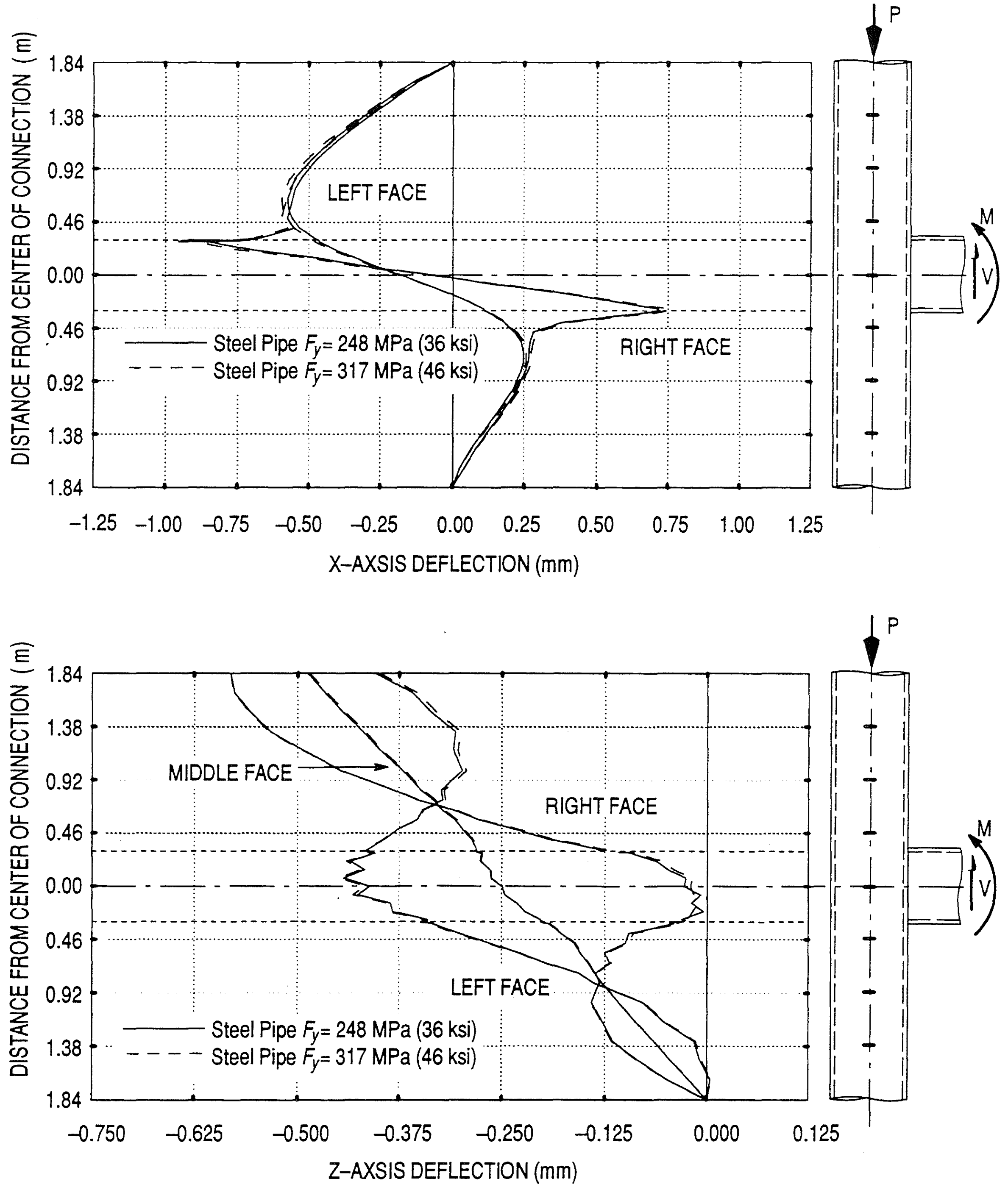

Figure A.22. Displacement of the Steel Pipe, Connection *Type IV:* Steel Grade Effect

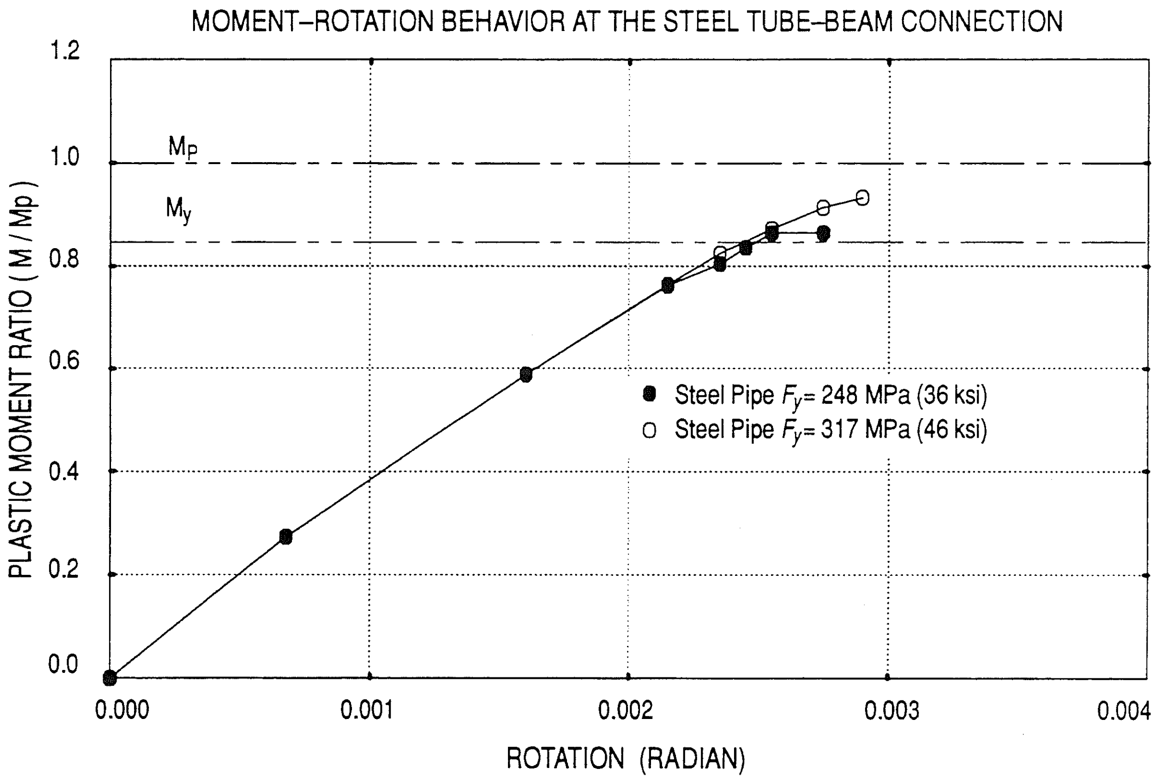

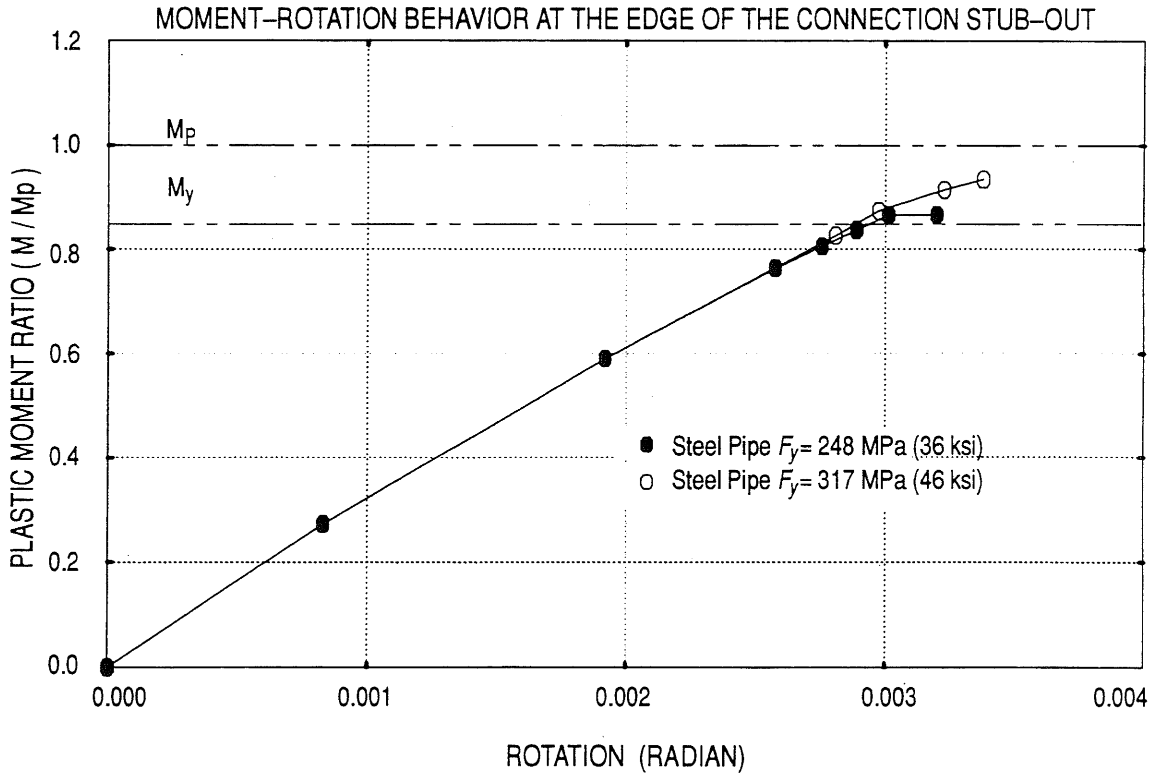

Figure A.23. Analytical Moment Rotation Behavior Connection *Type IV:* Steel Grade Effect

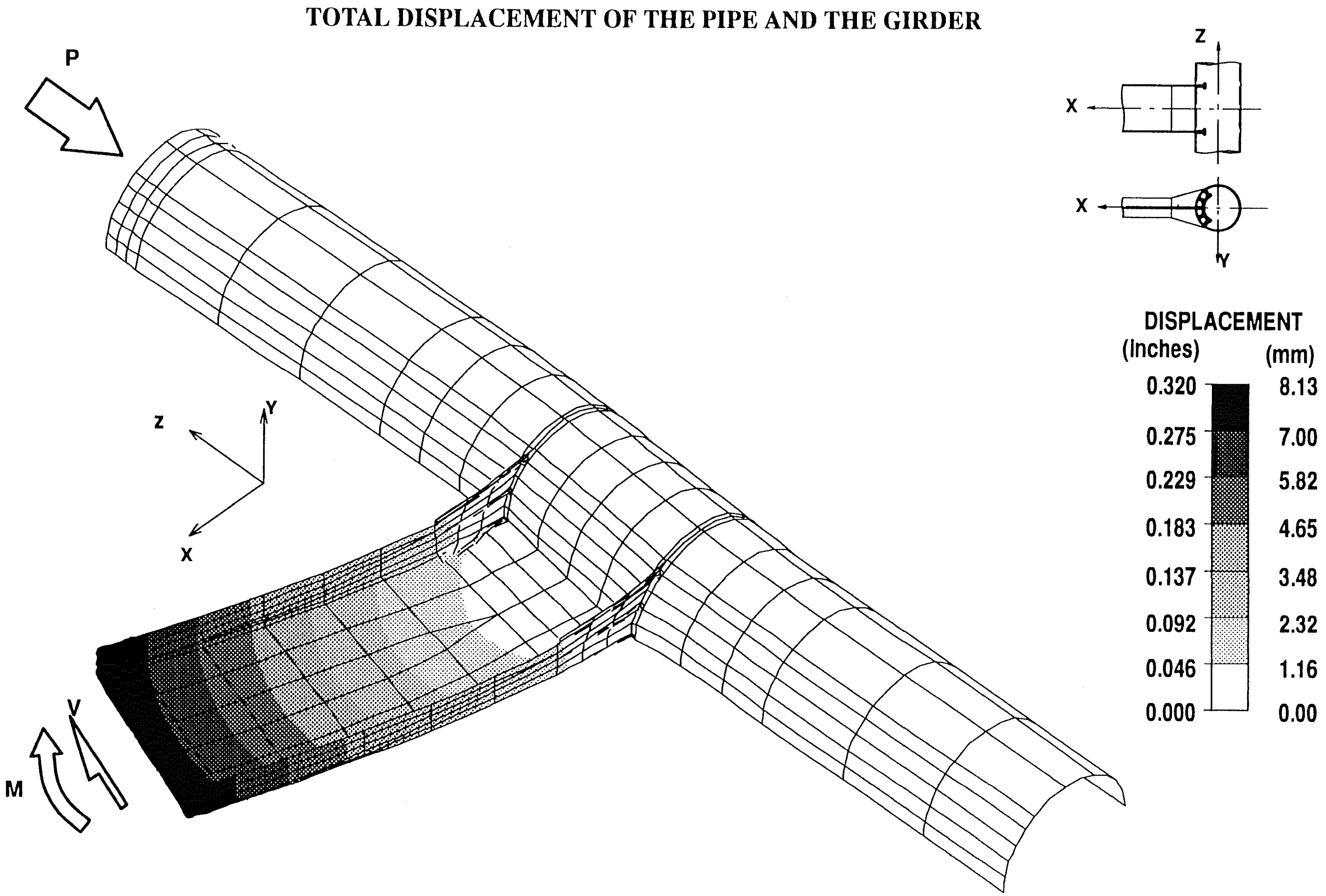

Figure A.24. Total Displacement and the Deformed Shape of the Tube and the Girder, Connection *Type IV*

CONCRETE CORE MINIMUM PRINCIPAL STRESS

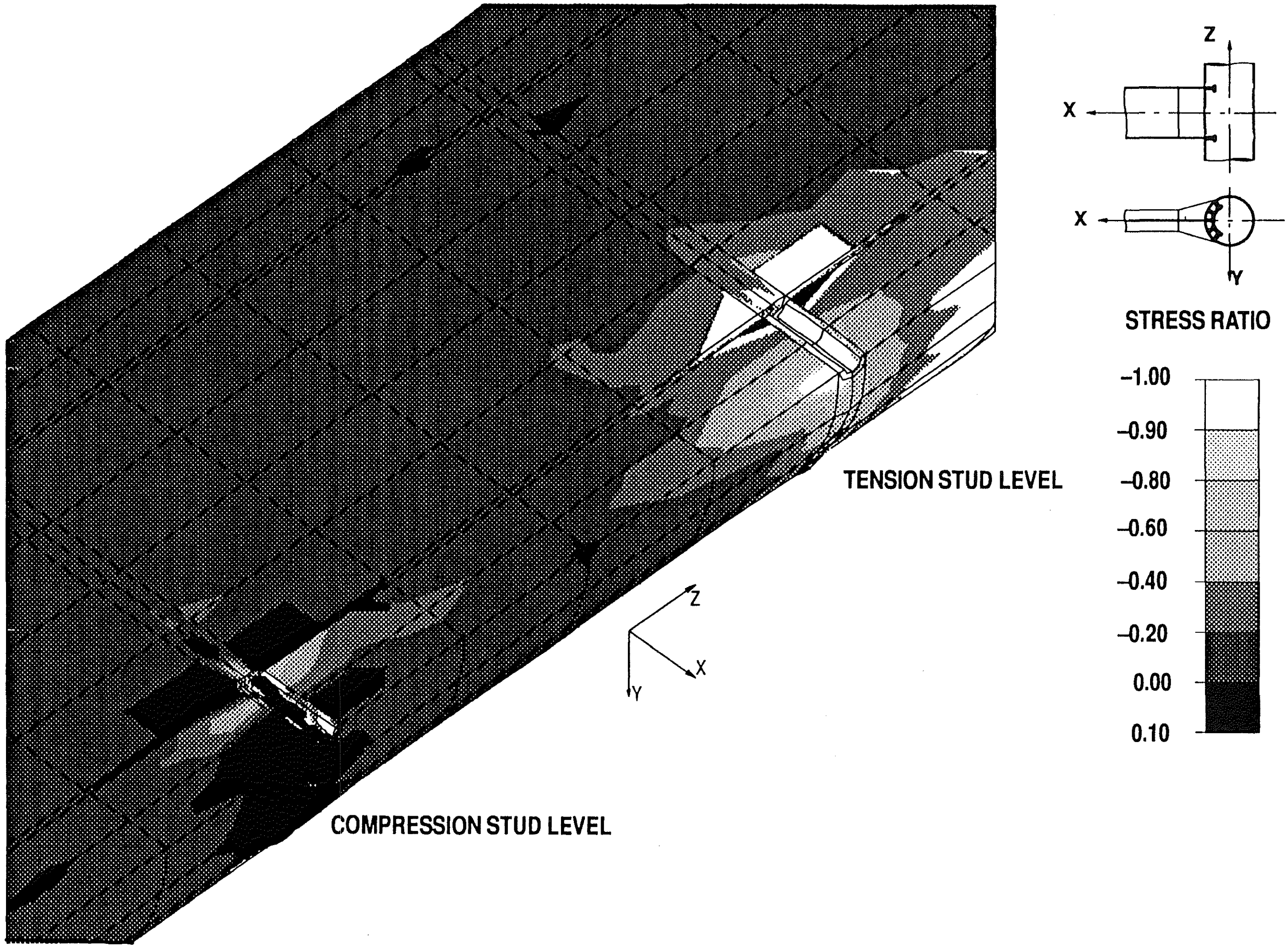

Figure A.25. Minimum Principal Stress Ratio in the Concrete Core, Connection *Type IV*

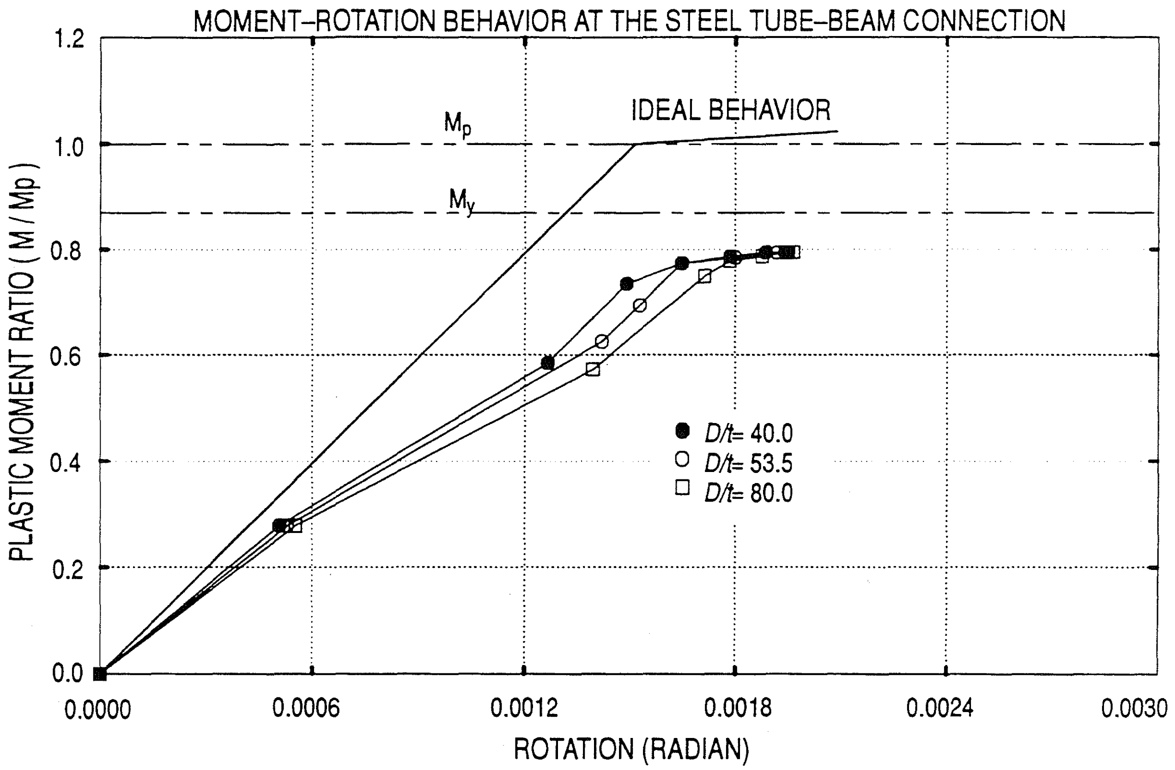

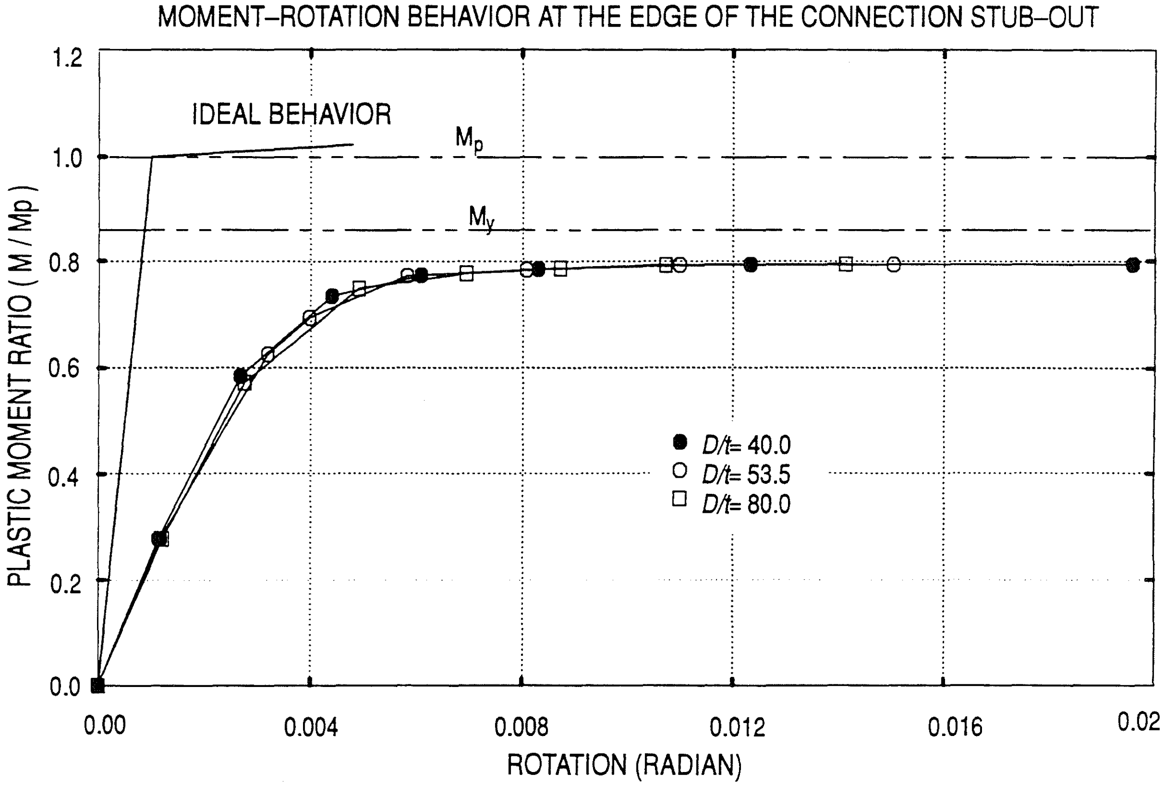

Figure A.26. Analytical Moment–Rotation Behavior, Connection *Type V: D/t* Effect

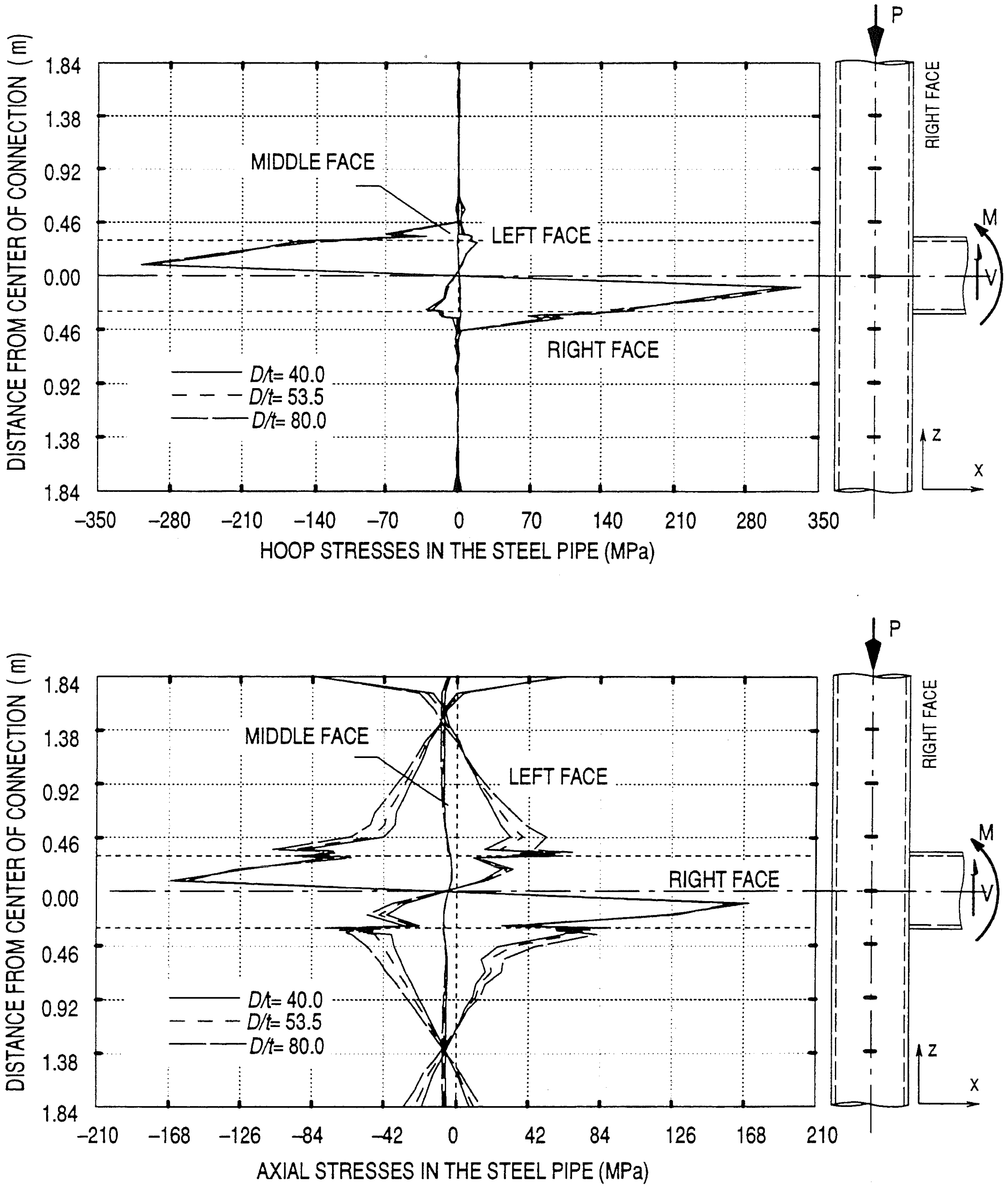

Figure A.27. Stresses in the Steel Pipe, Connection *Type V: D/t* Effect

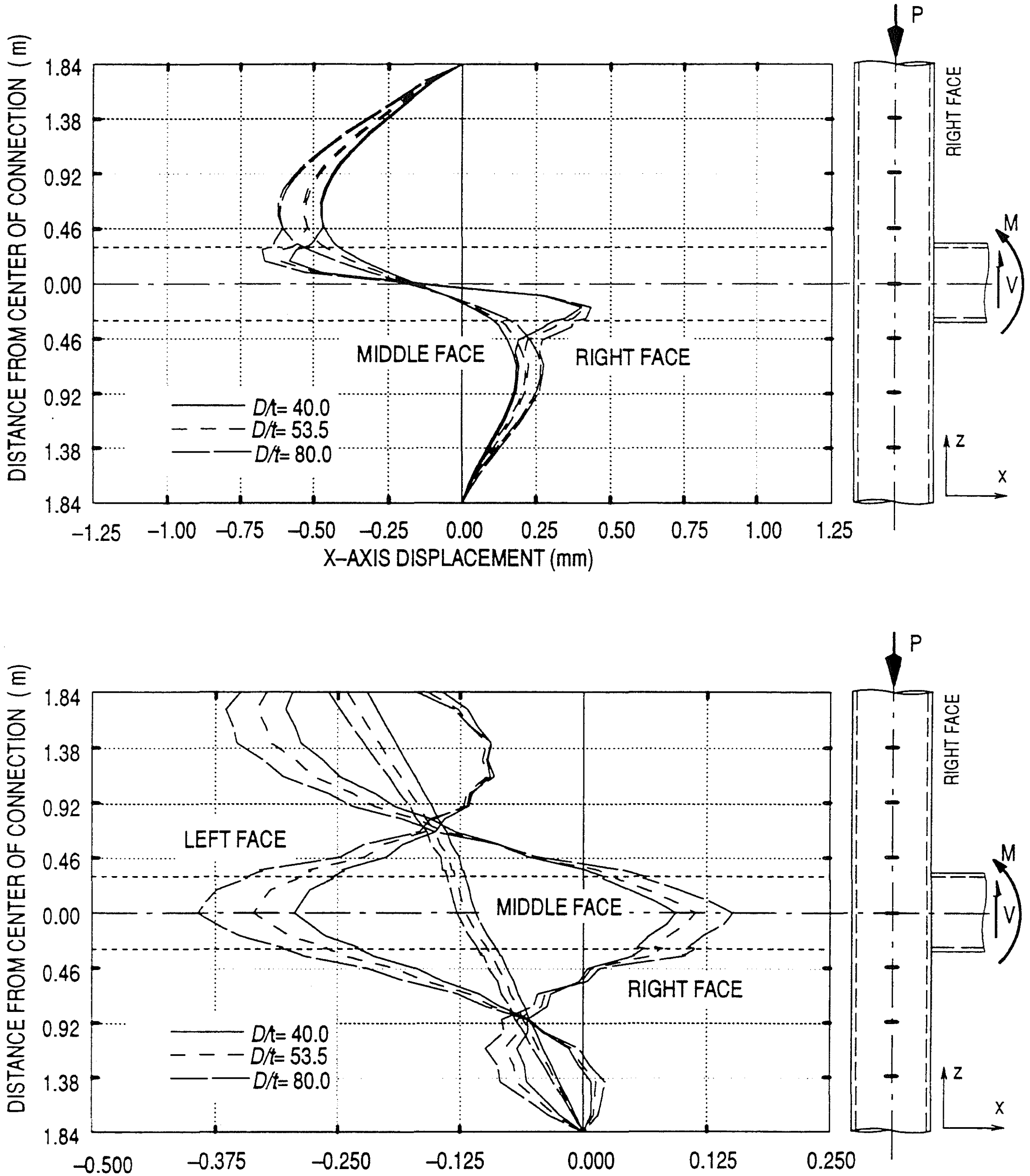

Figure A.28. Displacement of Tubular Columns, Connection *Type V: D/t* Effect

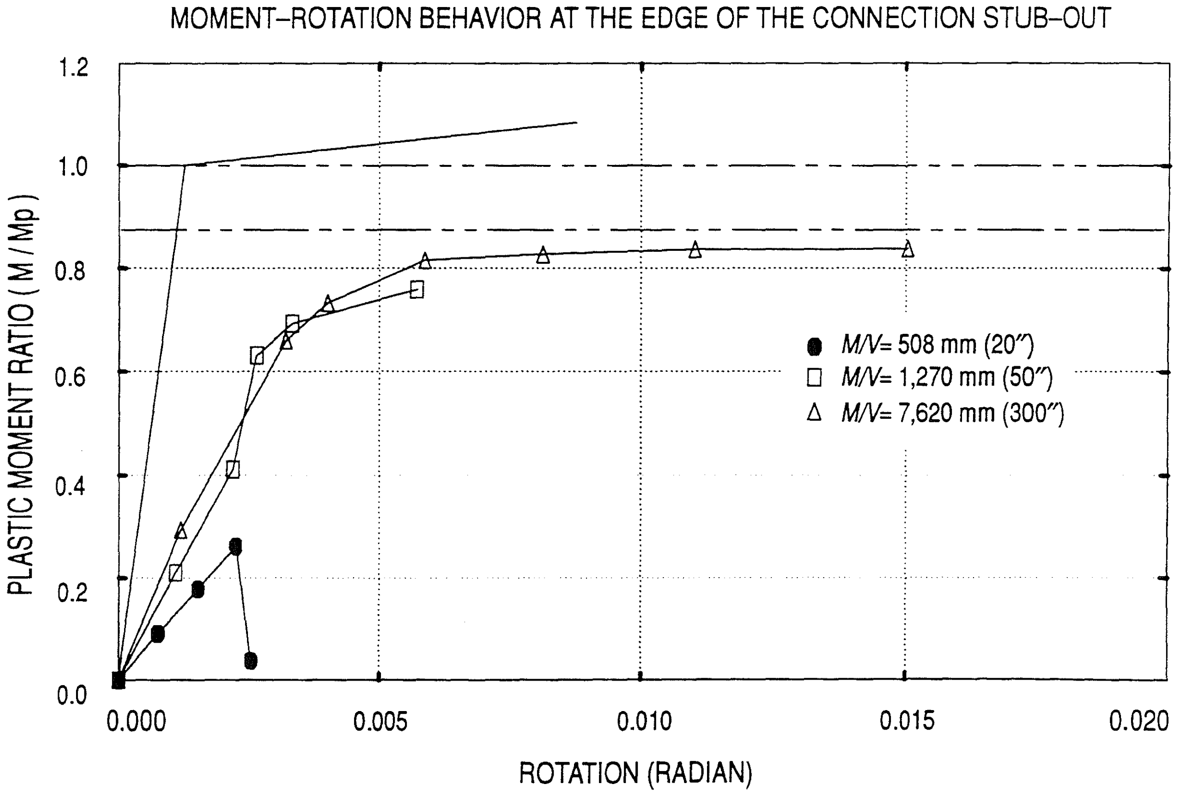

Figure A.29. Analytical Moment–Rotation Behavior, Connection *Type V: M/V* Ratio Effect

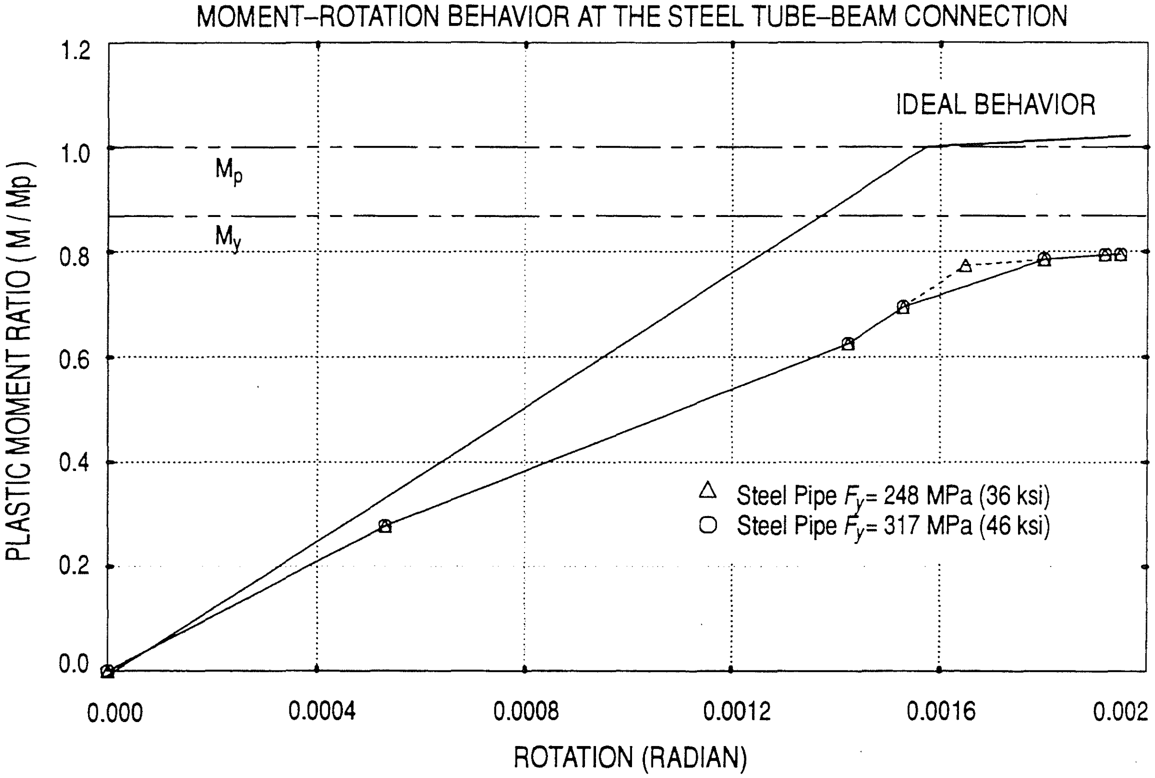

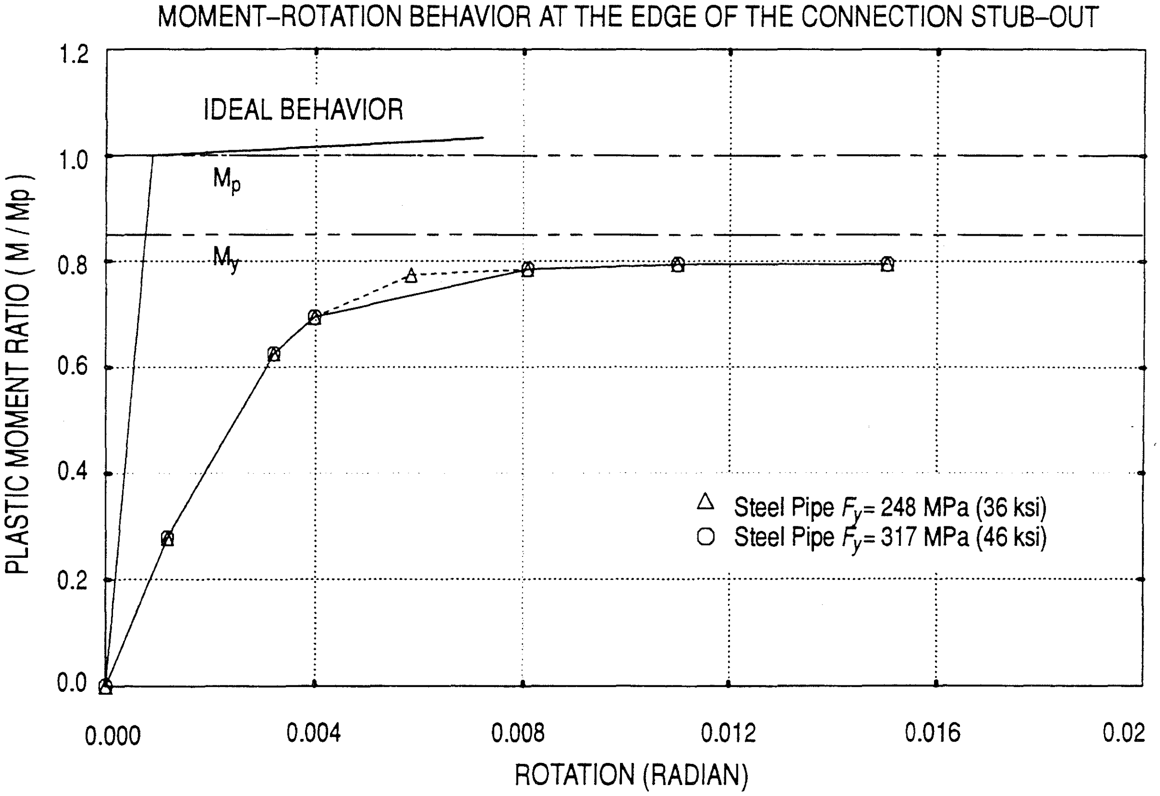

Figure A.30. Analytical Moment–Rotation Behavior, Connection *Type V:* Steel Grade Effect

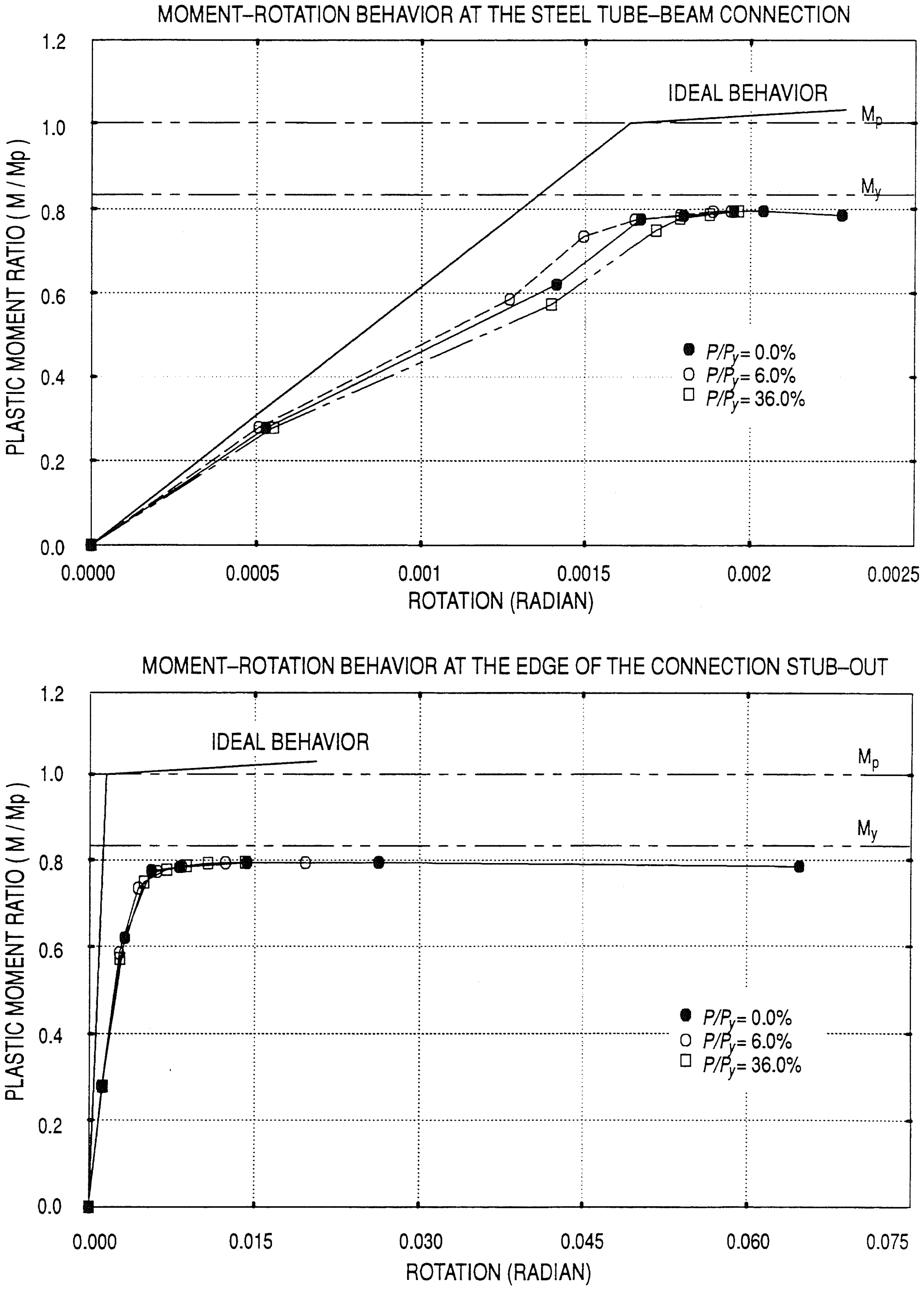

Figure A.31. Analytical Moment–Rotation Behavior, Connection *Type V:* Load Ratio Effect

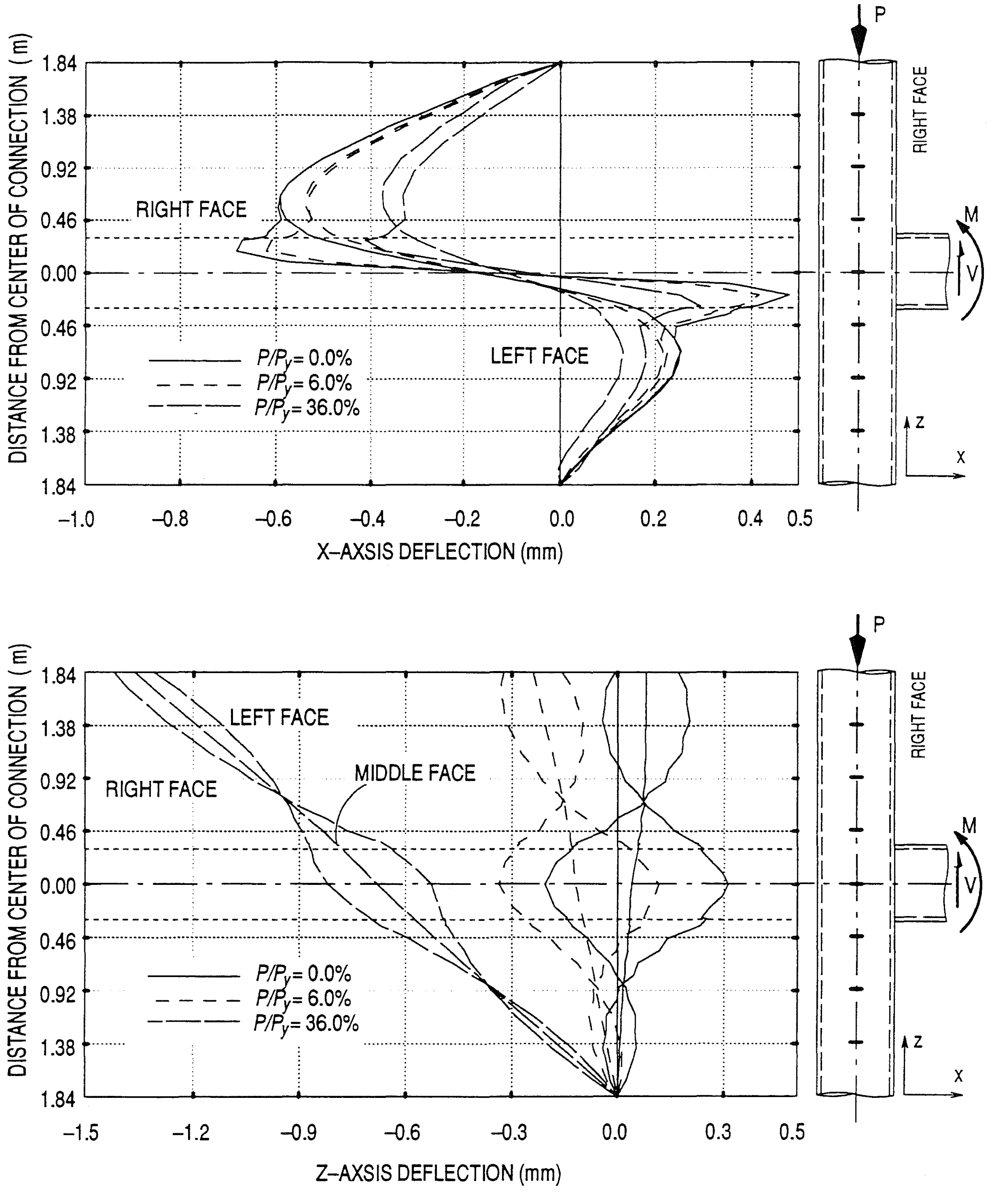

Figure A.32. Displacement of the Steel Pipe, Connection *Type V:* Load Ratio Effect

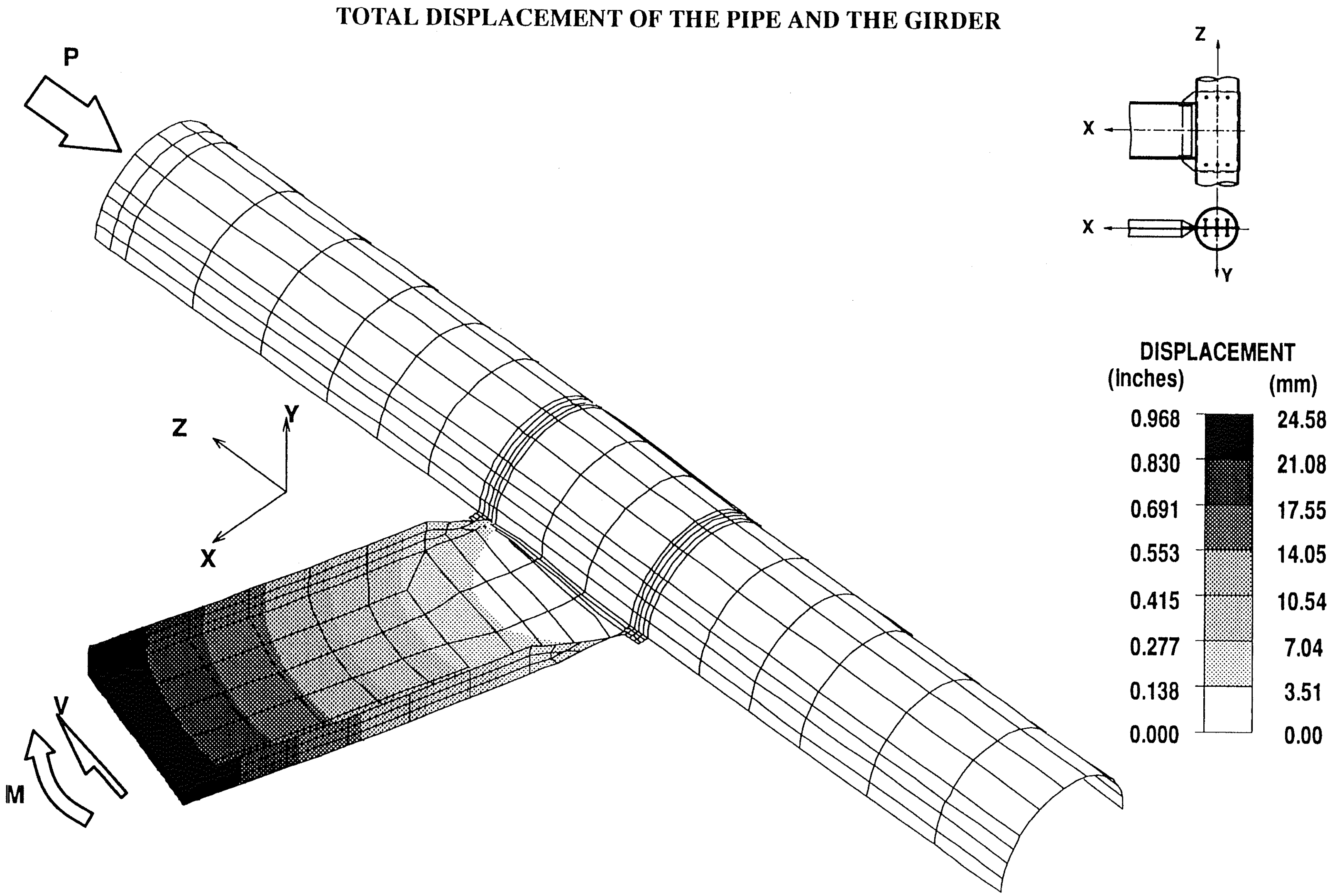

Figure A.33. Total Displacement and the Deformed Shape of the Tube and the Girder, Connection *Type V*

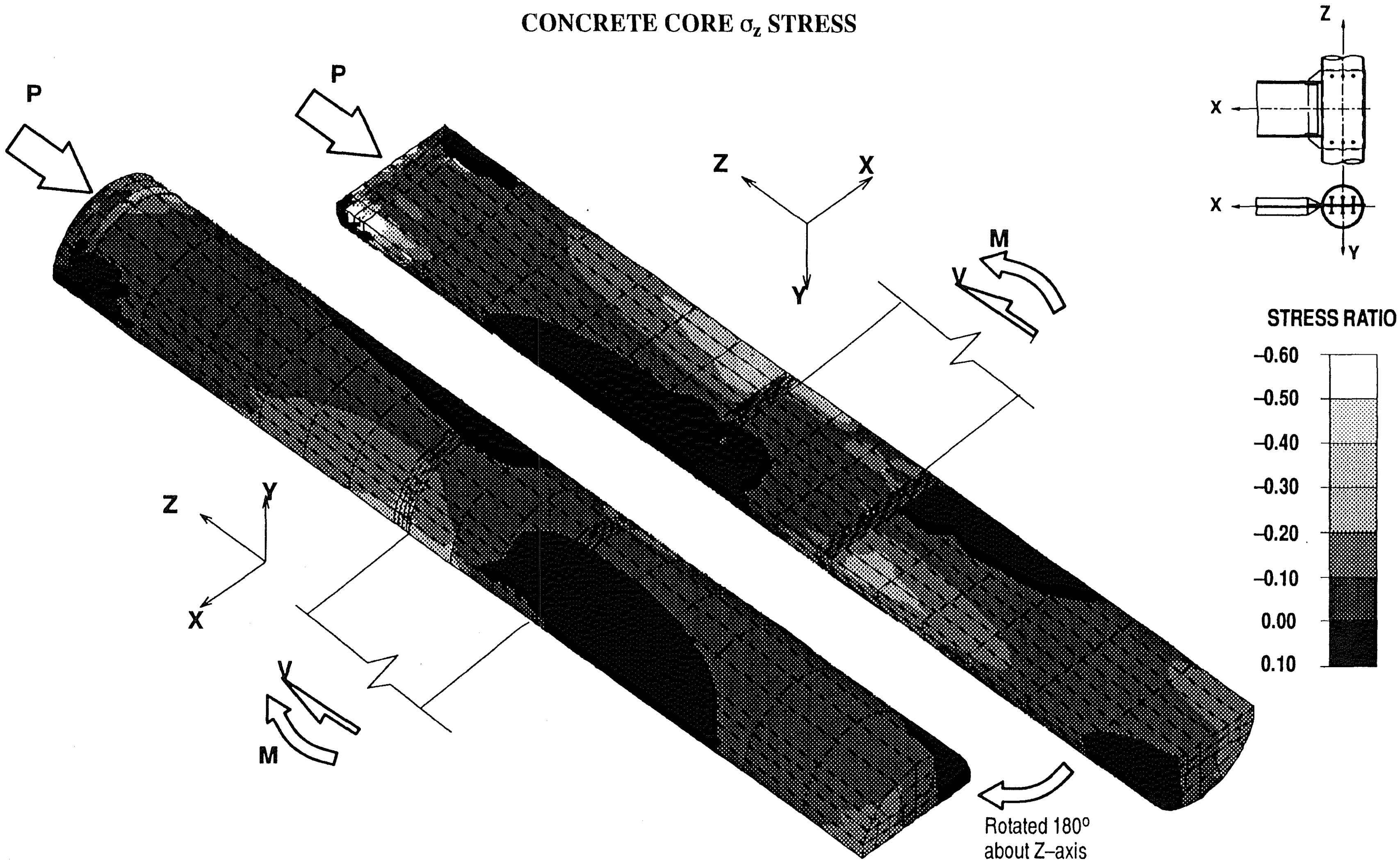

Figure A.34. Axial Stress Ratio in the Concrete Core, Connection *Type V*

WEB-PLATE τ_{xz} STRESS

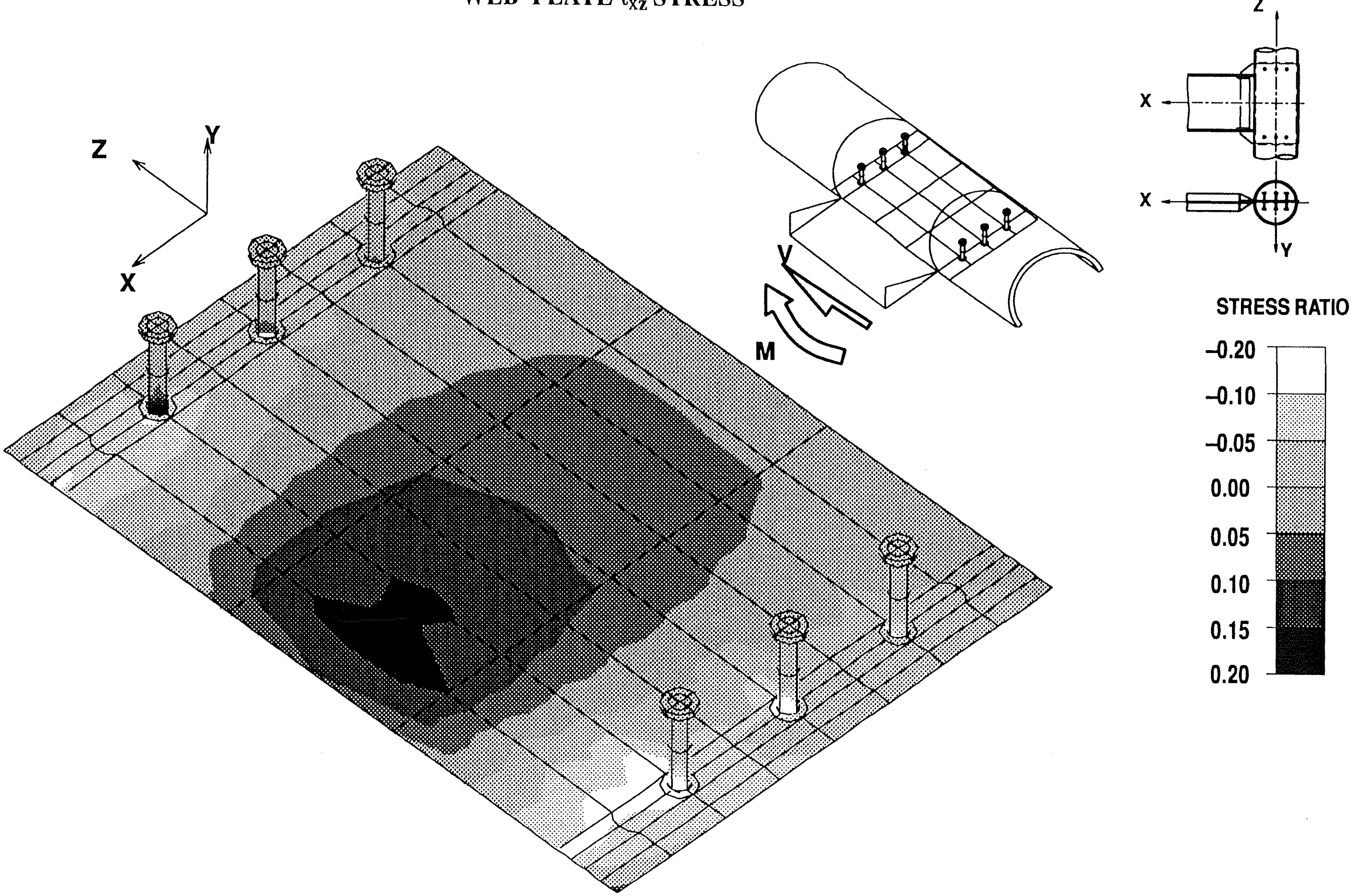

Figure A.35. Web Plate Shear Stress Ratio, Connection *Type V*

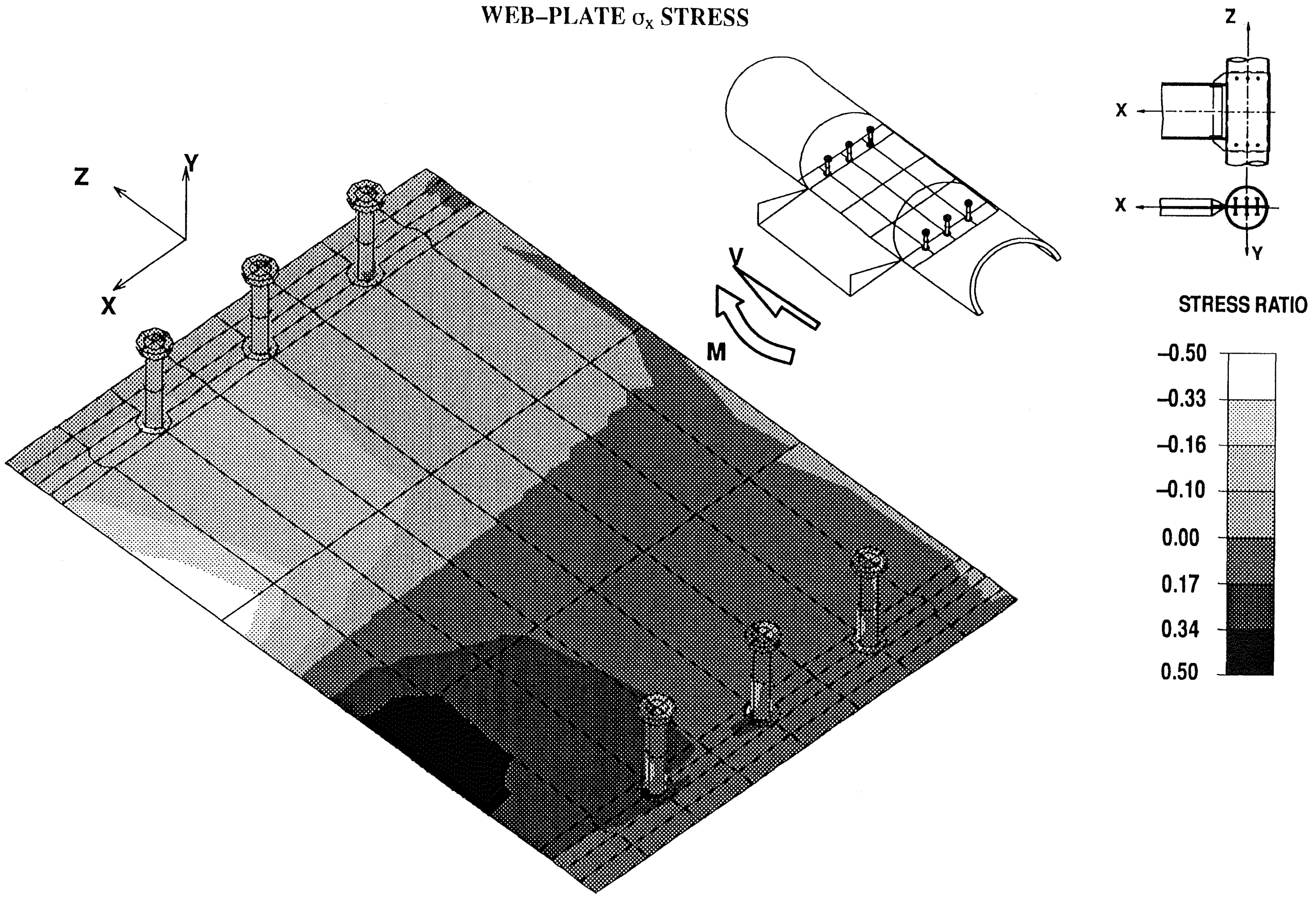

WEB-PLATE σ_x STRESS

Figure A.36. Web Plate Flexural Stress Ratio, Connection *Type V*

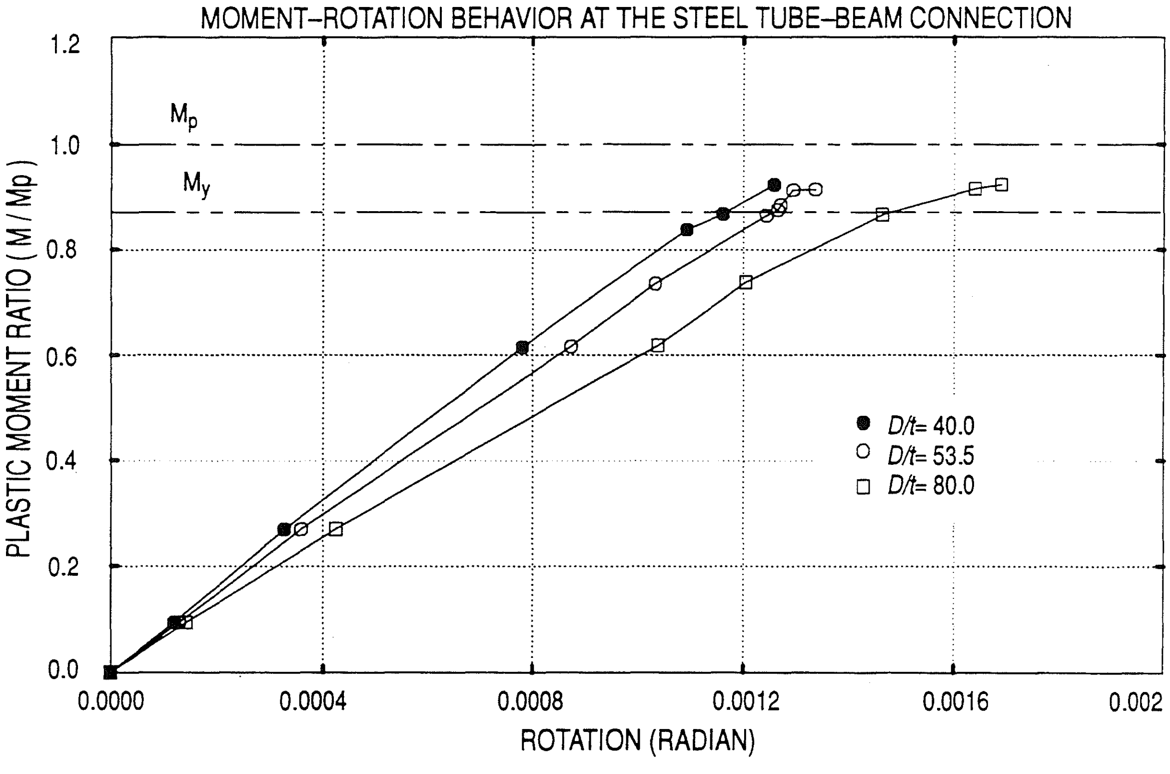

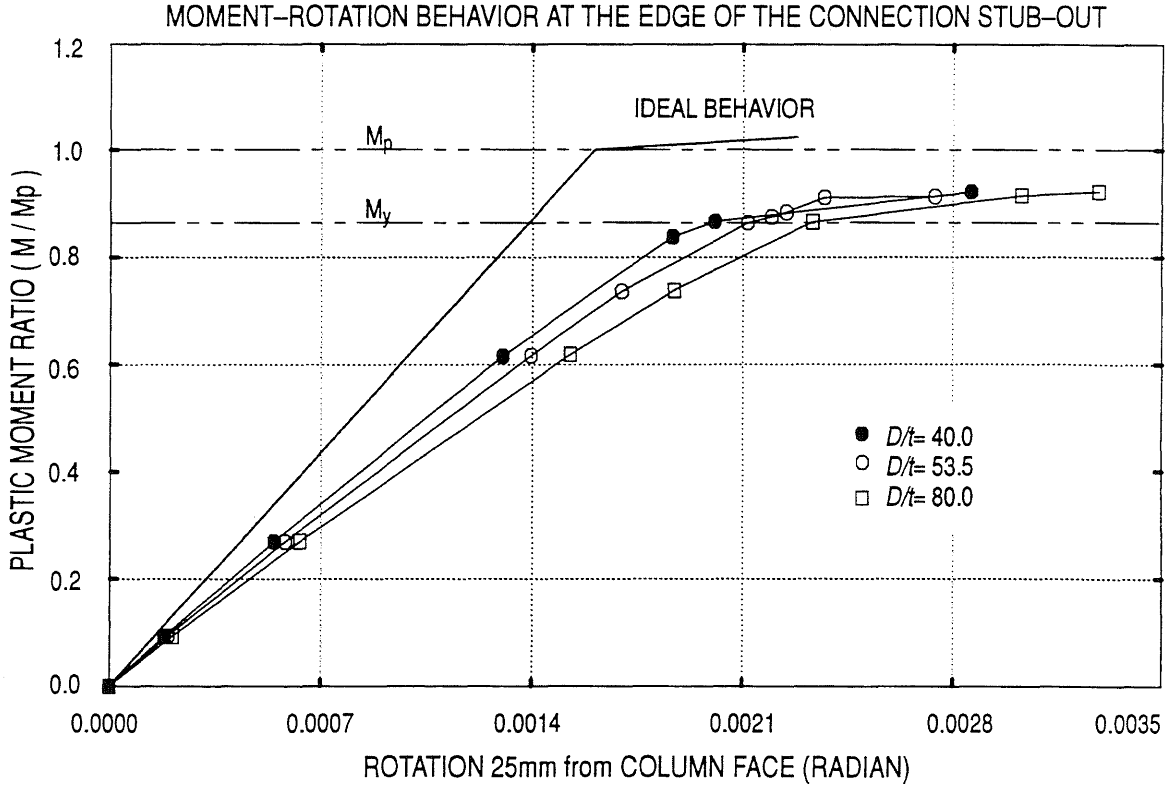

Figure A.37. Analytical Moment–Rotation Behavior, Connection *Type VII: D/t* Effect

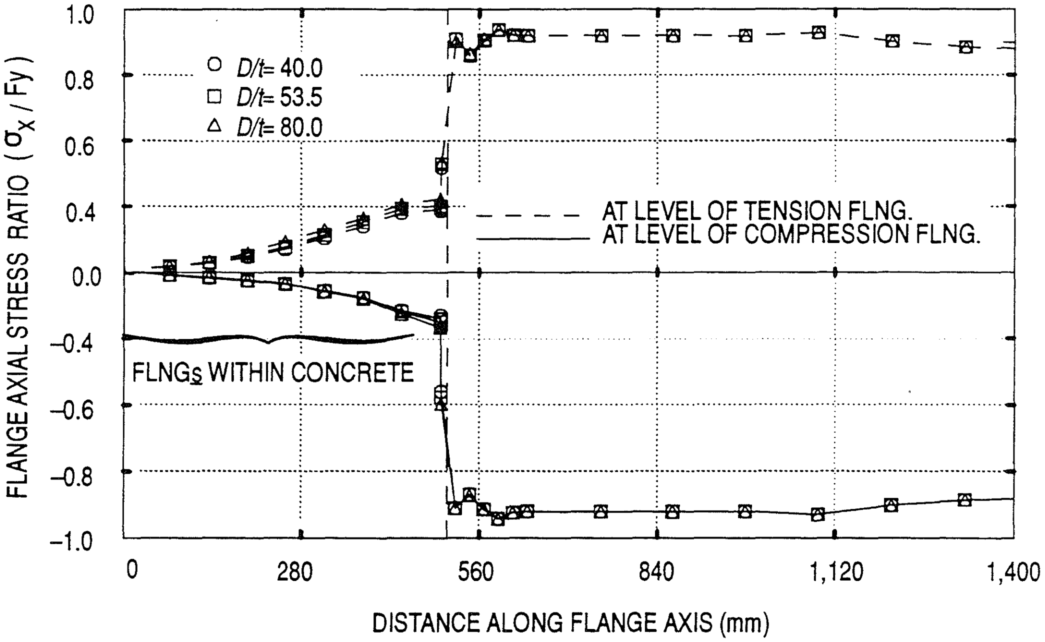

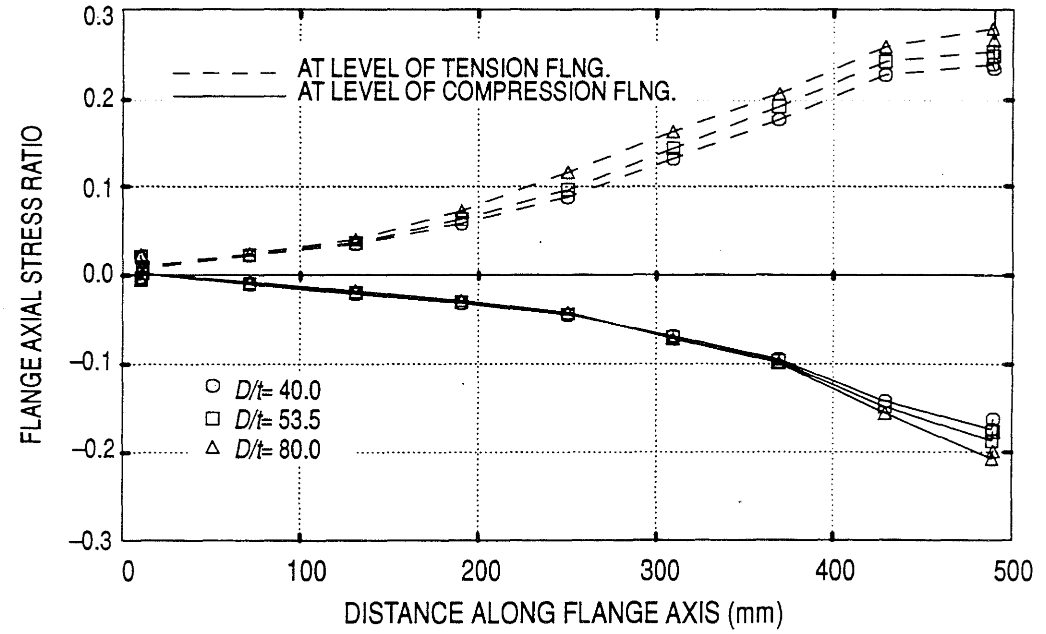

Figure A.38. Variation of Axial Stresses along Girder Flanges, Connection *Type VII: D/t* Effect

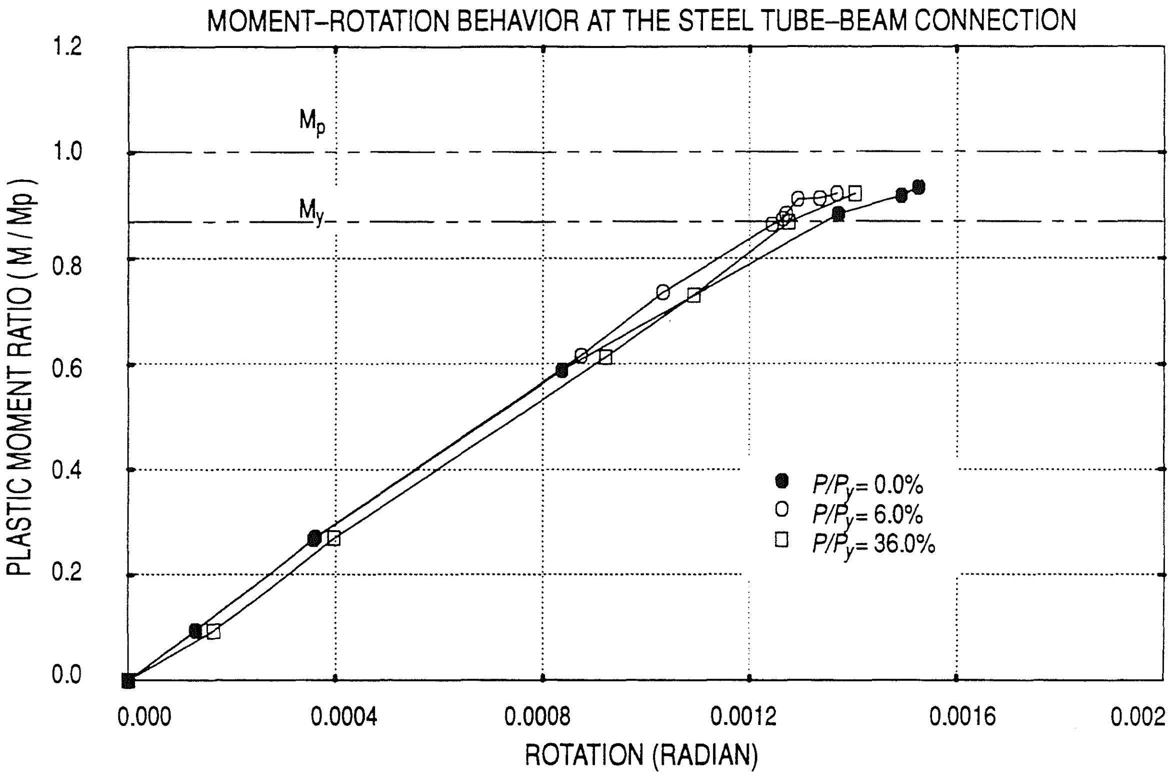

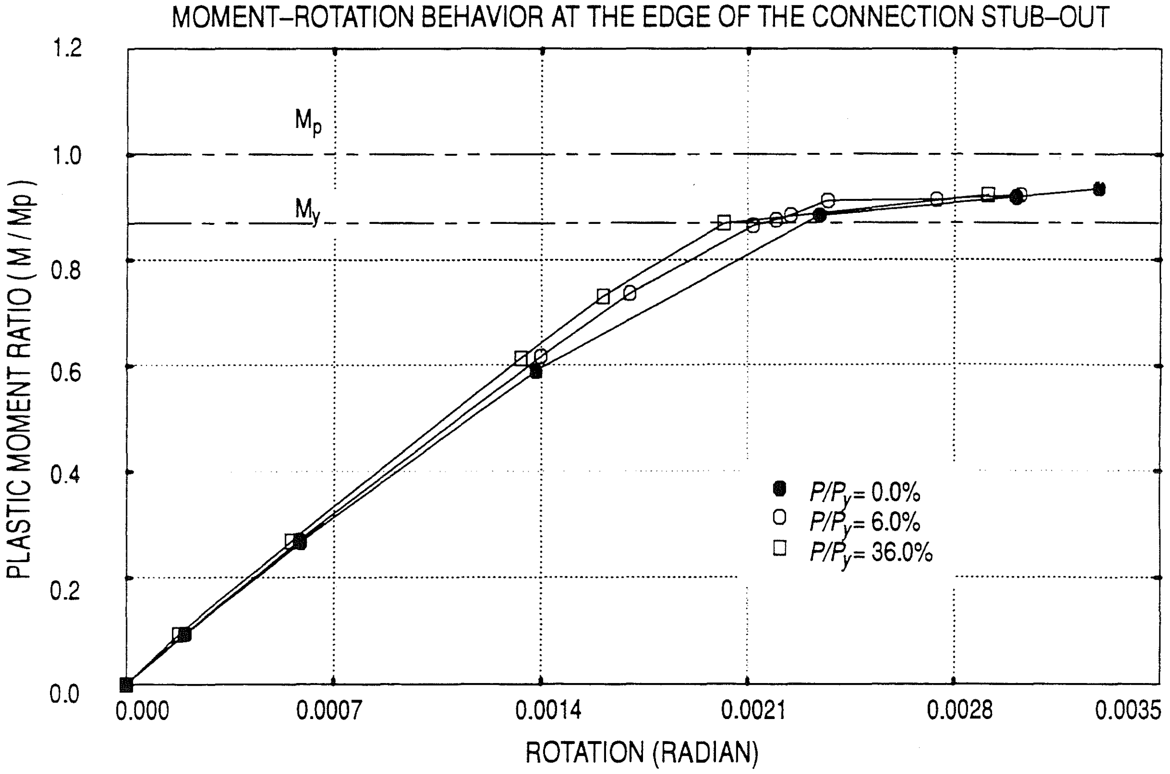

Figure A.39. Analytical Moment Rotation Diagram, Connection *Type VII:* Load Ratio Effect

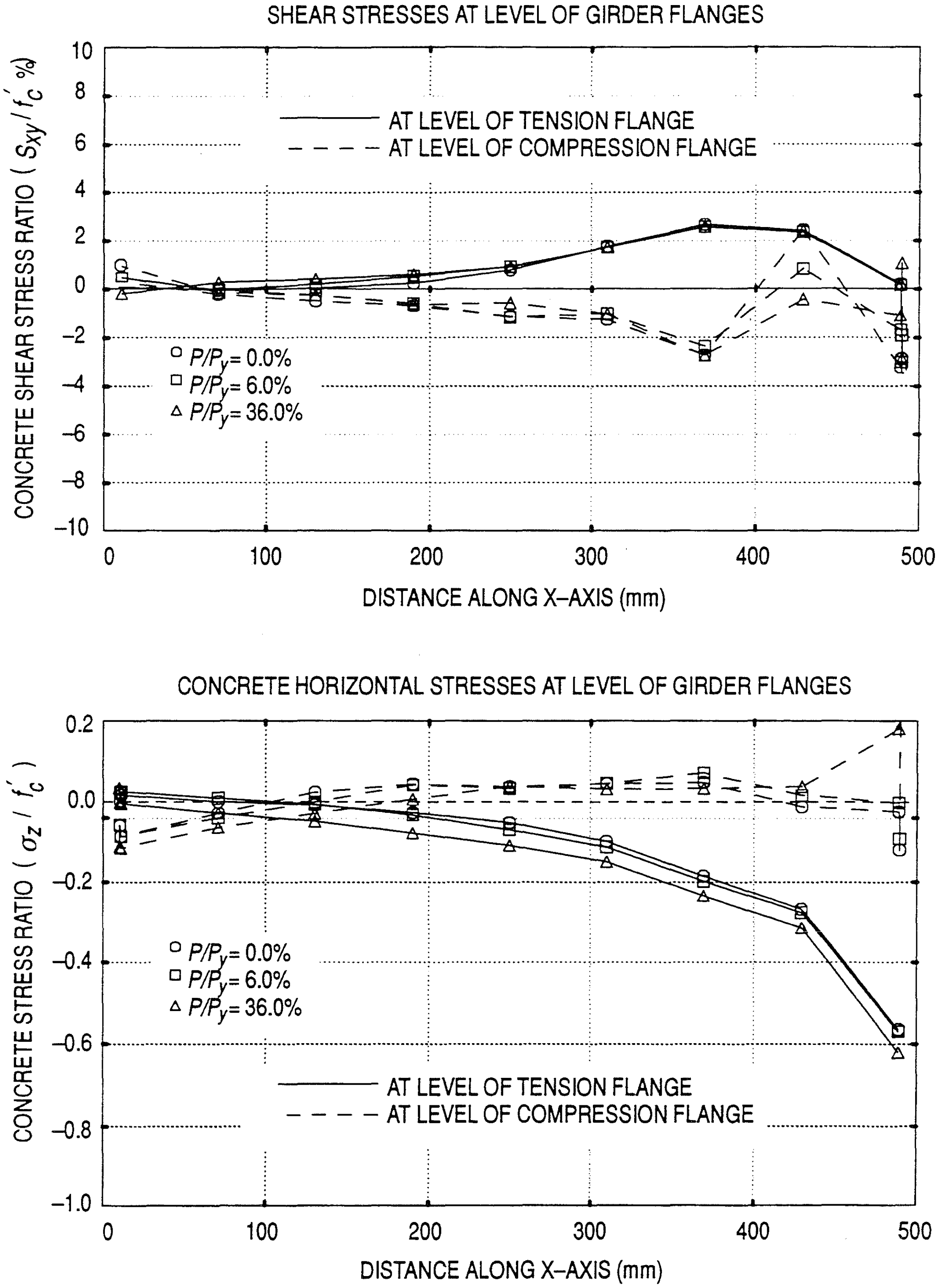

Figure A.40. Concrete Stress, Connection *Type VII:* Load Ratio Effect

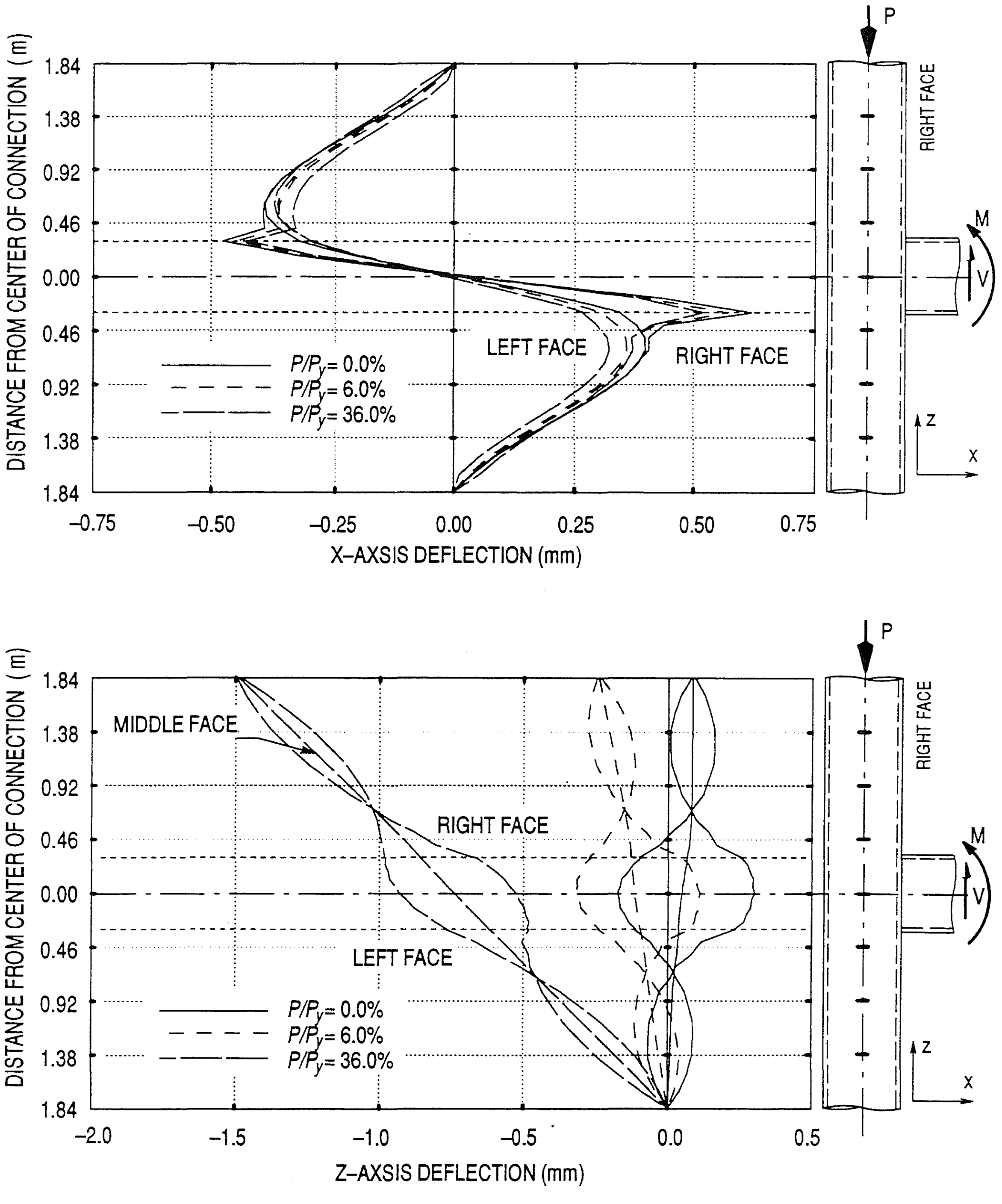

Figure A.41. Displacement of the Steel Pipe, Connection *Type VII:* Load Ratio Effect

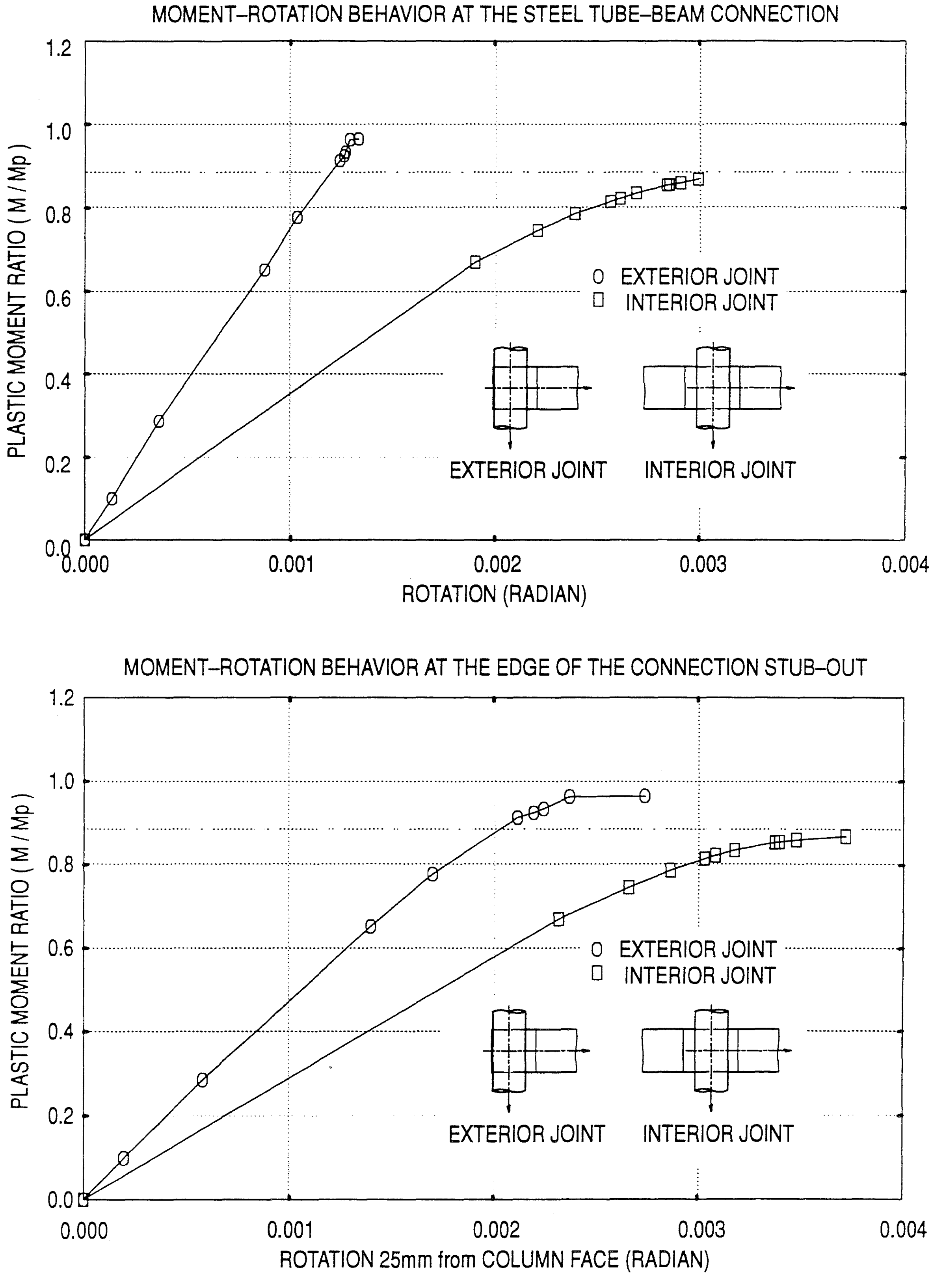

Figure A.42. Analytical Moment Rotation Behavior, Connection *Type VII*

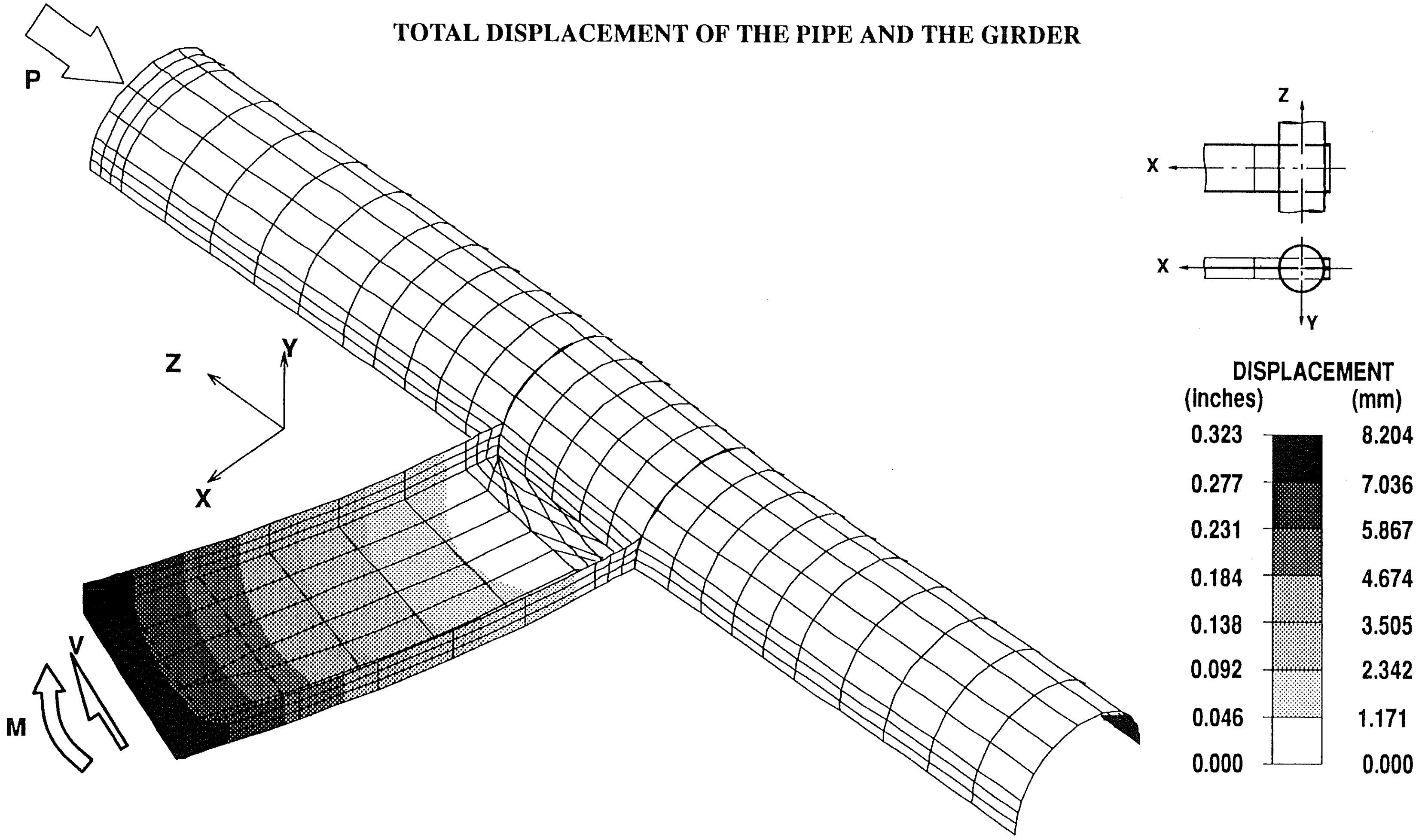

Figure A.43. Total Displacement and Deformed Shape of the Tube and the Girder, Connection *Type VII*

X–DIRECTION DISPLACEMENT OF THE CONCRETE CORE

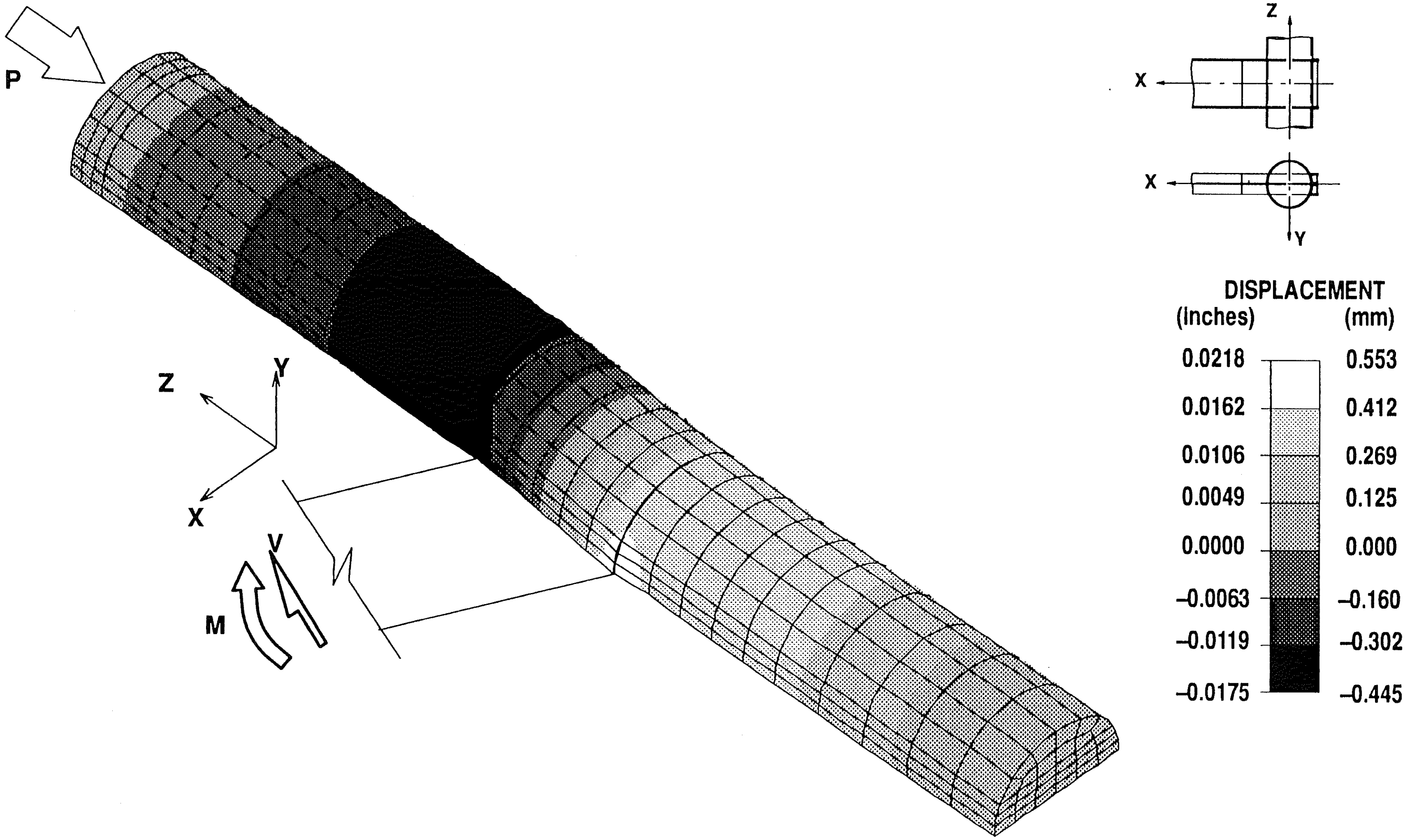

Figure A.44. X–Direction Displacement and Deformed Shape of the Concrete Core, Connection *Type VII*

CONCRETE CORE σ_z STRESS

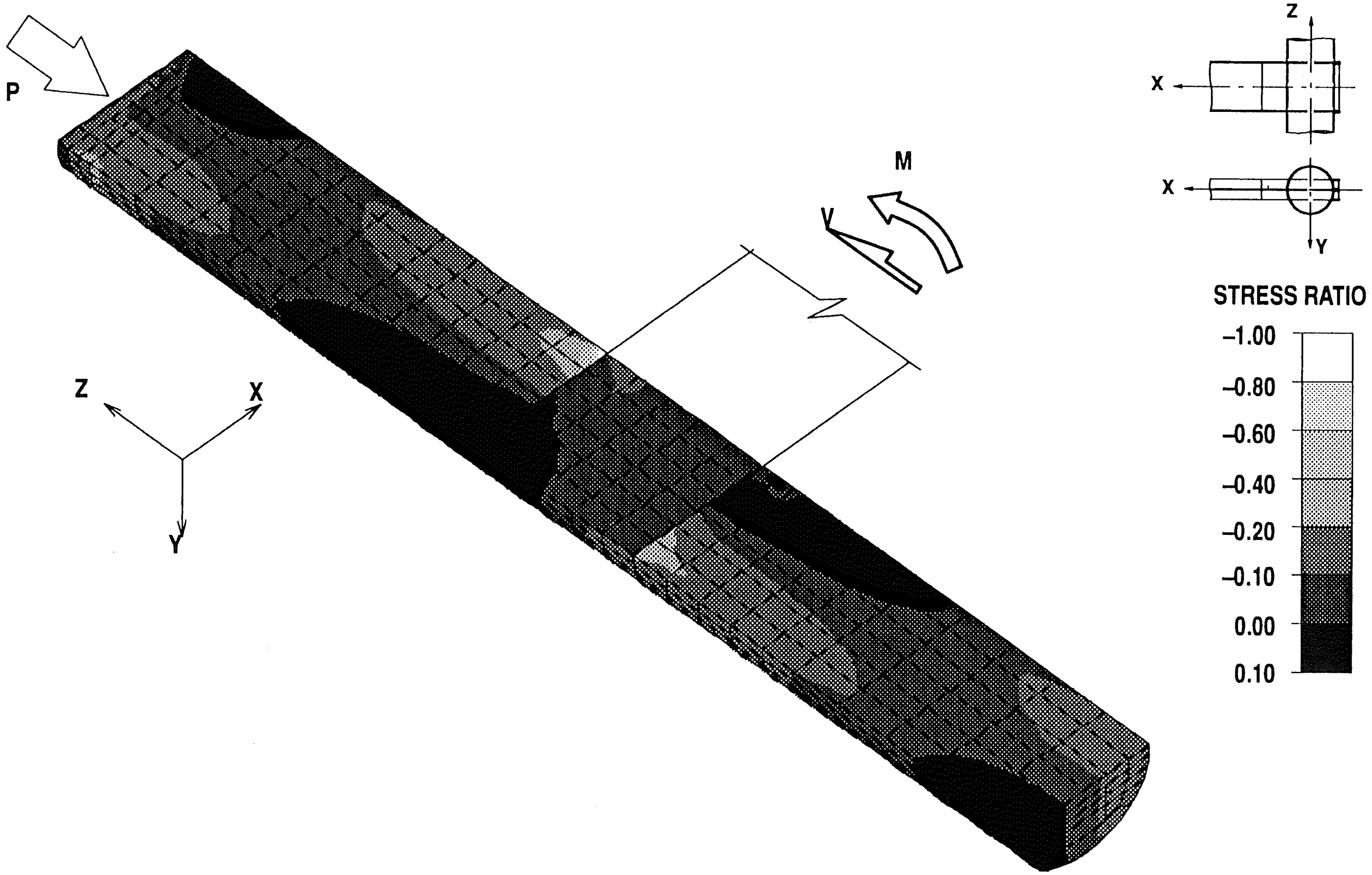

Figure A.45. Longitudinal Stress Ratio in the Concrete Core, Connection *Type VII*

APPENDIX B

EXPERIMENTAL INVESTIGATION

The data obtained from the strain gages and *LVDTs* used in this research project are presented in this Appendix. For convenience, most of the results were normalized in order to present them in a dimensionless format.

The figures present in this Appendix include:

1. The steel pipe strains as measured by strain gages applied to the tube skin,
2. The lateral pipe displacements as measured by *LVDTs* attached at the level of pipe longitudinal center–line.

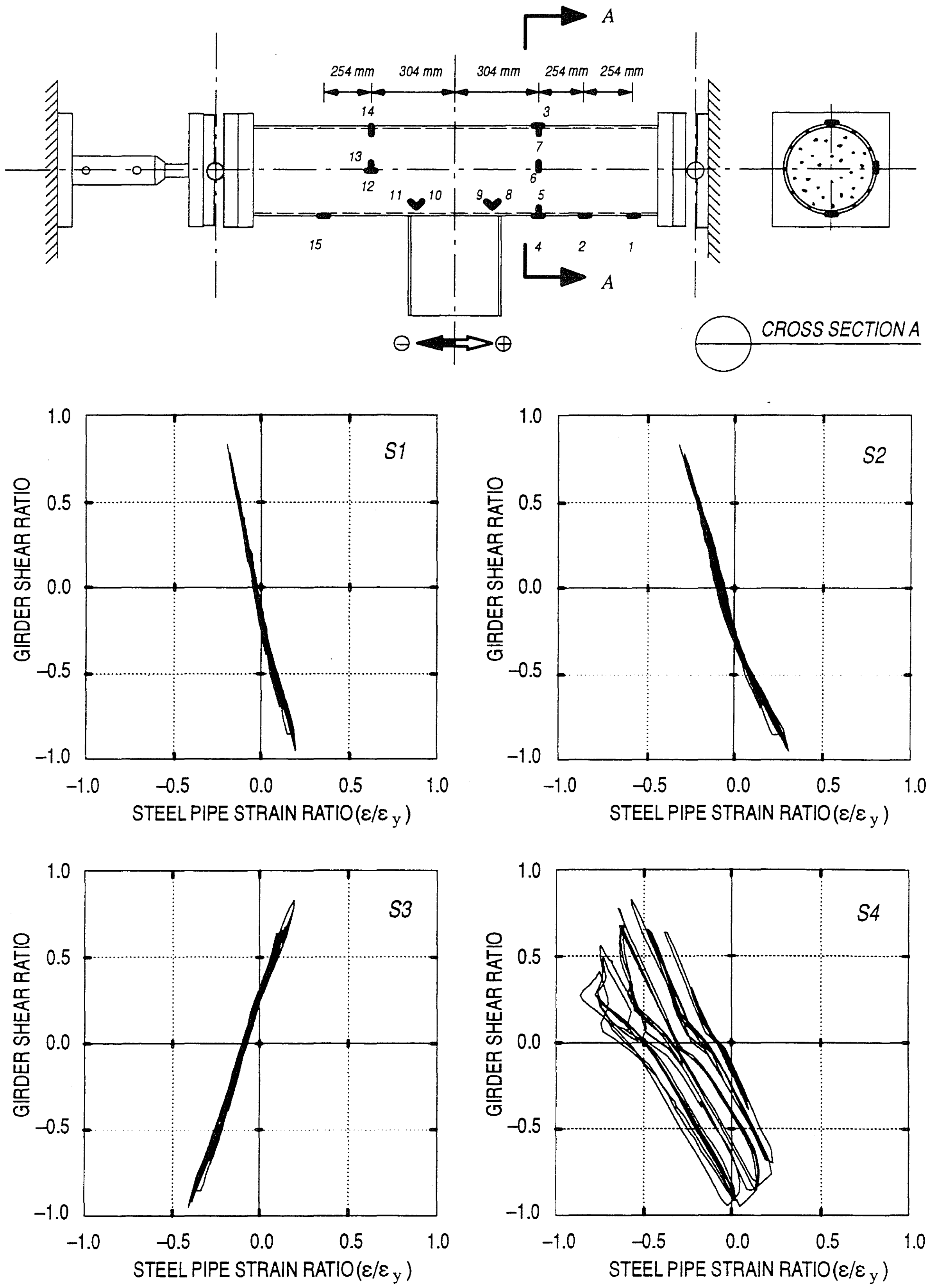

Figure B.1 a. Measured Strain in the Steel Pipe for Connection *Type I*

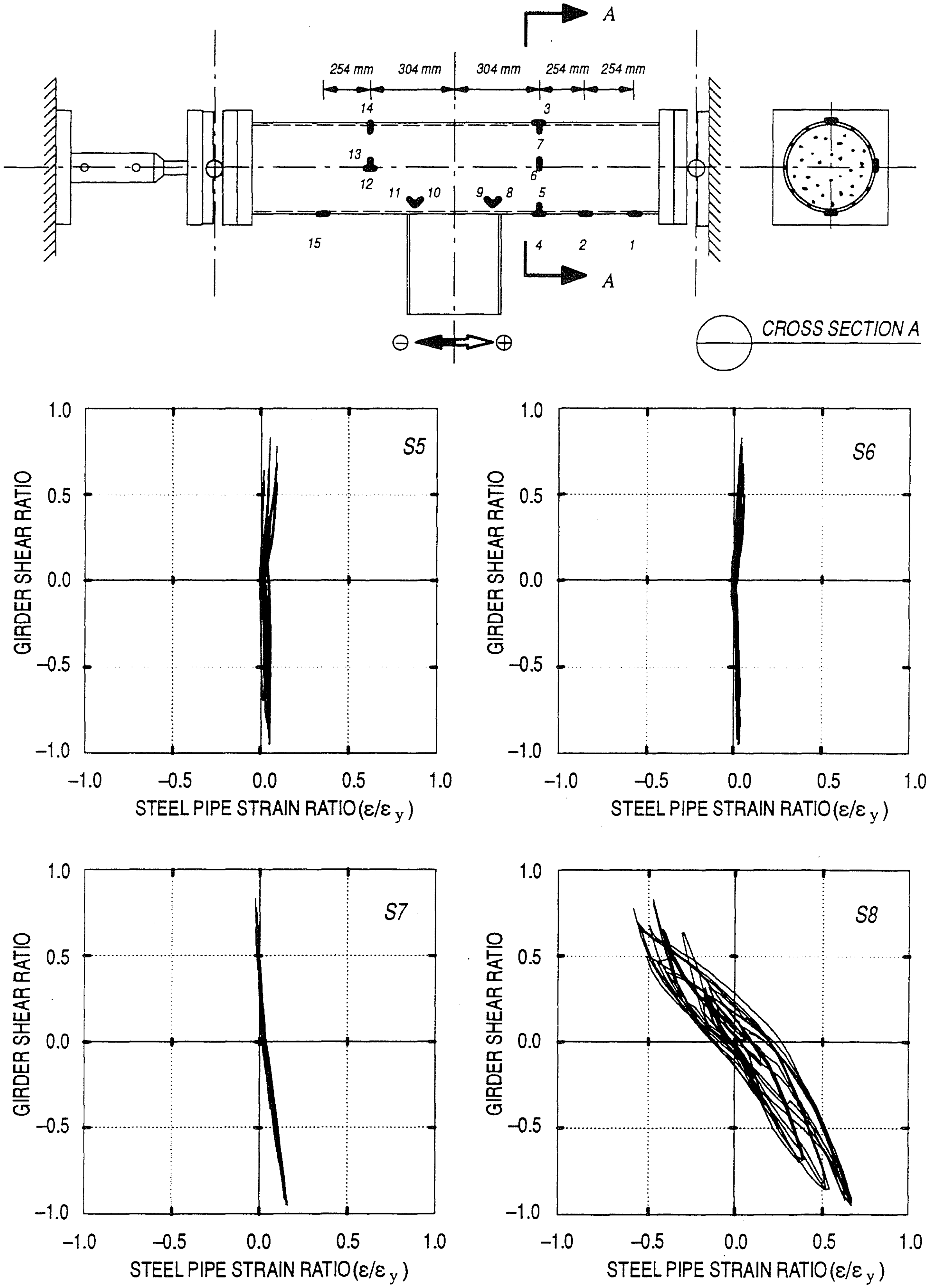

Figure B.1 b. Measured Strain in the Steel Pipe for Connection *Type I*

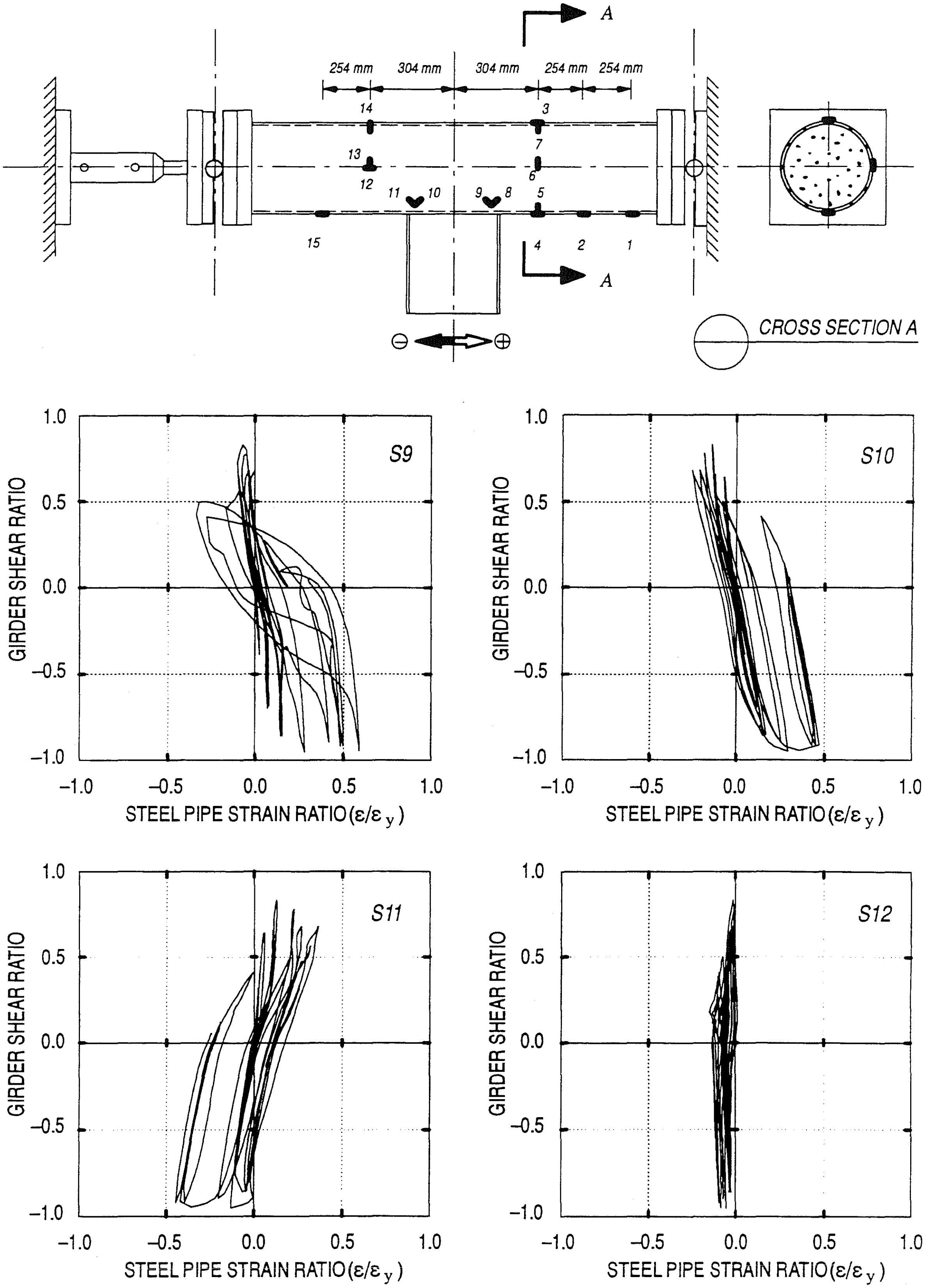

Figure B.1 c. Measured Strain in the Steel Pipe for Connection *Type I*

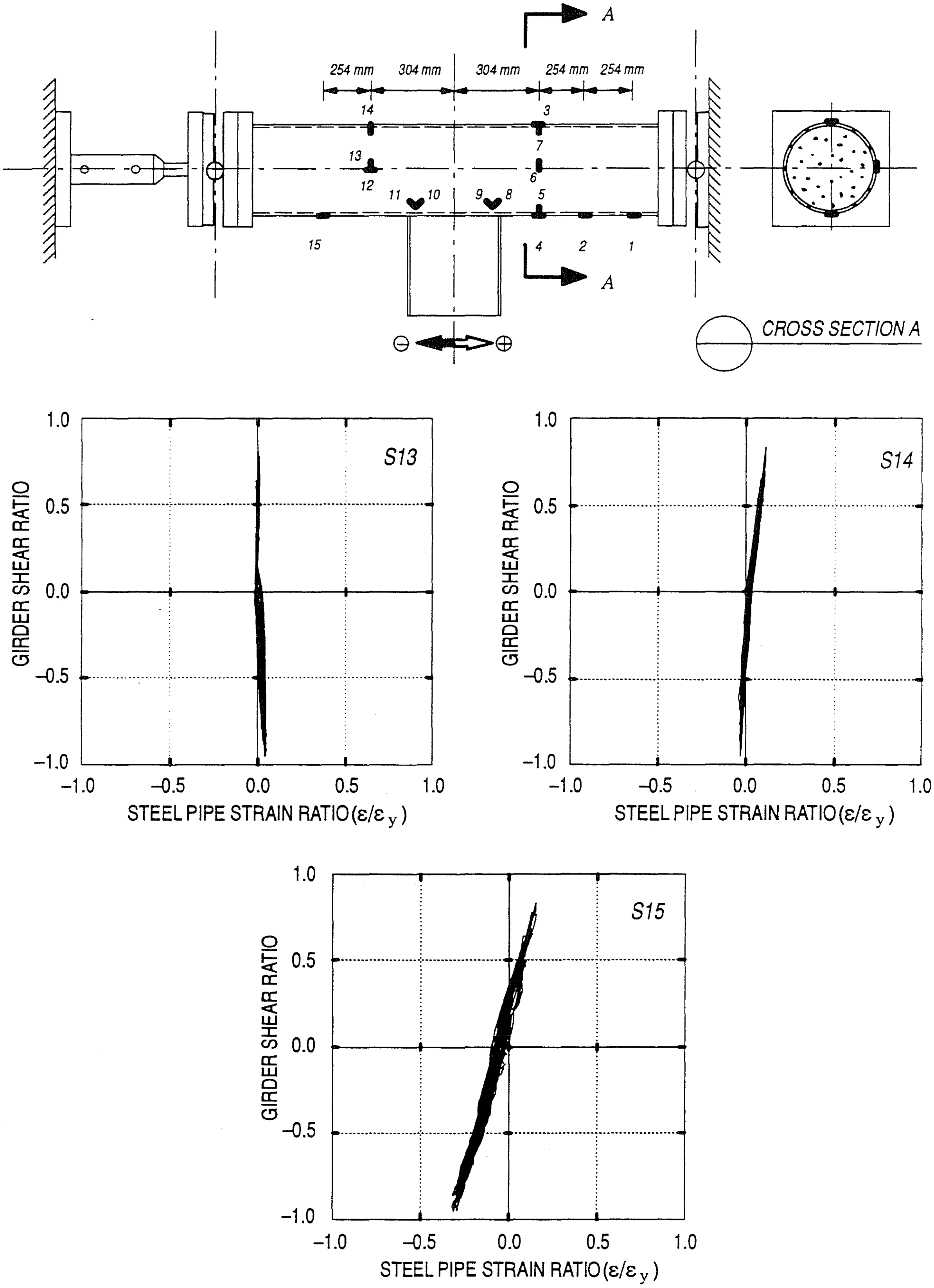

Figure B.1 d. Measured Strain in the Steel Pipe for Connection *Type I*

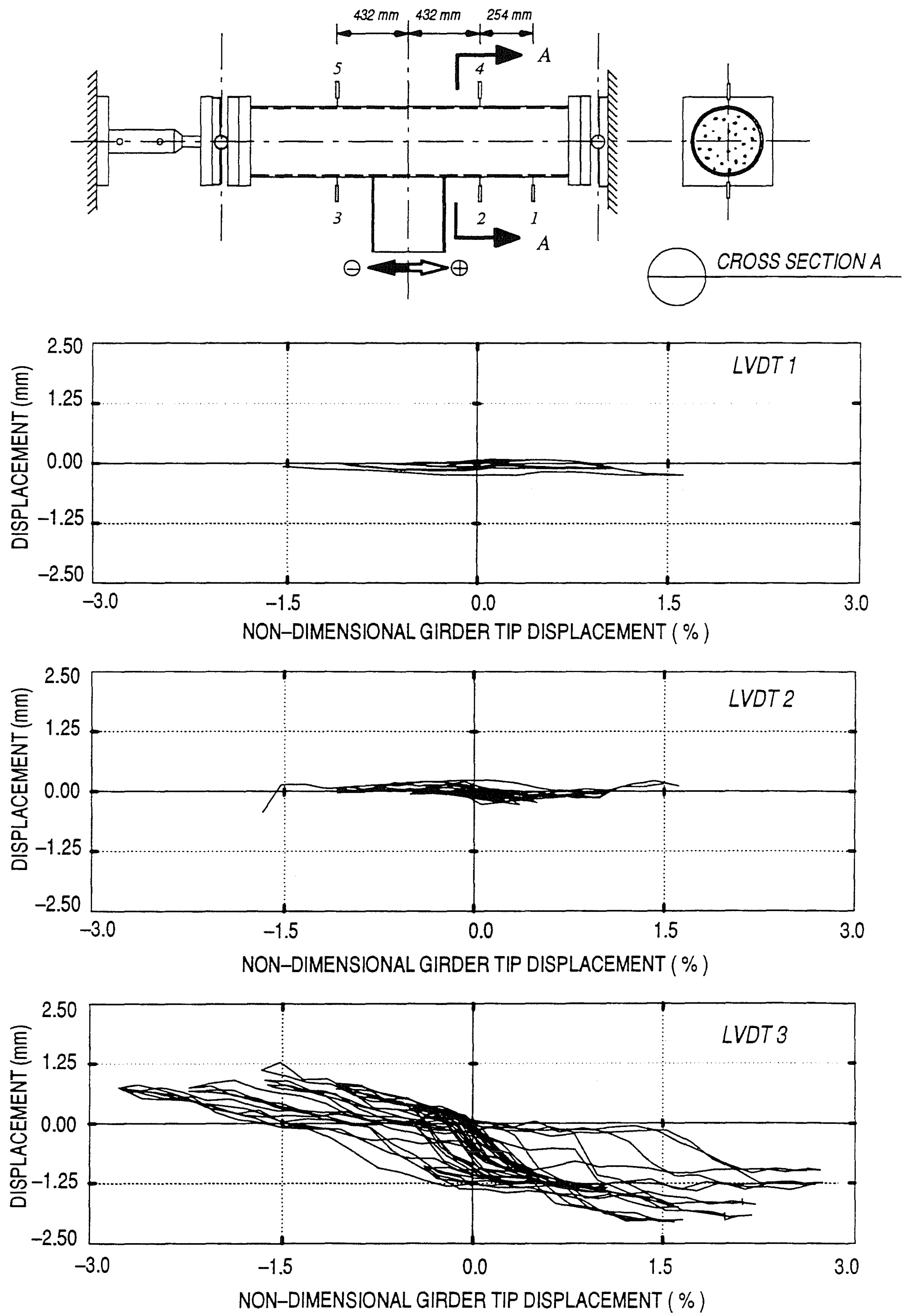

Figure B.2 a. Lateral Steel Pipe Displacement for Connection *Type I*

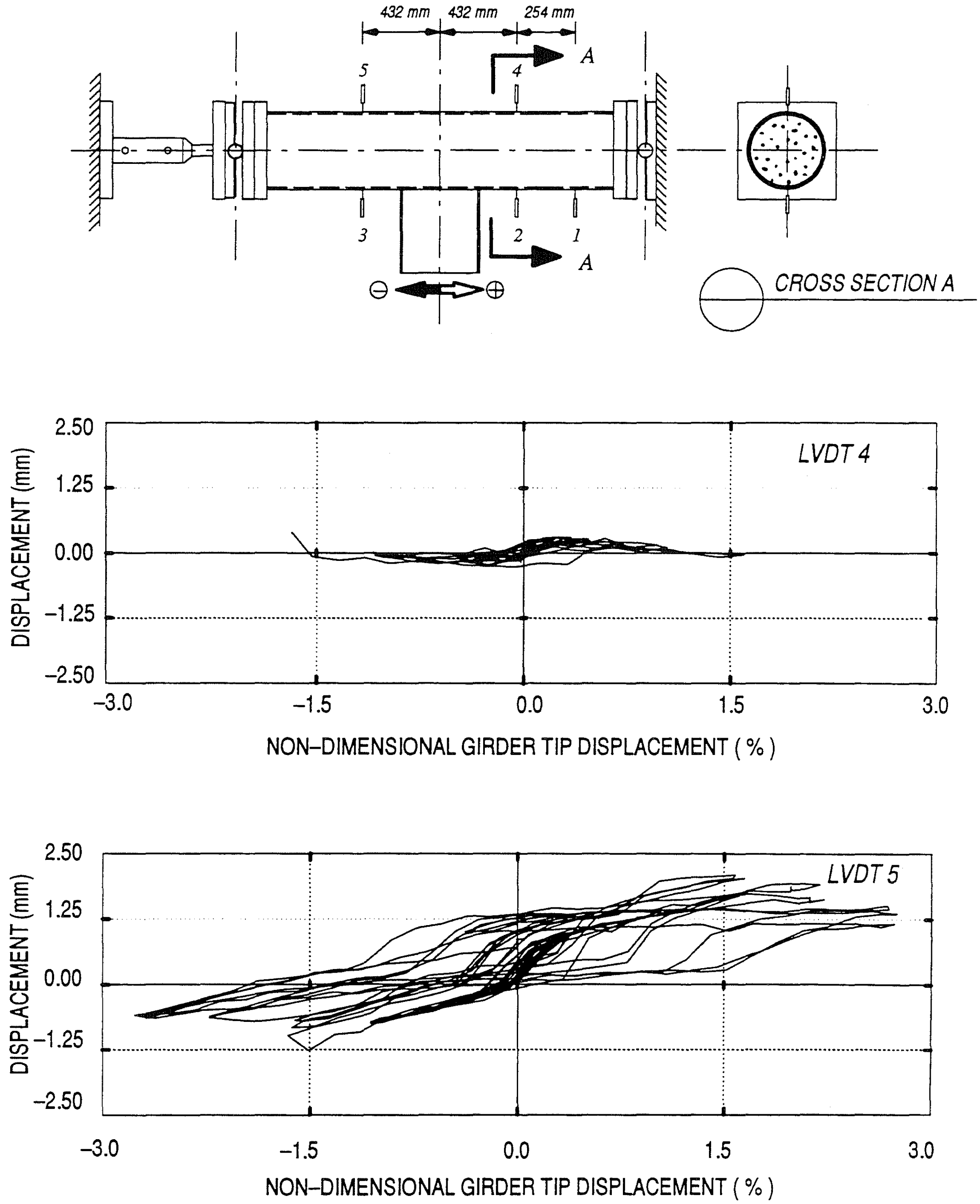

Figure B.2 b. Lateral Steel Pipe Displacement for Connection *Type I*

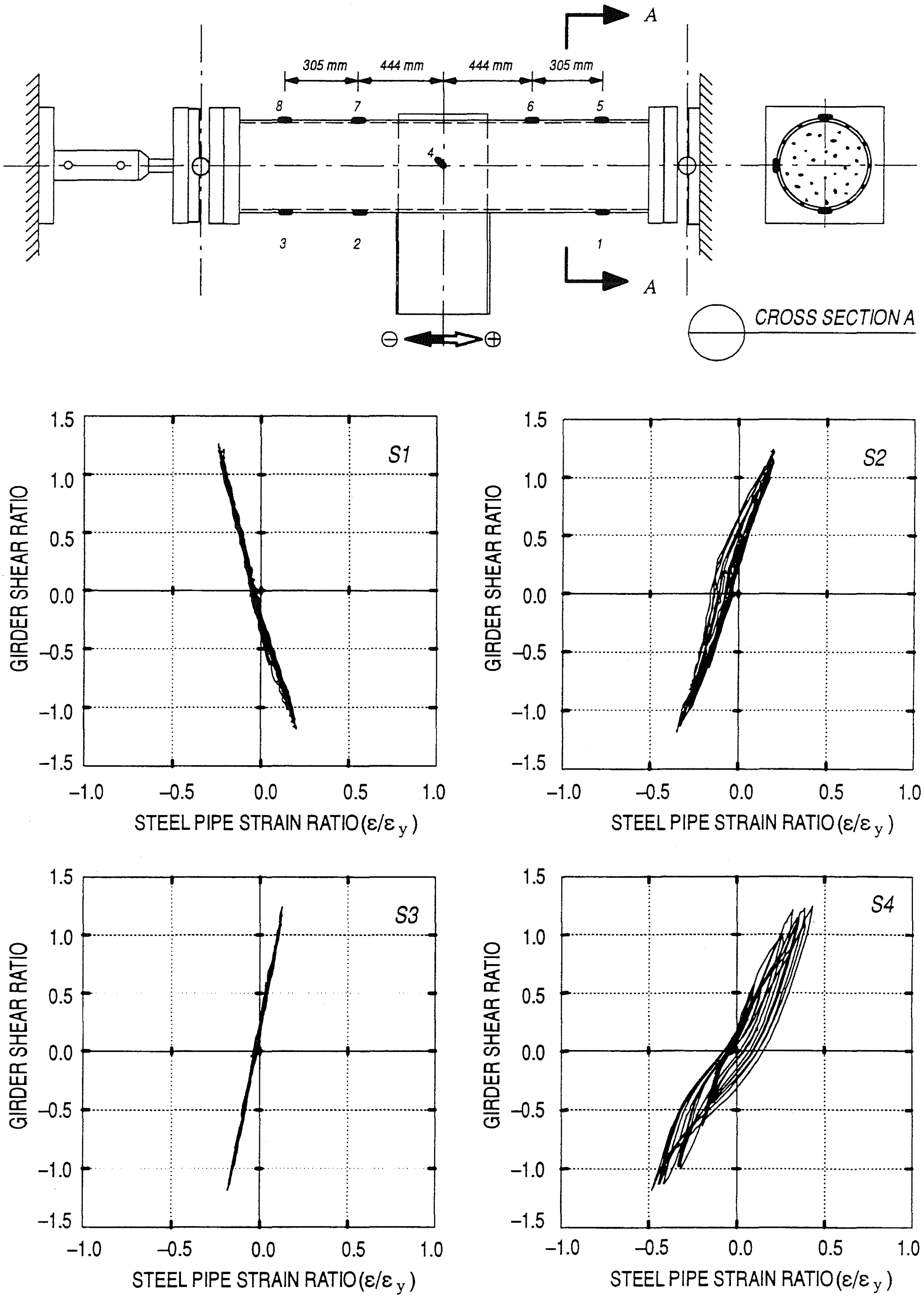

Figure B.3 a. Measured Strain in the Steel Pipe for Connection *Type IA*

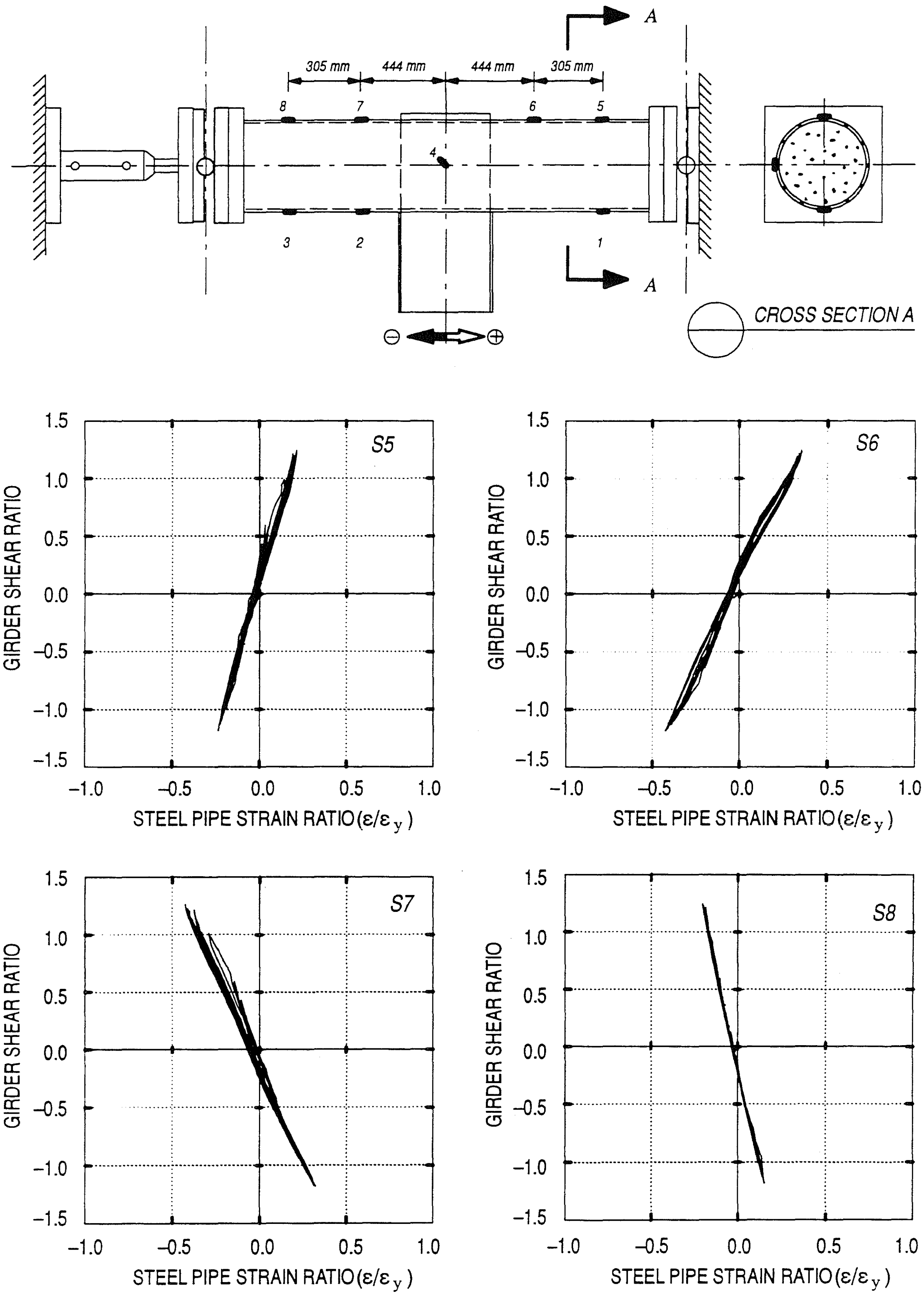

Figure B.3 b. Measured Strain in the Steel Pipe for Connection *Type IA*

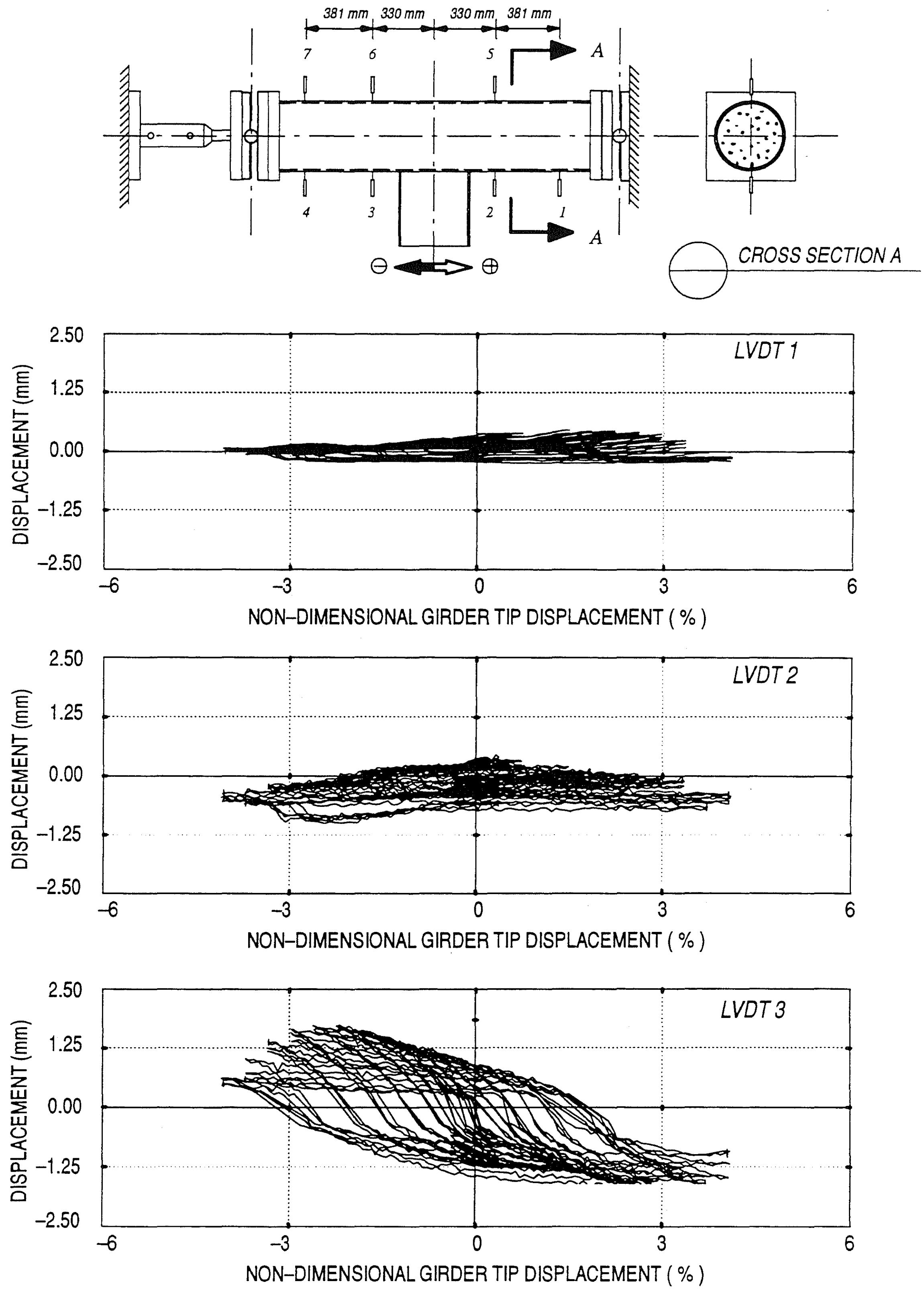

Figure B.4 a. Lateral Displacement of the Composite Column, Connection *Type IA*

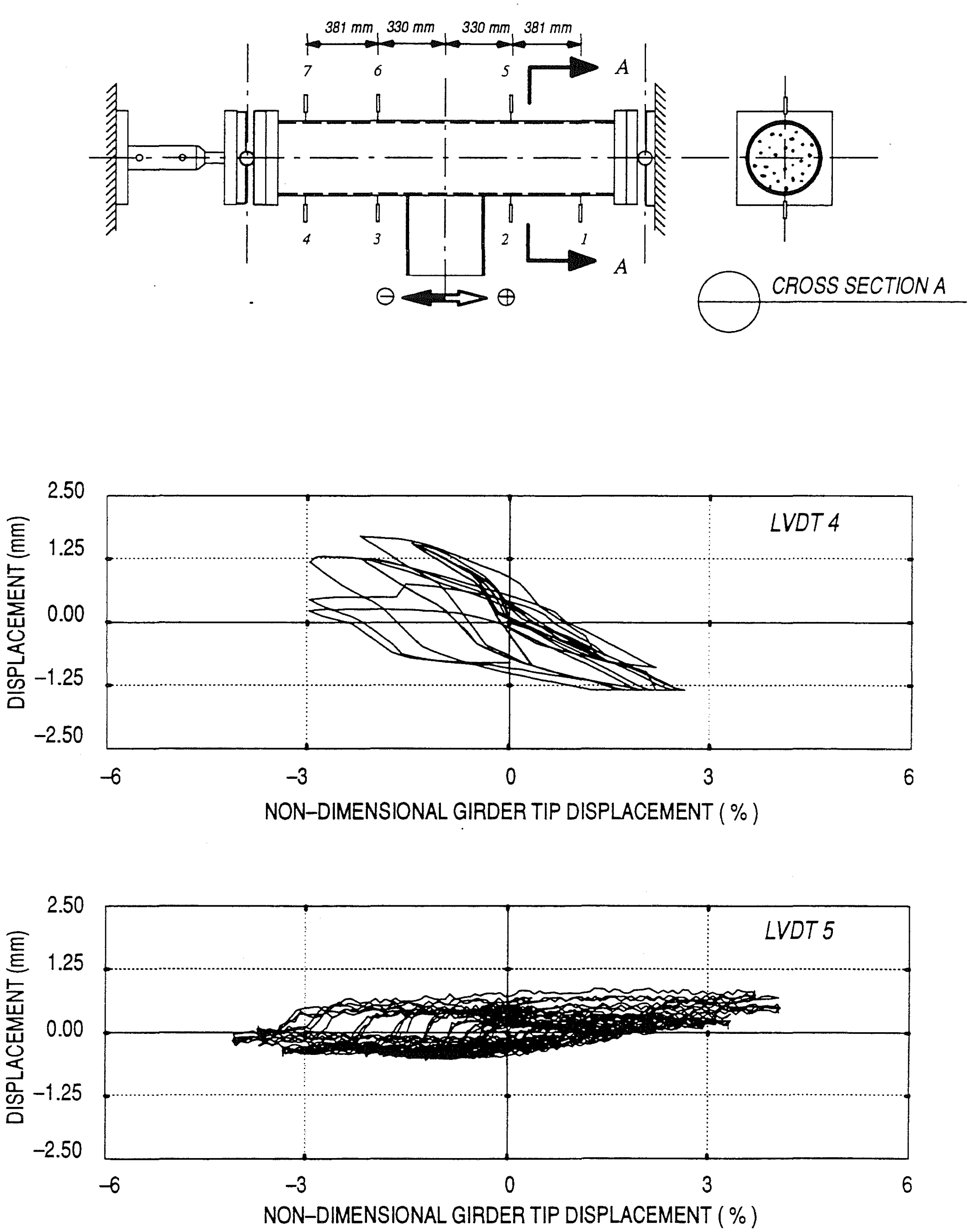

Figure B.4 b. Lateral Displacement of the Composite Column, Connection *Type IA*

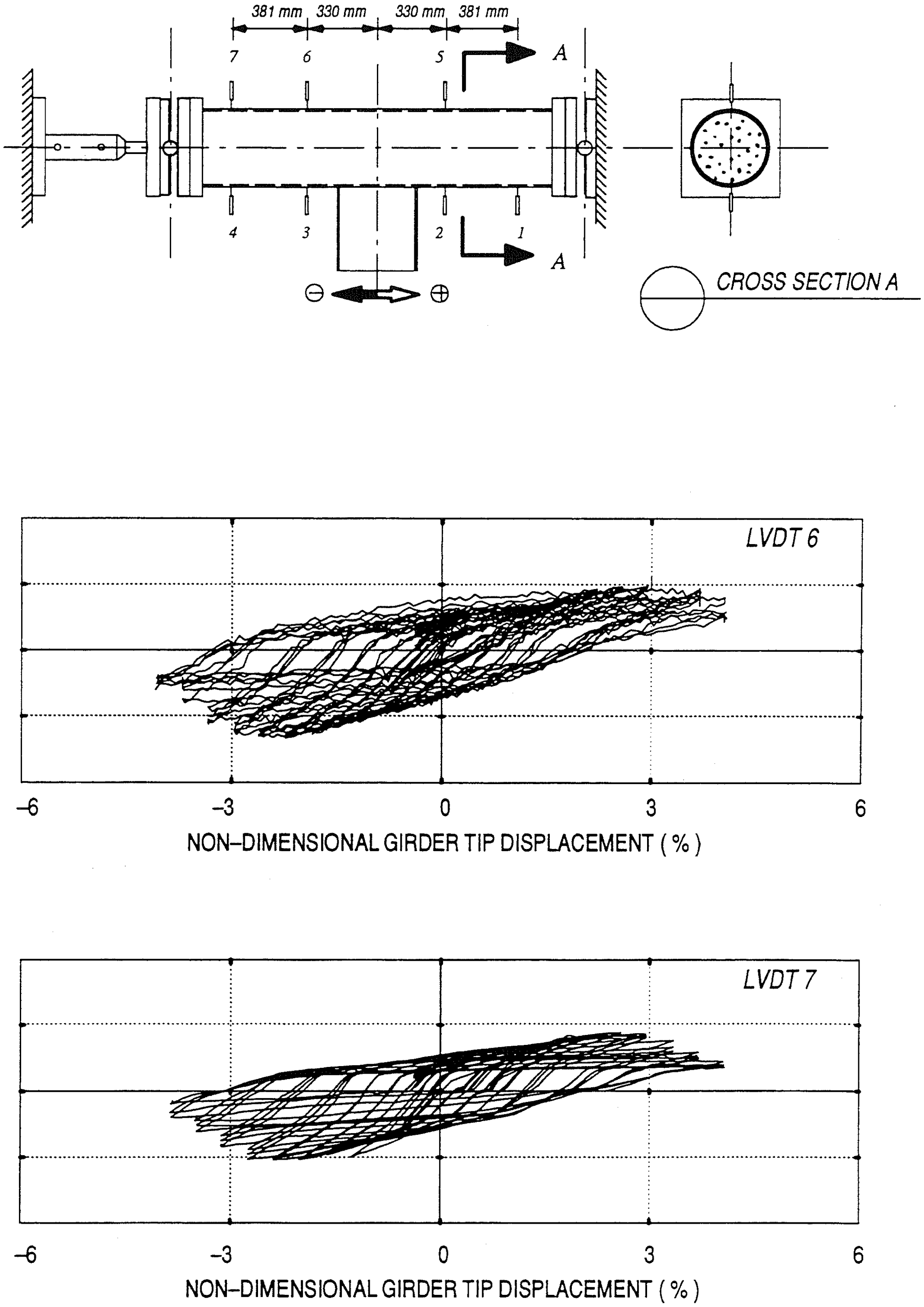

Figure B.4 c. Lateral Displacement of the Composite Column, Connection *Type IA*

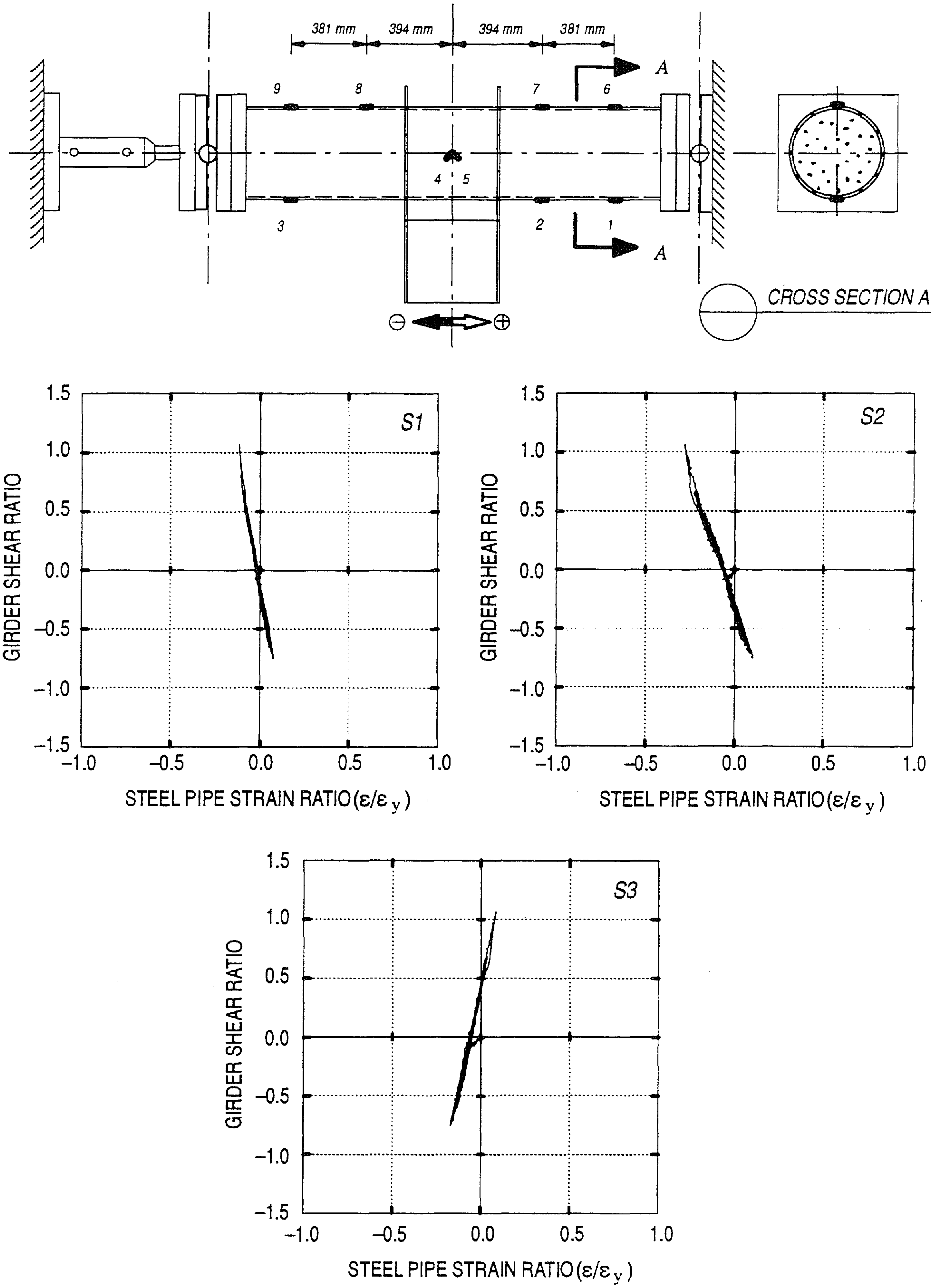

Figure B.5 a. Measured Strain in the Steel Pipe for Connection *Type II*

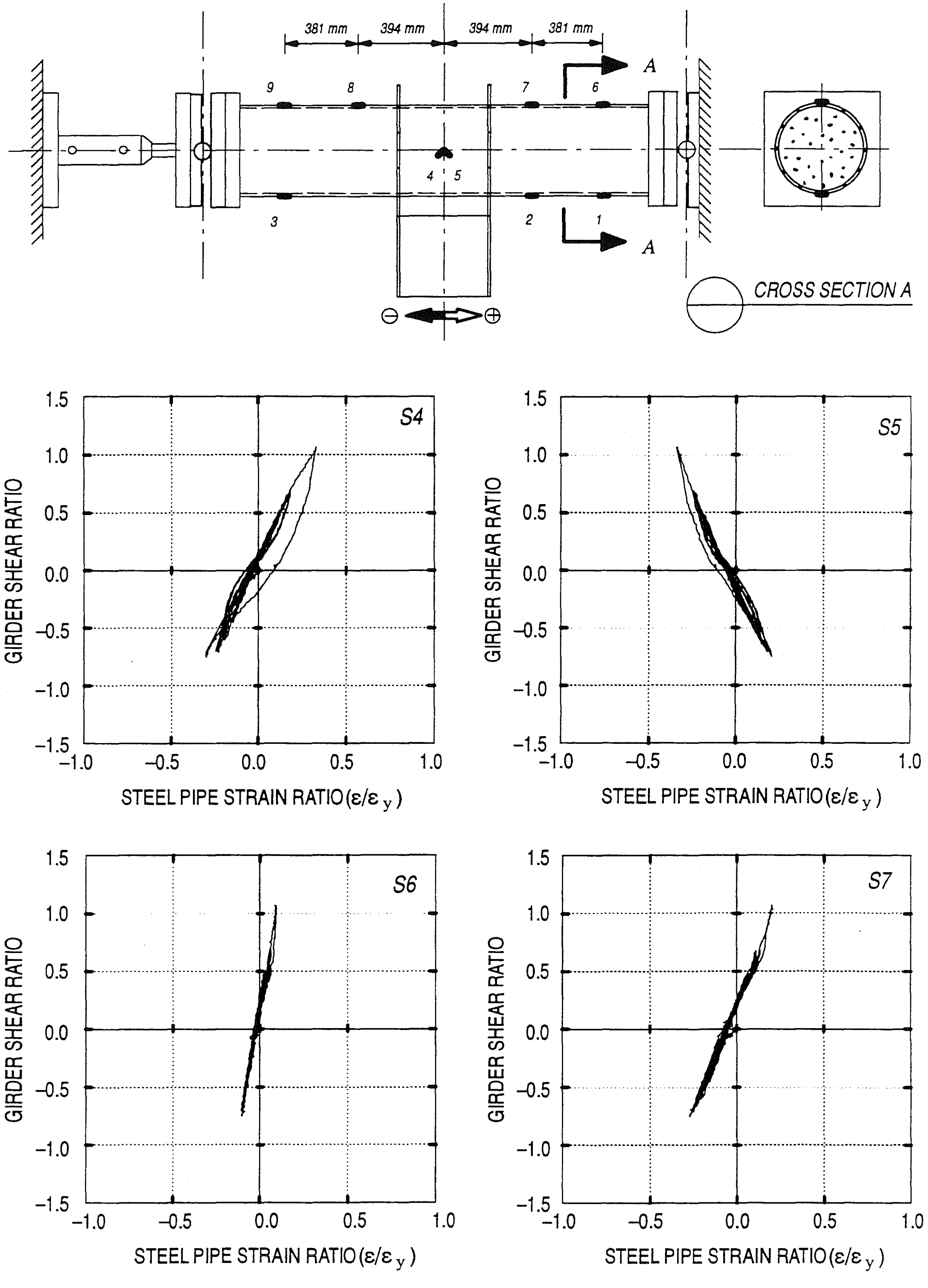

Figure B.5 b. Measured Strain in the Steel Pipe for Connection *Type II*

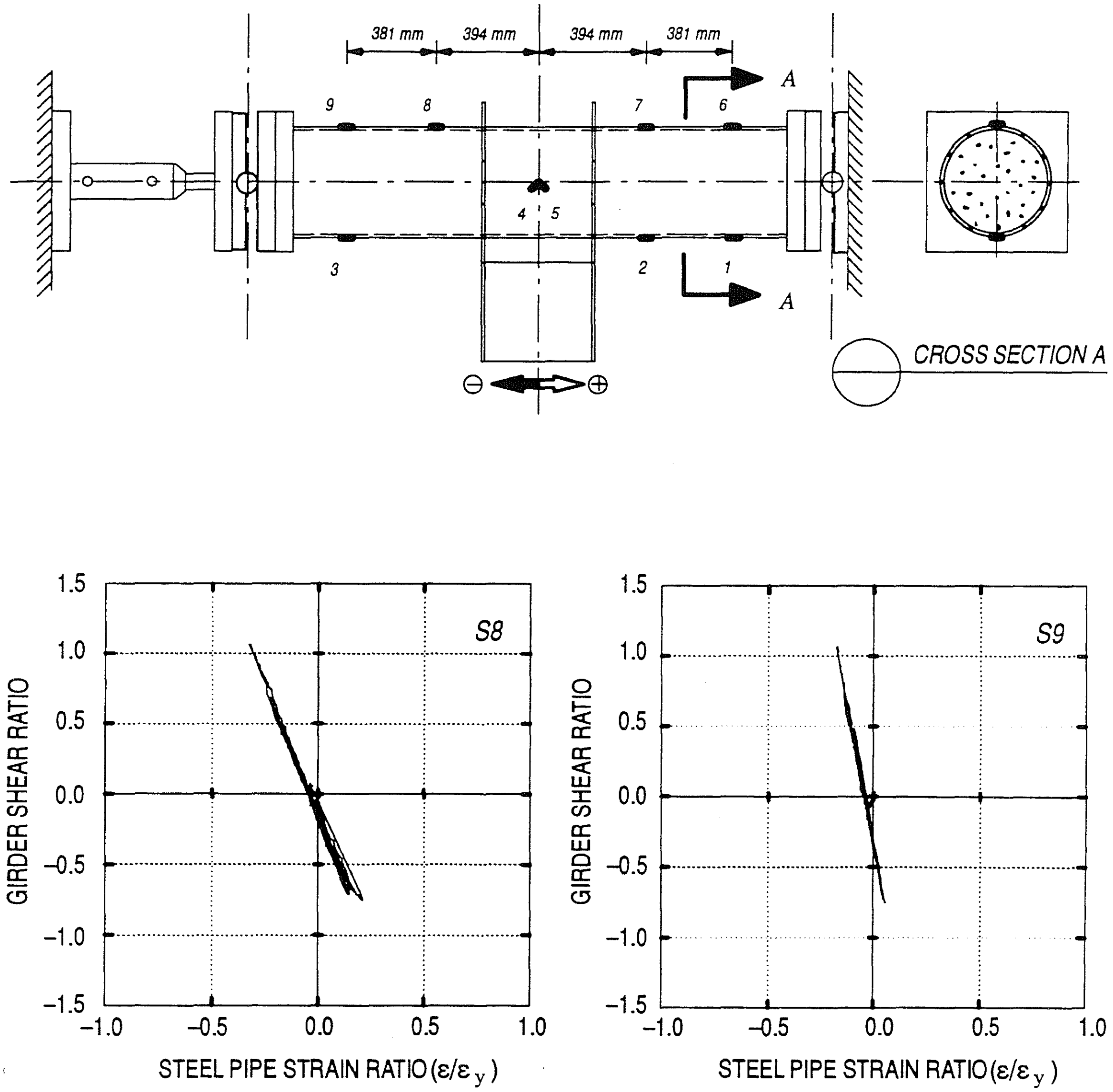

Figure B.5 c. Measured Strain in the Steel Pipe for Connection *Type II*

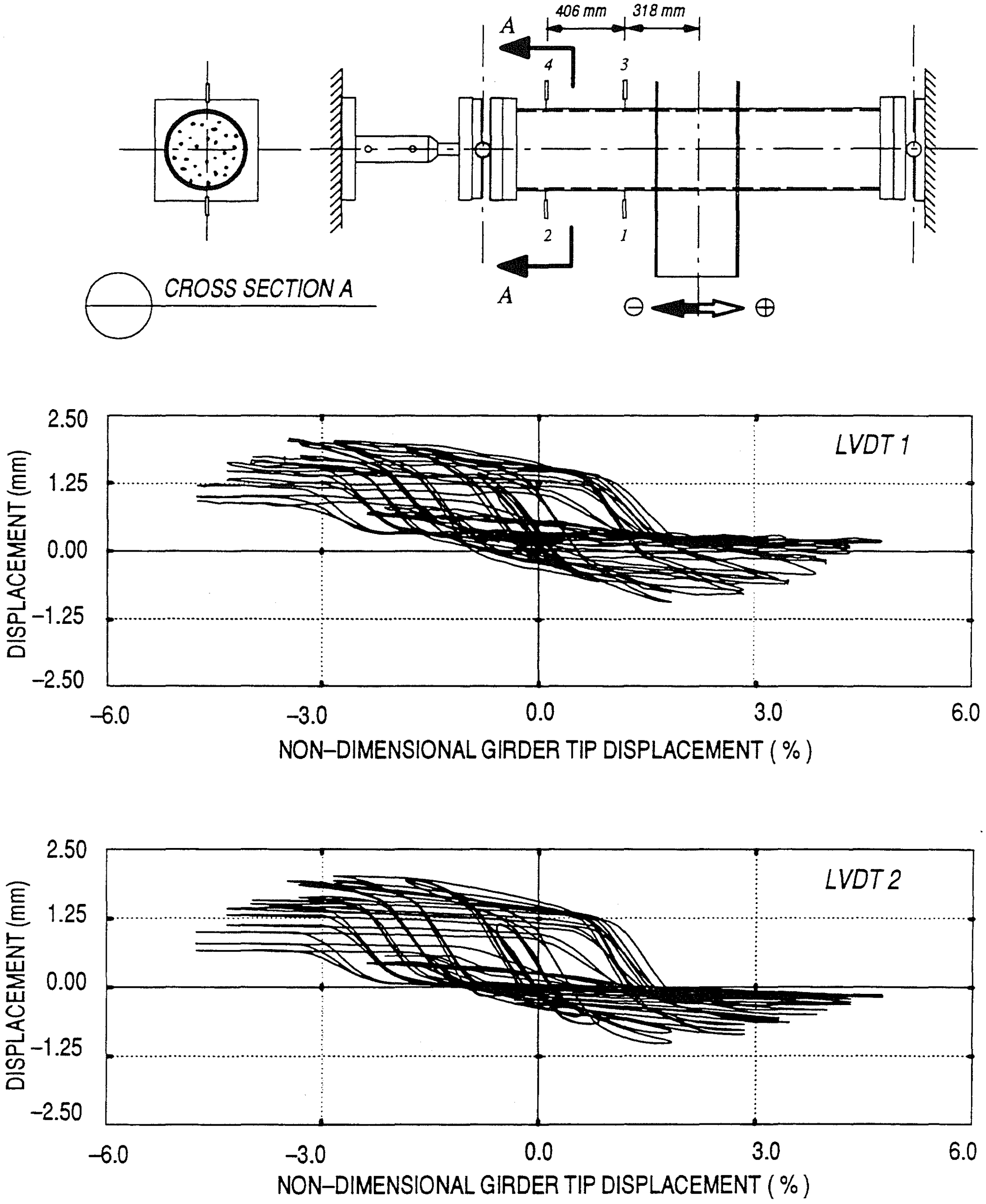

Figure B.6 a. Lateral Displacement of the CFT for Connection *Type II*

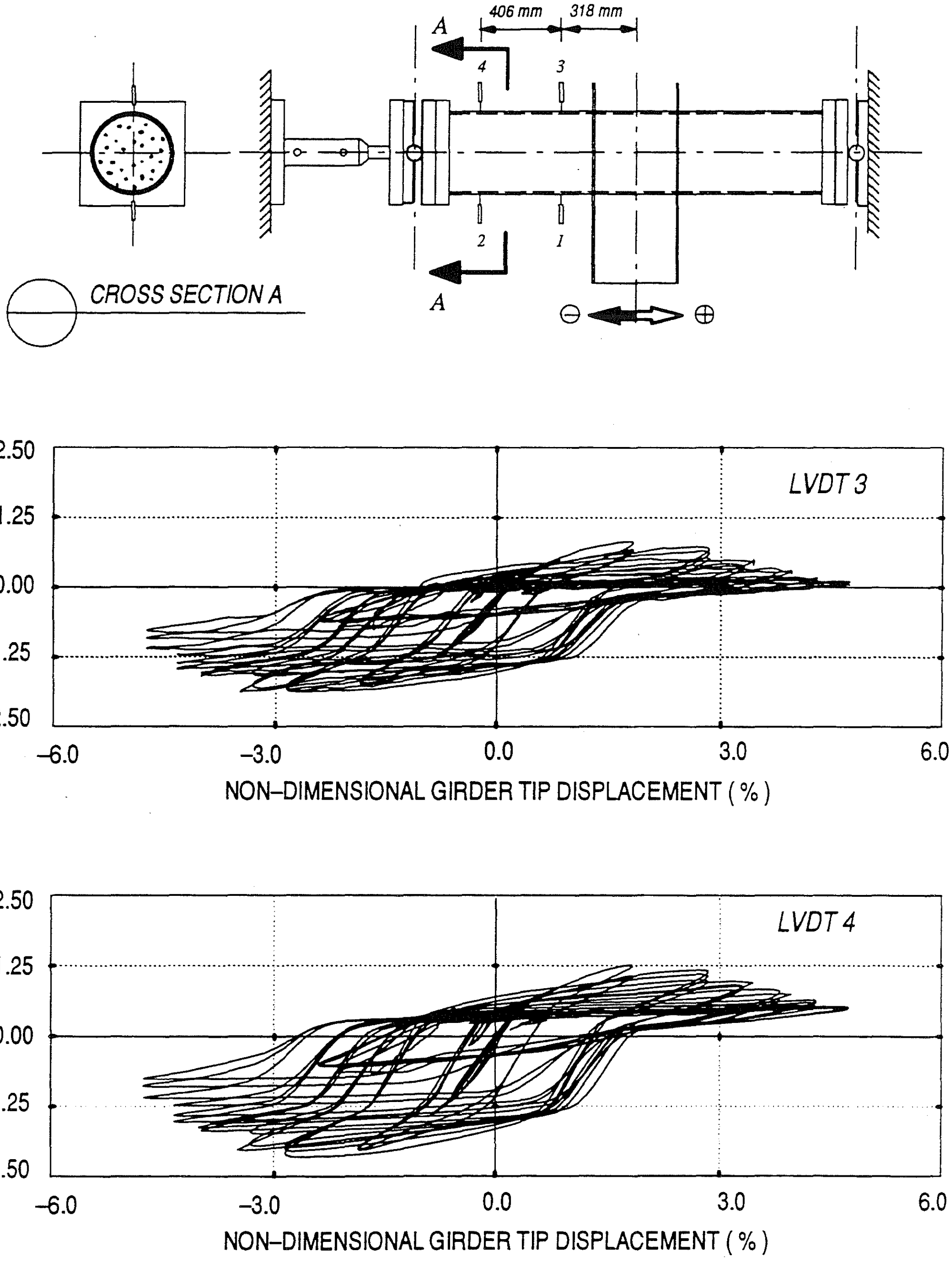

Figure B.6 b. Lateral Displacement of the CFT for Connection *Type II*

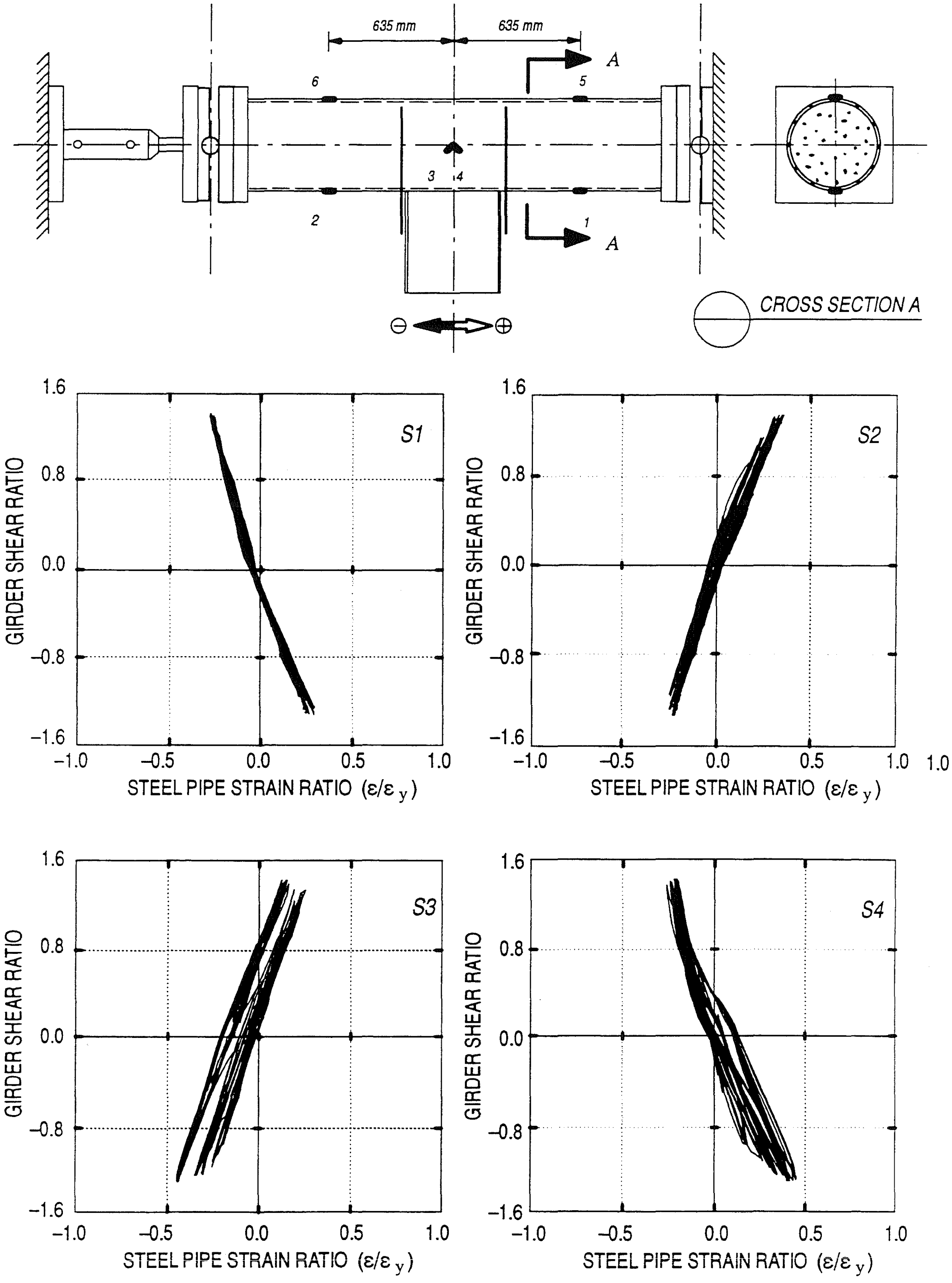

Figure B.7 a. Measured Strain in the Steel Pipe for Connection *Type III*

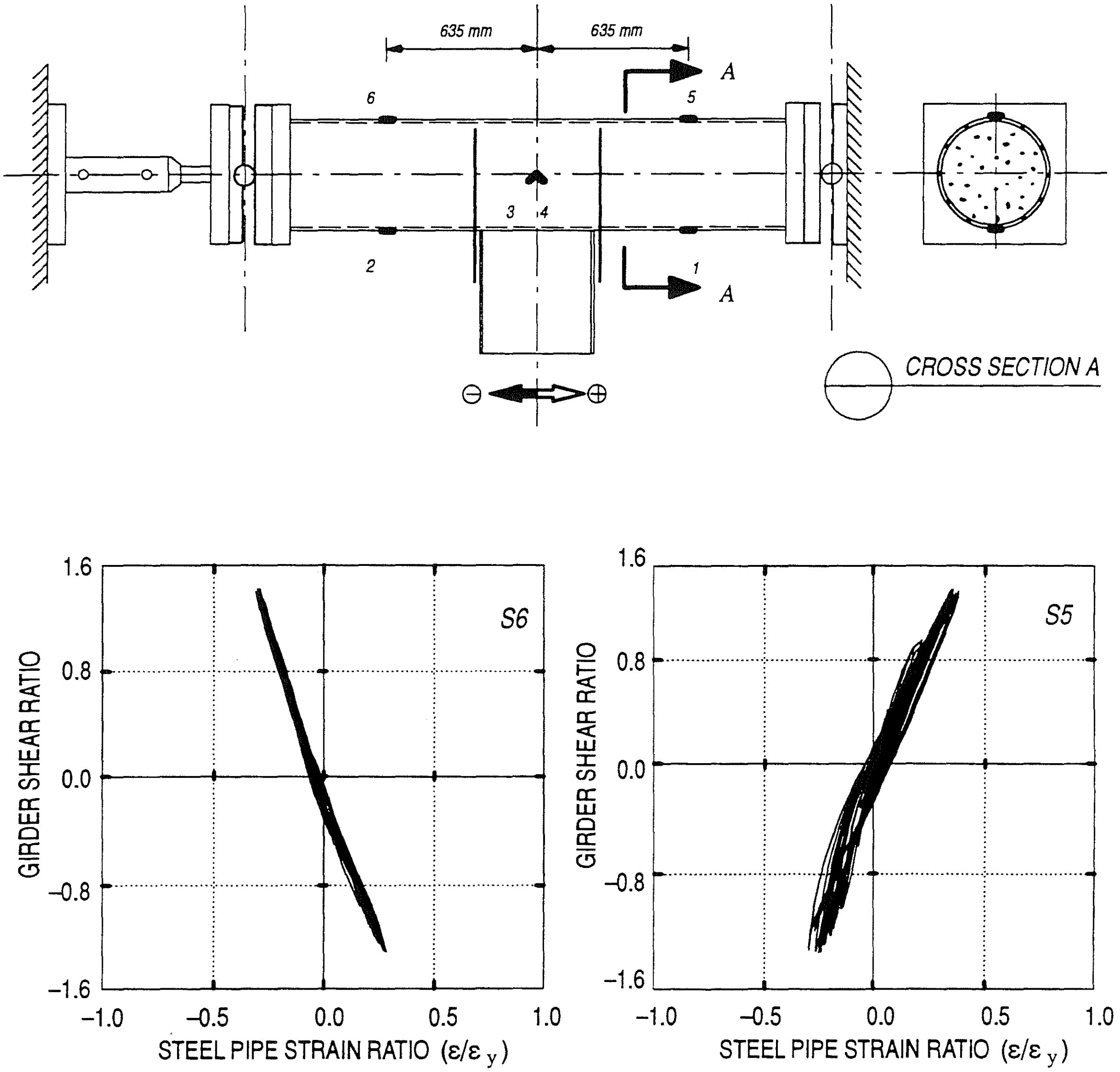

Figure B.7 b. Measured Strain in the Steel Pipe for Connection *Type III*

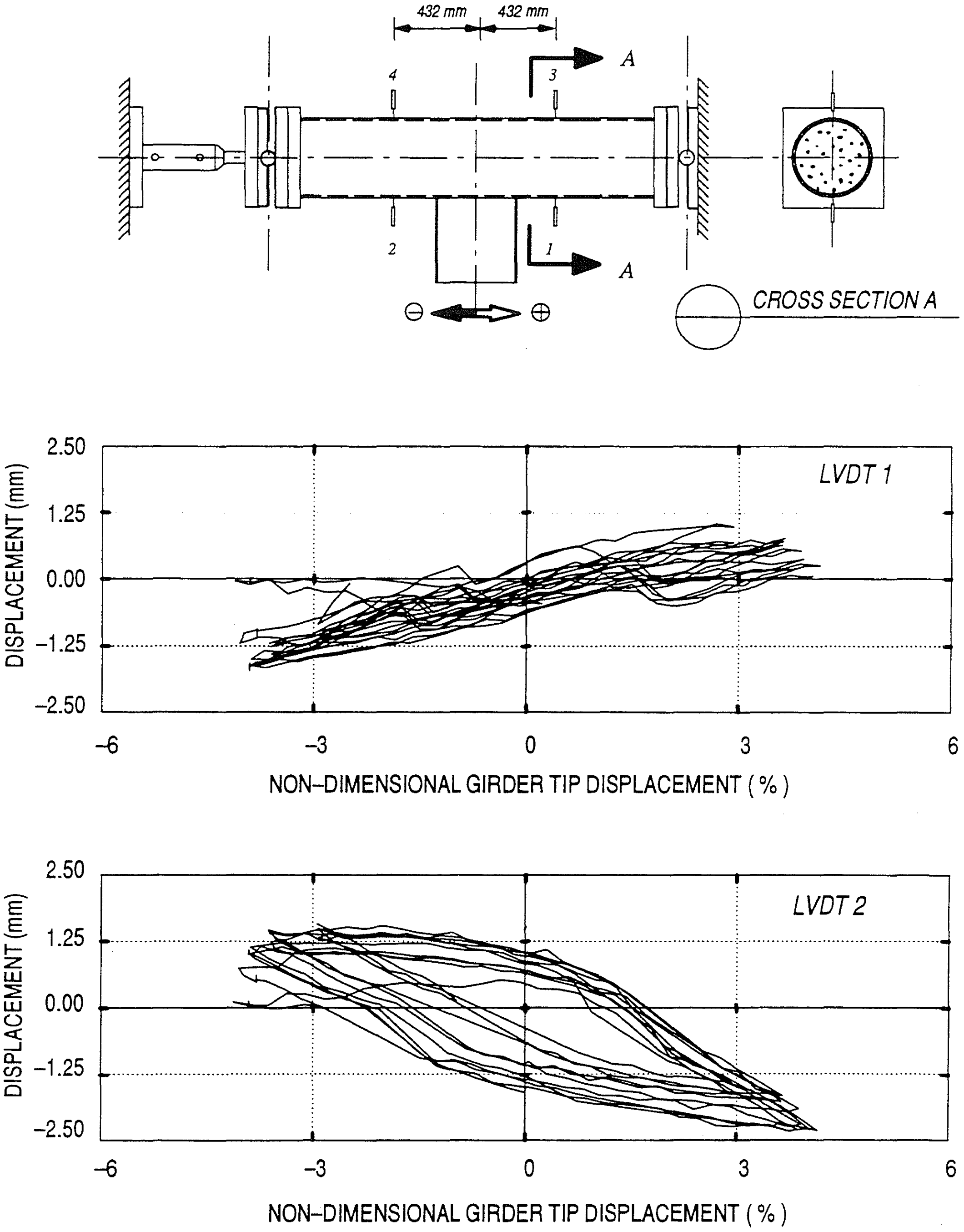

Figure B.8 a. Lateral Displacement of the CFT for Connection *Type III*

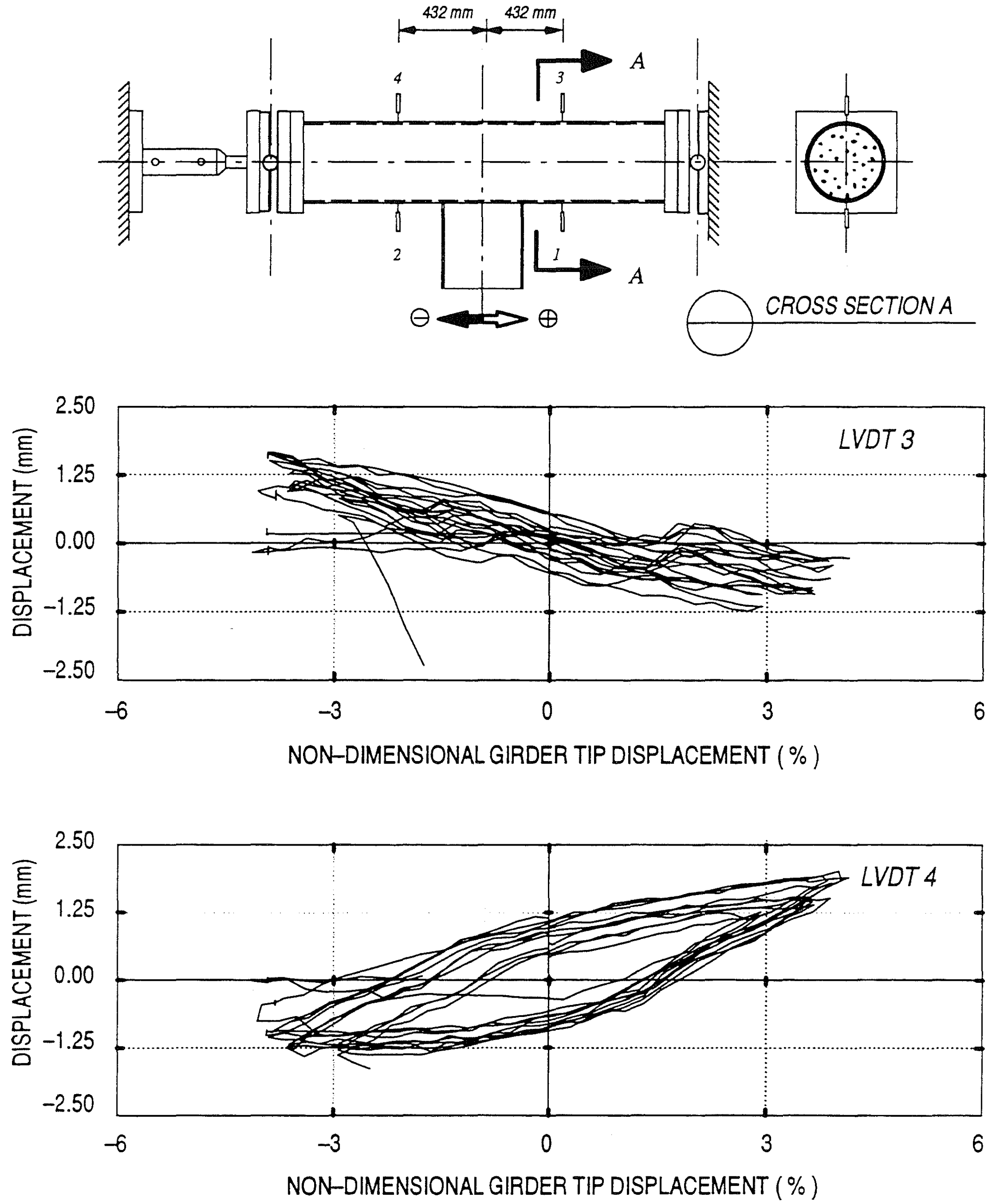

Figure B.8 b. Lateral Displacement of the CFT for Connection *Type III*

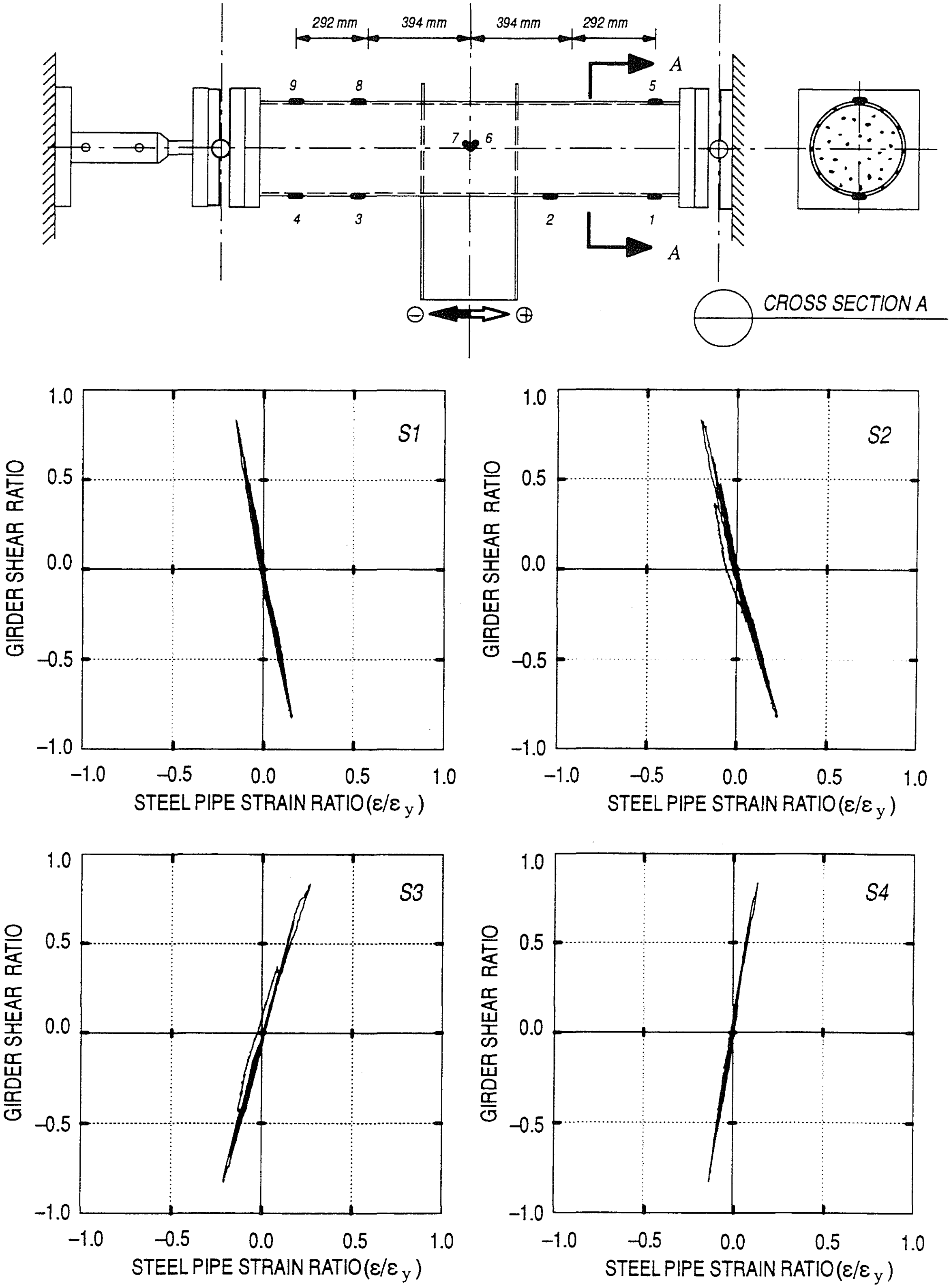

Figure B.9 a. Measured Strains in the Steel Pipe for Connection *Type VI*

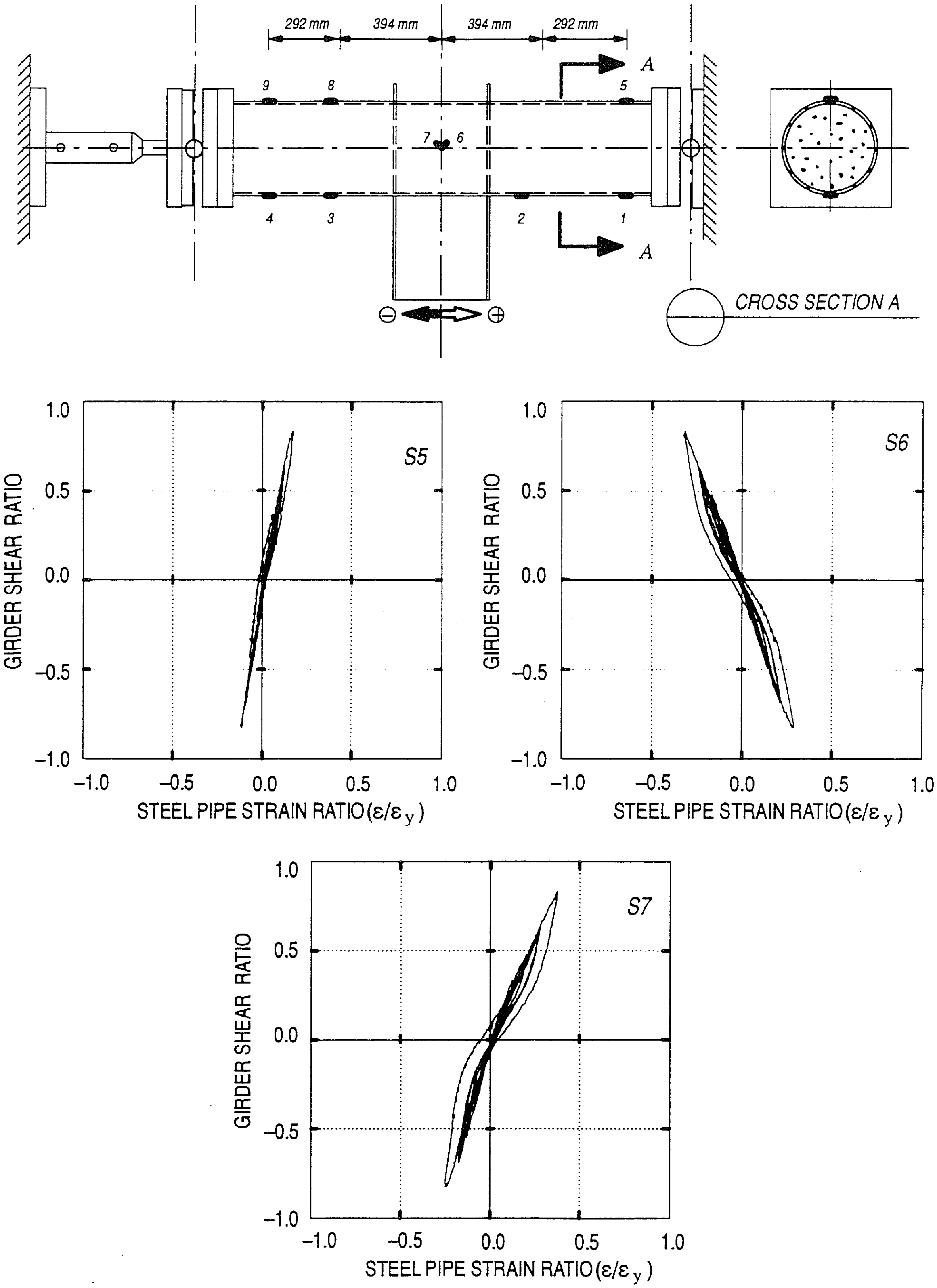

Figure B.9 b. Measured Strains in the Steel Pipe for Connection *Type VI*

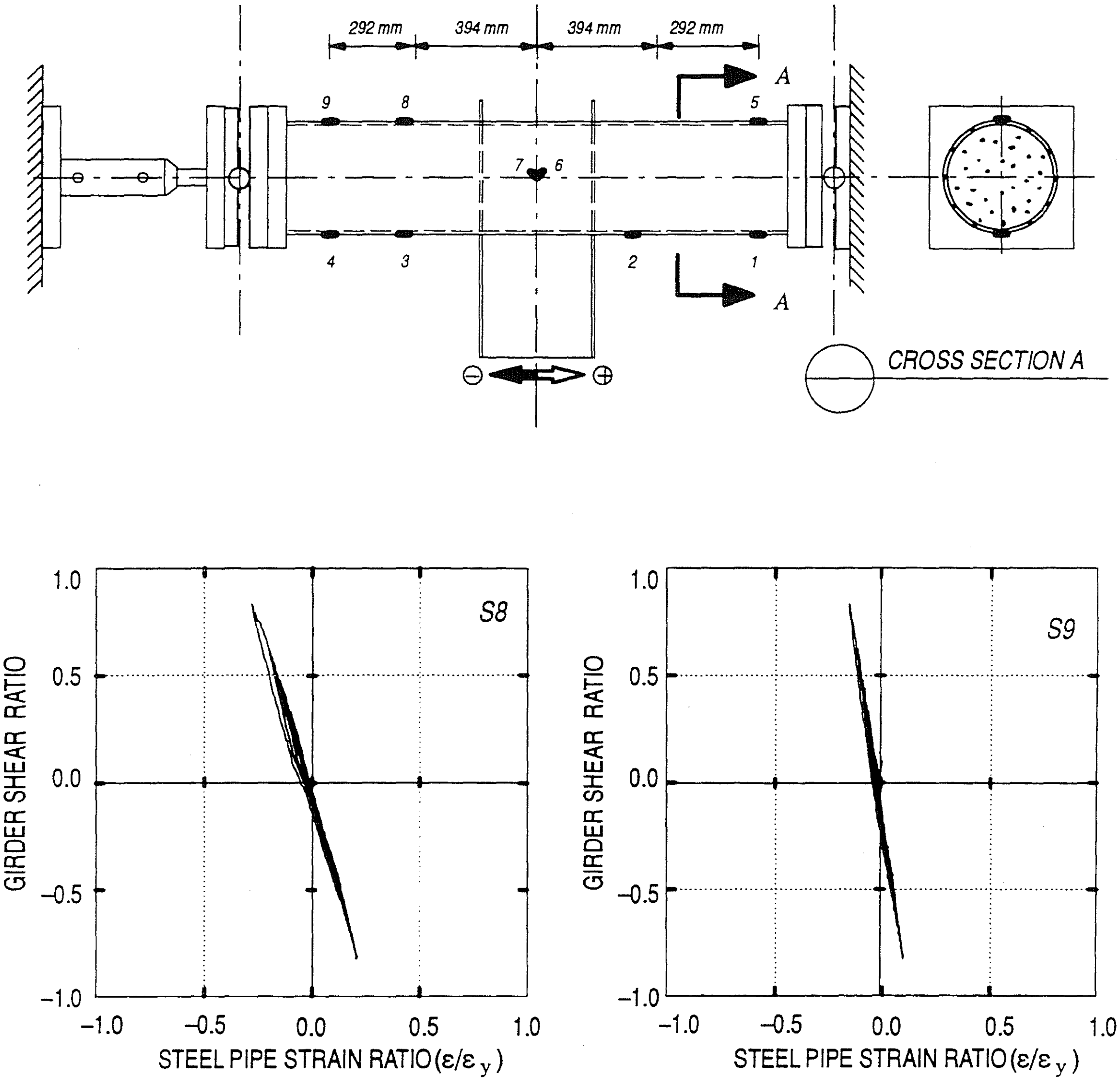

Figure B.9 c. Measured Strains in the Steel Pipe for Connection *Type VI*

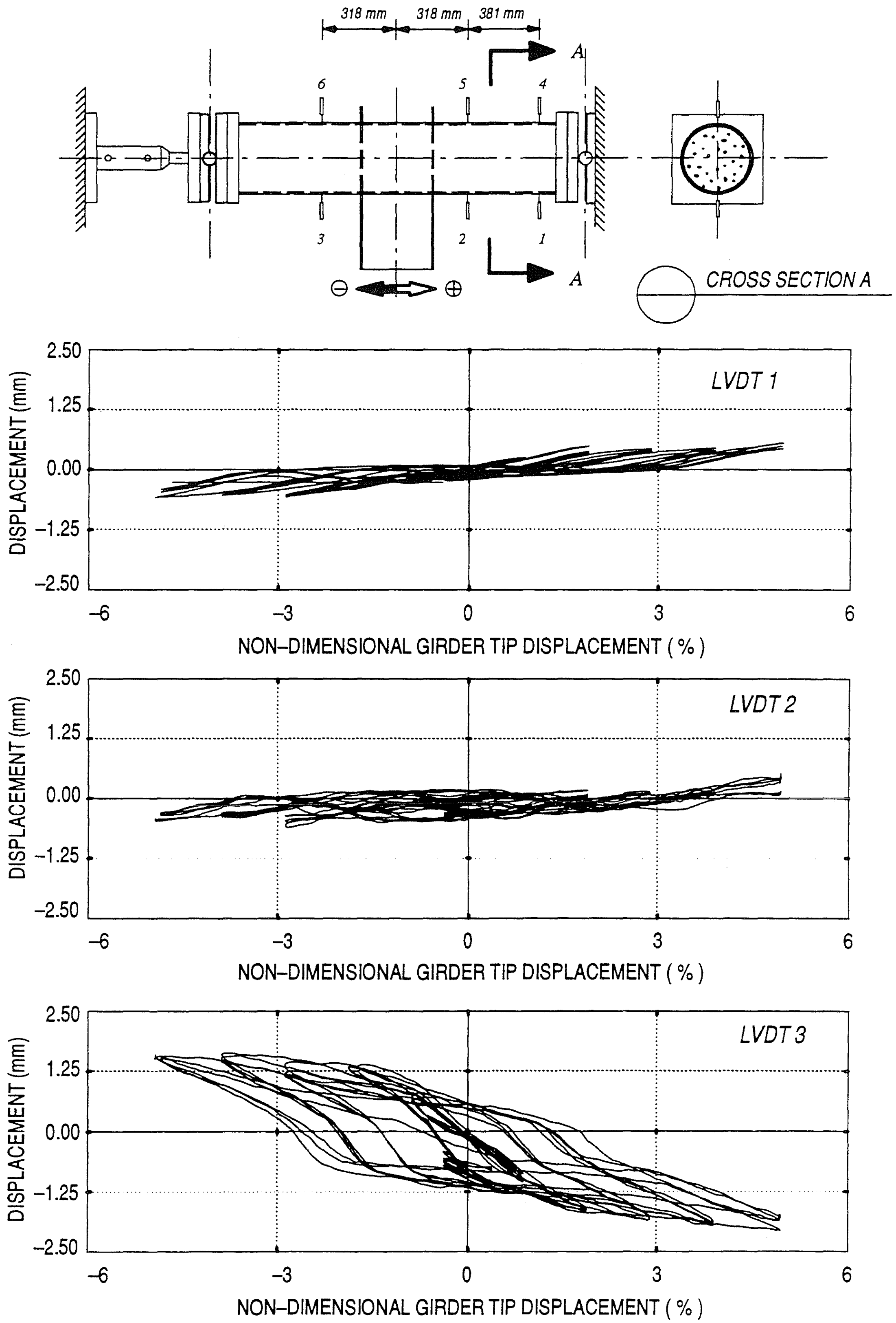

Figure B.10 a. Lateral Displacement of the CFT for Connection *Type VI*

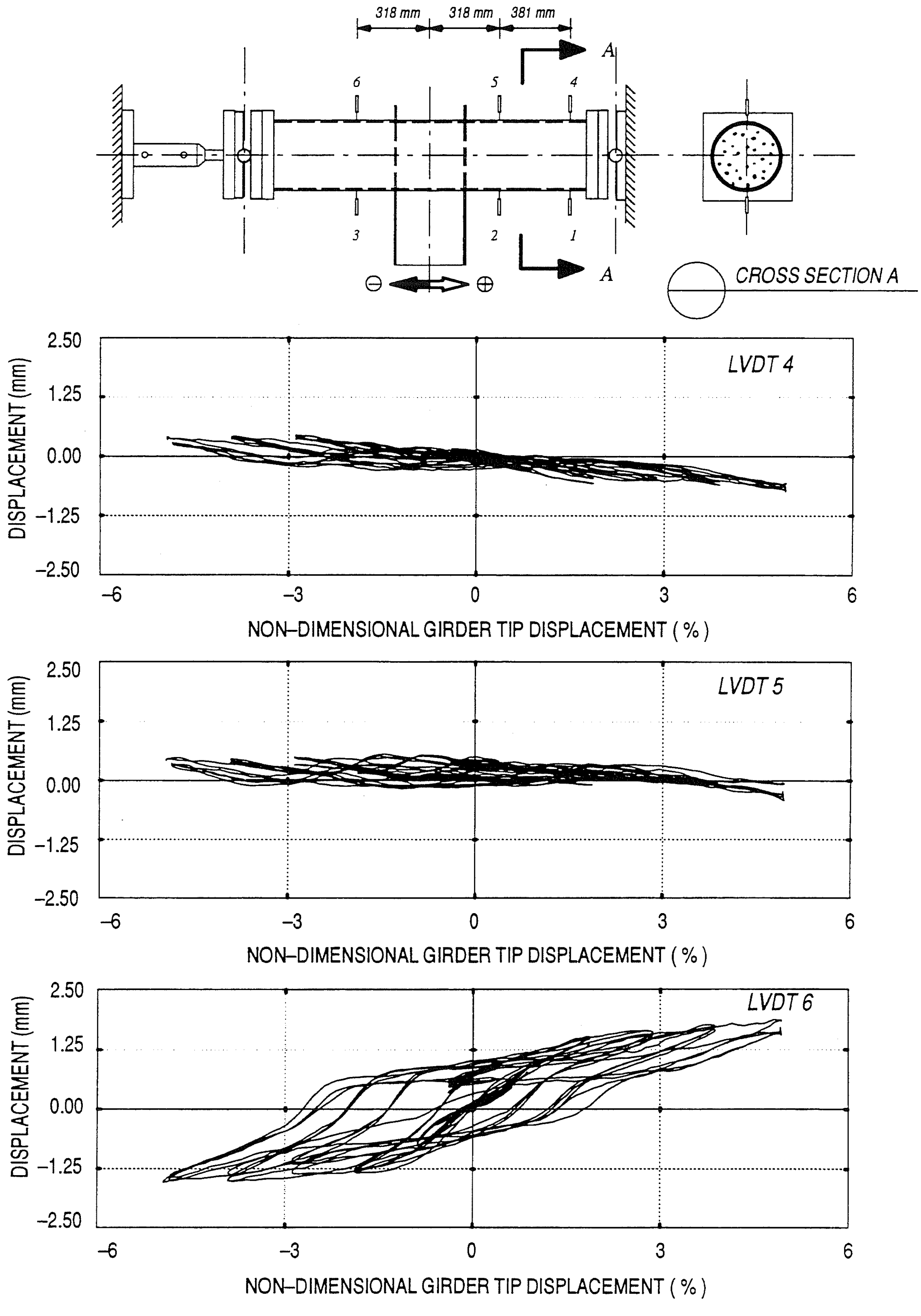

Figure B.10 b. Lateral Displacement of the CFT for Connection *Type VI*

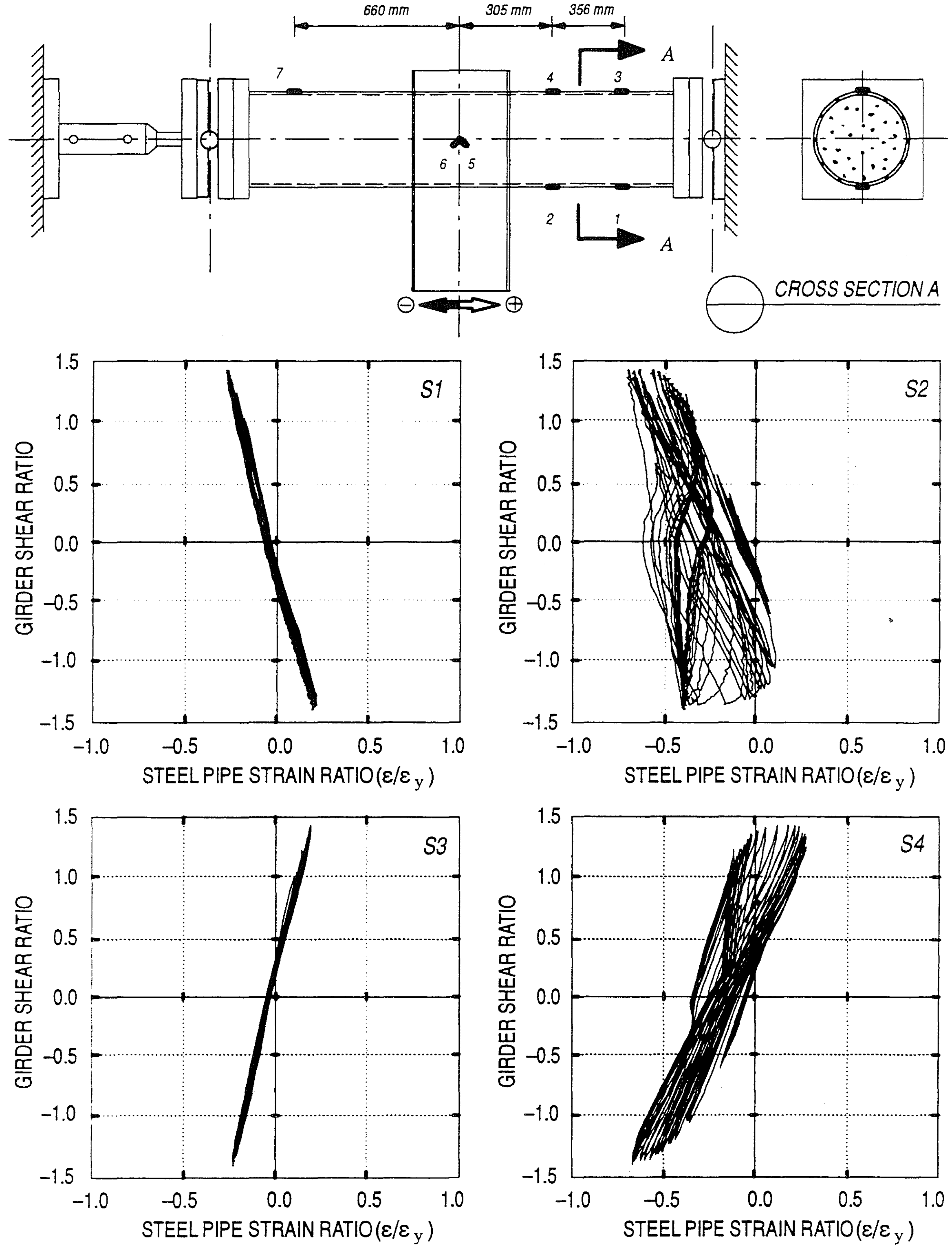

Figure B.11 a. Measured Strains in the Steel Pipe for Connection *Type VII*

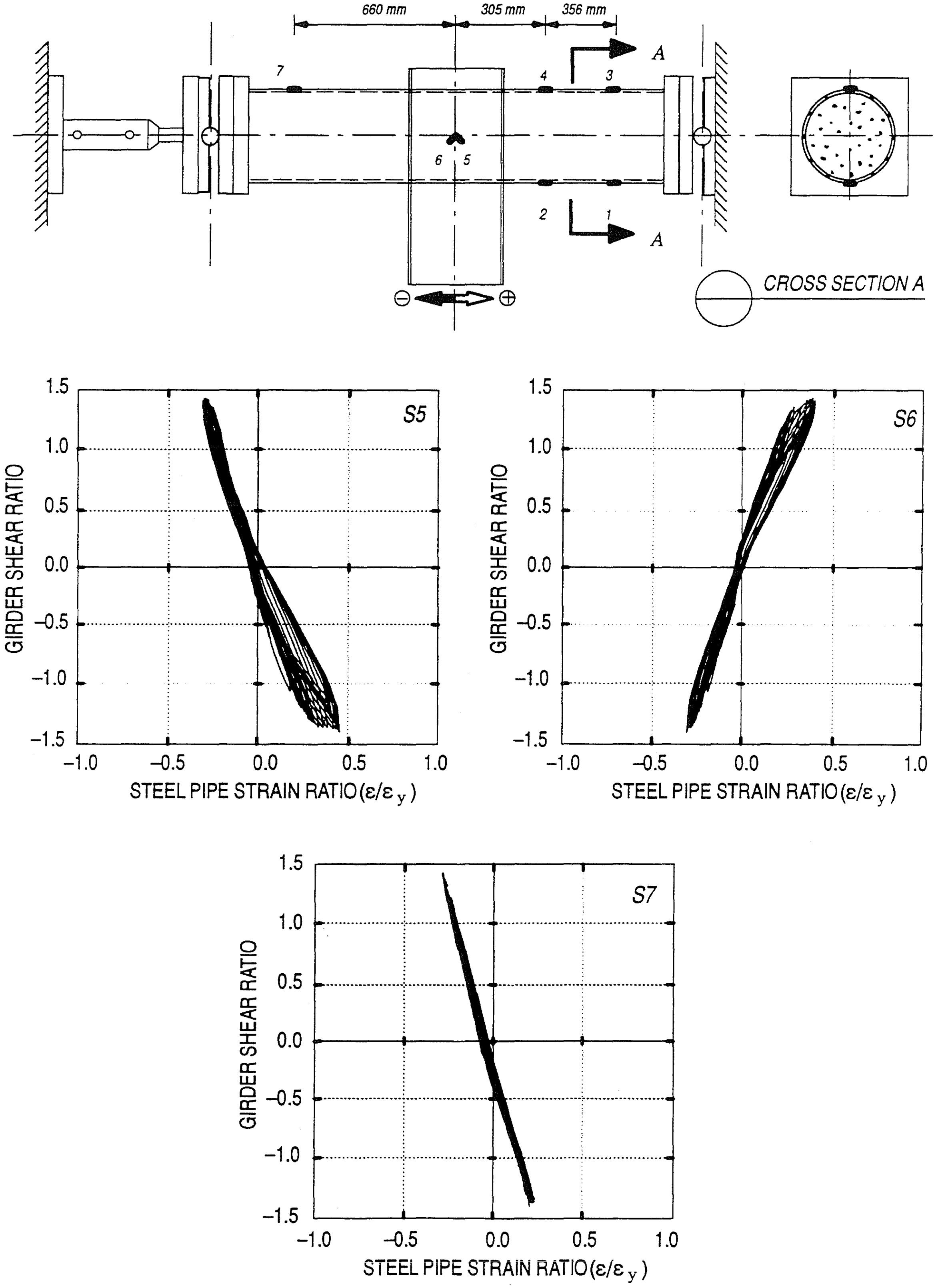

Figure B.11 b. Measured Strains in the Steel Pipe for Connection *Type VII*

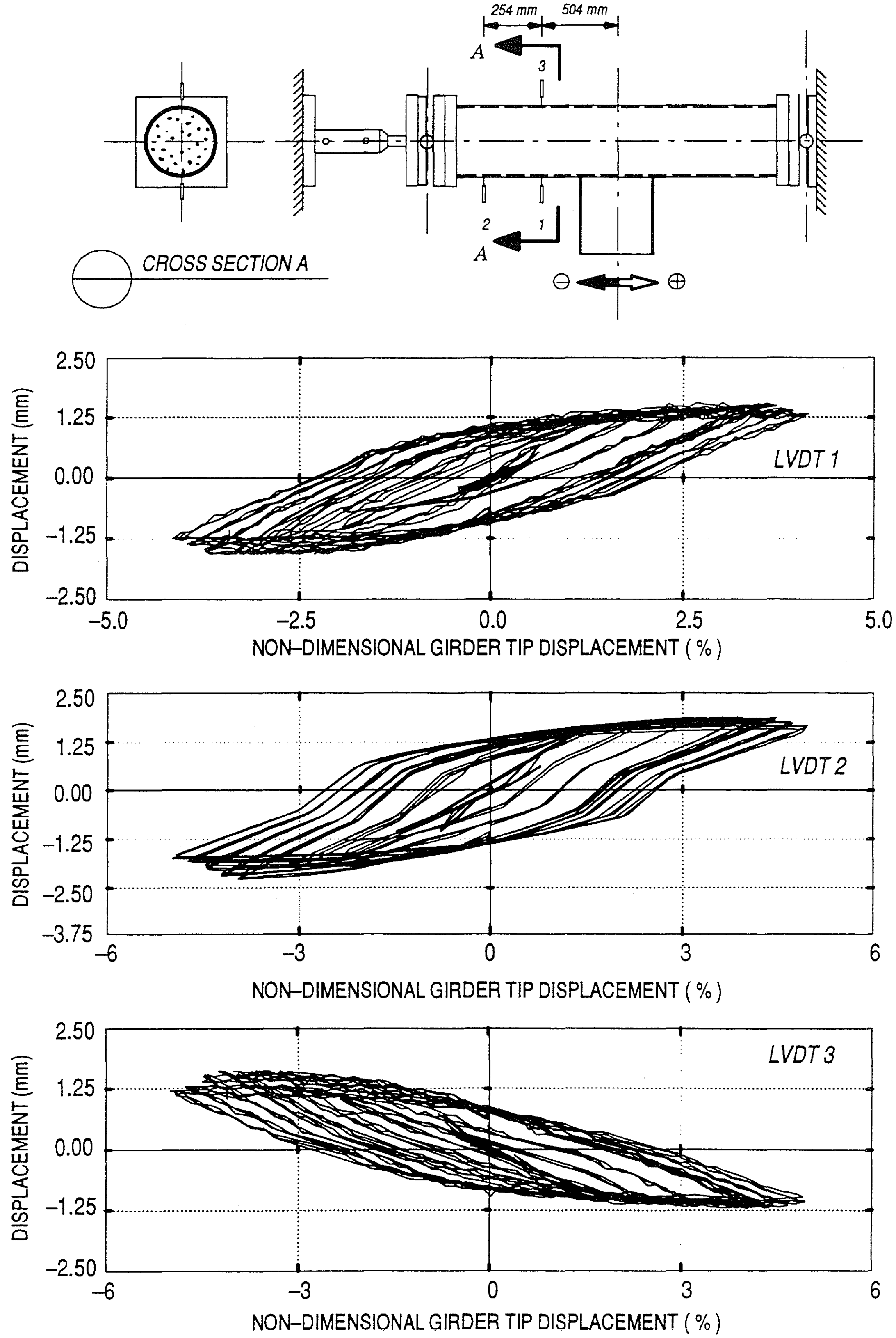

Figure B.12. Lateral Displacement of the CFT for Connection *Type VII*

APPENDIX C

TEST APPARATUS DEFORMATIONS

The imposed displacement at the girder tip and the deformations of the CFT column were modified to eliminate any effects from the test apparatus deformations. The deformations of the test apparatus and the variation of the CFT axial load during the test are presented in this appendix.

In general, the deformations of the test apparatus were less than 2.5 mm (0.1″). Less than one–fifth of this displacement was due to the elastic deformation of the channels, and the reset was due to the elastic bending of the end plates that attached the channels to the reaction block. Mechanical dial gages were used to monitor the test apparatus deformations while testing connection *Type I*, therefore, no graphical data are shown for this specimen in this appendix.

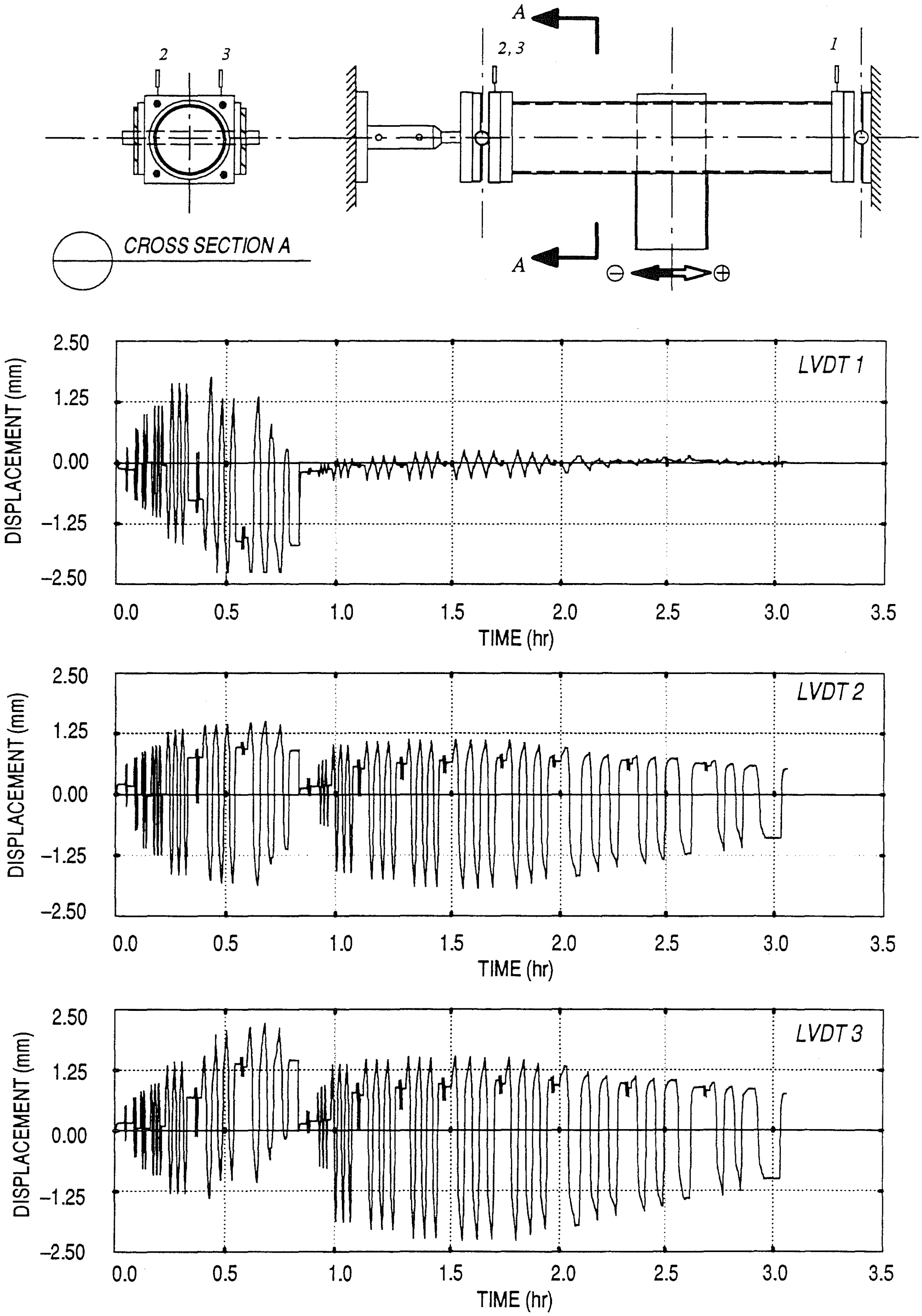

Figure C.1. Displacement of the Test Apparatus for Connection *Type IA*

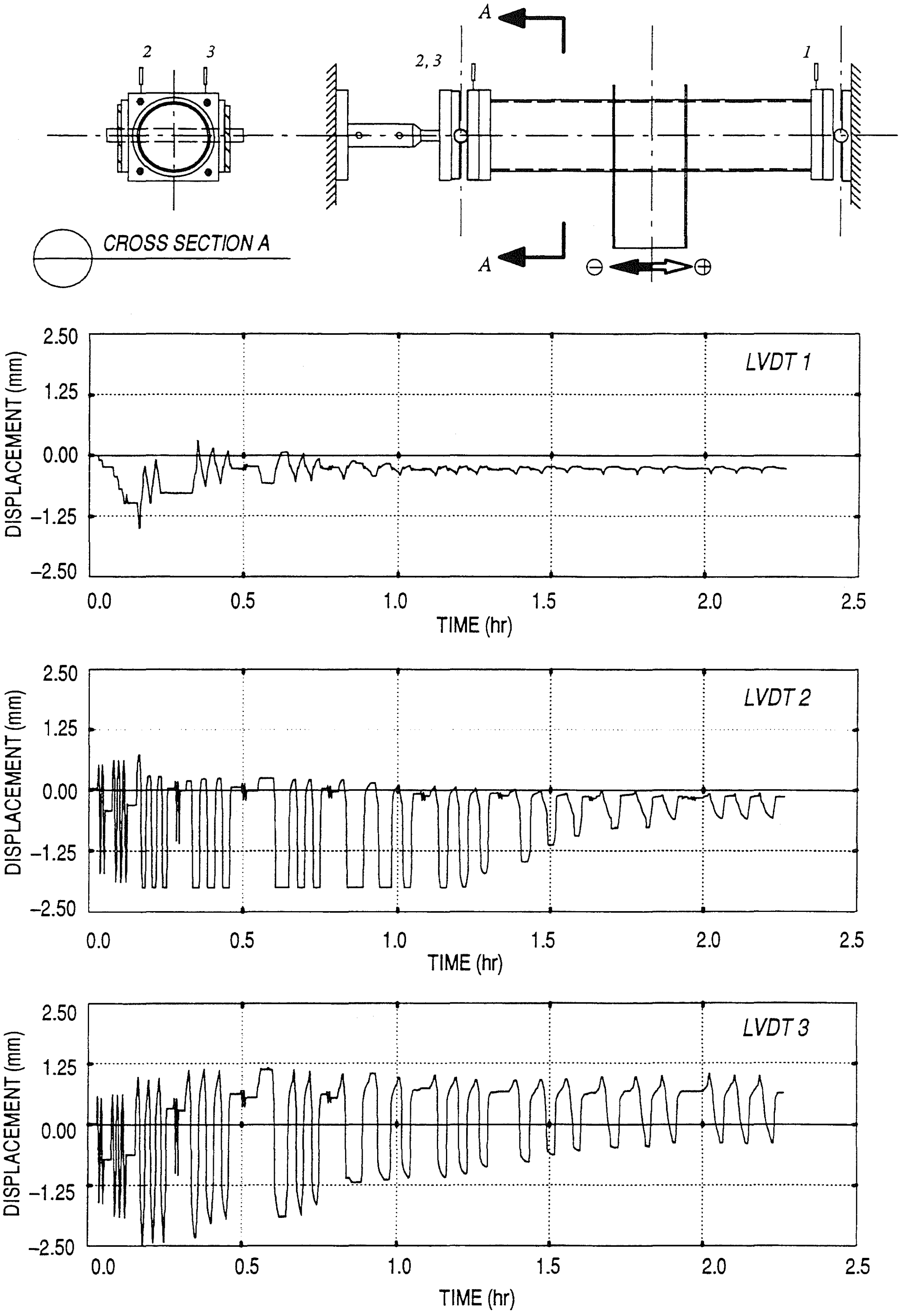

Figure C.2. Displacement of the Test Apparatus for Connection *Type II*

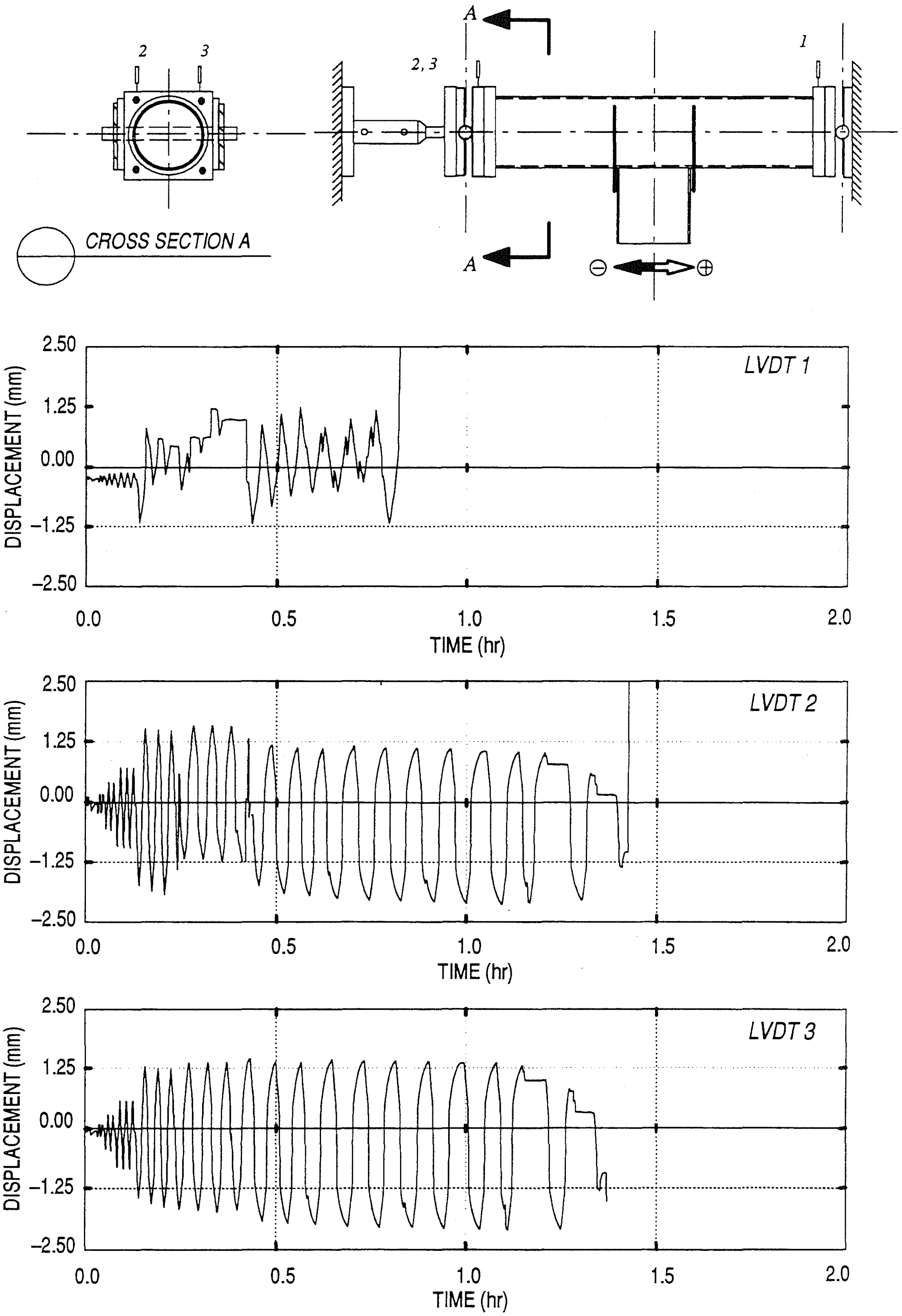

Figure C.3. Displacement of the Test Apparatus for Connection *Type III*

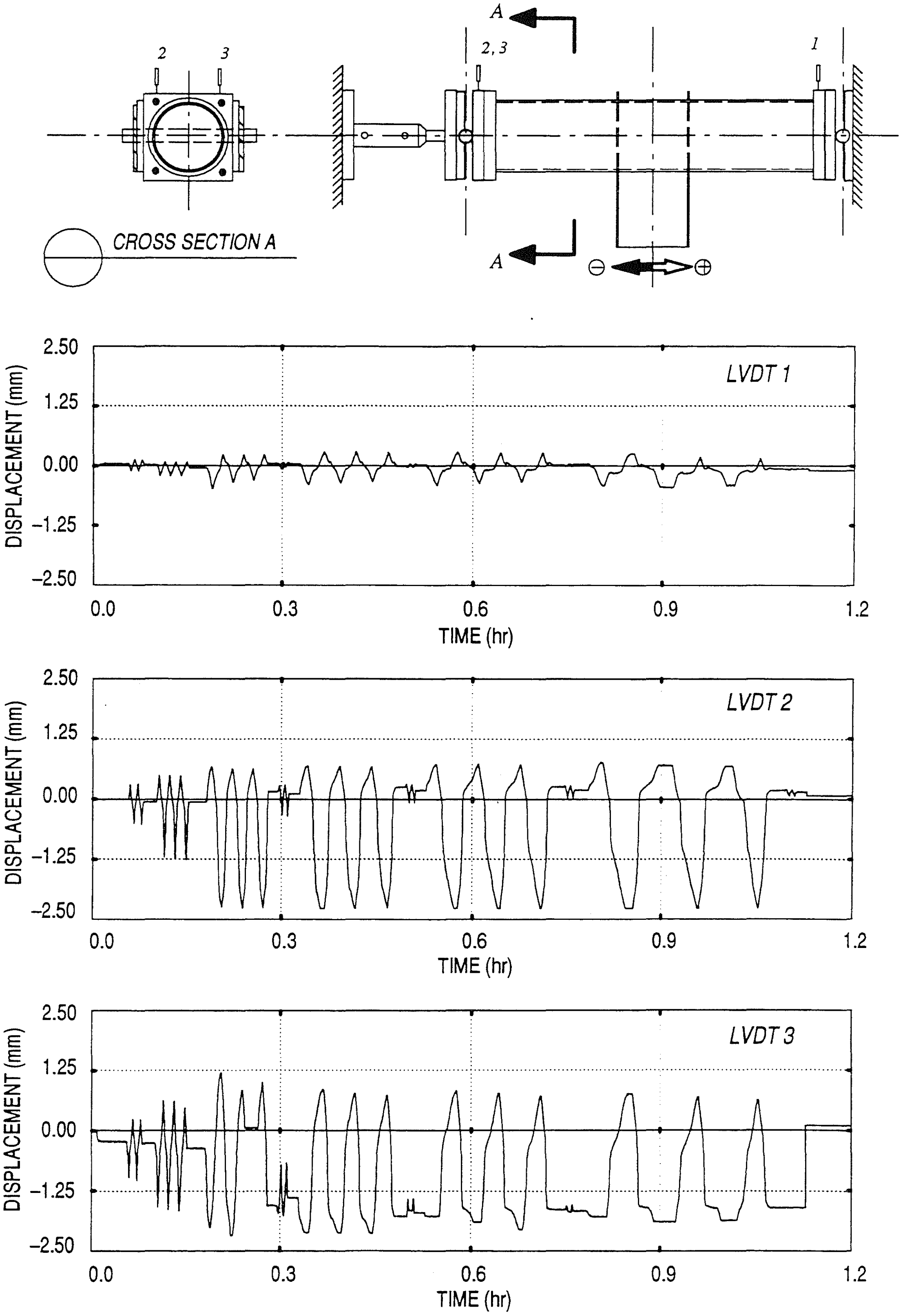

Figure C.4. Displacement of the Test Apparatus for Connection *Type VI*

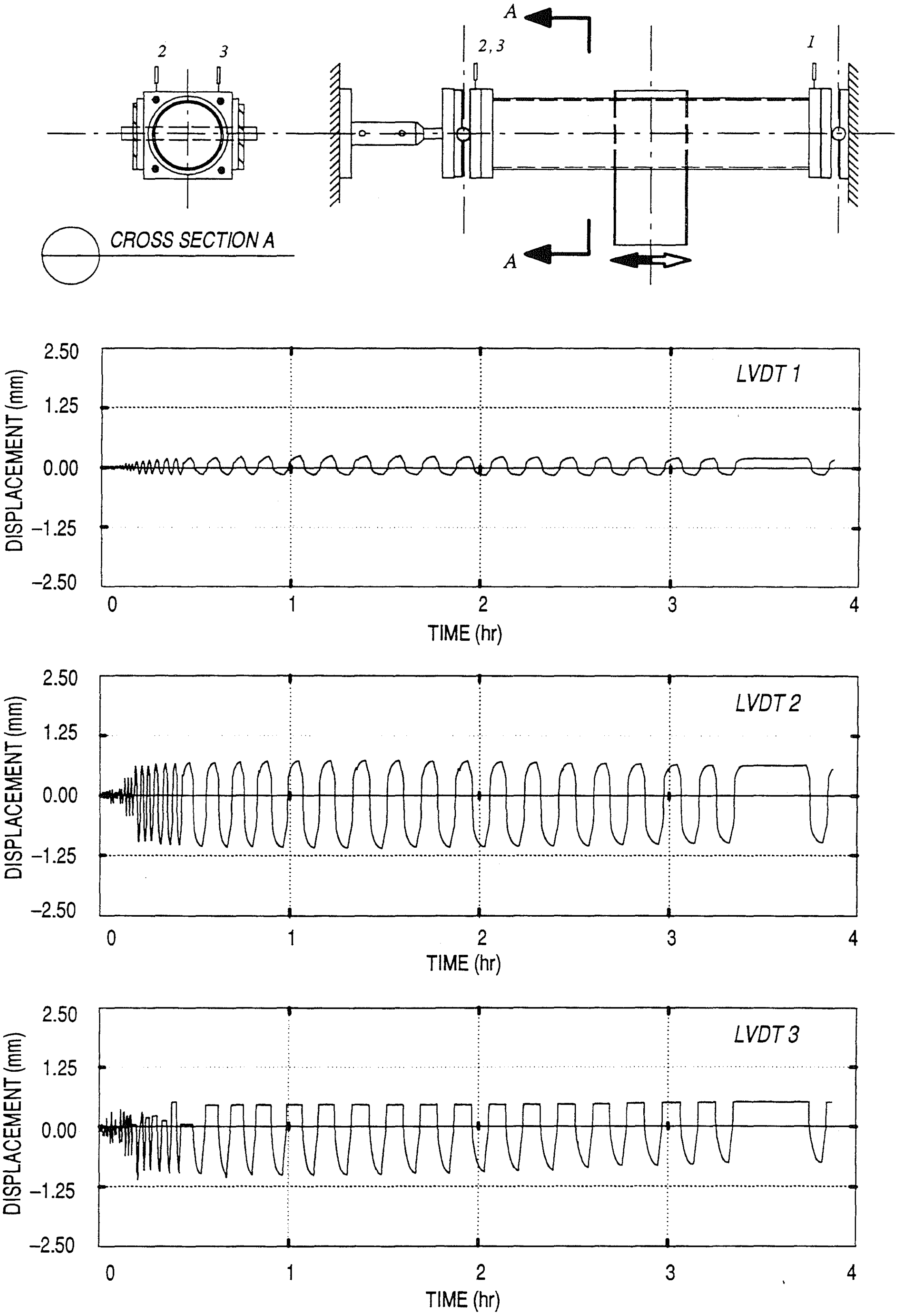

Figure C.5. Displacement of the Test Apparatus for Connection *Type VII*

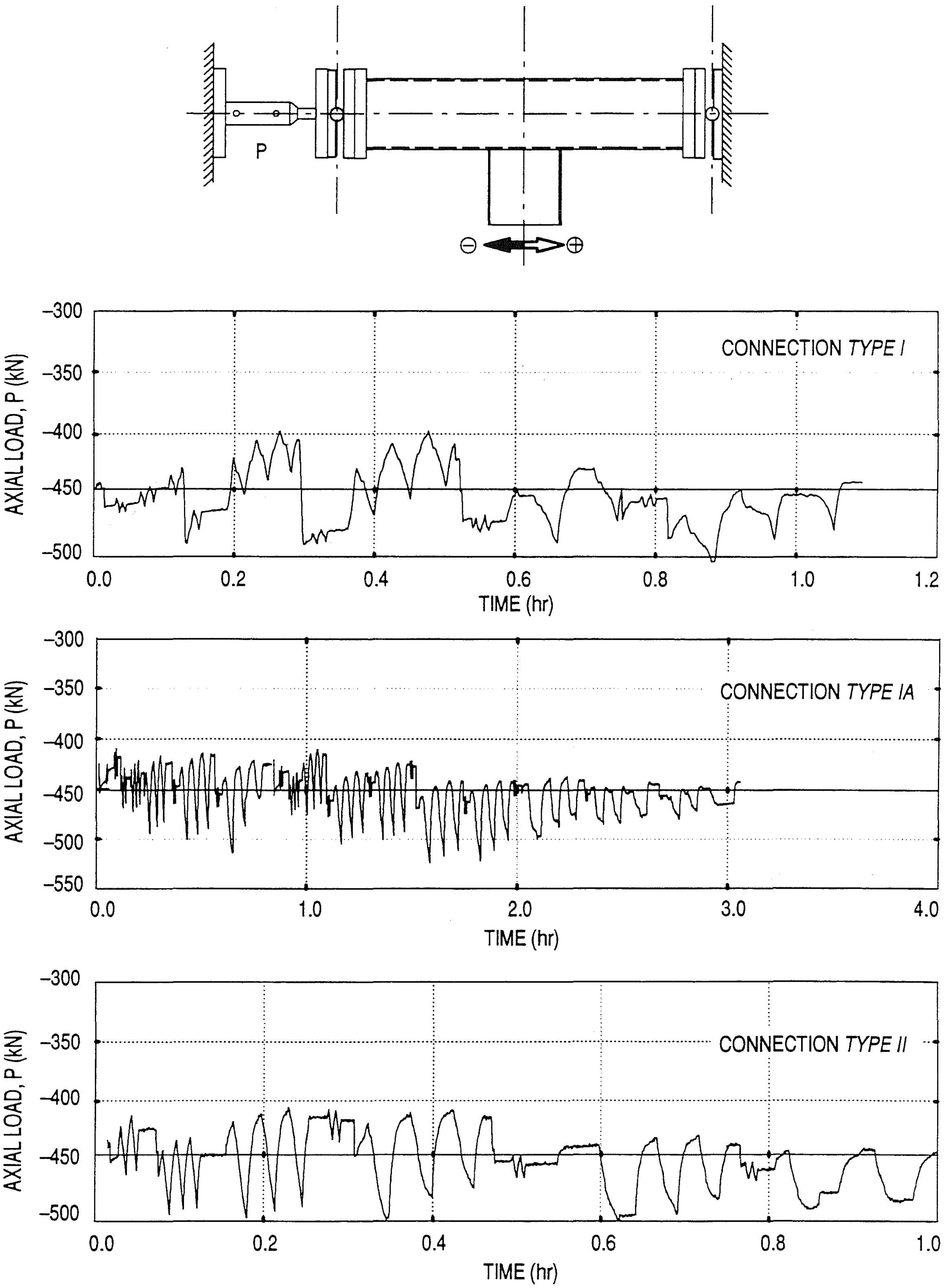

Figure C.6. Variation of the CFT Axial Load During the Test

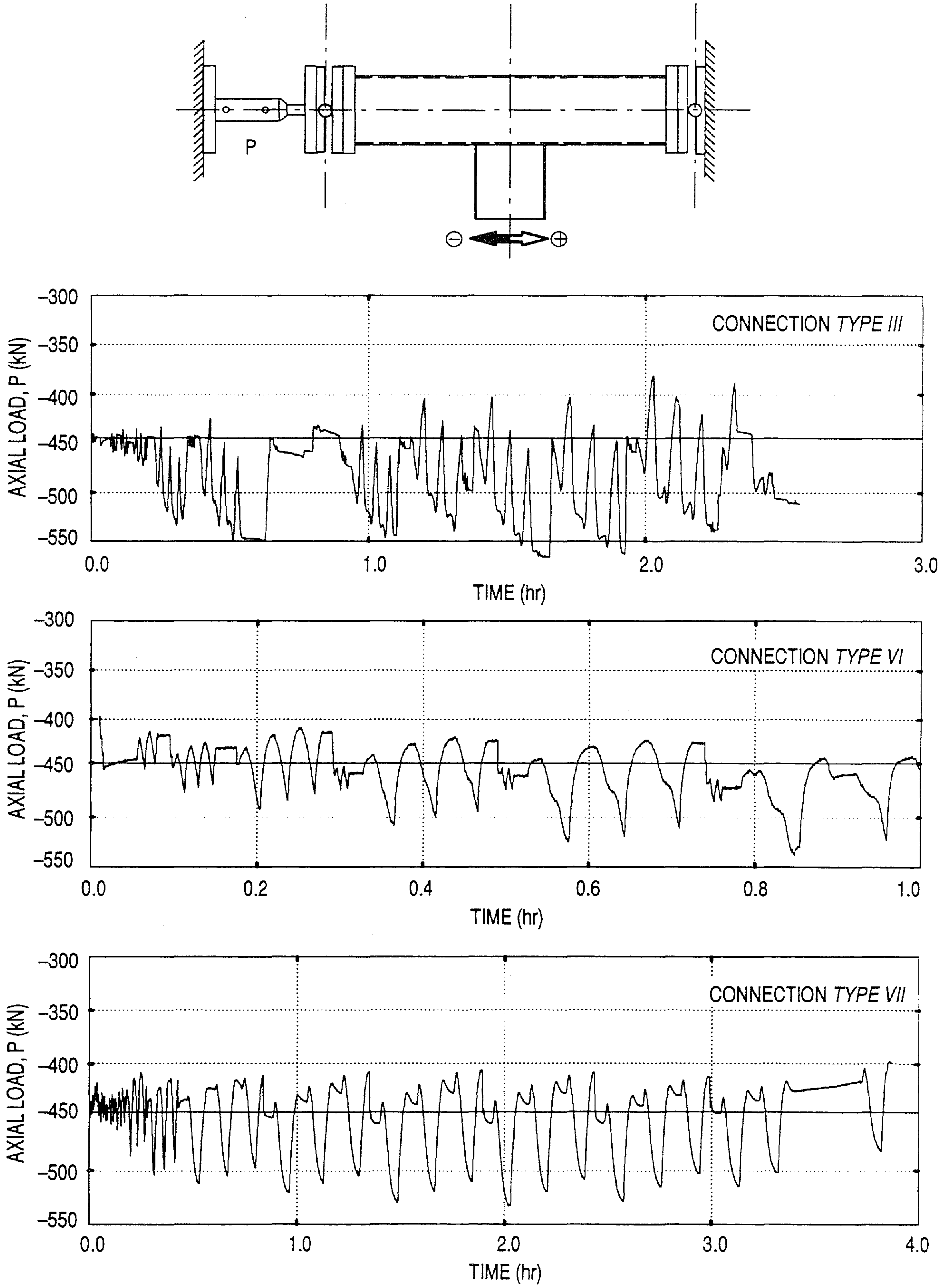

Figure C.6. Variation of the CFT Axial Load During the Test, *continued*

VITA

The author was born on April 25, 1966 in Saudi Arabia. In 1989 he received a B.S. degree in civil engineering from Jordan University of Science and Technology (JUST), and in 1992, he received an M.S. degree in civil engineering from the same university. In 1993, the author enrolled in the Ph.D. program in civil engineering at the University of Illinois at Urbana–Champaign (UIUC). Yousef Alostaz started his professional career in 1988 as a supervising engineer at the engineering office at JUST. Between 1989 and 1992, he worked as a research assistant at JUST. After joining the UIUC, he worked as a research assistant between 1994 and 1997.